Experimental Aerodynamic Characteristics of Two V/STOL Fighter/Attack Aircraft Configurations at Mach Numbers From 0.4 to 1.4

Walter P. Nelms
Donald A. Durston, Ames Research Center, Moffett Field, California
J. R. Lummus, General Dynamics, Fort Worth Division, Fort Worth, Texas



National Aeronautics and Space Administration

Ames Research Center Moffett Field, California 94035



Experimental Aerodynamic Characteristics of Two V/STOL Fighter/Attack Aircraft Configurations at Mach Numbers From 0.4 to 1.4

Walter P. Nelms
Donald A. Durston, Ames Research Center, Moffett Field, California
J. R. Lummus, General Dynamics, Fort Worth Division, Fort Worth, Texas



Ames Research Center Moffett Field, California 94035



TABLE OF CONTENTS

	Page
NOMENCLATURE	v
SUMMARY	1
INTRODUCTION	2
TEST FACILITY	. 2
MODEL DESCRIPTION	3 3 3
TEST CONDITIONS AND PROCEDURES	3
RESULTS AND DISCUSSION	4 5 6 7 8
CONCLUDING REMARKS	8
REFERENCES	10
TABLES	11
FIGURES	15



NOMENCLATURE

The axis system and sign conventions are shown in figure 1. The longitudinal characteristics are presented in the stability-axis coordinate system and the lateral-directional characteristics are presented in the body-axis coordinate system.

- A aspect ratio
- a.c. aerodynamic center
- B.L. buttockline, spanwise distance from model centerline
- b wing span
- $\textbf{C}_{\textbf{A}_{\textbf{TNT}}}$ internal (duct) axial force coefficient
- C_D drag coefficient, drag/qS
- C_I lift coefficient, lift/qS
- $C_{\widetilde{L}_{\sim}}$ lift curve slope
- Compared to the coefficient, rolling moment/qSb
- $C_{\ell_{\mathcal{Q}}}$ lateral stability derivative
- C_m pitching-moment coefficient, pitching moment/qS \bar{c}
- C_{m_0} zero-lift pitching moment
- $C_{
 m N_{TNT}}$ internal (duct) normal-force coefficient
- $\mathtt{C}_{\mathtt{n}}$ yawing-moment coefficient, yawing moment/qSb
- C_{ng} directional stability derivative
- C_R root chord
- C_T tip chord
- Cy side-force coefficient, side force/qS
- $C_{Y_{\mathcal{Q}}}$ side-force derivative
- c wing mean aerodynamic chord
- F.S. fuselage station
- H.L. hinge line

- L/D lift-to-drag ratio
- M free-stream Mach number
- Re/L unit Reynolds number
- S wing area
- S.S. span station
- W.L. waterline, vertical distance from model centerline
- α angle of attack
- β angle of sideslip
- Λ sweep angle

Configuration Code

Note: Since there were no strake options on the RALS configuration, \mathbf{B}_2 includes both body and strake.

Component	Ejector	RALS
Body	B ₁	B ₂
Strake		
Baseline	S ₁	
High-sweep	S_2	
Off	S ₃	
Nacelles	N	N
Wing	W_1	W ₂
Canard longitudinal location		
Mid (baseline)	C ₁	C 1
Forward	C2	C_2
Aft	C ₃	C 3
Vertical tail and dorsal	V	v

Flap deflection and incidence of all-movable surfaces (common to both configurations)

	Wing	Canard	Vertical Tail
Leading-edge flap	LE-W	LE-C	
Trailing-edge flap	TE-W	TE-C	
Incidence (of all-movable surfaces)		Canard	Vert

EXPERIMENTAL AERODYNAMIC CHARACTERISTICS OF TWO V/STOL

FIGHTER/ATTACK AIRCRAFT CONFIGURATIONS

AT MACH NUMBERS FROM 0.4 TO 1.4

Walter P. Nelms and Donald A. Durston
Ames Research Center

and

J. R. Lummus General Dynamics, Fort Worth Division

SUMMARY

A wind-tunnel test was conducted at Ames Research Center to measure the aerodynamic characteristics of two horizontal-attitude takeoff and landing V/STOL fighter/attack aircraft concepts. The concepts were developed by the General Dynamics Corporation, Fort Worth Division, during a contract study for Ames Research Center and the David Taylor Naval Ship Research and Development Center (DTNSRDC). One aircraft concept was configured to use an ejector to provide propulsive lift; the other used separately ducted and heated fan air to provide propulsive lift (remote augmentation lift system (RALS)). Neither of these propulsive lift devices was simulated during the tests reported here. The tests did investigate the aerodynamic uncertainties for these concepts over a Mach number range from 0.2 to 2.0. The present report covers tests, conducted in the Ames 11-Foot Transonic Wind Tunnel, for Mach numbers from 0.4 to 1.4.

The test results show the plotted effects of varying the angle of attack $(0^{\circ} \text{ to } 27^{\circ})$, angle of sideslip $(-4^{\circ} \text{ to } +8^{\circ})$, Mach number (0.4 to 1.4), Reynolds number $(9.8 \times 10^6 / \text{m to } 23.0 \times 10^6 / \text{m} (3.0 \times 10^6 / \text{ft to } 7.0 \times 10^6 / \text{ft}))$, and configuration buildup. In addition, the effects of wing trailing-edge flap deflections, canard incidence, and vertical tail deflections are presented. Variable canard longitudinal location and different shapes of the inboard nacelle-body strakes were also investigated. The results indicate that high lift characteristics ($C_{L_{max}} \approx$ 2.0) can be obtained with the baseline configurations of both models over most of the Mach number range. This is attributable to a combination of the beneficial effect of the inboard strake vortices over the wide body and the favorable interaction between the canard and wing flows. The baseline configurations exhibited relatively high longitudinal instability at low Mach numbers (over 28% at Mach number 0.4); they became nearly neutrally stable at supersonic speeds. Trailing-edge wing flaps were found to be the most effective trimming devices on both models. Variable canard incidence contributed somewhat, but lost effectiveness at the higher incidence angles (-20°) or at moderate aircraft angles of attack $(12^{\circ}-15^{\circ})$.

Longitudinal stability was increased for the ejector configuration by an aft movement of the canard and by a reduction in the planform size of the strakes. In general, however, the canard located midway between the aft and forward location and the baseline strakes produced the most favorable lift and drag characteristics. Likewise, on the RALS configuration, the midcanard location gave the higher lift, and the aft position produced the greater longitudinal stability.

INTRODUCTION

Ames Research Center has a number of research programs under way to develop aerodynamic and aerodynamic-propulsion integration technology for V/STOL fighter/attack aircraft of the post-1990 time period. One of these programs was a contract study that was jointly sponsored with the David Taylor Naval Ship Research and Development Center and the Naval Air Systems Command. In Phase I of the program, four contractors provided conceptual designs, estimated the aerodynamics of the designs, identified aerodynamic uncertainties, and proposed a wind-tunnel program to explore these uncertainties. References 1 through 5 give the detailed results of this Phase I effort, and reference 6 presents a summary of these studies and of several other related programs at Ames. In Phase II of the program, two contractors designed and built wind-tunnel models for tests in the Ames Unitary and 12-Foot Wind Tunnels; the tests cover a Mach number range of 0.2 to 2.0.

This report presents the results of transonic tests of two models designed and built in Phase II by the General Dynamics Corporation (ref. 1). Two concepts were investigated, both of which were horizontal-attitude take-off and landing V/STOL fighter/attack aircraft. One model was a representation of a V/STOL fighter aircraft employing a jet diffuser ejector for its propulsive lift system; the other model represents an aircraft featuring engine air ducting to a forward combustor and nozzles (remote augmentation lift system (RALS)).

The experimental investigation documented in this report was conducted in the Ames 11-Foot Transonic Wind Tunnel over a Mach number range of 0.4 to 1.4. The Reynolds number was held constant at $9.84\times10^6/m$ ($3.0\times10^6/ft$). Angle of attack was varied up to approximately 27° and angles of sideslip ranged from -4° to +8°. Model variations investigated included component buildup, canard longitudinal location, inboard strake shape, and deflections of the canard, wing trailing-edge flaps, and vertical tail.

TEST FACILITY

The tests were conducted in the Ames 11-Foot Transonic Wind Tunnel, which is a variable-density, closed-circuit, continuous-flow facility. This tunnel has an adjustable nozzle (two flexible walls) and a slotted test section to permit transonic testing over a Mach number range that is continuously variable from 0.4 to 1.4.

MODEL DESCRIPTION

Two models were tested, one representative of a V/STOL fighter/attack aircraft using a jet diffuser ejector for its vertical lift system (identified as configuration E205) and the other representative of a concept with a remote augmentation lift system (RALS) for vertical takeoff and landing (configuration R104). The models were 9.39-percent scaled versions of the conceptual aircraft described in reference 1.

Configuration E205

A three-view drawing of the wind-tunnel model simulating a V/STOL fighter with a jet diffuser ejector vertical lift system (model E205) is shown in figure 2(a). Pertinent dimensions, areas, and other parameters are presented in table 1 and in figures 2(b) and 2(c). Figure 2(d) gives a cross-sectional area distribution of the wind-tunnel model. Photographs of the model and its installation in the 11-Foot Wind Tunnel are shown in figure 3.

Parametric variations available on the model (not all were investigated in the present test) included: component buildup, variable wing outboard and inboard trailing-edge flaps, variable wing leading-edge flaps, a variable incidence canard with variable leading- and trailing-edge flaps, three longitudinal canard locations, three inboard nacelle/body strake shapes, and an all-movable vertical tail. A wing-root bending moment gage was installed to obtain an indication of buffet onset. The term baseline configuration as used herein refers to the model with the mid-canard location (fig. 2(a)) and the baseline strake (S₁ in fig. 2(c)).

Configuration R104

Figure 4(a) is a three-view drawing of the wind-tunnel model of a V/STOL fighter employing RALS for vertical lift. Pertinent dimensions, areas, and other parameters are given in table 2 and in figure 4(b). Figure 4(c) shows the cross-sectional-area distribution of the wind-tunnel model. Photographs of the model and of the model installed in the Ames 11-Foot Transonic Wind Tunnel are presented in figure 5.

The parametric variations on the R104 configuration were the same as those of the E205 model except that only one inboard nacelle/body strake shape was available. The baseline configuration again has the mid-canard location (fig. 4(a)).

TEST CONDITIONS AND PROCEDURES

Tests were conducted at Mach numbers of 0.4 to 1.4 at a constant unit Reynolds number of 9.84×10^6 /m $(3.0 \times 10^6$ /ft). Angle of attack was varied up

to the maximum allowable loading (about 27° at the lower Mach numbers), using a +12.5° bent sting arrangement; angle of sideslip ranged from -4° to +8°. The angles of attack and angles of sideslip were corrected for wind-tunnel flow misalignment and for balance and sting deflections caused by aerodynamic loads. Runs to evaluate Reynolds number effects were made at Mach numbers 0.6, 0.9, and 1.2 for the E205 configuration.

The models were sting-supported through the base of the fuselage body on a 2.5-in. six-component strain-gage balance. The moment reference center for both models was located longitudinally at 3 percent of the mean aerodynamic chord, which represents a fuselage station of 0.737 m (29.002 in.) on the E205 model, and a fuselage station of 0.748 m (29.463 in.) on the R104 model. Measured axial forces have been adjusted to a condition corresponding to that of having free-stream static pressure acting on the fuselage cavity and on the base areas of the two nacelle choke plugs.

The data presented in this report have been adjusted for internal forces acting in the flow-through nacelles. These internal axial and normal forces were derived from a series of runs employing a duct exit rake in both nacelles. These rakes, each with 20 total head tubes, were calibrated prior to the test against known mass flows measured by standard ASME nozzles. The duct exit static pressures were measured during the internal flow survey, using a series of orifices located around the periphery of the nacelle choke plugs. Figure 6 shows the rake installation on the E205 model in the 11-Foot Tunnel. The resulting internal force coefficients that have been applied to the data are presented in table 3 (E205) and table 4 (R104) as a function of Mach number and angle of attack.

To assure an all turbulent boundary layer, transition strips consisting of a random distribution of 0.0175-0.0208-cm (0.0069-0.0082-in.) sieved glass spheres were placed near the leading edges of the wing, canard, and vertical tail, around the fuselage nose, and around the nacelle leading edges. Experience with the 11-Foot Wind Tunnel has shown that grit of this size would produce a turbulent boundary layer on the model, at the conditions of the test, without causing grit-associated drag.

RESULTS AND DISCUSSION

Experimental aerodynamic data for the two models are presented in figures 7 through 120. The E205 model results are shown in figures 7 through 80 and the R104 results are presented in figures 81 through 120.

To expedite publication of the data, only a brief description of the test results is presented in the following sections. An in-depth analysis of the data and comparison with theoretical estimates will be reported in subsequent publications.

Baseline E205 Configuration

Longitudinal characteristics (zero deflection on all surfaces)- The effect of Mach number on the longitudinal characteristics of the baseline configuration is presented in figure 7. Maximum permissible loading of the balance and sting limited angle of attack to about 25° to 27° at subsonic speeds and to about 20° at supersonic speeds. Lift coefficients continued to increase to these angles of attack at all test Mach numbers, and maximum lift could not be reached. Summary data for the effects of Mach number are given in figure 8.

Figures 9-11 show the effect of variations in Reynolds number at Mach numbers of 0.6, 0.9, and 1.2, respectively. Little or no effect on the longitudinal characteristics is displayed for the Reynolds number range that could be achieved in the 11-Foot Wind Tunnel within permissible maximum loading.

Longitudinal aerodynamic characteristics resulting from model component buildup are presented in figures 12 through 19. The body-nacelle-alone configuration exhibited relatively high lift coefficients (up to 0.9) resulting from a favorable interaction of the inboard nacelle/body strake on the wide area between the nacelles. Addition of the wing further increased this lift; the canard, through favorable interaction with the wing, improved both the lift and drag up to the maximum angles of attack of the test. It is believed that the high lift coefficients generated by this model are due to a combination of the favorable interaction of the inboard strake on the wide body together with the favorable interaction of the canard on the wing. The effects of component buildup on pitching moment coefficient were essentially as would be expected by locating lifting areas fore and aft of the moment reference center. Figure 20 presents a summary of the Mach number effects on longitudinal aerodynamics for a buildup of model components.

Lateral/directional characteristics- Figures 21-23 show the lateral/directional aerodynamic characteristics at various angles of attack for the baseline configuration. The model produced positive directional stability (+Cn $_{\beta}$) and positive effective dihedral (-C $_{\lambda\beta}$) up to angles of attack of about 17° at Mach 0.6. At Mach 0.9, Cn $_{\beta}$ is positive to about 10° and the effective dihedral is positive at all angles of attack. At Mach number 1.2, changes in directional stability are exhibited between β = ±2° at positive angles of attack.

Canard-off effects on the lateral/directional characteristics of the baseline configuration are shown for two angles of attack in figures 25 and 26 for Mach numbers 0.9 and 1.2, respectively.

Trim characteristics- Figures 27 through 35 present the trim characteristics of the baseline configuration. Canard incidence variations (0°, $\pm 10^{\circ}$, -20°) and canard-off are shown for three wing trailing-edge flap deflections (0°, 10° , 25°) at Mach numbers of 0.6, 0.9, and 1.2. For these runs, the wing outboard and inboard trailing-edge flaps were deflected as a unit.

Although available, canard incidence of +20° and wing trailing-edge flap deflection of 20° were not run in order to conserve test time. Likewise, the effects on trim of canard leading- and trailing-edge flap deflections and wing leading-edge flap deflection (all available on the model) were not investigated during this tunnel entry, due to limited test time.

Figures 36 through 38 present some of the previous data replotted to show the effectiveness of the trailing-edge flap as a trimming device. The longitudinal aerodynamic characteristics are shown for three flap deflections (0°, 10°, 25°) with zero canard incidence at Mach numbers of 0.6, 0.9, and 1.2.

The results of the trim investigation indicate that the configuration could be trimmed over a range of angle of attack, using a combination of wing trailing-edge flap deflection and canard incidence. Of the two surfaces, the wing trailing-edge flaps proved to be the most effective trimming device. For the subsonic speeds, the canard became essentially ineffective at the negative deflections at relatively low angles of attack. This would suggest that for this particular configuration the canard would be scheduled with angle of attack and Mach number to give the most favorable interaction with the wing (provide the highest L/D), and the wing trailing-edge flaps would be used as the primary surface to provide trim.

Vertical tail effects- The longitudinal and lateral/directional aerodynamic characteristics resulting from deflection of the vertical tail are presented in figures 39 through 42 for Mach numbers 0.9 and 1.2. As expected, the vertical tail deflection is seen (figs. 39 and 40) to have little effect on the longitudinal characteristics, with the most significant effect being an increase in \mathcal{C}_{D} and a reduction in L/D for the higher deflections.

The lateral/directional characteristics are shown in figures 41 and 42 for vertical-tail-off and for deflections of 0°, 5°, and 15° at two angles of attack for each Mach number. The results indicate that deflecting the vertical tail was effective in producing significant control forces over the angle-of-attack and angle-of-sideslip ranges of the test.

It should be noted that when an angle of attack is given in a figure caption, it is only the nominal value; more accurate angles (to within $\pm 0.5^{\circ}$) are given at the top of each plot page.

Effects of Alternative Components

Canard location effects— The effect on the longitudinal aerodynamic characteristics of varying the canard longitudinal location (see fig. 2(a) for positions) is given in figures 43 through 69. Data are presented for canard deflections of 0° and $\pm 10^\circ$ at Mach numbers of 0.6, 0.9, and 1.2 for each of the three strake options (baseline, high-sweep, and "off" as shown in fig. 2(c)). The most pronounced effect of canard location is seen in the pitching moment, where the forward canard (C_2) accounts for the greater instability, as expected. The mid-canard (C_1) generally has the most favorable lift and drag of the three positions over the range of strake options and Mach numbers.

Lateral/directional characteristics are shown in figures 70 through 73 at two angles of attack, with and without the vertical tail, for Mach numbers of 0.9 and 1.2. There are some slight differences in these characteristics among the three canard locations; the trends and magnitude of the differences vary with Mach number and angle of attack.

Strake effects— The longitudinal aerodynamic effects due to the strake variations on the model (fig. 2(c)) are presented in figures 74 through 76 for Mach numbers of 0.6, 0.9, and 1.2. The canard was held at the midposition at 0° of incidence for these plots. With the baseline strake, the model L/D is greater, relative to the high-sweep and strake "off" configurations. However, a penalty is incurred in the pitching moment because of the baseline strake contributing to more longitudinal instability. This is primarily due to the slight increase in forward planform area of the baseline strake over the others (see fig. 2(c)).

The lateral/directional characteristics for the strake variations are plotted in figures 77 through 80 in a sequence similar to that for the canard location effects. Generally, the baseline strake configuration is slightly more stable than the other two in terms of yawing and rolling moments. There is little difference in side force due to the three strake variations.

Baseline R104 Configuration

Longitudinal characteristics (zero deflection on all surfaces)— The effect of Mach number on the longitudinal characteristics of the baseline configuration is presented in figure 81, and summary data are given in figure 82. In general, the results are similar to those previously discussed for the E205 configuration. However, the R104 configuration has higher minimum drag than the E205 configuration at supersonic speeds. It is felt that this increased drag is due to (1) changes from the flight vehicle lines as a result of using the E205 nose and cockpit section on the R104 model (to reduce costs), which resulted in a "necked down" section aft of the cockpit (see fig. 4(a)); (2) inefficient flow in the top channels between the aft portion of the nacelles and fuselages (these channels are narrower on the R104 configuration); and (3) an area distribution on the R104 configuration that exhibits greater peakedness (compare figs. 4(c) and 2(d)).

Longitudinal aerodynamic characteristics resulting from model component buildup are shown in figures 83 through 90; figure 91 presents a summary with Mach number. A canard-on with wing-off configuration, added to this series of runs, was not used during tests of the E205 model. Otherwise, the results are similar to those of the E205 configuration with exception of the aforementioned minimum drag difference.

Lateral/directional characteristics- Figures 92-94 show the lateral/directional aerodynamic characteristics at various angles of attack for the baseline configuration. The results are similar to those of the E205 configuration, except that the R104 concept appears to be slightly more directionally unstable at the higher angles of attack. Also, the changes in

directional stability exhibited by the E205 model between $\beta=\pm2^{\circ}$ at Mach number 1.2 are not as evident on the R104 configuration. Figure 95 presents a summary with angle of attack of these basic lateral/directional characteristics.

Canard-off effects on the lateral/directional characteristics of the baseline R104 configuration are shown for two angles of attack in figures 96 and 97 for Mach numbers 0.9 and 1.2, respectively.

Trim characteristics- Figures 98 through 106 present the trim characteristics of the baseline R104 configuration, using canard incidence and wing trailing-edge flap deflections. Canard incidence variations (0°, ±10°, -20°) and canard-off are shown for three wing trailing-edge flap deflections (0°, 10°, and 25°) at Mach numbers of 0.6, 0.9, and 1.2. Figures 107 through 109 show directly the effectiveness of the wing trailing-edge flap as a trimming surface. Generally the trim characteristics are similar to those of the E205 configuration, with some minor differences noted by comparison of the appropriate figures.

Vertical tail effects- The effects of vertical tail deflection on the longitudinal characteristics are presented in figures 110 and 111, and the lateral/directional results are shown in figures 112 and 113. These results are again similar to those of the E205 configuration, with some minor differences at the higher angles of attack, particularly at Mach number 1.2.

Effects of Canard Location

Figures 114 through 116 present the longitudinal aerodynamic effects of moving the canard forward and aft of the baseline mid-location (see fig. 4(a) for positions). The results are shown for Mach numbers 0.6, 0.9, and 1.2 with all control surfaces at zero deflection. Both alternative canard positions resulted in a slight loss in lift at the highest angles of attack, with the aft location generally producing the greater loss. The most notable effect of canard longitudinal location was the changes in stability where an aft movement of the canard reduced the instability of the model at all Mach numbers.

The effect of canard location on the lateral/directional characteristics, for Mach numbers 0.9 and 1.2 and at two angles of attack, is shown in figures 117-120. Both vertical tail-on and tail-off results are presented.

CONCLUDING REMARKS

Tests were conducted in the Ames 11-Foot Transonic Wind Tunnel at Mach numbers from 0.4 to 1.4 on two models representative of V/STOL fighter/attack aircraft configurations. Both were horizontal-attitude takeoff and landing concepts developed by the General Dynamics Corporation. The concepts differed in their approach to propulsive lift; one used a jet diffuser ejector system for vertical lift and the other a remote augmentation lift system (RALS).

Detailed effects of varying the angle of attack (up to 27°), angle of sideslip (-4° to +8°), Mach number, Reynolds number, and configuration buildup were investigated. In addition, the effects of wing trailing-edge flap deflections, canard incidence, and vertical-tail deflections were explored. Variable canard longitudinal location and different shapes of the inboard nacelle/body strakes were also investigated. Results from these tests indicate the following:

- 1. The models produced high lift coefficients ($C_{L_{max}} \approx 2.0$), which could be attributed to a favorable interaction between the canard and wing and between the inboard strake and the wide body. Maximum lift was not achieved within the test angle-of-attack limits of about 27°.
- 2. Addition of the canard increased lift coefficients and improved the drag polars at high angles of attack; however, it also increased the instability of both configurations.
- 3. Both models in the baseline configurations exhibited relatively high longitudinal instability at low Mach numbers (over 28 percent at Mach number 0.4). At supersonic speeds, the ejector concept became nearly neutrally stable, and the RALS configuration was still about 8 to 10 percent unstable.
- 4. The baseline configurations of both concepts had positive directional stability to angles of attack of about 17° at a Mach number of 0.6 and 10° at a Mach number of 0.9. At Mach 1.2, the ejector configuration was directionally stable to an angle of attack of about 6° ; the RALS concept was stable to an angle of attack of about 14° .
- 5. Using a combination of wing trailing-edge flap deflection and canard incidence, both configurations could be trimmed to an angle of attack of about 12° subsonically and to about 16° to 20° at Mach 1.2.
- 6. Wing trailing-edge flaps were found to be the most effective trimming surfaces, for the canard lost effectiveness at the higher negative incidence angles.
- 7. In general, the canard in the mid-longitudinal position and the baseline strakes produced the most favorable lift and drag characteristics for the ejector configuration. Likewise, the mid-canard location gave the higher lift for the RALS concept.
- 8. Longitudinal stability was increased for the jet diffuser ejector configuration by an aft movement of the canard and by a reduction in the planform size of the strakes. On the RALS concept, the aft canard location also produced the greater longitudinal stability.

REFERENCES

- 1. Lummus, J. R.: Study of Aerodynamic Technology for VSTOL Fighter/Attack Aircraft. NASA CR-152128, 1978.
- 2. Burhans, W. R. et al.: Study of Aerodynamic Technology for VSTOL Fighter/ Attack Aircraft. NASA CR-152129, 1978.
- 3. Brown, S. H.: Study of Aerodynamic Technology for VSTOL Fighter/Attack Aircraft Horizontal Attitude Concept. NASA CR-152130, 1978.
- 4. Gerhardt, H. A.; and Chen, W. S.: Study of Aerodynamic Technology for VSTOL Fighter/Attack Aircraft Vertical Attitude Concept. NASA CR-152131, 1978.
- 5. Driggers, H. H.: Study of Aerodynamic Technology for VSTOL Fighter/ Attack Aircraft. NASA CR-152132, 1978.
- 6. Nelms, W. P.: Studies of Aerodynamic Technology for VSTOL Fighter/ Attack Aircraft. AIAA Paper 78-1511, Los Angeles, Calif., 1978.

TABLE 1.- GEOMETRY OF E205 CONFIGURATION

	Wing	Horizontal canard (mid-position)	Vertical tail			
Airfoil at CR CT Theoretical area, m² (ft²) MAC, m (in.) Aspect ratio Taper ratio Root chord, m (in.) Tip chord, m (in.) Span, m (in.) Dihedral Incidence Hinge line at B.L. F.S. W.L. Hinge-line sweep Leading-edge sweep Trailing-edge sweep Body length, 153 m (60.10 in.)	NACA-64A204 NACA-64A204 0.315 (3.3858) 0.340 (13.398) 3.62 0.190 0.495 (19.505) 0.094 (3.706) 1.067 (42.010) 0° 40° 4°58' -	$0.0315 (0.3390)^{\alpha}$ $0.183 (7.197)$ 1.08^{α} 0.37 $0.249 (9.815)$	5.3% biconvex 4.0% biconvex 0.0389 (0.4188) 0.184 (7.256) 1.27 0.43 0.245 (9.638) 0.105 (4.144) 0.222 (8.751) - 0 1.252 (49.297) 0.403 (15.869) 0° 47°30' 24°52' -			

 $[\]overline{a}$ Area of one panel.

TABLE 2.- GEOMETRY OF R104 CONFIGURATION

	Wing	Horizontal canard (mid-position)	Vertical tail				
Airfoil at CR CT Theoretical area, m² (ft²) MAC, m (in.) Aspect ratio Taper ratio Root chord, m (in.) Tip chord, m (in.) Span, m (in.) Dihedral Incidence Hinge-line at B.L. F.S. W.L. Hinge-line sweep Leading-edge sweep Trailing-edge sweep Body length, 147 m (57.90 in.)	NACA-64A204 NACA-64A204 0.293 (3.154) 0.330 (12.973) 3.57 0.1966 0.479 (18.851) 0.094 (3.706) 1.023 (40.270) 0° 40° 4°58'	NACA-64A005 NACA-64A003 0.0315 (0.3390) ^a 0.183 (7.197) 1.08 ^a 0.37 0.249 (9.815) 0.092 (3.631) 0.184 (7.261) 0° - 0.206 (8.126) 0.620 (24.414) 0.396 (15.587) -1°46' 45° 8°26' -	5.3% biconvex 4.0% biconvex 0.0389 (0.4188) 0.184 (7.256) 1.27 0.43 0.254 (9.638) 0.105 (4.144) 0.222 (8.751) 1.247 (49.110) 0.377 (14.836) 0° 47°30' 24°52' -				

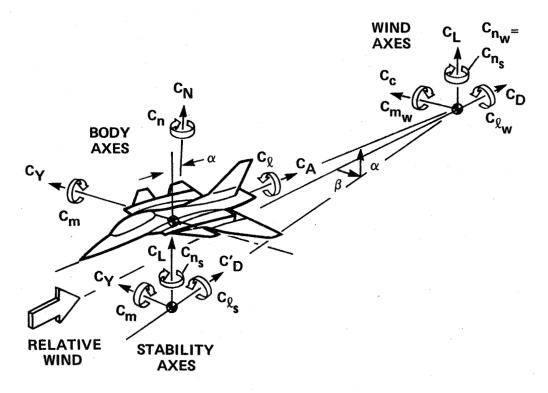
 $[\]alpha$ Area of one panel.

TABLE 3,- INTERNAL FORCE COEFFICIENTS OF E205 CONFIGURATION (Values are totals of both ducts)

	1.40	-0.00252	.00145	.00045	.00121	.00360	96000.	.00647	.00072	00600.	.00047	.01135	.00030	.01364	.00026	.01575	.00032	.01575	.00040	.01575	.00045
	1.20	-0.00252	86000.	.00045	.00065	.00341	.00043	.00610	.00034	.00855	.00035	.01072	.00043	.01266	.00052	.01452	.00063	.01627	.00074	.01627	.000080
	1.10	-0.00225	.00077	.00045	.00053	.00320	.00051	.00589	.00064	.00831	,00084	.01032	.00108	.01220	.00137	.01397	.00169	.01563	.00205	.01640	.00222
Mach number	0.95	-0.00225	98000.	.00045	92000.	.00306	.00080	.00570	.00110	.00817	.00156	.01022	.00215	.01202	.00285	.01354	.00357	.01495	.00439	.01557	.00484
Mach	6.0	-0.00240	.00080	.00045	.00079	.00327	.00085	.00585	.00131	.00814	.00204	.01020	.00275	.01210	.00346	.01351	.00419	.01458	.00491	.01496	.00525
	0.8	-0.00240	.00111	.00045	.00109	.00327	.00108	.00585	.00202	.00819	.00310	.01033	.00416	.01220	.00524	.01376	.00633	.01502	.00742	.01550	.00795
	9.0	-0.00240	.00141	.00045	.00143	.00327	.00168	.00585	.00316	.00819	.00475	.01033	.00640	.01220	.00807	.01376	06600.	.01502	.01180	.01550	.01276
	0.4	-0.00240	.00167	.00045	.00175	.00327	.00205	.00585	.00389	.00814	.00572	.01020	.00757	.01202	.00950	.01345	.01148	.01454	.01355	.01496	.01460
4	Augle of actack, force coefficient	-4°, CN _{TNT}	CATNT	O°, CNTNT	CAINT	4°, CN _{TNT}	CATNT	8°, C _{NTNT}	CATNT	12°, CNINT	CAINT	16°, CN _{TNT}	CAINT	20°, CNTNT	CATNT	24°, CNINT	CATNT	28°, C _{NTNT}	CAINT	30°, C _{NINT}	$c_{ m A_{INT}}$

TABLE 4.- INTERNAL FORCE COEFFICIENTS OF R104 CONFIGURATION (Values are totals of both ducts)

													<u> </u>				بنبسيحب					وحب منسست
		1.40	-0.00271	.00156	.00048	.00130	.00386	.00103	.00695	.00077	99600.	.00050	.01218	.00032	.01464	.00028	.01691	.00034	.01691	.00043	.01691	.00048
		1.25	-0.00271	.00105	.00048	.00070	.00366	.00046	.00655	.0036	.00918	.00038	.01151	97000.	.01359	.00056	.01559	89000.	.01747	62000.	.01747	.00086
		1.10	-0.00242	.00083	.00048	.00057	.00344	.00055	.00632	69000.	.00892	06000.	.01108	.00116	.01310	.00147	.01500	.00181	.01678	.00220	.01760	.00238
444497	Mach number	96.0	-0.00242	.00092	.00048	.00082	.00328	.00086	.00612	.00118	.00877	.00167	.01097	.00231	.01290	.00306	.01453	.00383	.01605	.00471	.01671	.00520
S OF DOC!!	Σ	6.0	-0.00258	98000.	.00048	.00085	.00351	.00085	.00628	.00141	.00874	.00219	.01095	.00295	.01299	.00371	.01450	.00450	.01565	.00527	.01606	.00564
(dates are cotate of both dates)		0.8	-0,00258	.00119	.00048	.00117	.00351	.00116	.00628	.00217	.00879	.00333	.001109	.00447	.01310	.00562	.01477	.00680	.01612	76200.	.01664	.00853
		0.6	-0.00258	.00151	.00048	.00154	.00351	.00180	.00628	.00339	.00879	.00510	.01109	.00687	.01310	99800	.01477	.01063	.01612	.01267	.01664	.01370
		0.4	-0.00258	.00179	.00048	.00188	.00351	.00220	.00628	.00418	.00874	.00614	.01095	.00813	.01290	.01020	.01444	.01232	.01561	.01455	.01606	.01567
	Angle of attack,	force coefficient	-4°, C _{NINT}	CAINT	0°, C _{NINT}	CAINT	4°, C _{NINT}	$c_{A_{\mathrm{INT}}}$	8°, C _{NINT}	$c_{A_{\mathrm{INT}}}$	12°, C _{NINT}	$c_{ m A_{INT}}$	16°, C _{NINT}	$c_{ m A_{INT}}$	20°, C _{NINT}	CAINT	24°, C _{NINT}	CAINT	28°, CNINT	CAINT	30°, C _{NINT}	$c_{ m A_{INT}}$

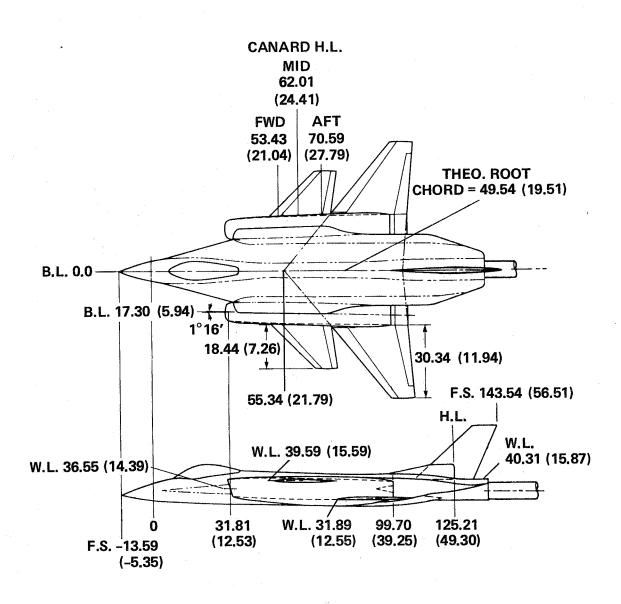


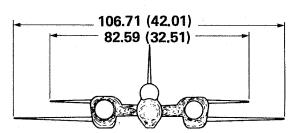
NOTE:

- 1. POSITIVE VALUES OF FORCE AND MOMENT COEFFICIENTS AND ANGLES ARE INDICATED.
- 2. ORIGINS OF WIND AND STABILITY AXES HAVE BEEN DISPLACED FROM CENTER OF GRAVITY FOR CLARITY.

 $+\beta$ (SIDESLIP) = $-\psi$ (YAW)

Figure 1.- Axis system and sign conventions.

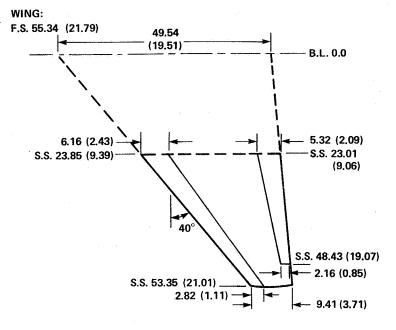


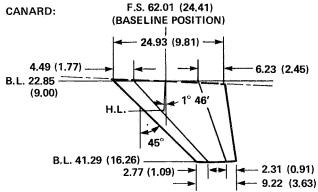


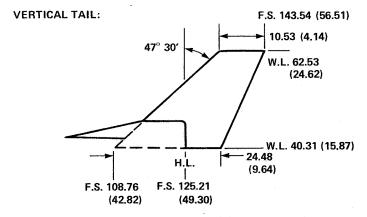
NOTE: ALL LINEAR DIMENSIONS ARE IN CENTIMETERS (INCHES).

(a) Three-view drawing.

Figure 2.- Details of the E205 wind-tunnel model.



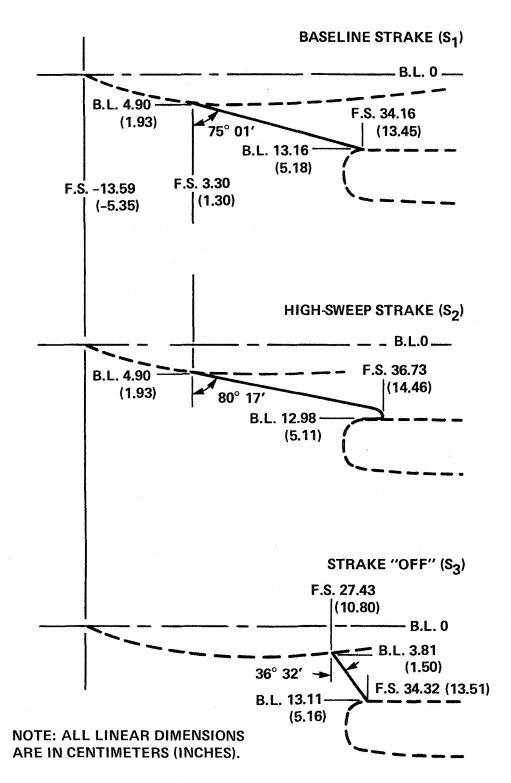




NOTE: ALL LINEAR DIMENSIONS ARE IN CENTIMETERS (INCHES).

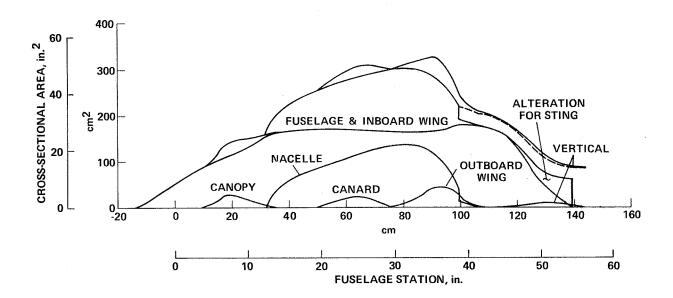
(b) Wing, canard and vertical tail detail.

Figure 2.- Continued.



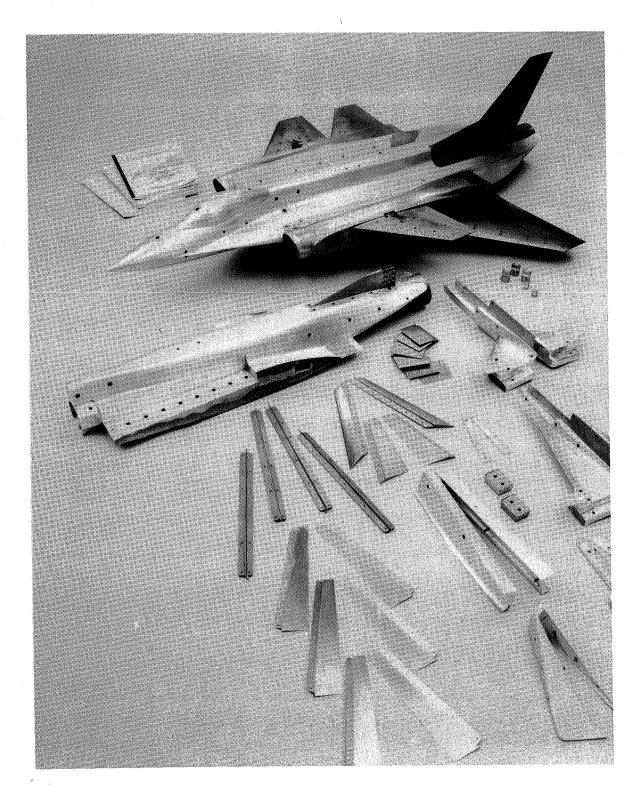
(c) Strake options.

Figure 2.- Continued.

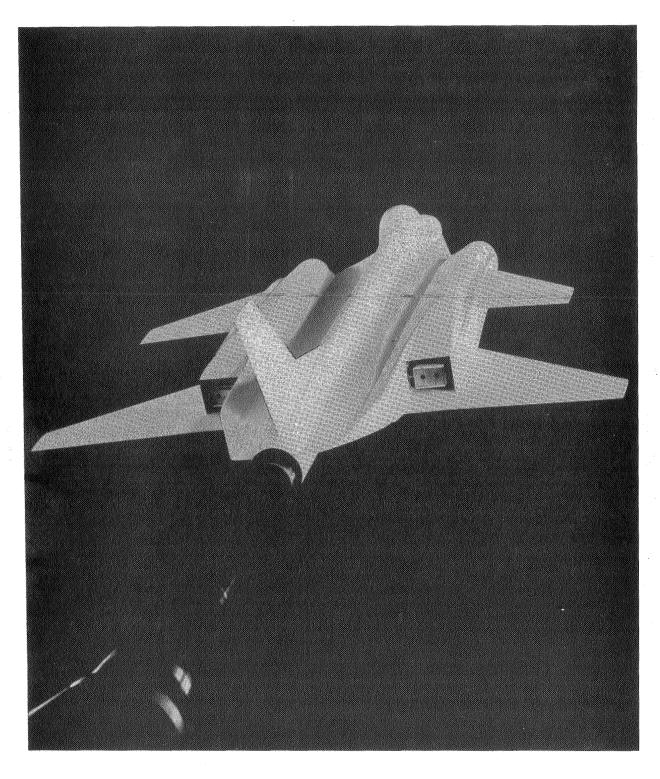


(d) Cross-sectional area distribution.

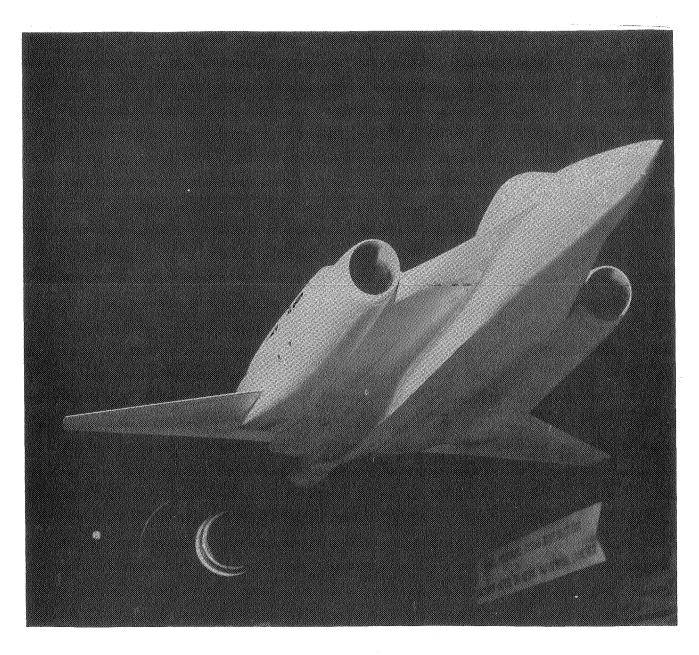
Figure 2.- Concluded.



(a) E205 model, R104 body, and components. Figure 3.- E205 model.

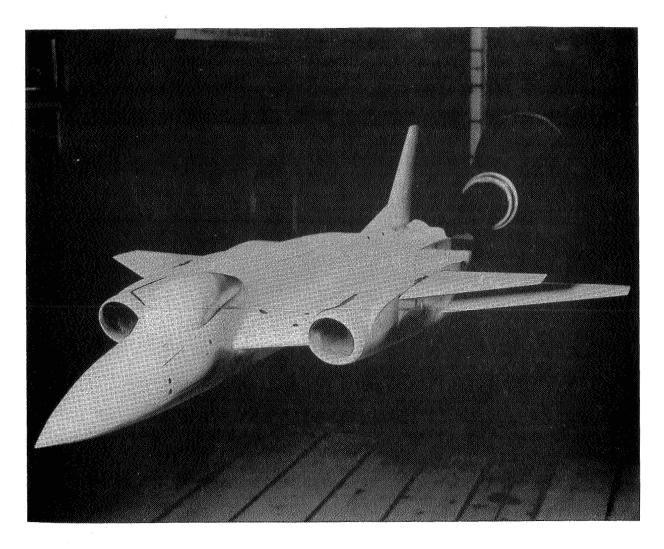


(b) E205 model installed in wind tunnel Figure 3.- Continued.



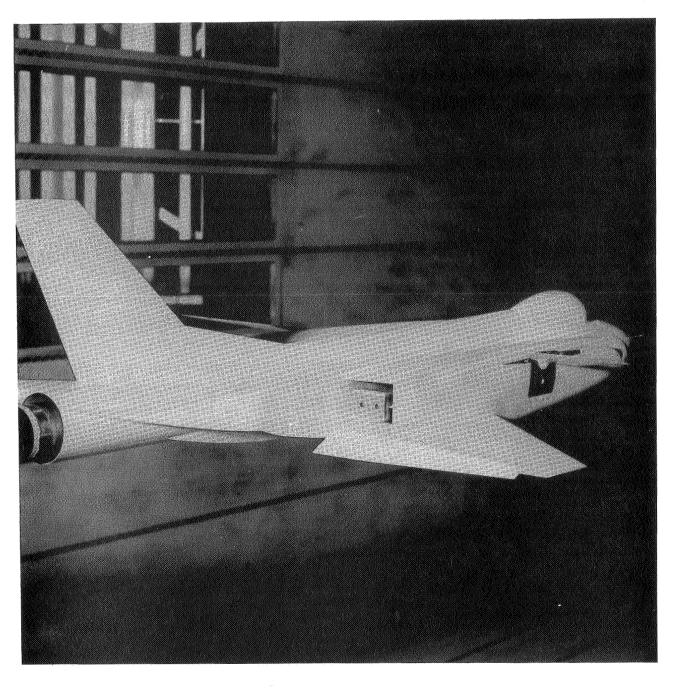
(c) $E205 \mod 2$ with canard off.

Figure 3.- Continued.

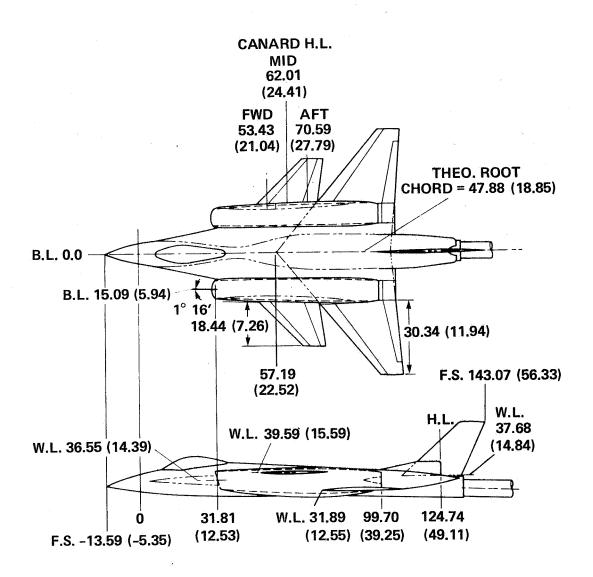


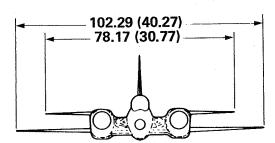
(d) E205 model with strake "off."

Figure 3.- Continued.



(e) E205 model with mid-canard at -10° , wing trailing-edge flaps at 25°. Figure 3.- Concluded.

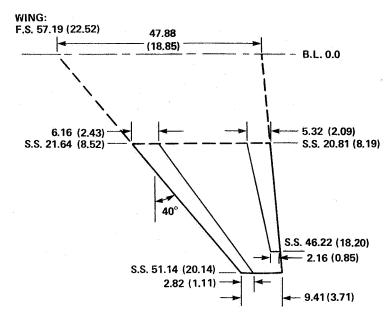


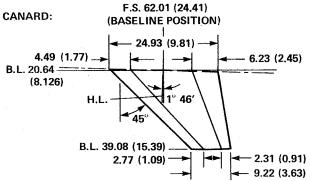


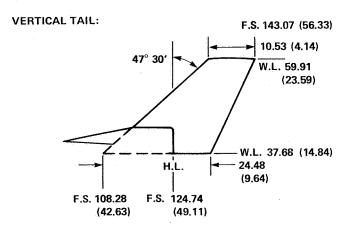
NOTE: ALL LINEAR DIMENSIONS ARE IN CENTIMETERS (INCHES).

(a) Three-view drawing.

Figure 4.- Details of R104 wind-tunnel model.



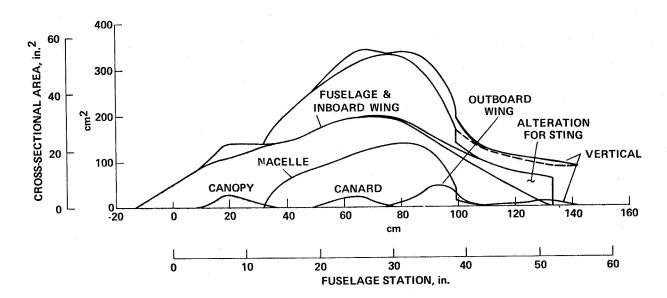




NOTE: ALL LINEAR DIMENSIONS ARE IN CENTIMETERS (INCHES).

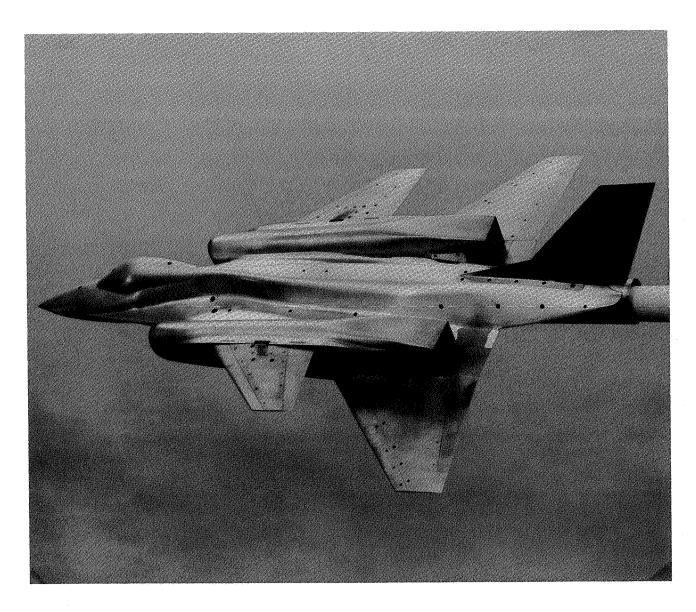
(b) Wing, canard, and vertical tail detail.

Figure 4.- Continued.



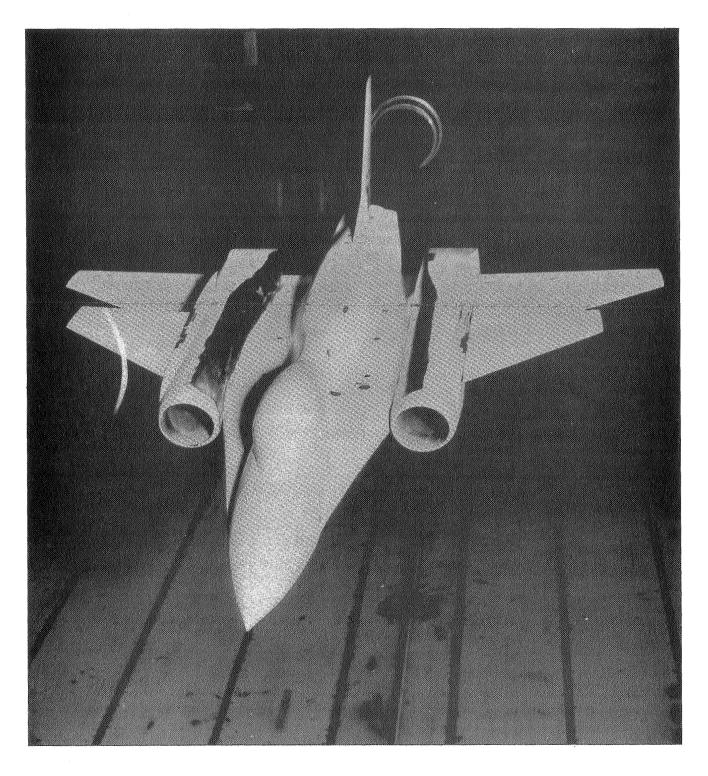
(c) Cross-sectional area distribution.

Figure 4.- Concluded.



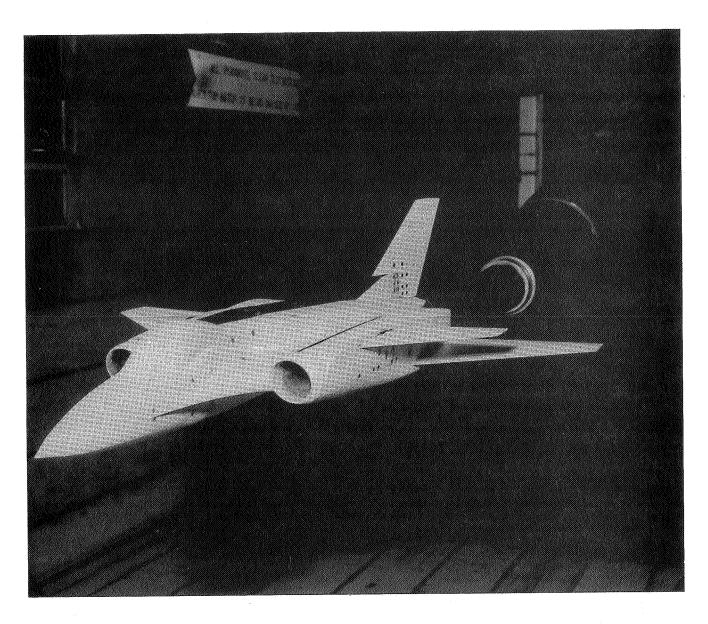
(a) R104 model.

Figure 5.- Views of R104 model.



(b) R104 model with forward canard.

Figure 5.- Continued.



(c) R104 model with vertical tail at 15°.

Figure 5.- Concluded.

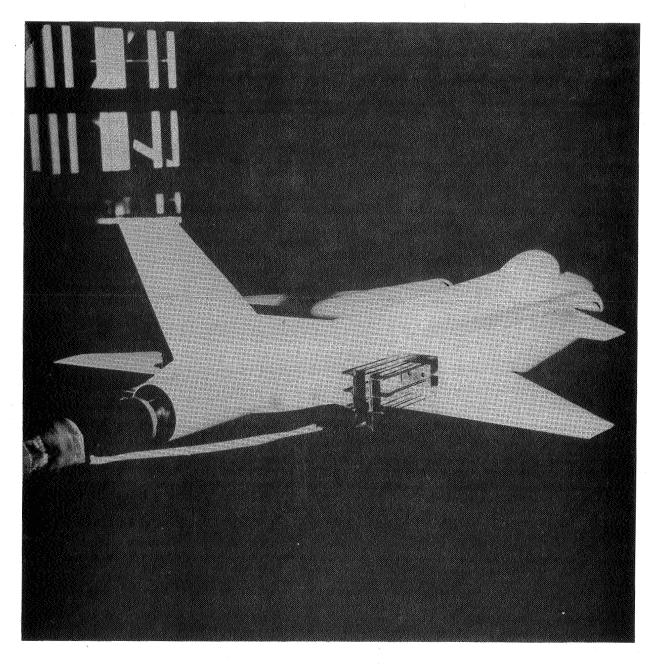
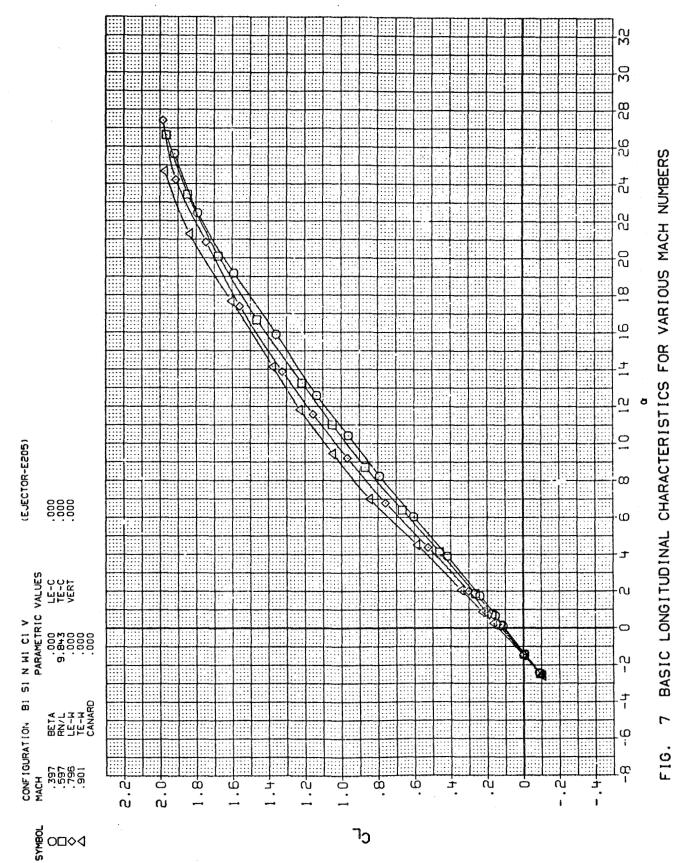
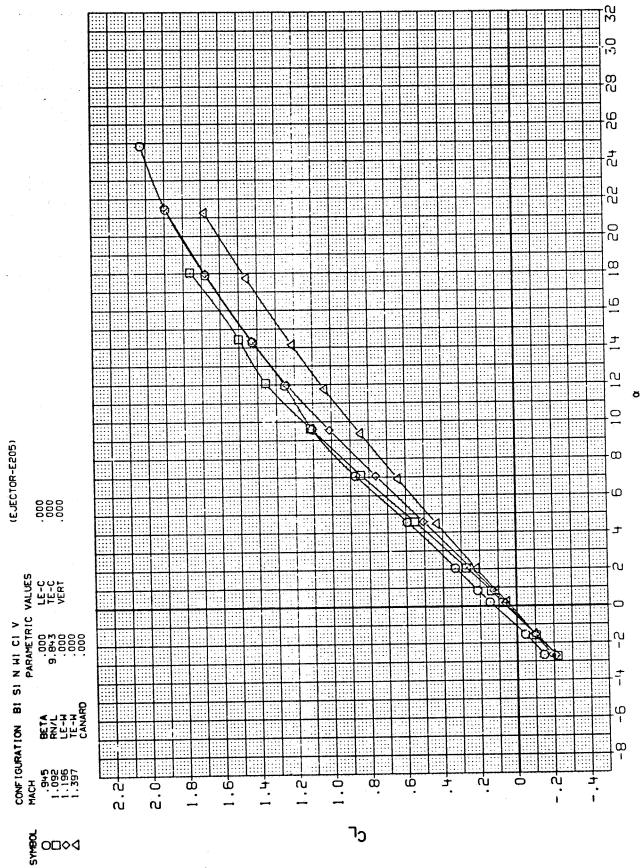
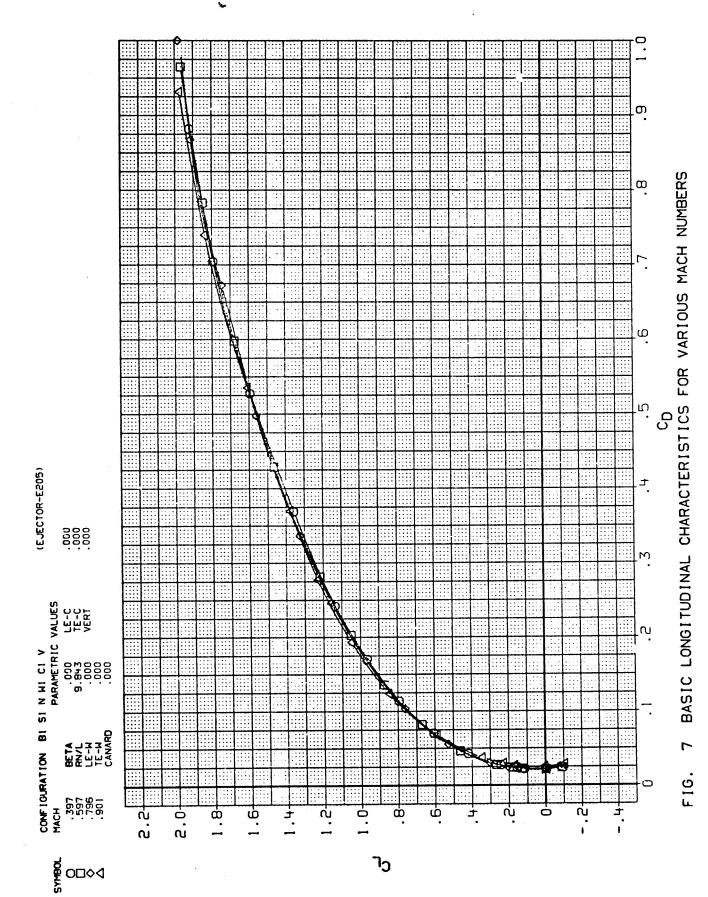


Figure 6.- Duct exit rake installation on E205 model.





7 BASIC LONGITUDINAL CHARACTERISTICS FOR VARIOUS MACH NUMBERS F16.



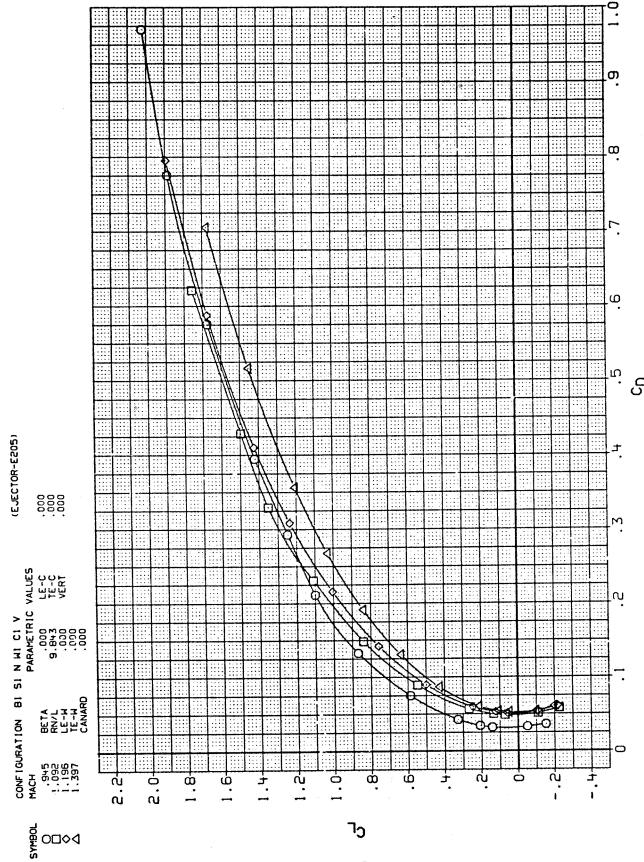
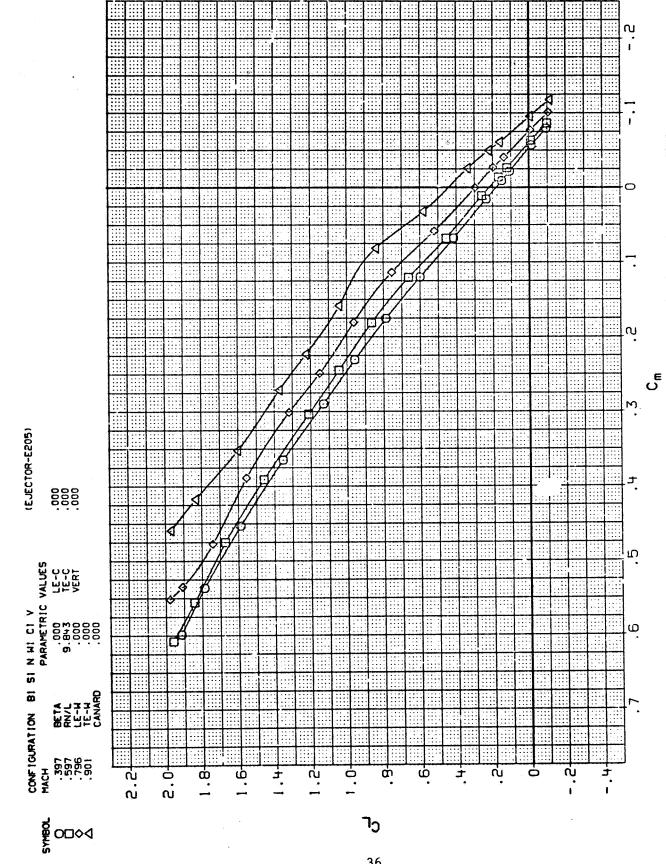
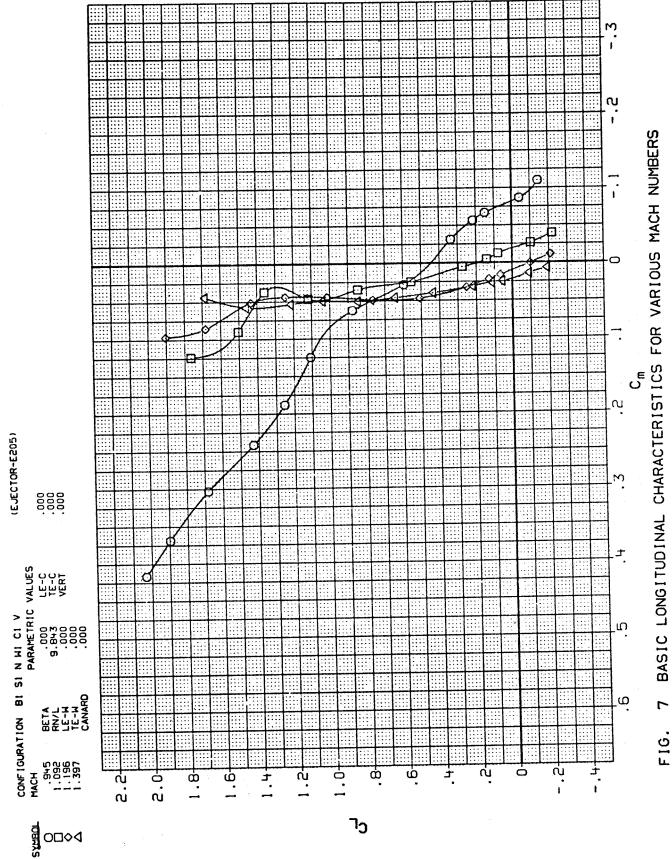


FIG. 7 BASIC LONGITUDINAL CHARACTERISTICS FOR VARIOUS MACH NUMBERS

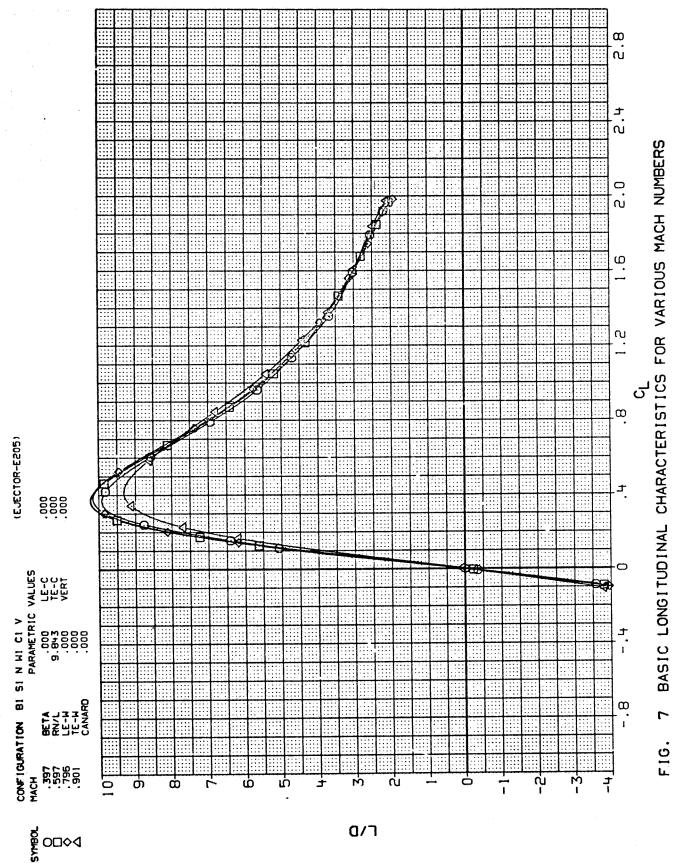


BASIC LONGITUDINAL CHARACTERISTICS FOR VARIOUS MACH NUMBERS F16.



37

F16.



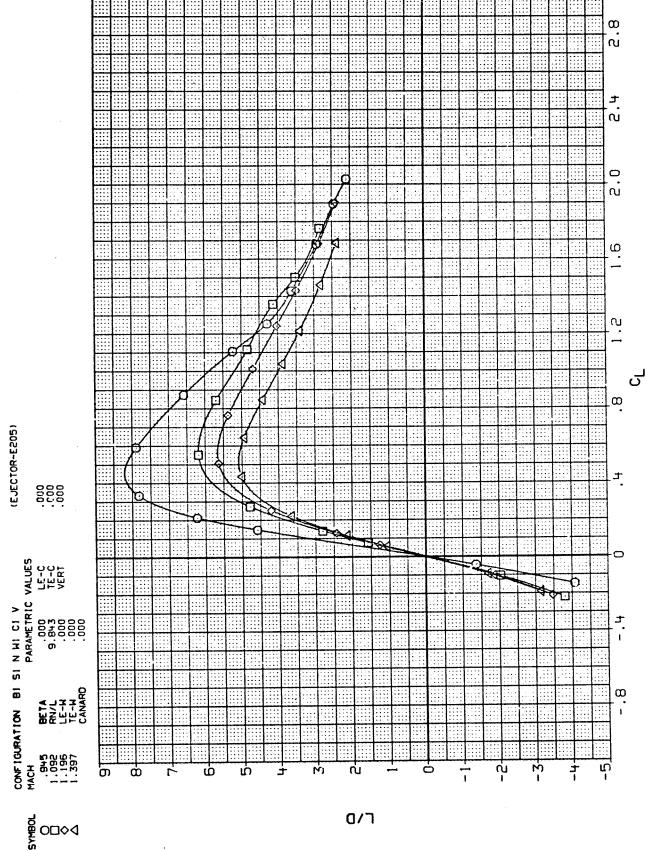
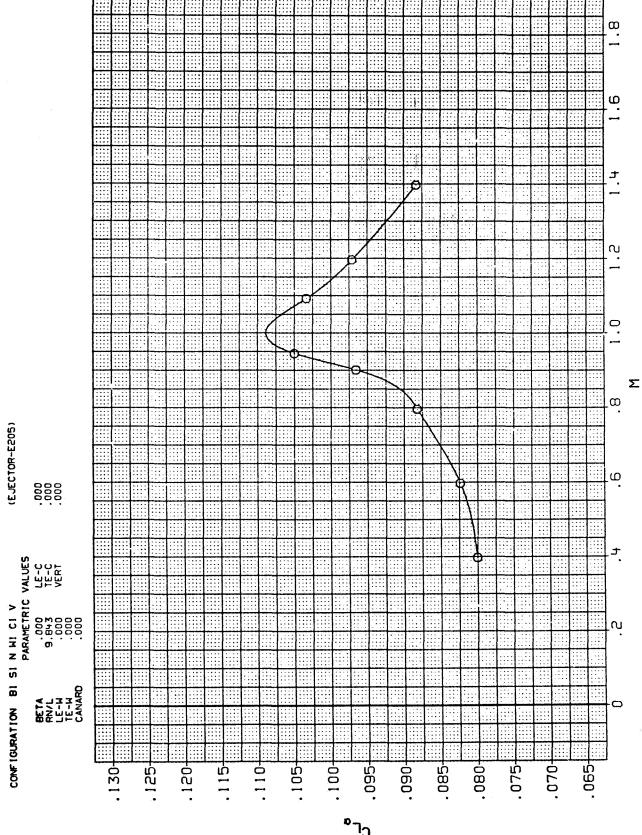
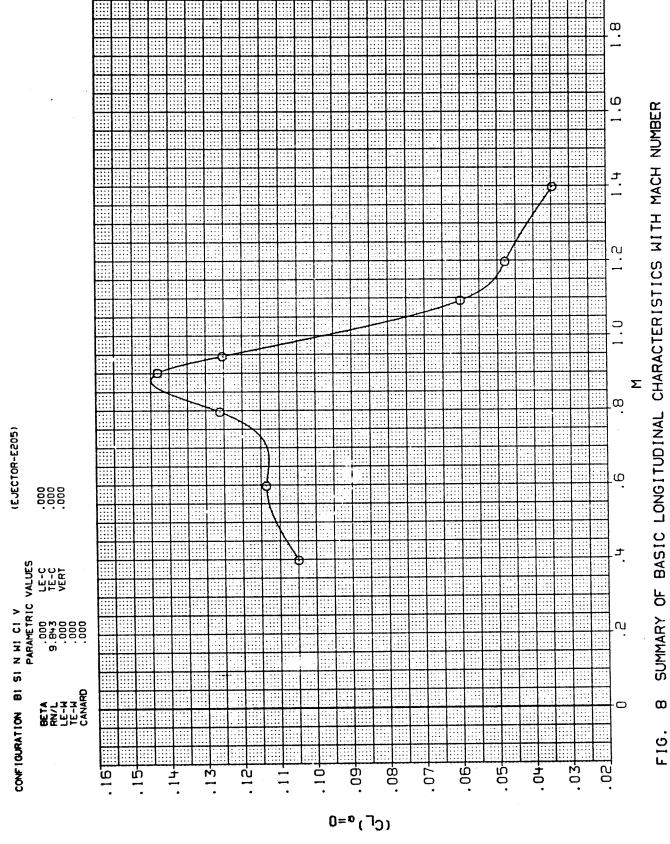


FIG. 7 BASIC LONGITUDINAL CHARACTERISTICS FOR VARIOUS MACH NUMBERS



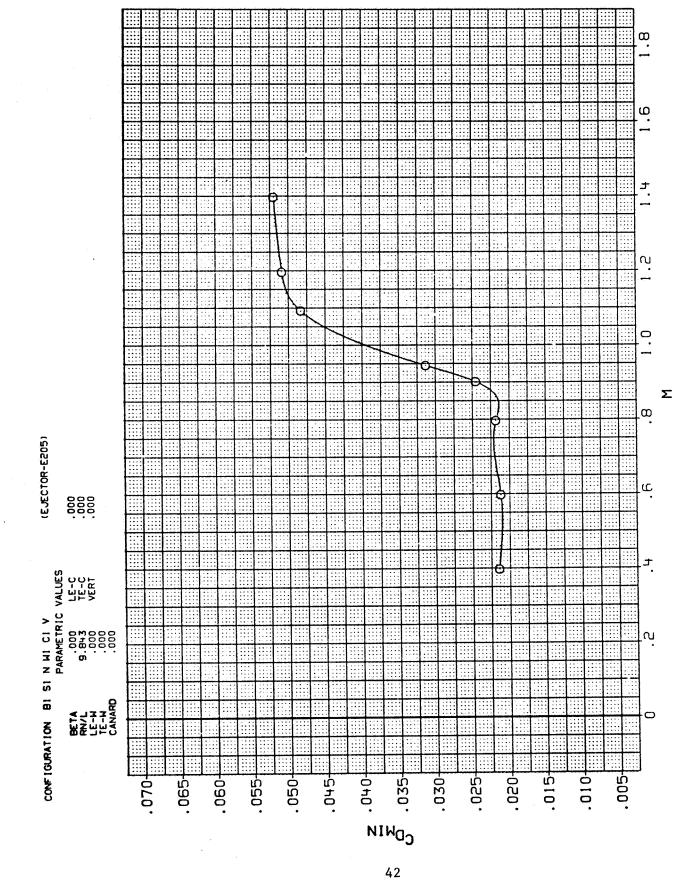
SUMMARY OF BASIC LONGITUDINAL CHARACTERISTICS WITH MACH NUMBER Φ F16.



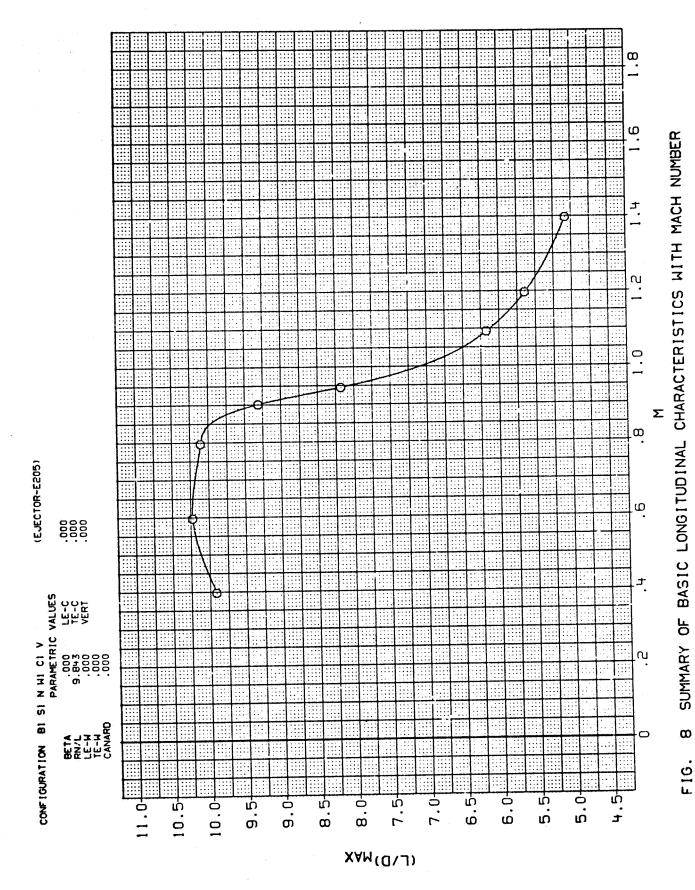
41

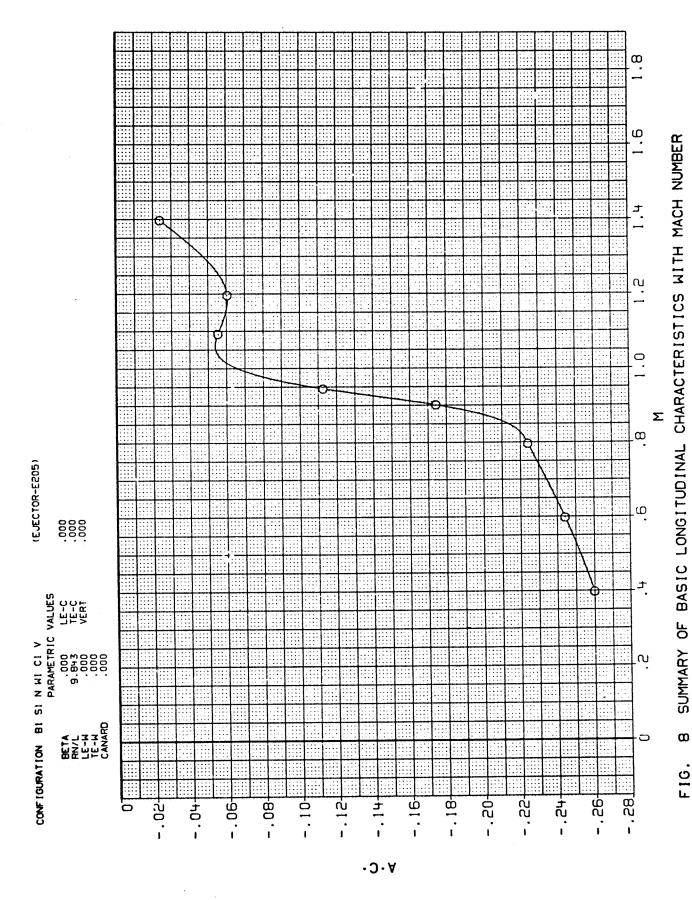
 $\boldsymbol{\omega}$

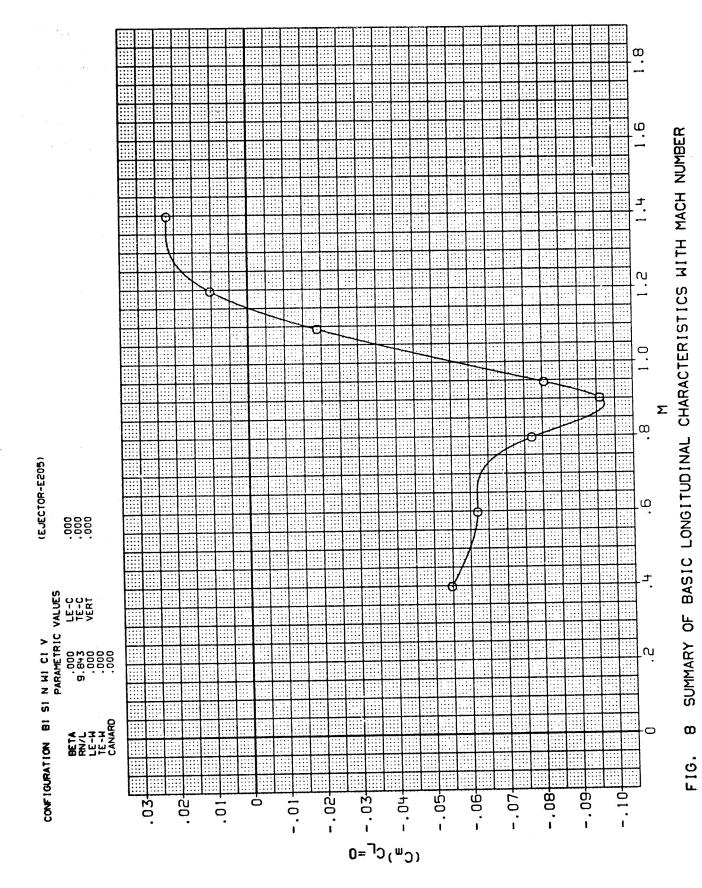
F16.

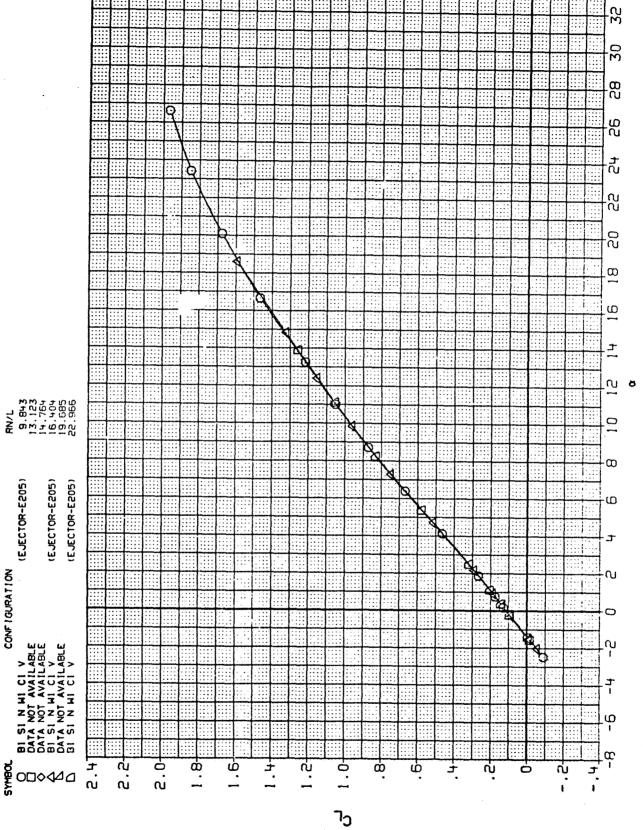


SUMMARY OF BASIC LONGITUDINAL CHARACTERISTICS WITH MACH NUMBER $\boldsymbol{\omega}$ F16.



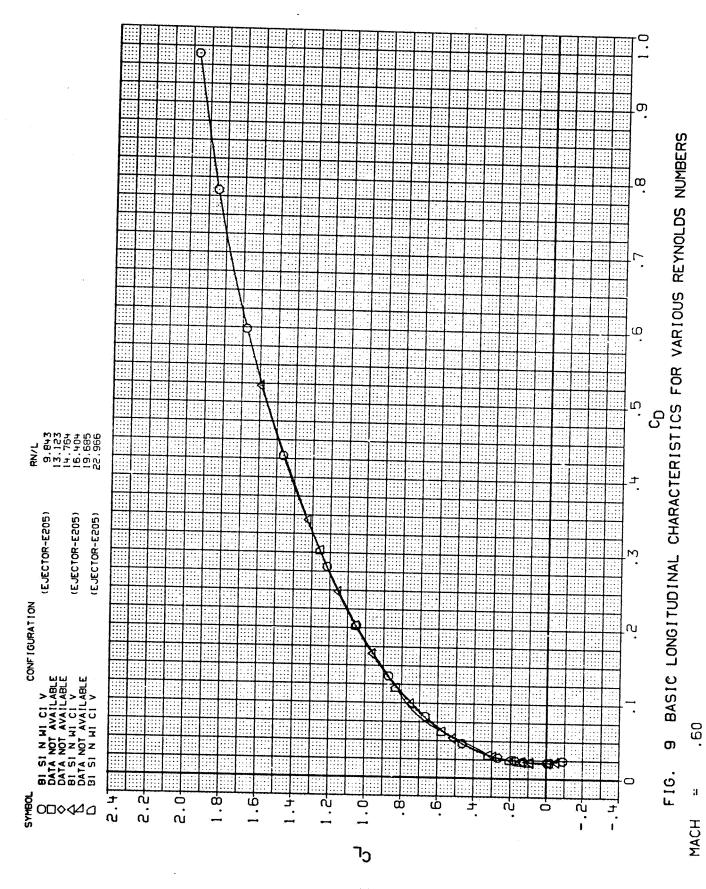


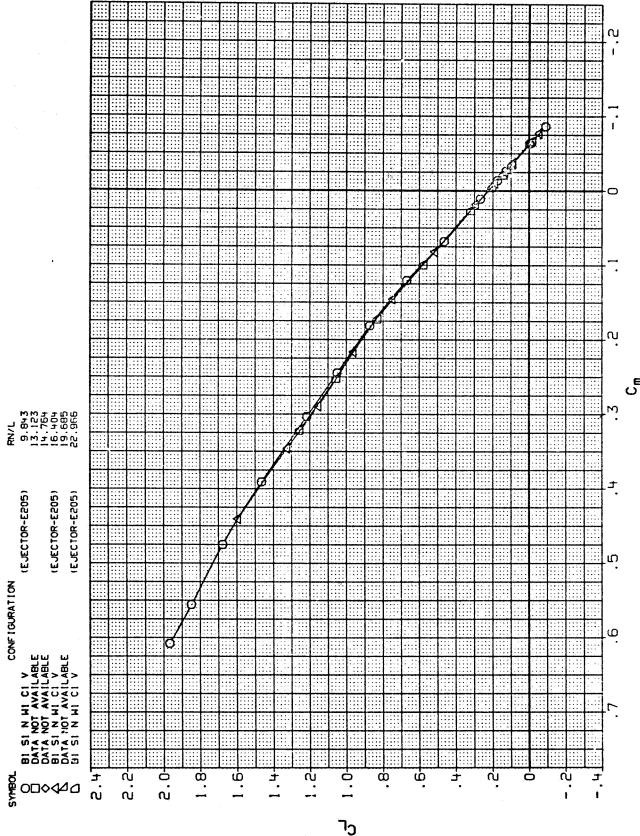




BASIC LONGITUDINAL CHARACTERISTICS FOR VARIOUS REYNOLDS NUMBERS ຓ F16. MACH

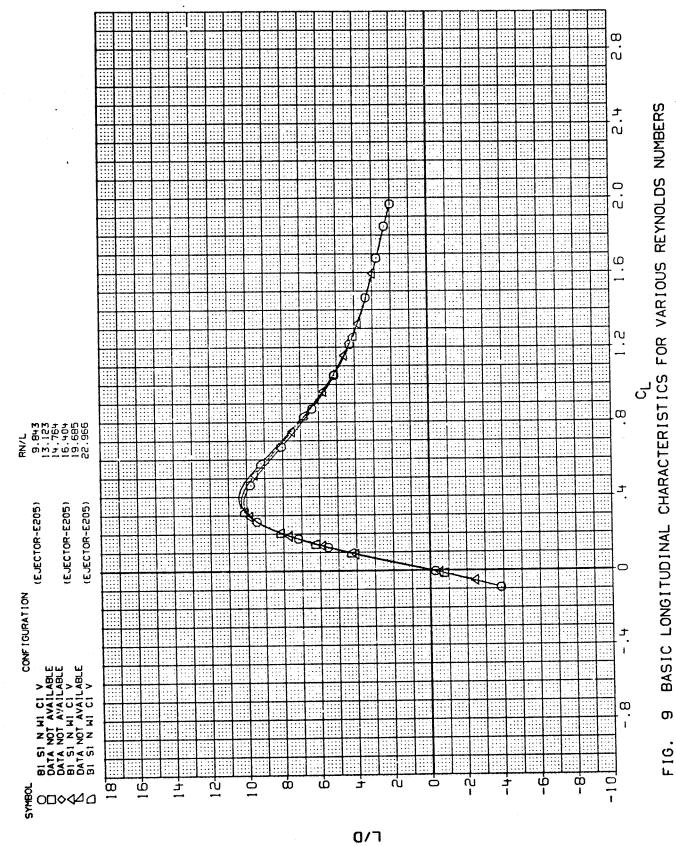
3



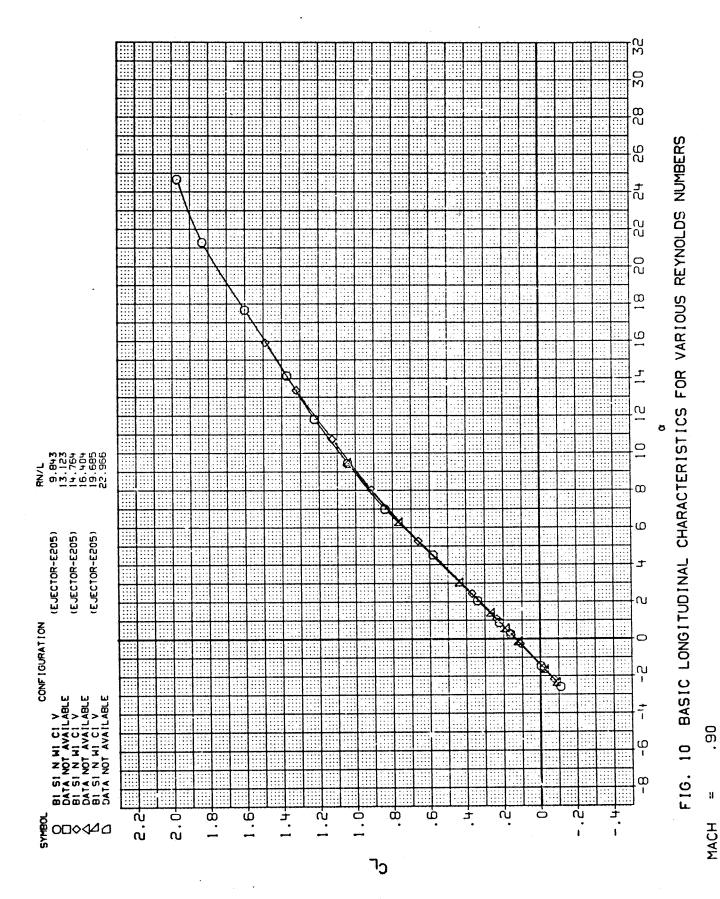


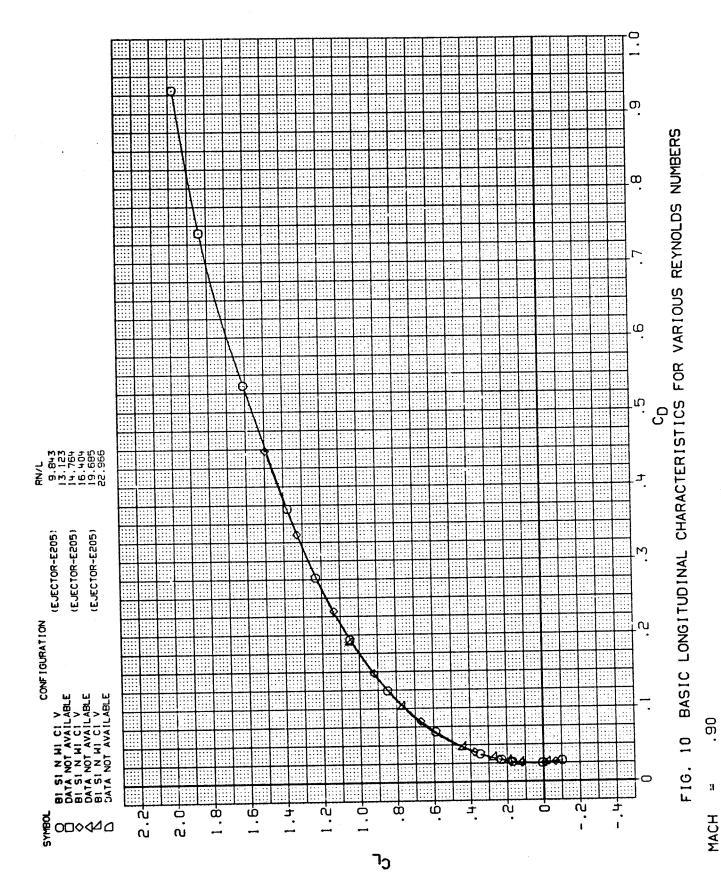
BASIC LONGITUDINAL CHARACTERISTICS FOR VARIOUS REYNOLDS NUMBERS ດ F16.

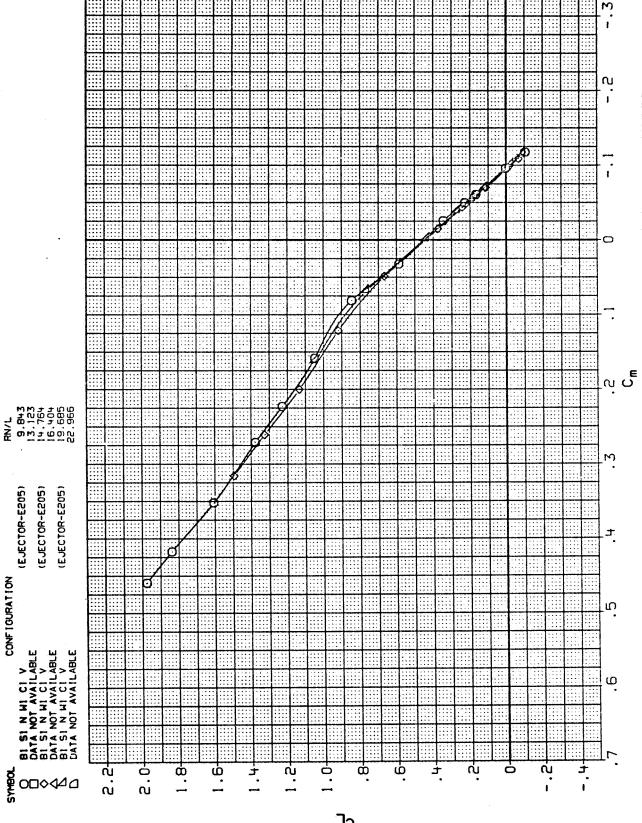
1



MACH = .60







BASIC LONGITUDINAL CHARACTERISTICS FOR VARIOUS REYNOLDS NUMBERS F16. 10

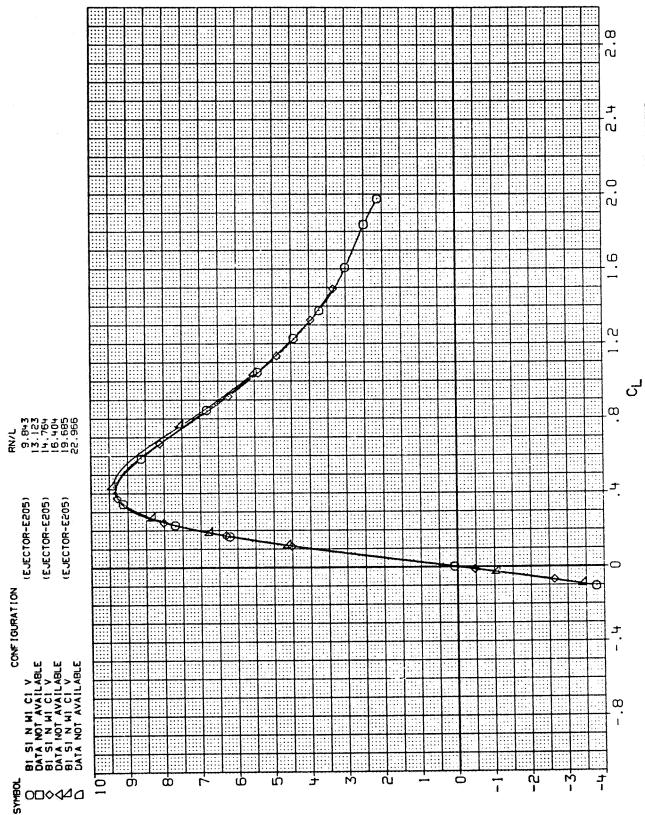


FIG. 10 BASIC LONGITUDINAL CHARACTERISTICS FOR VARIOUS REYNOLDS NUMBERS

90

۵/٦

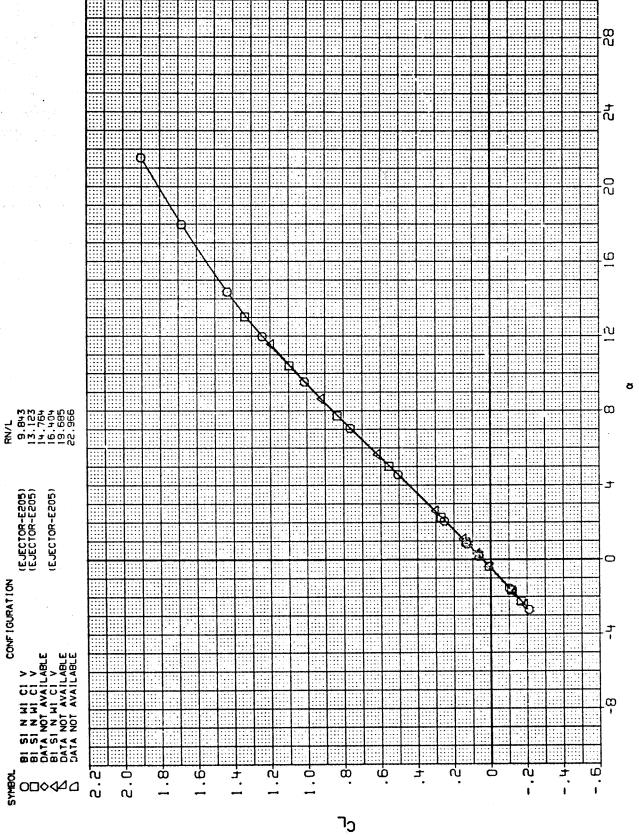


FIG. 11 BASIC LONGITUDINAL CHARACTERISTICS FOR VARIOUS REYNOLDS NUMBERS

11

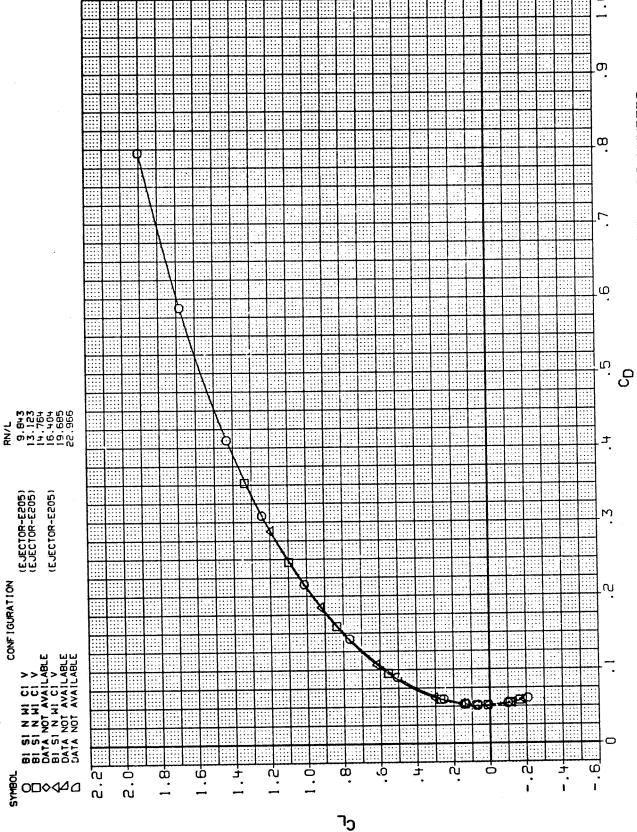


FIG. 11 BASIC LONGITUDINAL CHARACTERISTICS FOR VARIOUS REYNOLDS NUMBERS

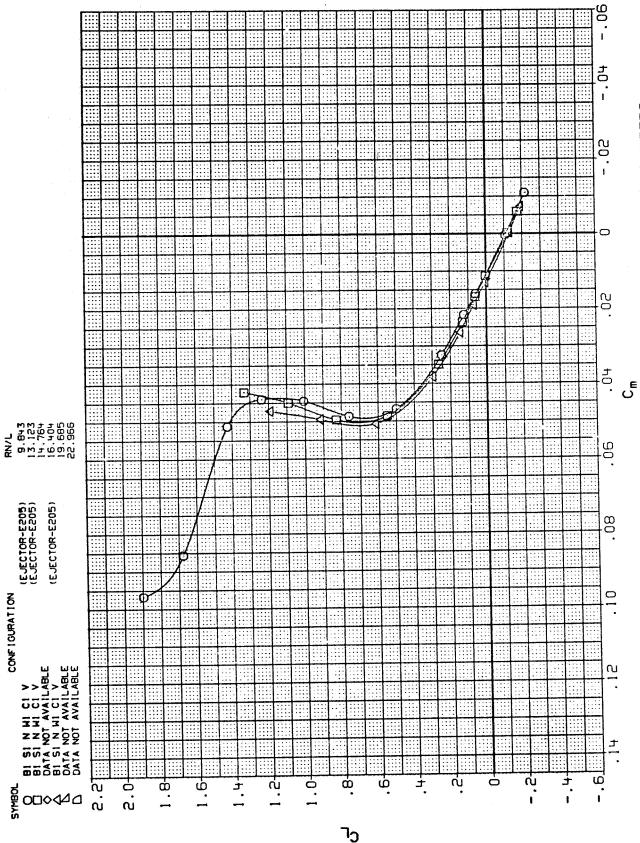


FIG. 11 BASIC LONGITUDINAL CHARACTERISTICS FOR VARIOUS REYNOLDS NUMBERS

H

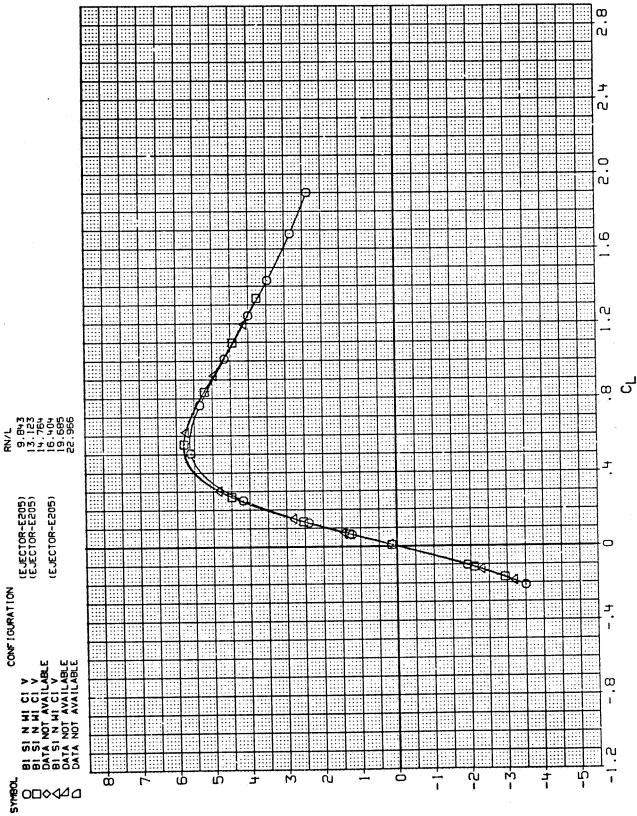


FIG. 11 BASIC LONGITUDINAL CHARACTERISTICS FOR VARIOUS REYNOLDS NUMBERS

3

רום

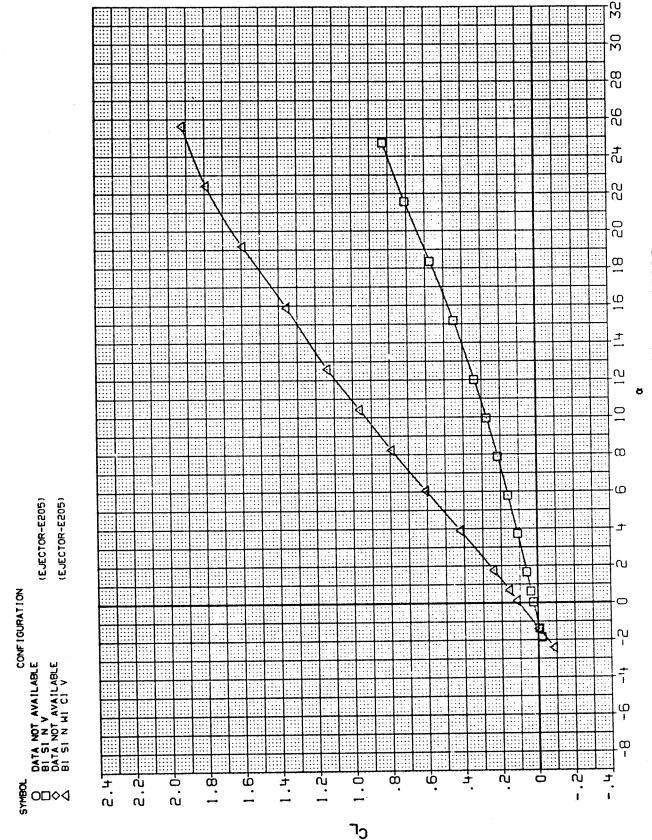
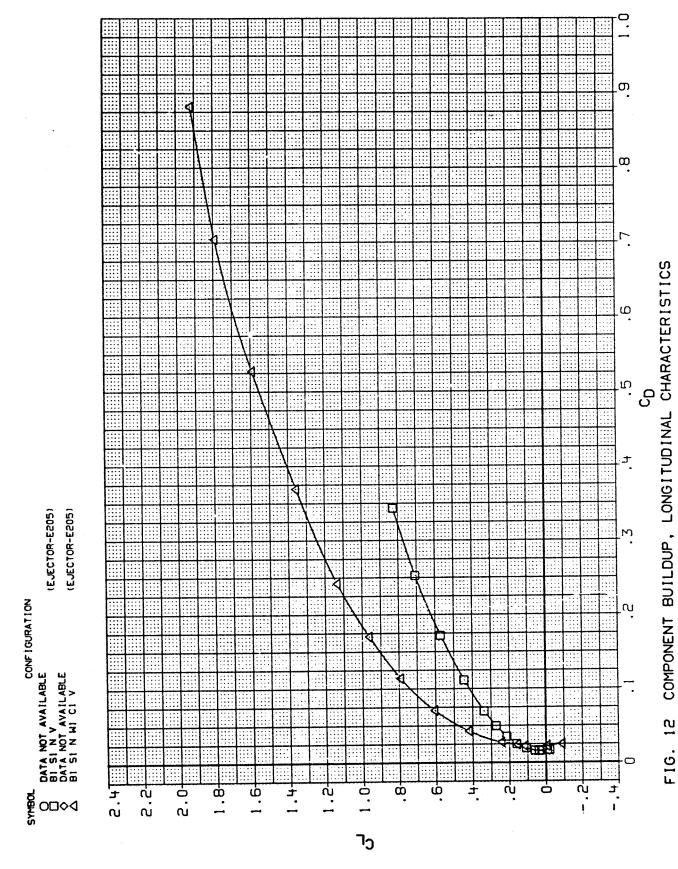
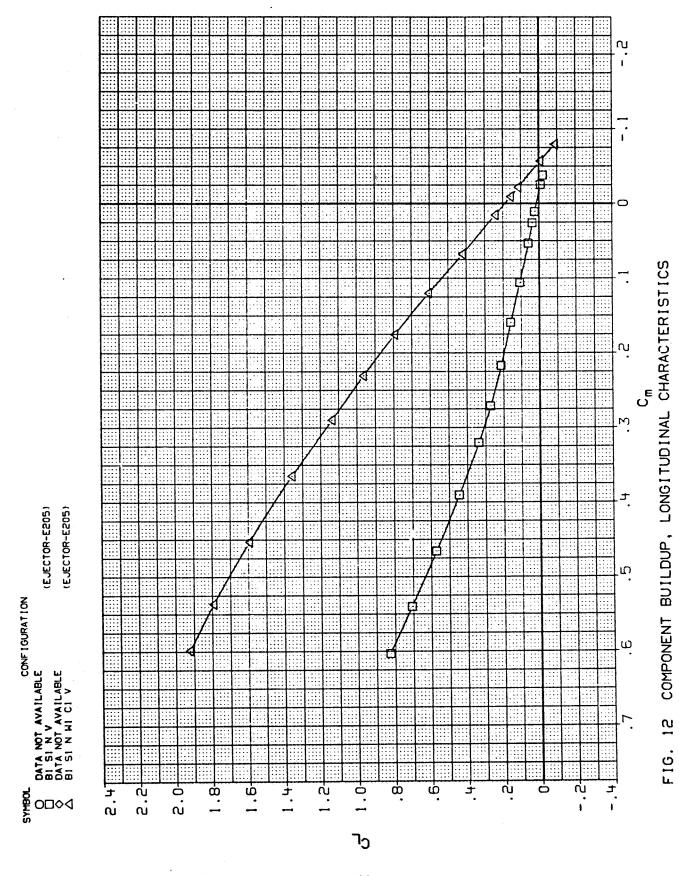


FIG. 12 COMPONENT BUILDUP, LONGITUDINAL CHARACTERISTICS



59



60

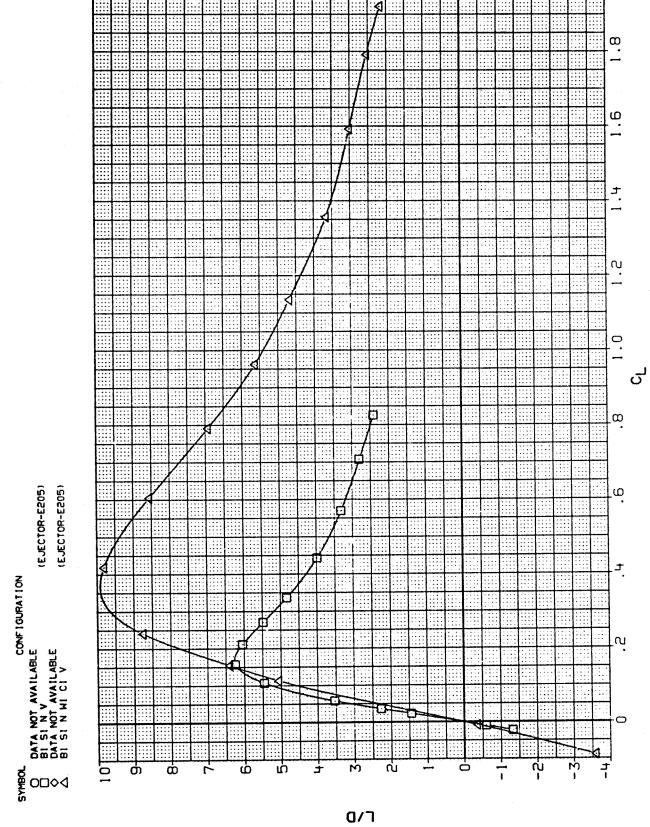
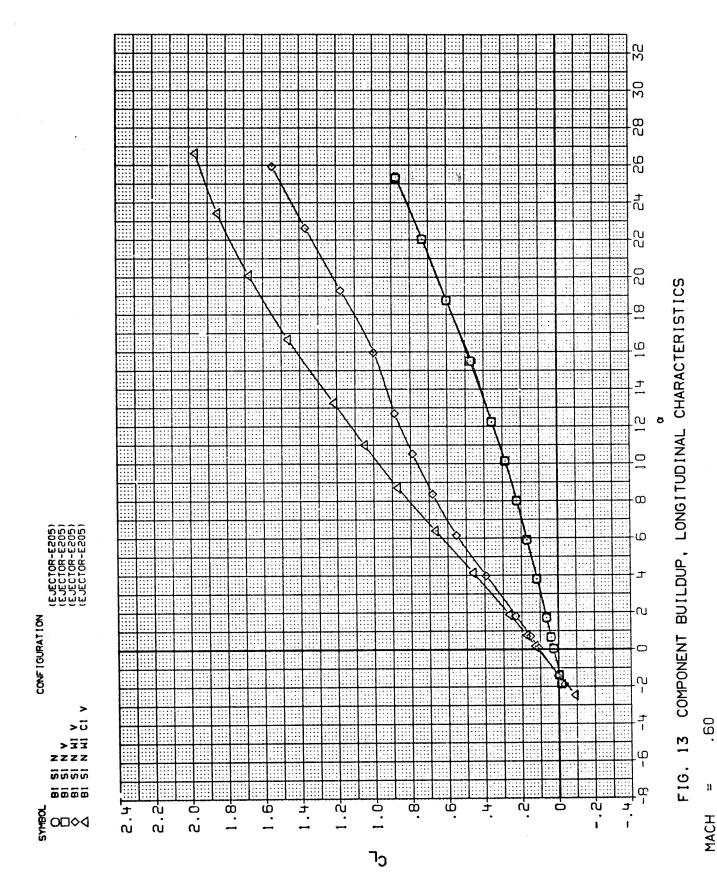


FIG. 12 COMPONENT BUILDUP, LONGITUDINAL CHARACTERISTICS



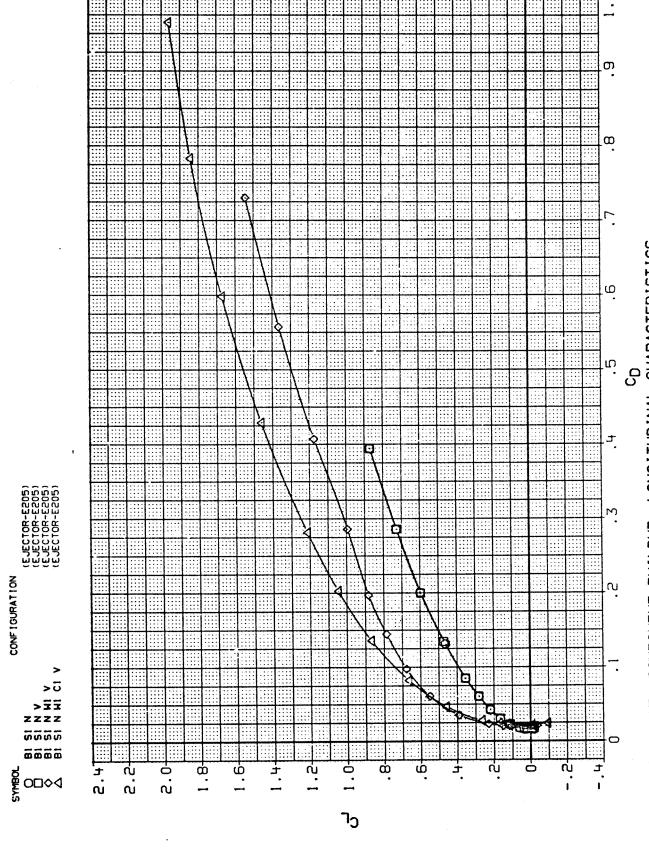
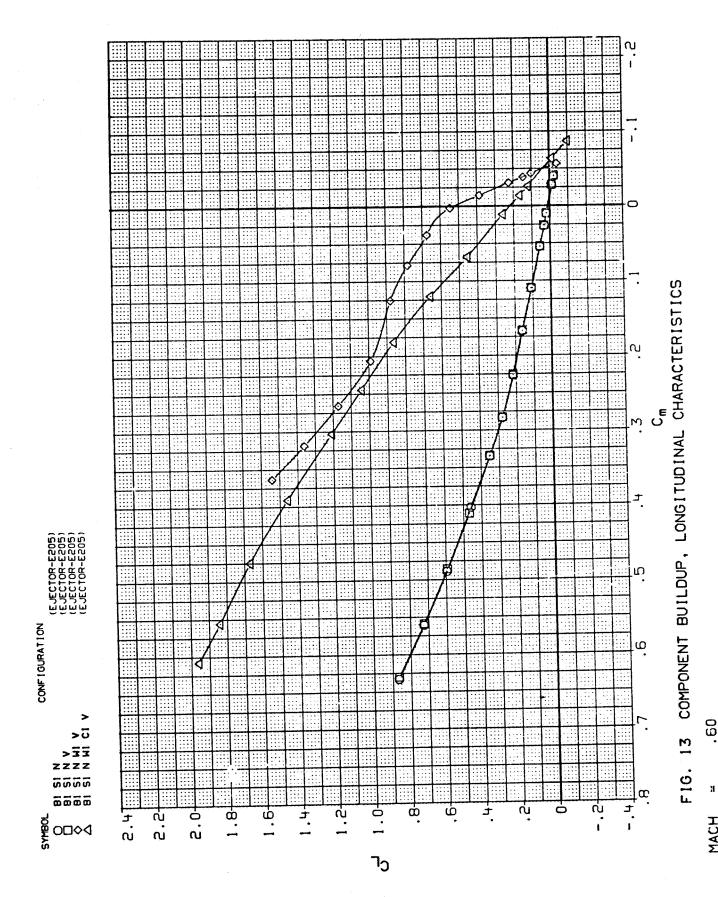


FIG. 13 COMPONENT BUILDUP, LONGITUDINAL CHARACTERISTICS

Н



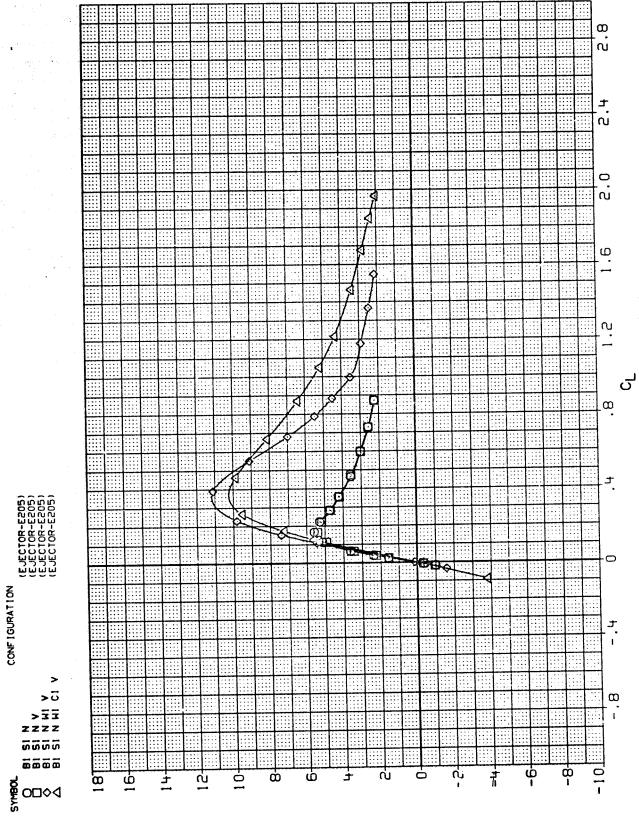


FIG. 13 COMPONENT BUILDUP, LONGITUDINAL CHARACTERISTICS

MACH

רום

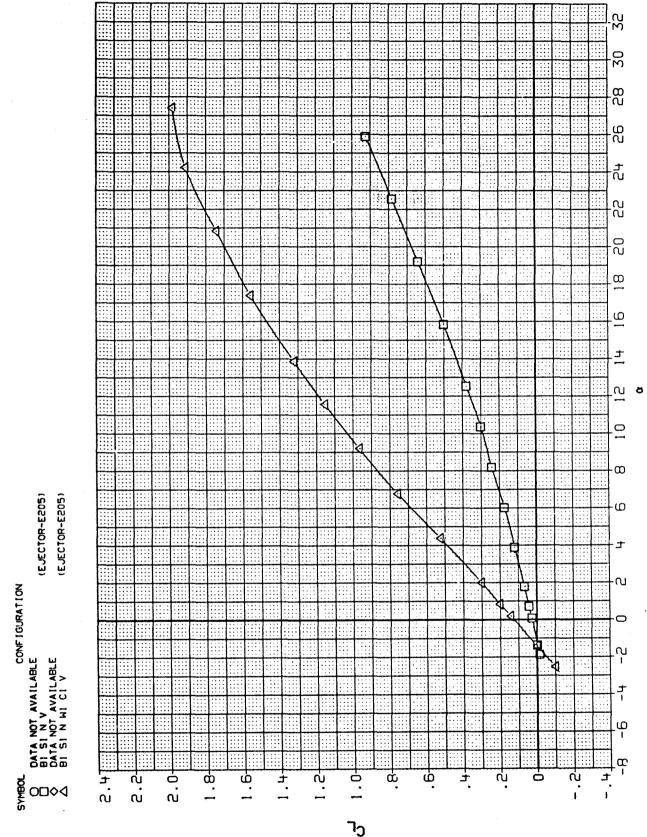


FIG. 14 COMPONENT BUILDUP, LONGITUDINAL CHARACTERISTICS

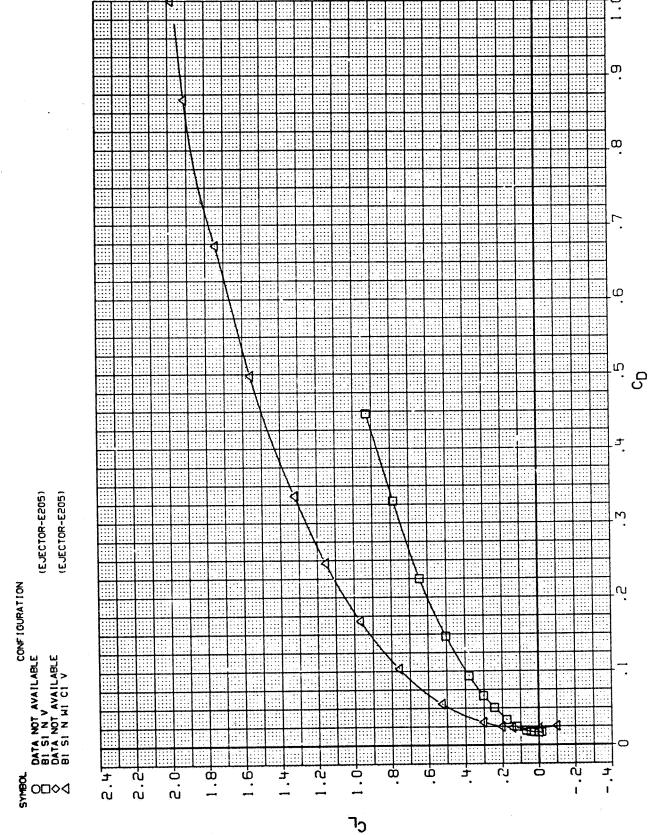
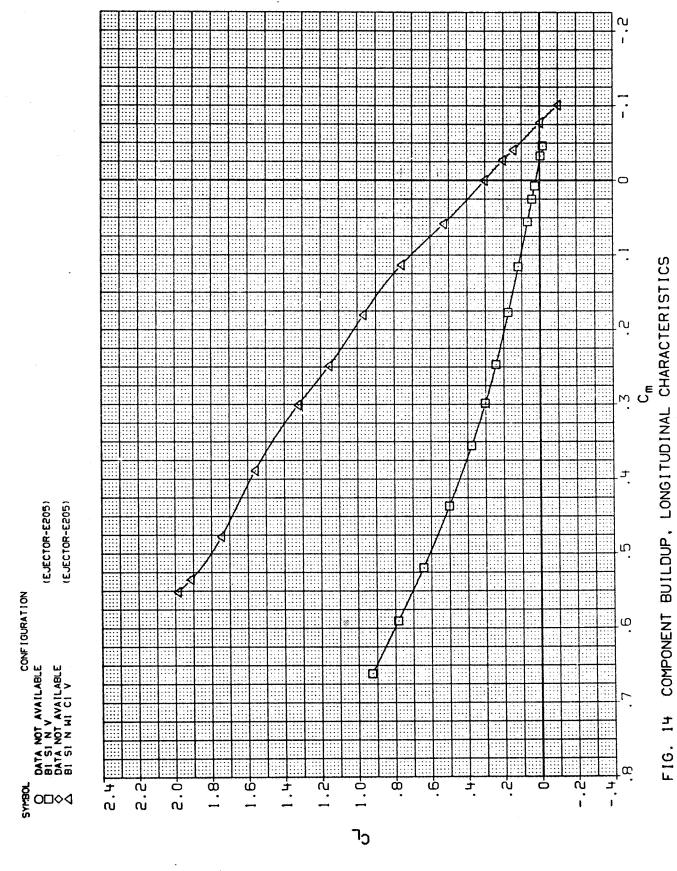
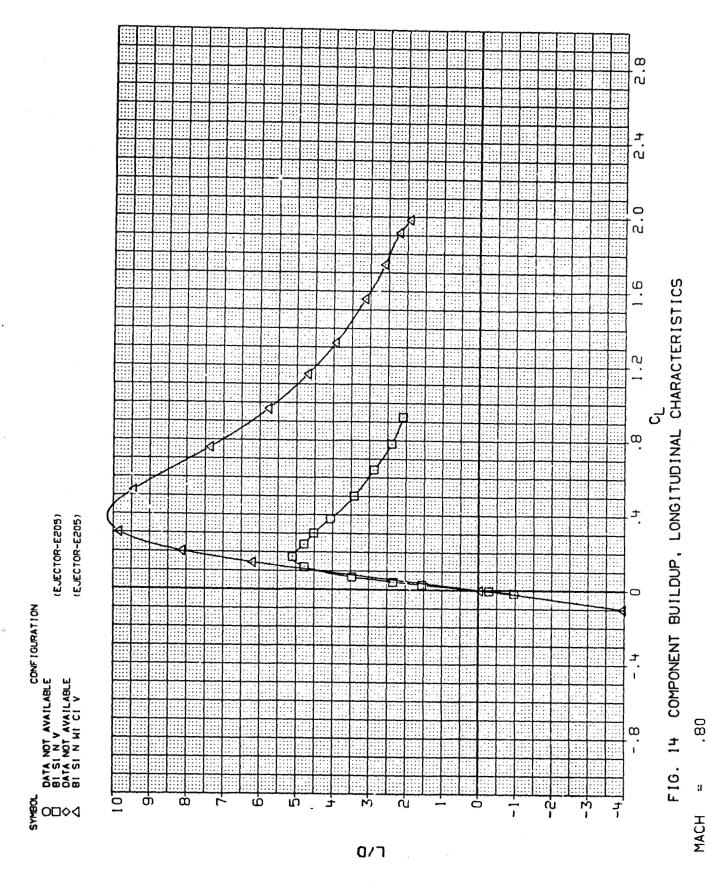
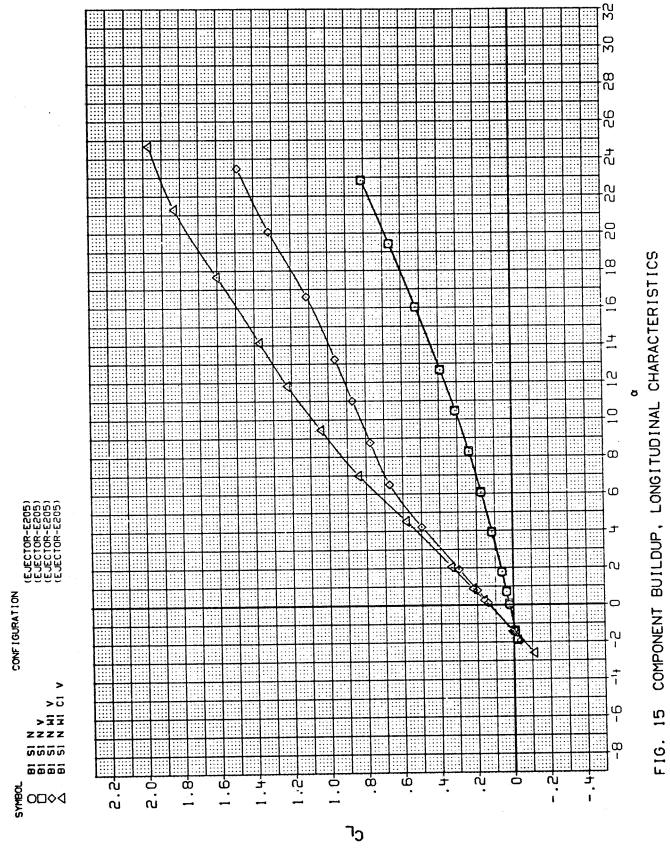


FIG. 14 COMPONENT BUILDUP, LONGITUDINAL CHARACTERISTICS

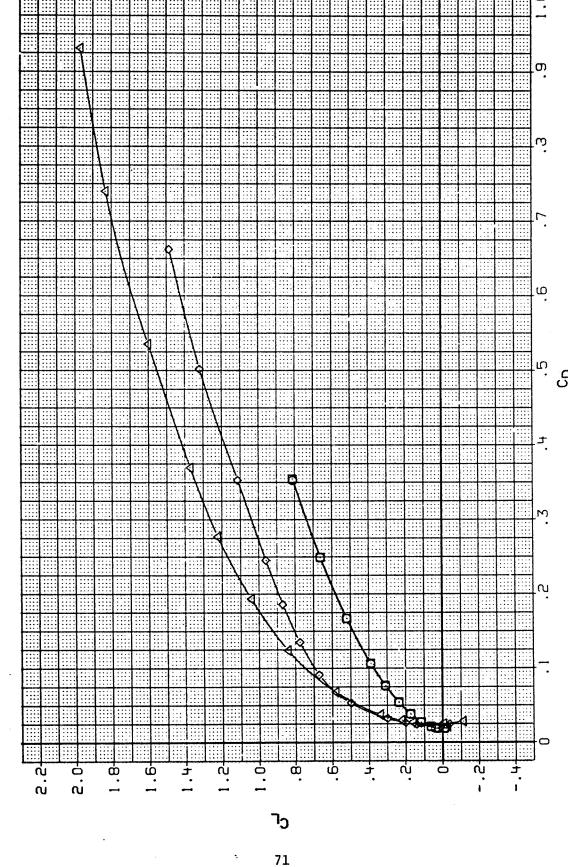


68





.



(EJECTOR-E205) (EJECTOR-E205) (EJECTOR-E205) (EJECTOR-E205)

>5 >==

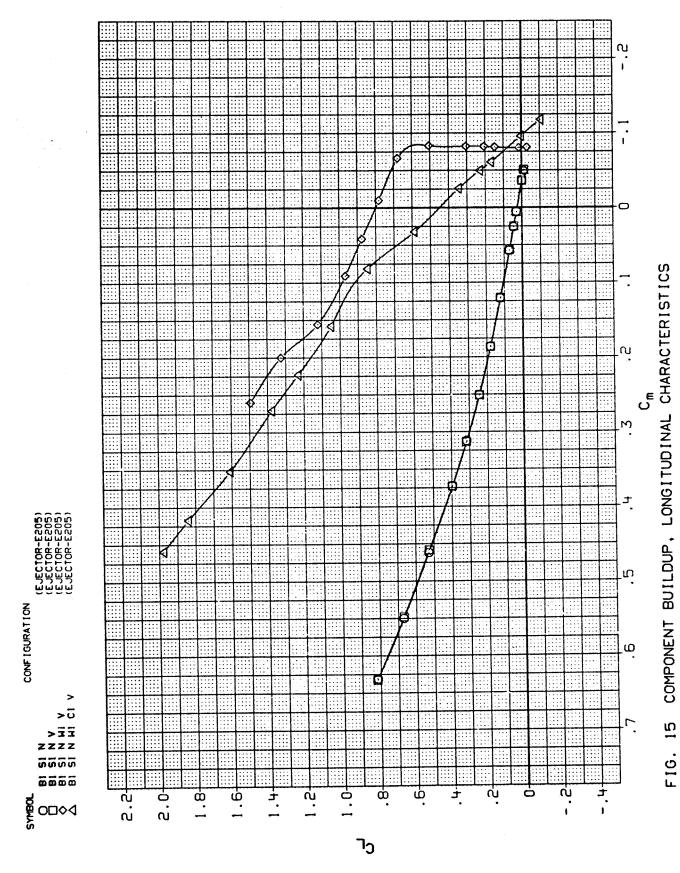
ខាលិល 8888

S P O□◊∢

CONFIGURATION

90 MACH

FIG. 15 COMPONENT BUILDUP, LONGITUDINAL CHARACTERISTICS



72

u

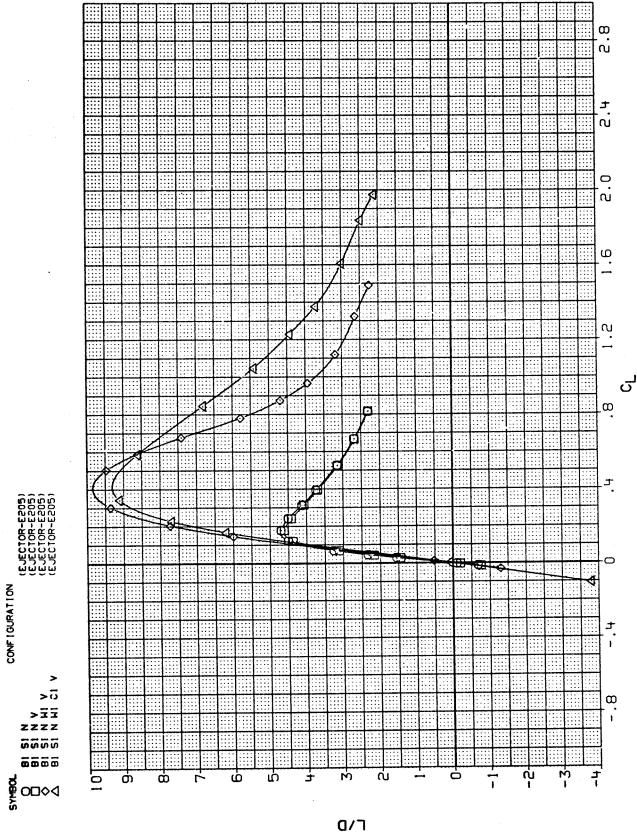


FIG. 15 COMPONENT BUILDUP, LONGITUDINAL CHARACTERISTICS

11

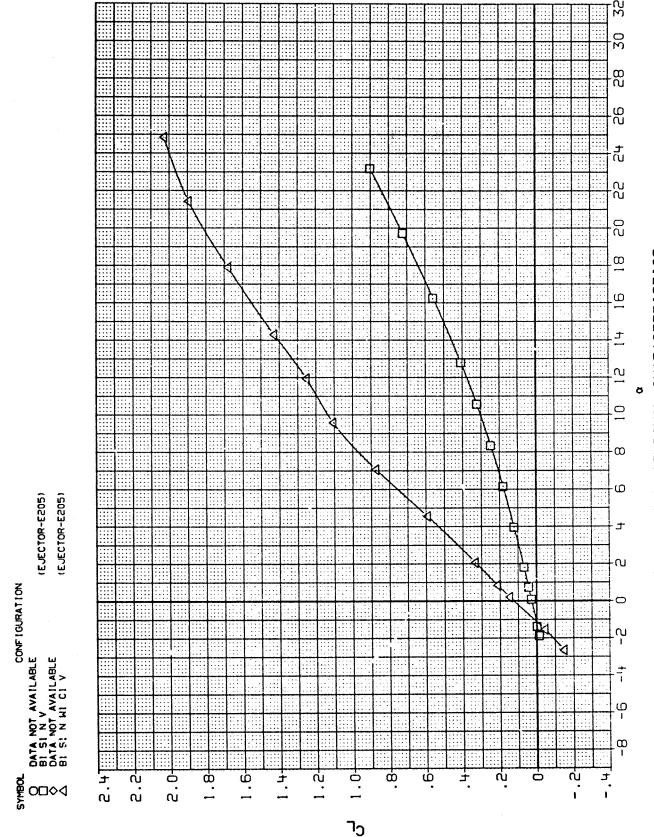
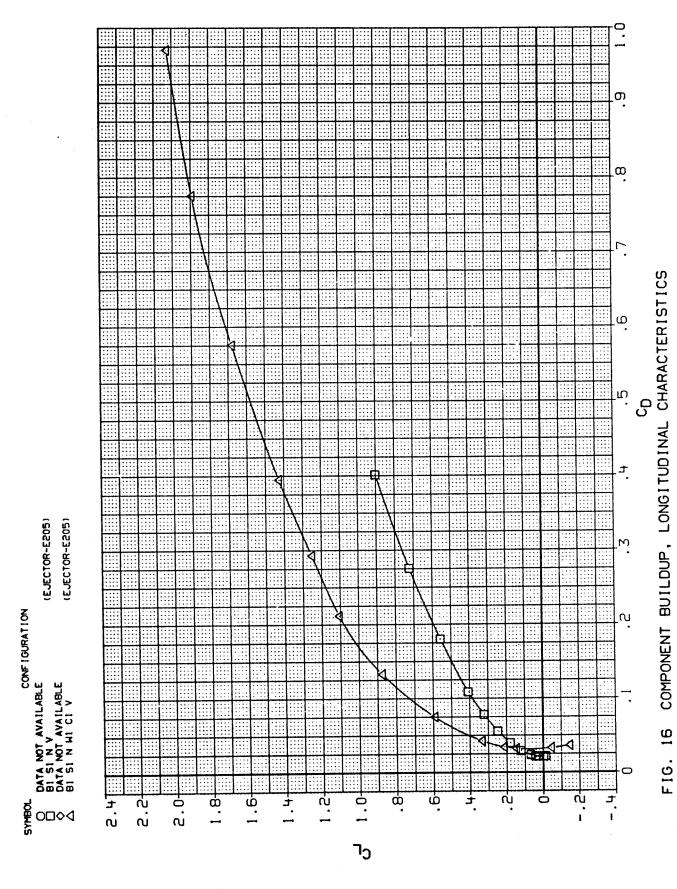
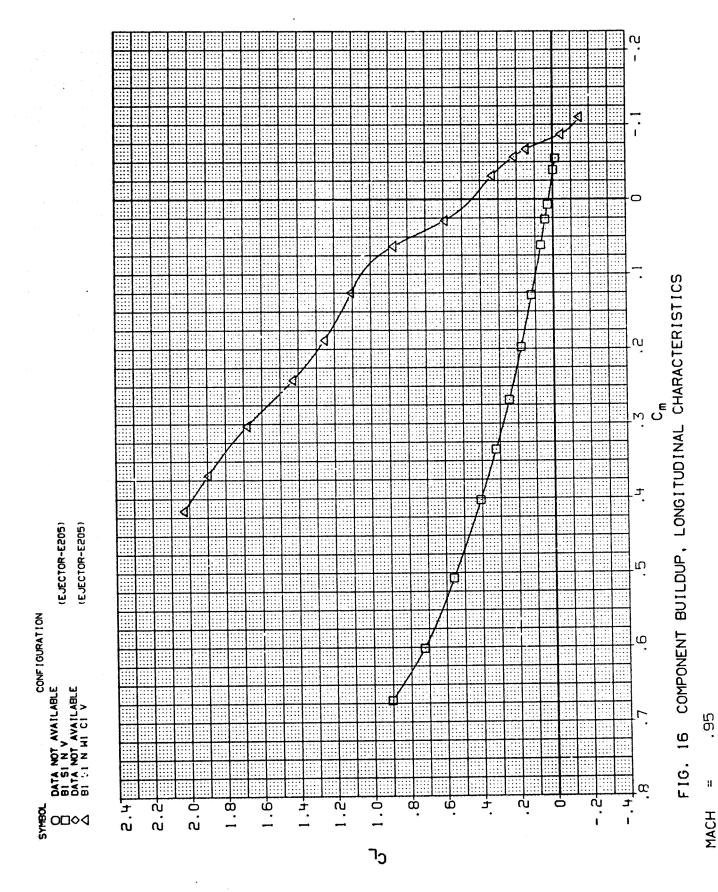


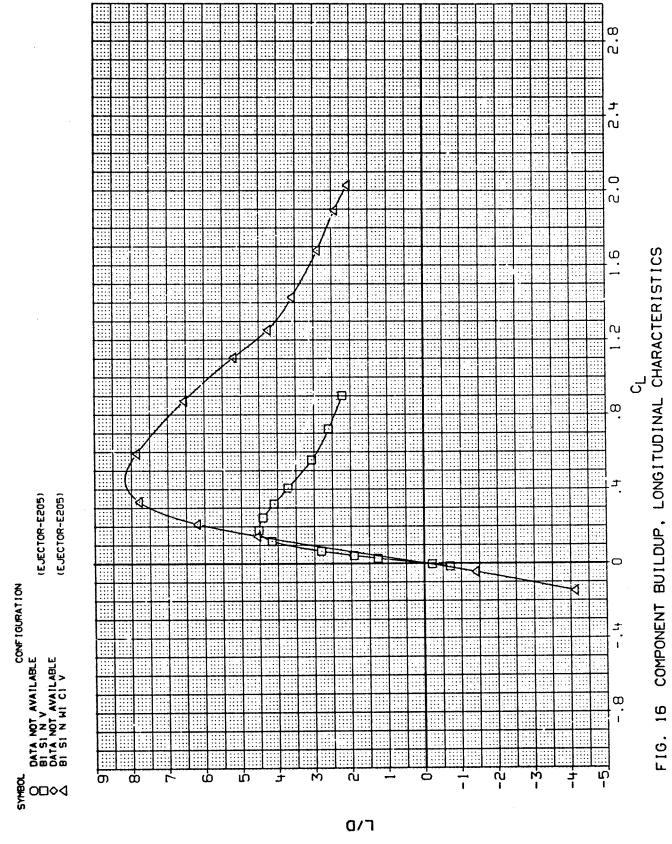
FIG. 16 COMPONENT BUILDUP, LONGITUDINAL CHARACTERISTICS



75

11





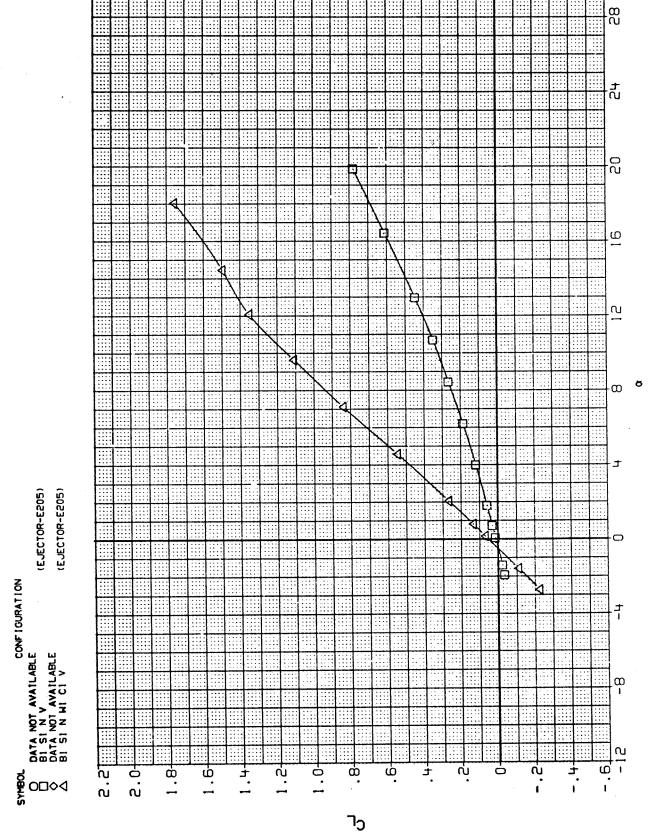
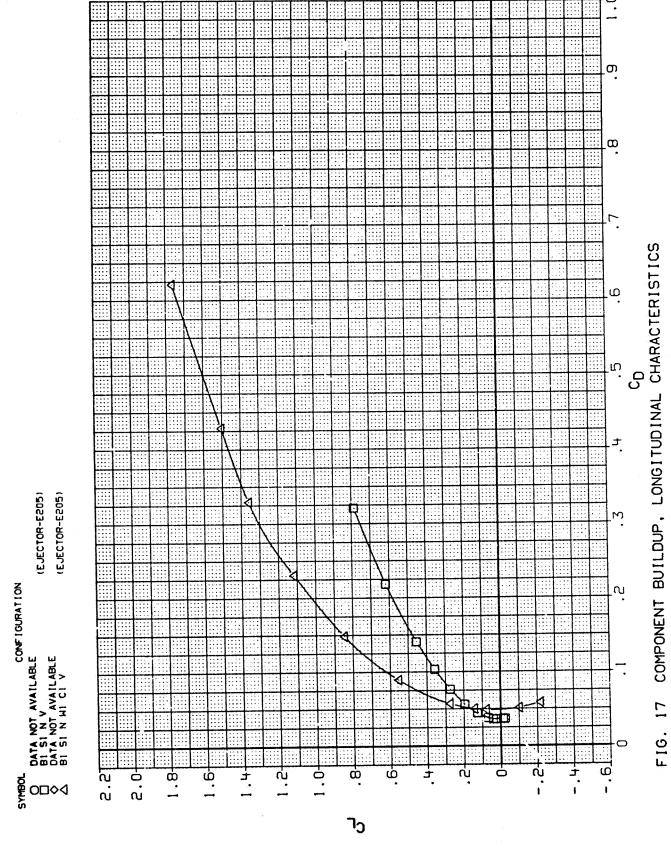


FIG. 17 COMPONENT BUILDUP, LONGITUDINAL CHARACTERISTICS



MACH = 1.10

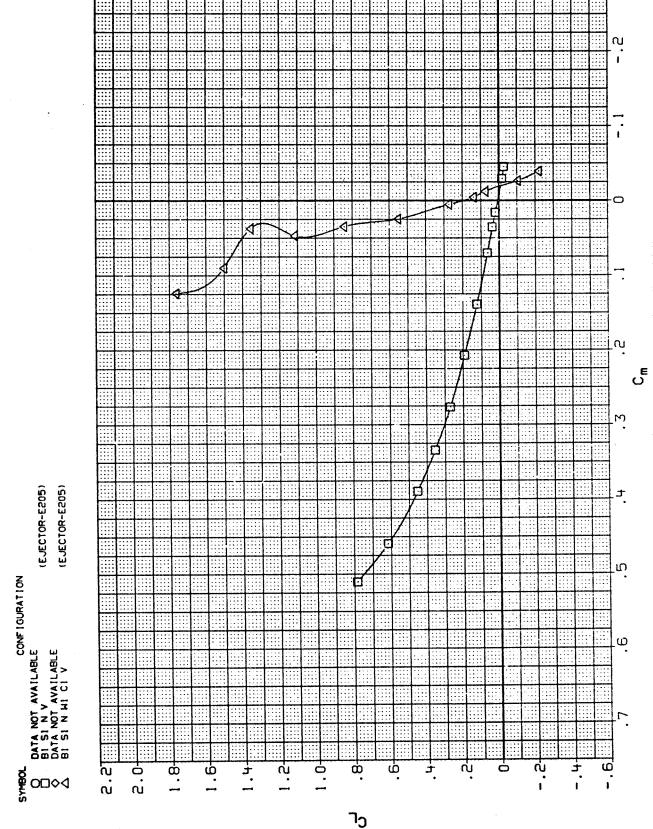


FIG. 17 COMPONENT BUILDUP, LONGITUDINAL CHARACTERISTICS

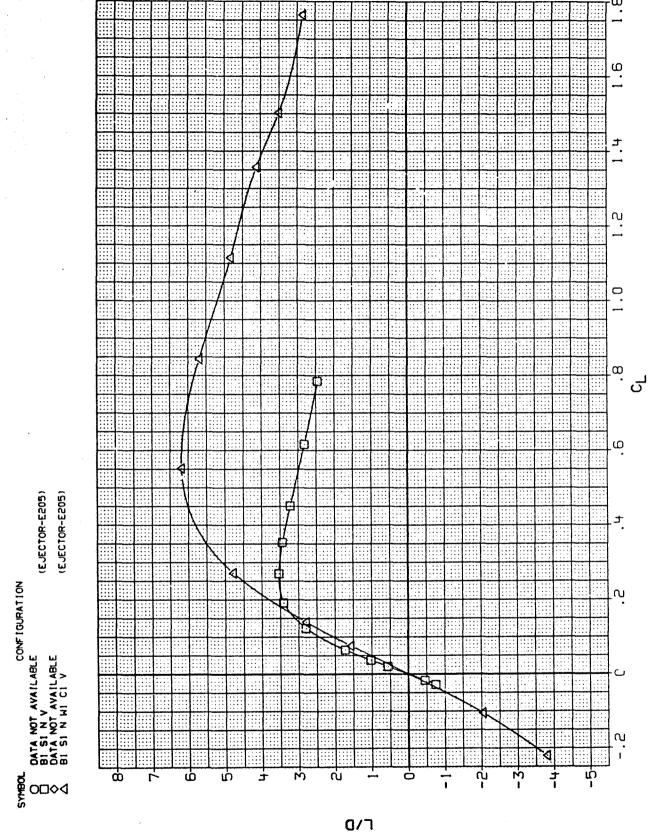


FIG. 17 COMPONENT BUILDUP, LONGITUDINAL CHARACTERISTICS

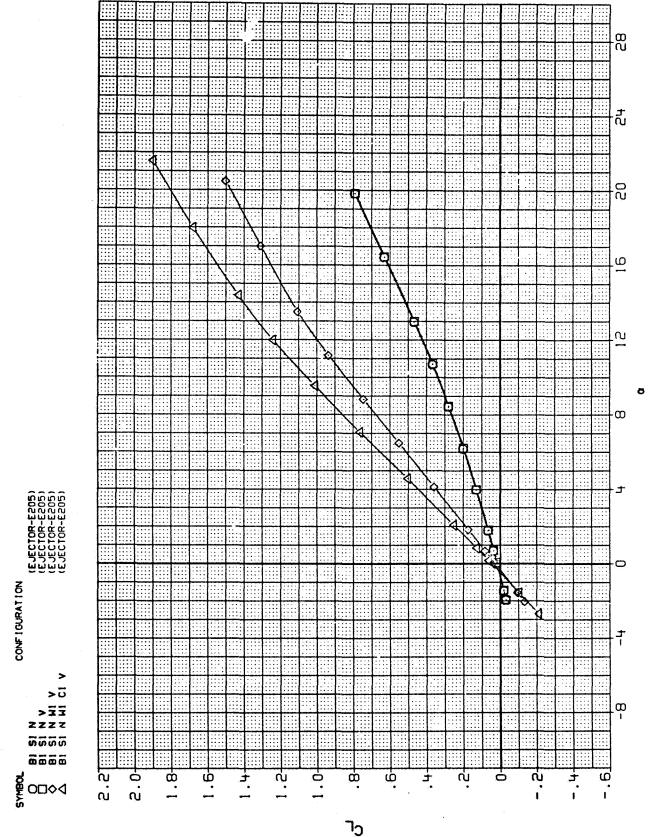
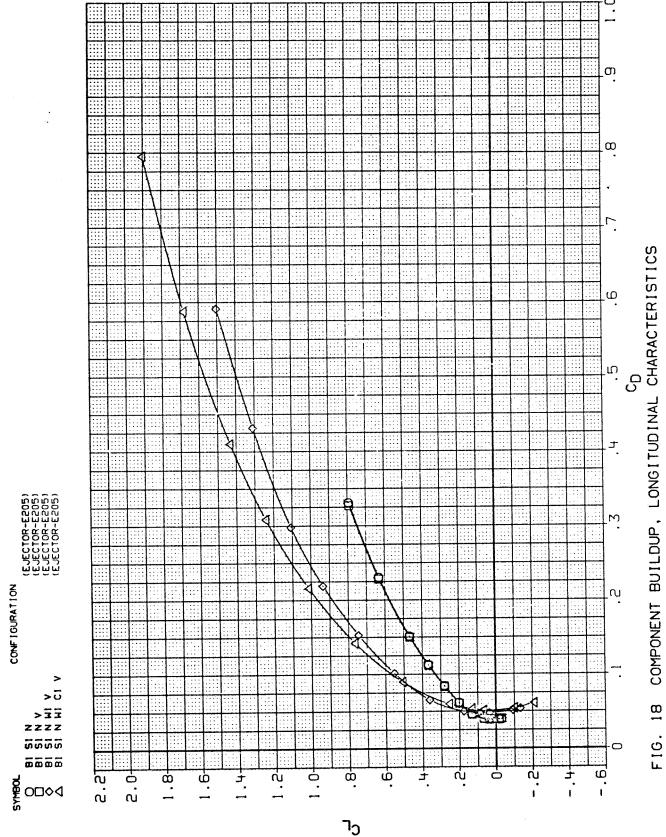
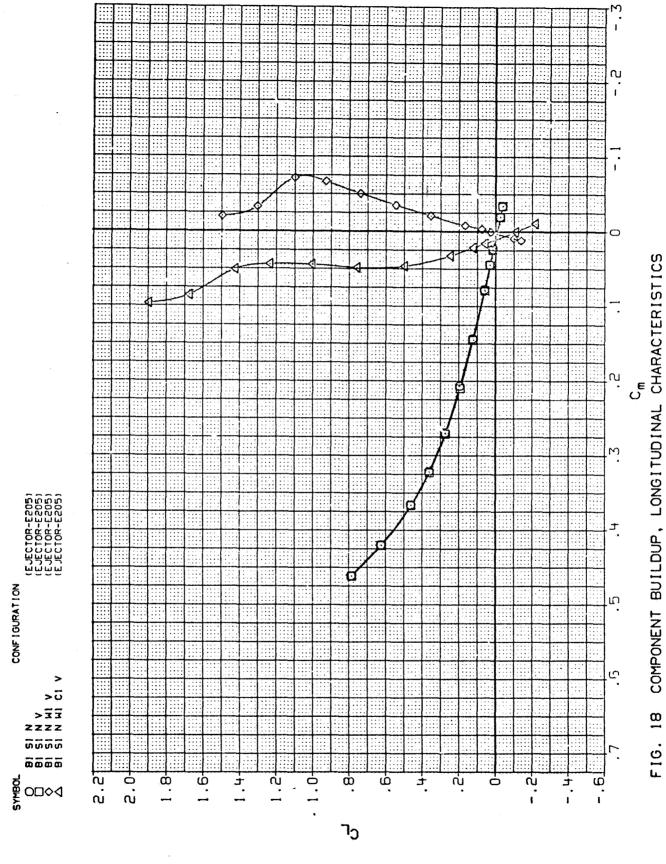


FIG. 18 COMPONENT BUILDUP, LONGITUDINAL CHARACTERISTICS



1.20



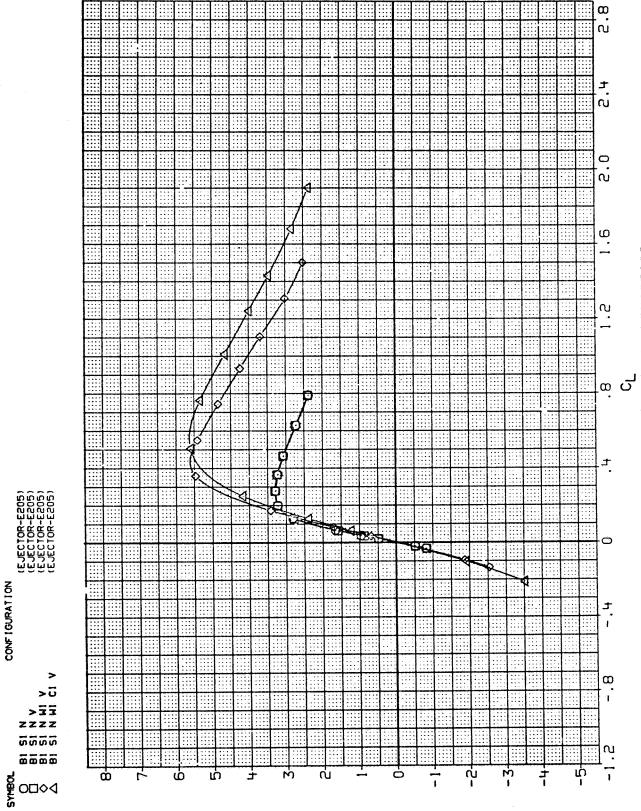


FIG. 18 COMPONENT BUILDUP, LONGITUDINAL CHARACTERISTICS

11

MACH

רום

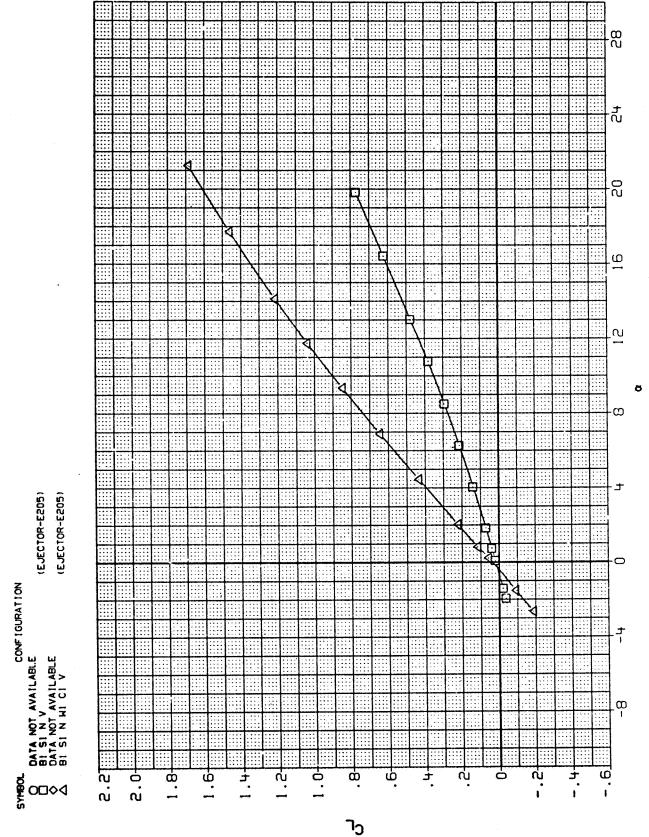
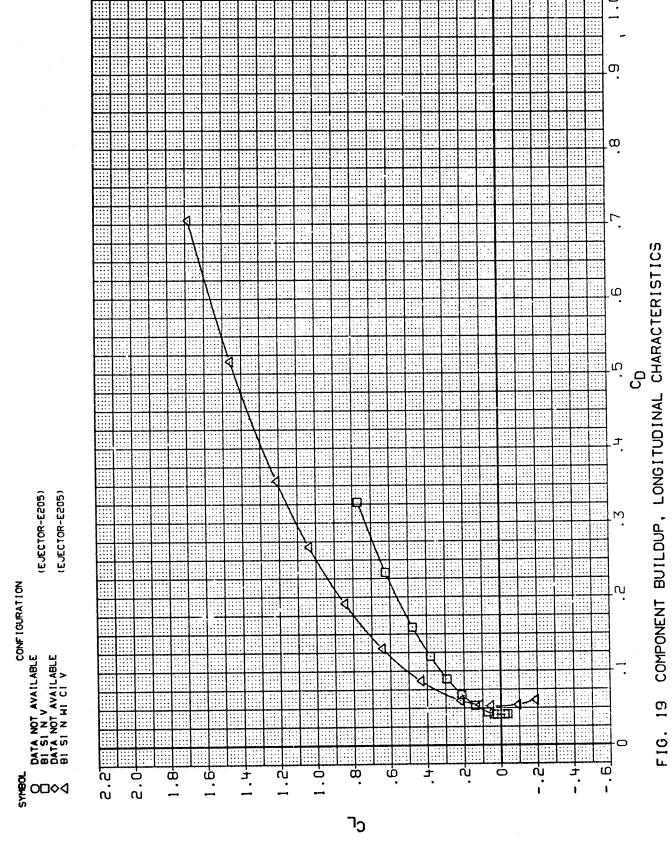
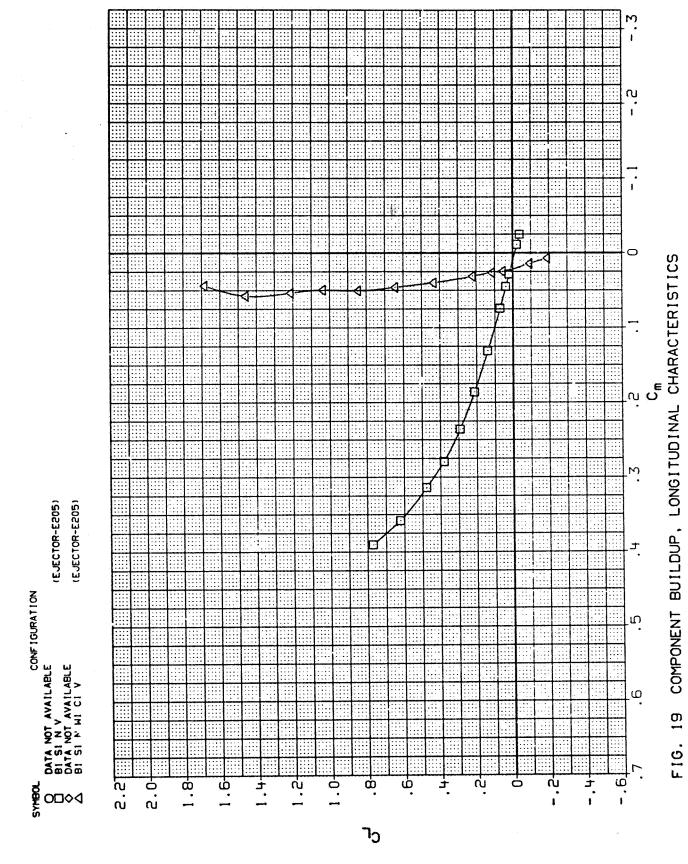


FIG. 19 COMPONENT BUILDUP, LONGITUDINAL CHARACTERISTICS



MACH = i



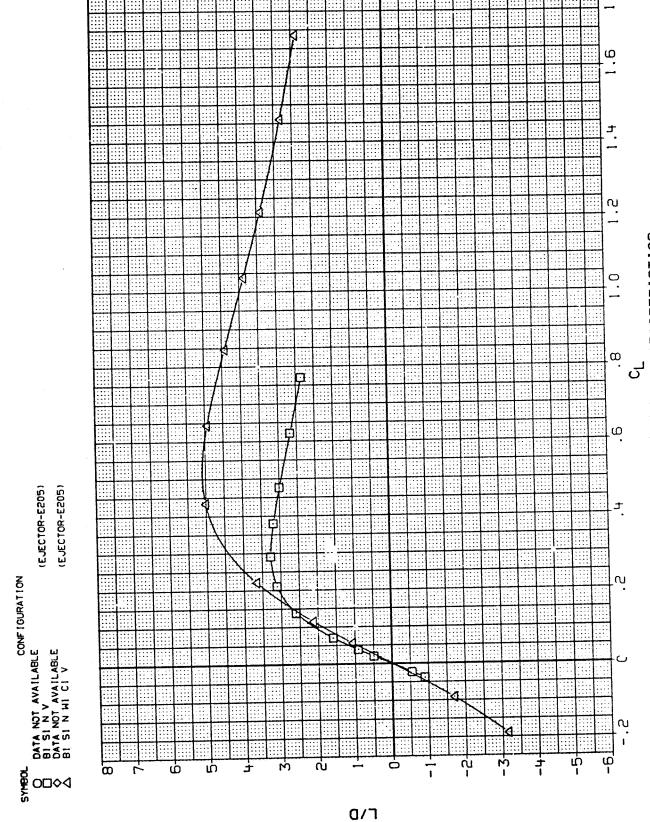


FIG. 19 COMPONENT BUILDUP, LONGITUDINAL CHARACTERISTICS

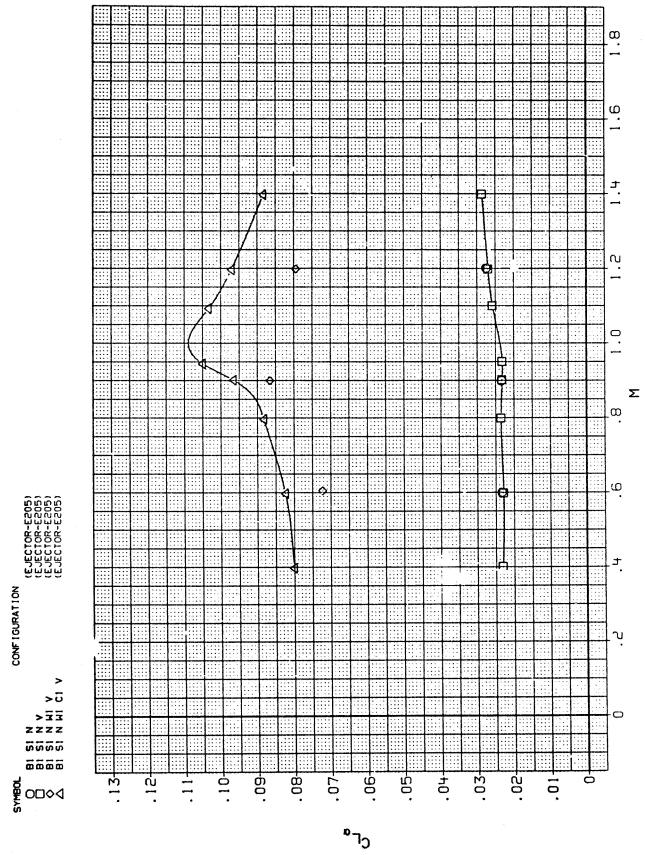


FIG. 20 SUMMARY OF COMPONENT BUILDUP WITH MACH NUMBER

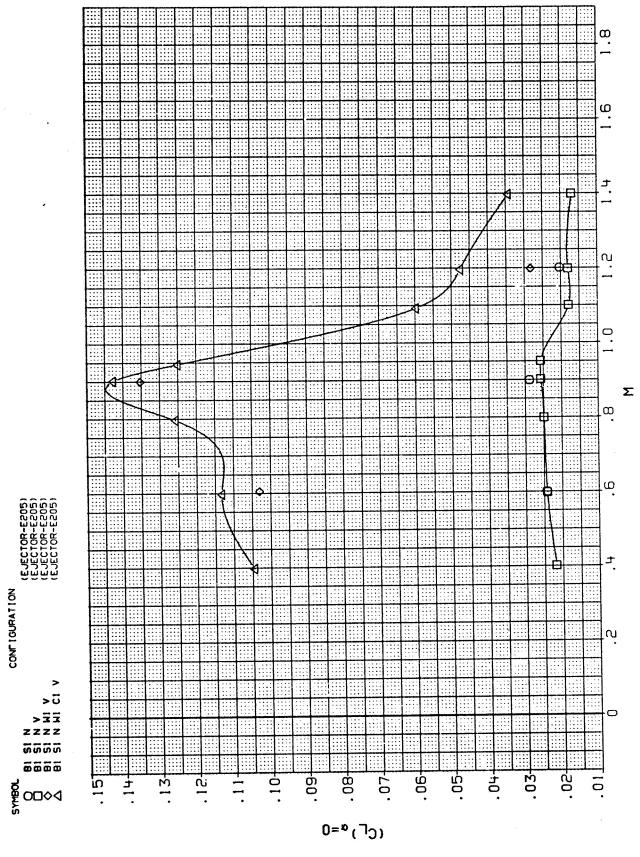
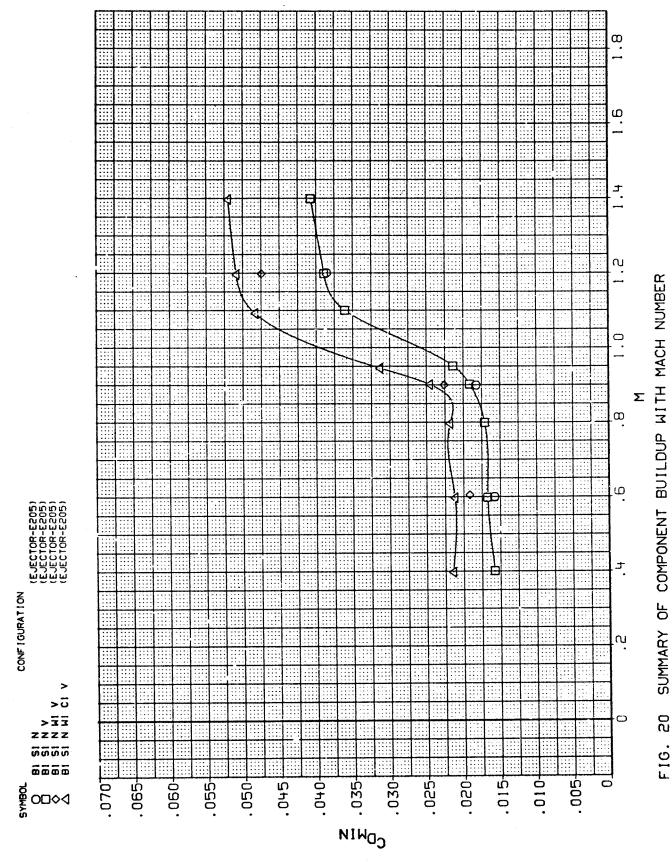
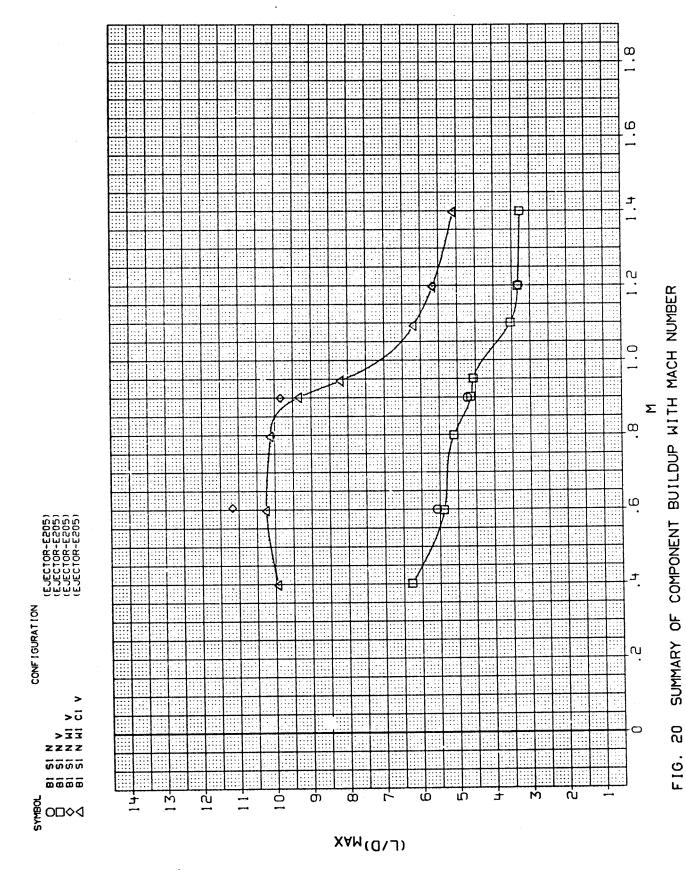
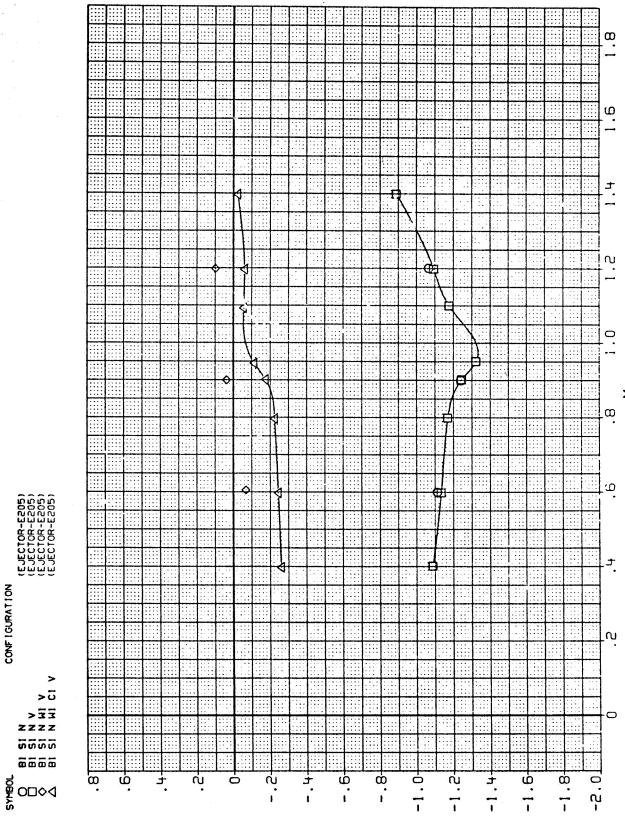


FIG. 20 SUMMARY OF COMPONENT BUILDUP WITH MACH NUMBER



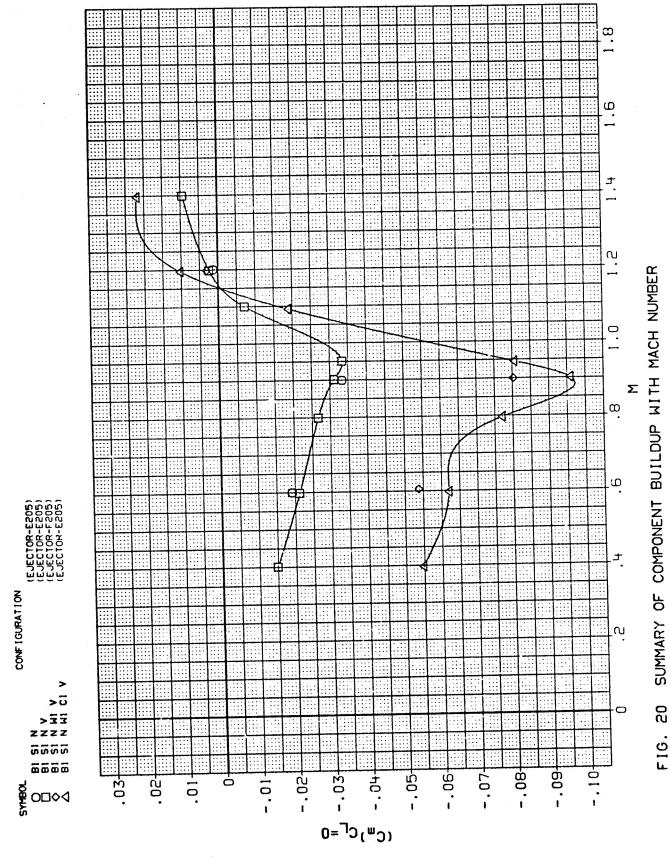




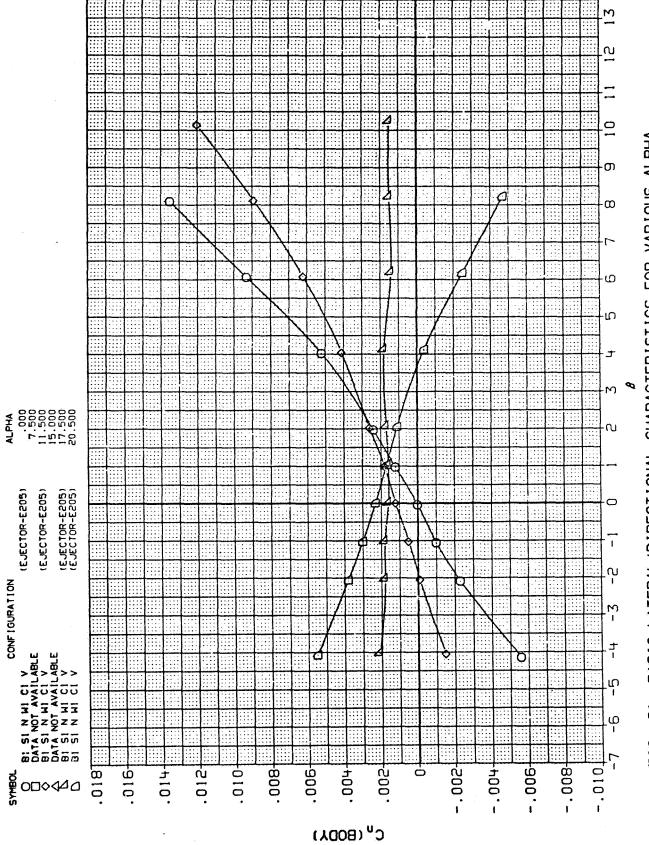
SUMMARY OF COMPONENT BUILDUP WITH MACH NUMBER

F16. 20

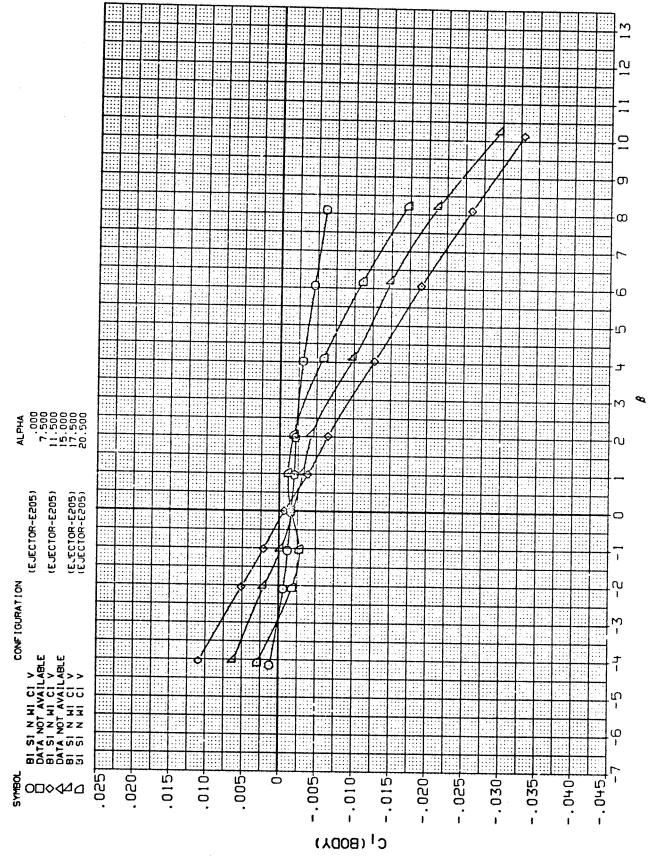
۰۵۰۸



F16. 20

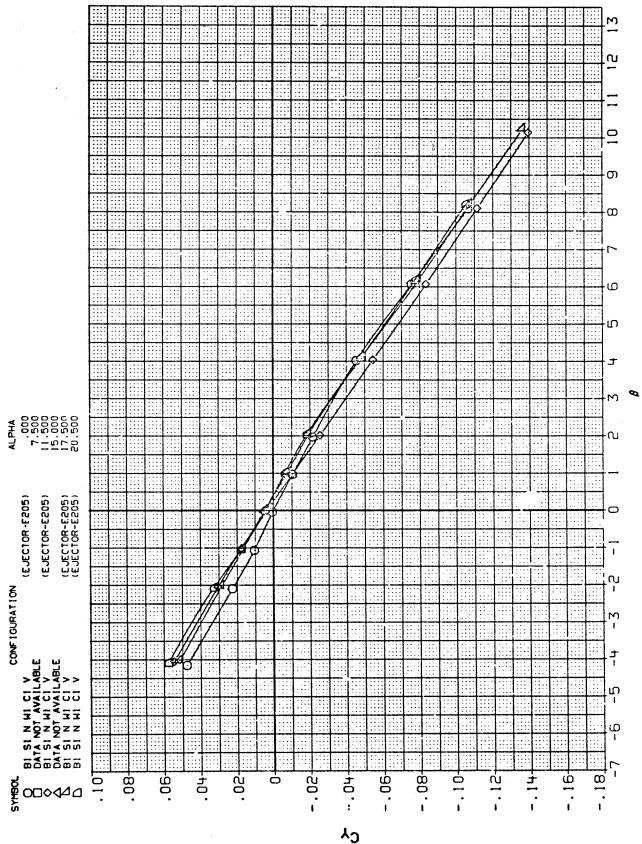


BASIC LATERAL/DIRECTIONAL CHARACTERISTICS FOR VARIOUS ALPHA ົດ F16.



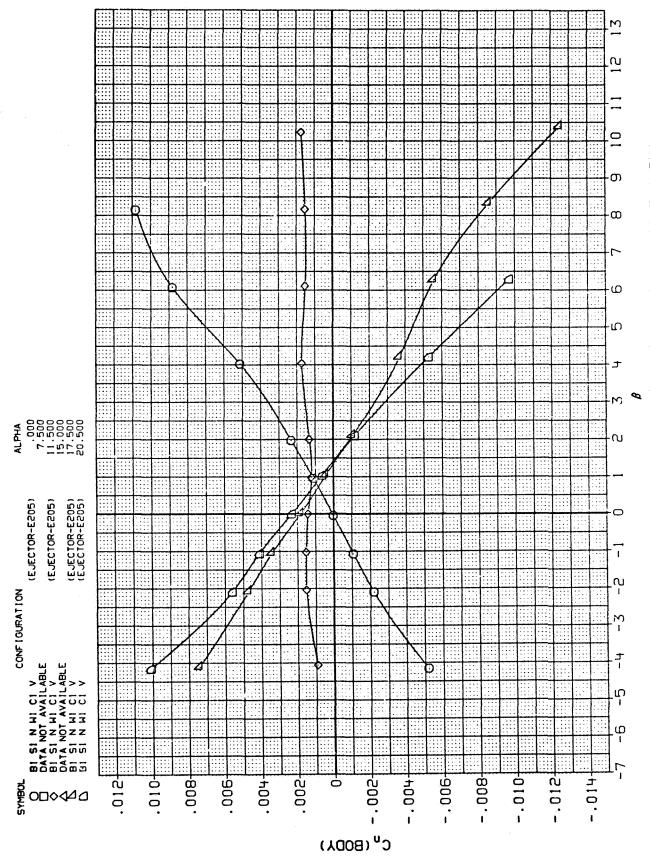
BASIC LATERAL/DIRECTIONAL CHARACTERISTICS FOR VARIOUS ALPHA ด F16.

11

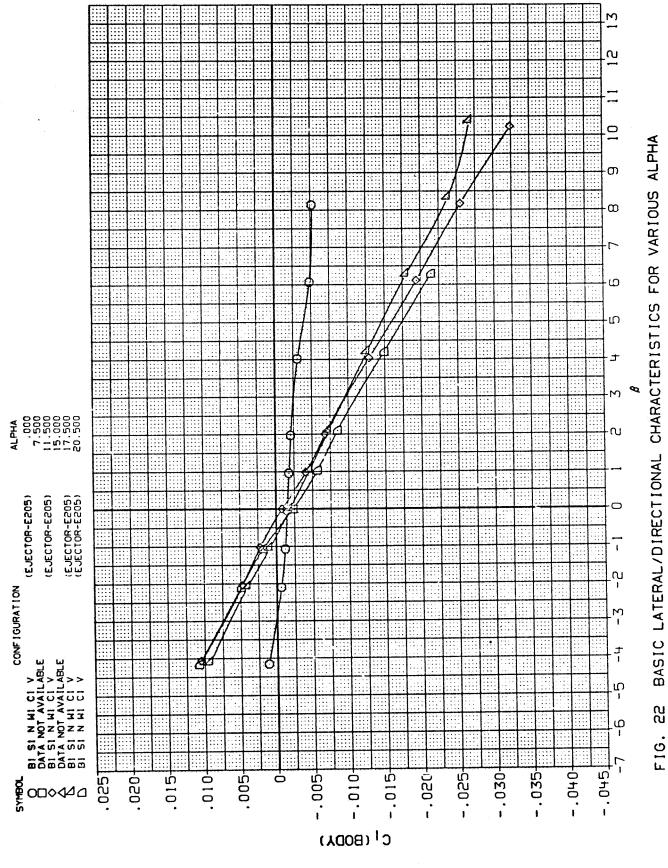


BASIC LATERAL/DIRECTIONAL CHARACTERISTICS FOR VARIOUS ALPHA ດ F16.

;1



BASIC LATERAL/DIRECTIONAL CHARACTERISTICS FOR VARIOUS ALPHA F1G. 22

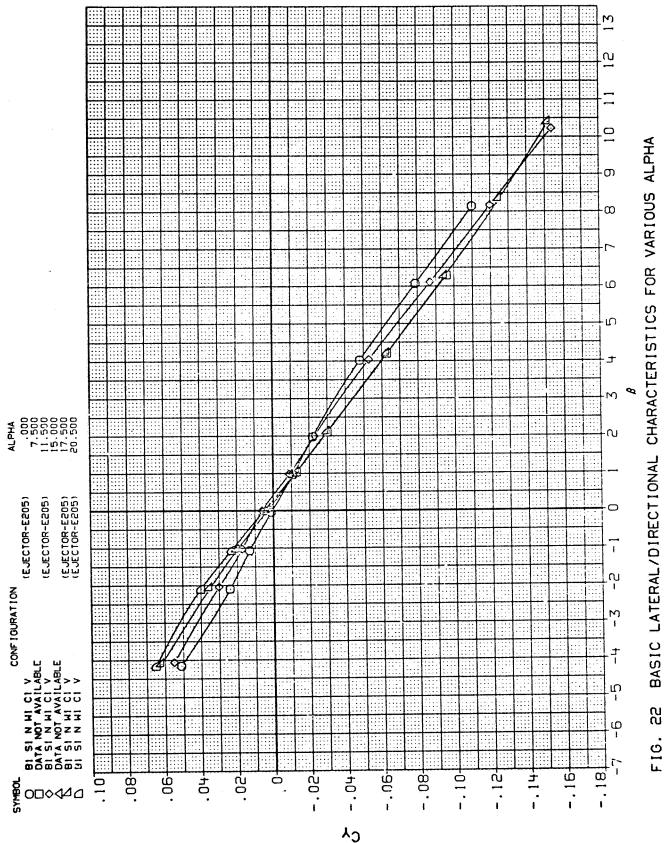


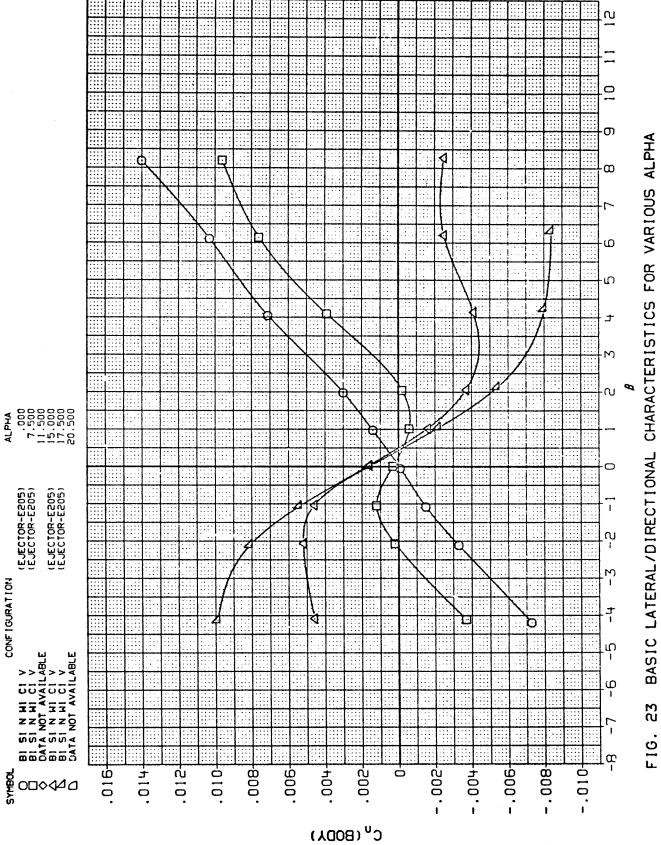
100

MACH

ດິດ

F16.





MACH

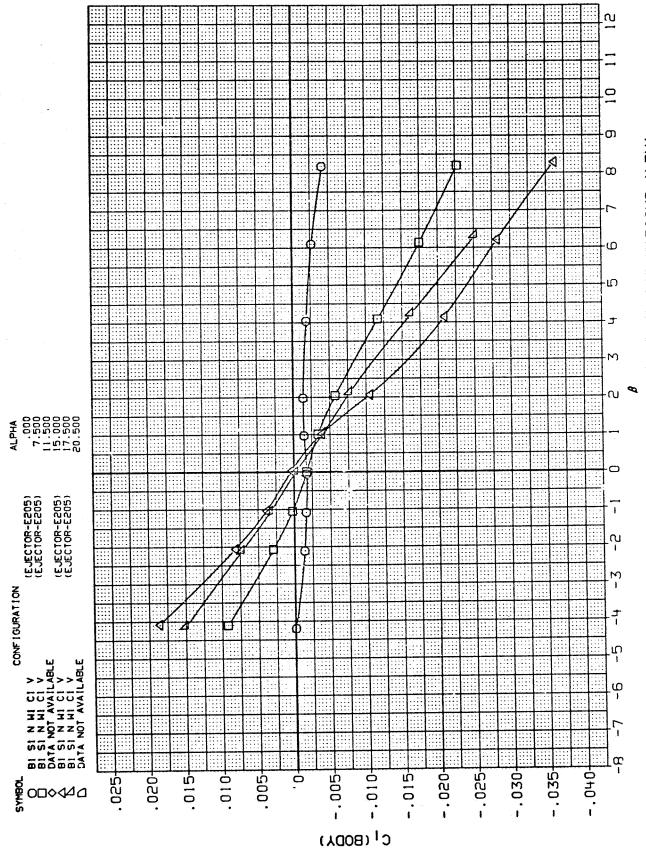
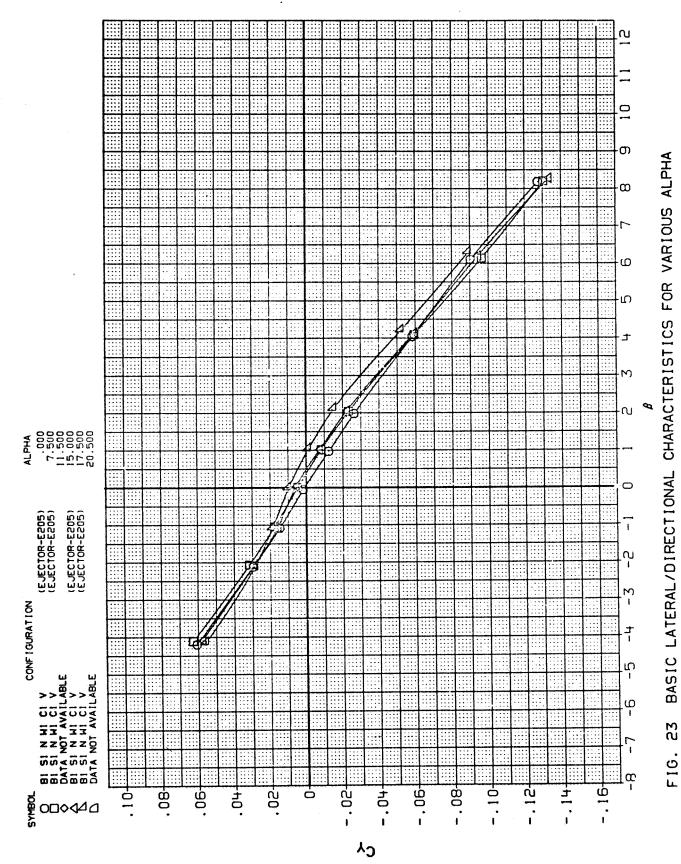
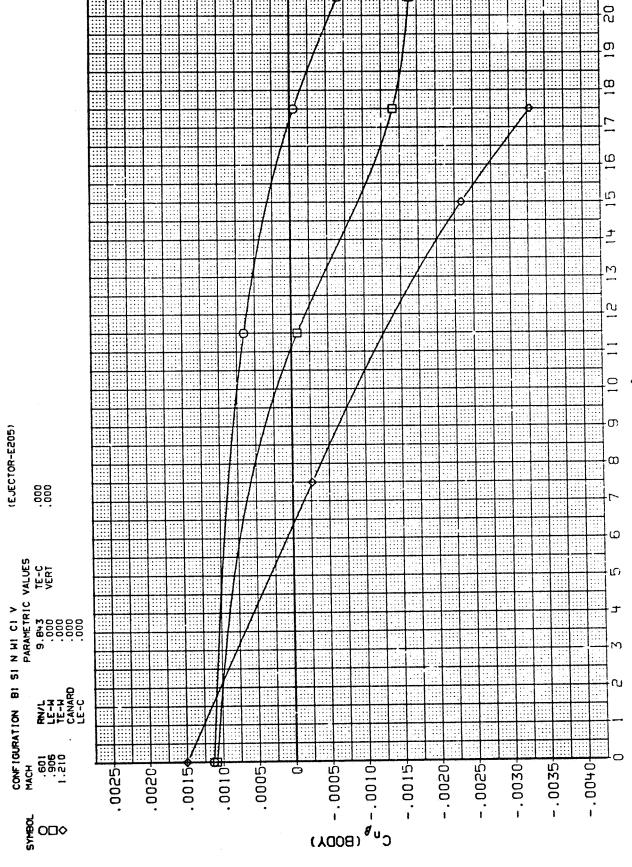


FIG. 23 BASIC LATERAL/DIRECTIONAL CHARACTERISTICS FOR VARIOUS ALPHA



1.20



SUMMARY OF BASIC LATERAL/DIRECTIONAL CHARACTERISTICS WITH ALPHA

F16. 24

105

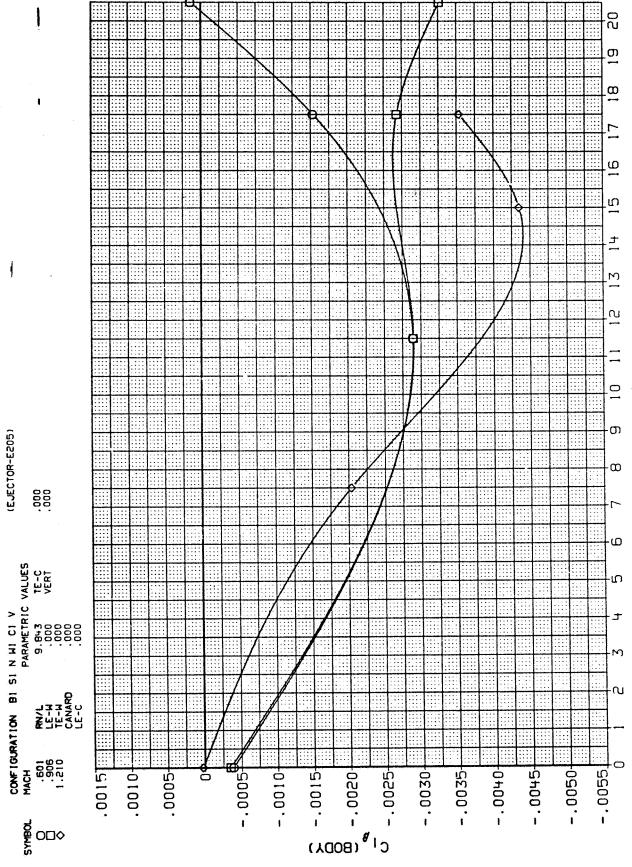
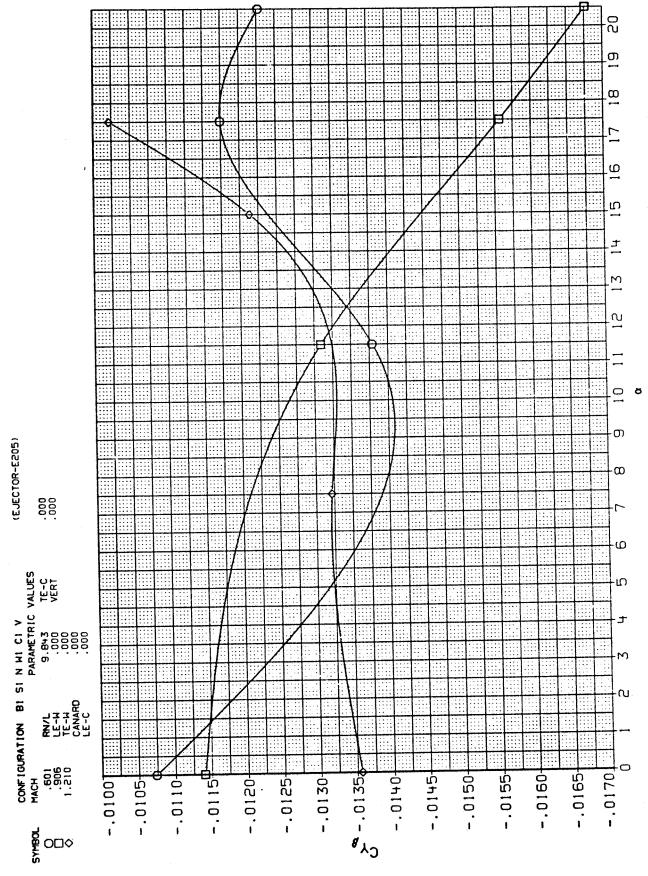


FIG. 24 SUMMARY OF BASIC LATERAL/DIRECTIONAL CHARACTERISTICS WITH ALPHA



SUMMARY OF BASIC LATERAL/DIRECTIONAL CHARACTERISTICS WITH ALPHA F1G. 24

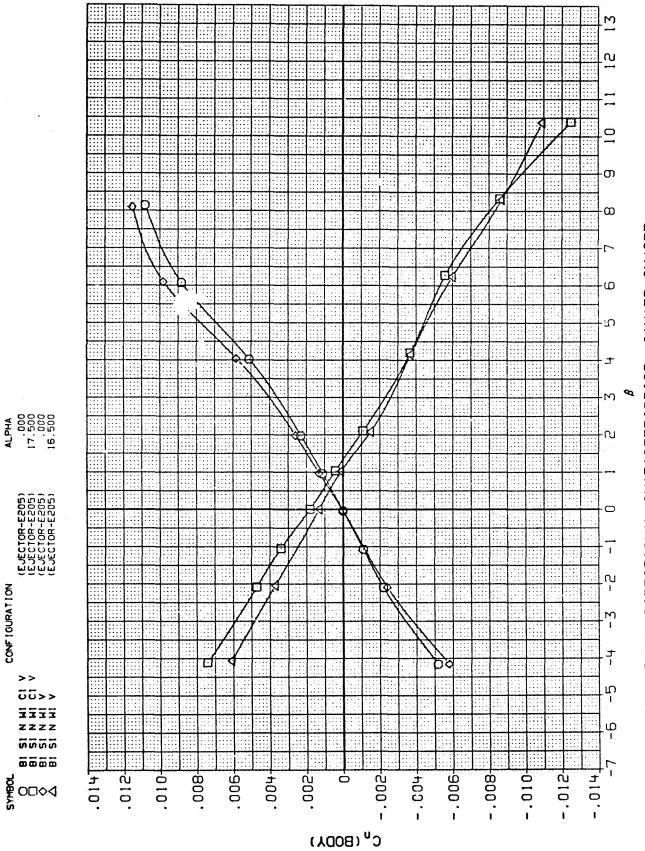
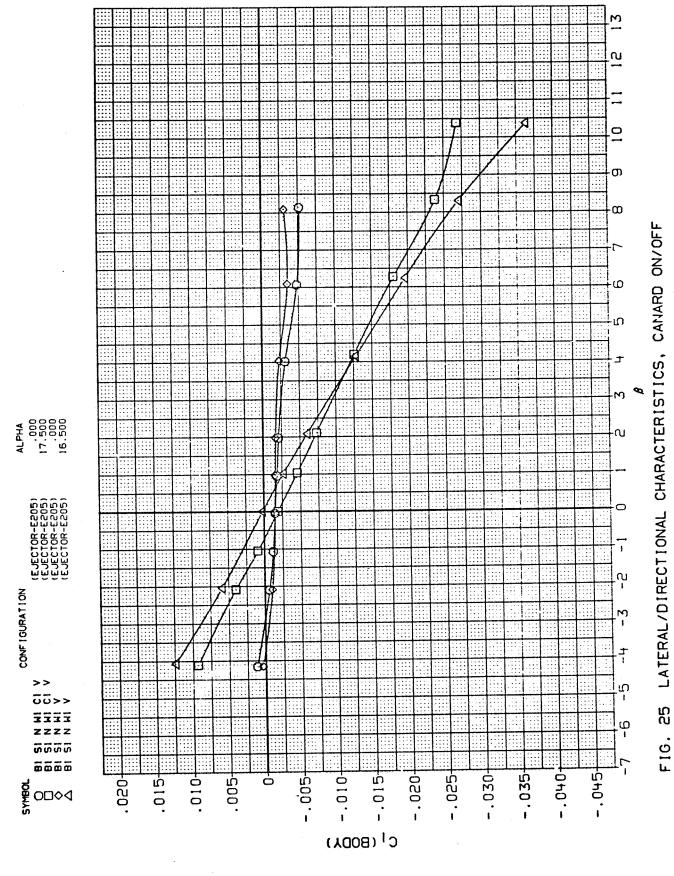
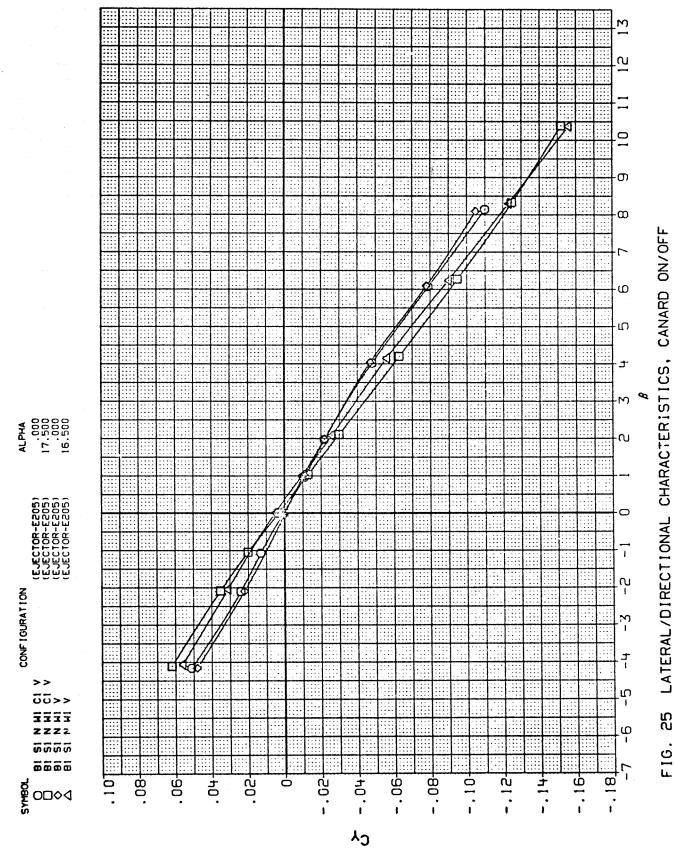
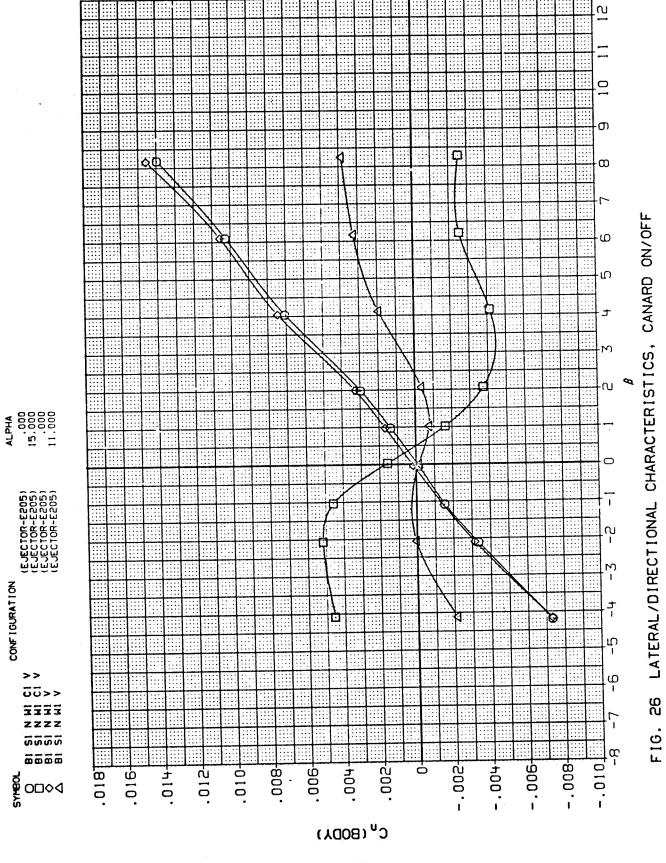


FIG. 25 LATERAL/DIRECTIONAL CHARACTERISTICS, CANARD ON/OFF





110



111

:1

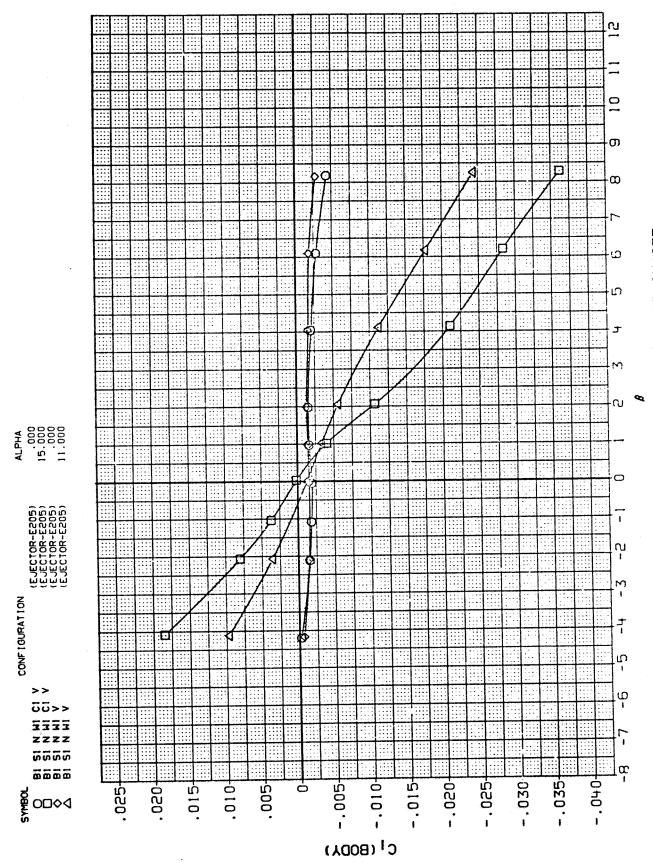
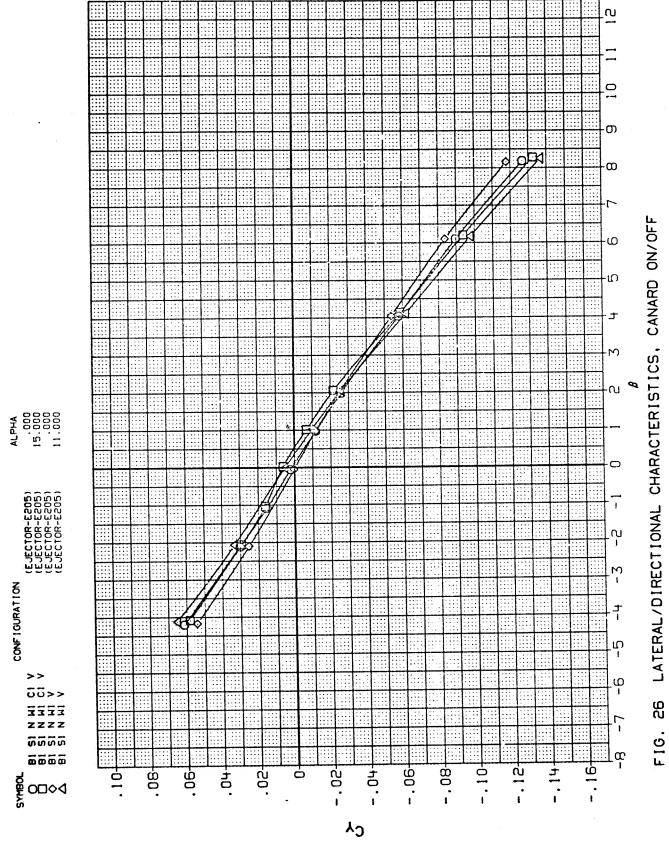
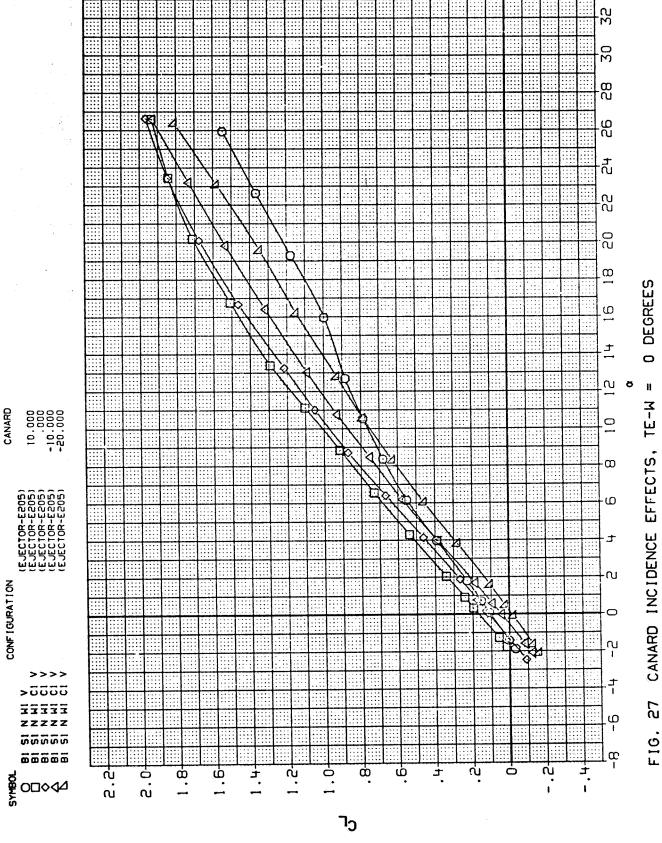


FIG. 26 LATERAL/DIRECTIONAL CHARACTERISTICS, CANARD ON/OFF



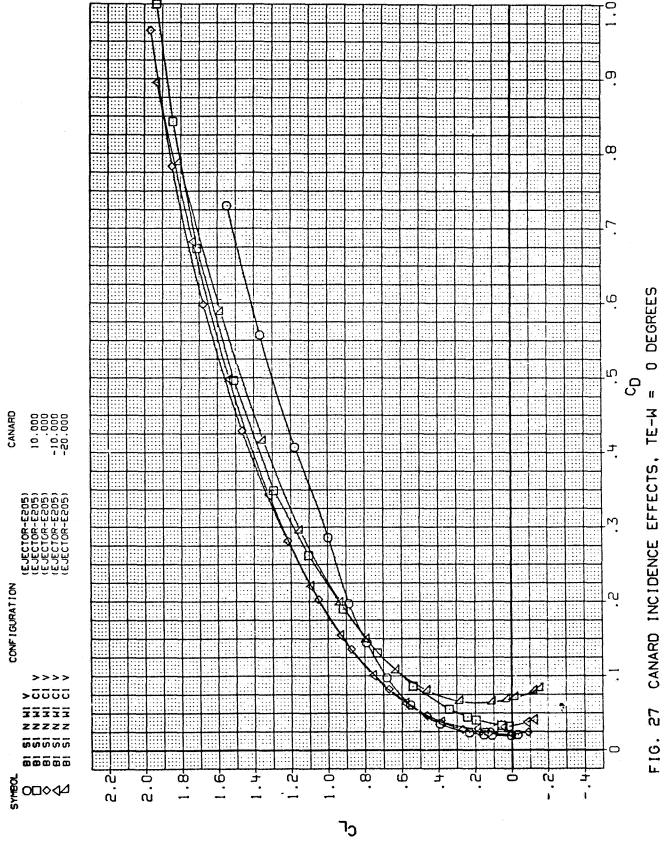
1.20 = 1.20



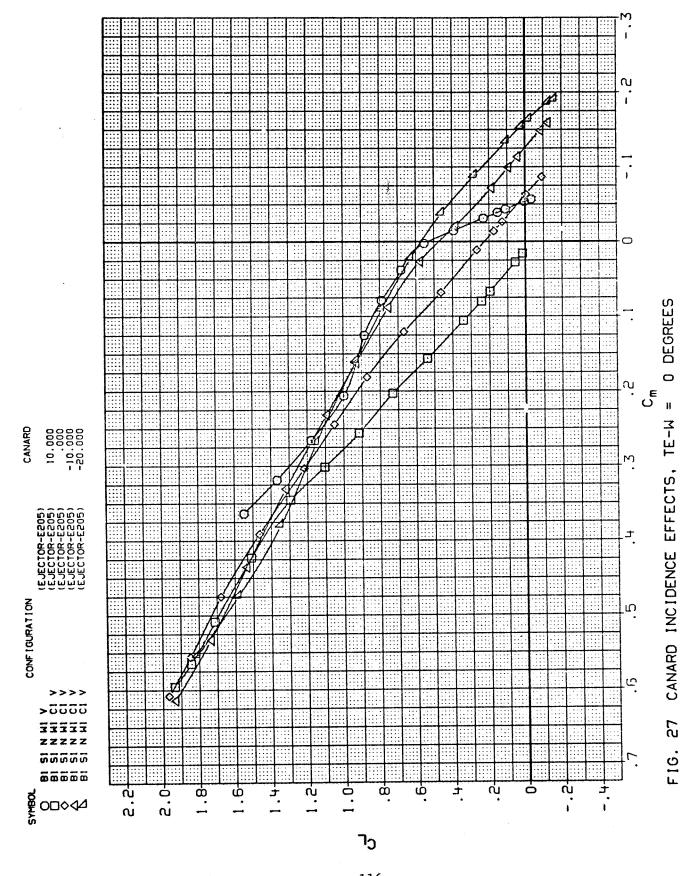
#

MACH

F16.



115



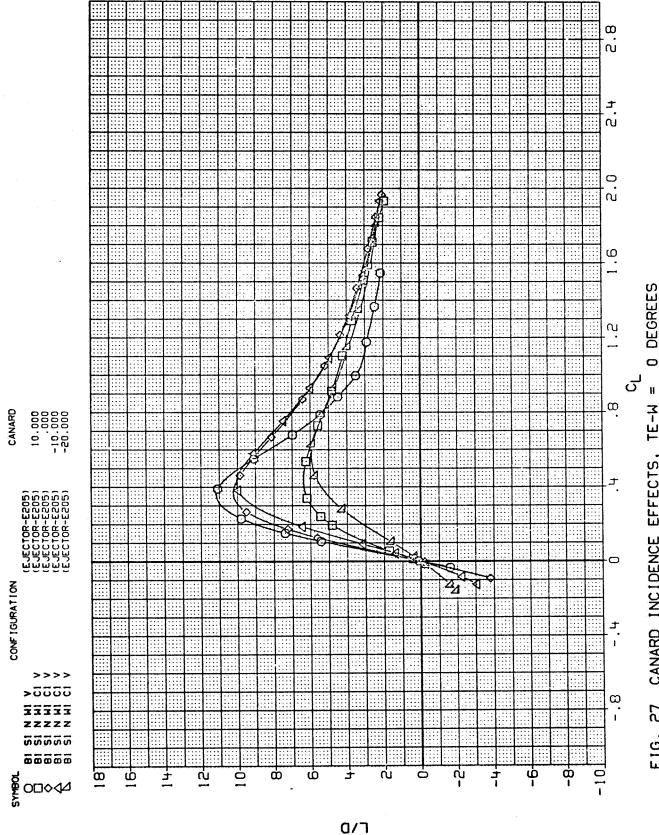


FIG. 27 CANARD INCIDENCE EFFECTS, TE-W

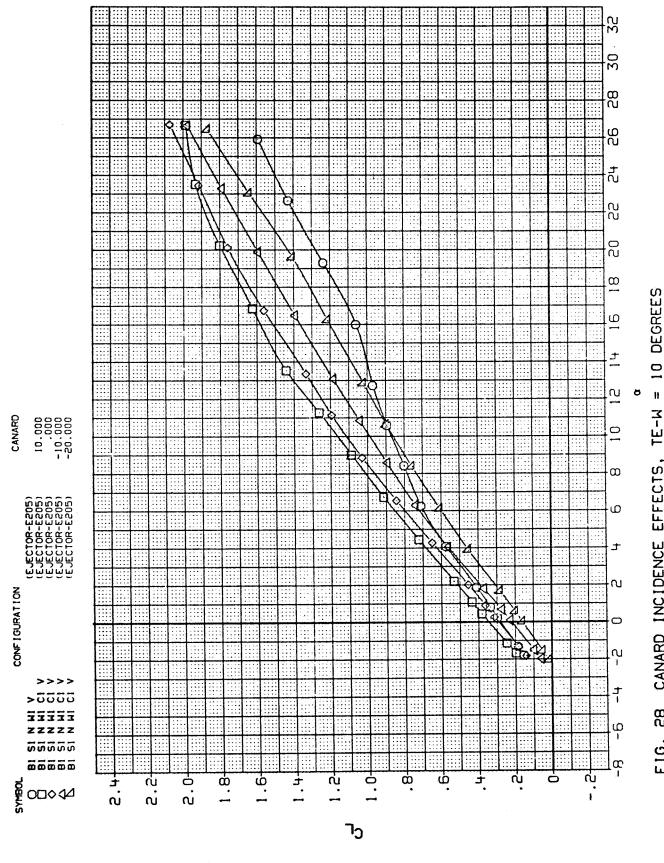
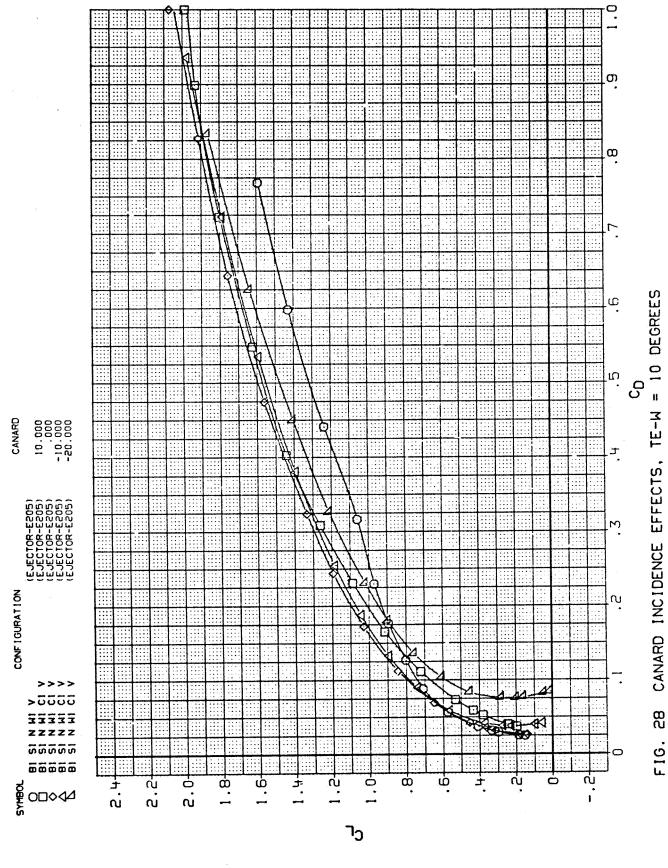
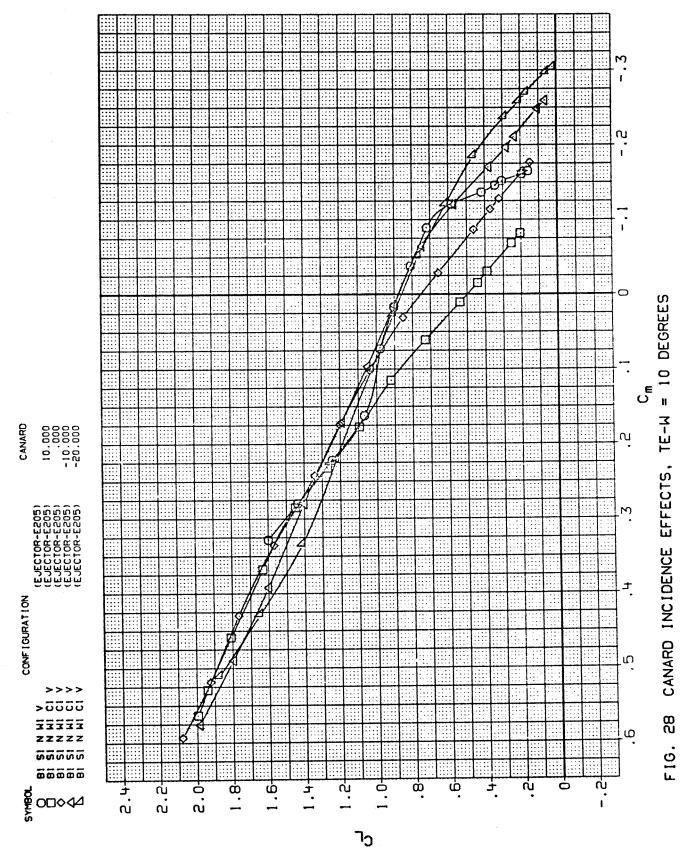


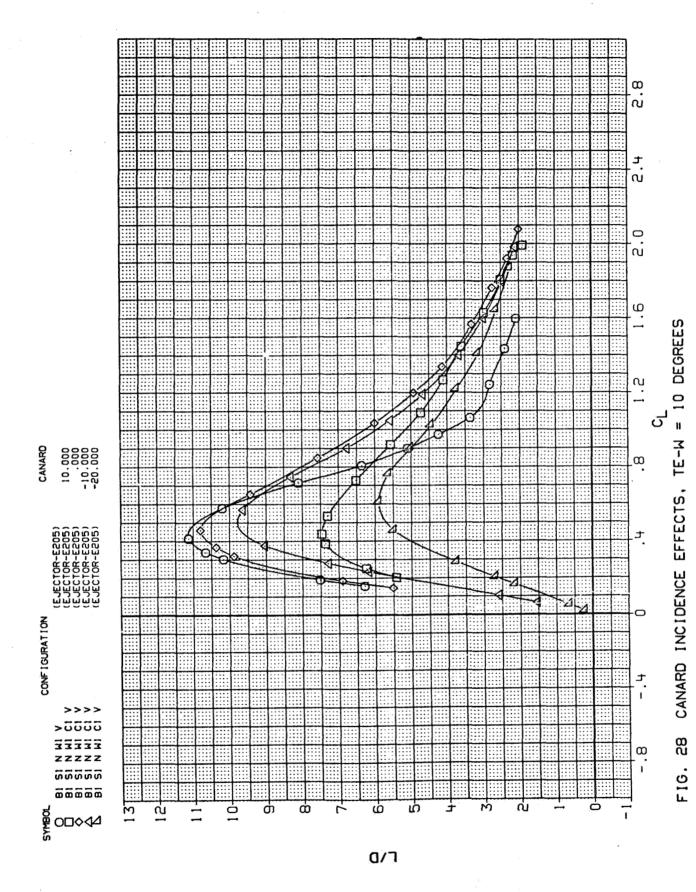
FIG. 28 CANARD INCIDENCE EFFECTS, TE-W



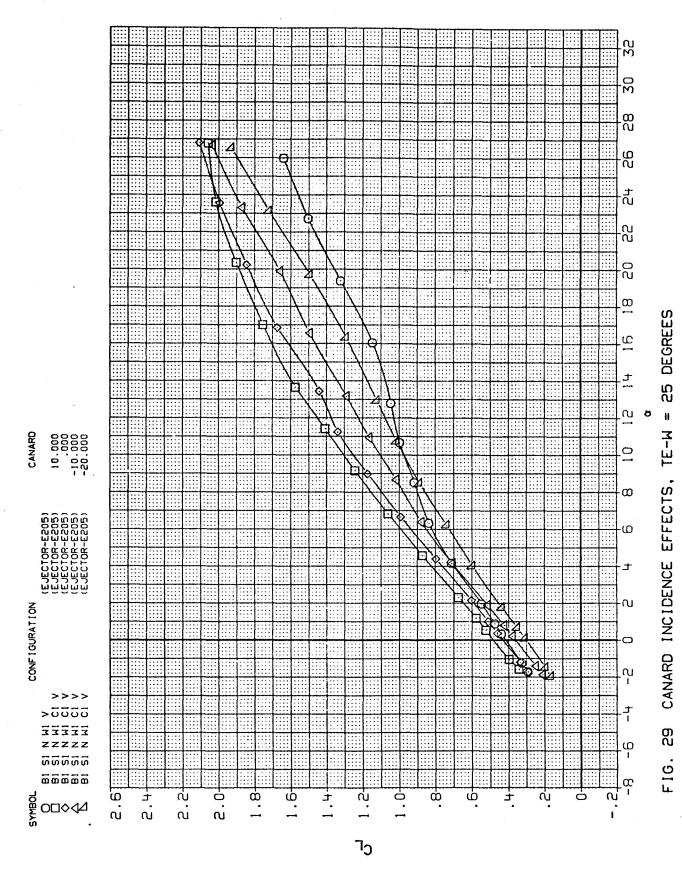
119

3

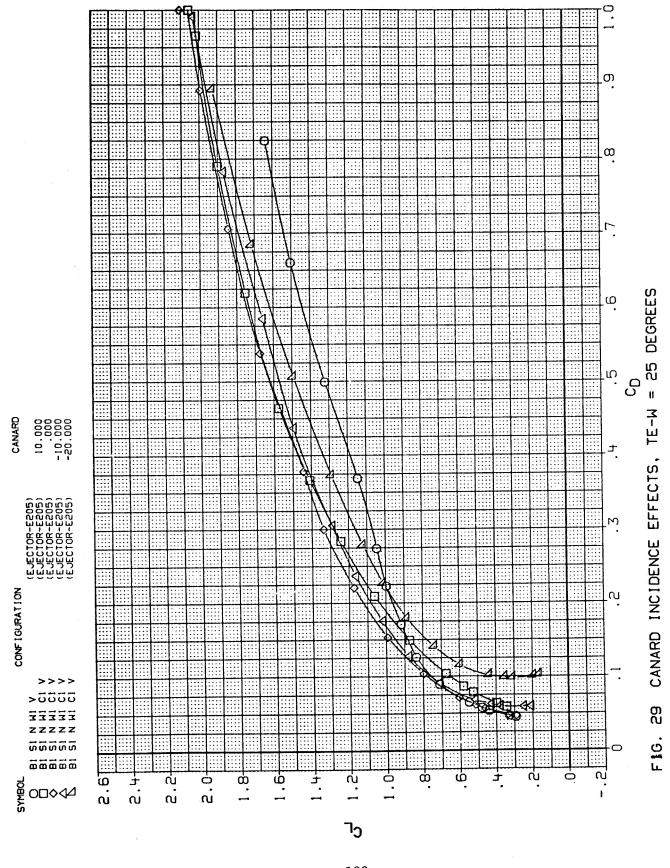


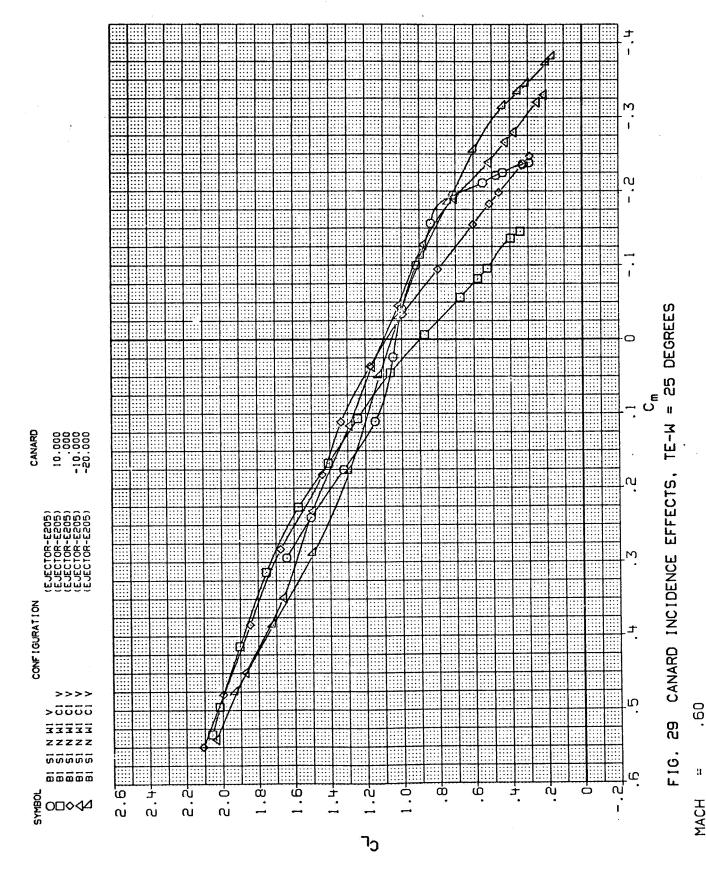


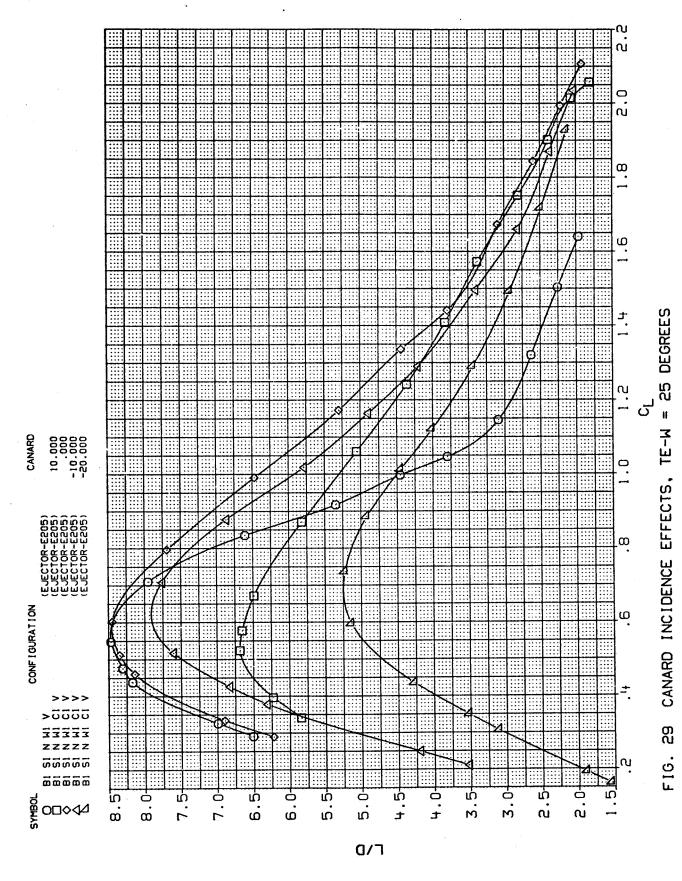
121



.60







125

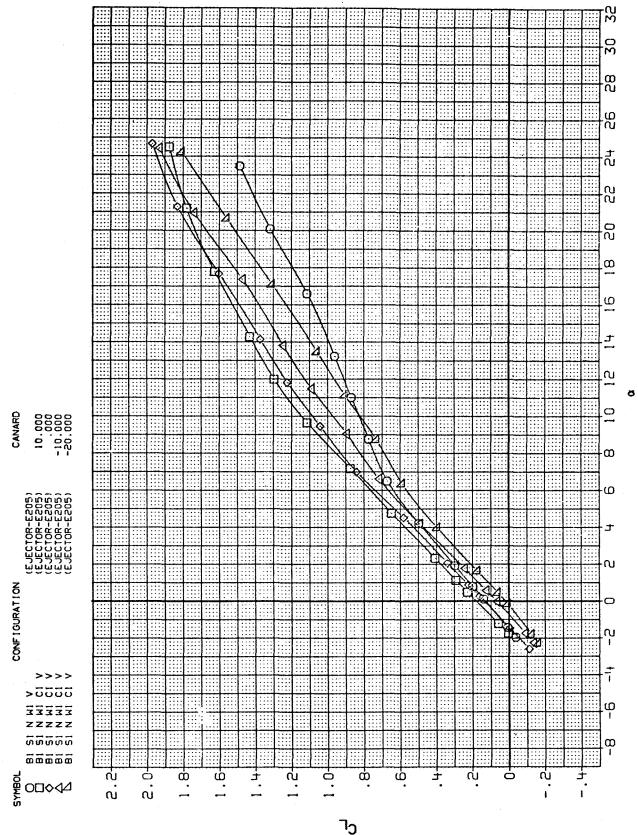
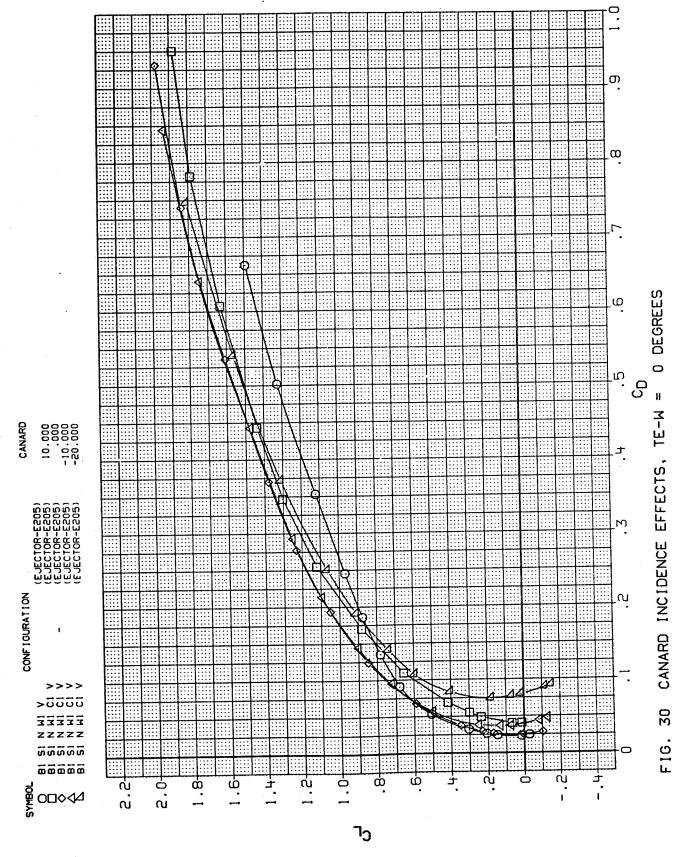
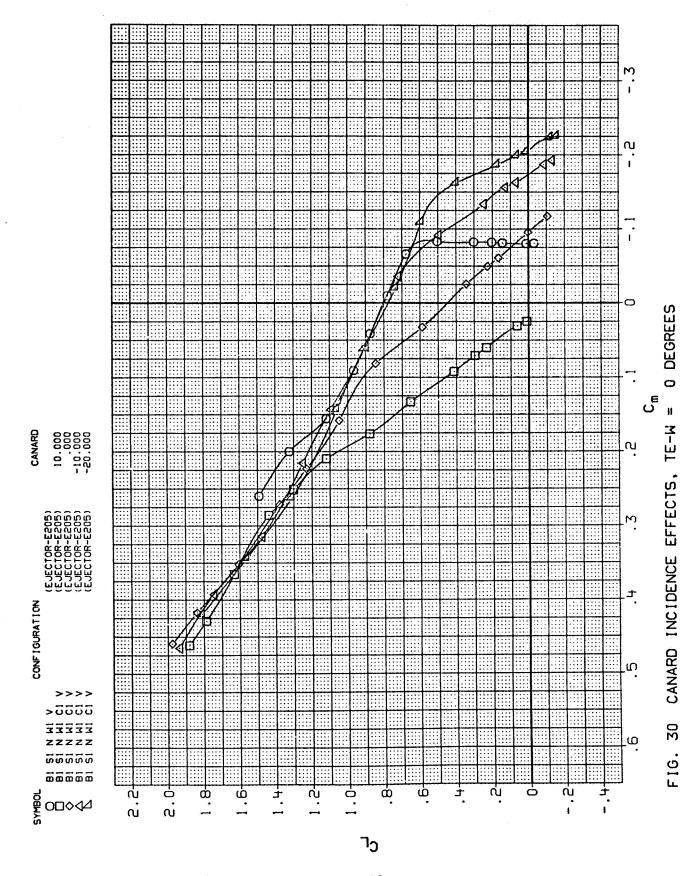
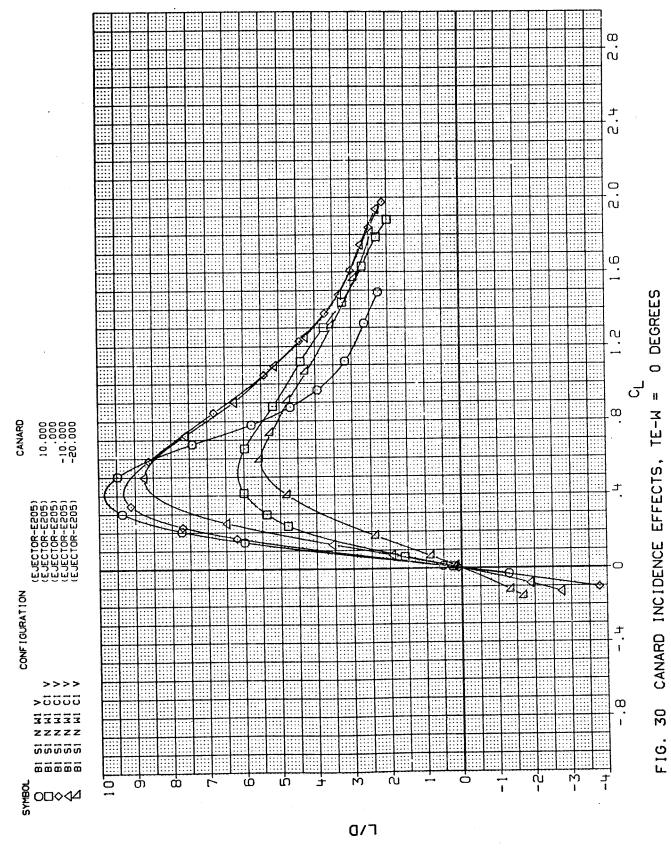


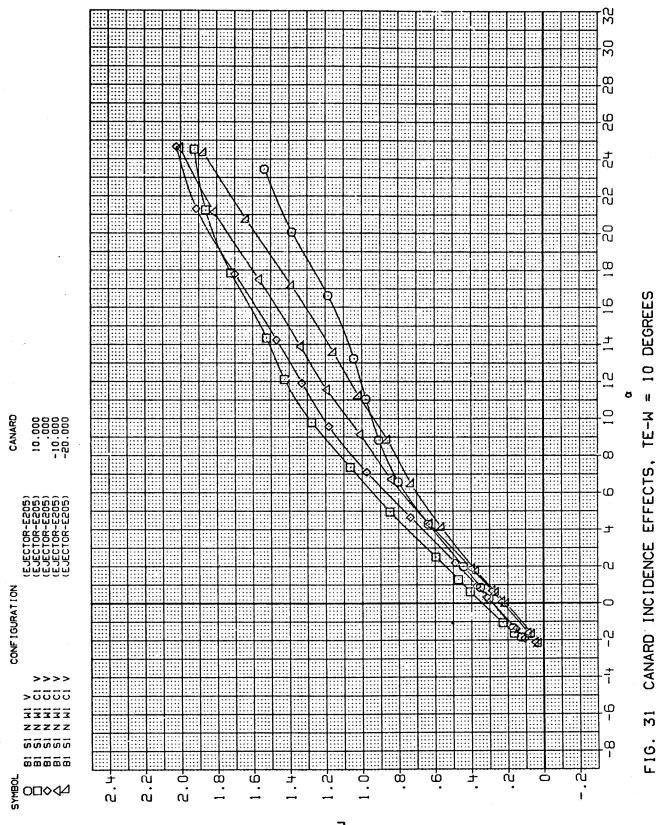
FIG. 30 CANARD INCIDENCE EFFECTS, TE-W = 0 DEGREES



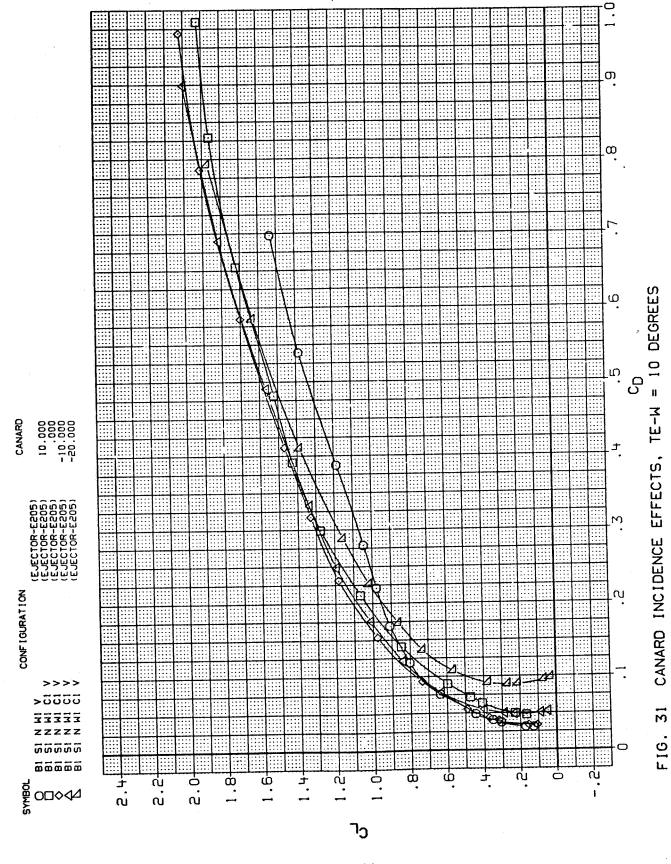


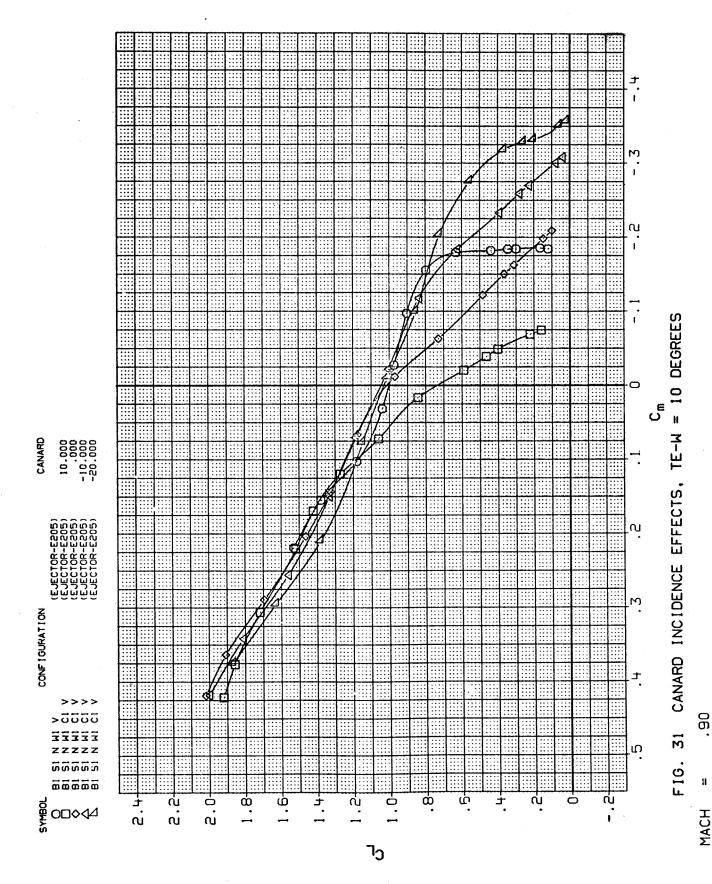
128





86. 31 F16.





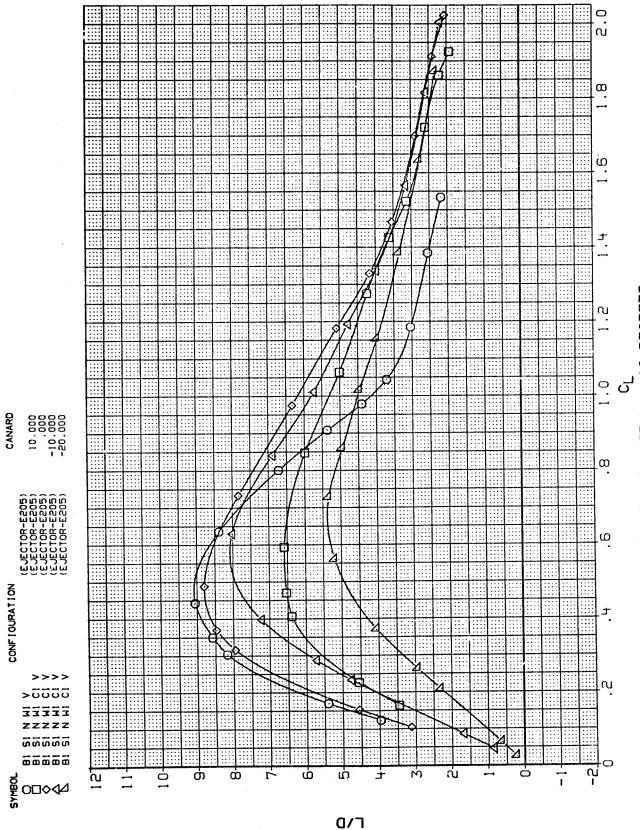
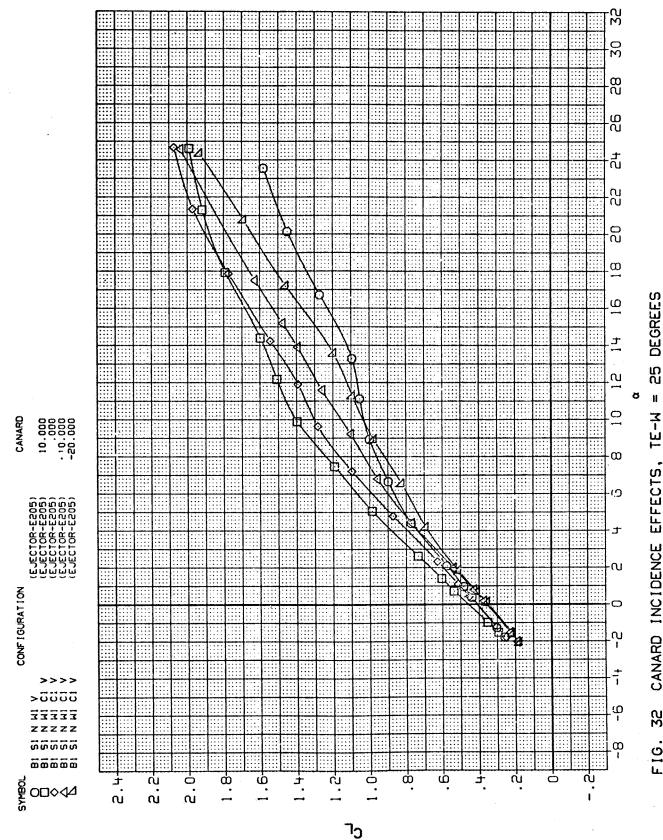
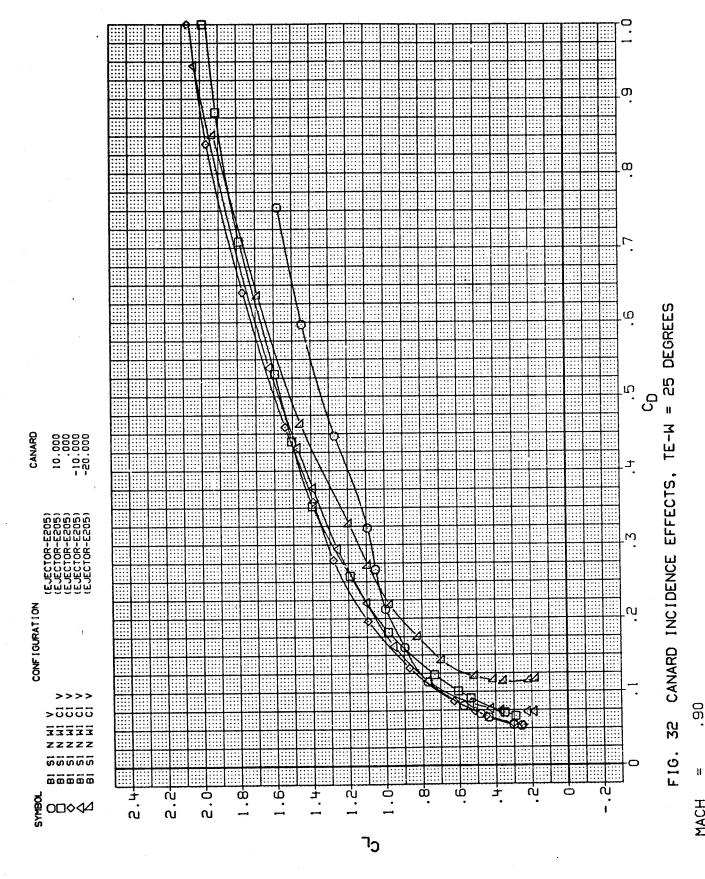
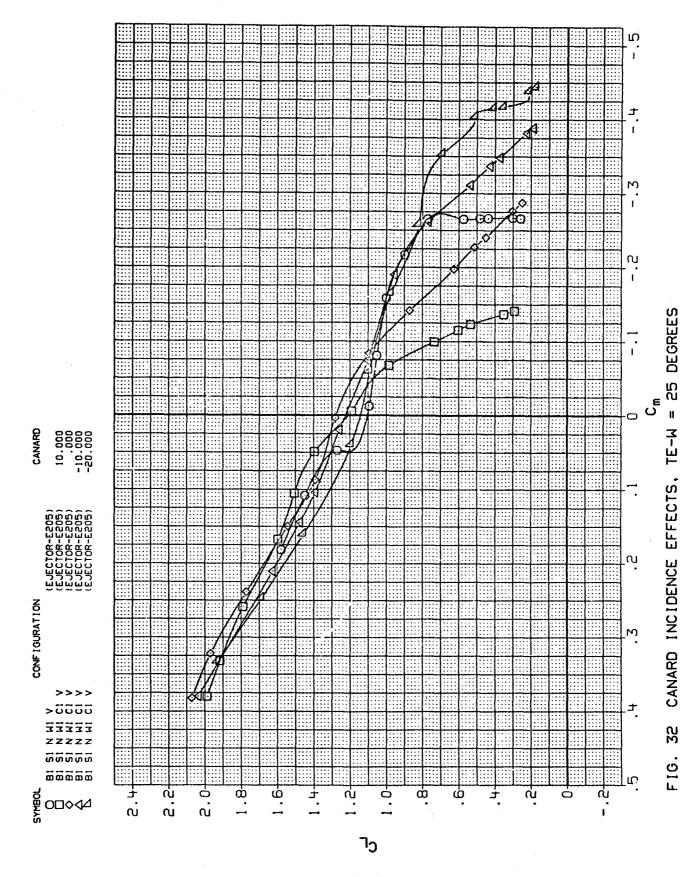


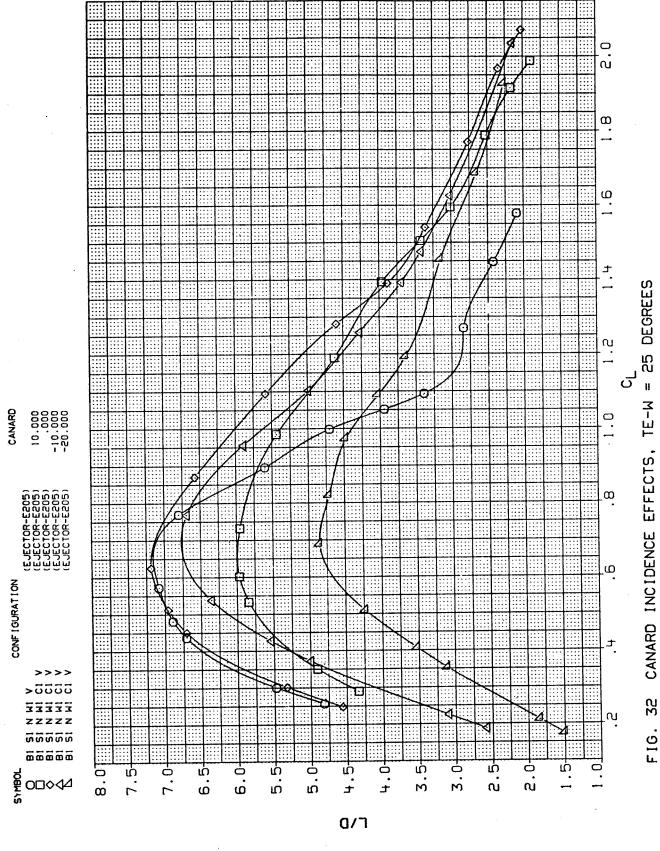
FIG. 31 CANARD INCIDENCE EFFECTS, TE-W = 10 DEGREES

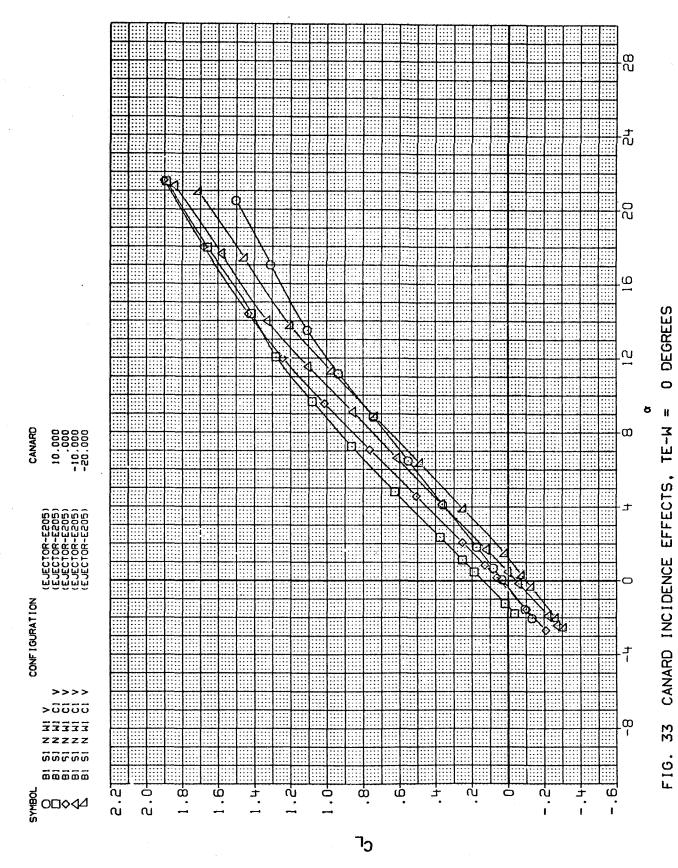


CANARD INCIDENCE EFFECTS, F16.

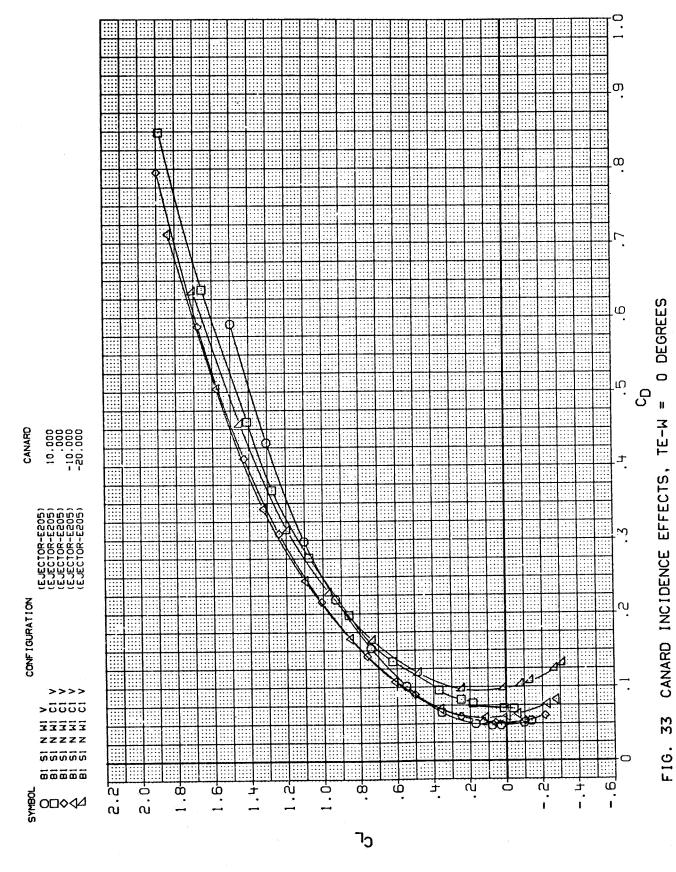


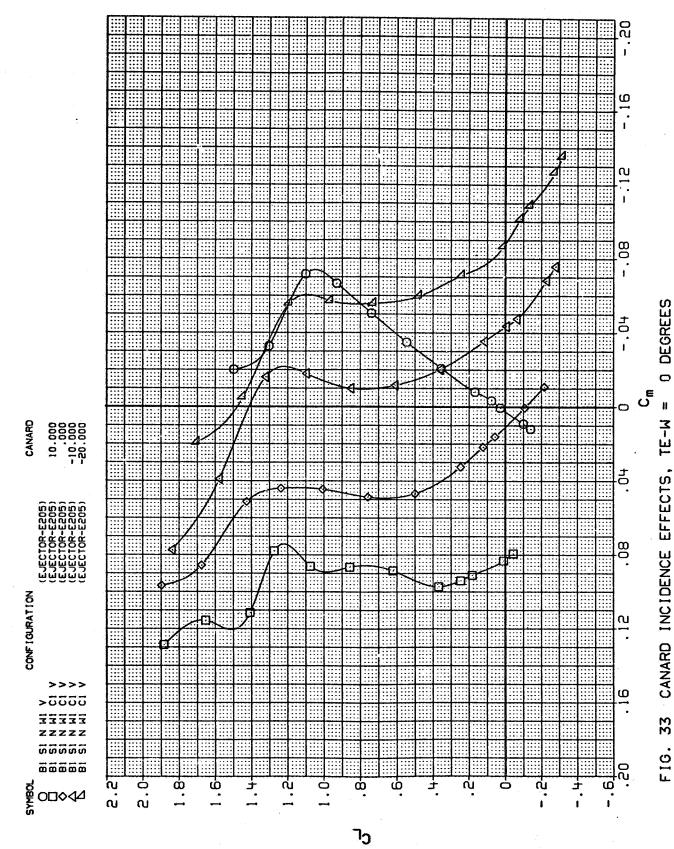




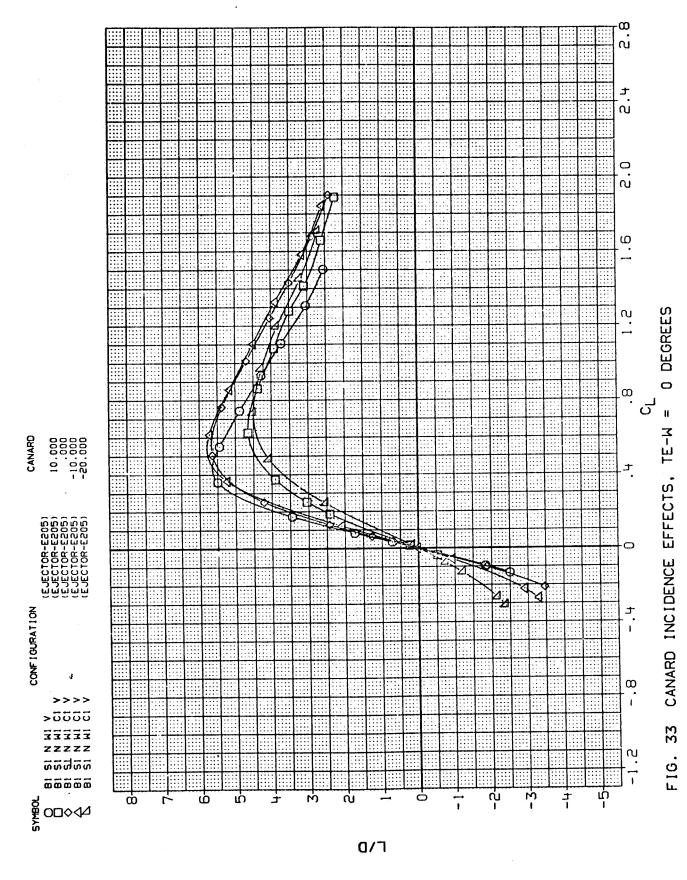


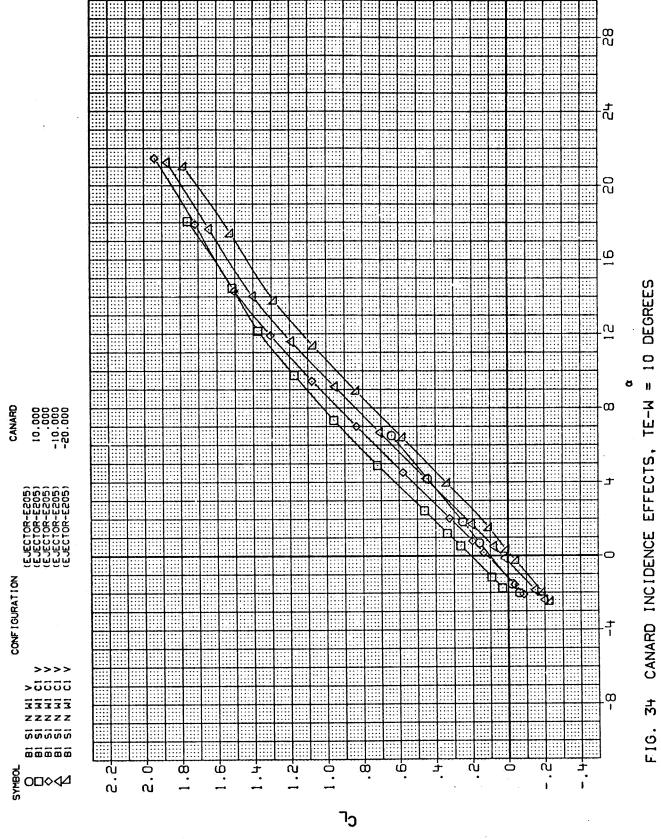
MACH = 1.20





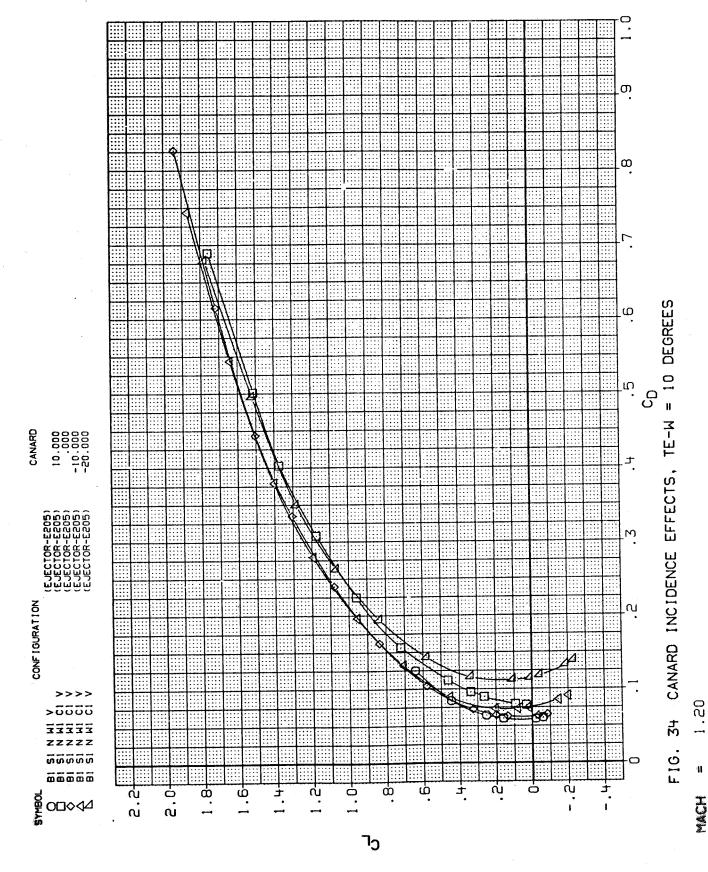
MACH = 1.20

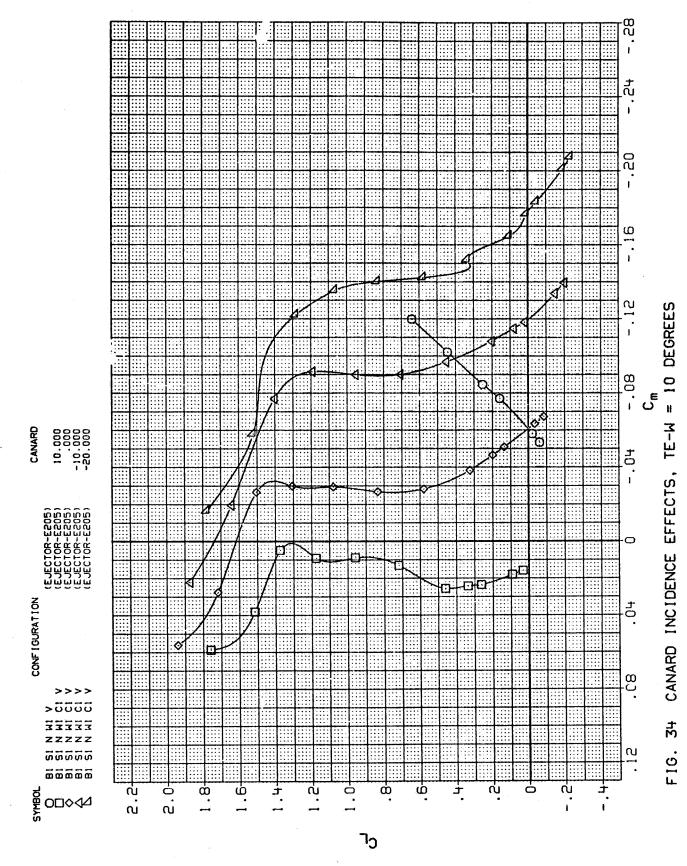




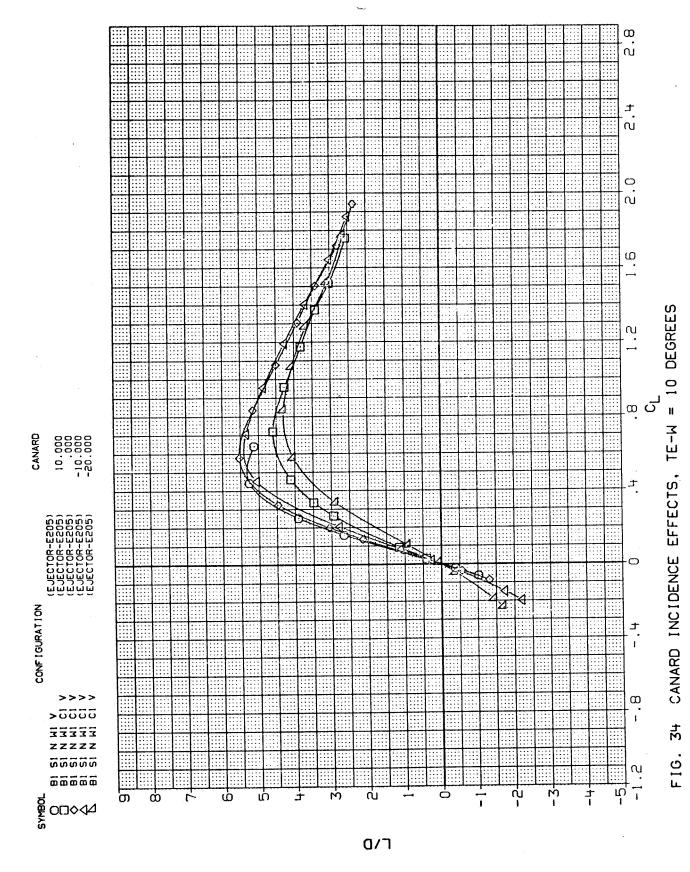
Ĥ

142





ACH = 1.2



MACH = 1.20

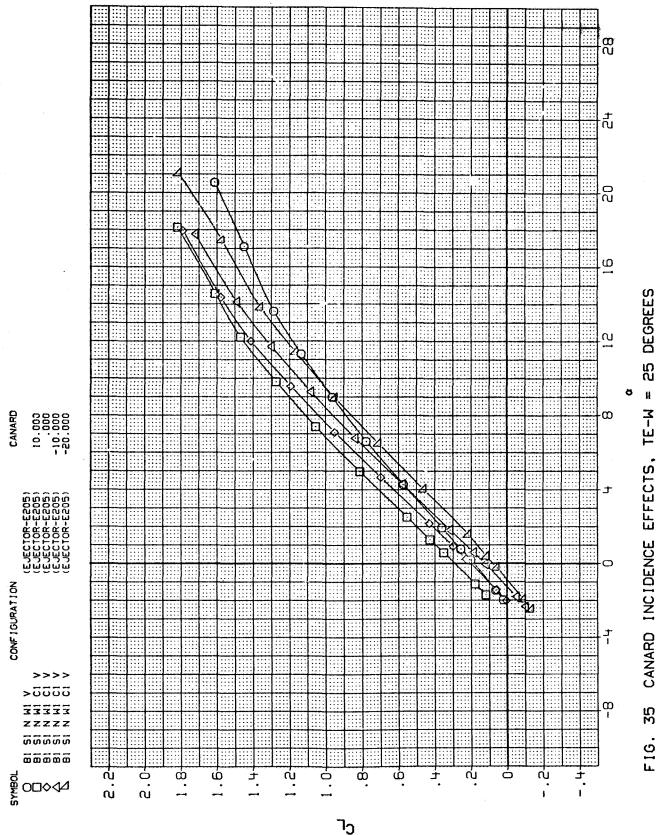
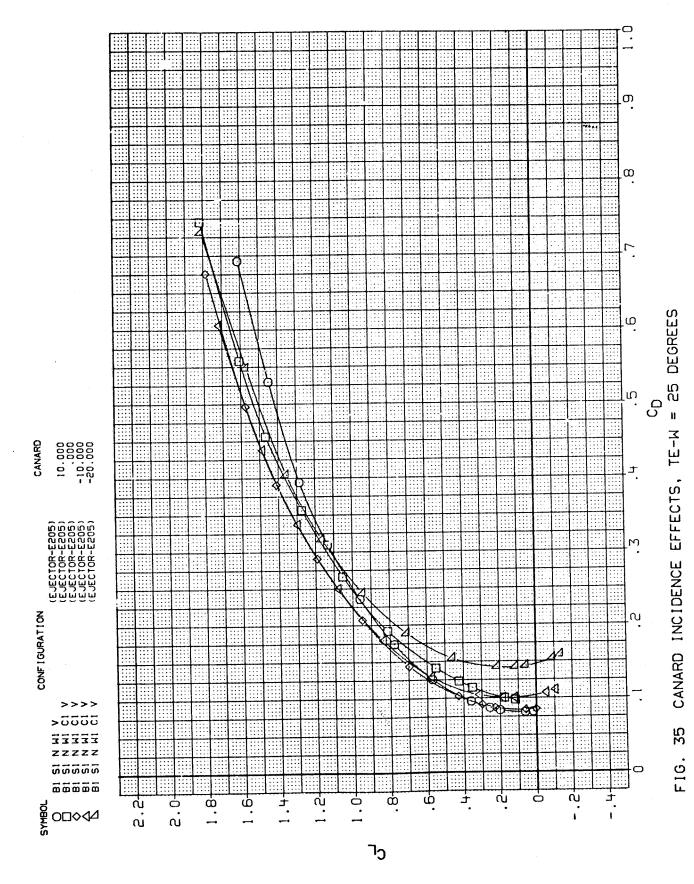
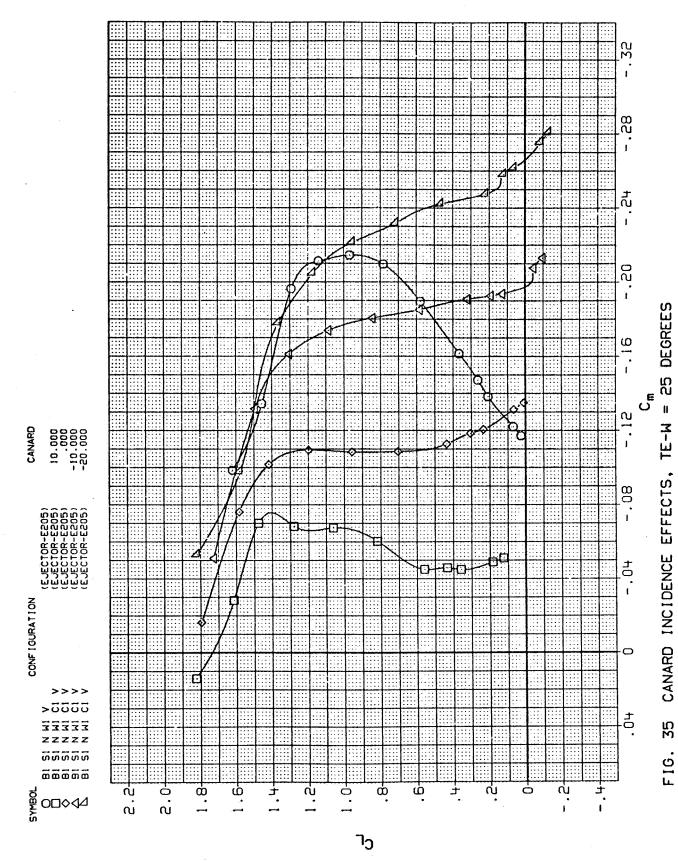


FIG. 35 CANARD INCIDENCE EFFECTS,

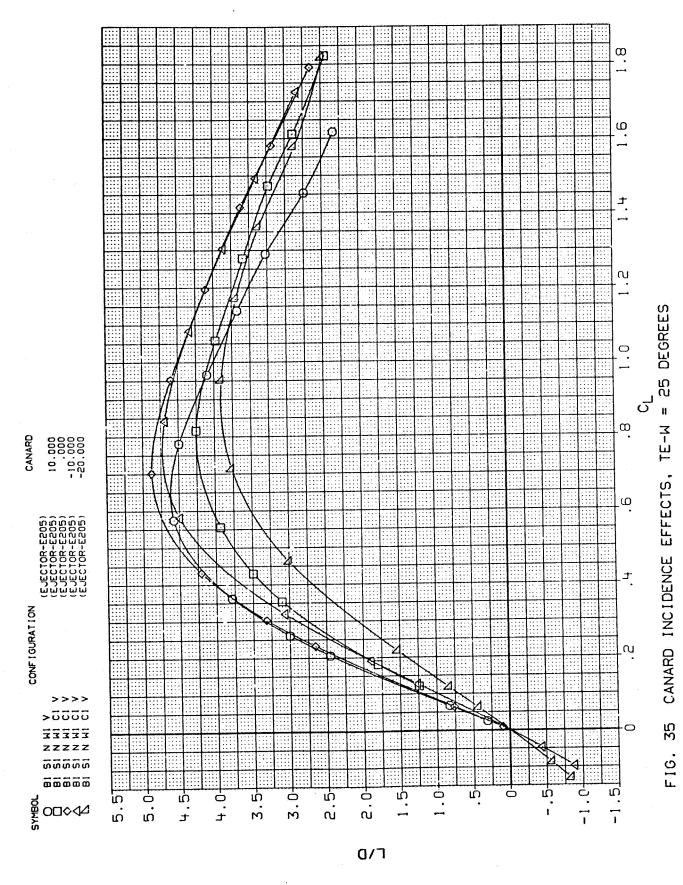


147

71



MACH = 1.20



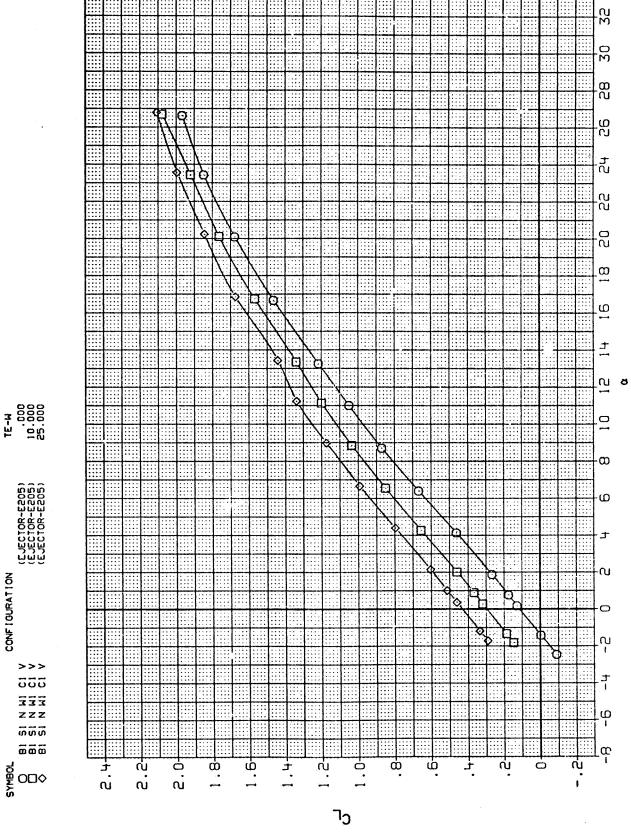
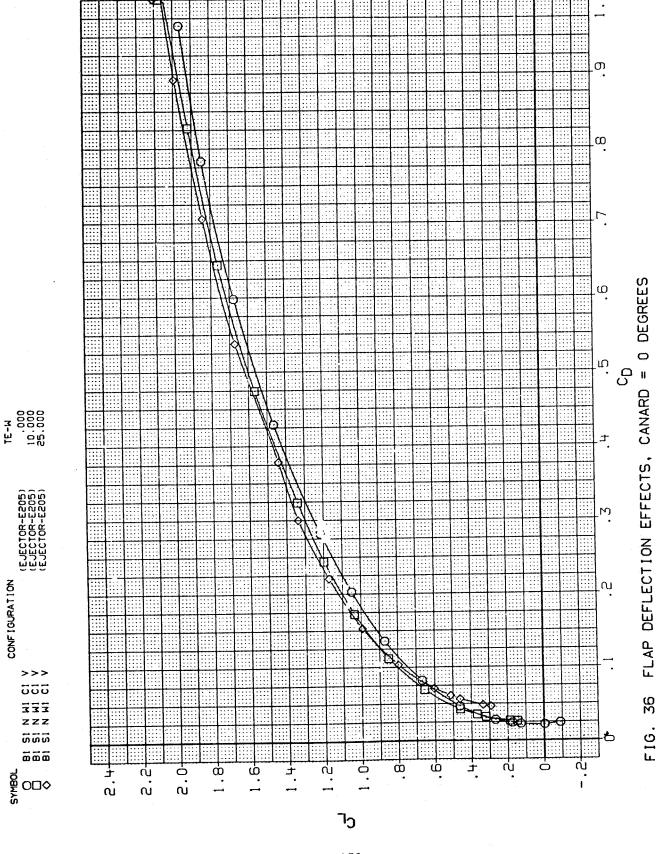


FIG. 36 FLAP DEFLECTION EFFECTS, CANARD = 0 DEGREES



11

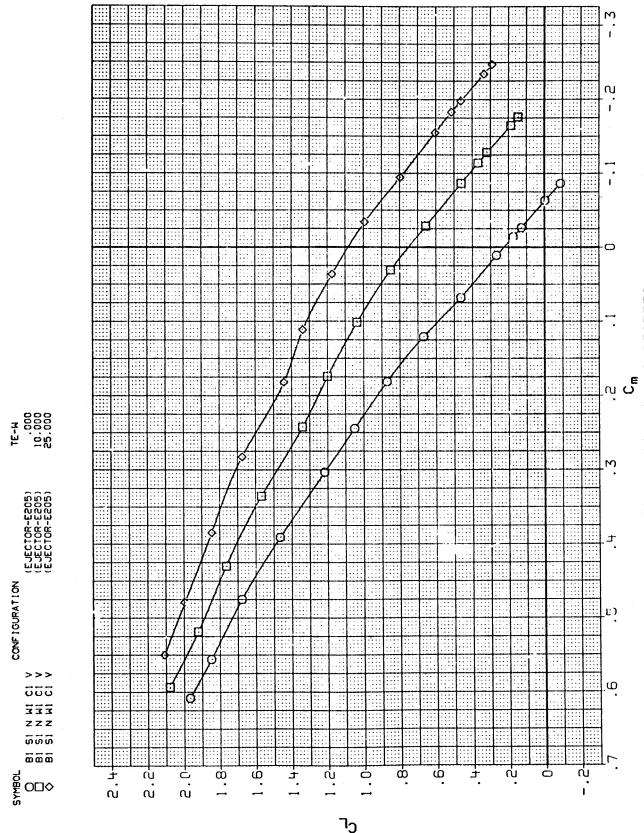


FIG. 36 FLAP DEFLECTION EFFECTS, CANARD = 0 DEGREES

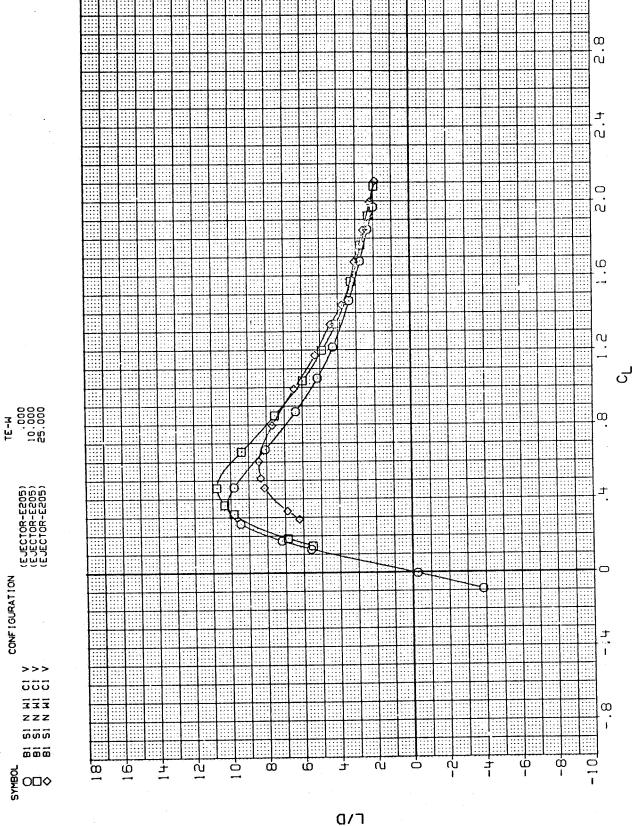


FIG. 36 FLAP DEFLECTION EFFECTS, CANARD = 0 DEGREES

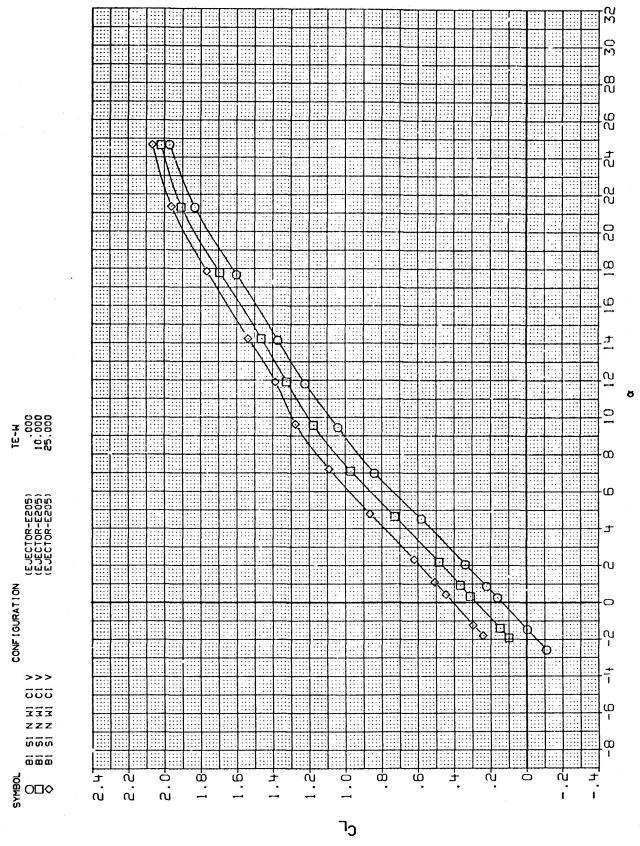
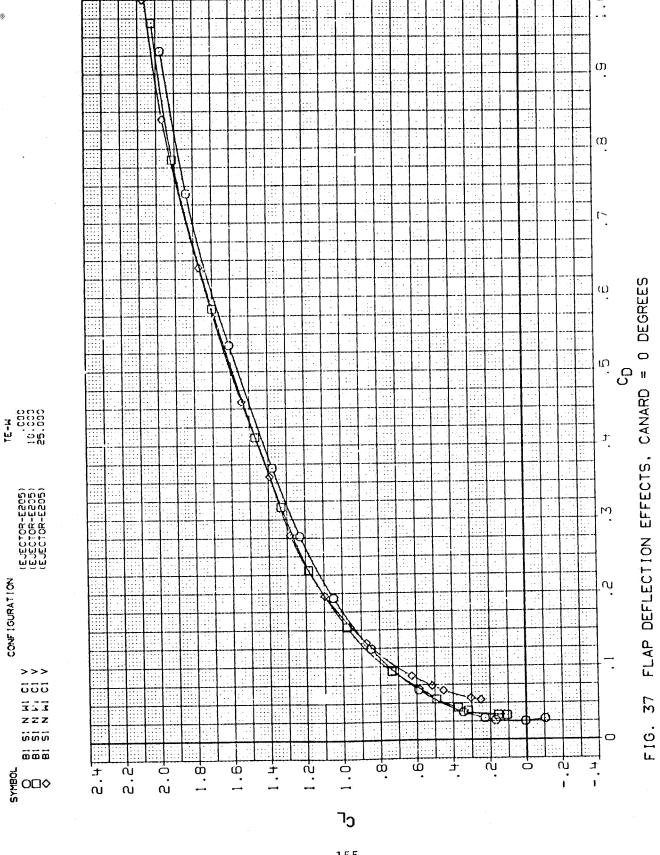
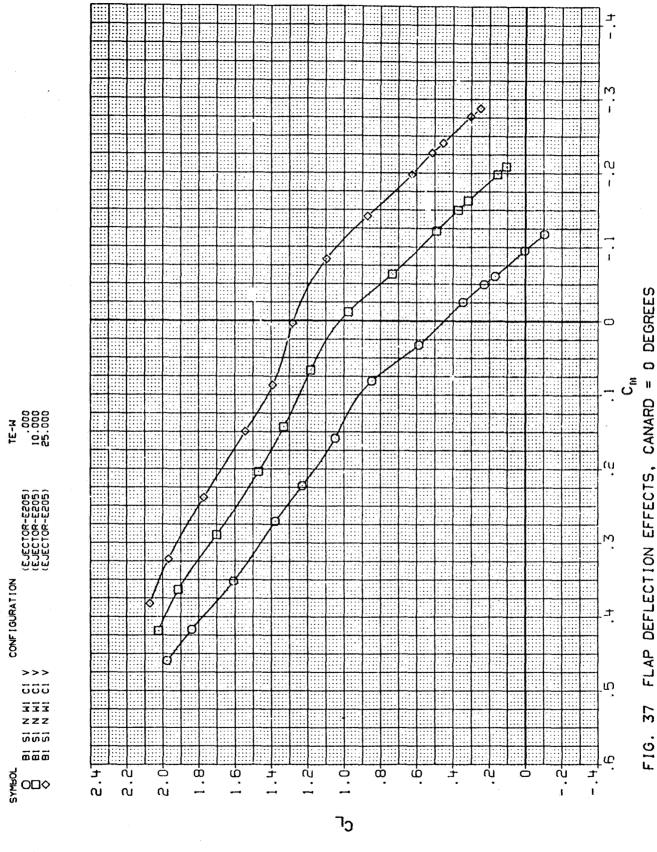


FIG. 37 FLAP DEFLECTION EFFECTS, CANARD = 0 DEGREES

1:

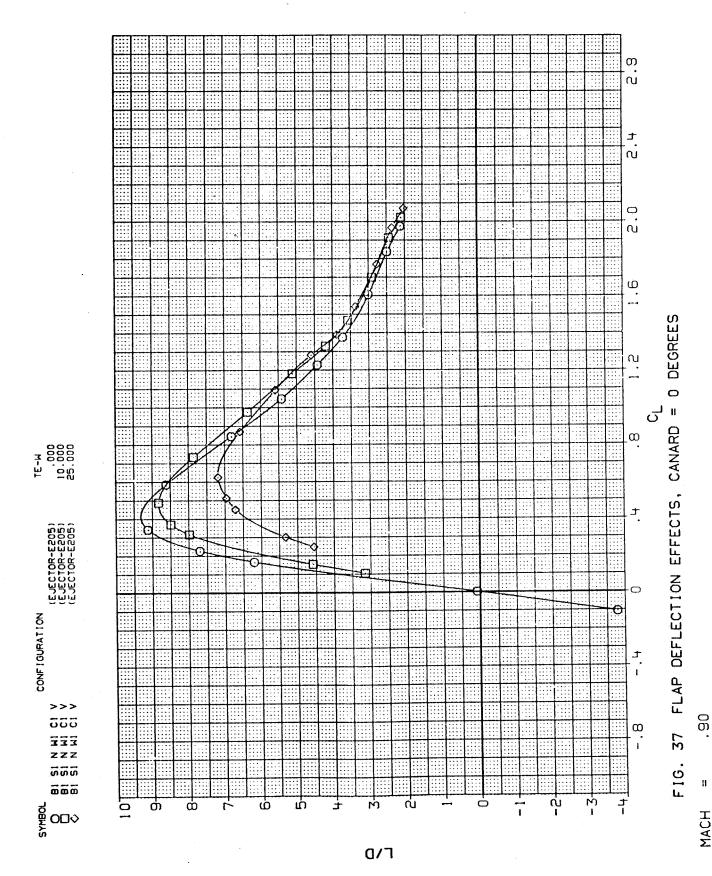


ш



156

H



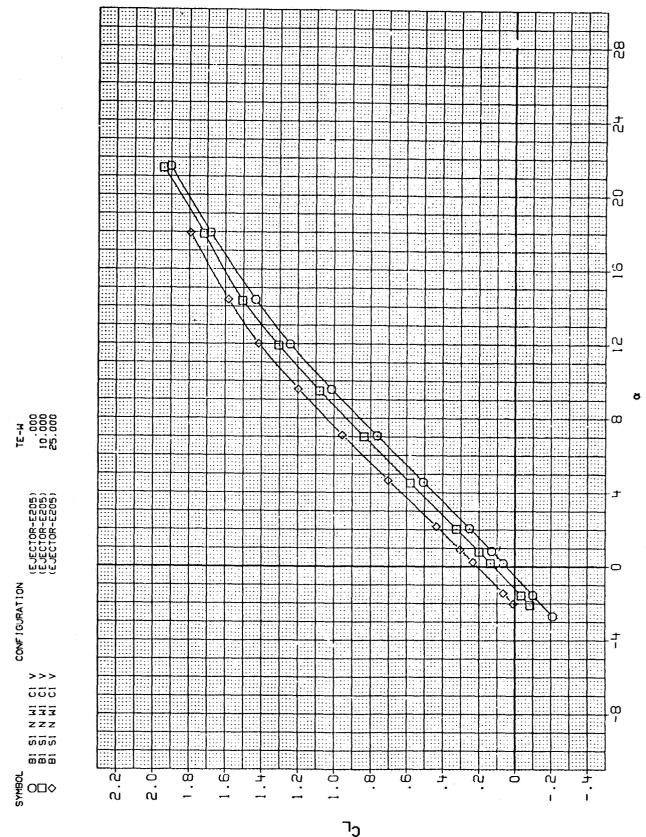
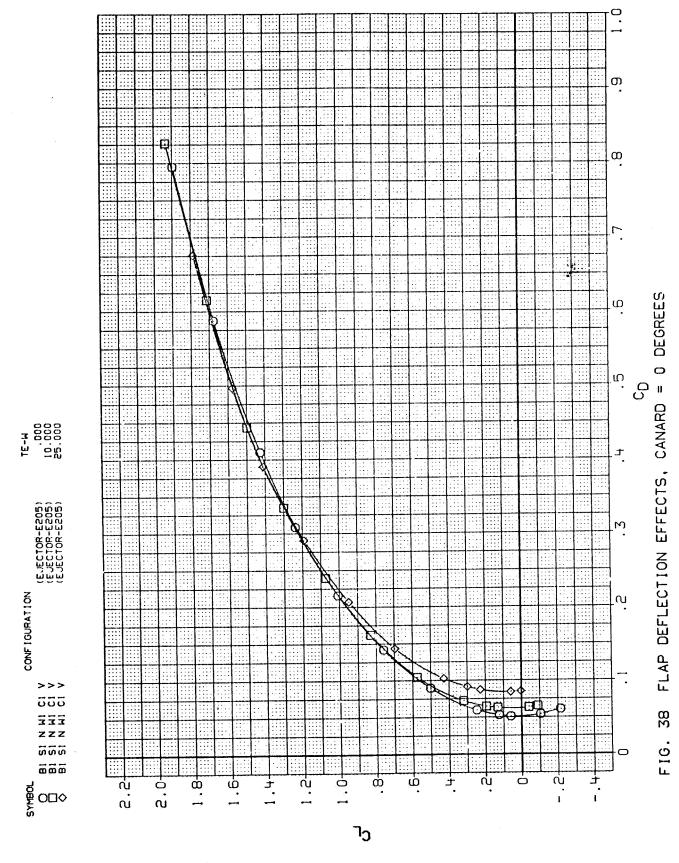


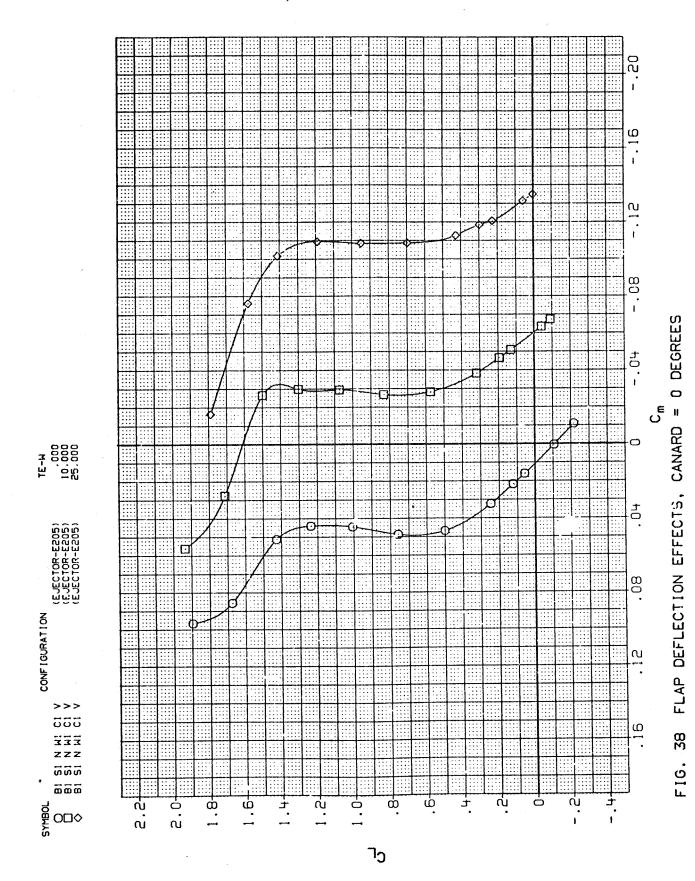
FIG. 38 FLAP DEFLECTION EFFECTS, CANARD = 0 DEGREES

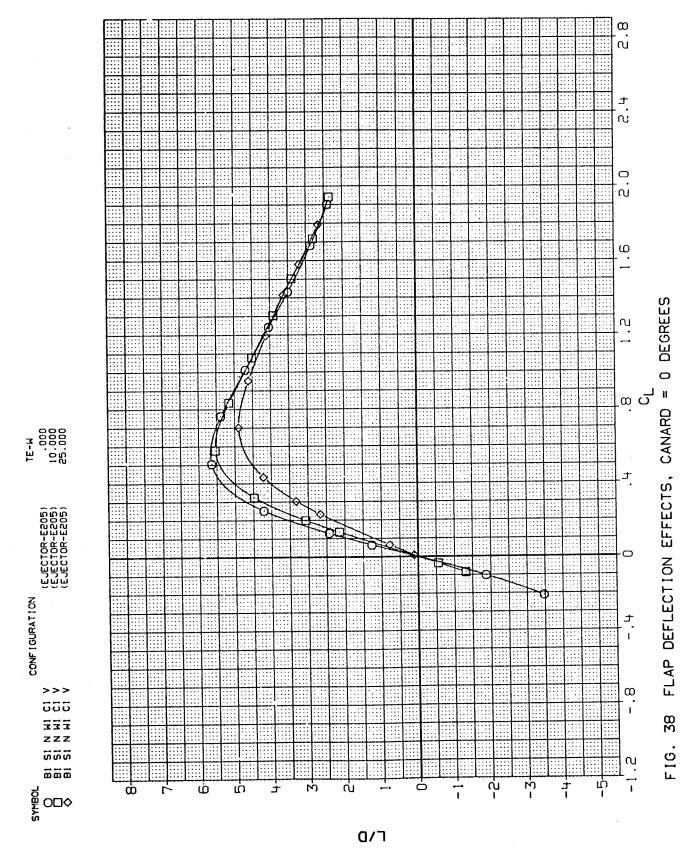
11

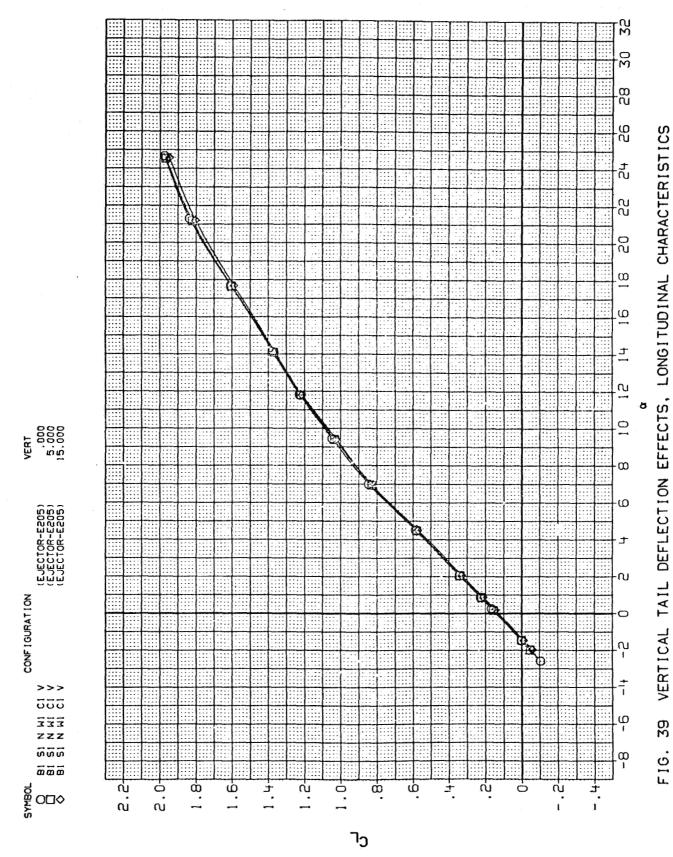


159

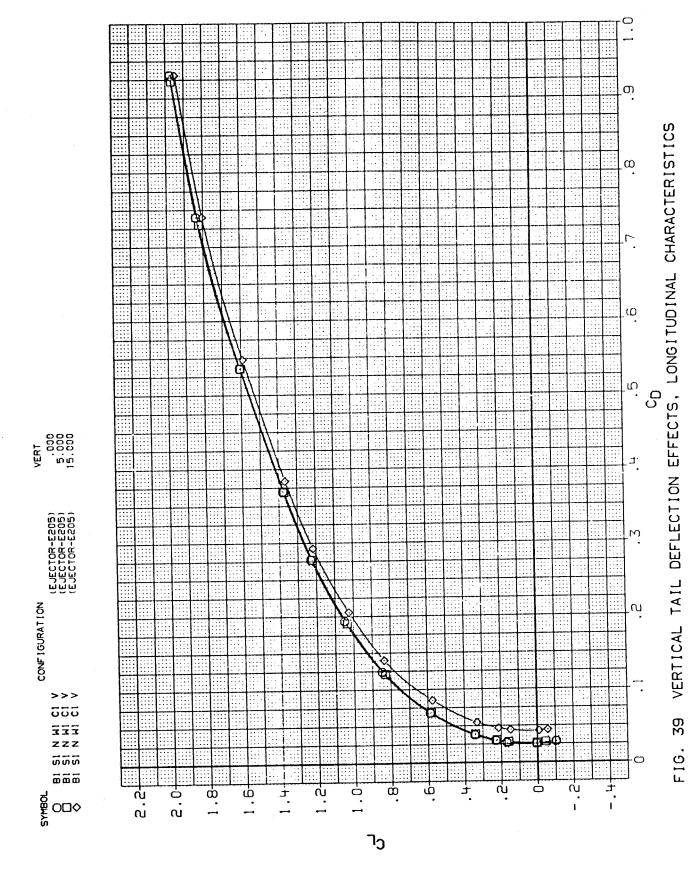
н



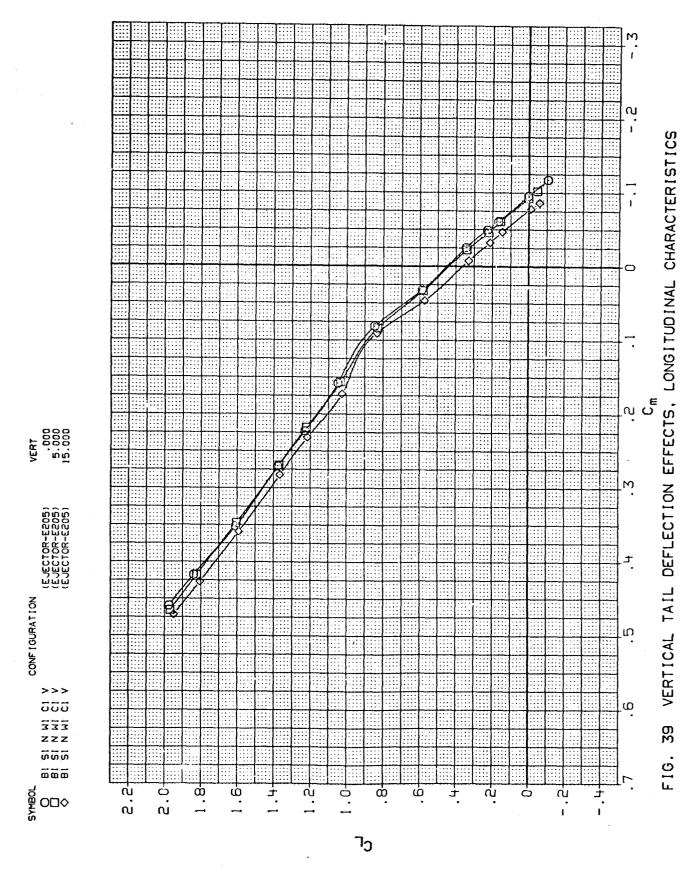




MACH = .90

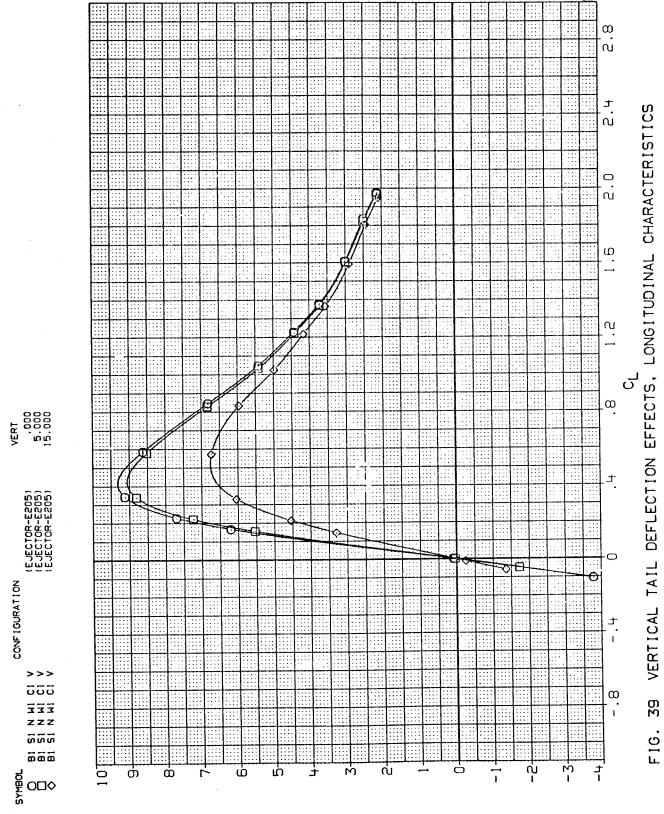


163



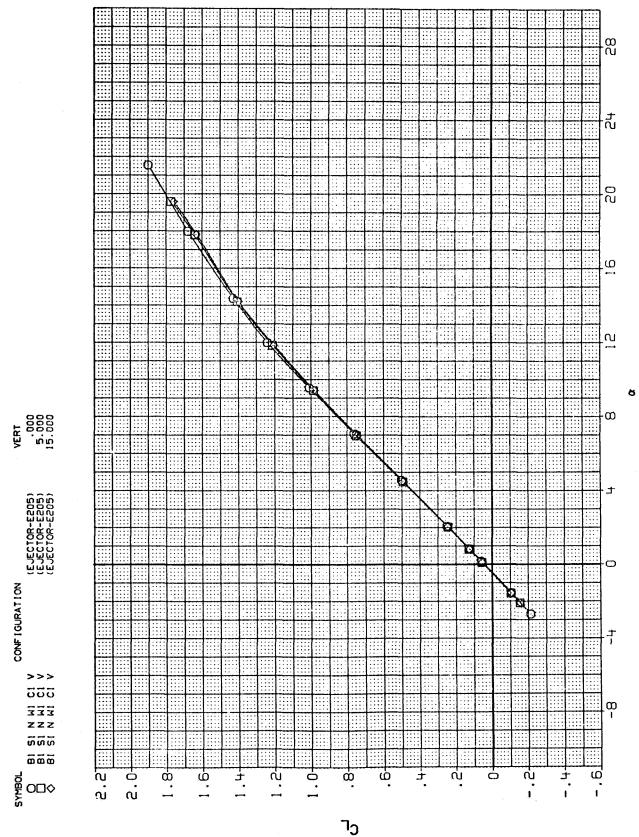
164

31



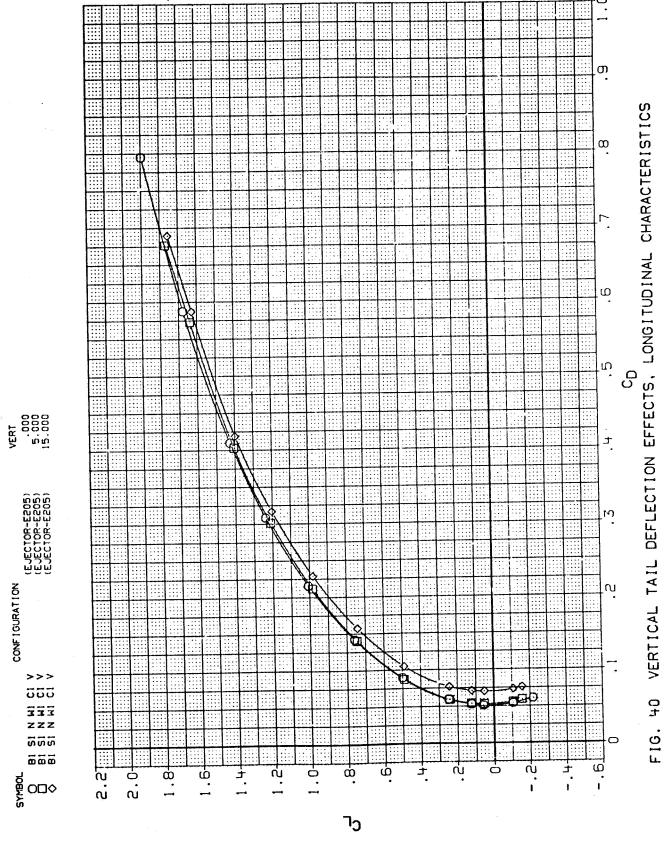
רום

Н



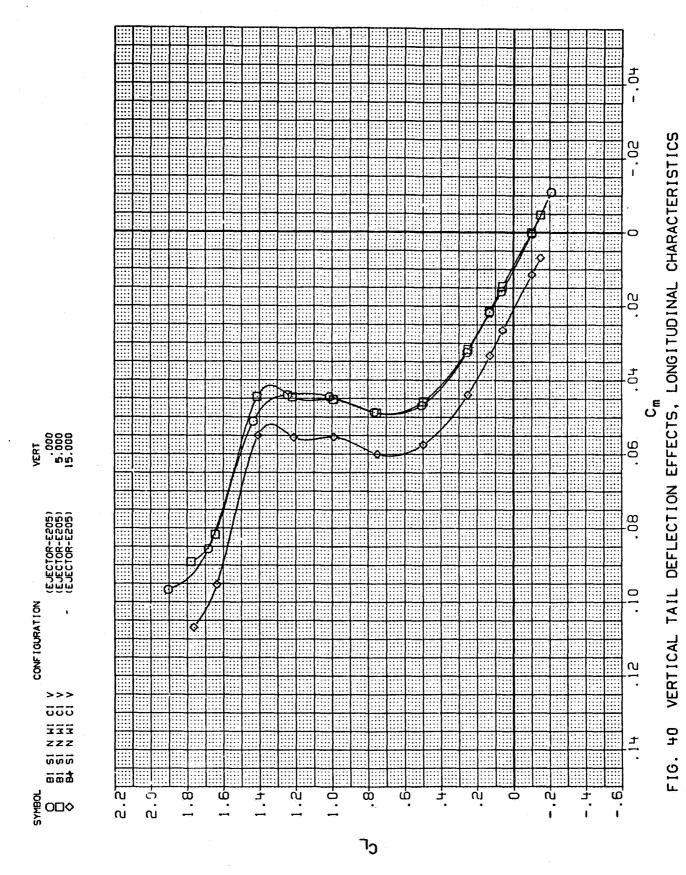
40 VERTICAL TAIL DEFLECTION EFFECTS, LONGITUDINAL CHARACTERISTICS F1G.

11



- -

ä



ACH = 1.20

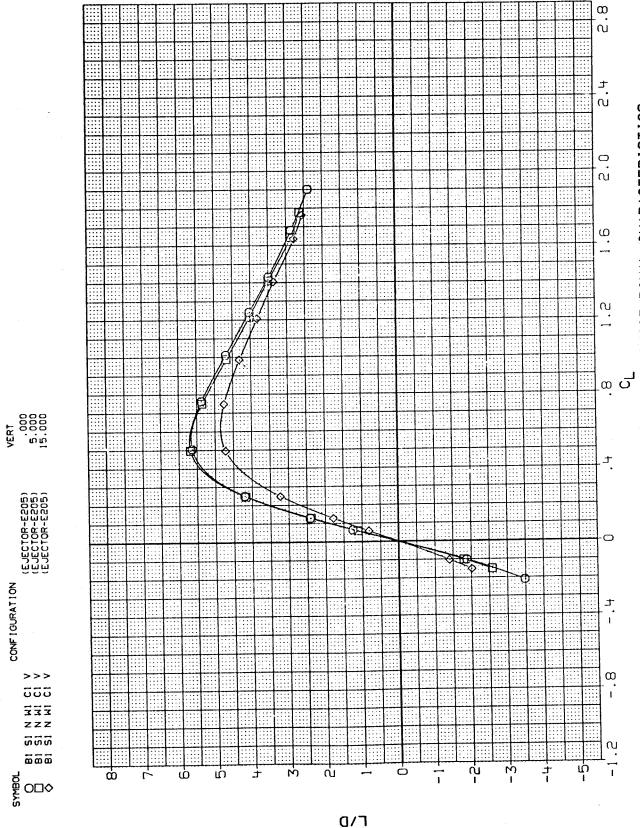
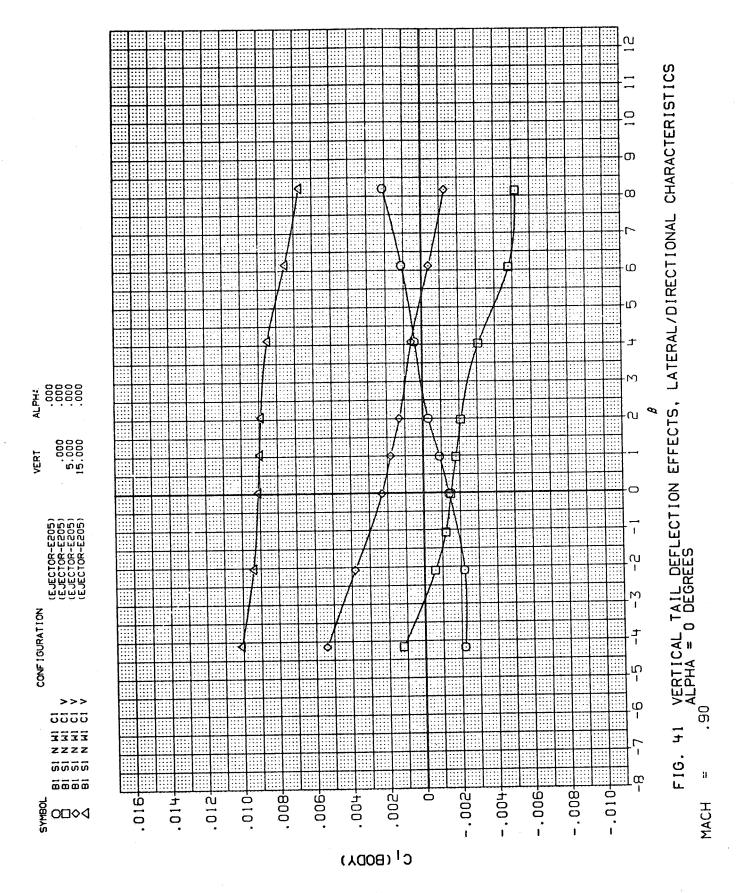
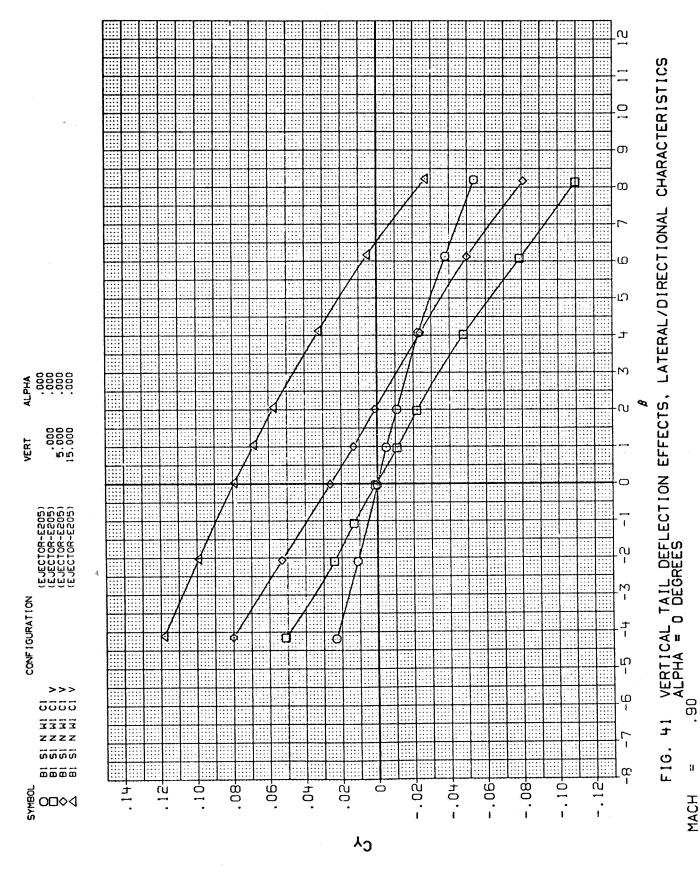
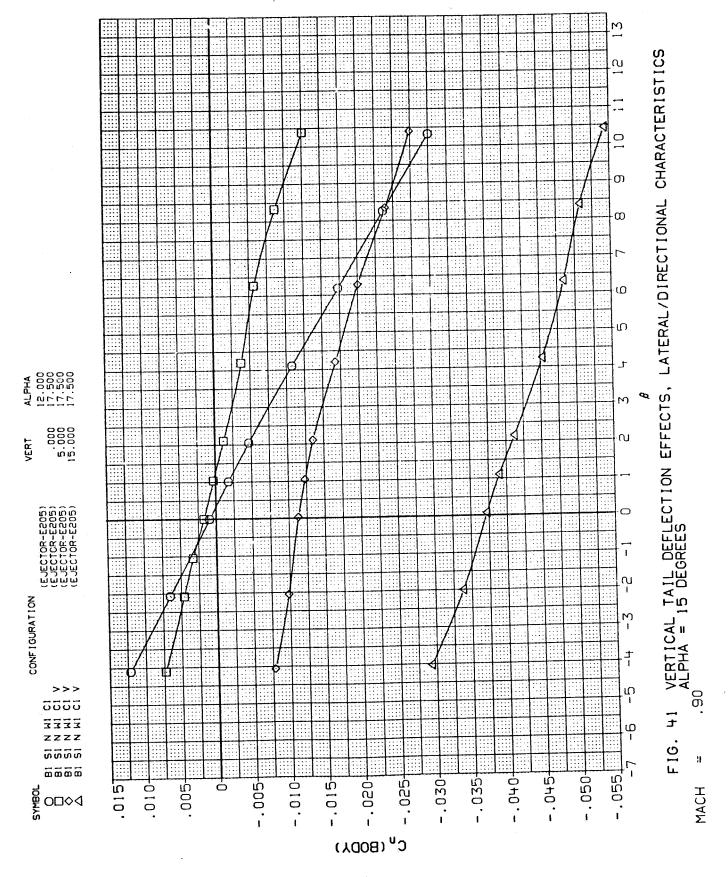


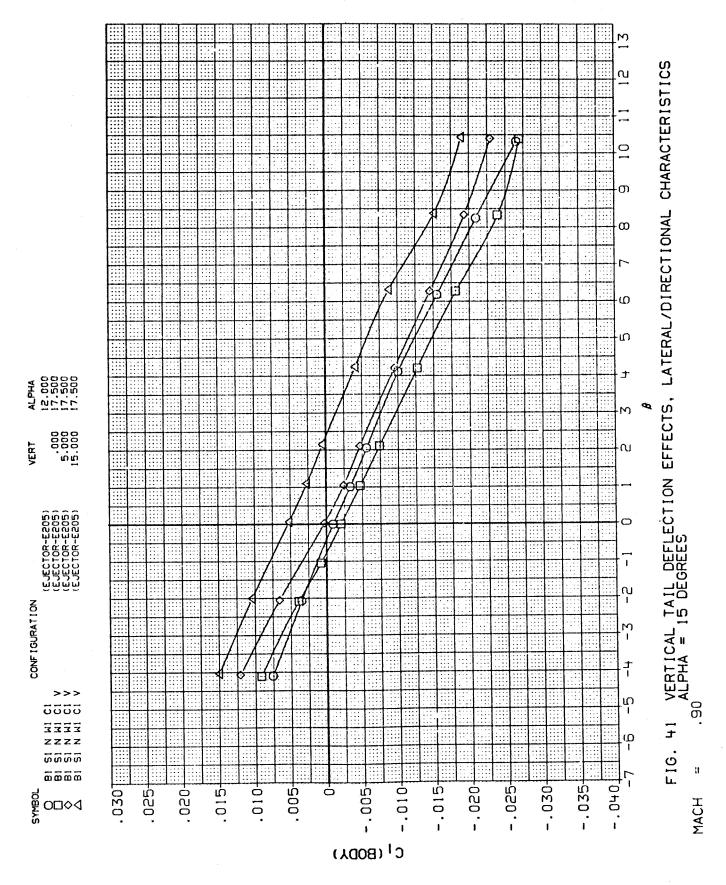
FIG. 40 VERTICAL TAIL DEFLECTION EFFECTS, LONGITUDINAL CHARACTERISTICS

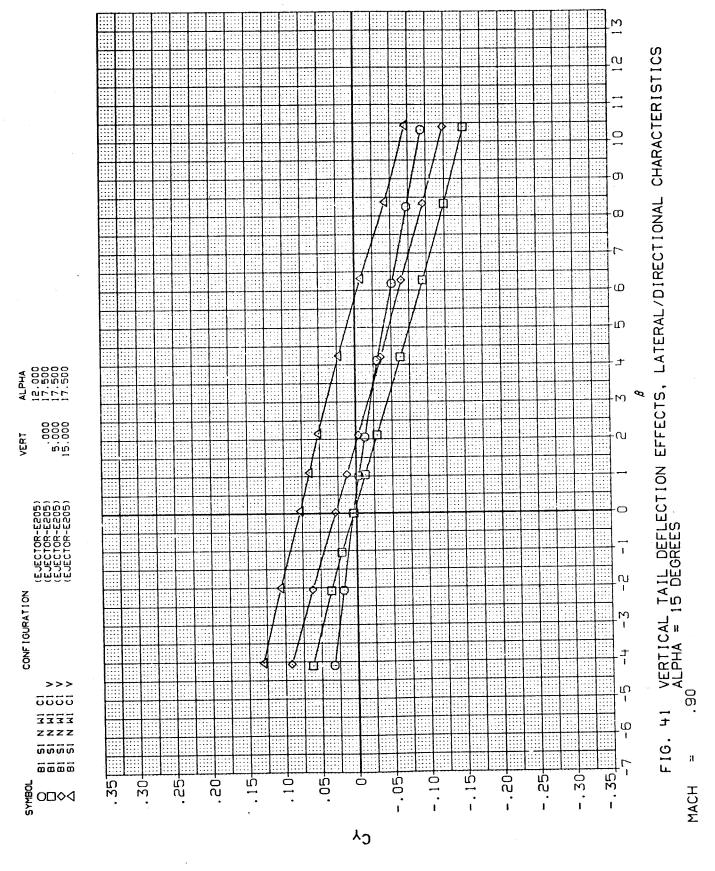
170

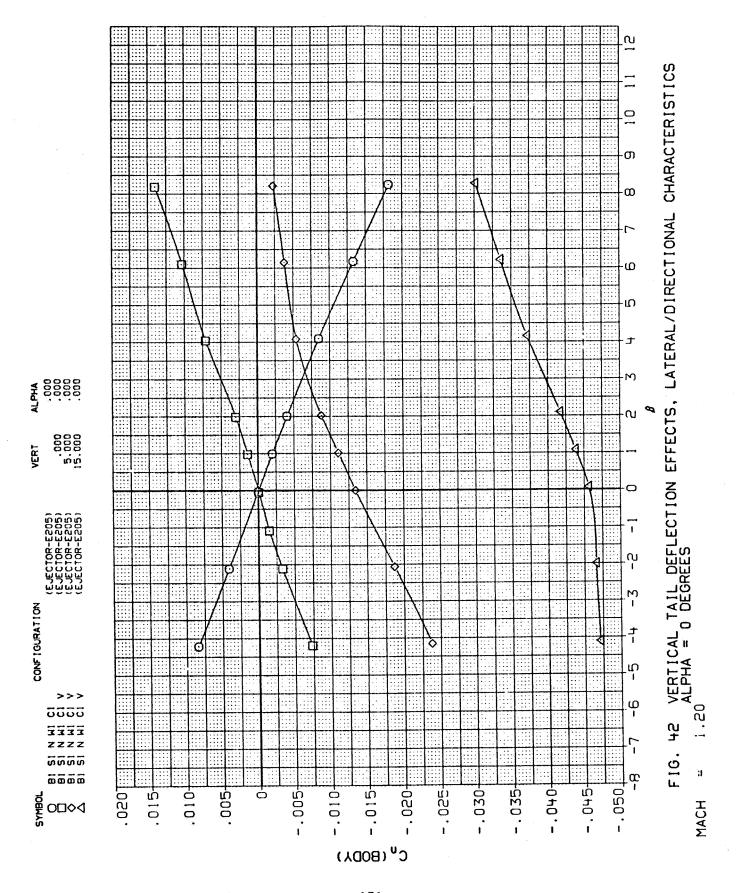


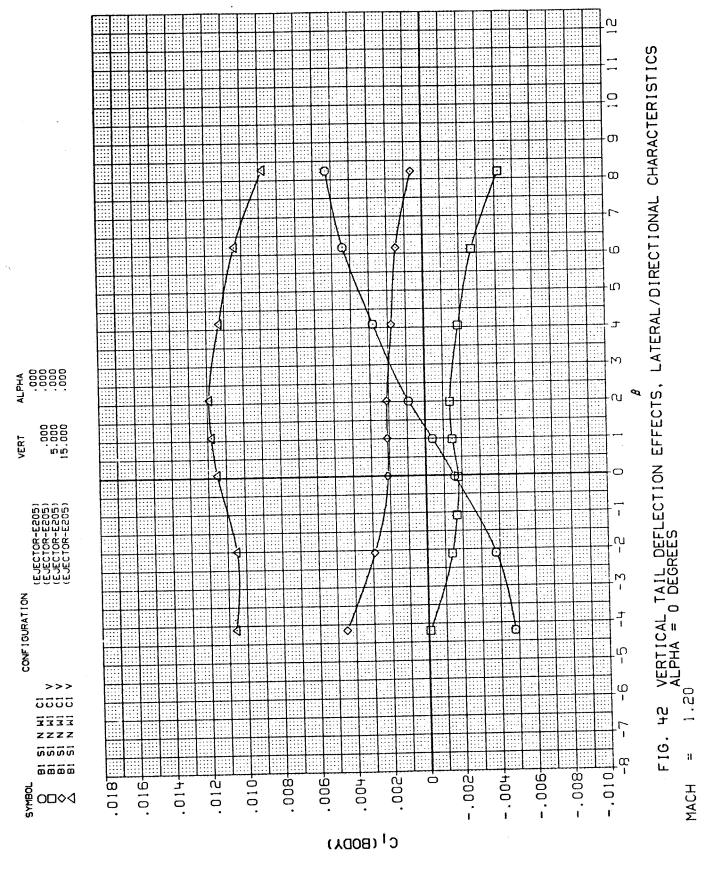


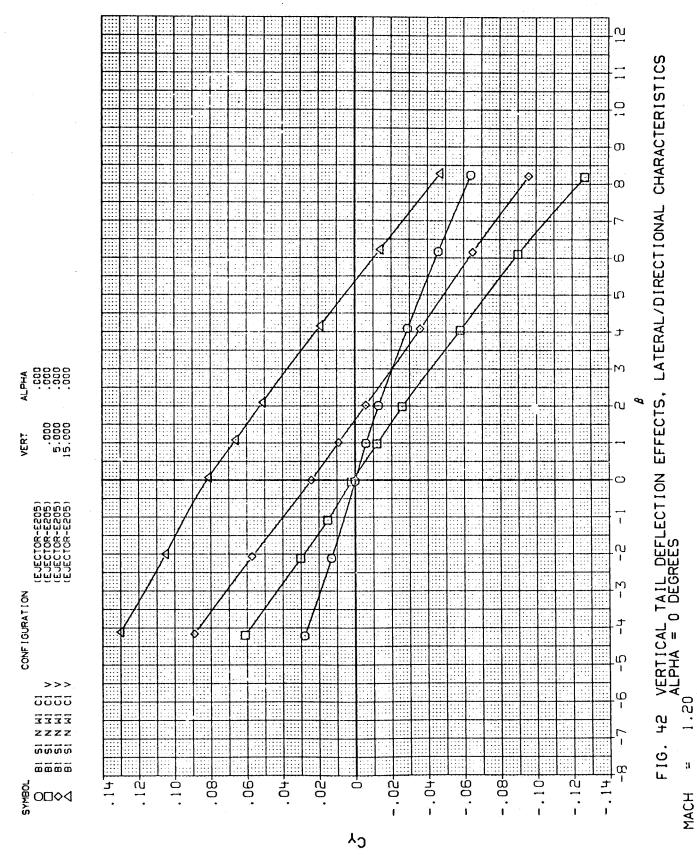


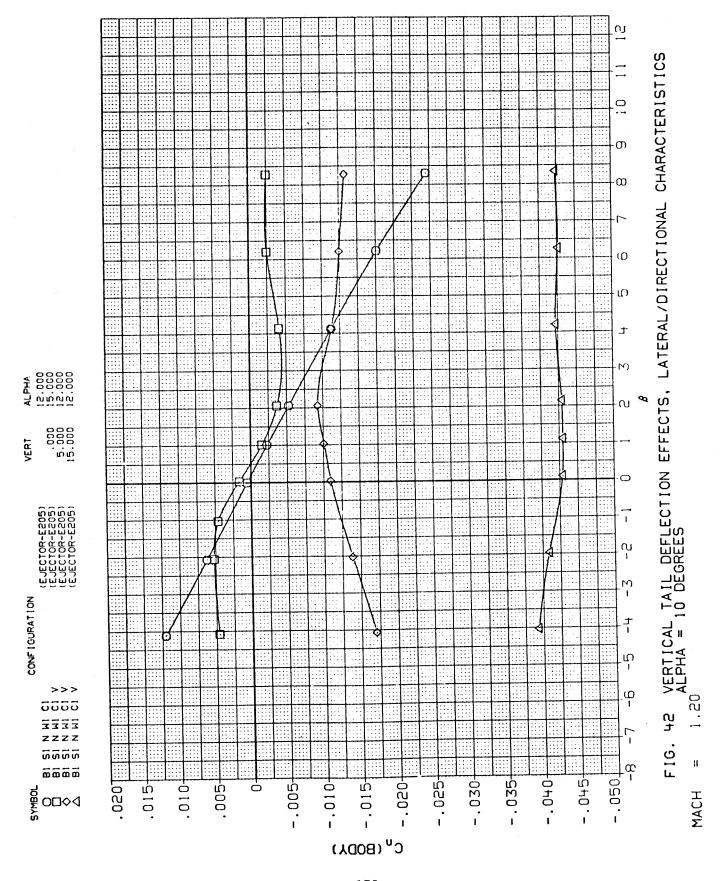


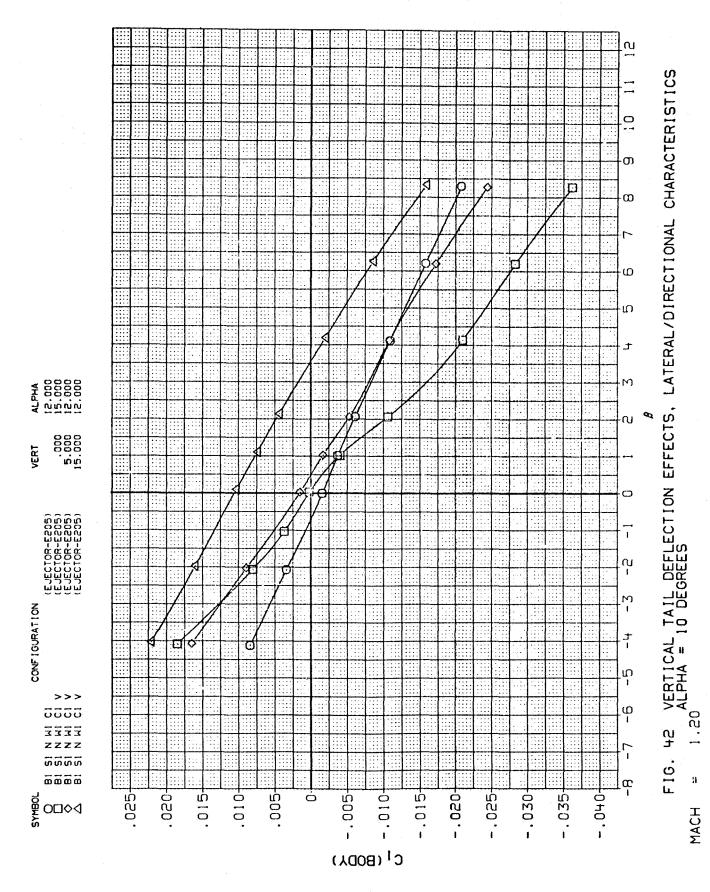


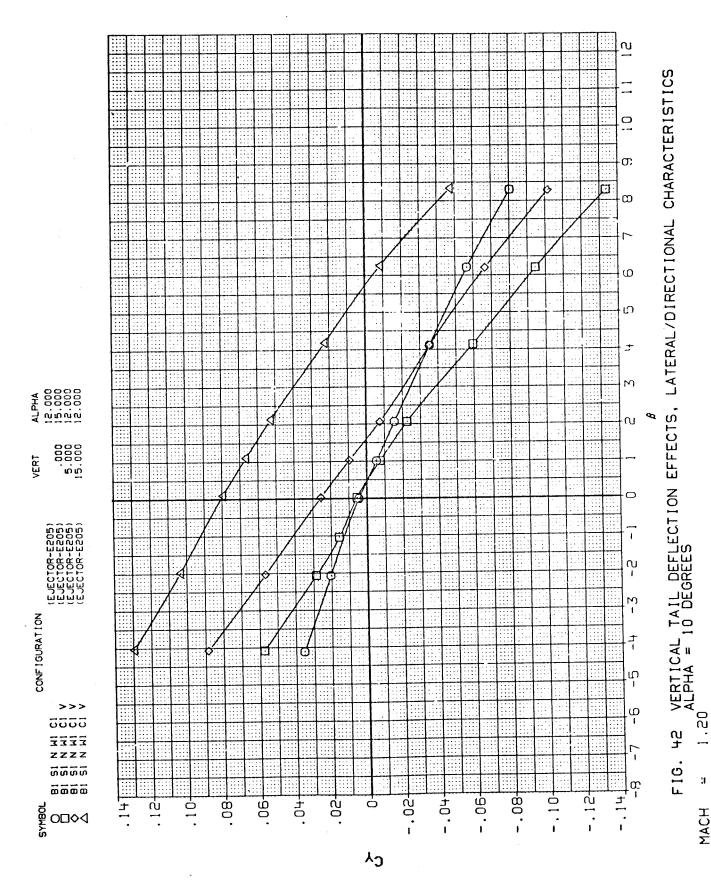


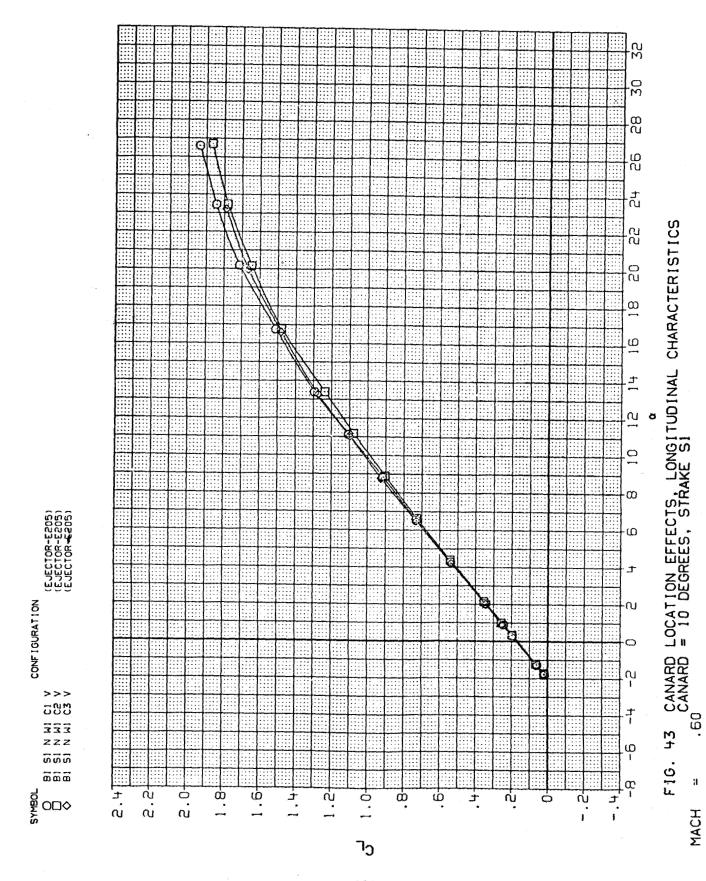


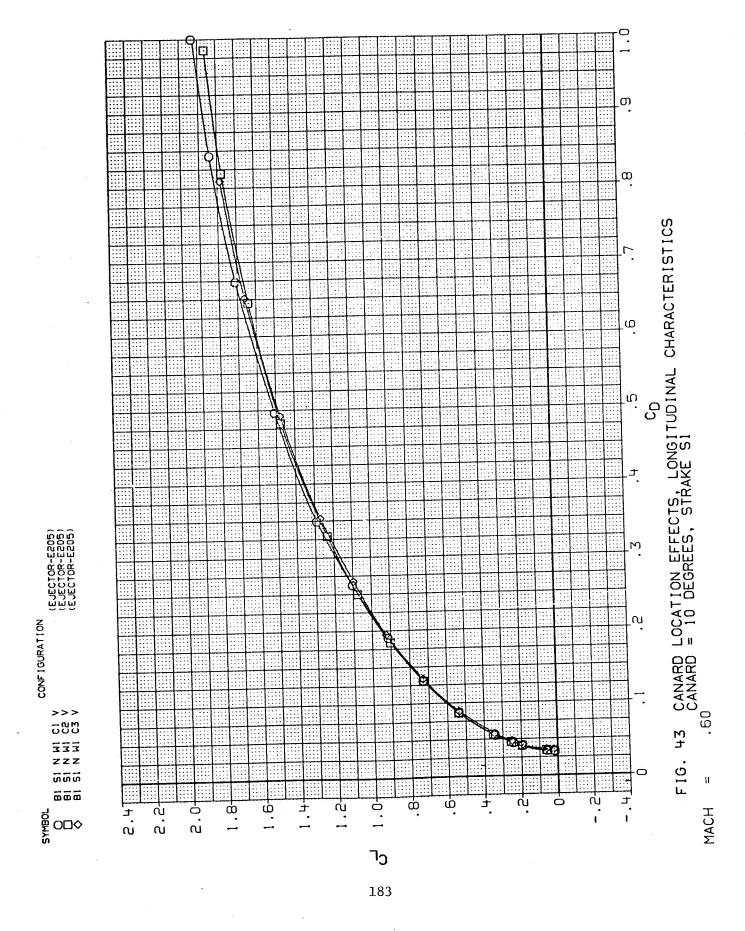


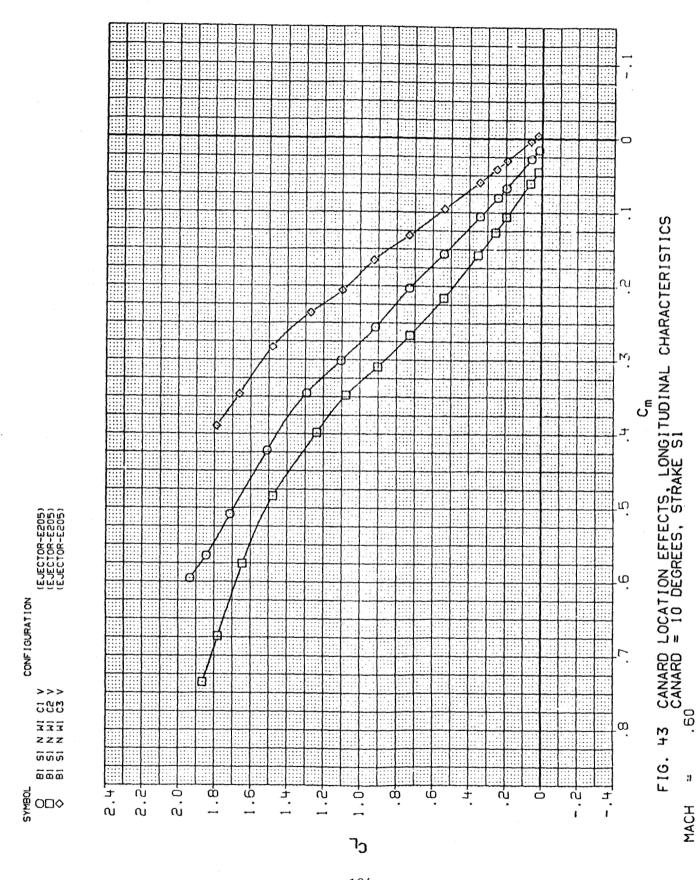


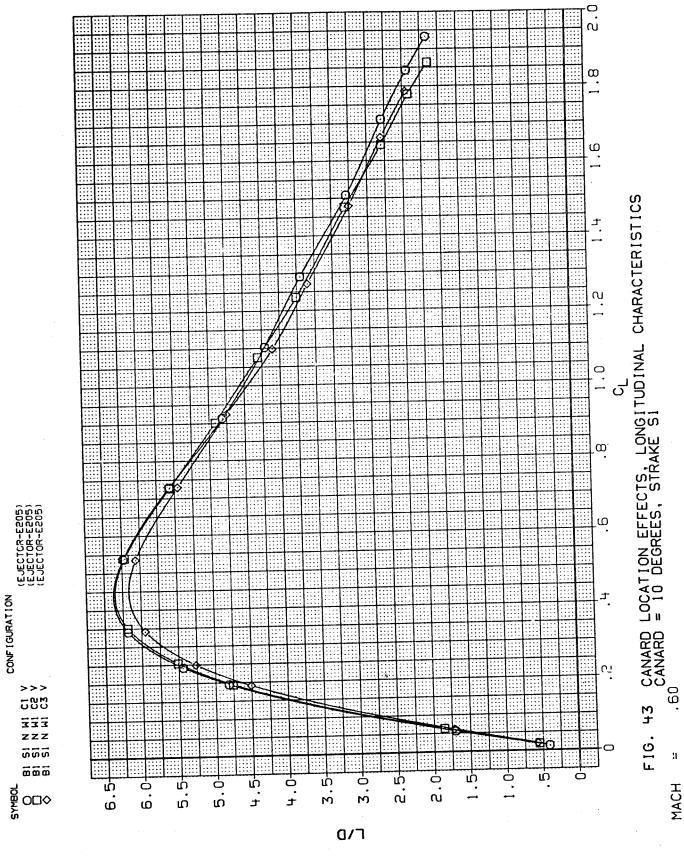


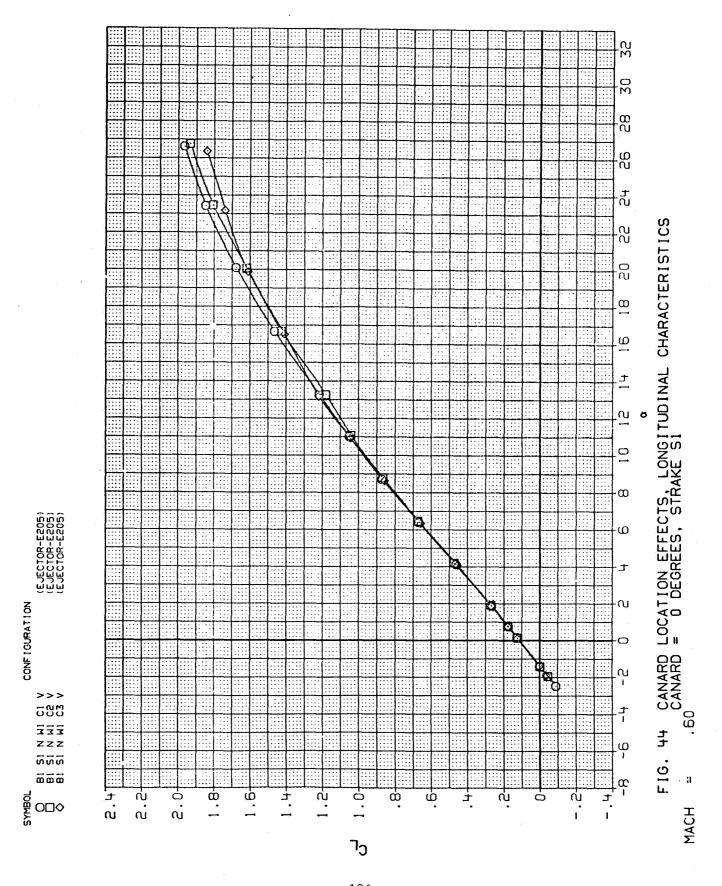


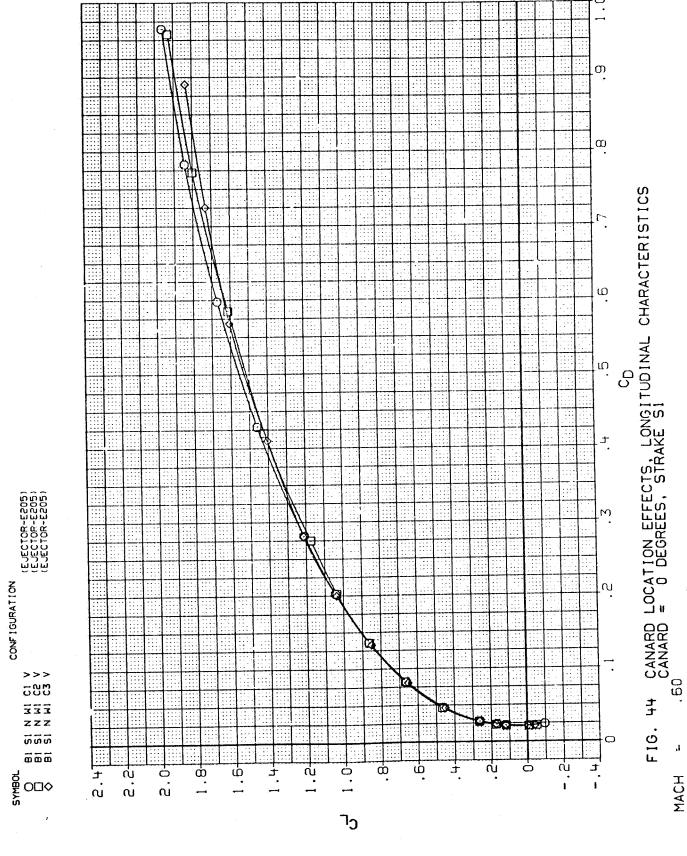


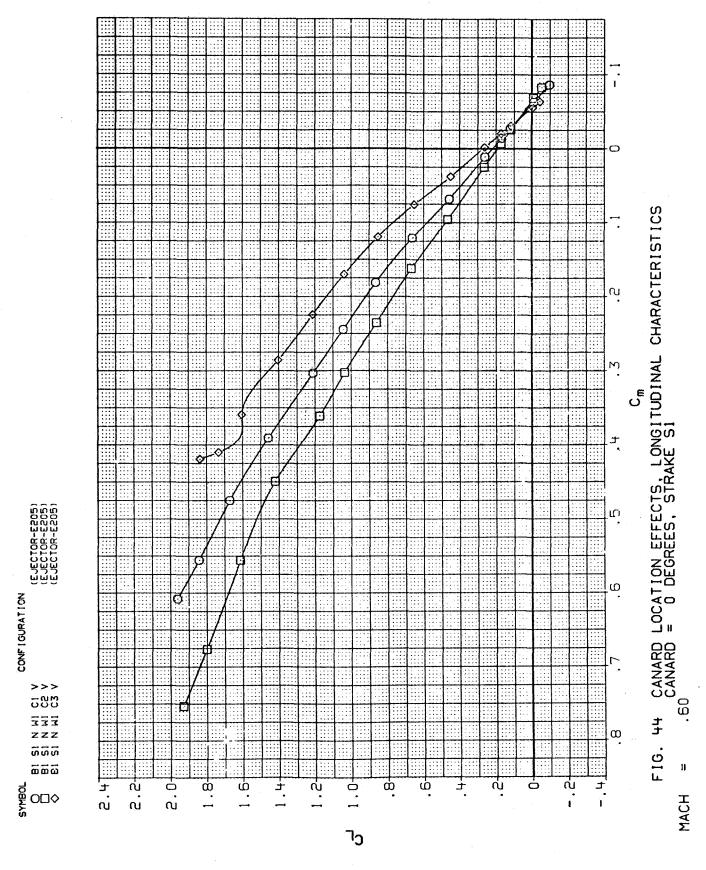


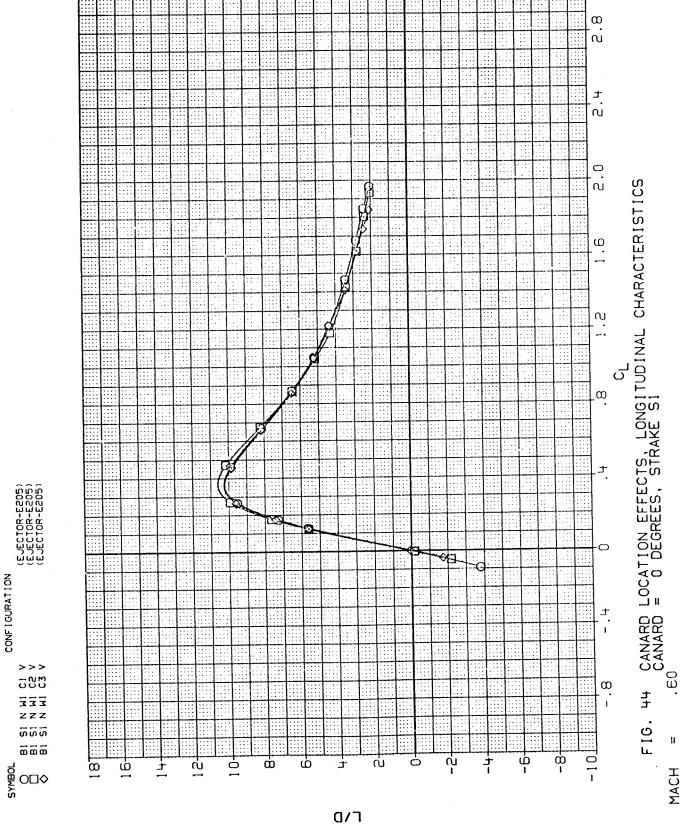


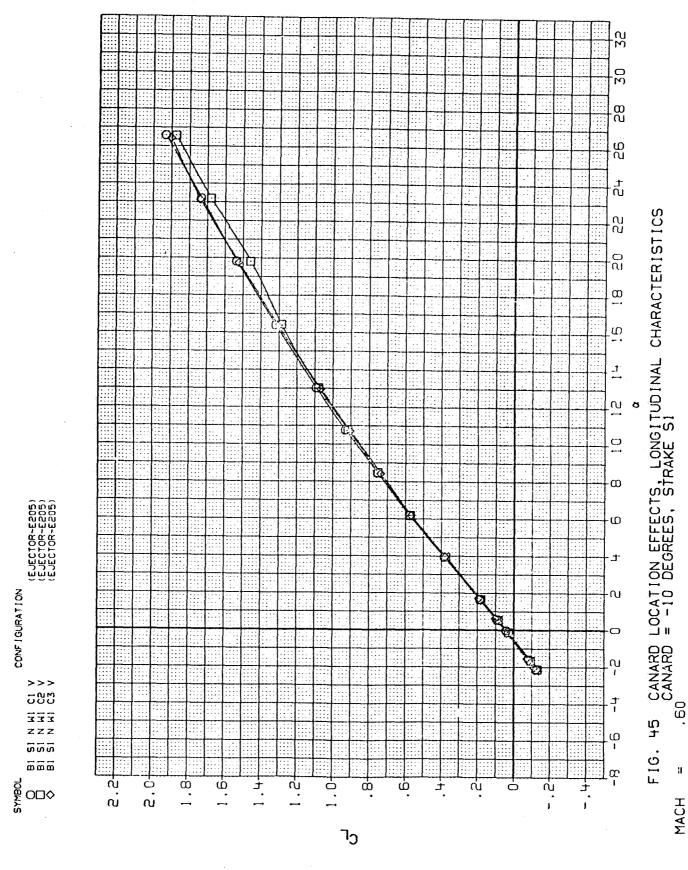


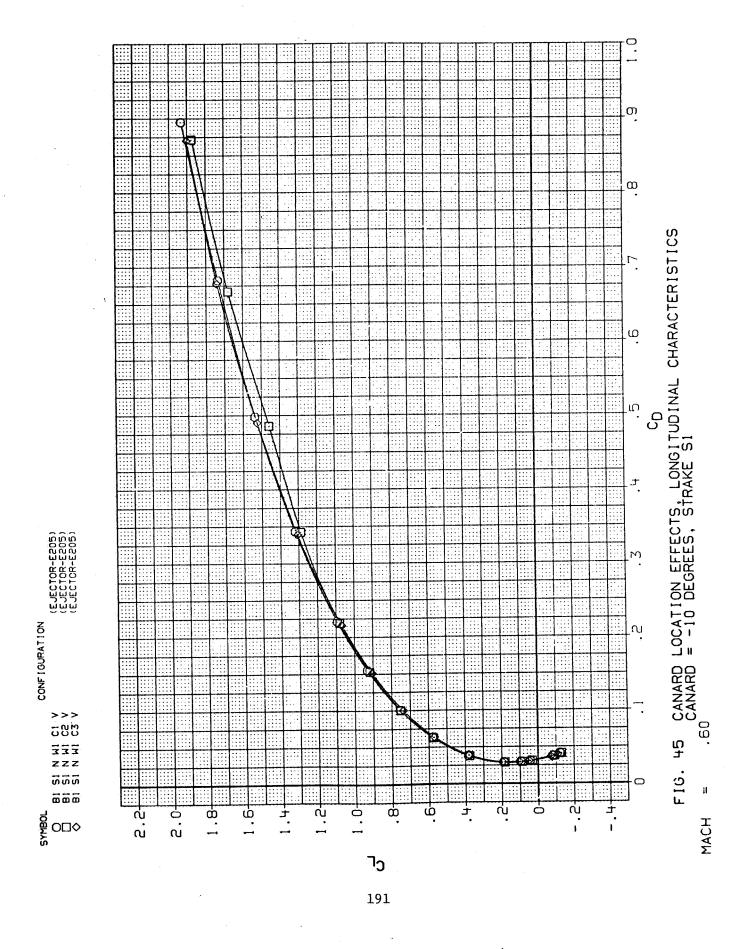


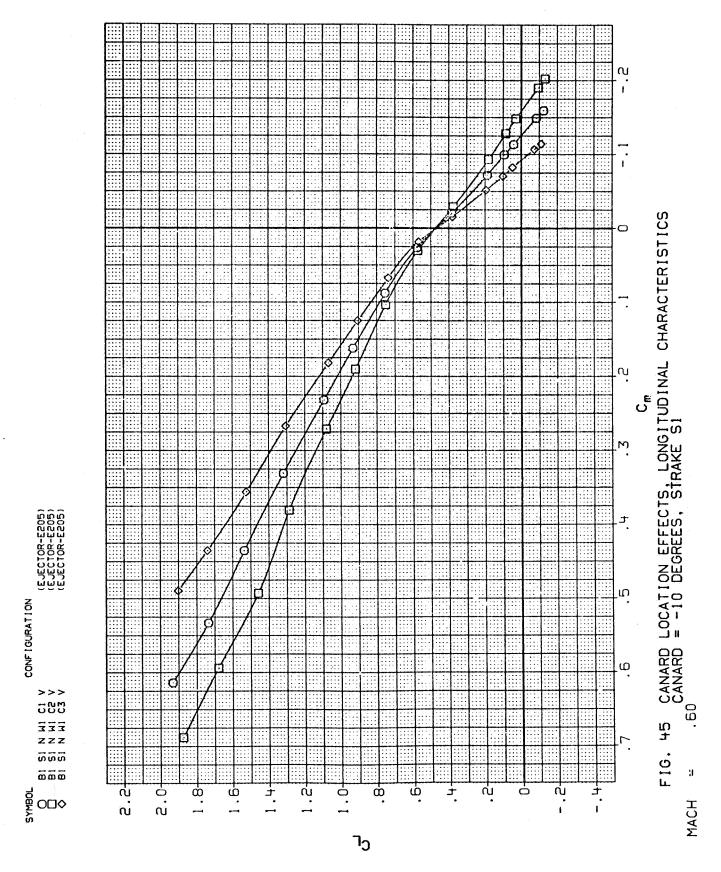


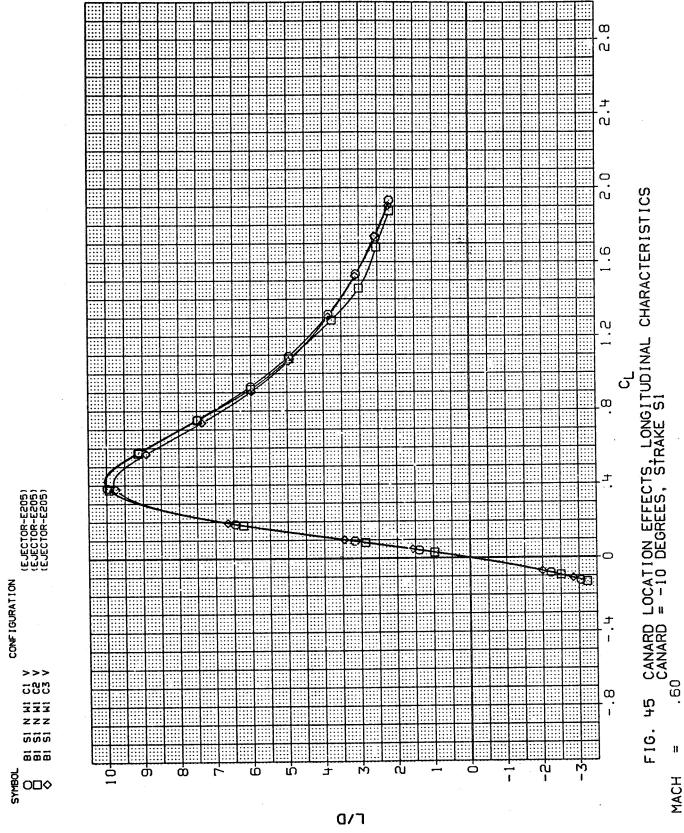


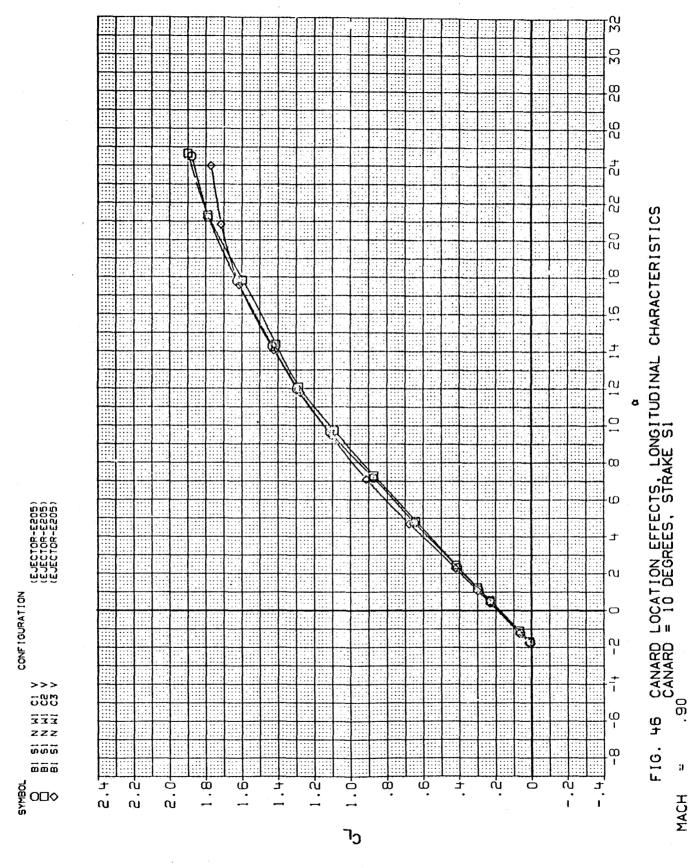


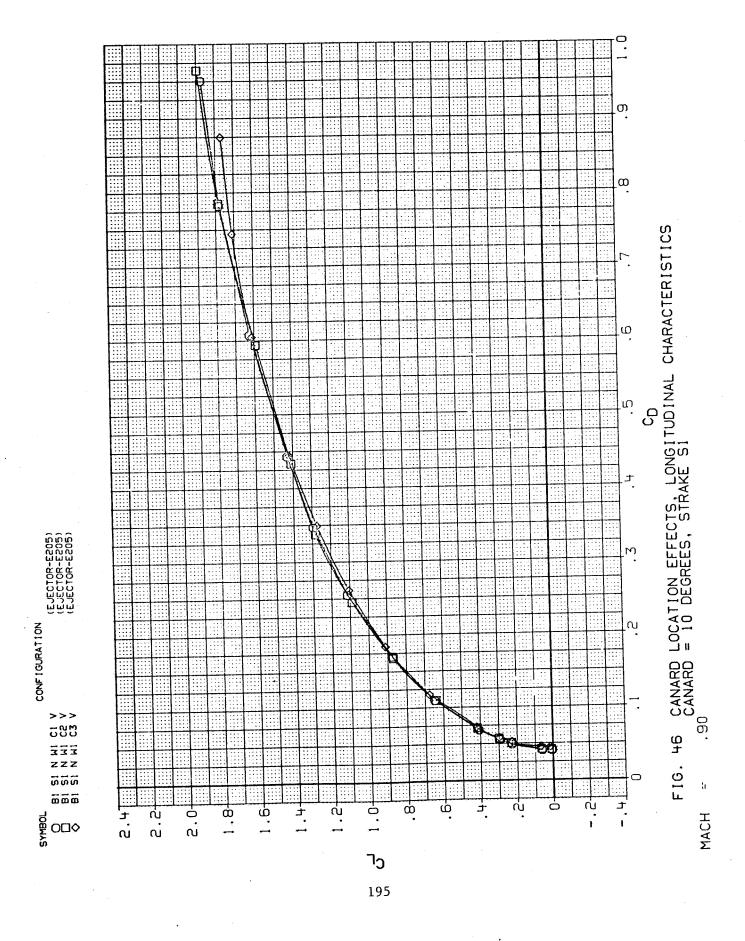


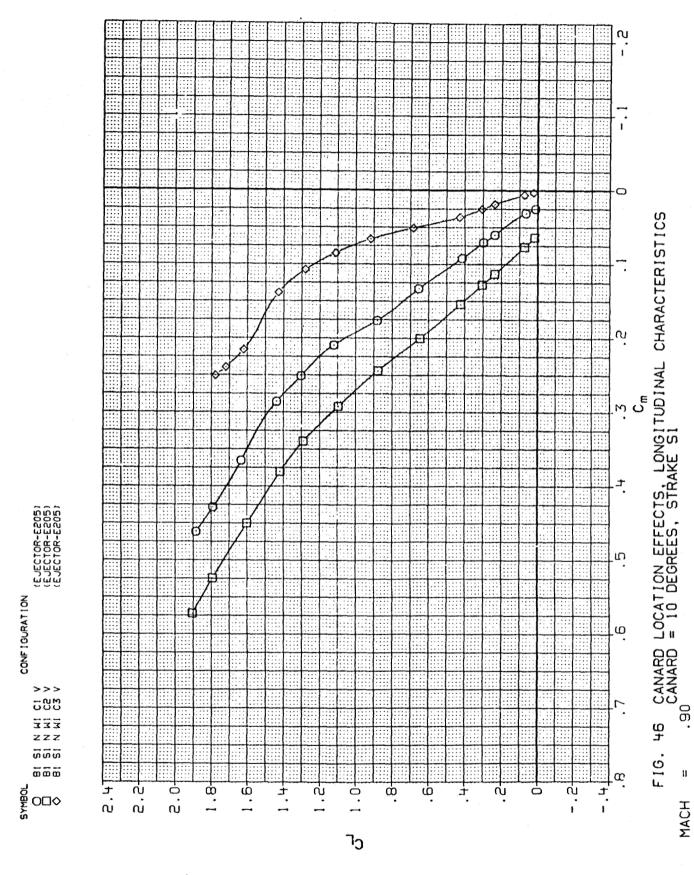


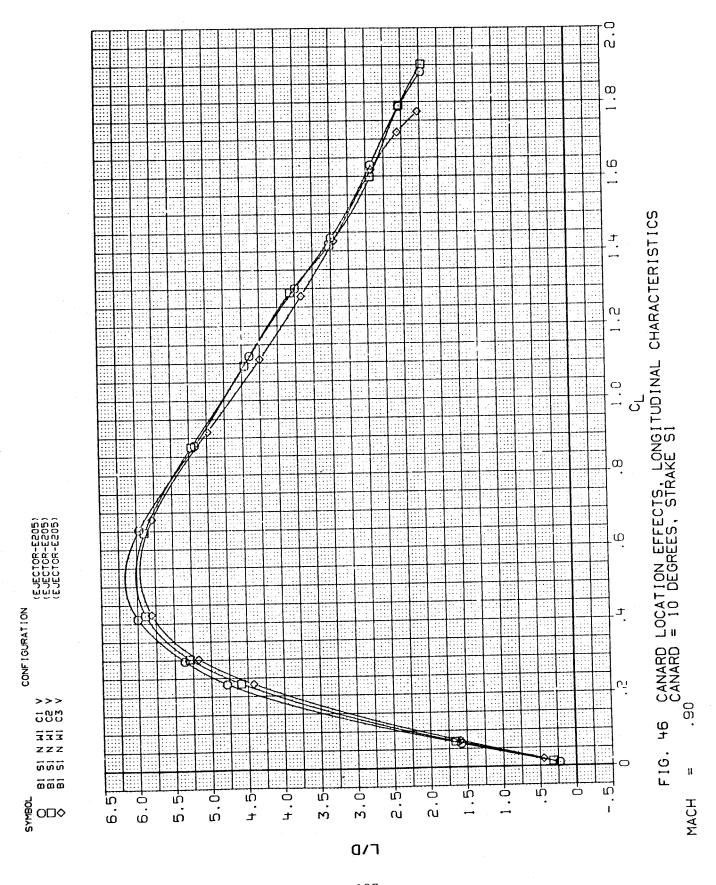


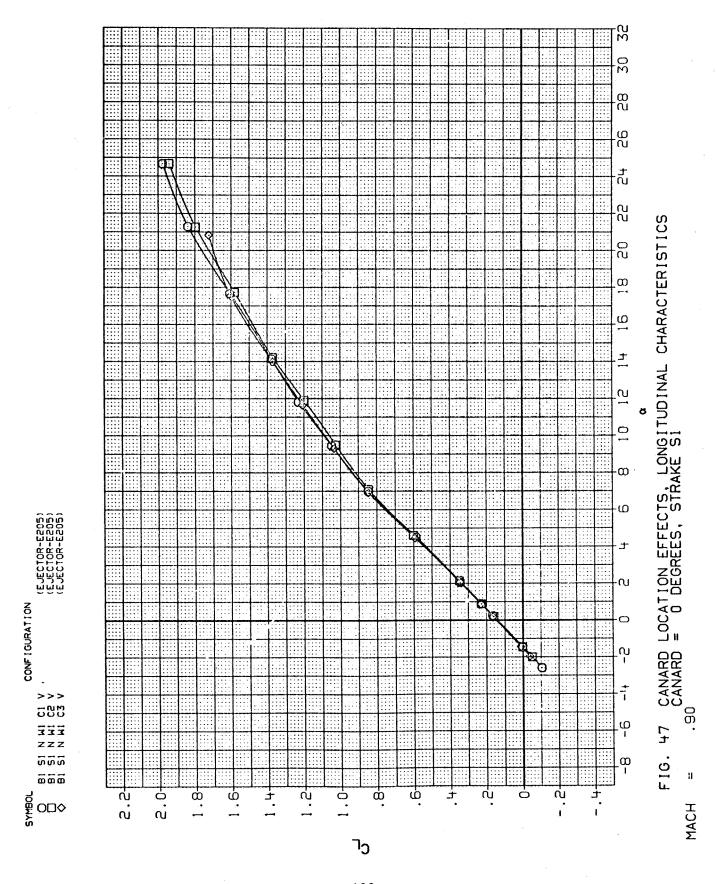


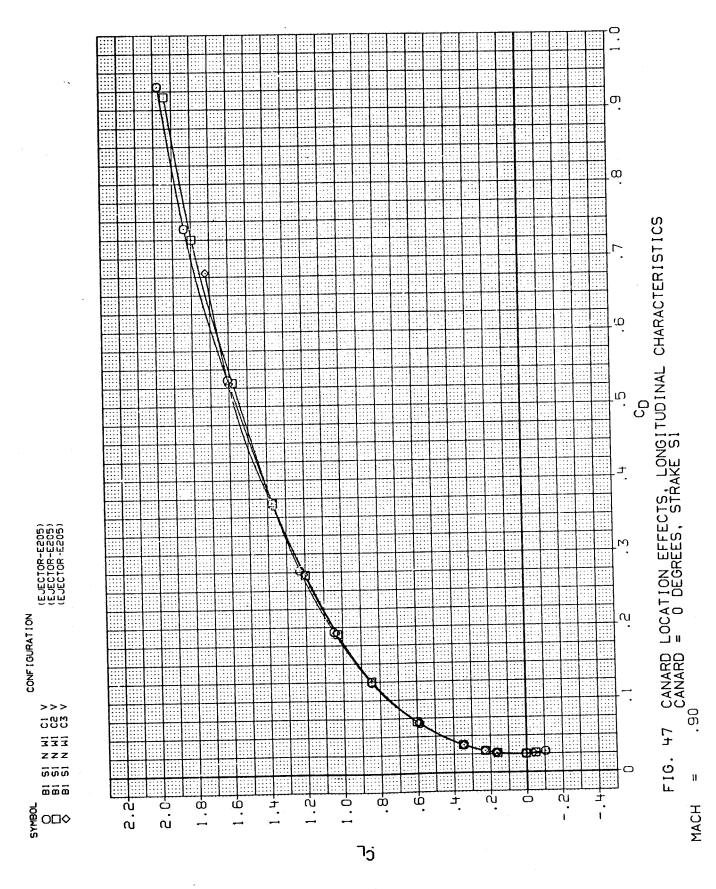


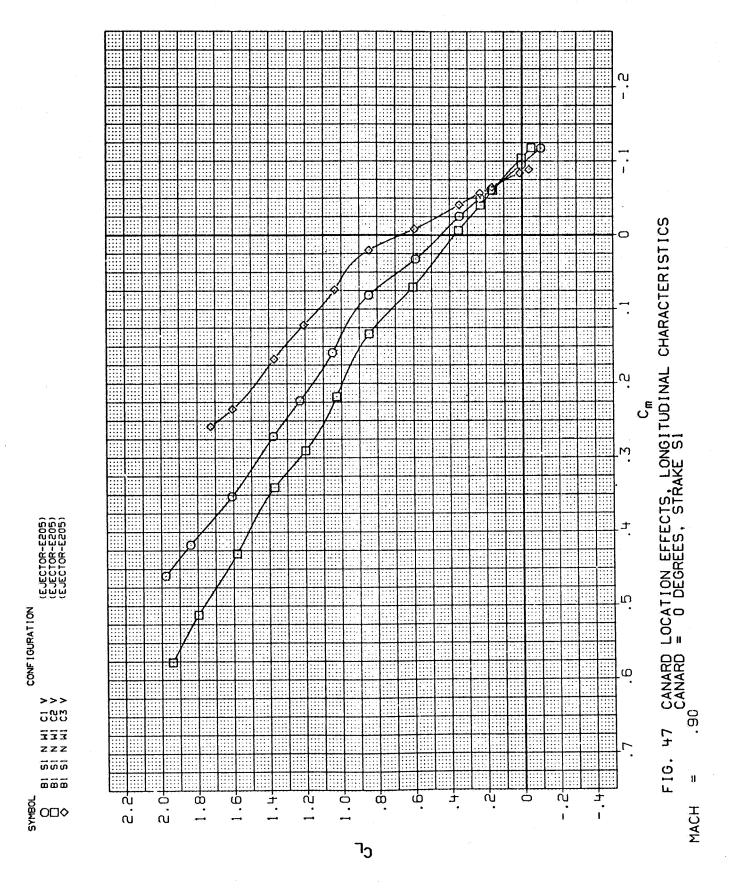


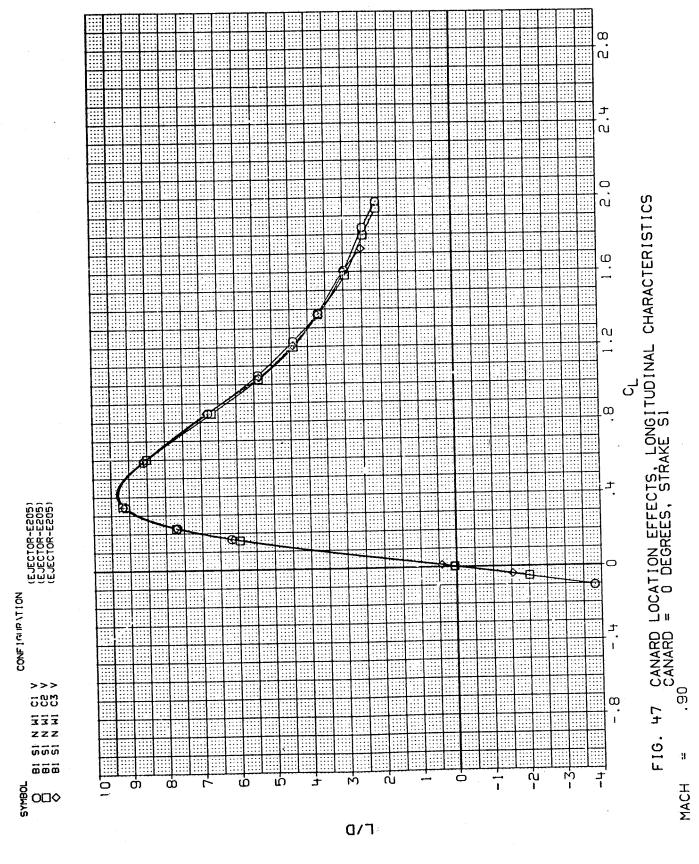


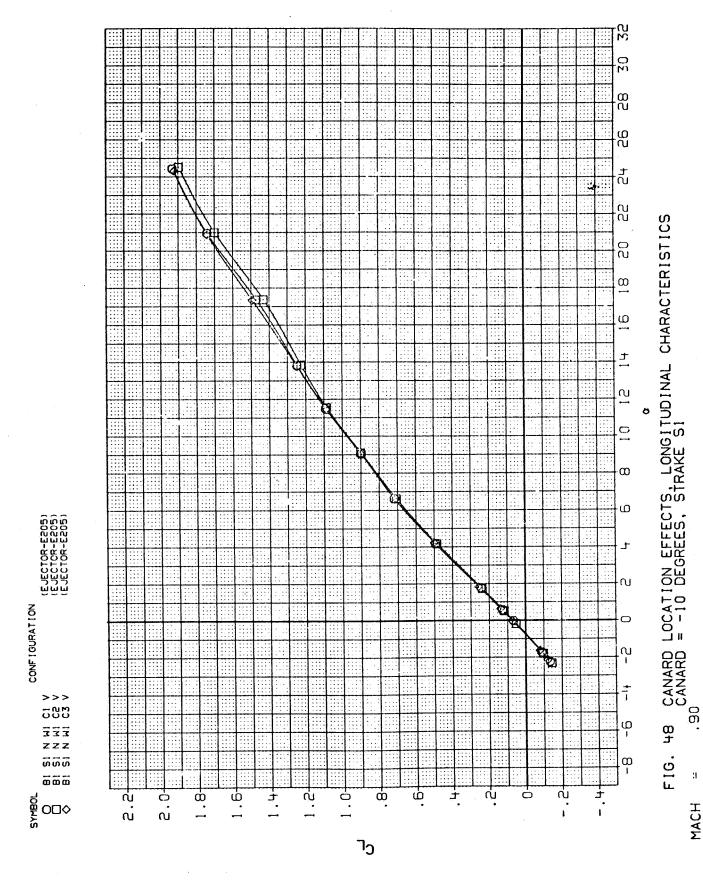


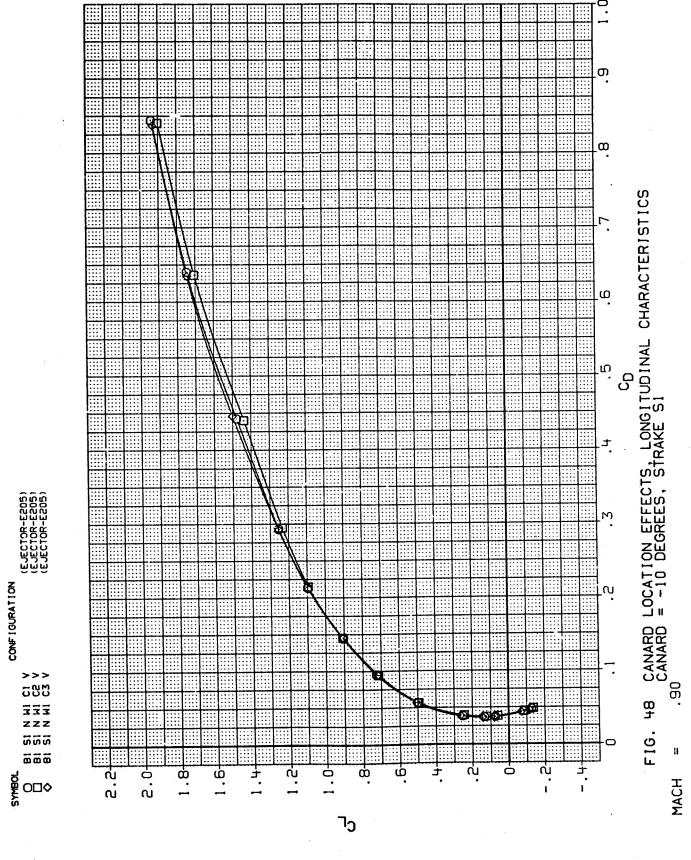


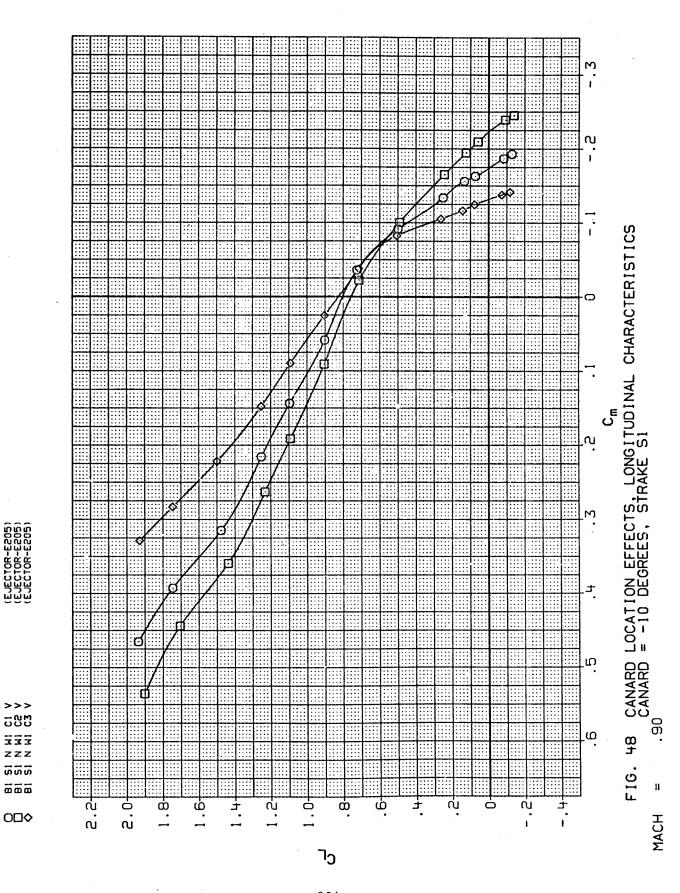




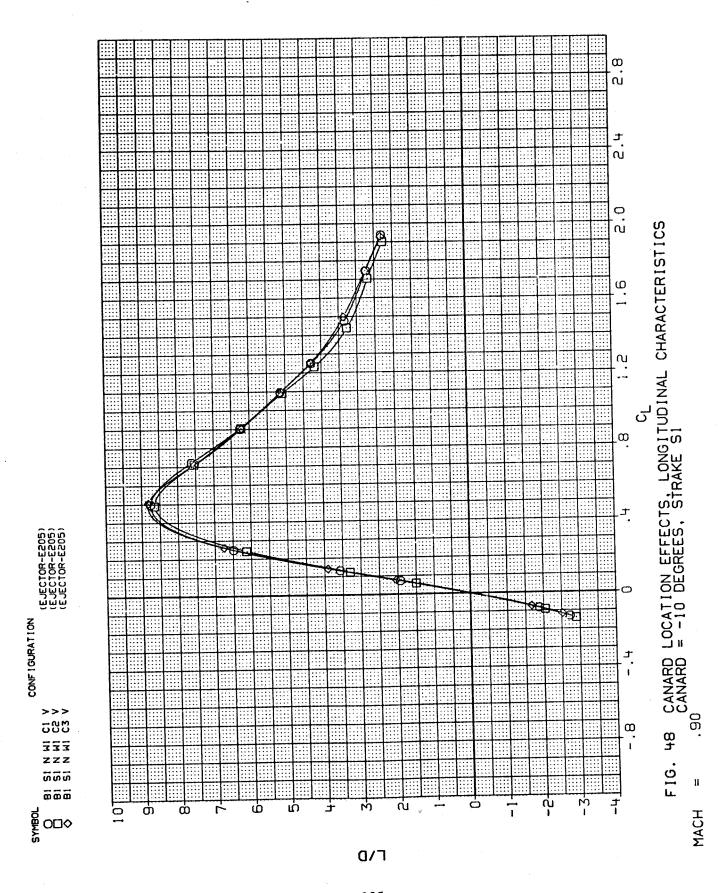


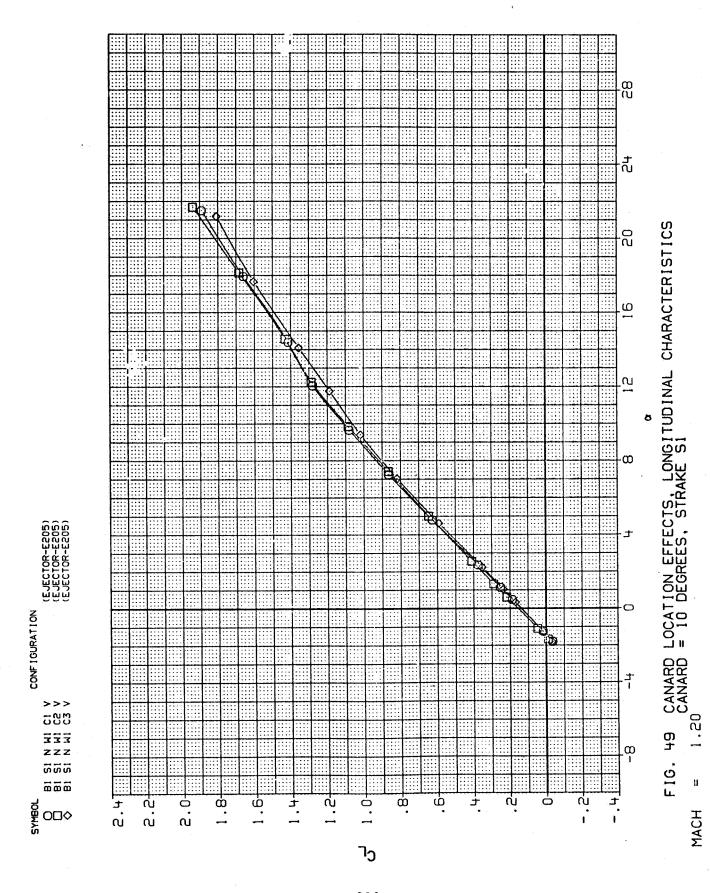


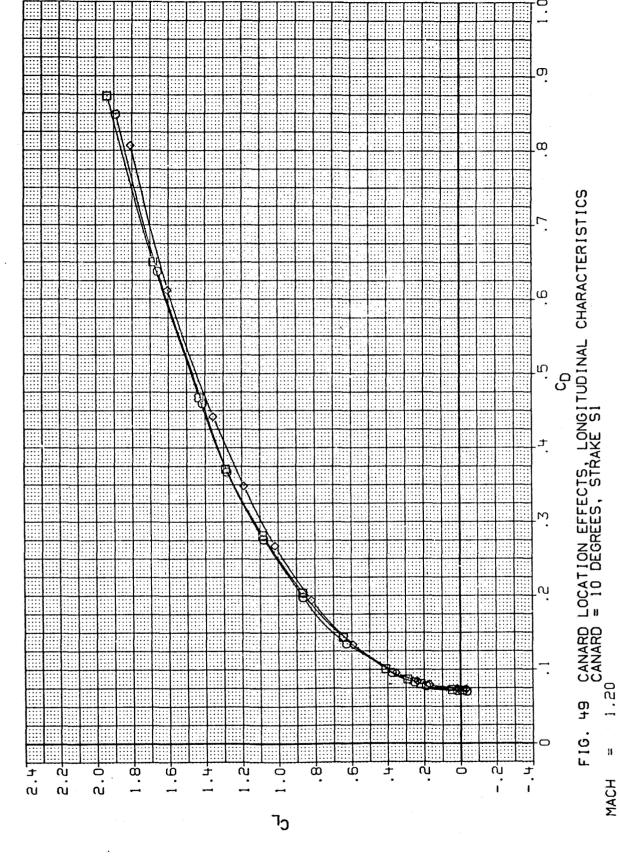




CONFIGURATION







11

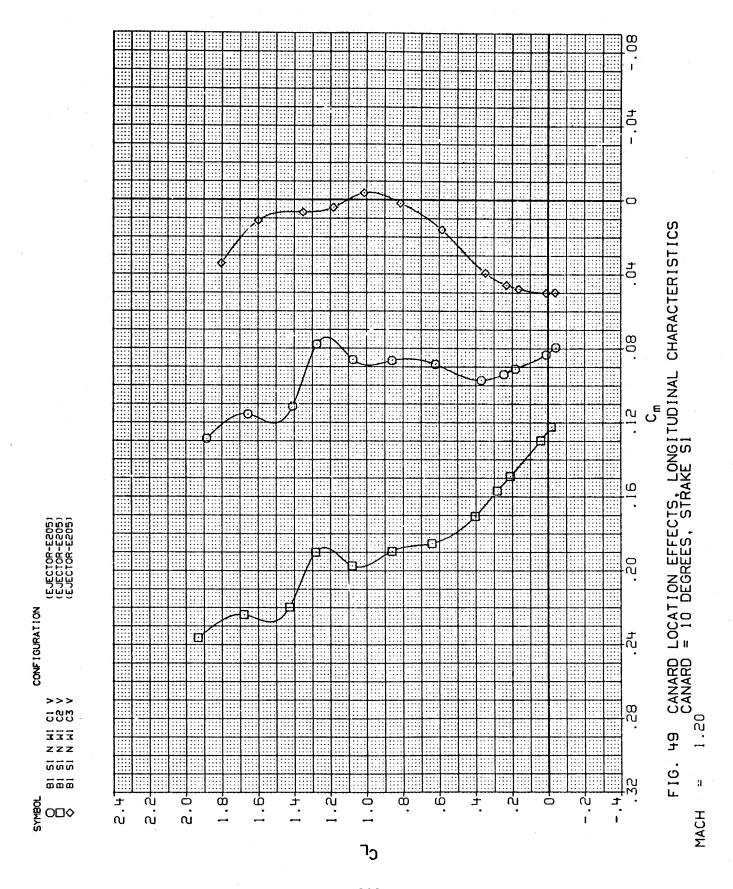
MACH

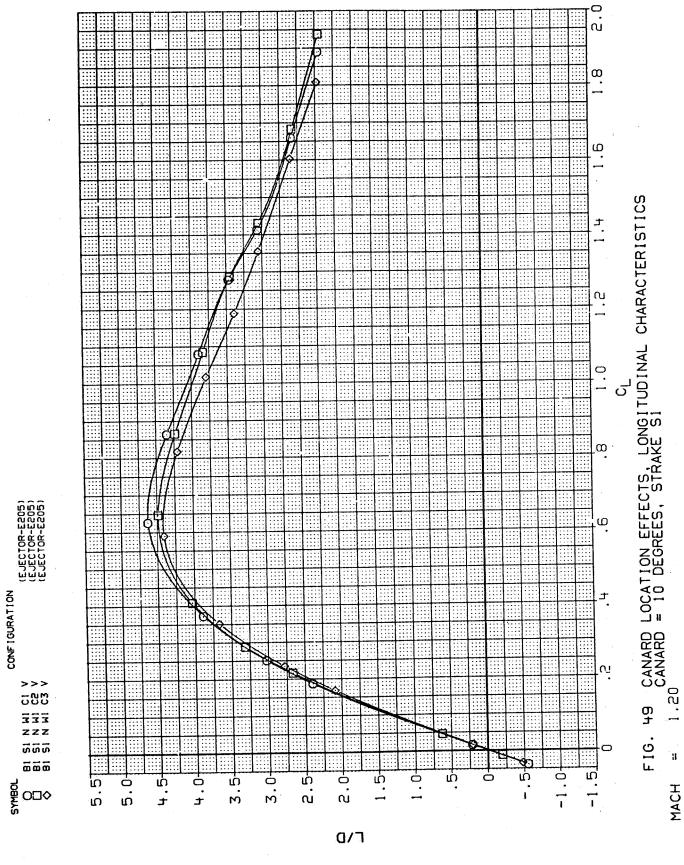
CONFIGURATION

>>> 200 333 ZZZ ខ្មួលខ្ម

 $\overline{\omega}$

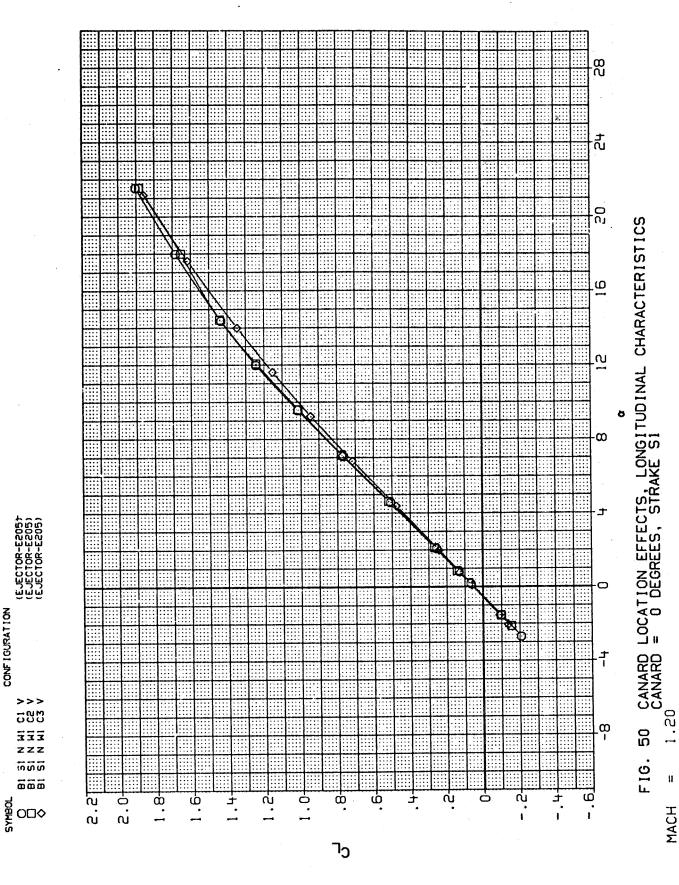
 $O\Box \Diamond$



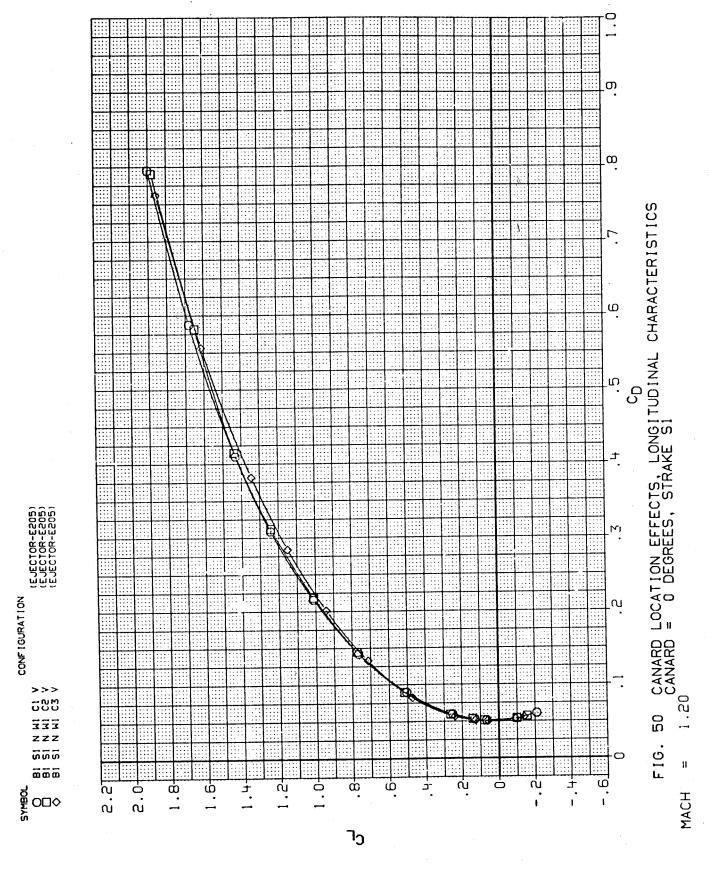


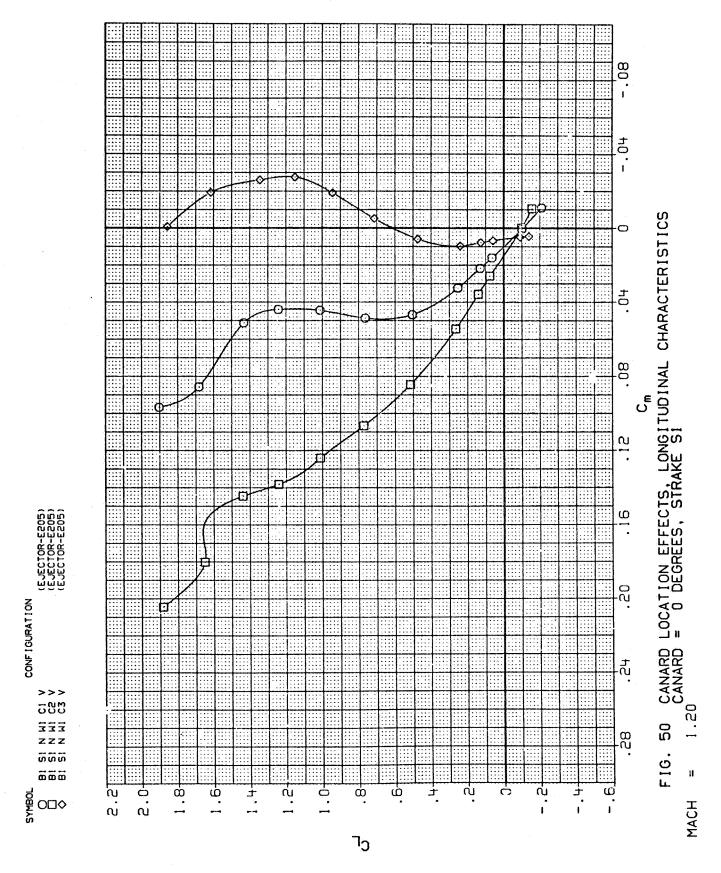
209

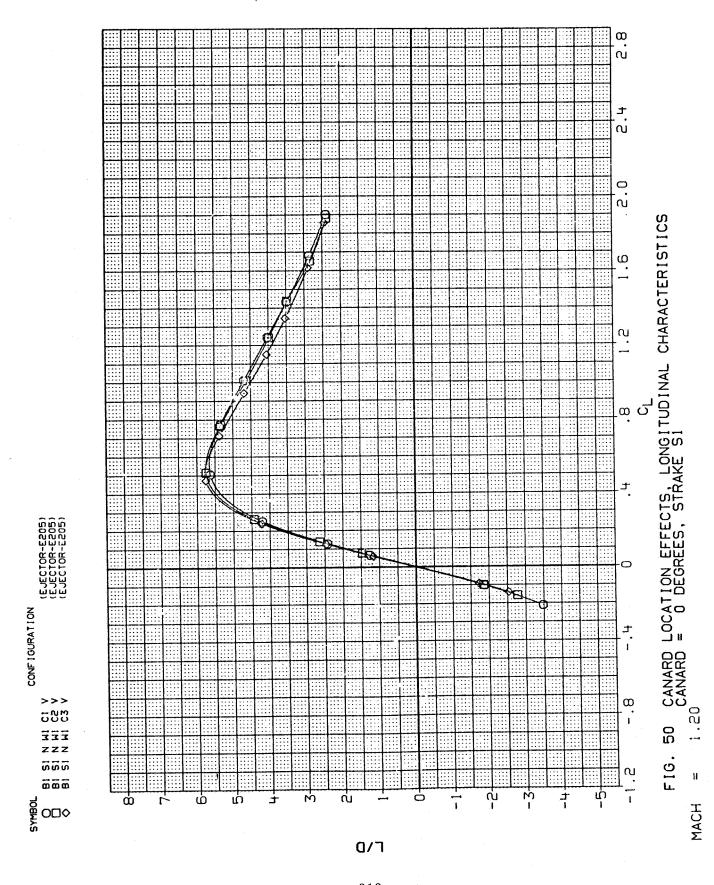
MACH

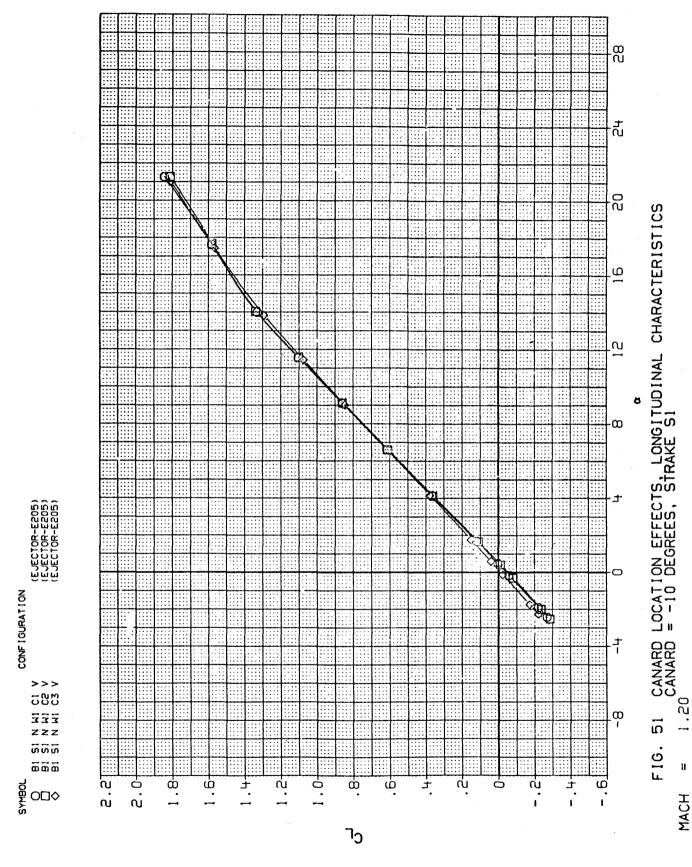


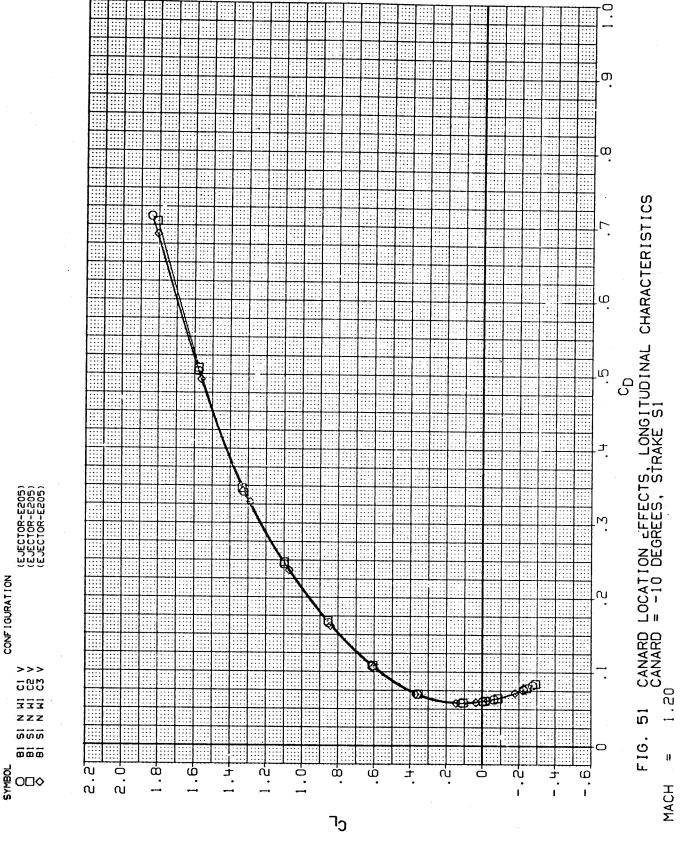
CONFIGURATION

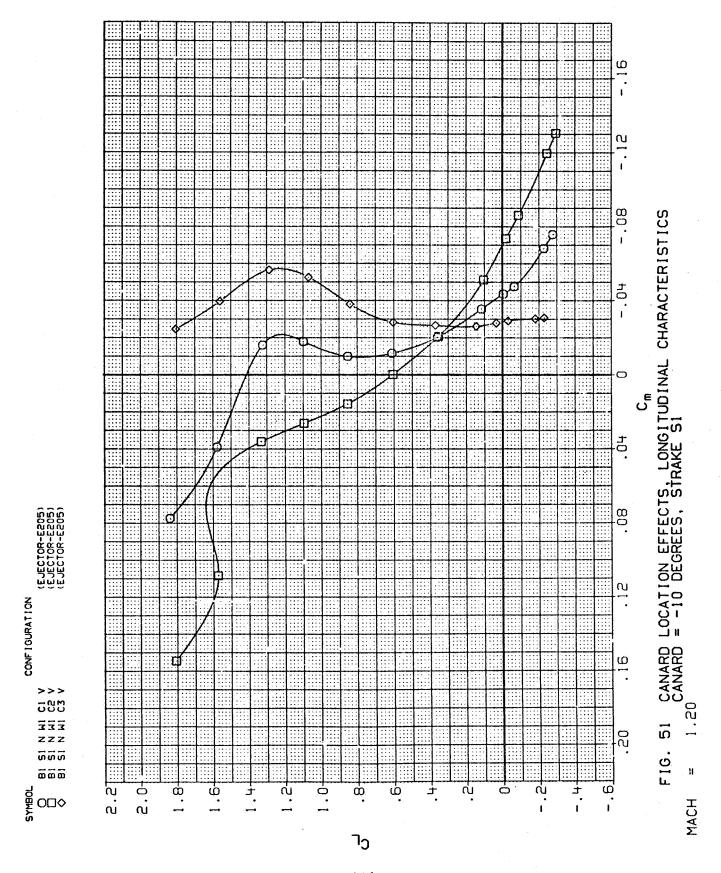


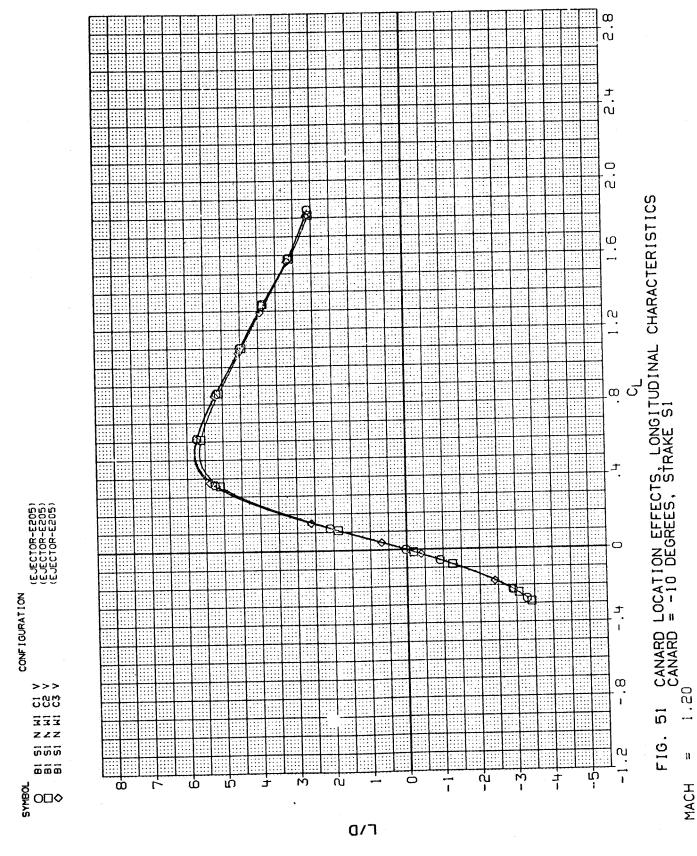


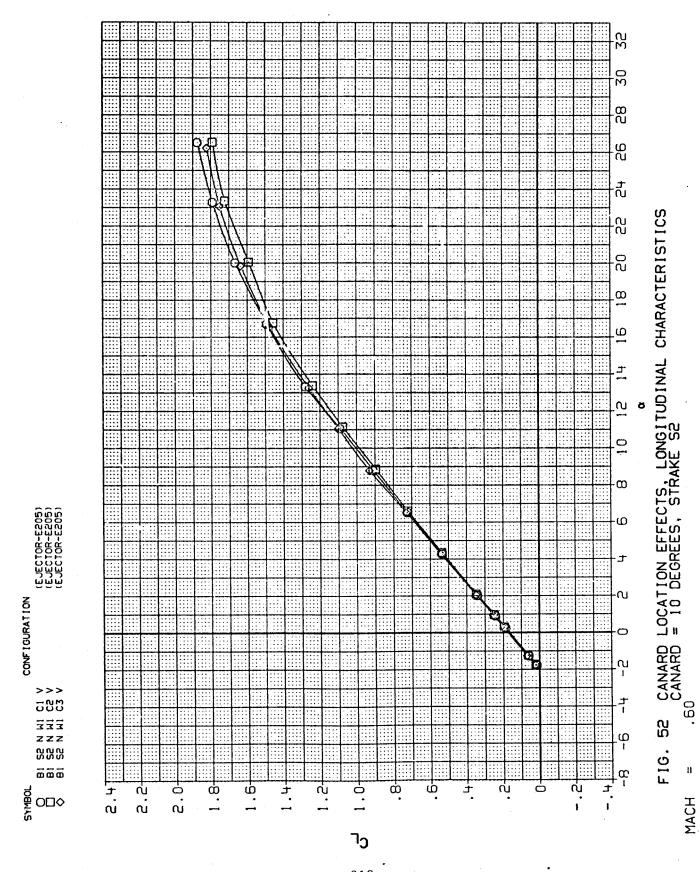




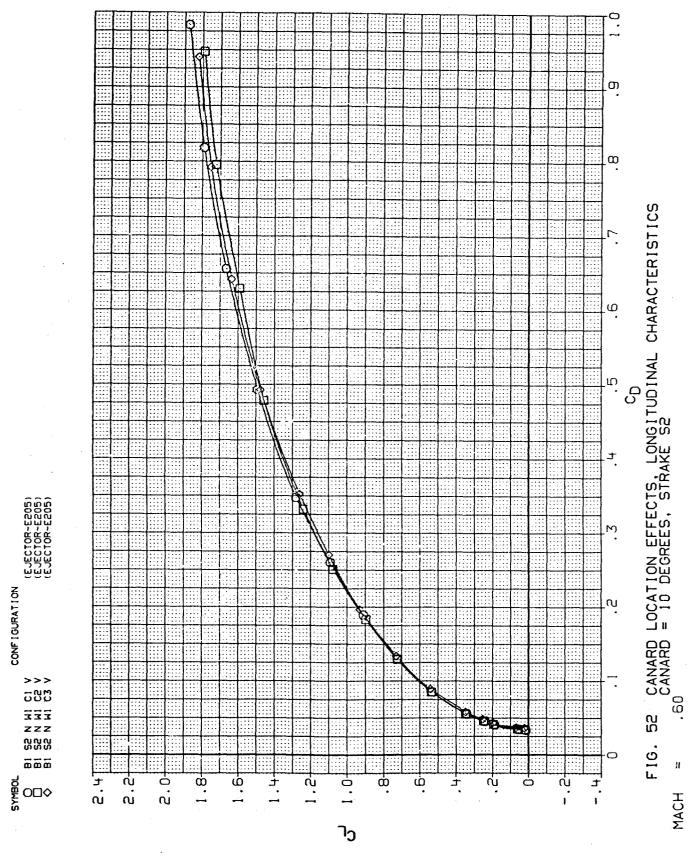


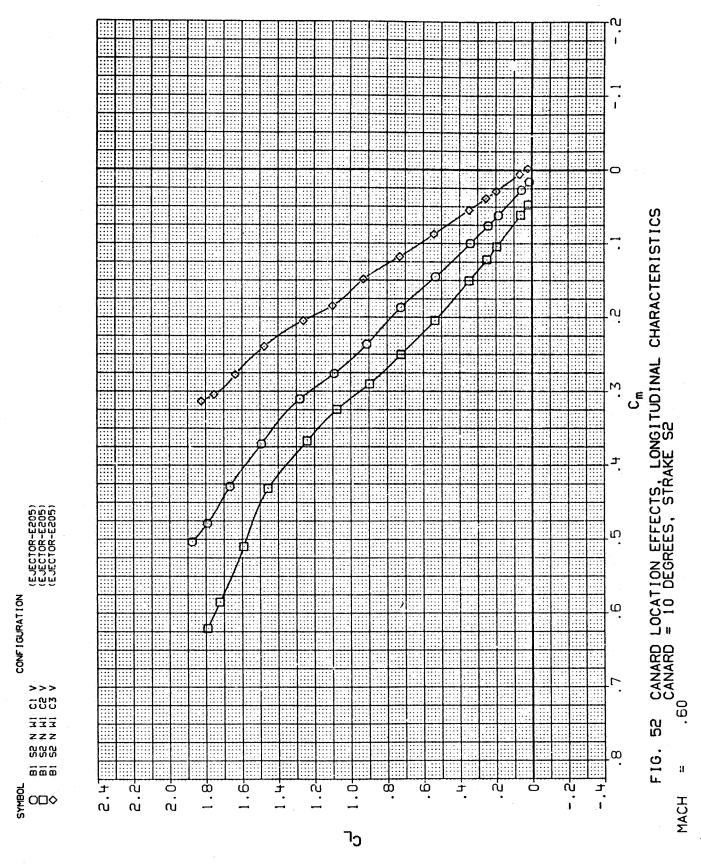


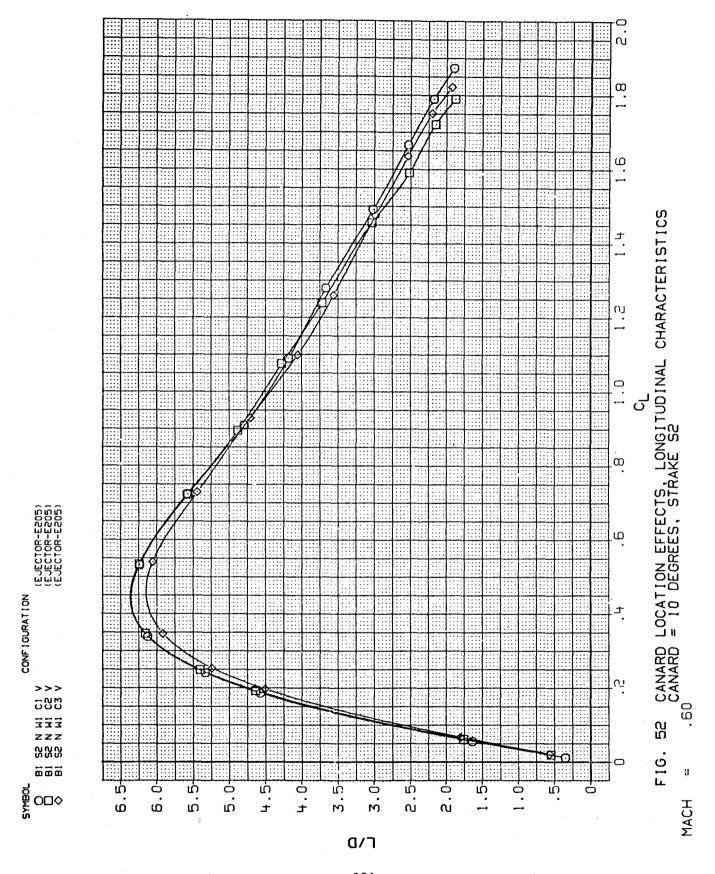


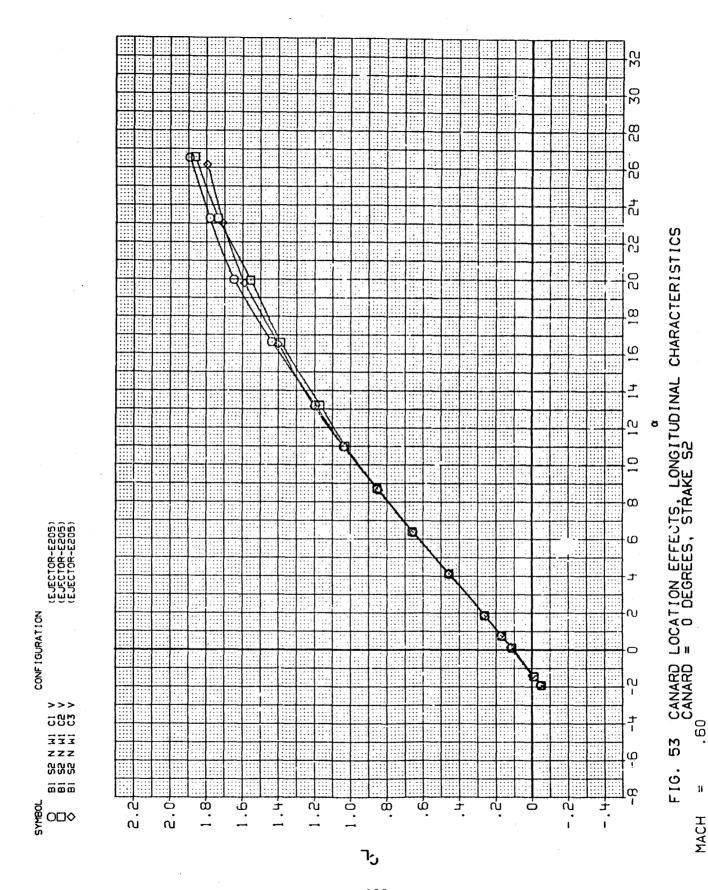


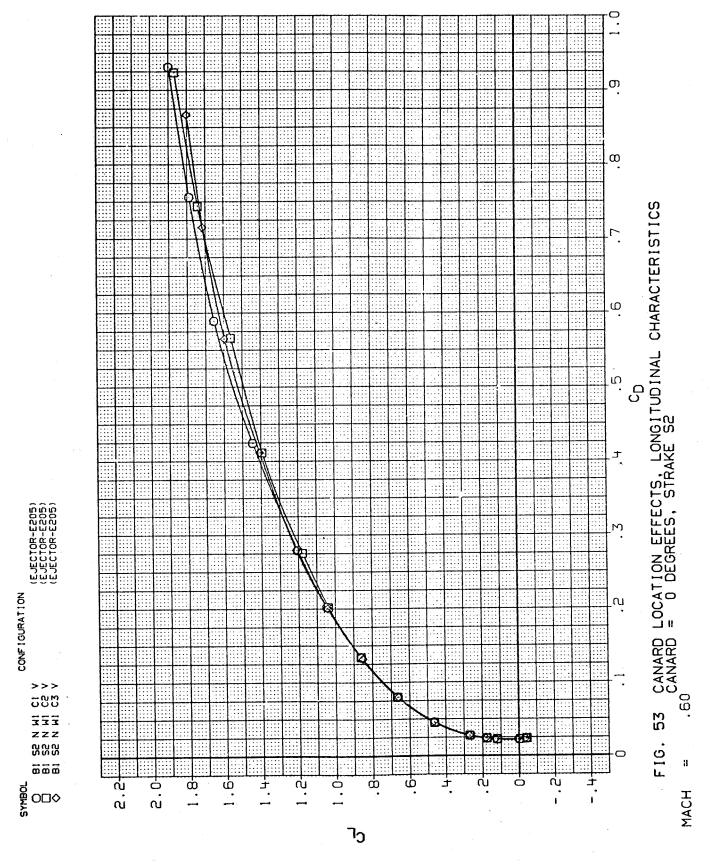
MACH

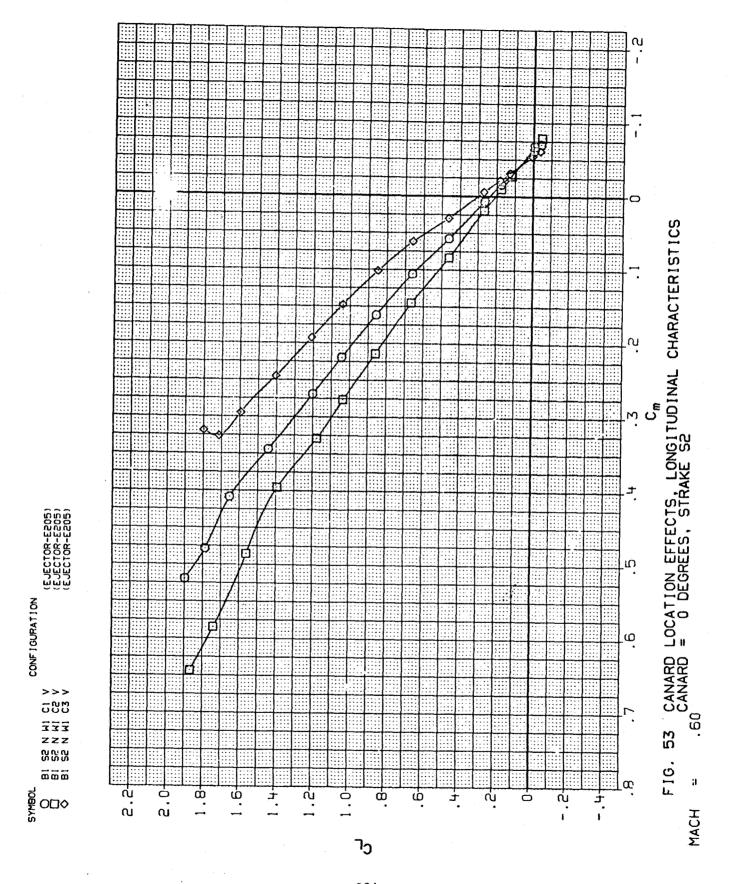


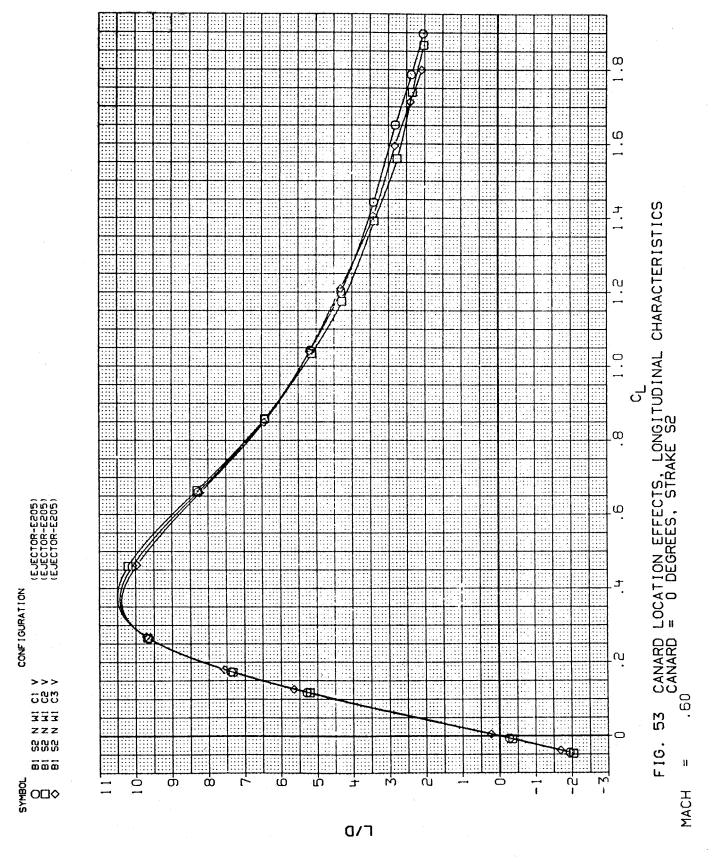


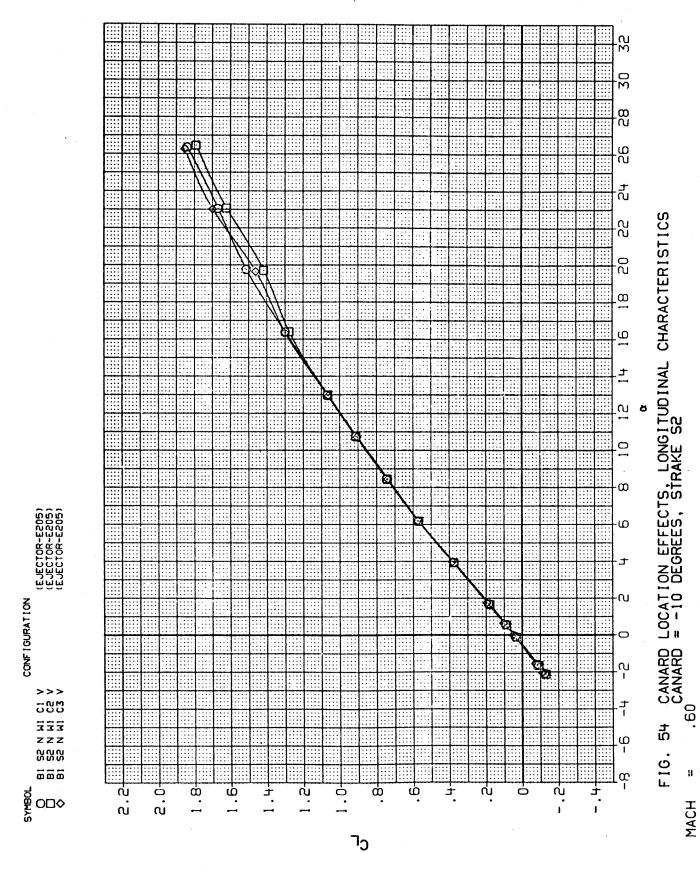


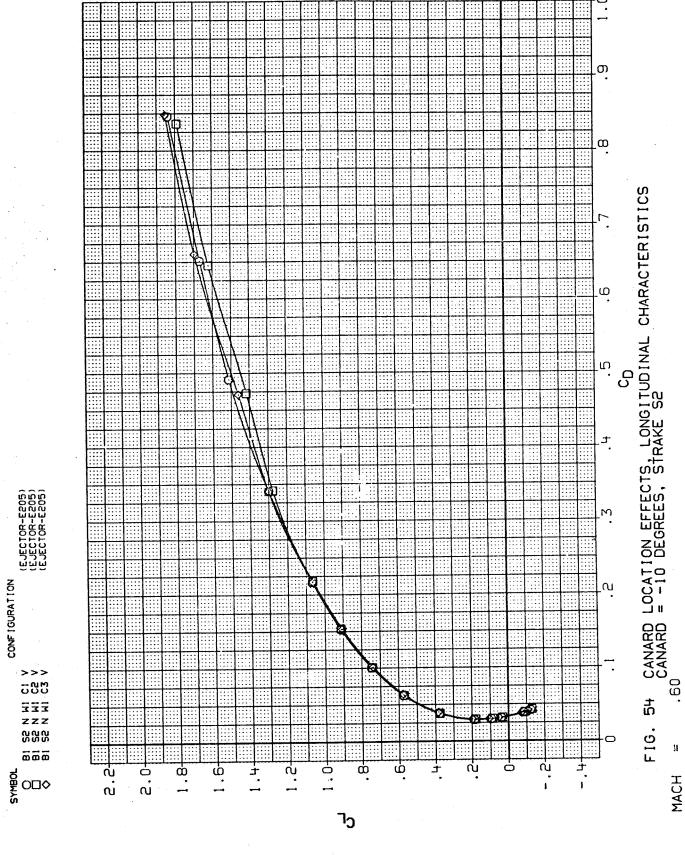


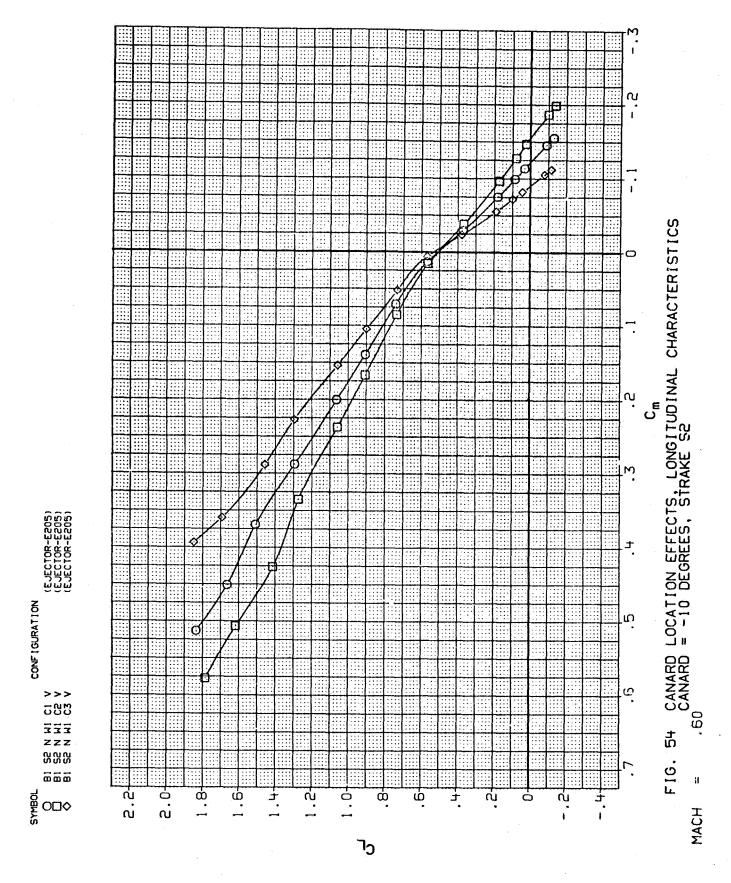


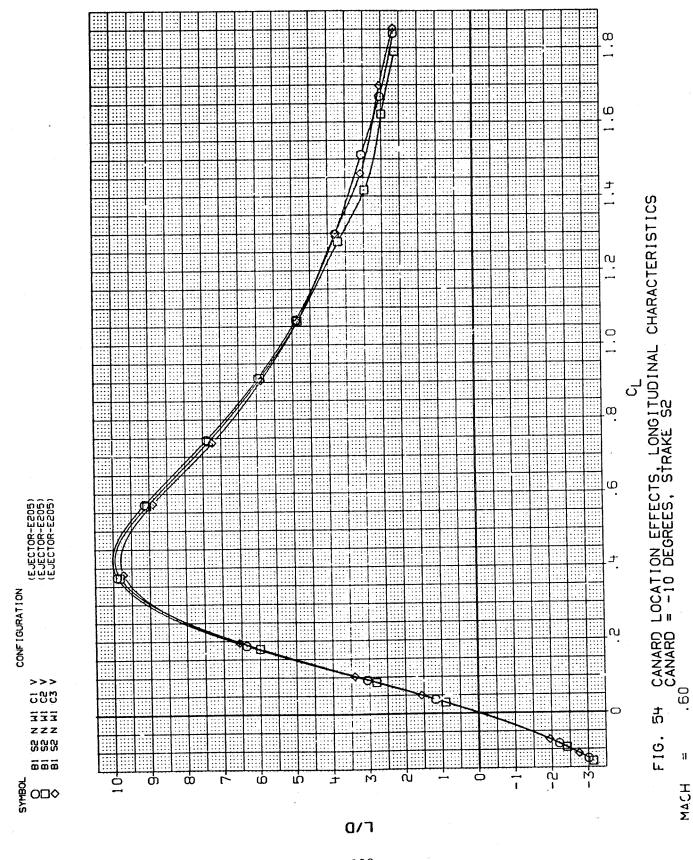


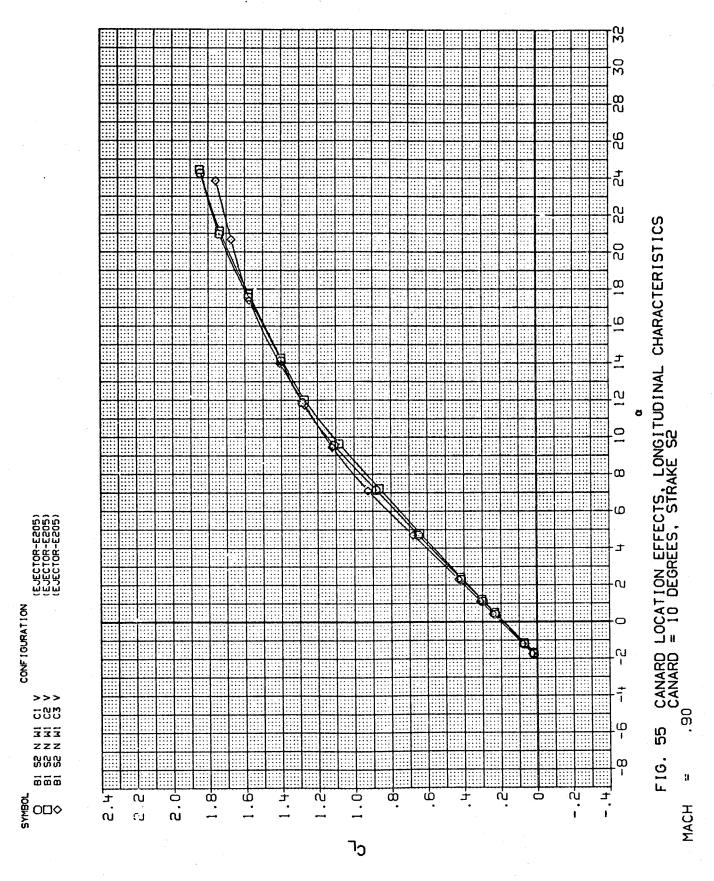


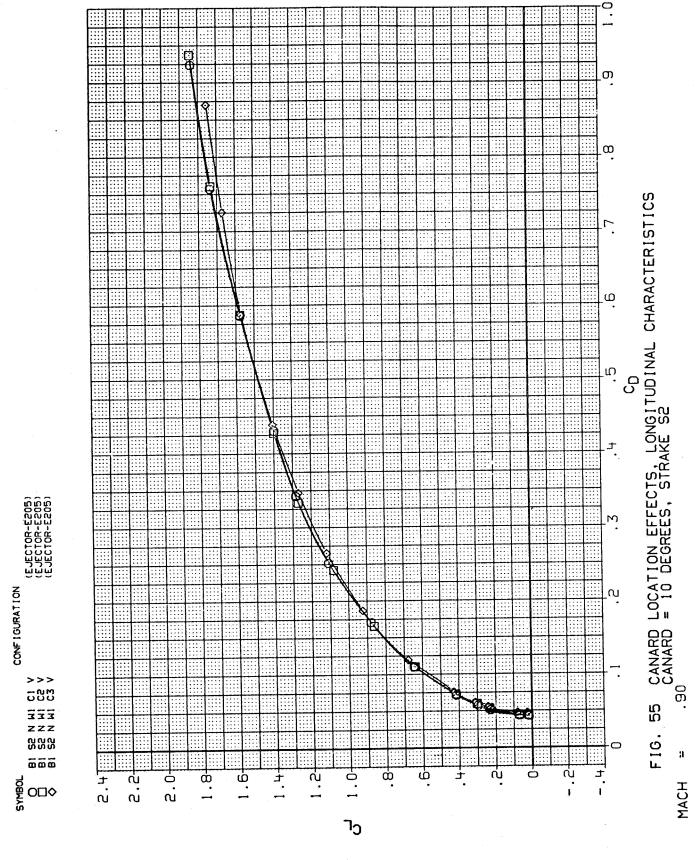


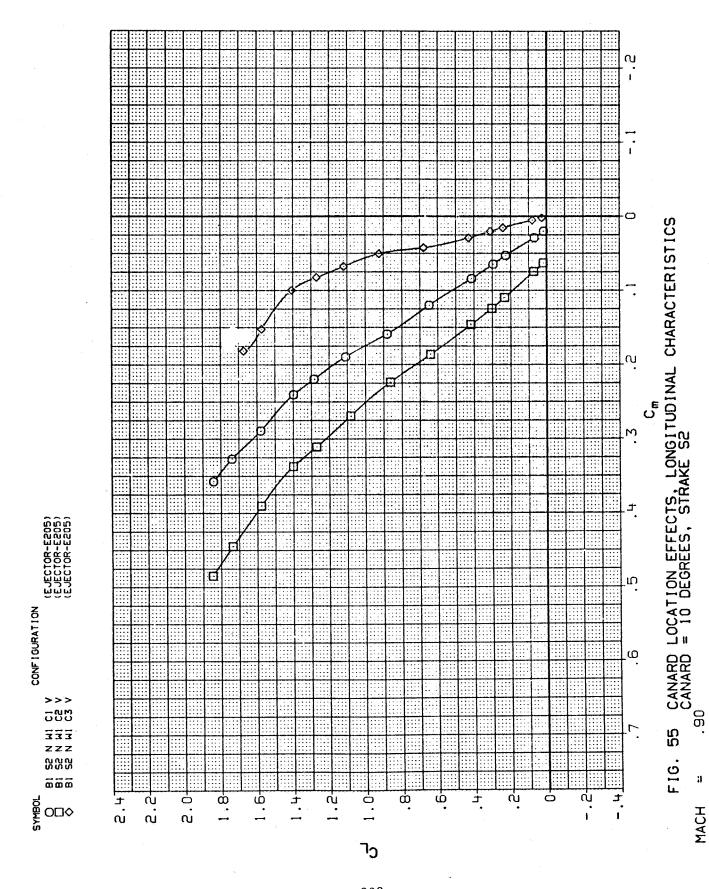


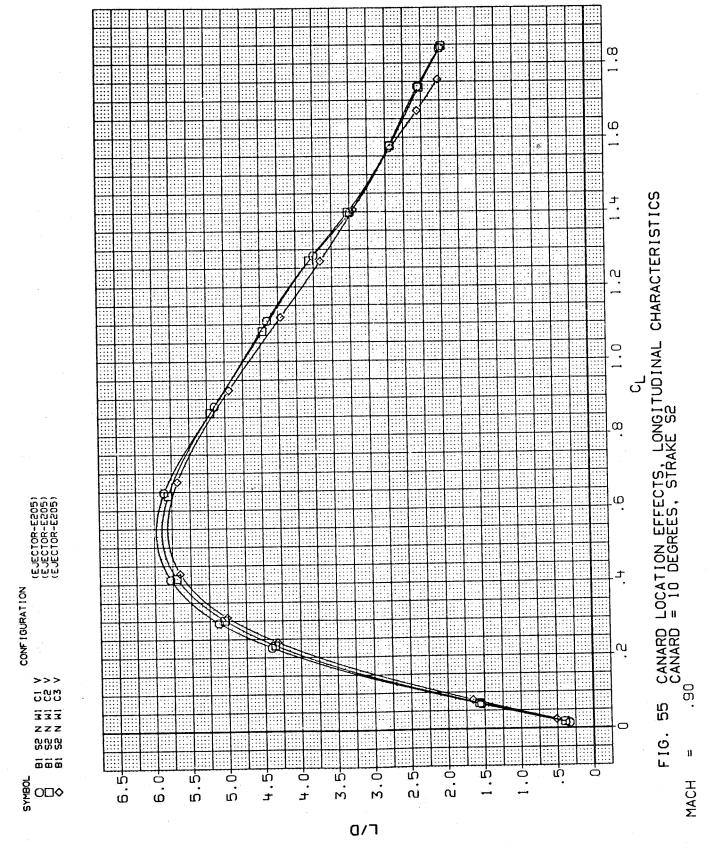


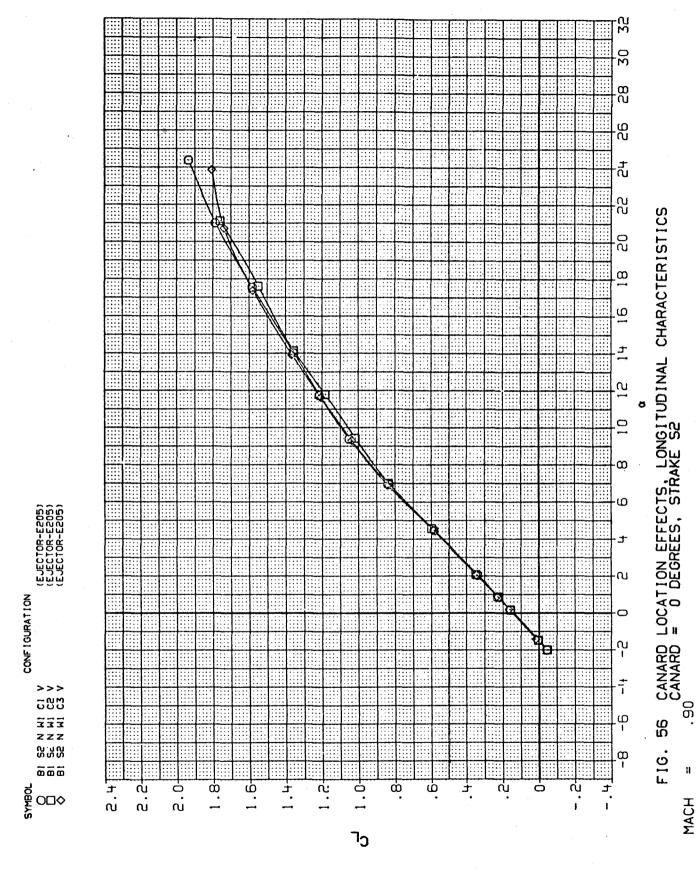


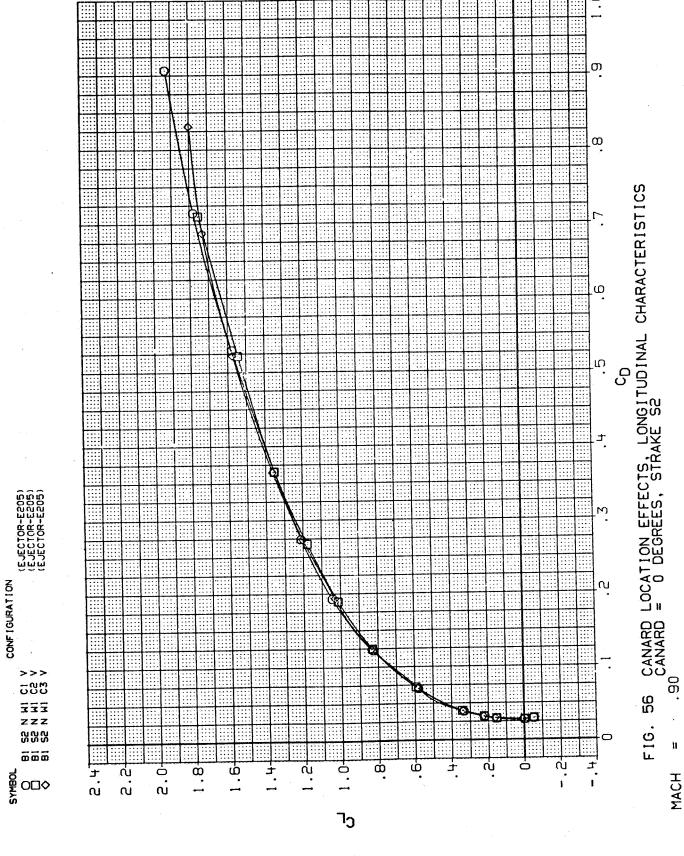


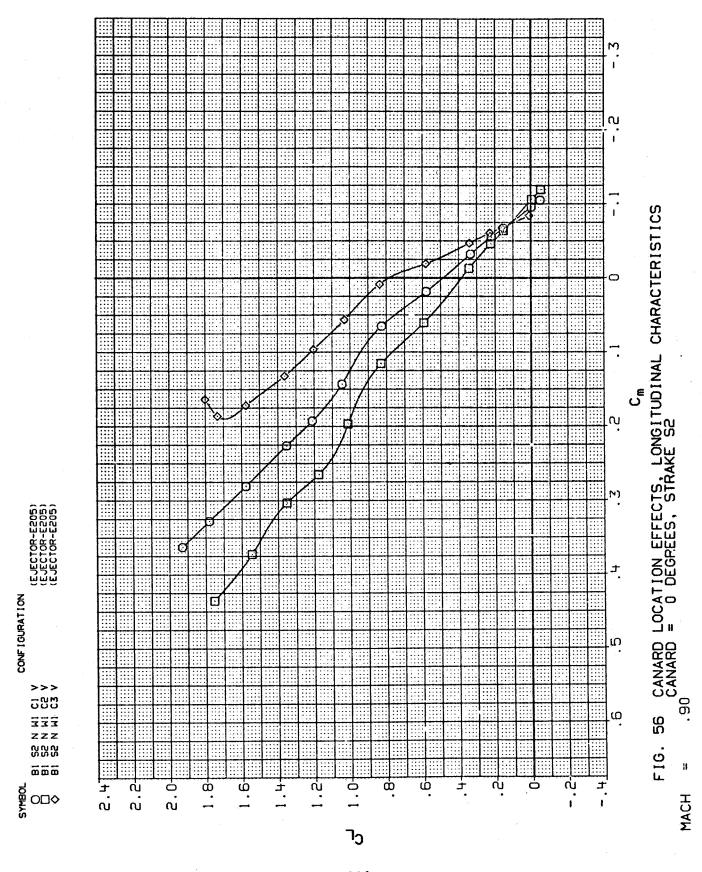


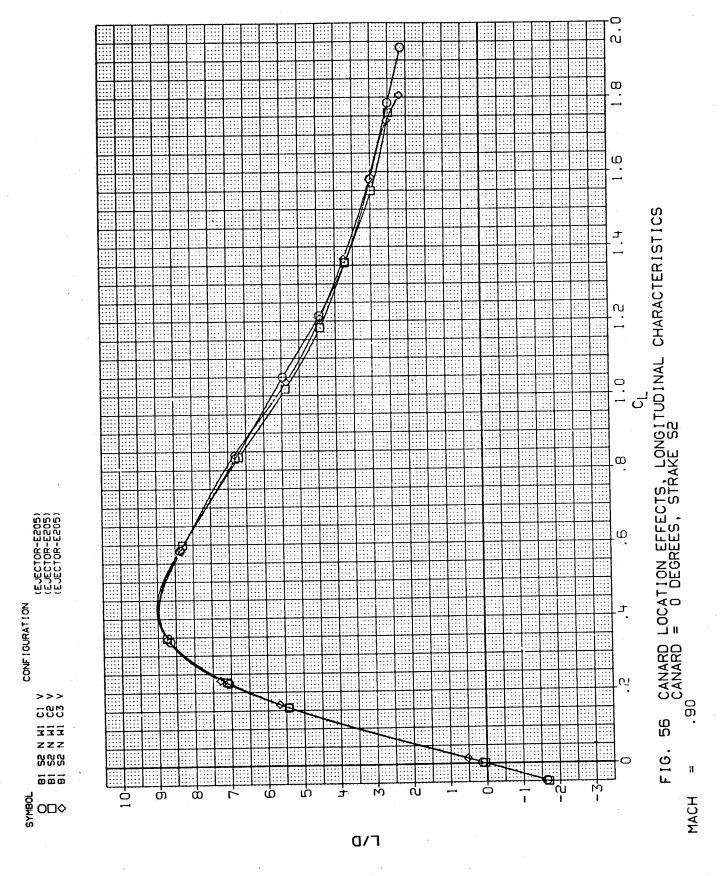


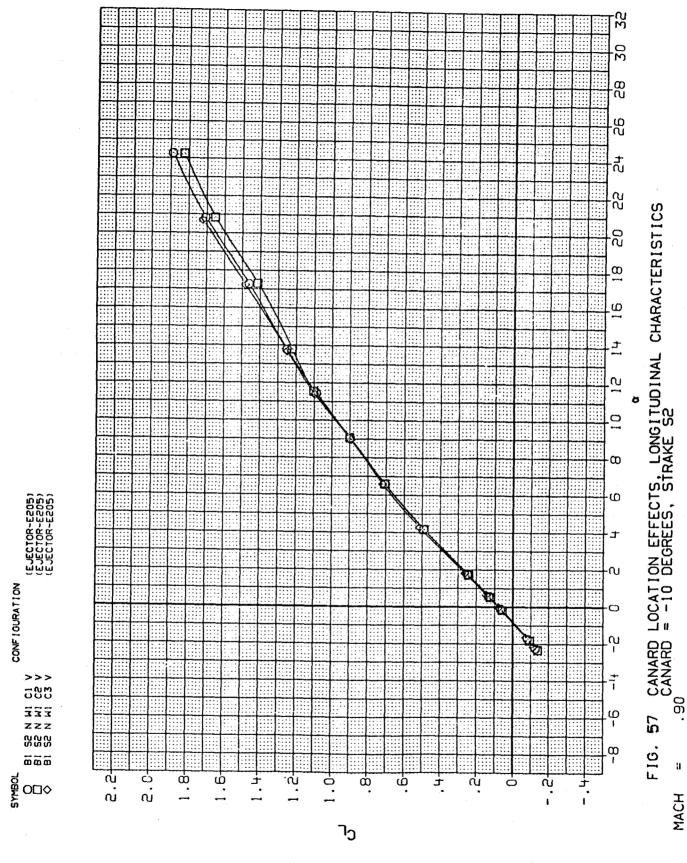






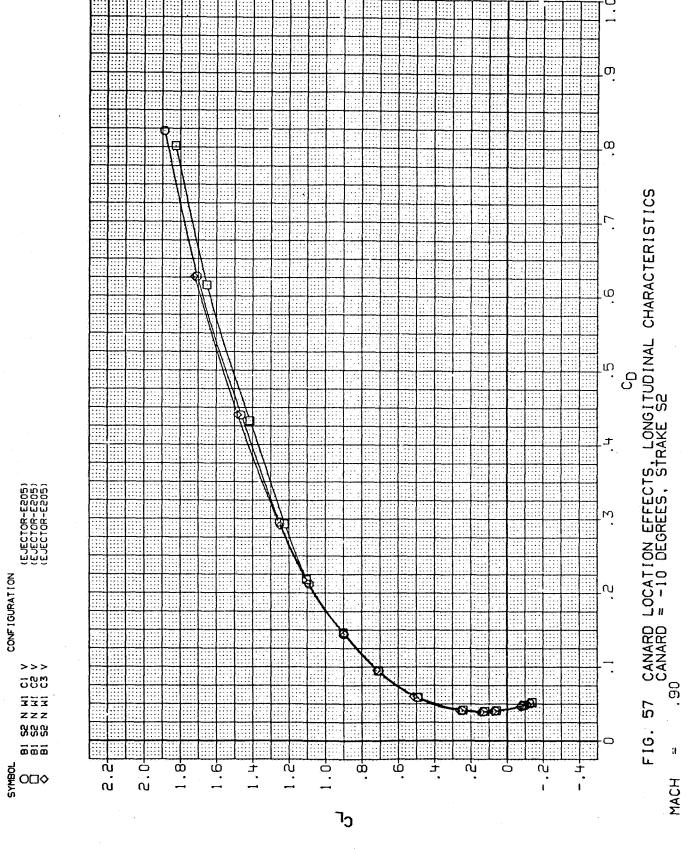


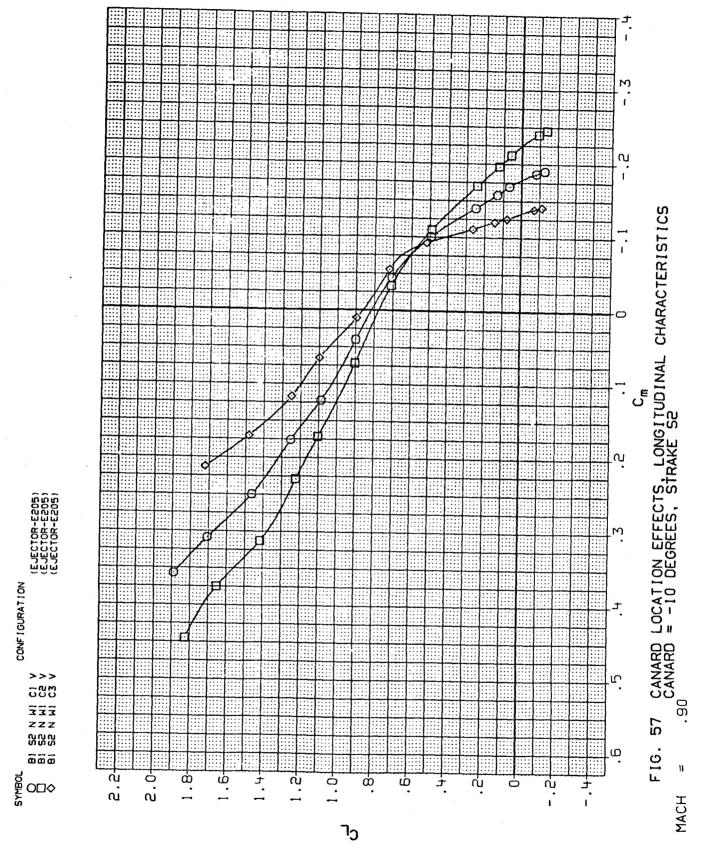


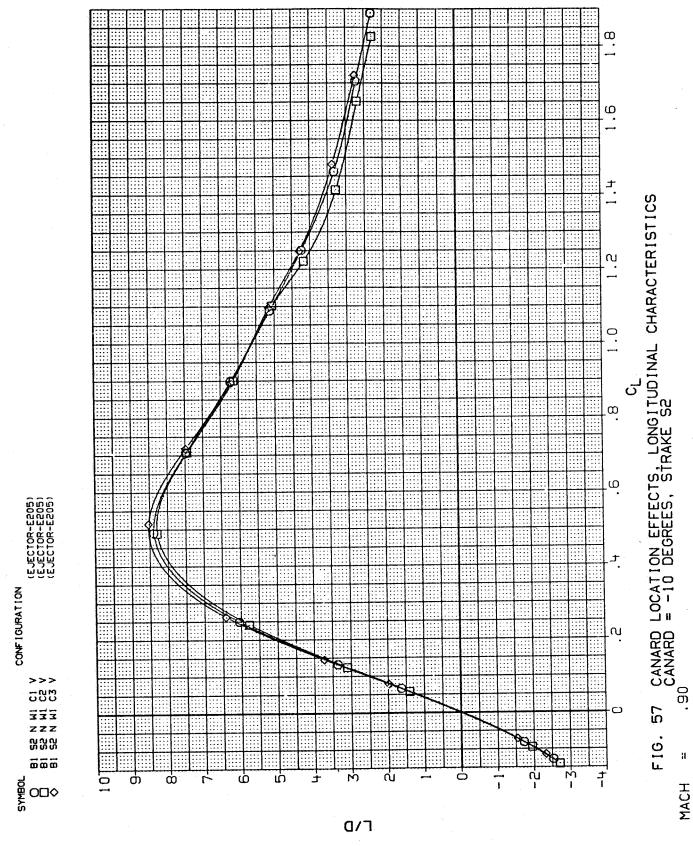


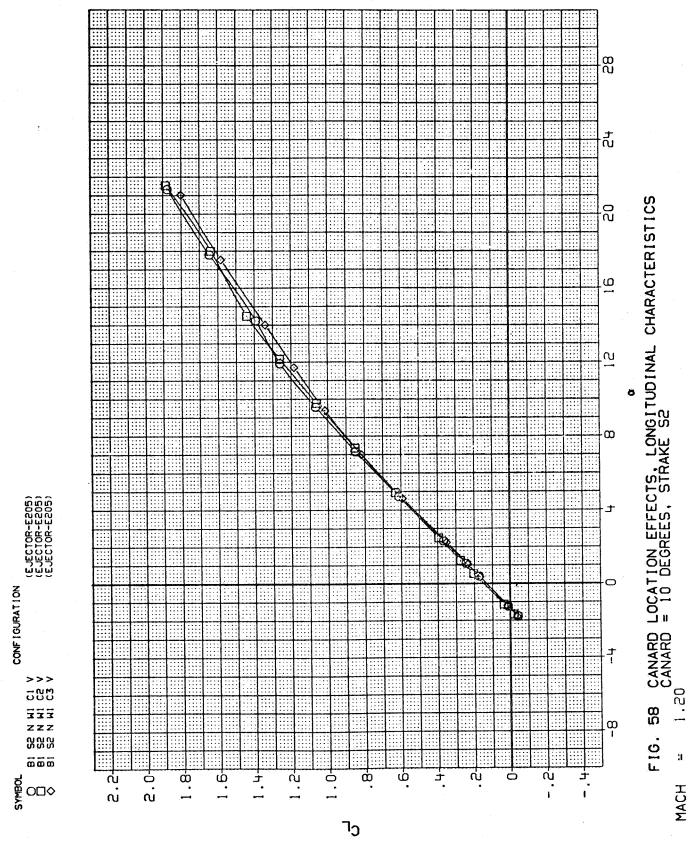
238

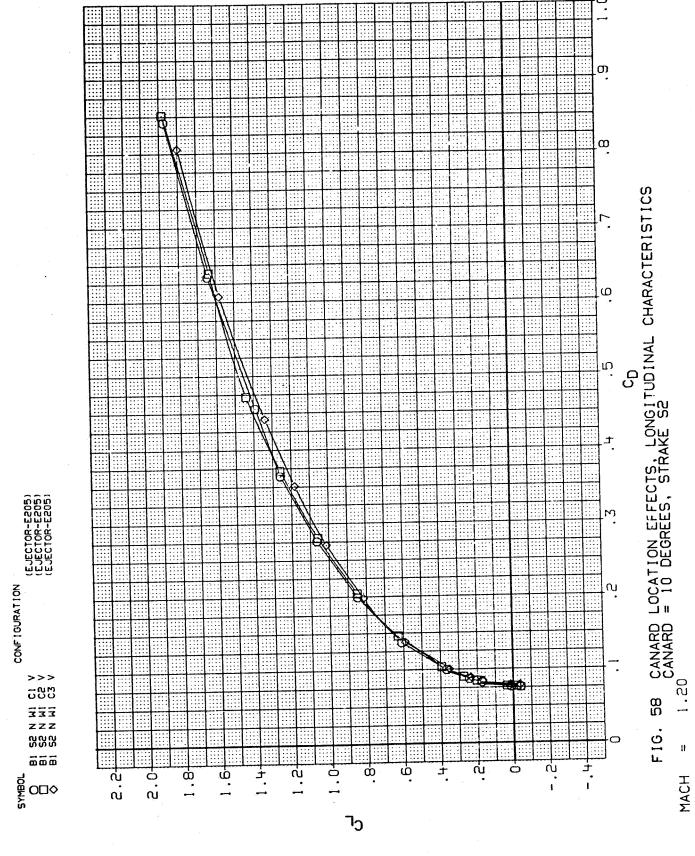
MACH

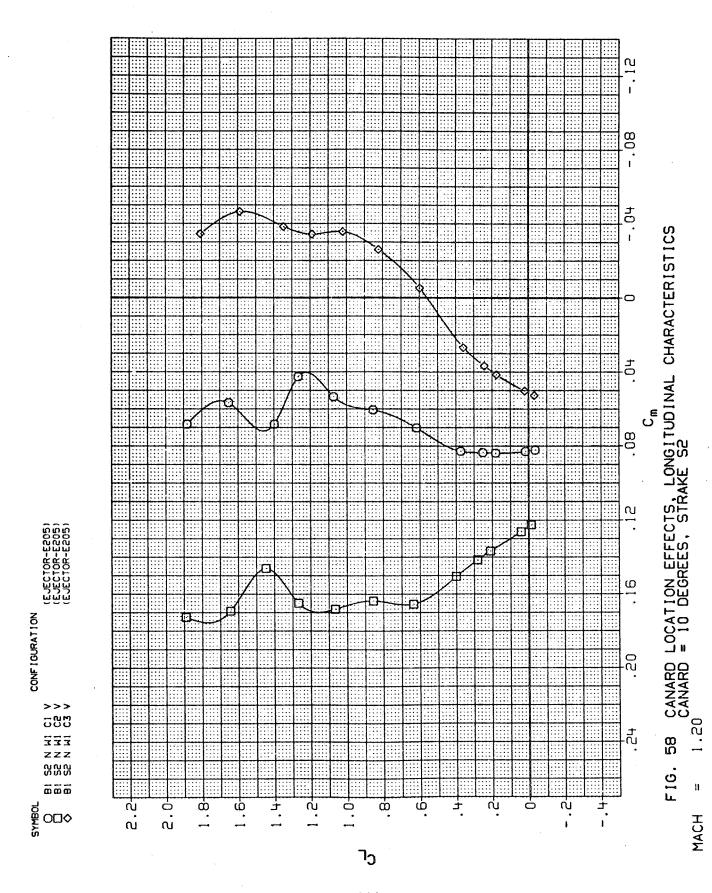


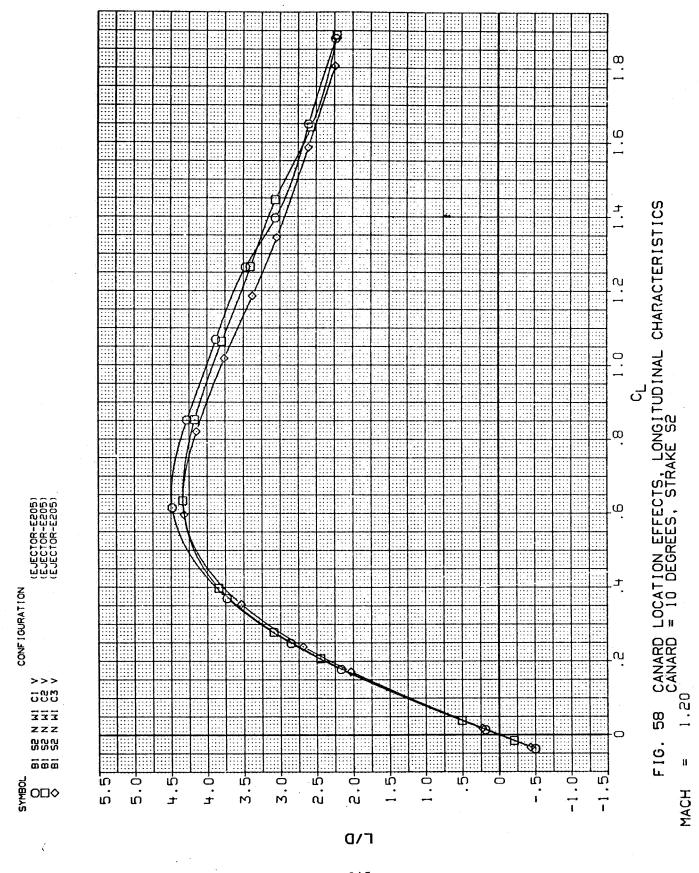




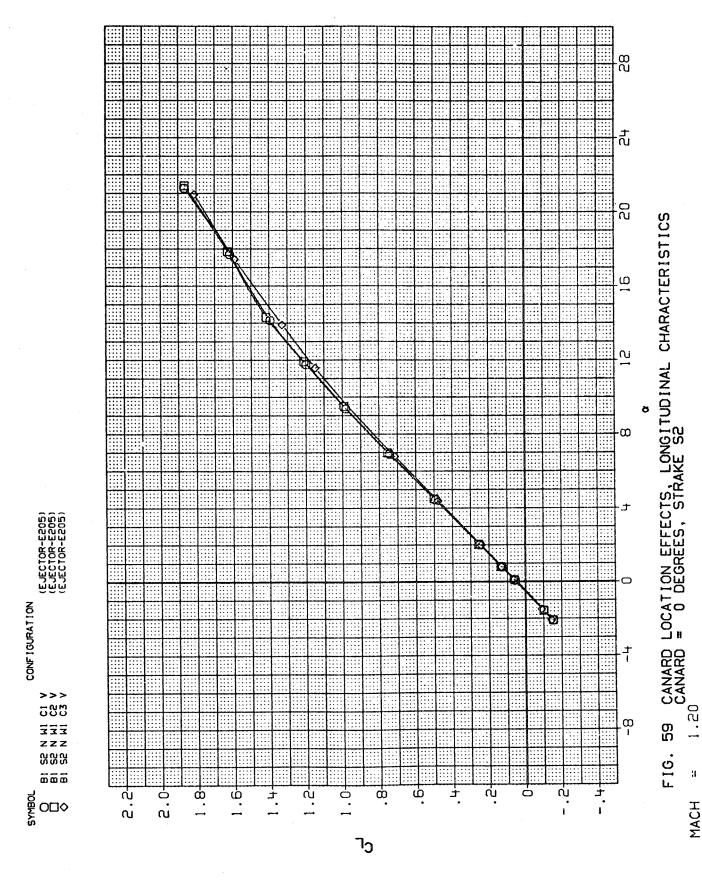


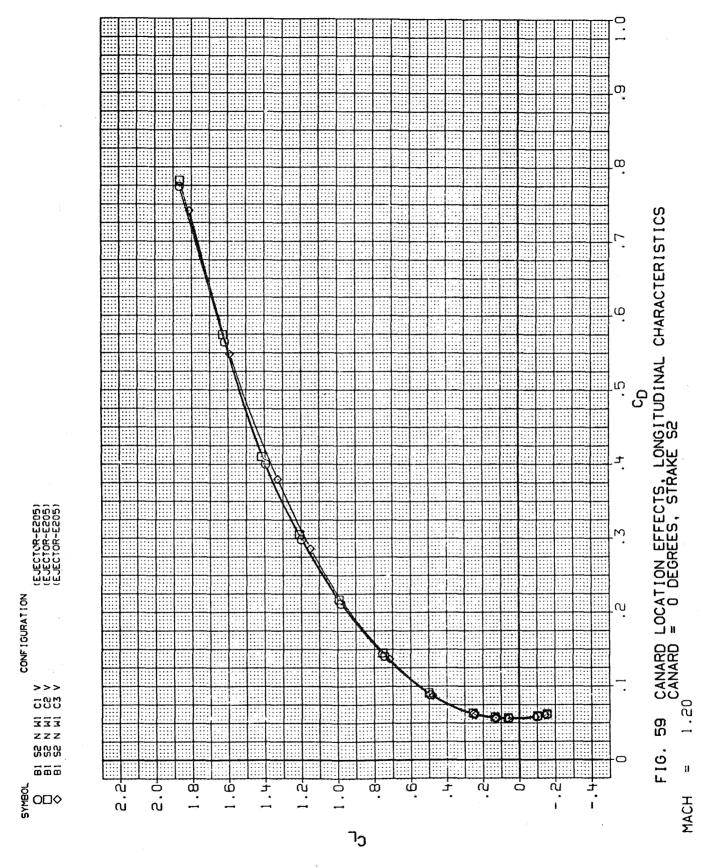


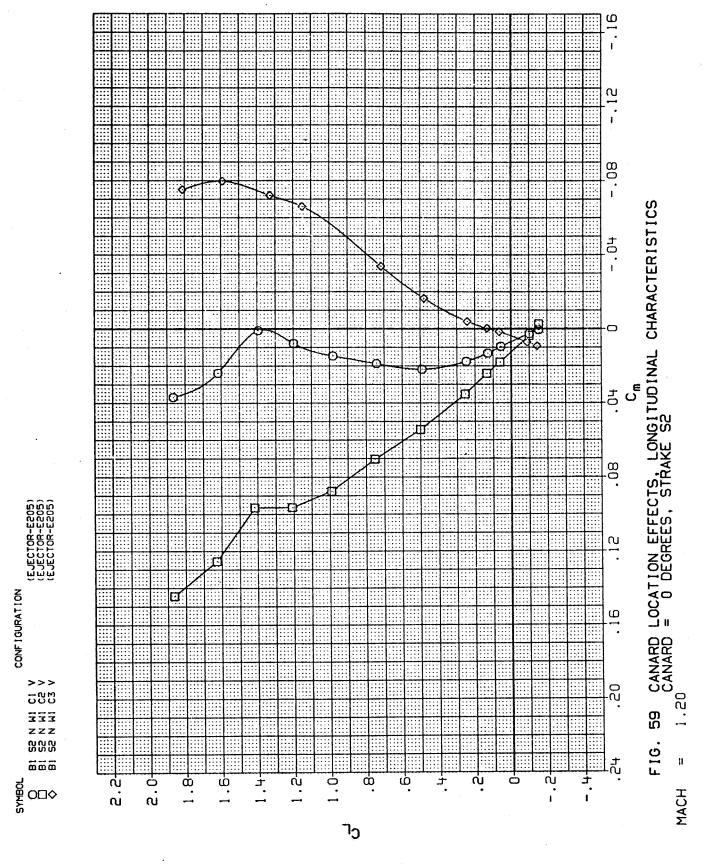


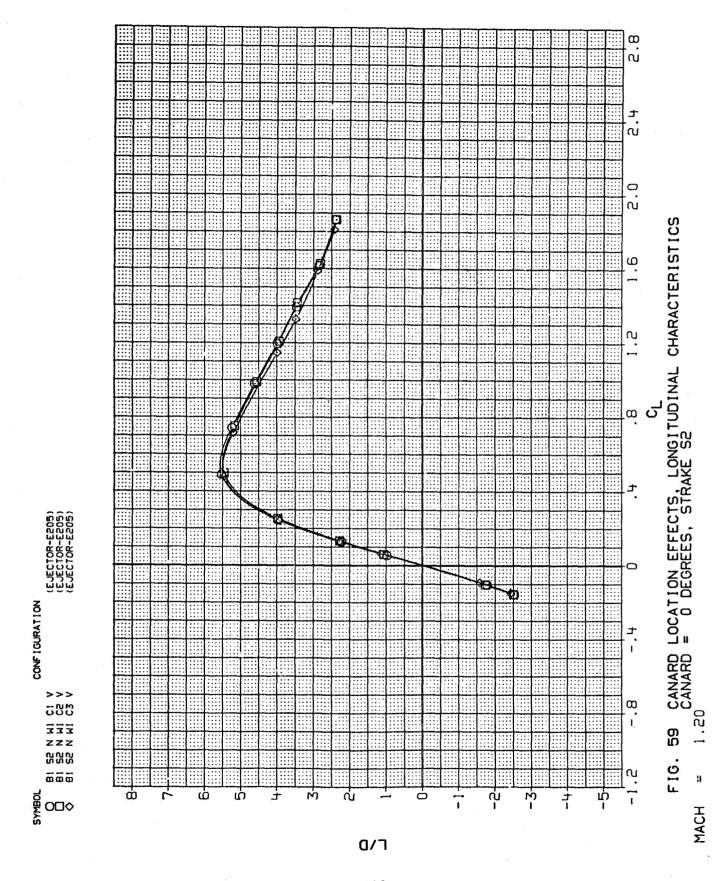


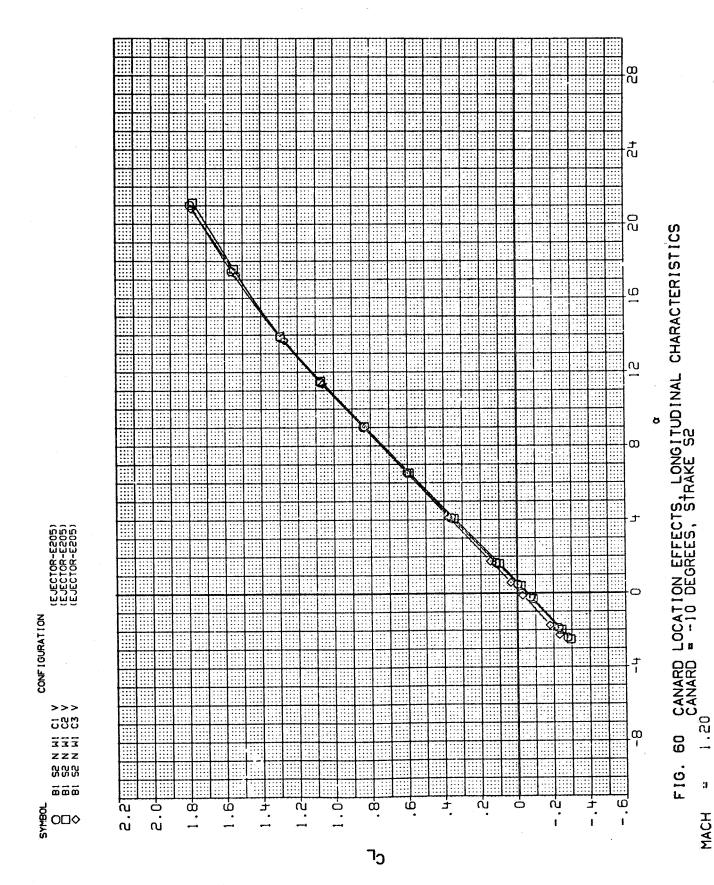
245



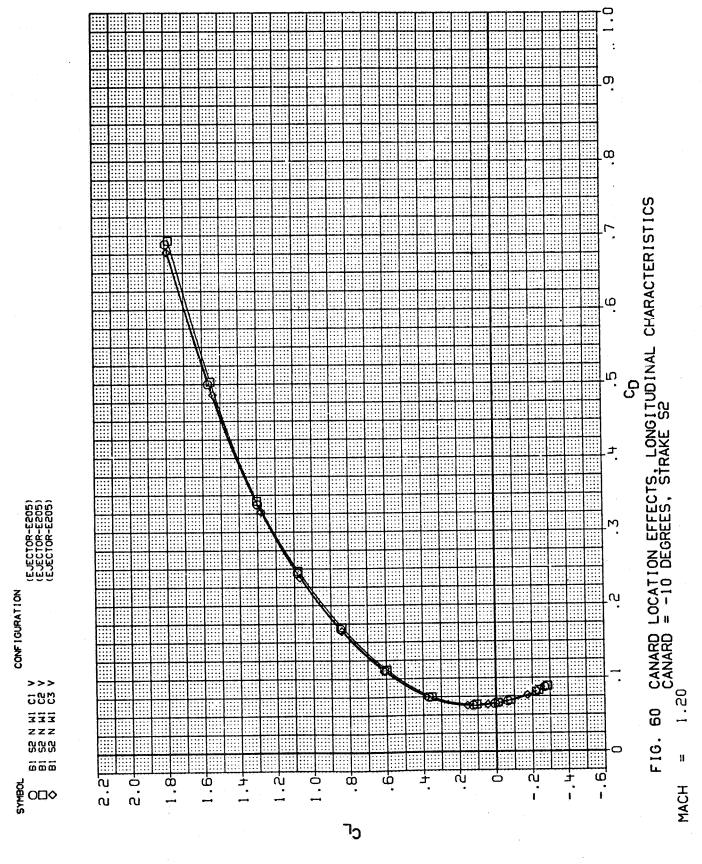


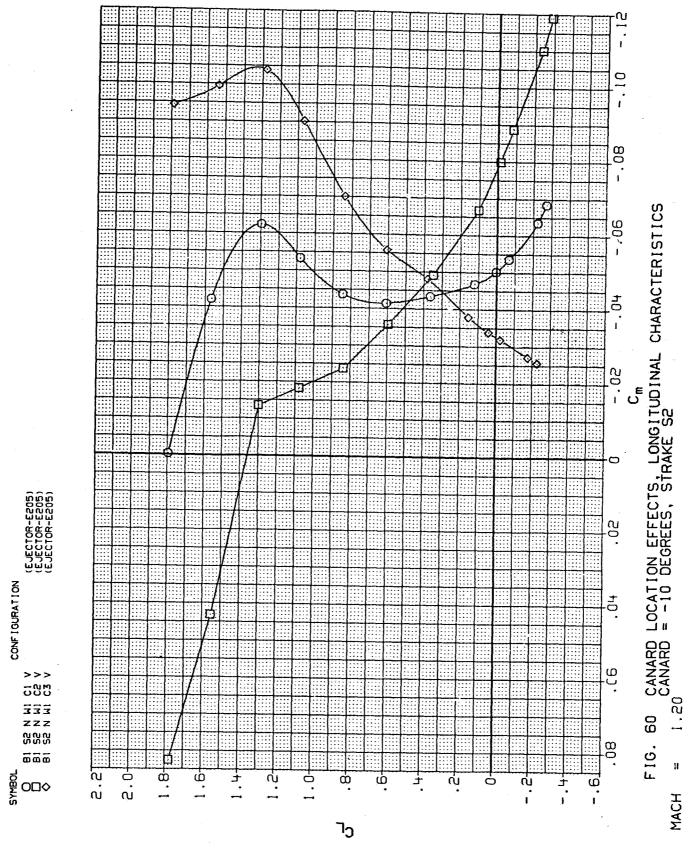


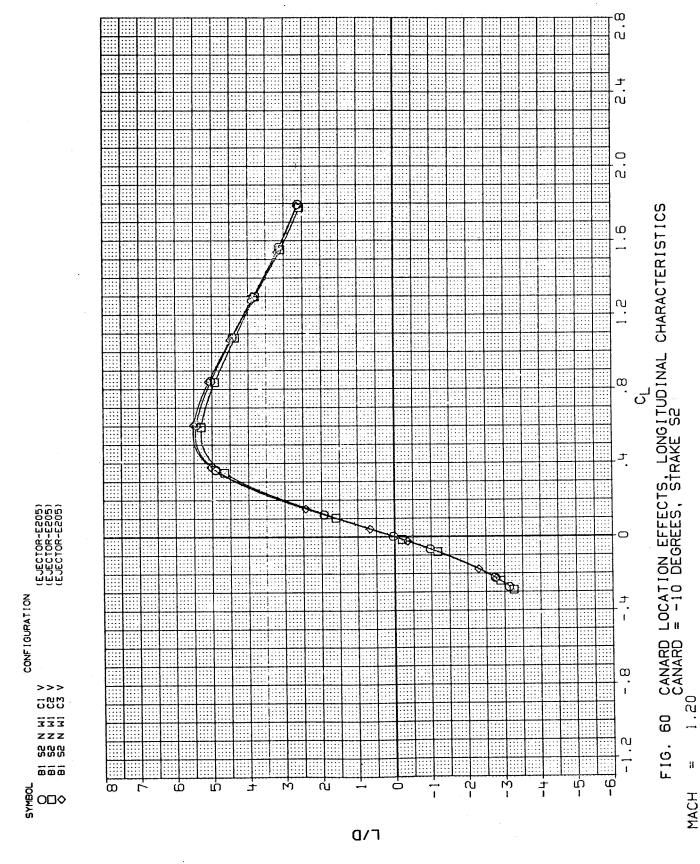


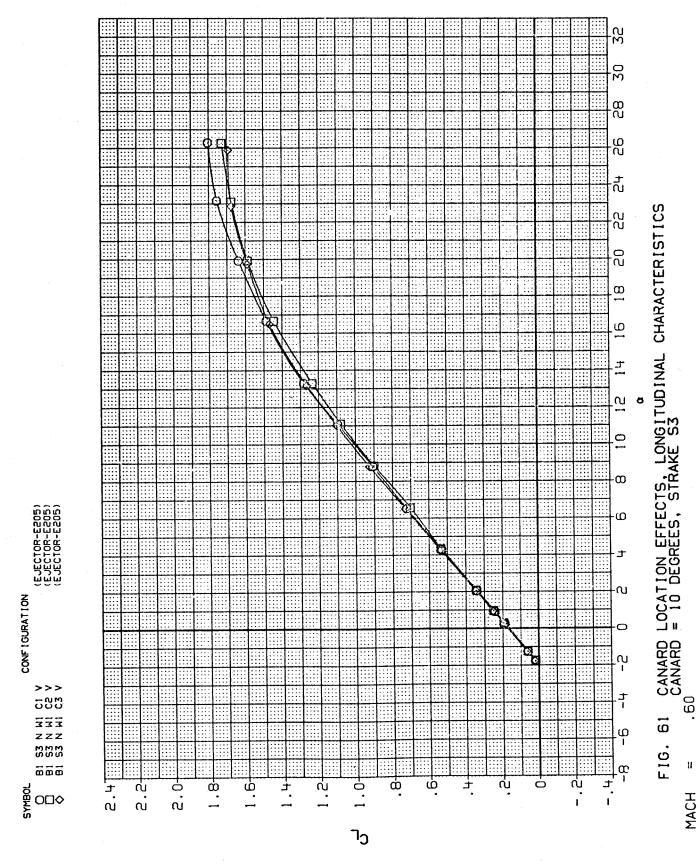


250

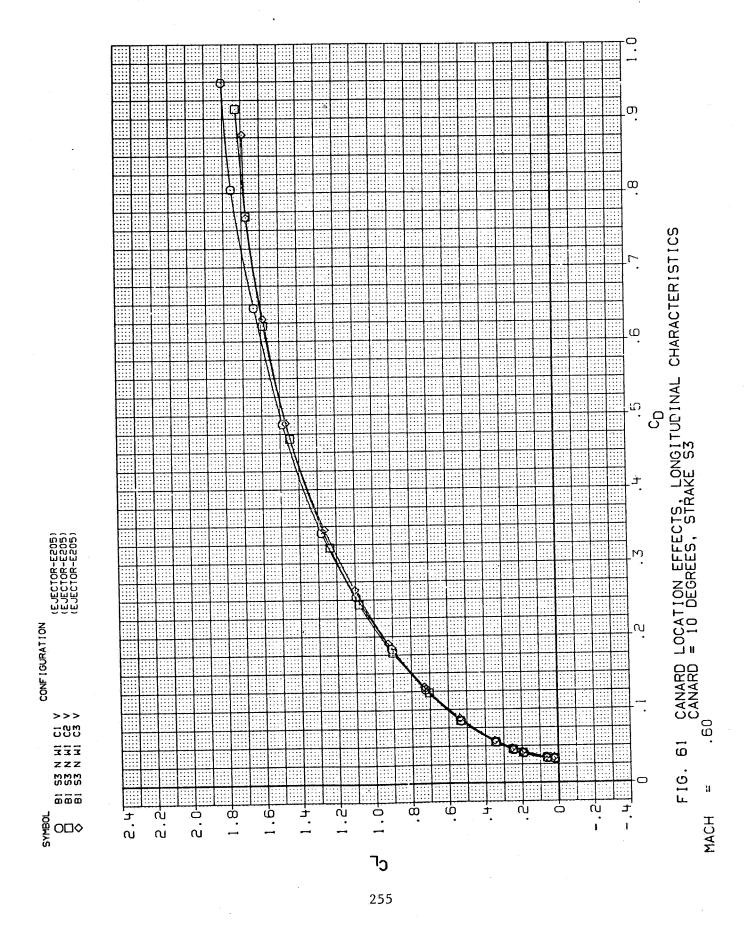


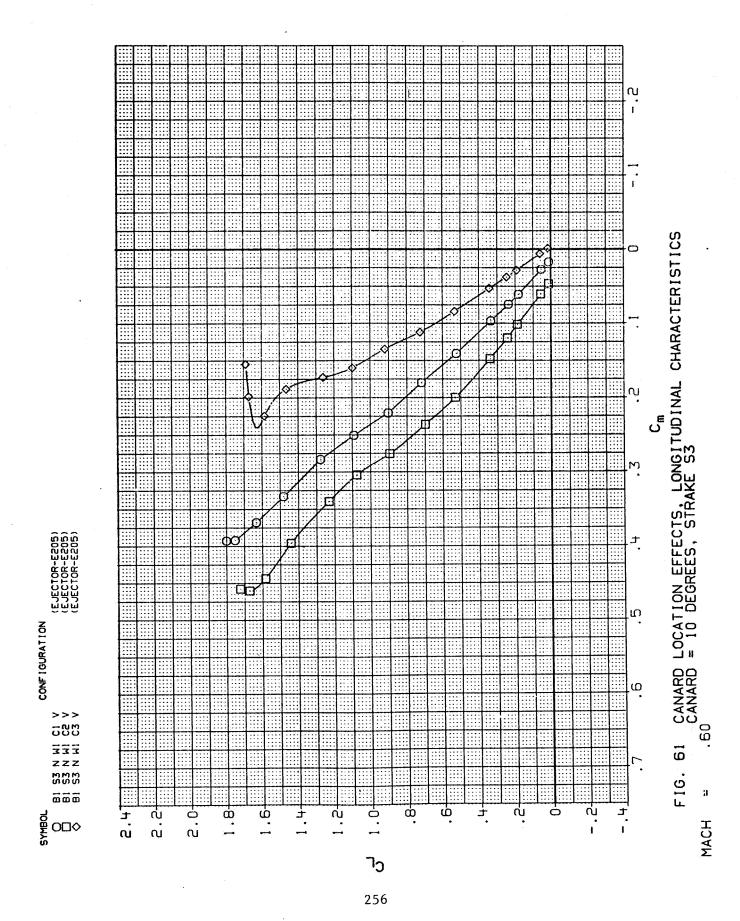


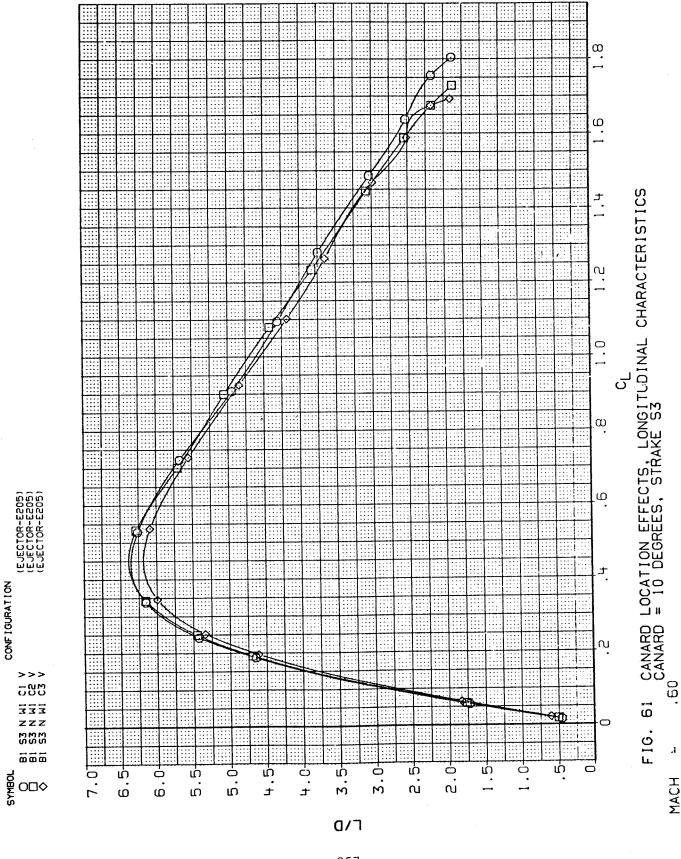


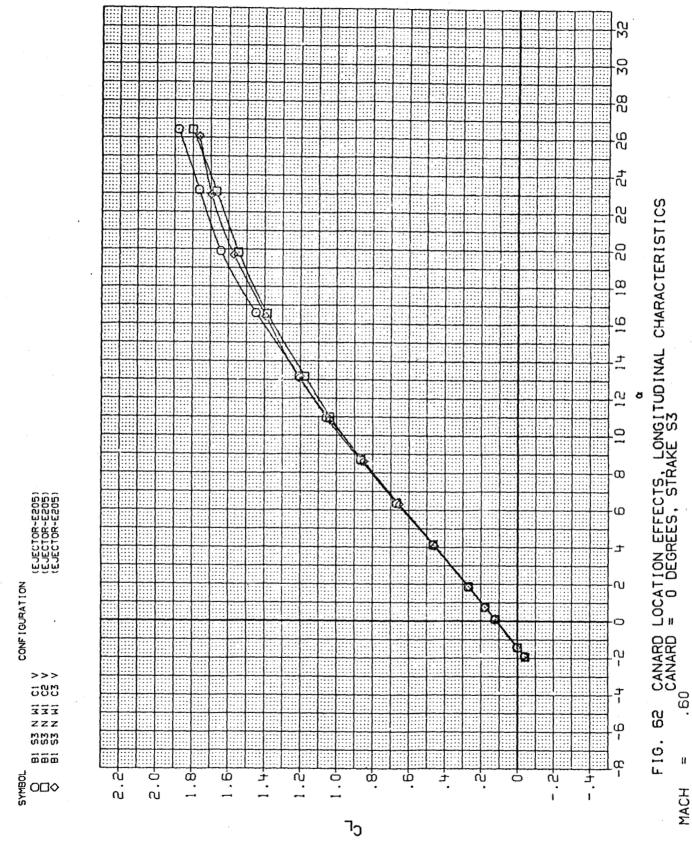


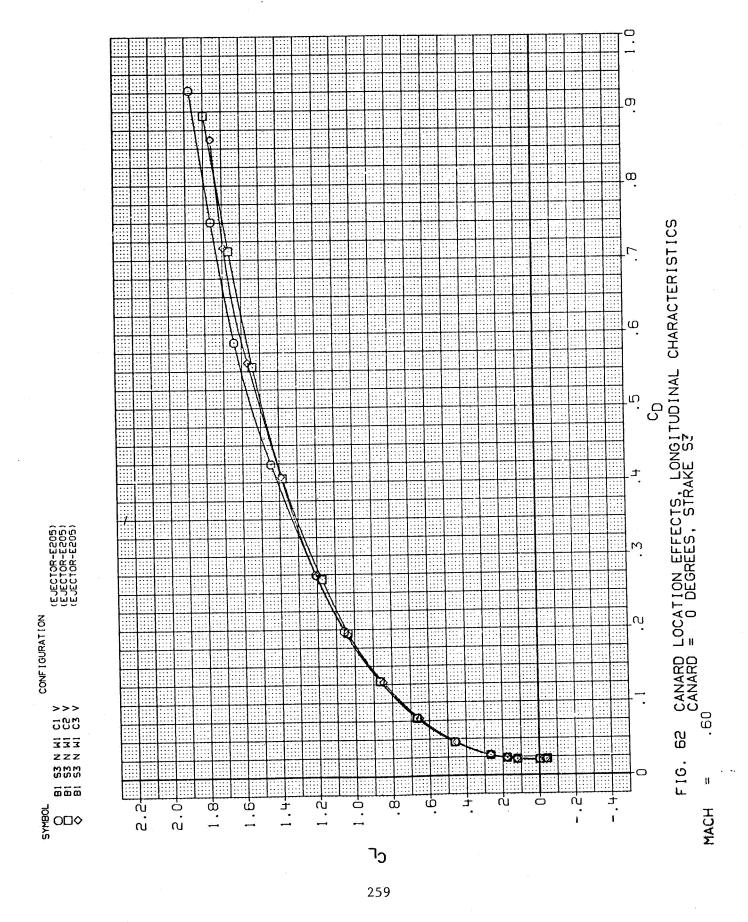
254

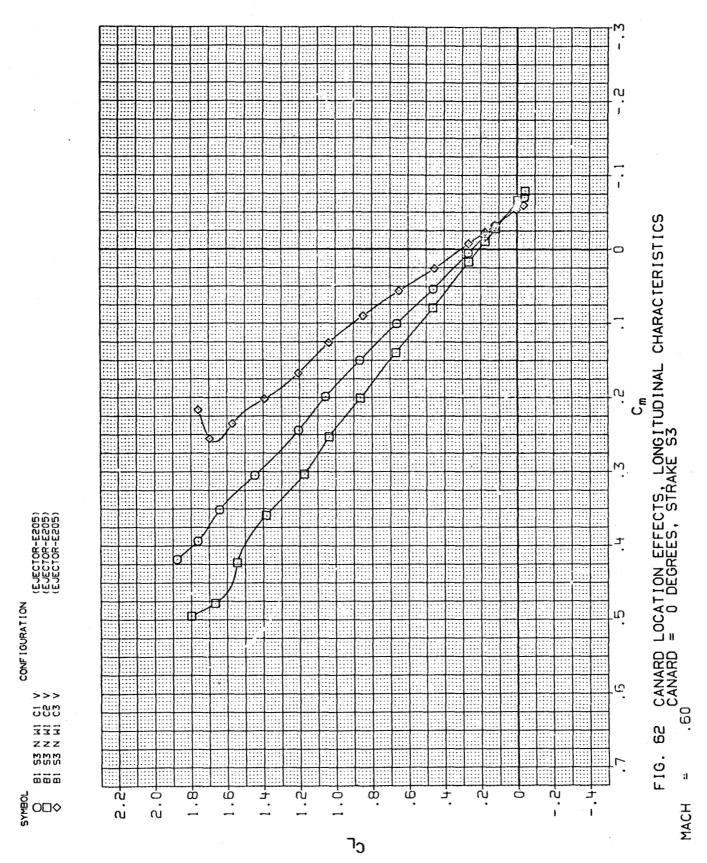


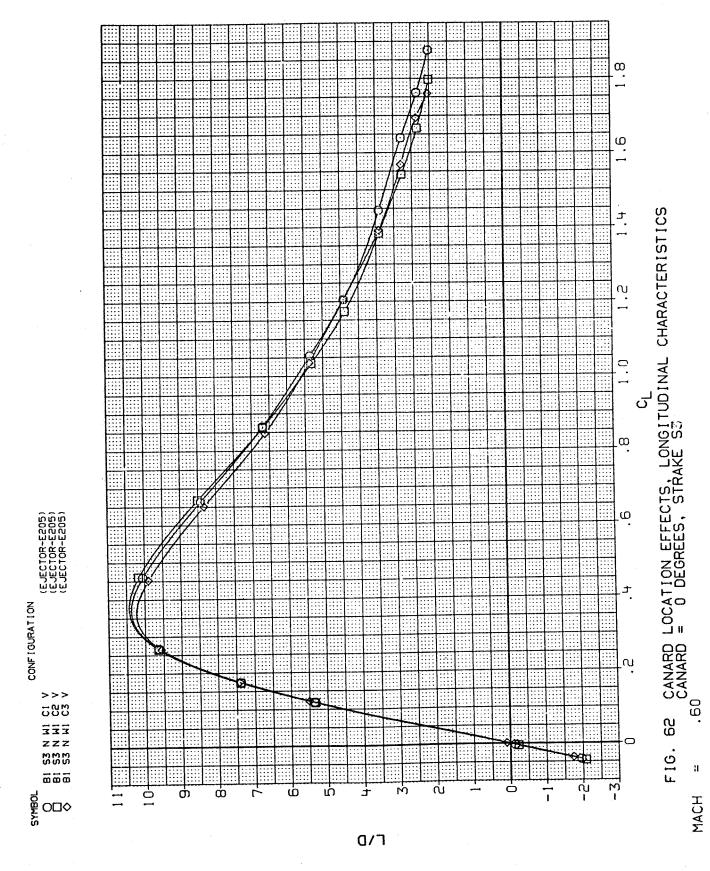


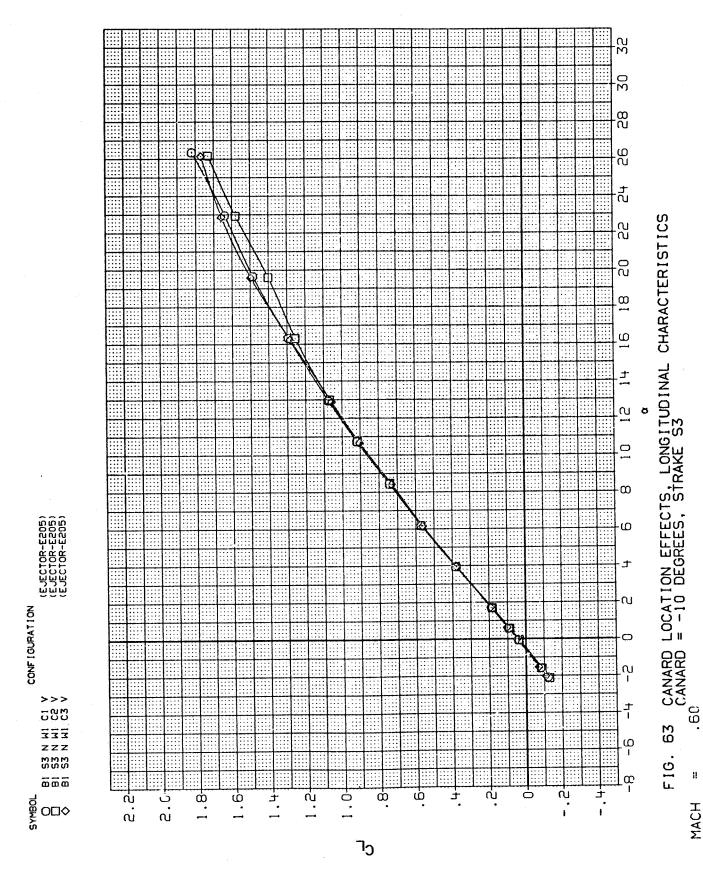


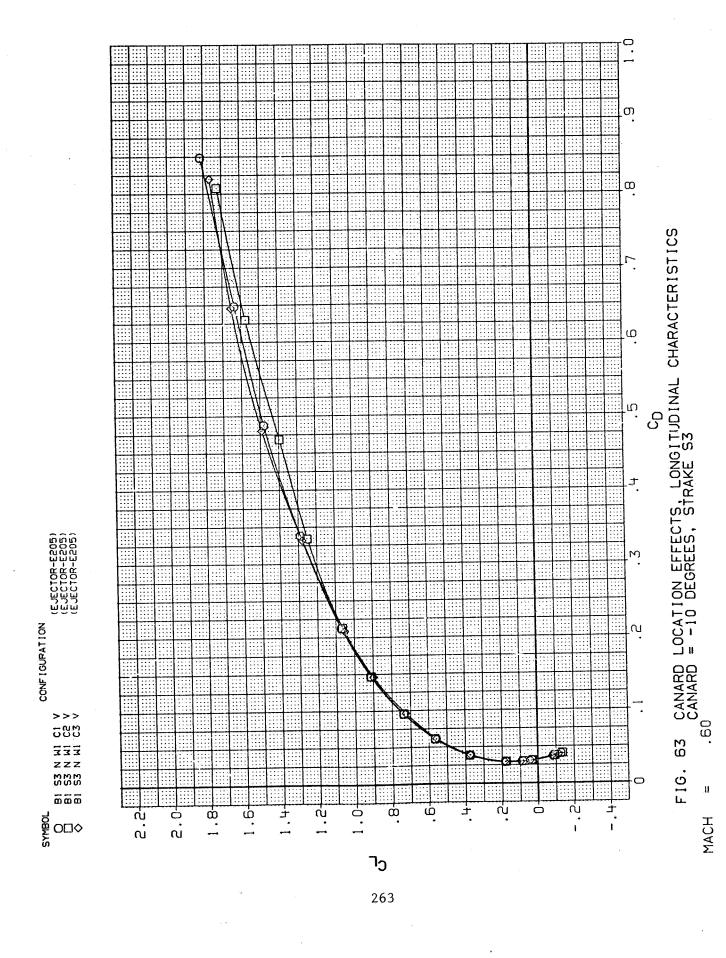


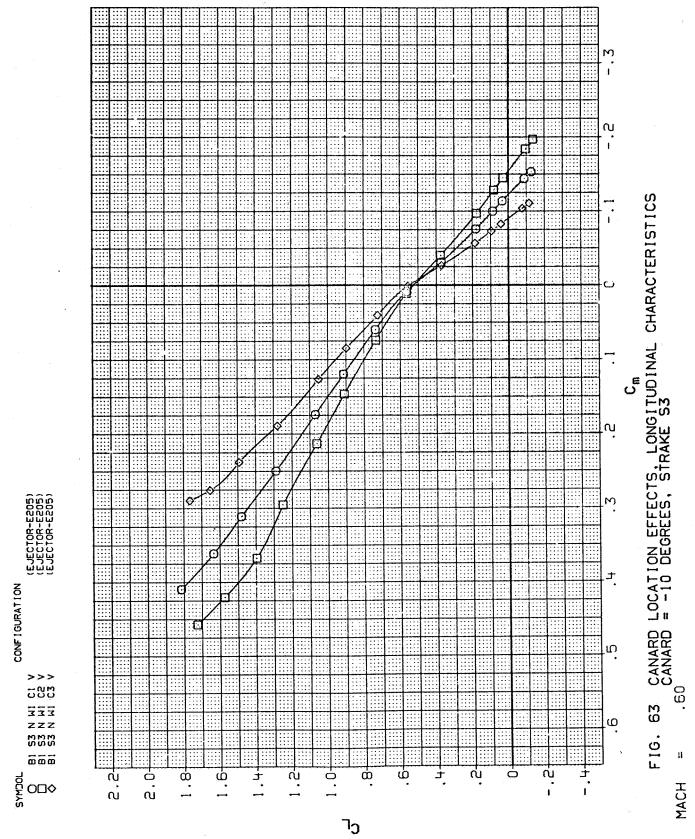




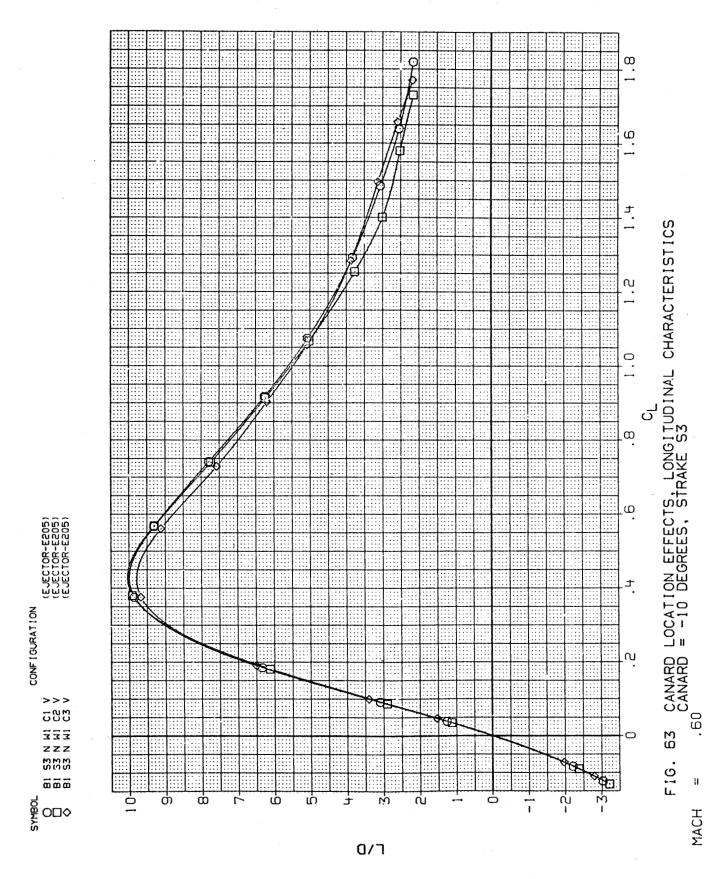


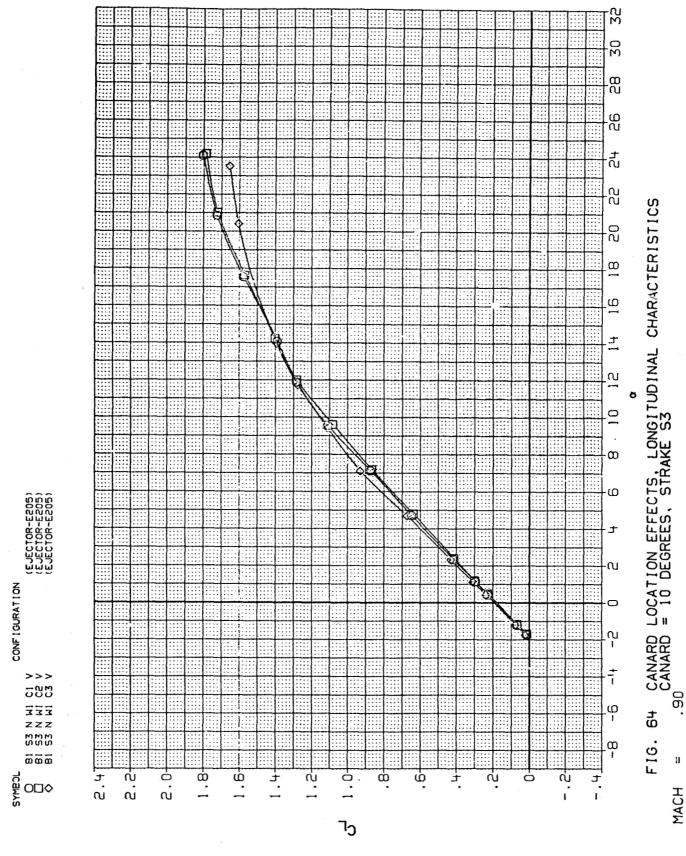




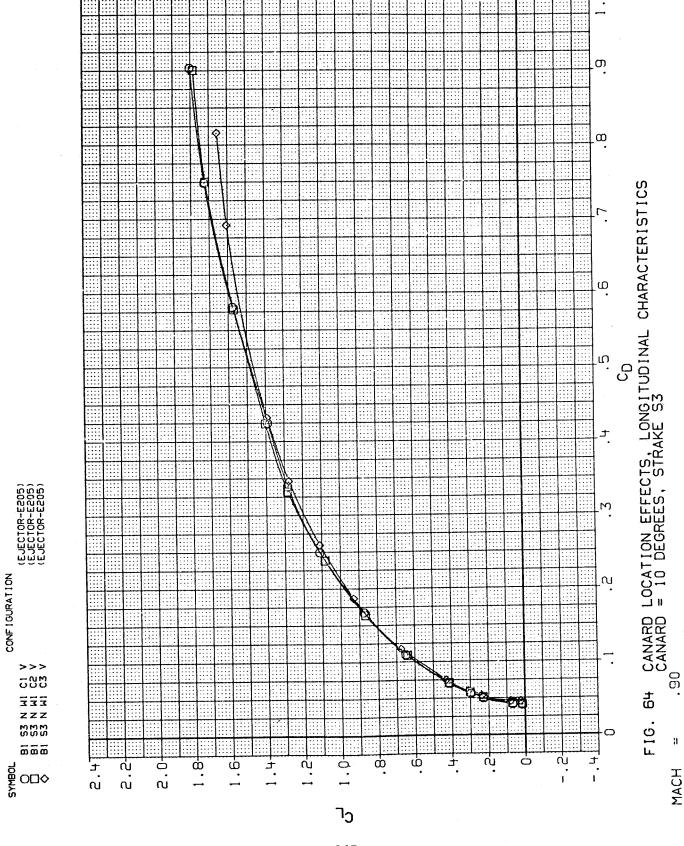


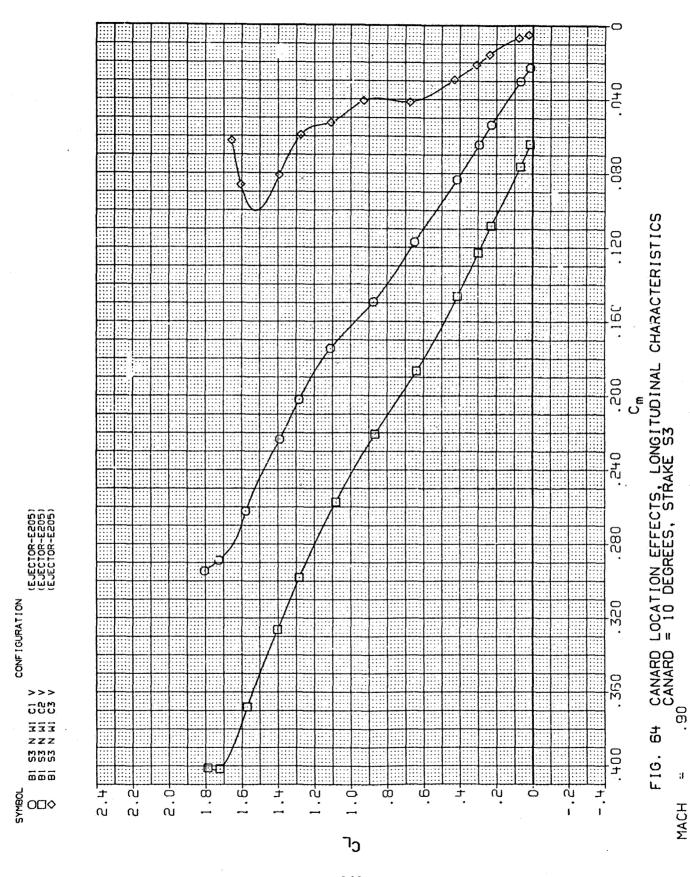
264

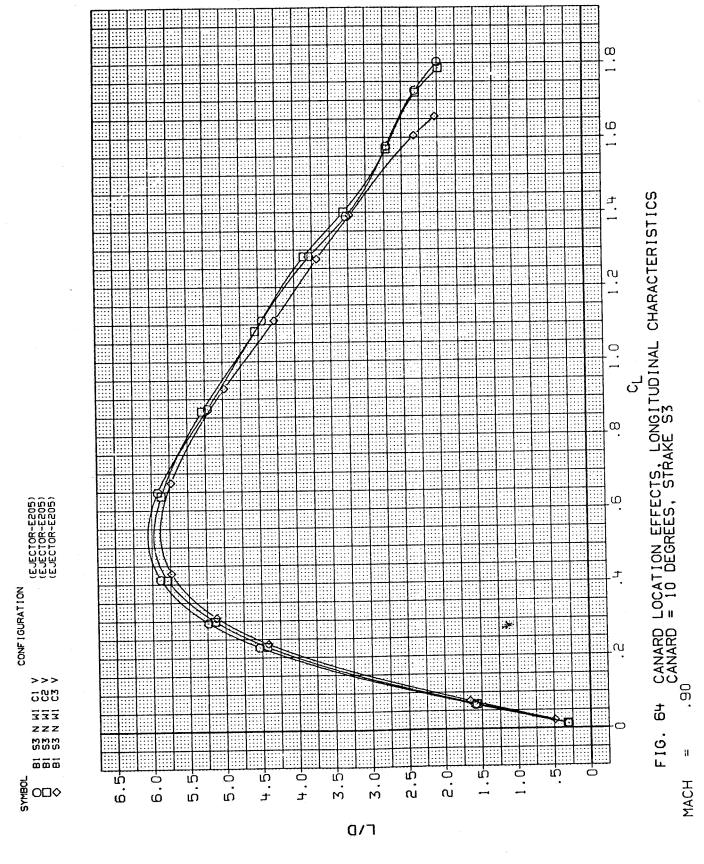


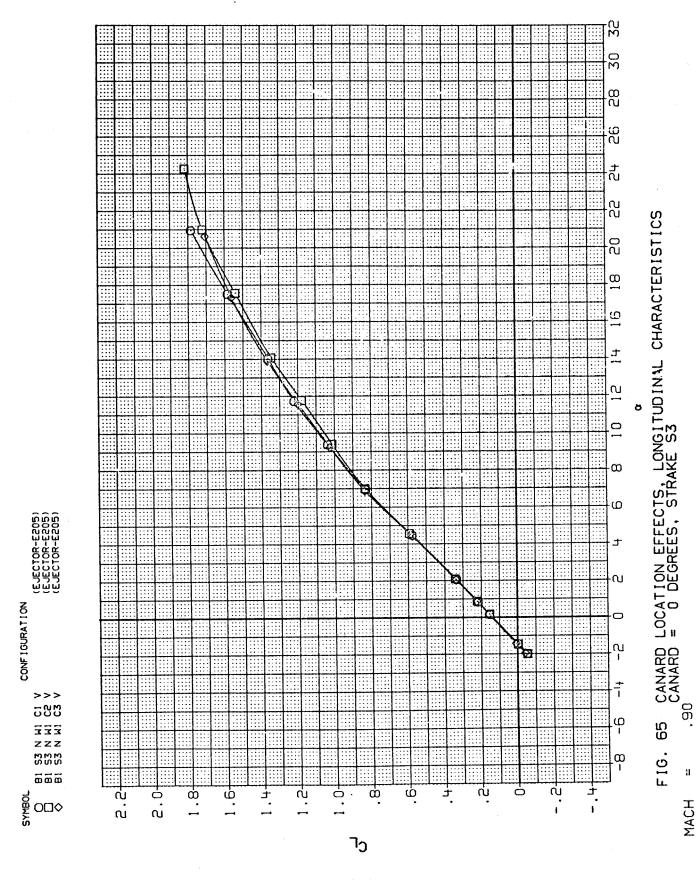


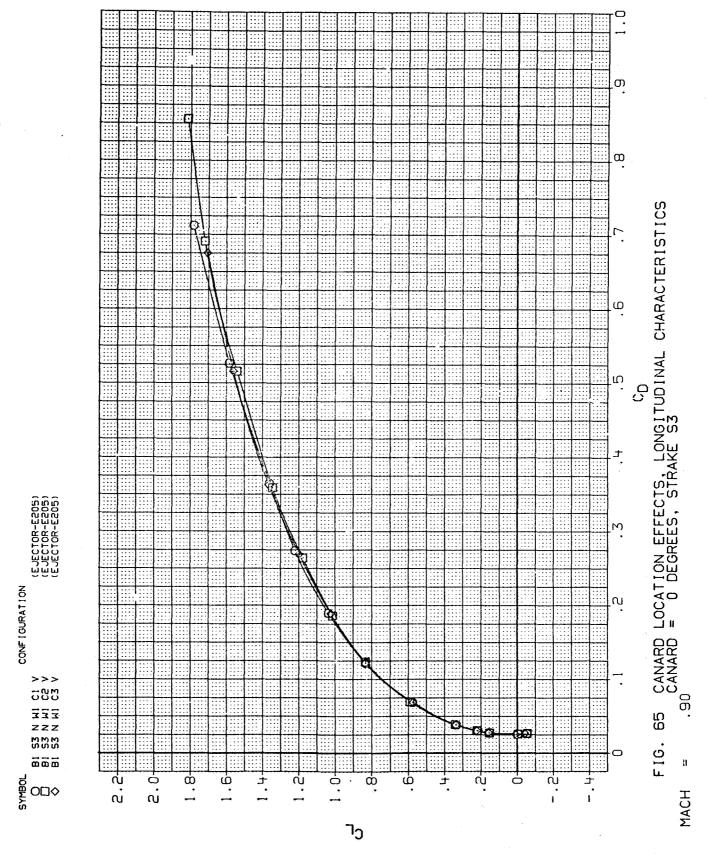
266

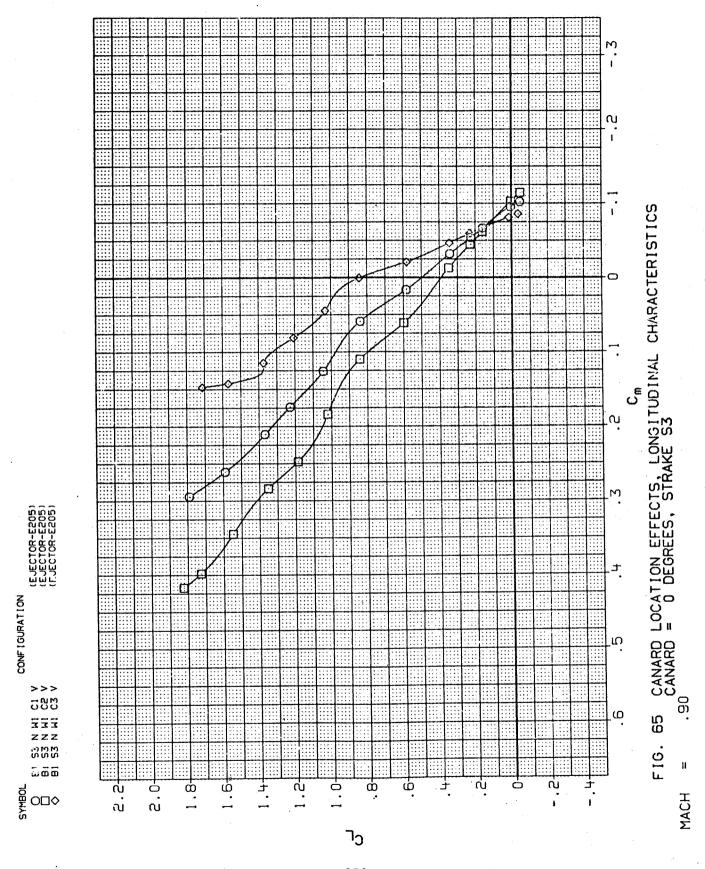


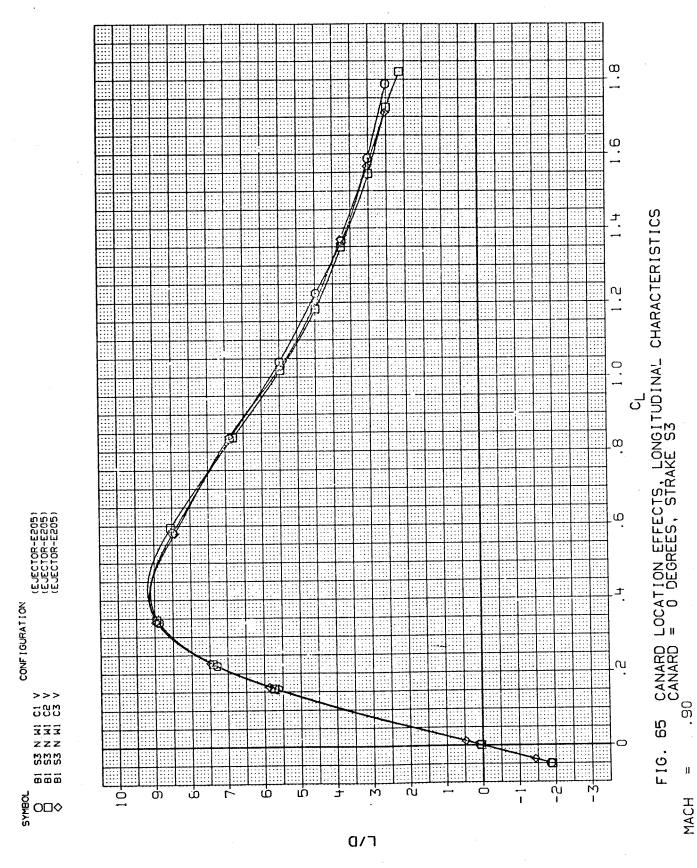


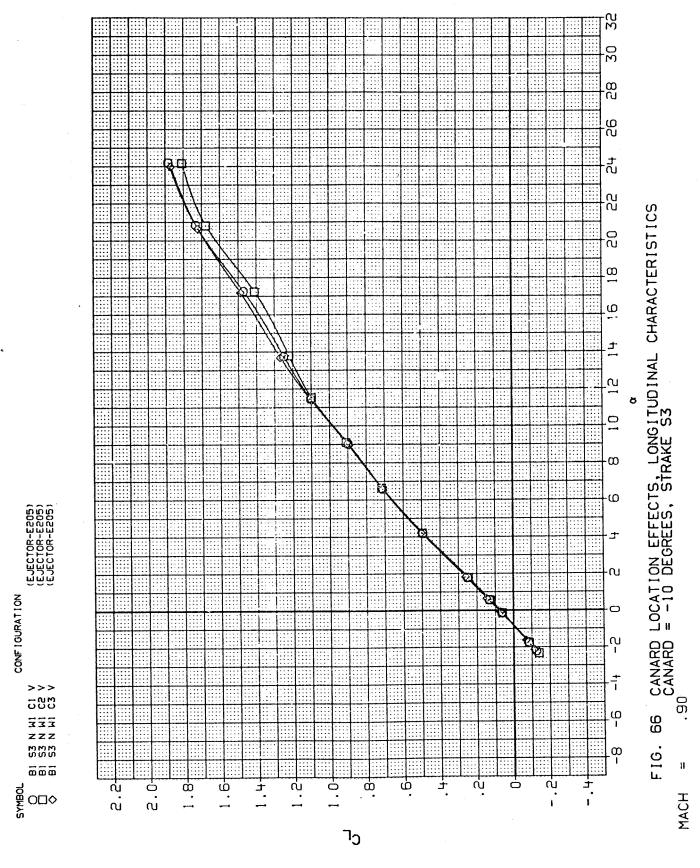


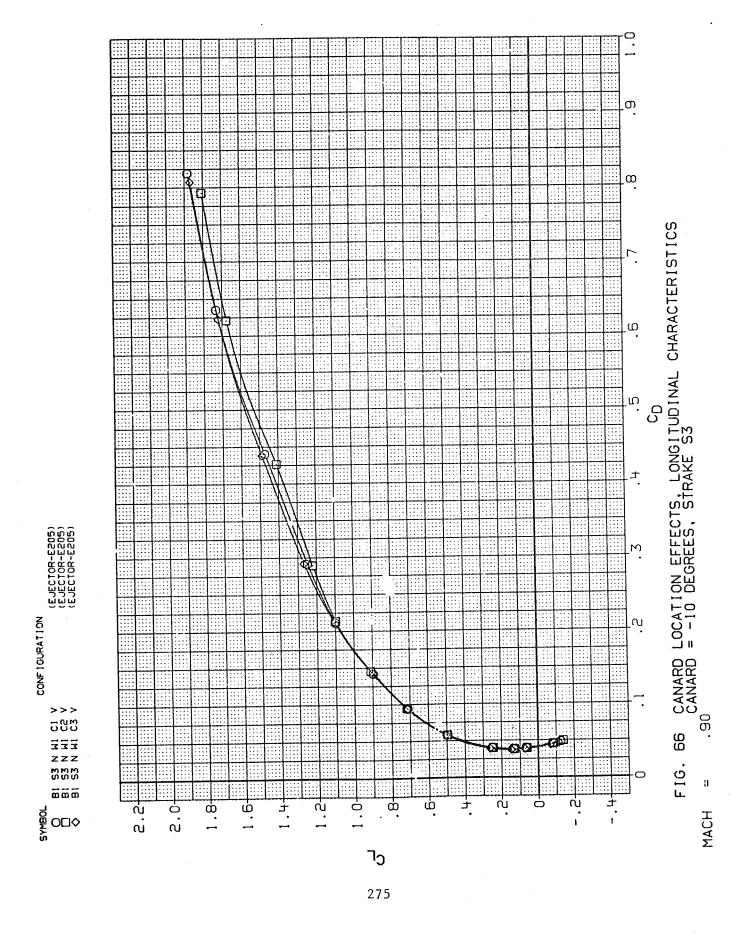


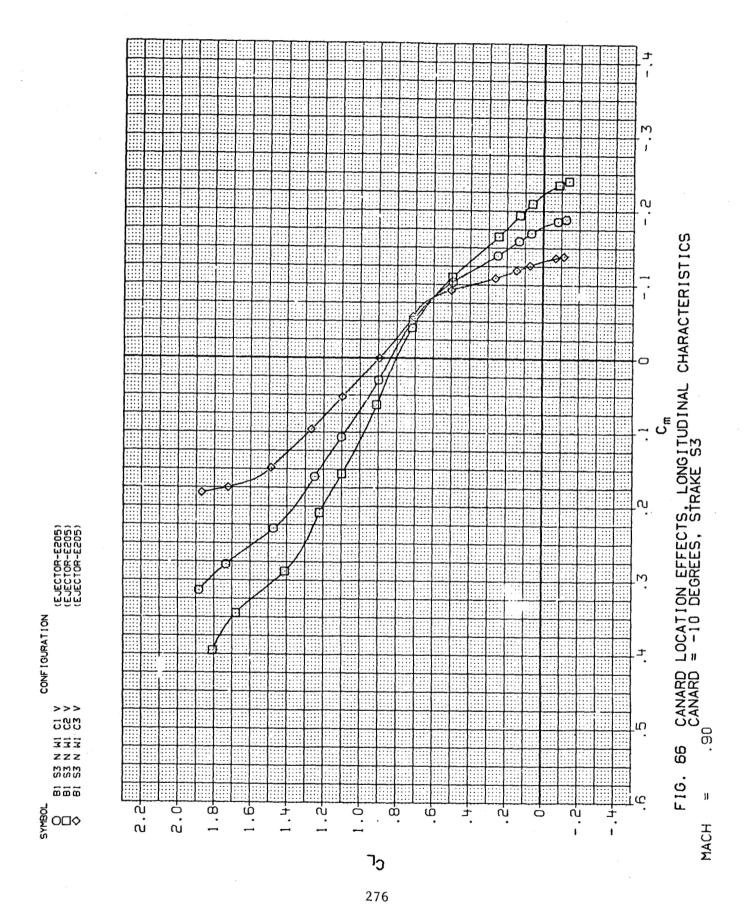


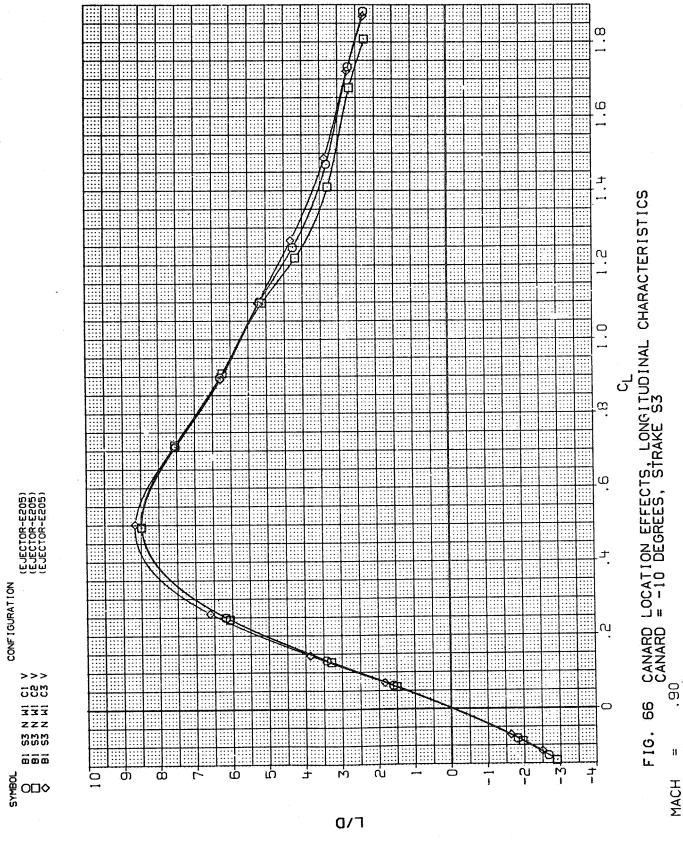


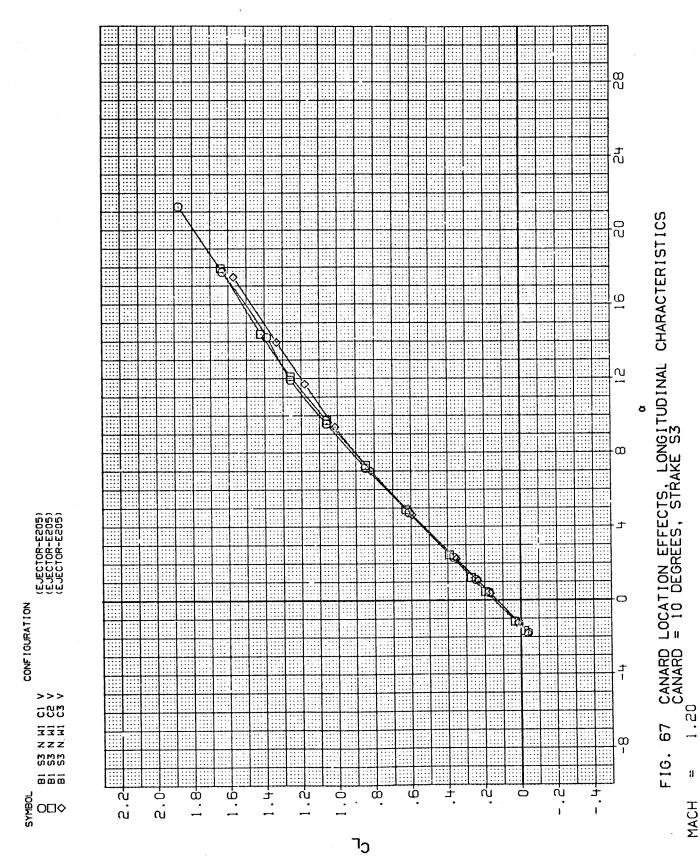




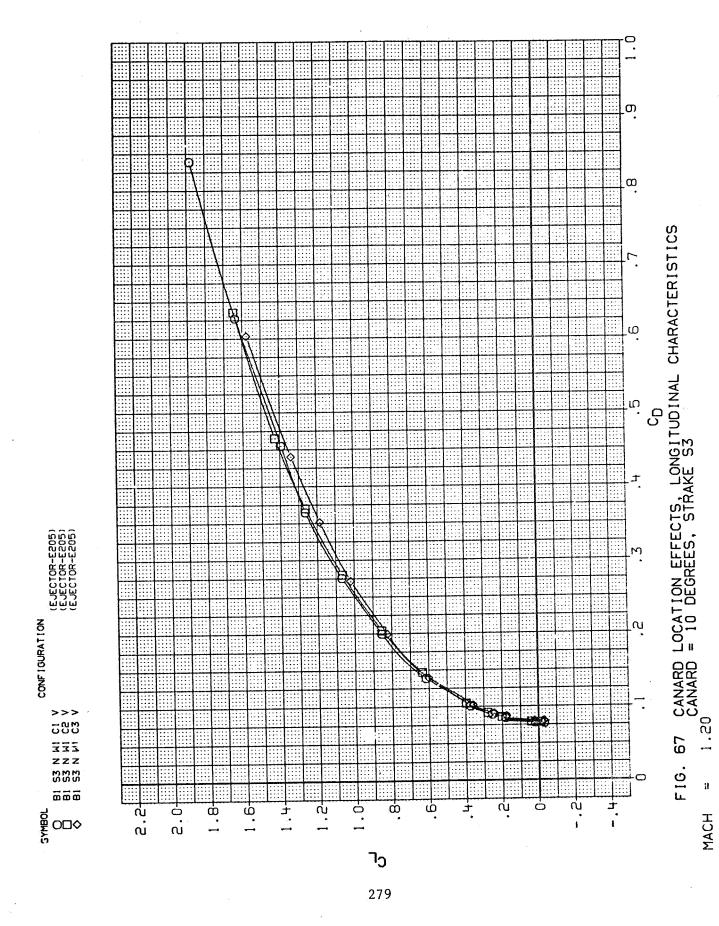


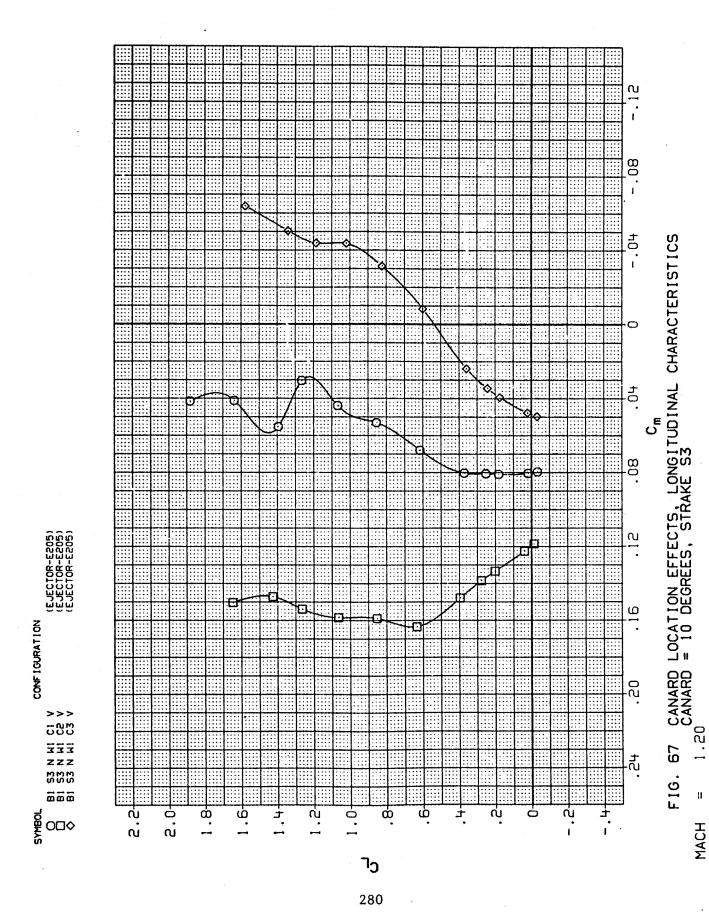


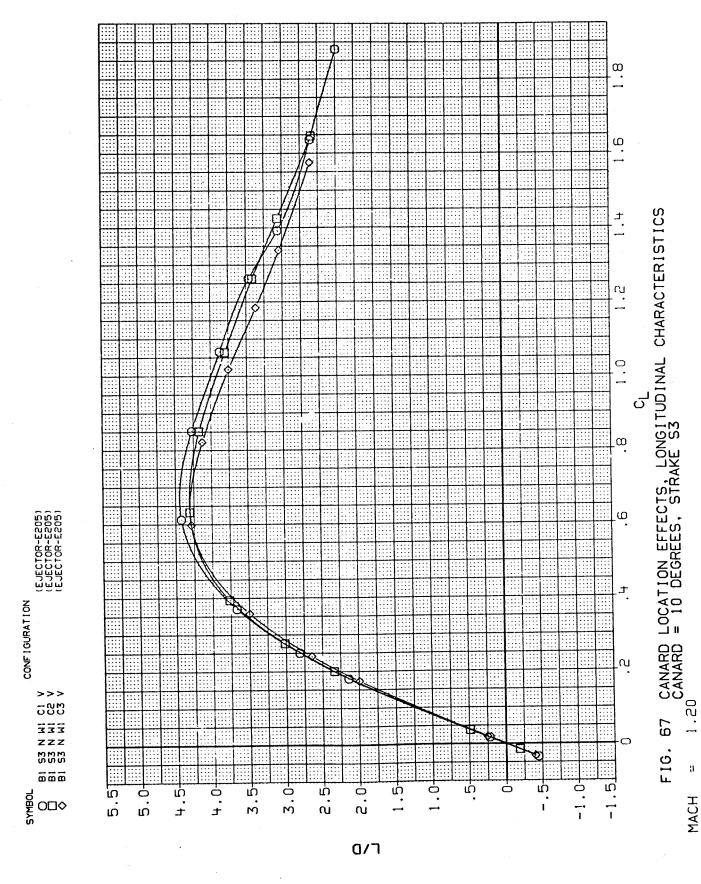




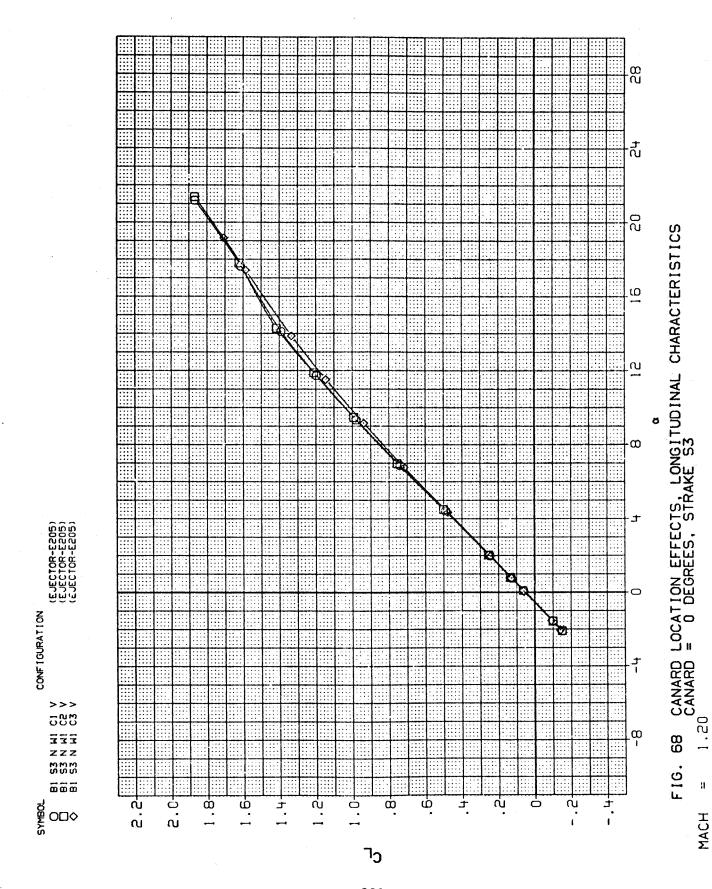
278

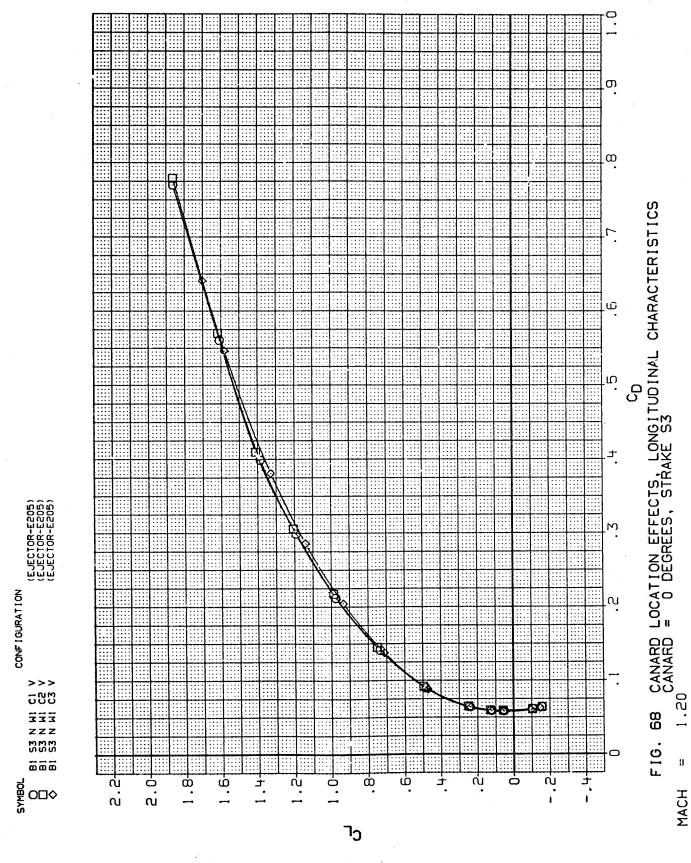




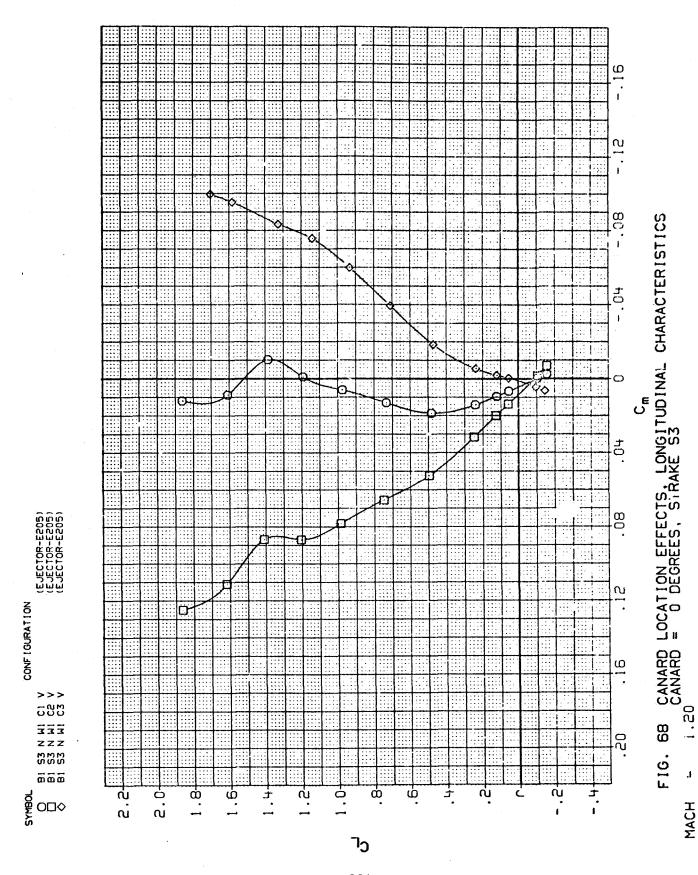


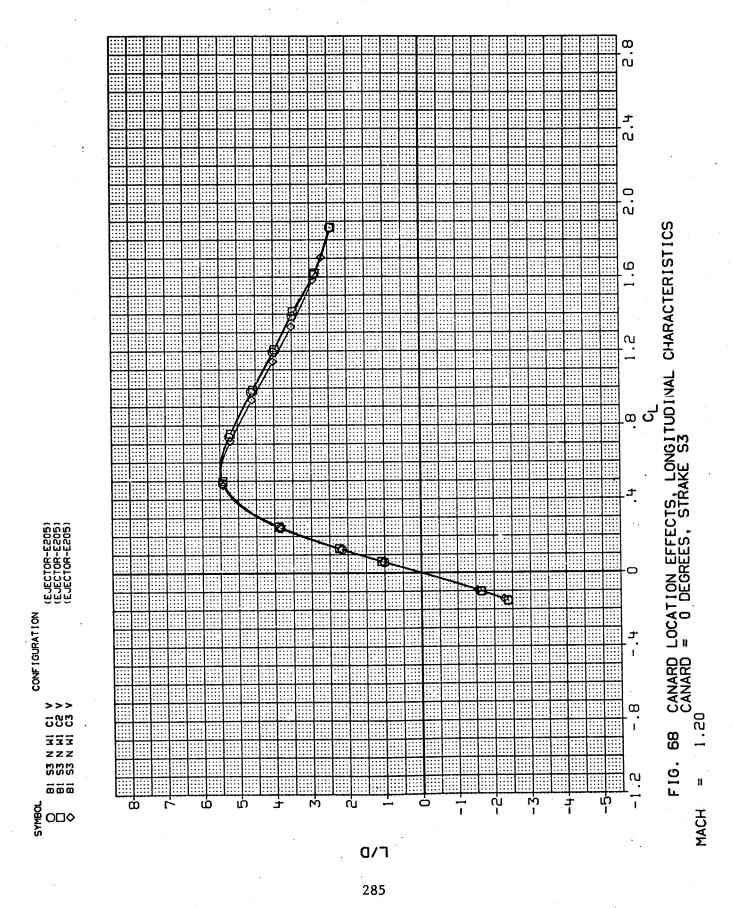
281

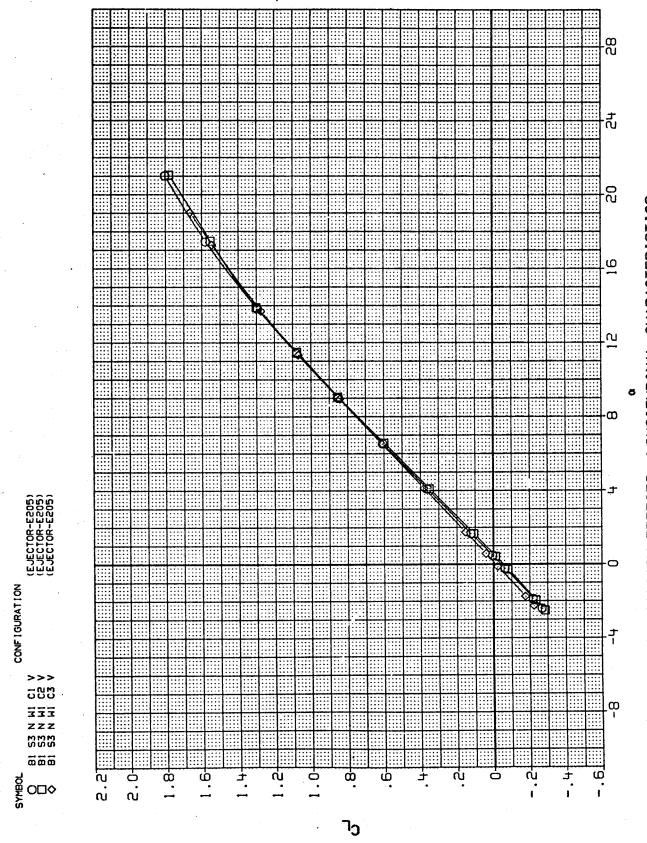




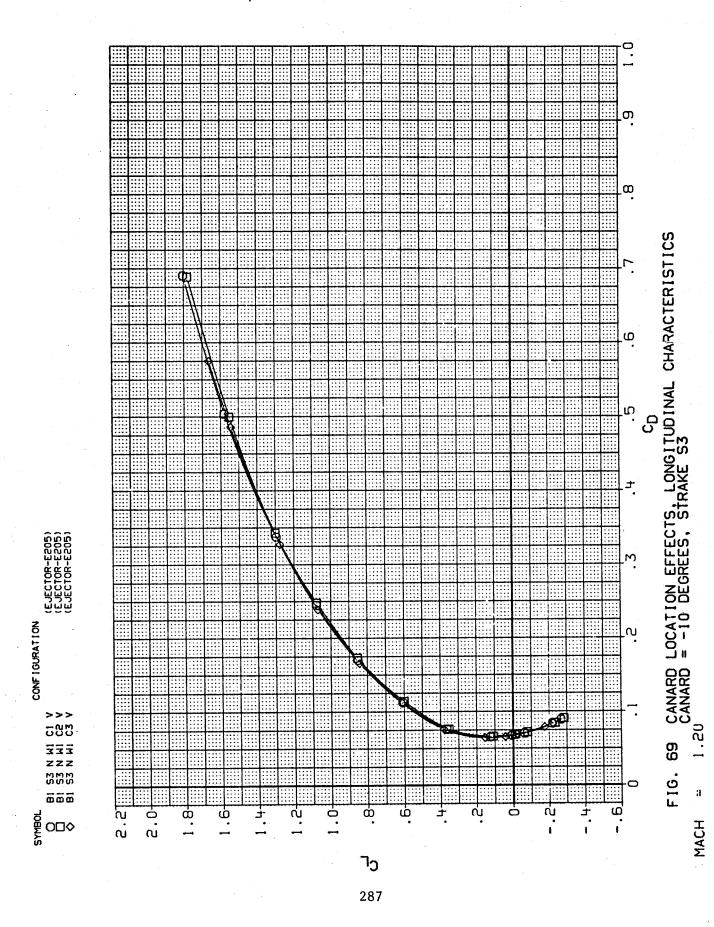
283

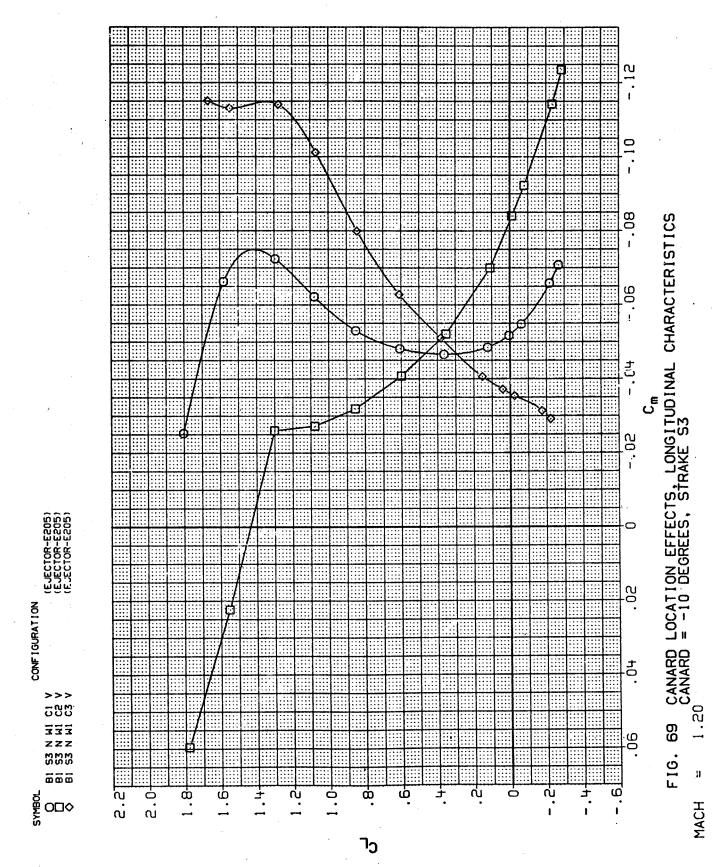




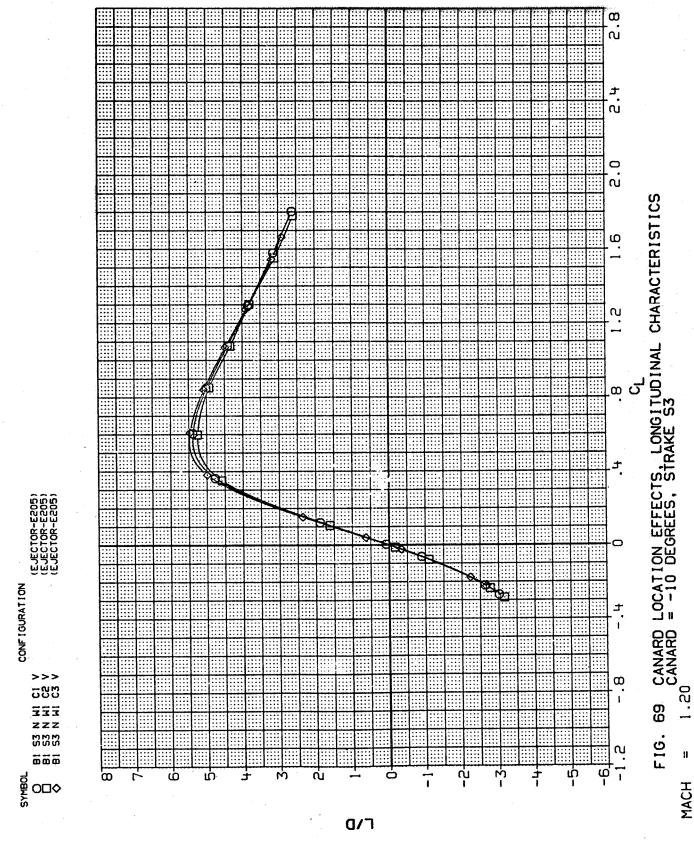


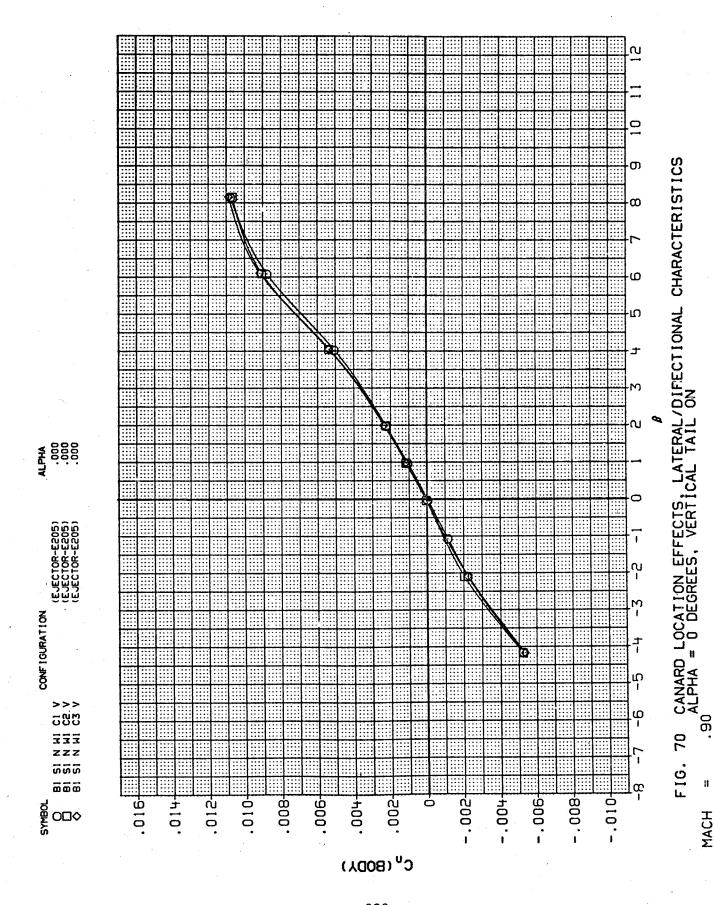
69 CANARD LOCATION EFFECTS, LONGITUDINAL CHARACTERISTICS CANARD = -10 DEGREES, STRAKE S3 1.20 :1 MACH

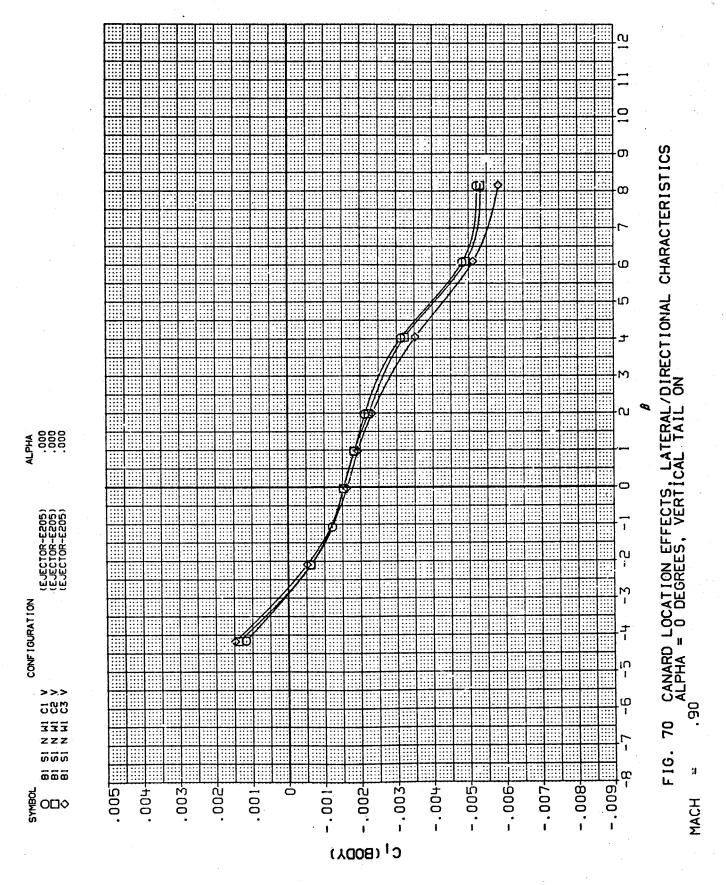


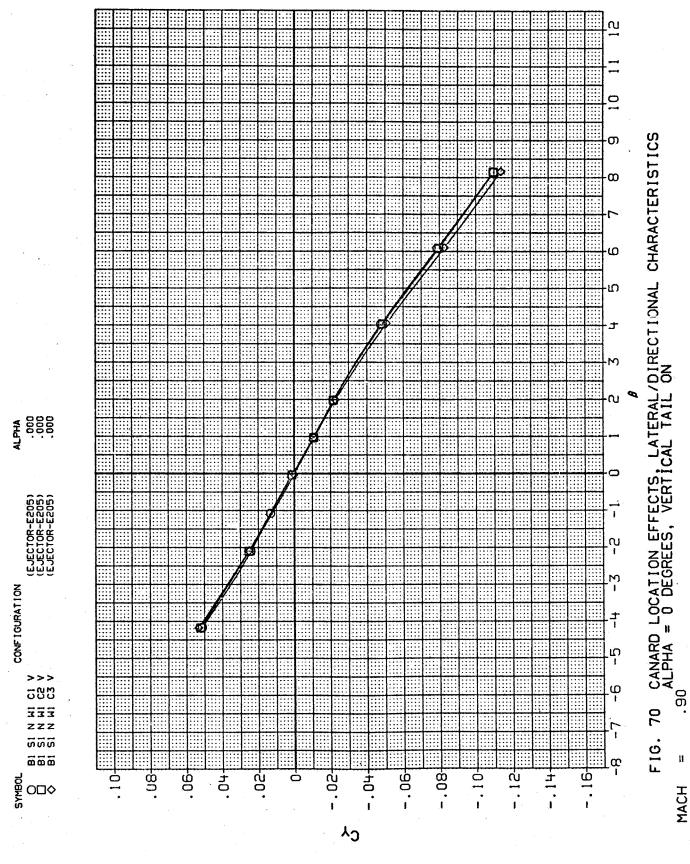


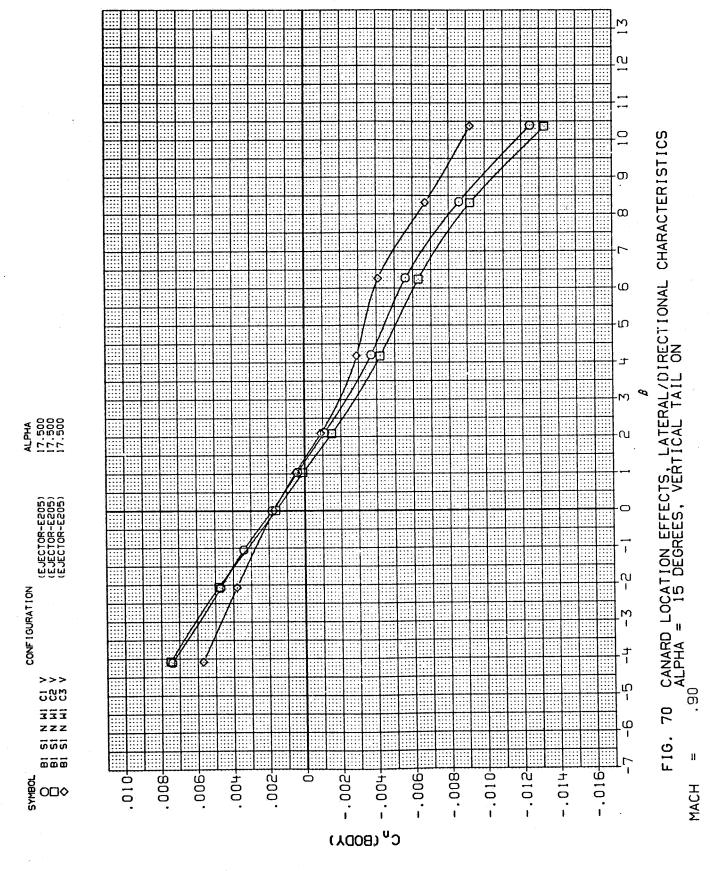
288

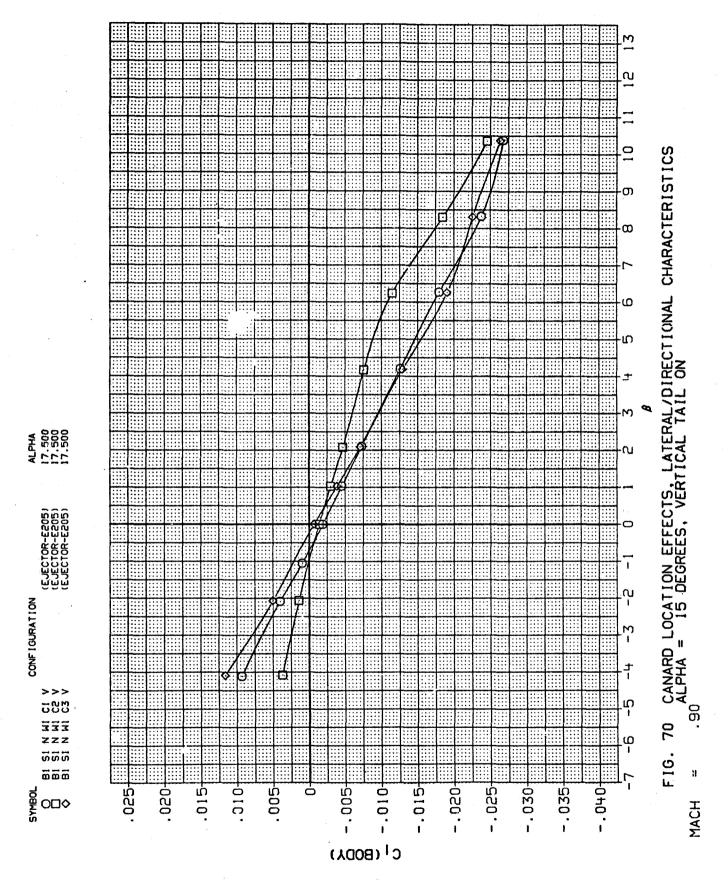


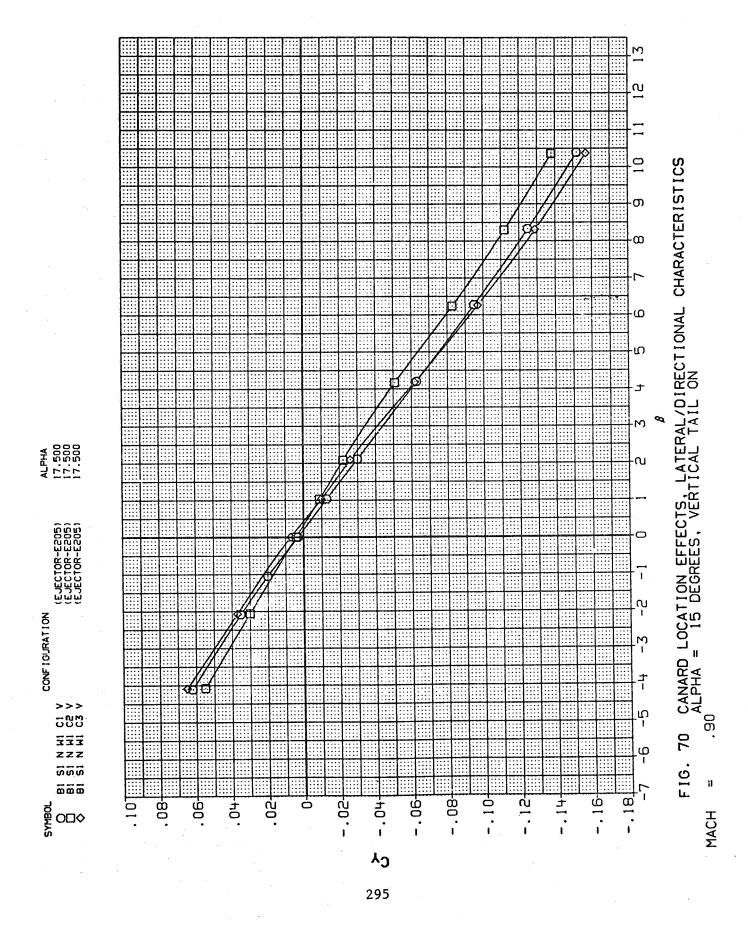


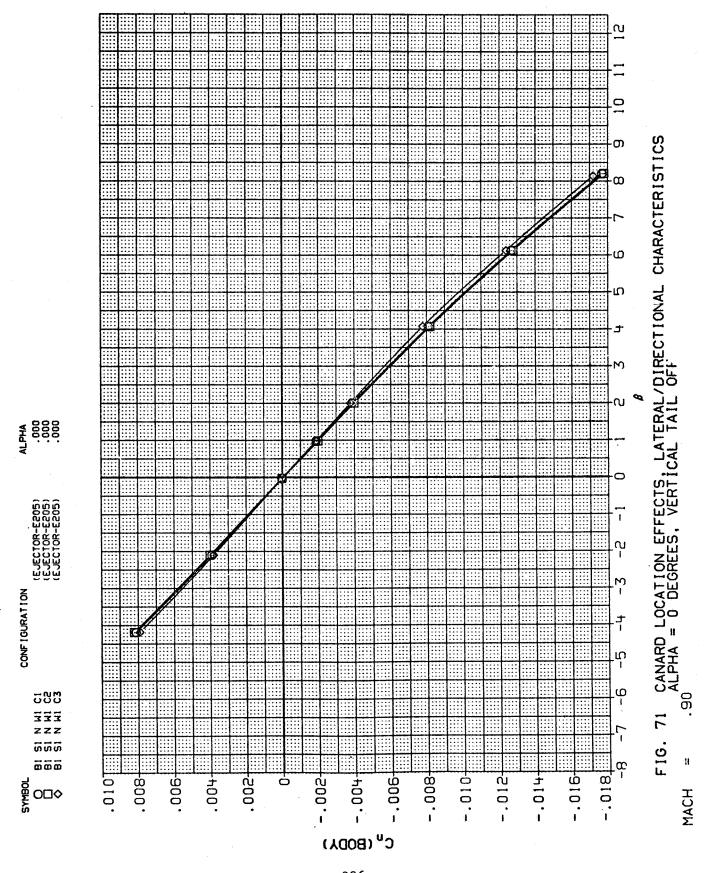


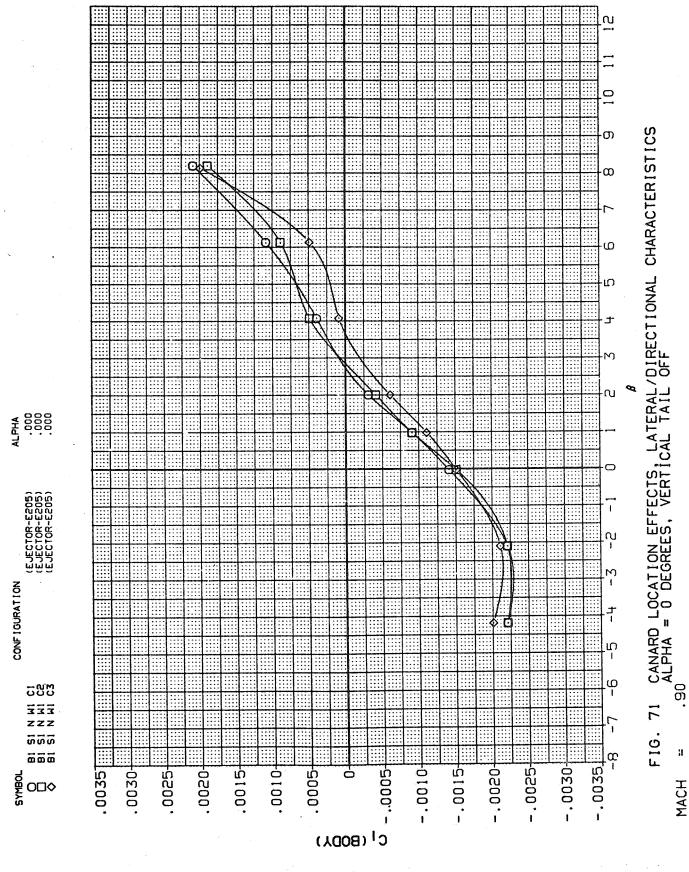




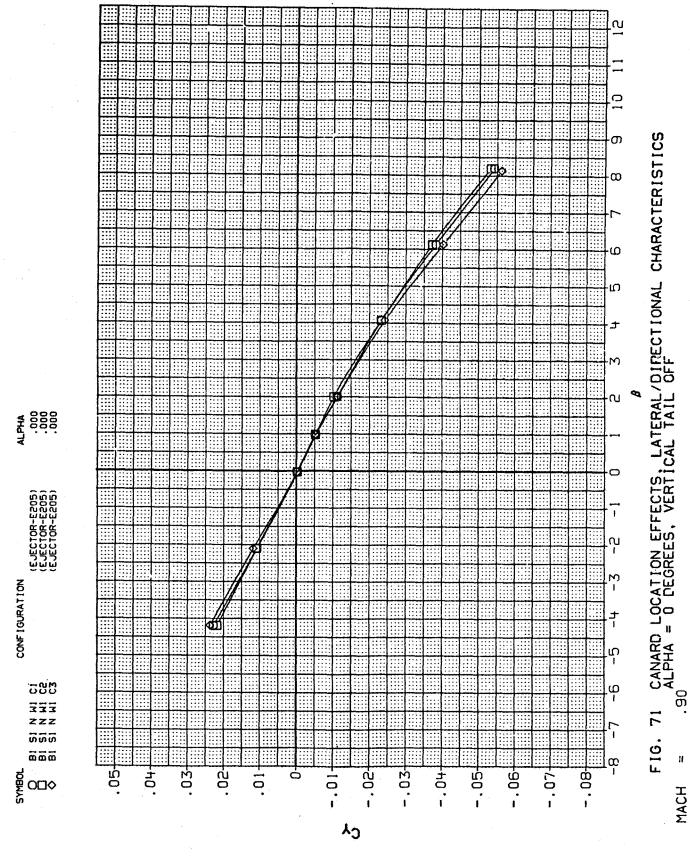


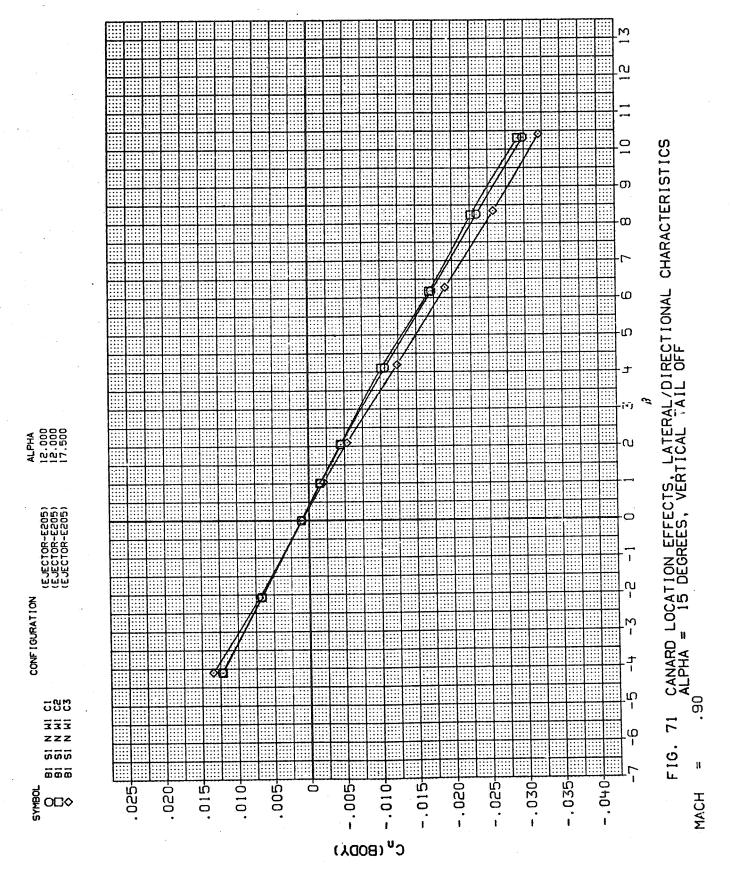


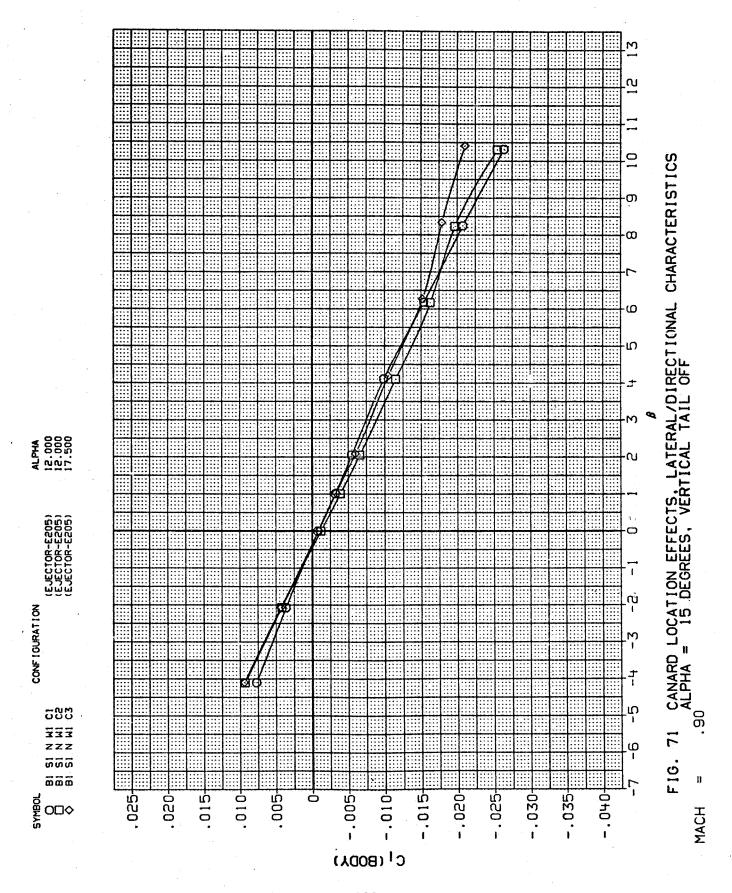


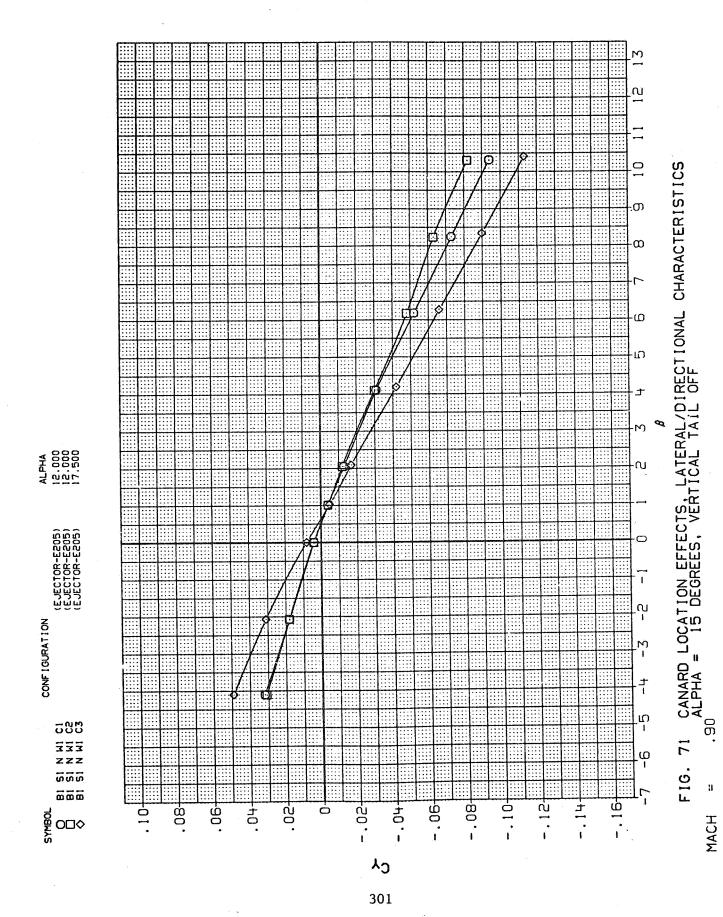


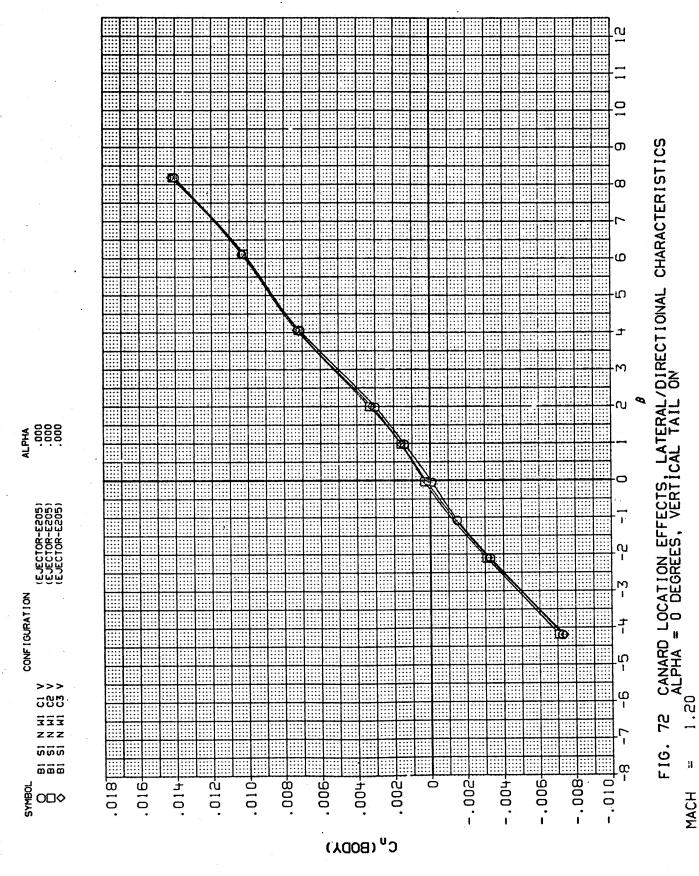
297

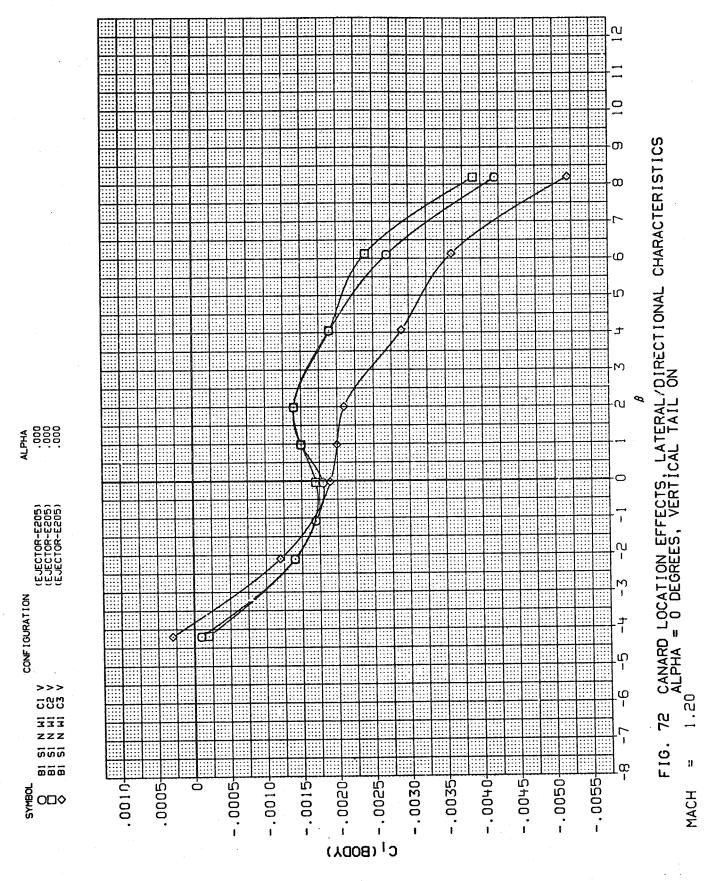


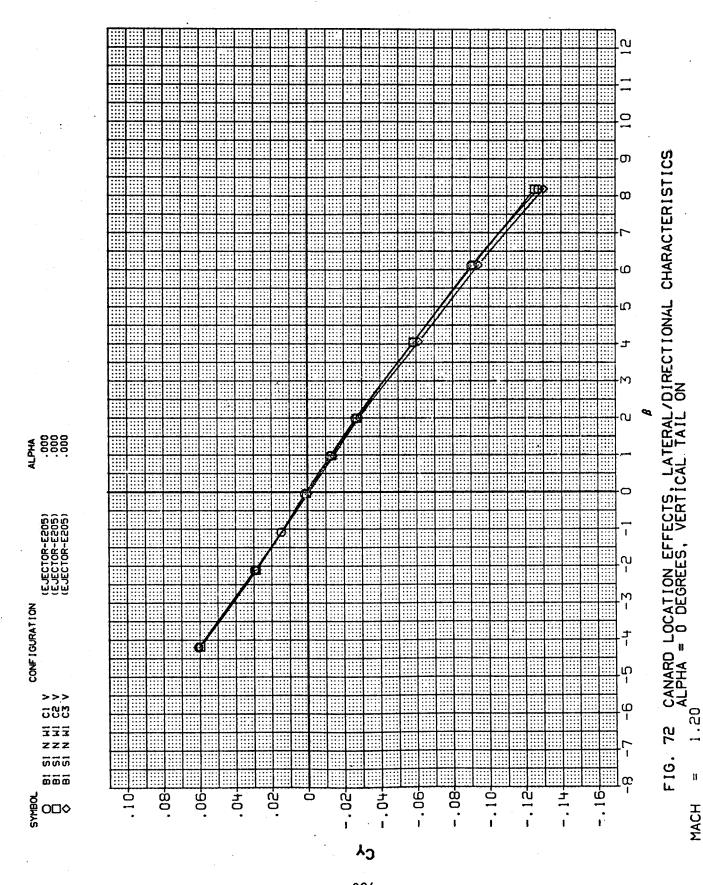


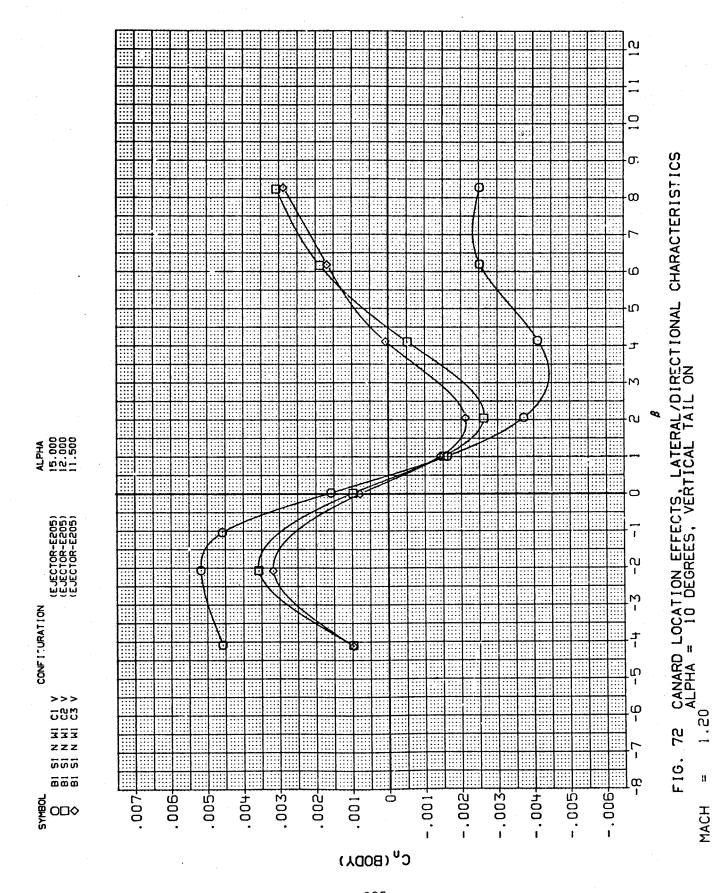


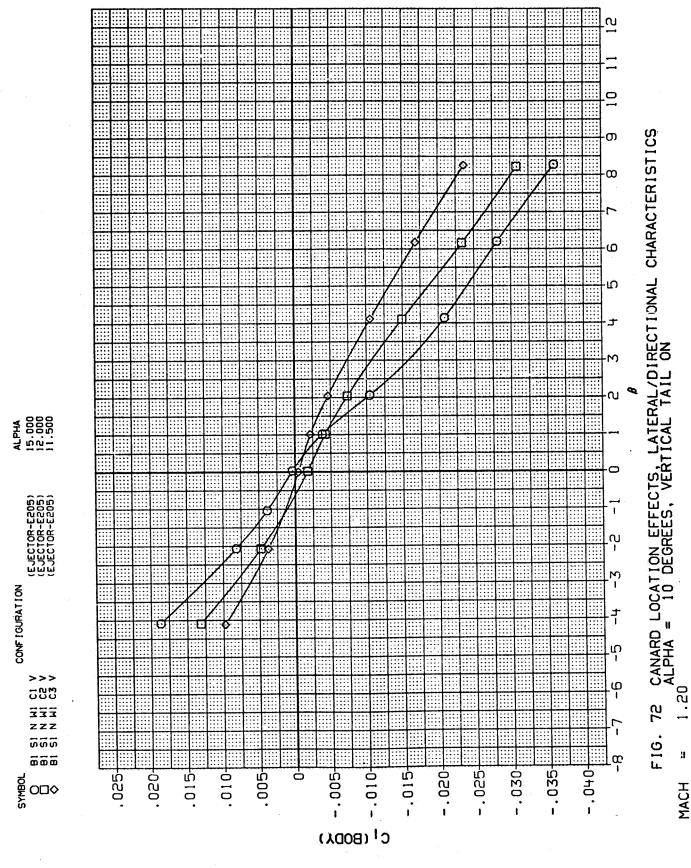


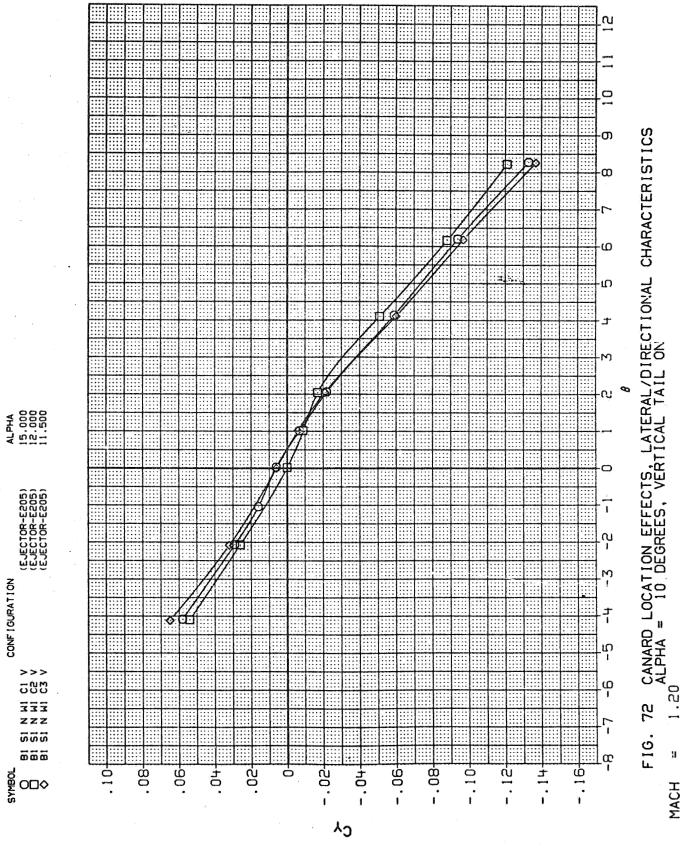


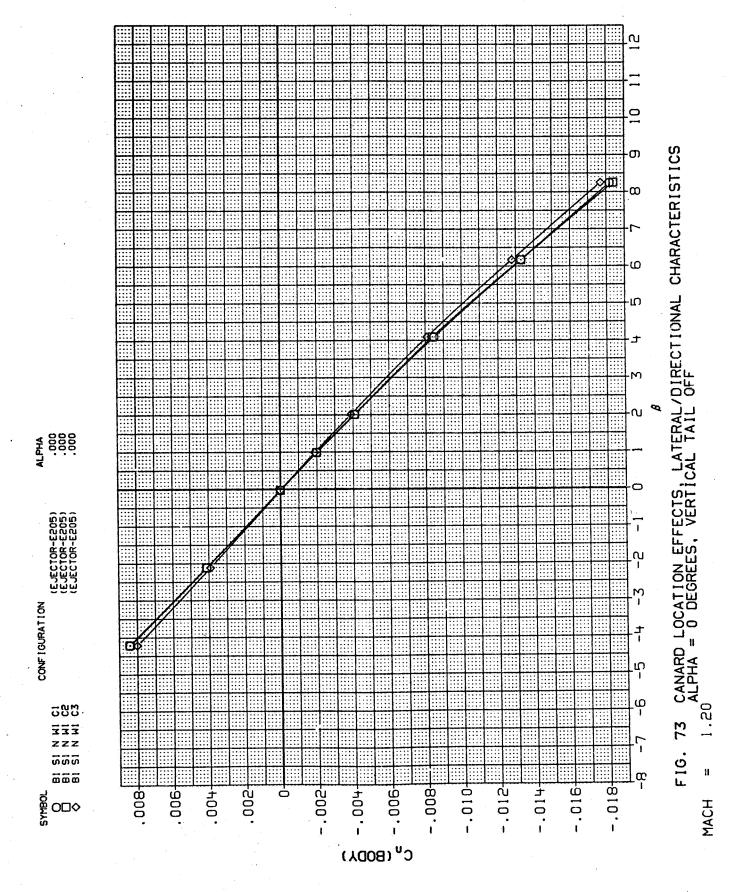


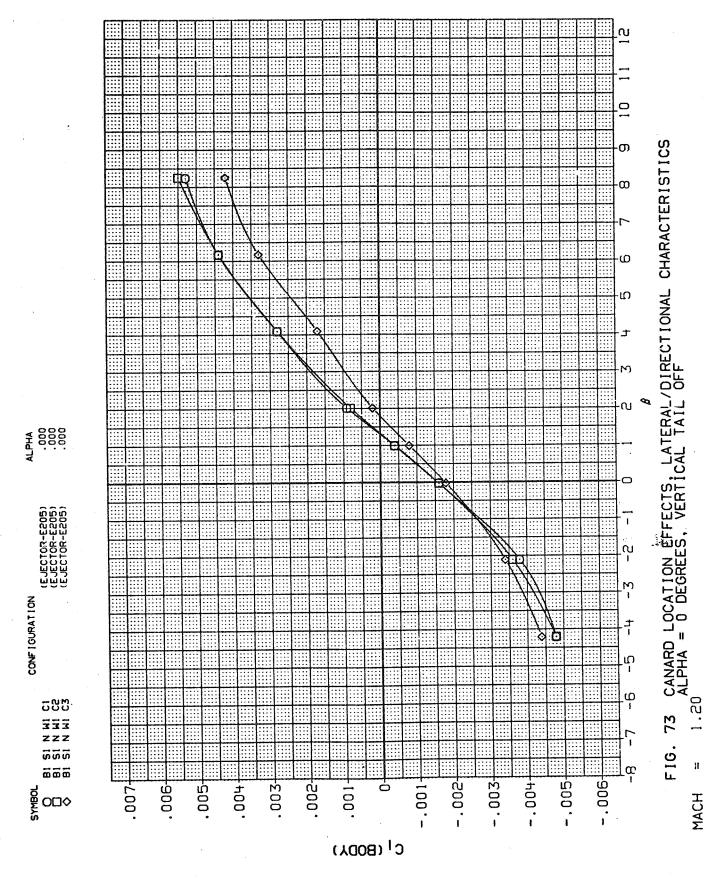


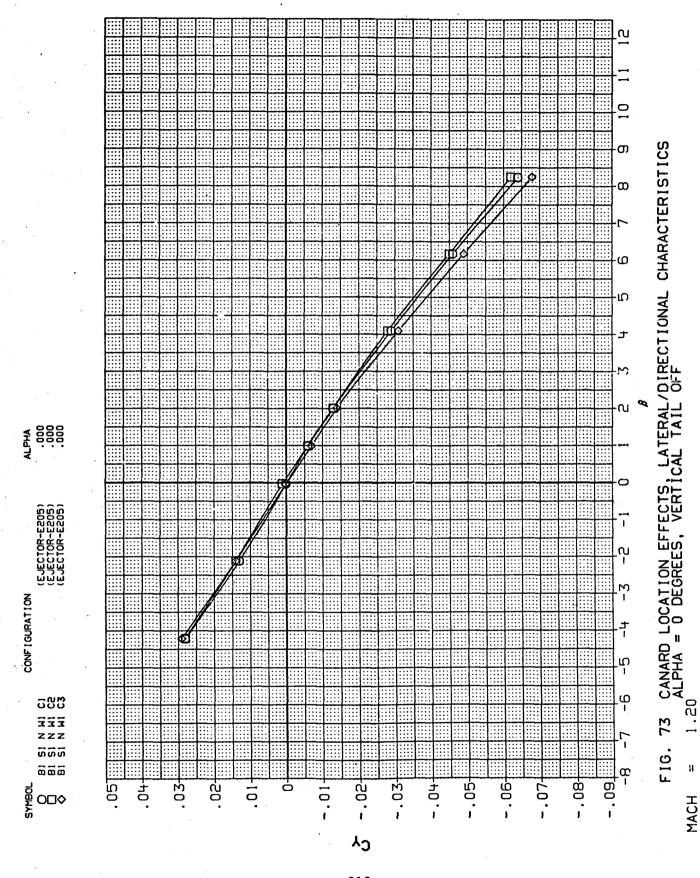




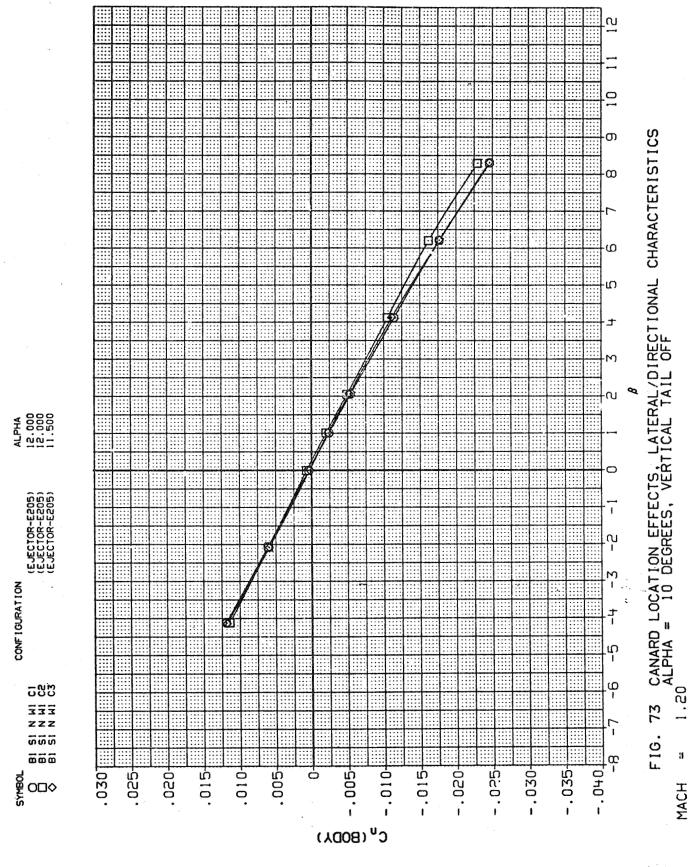




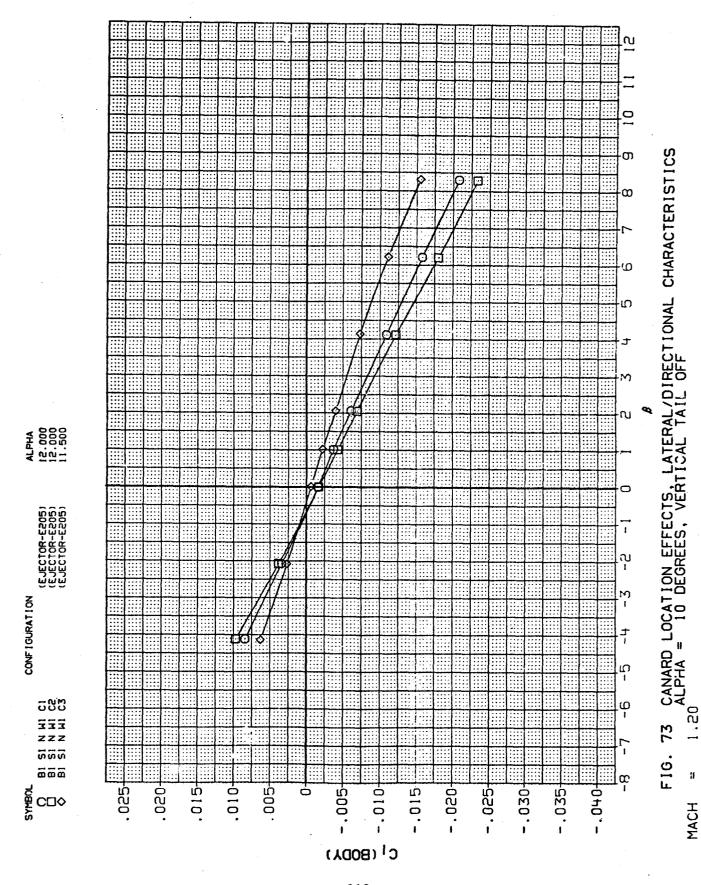


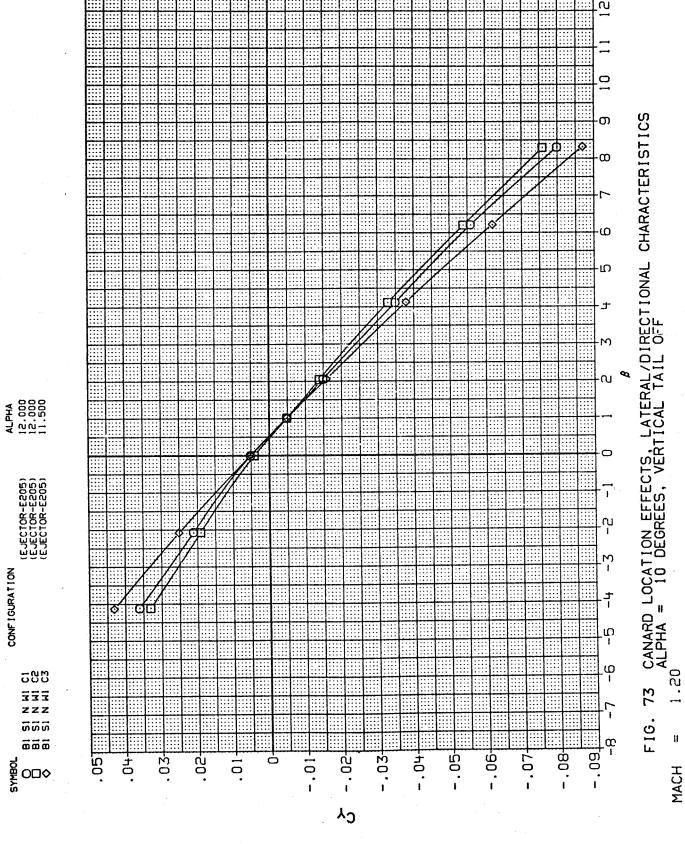


310



311





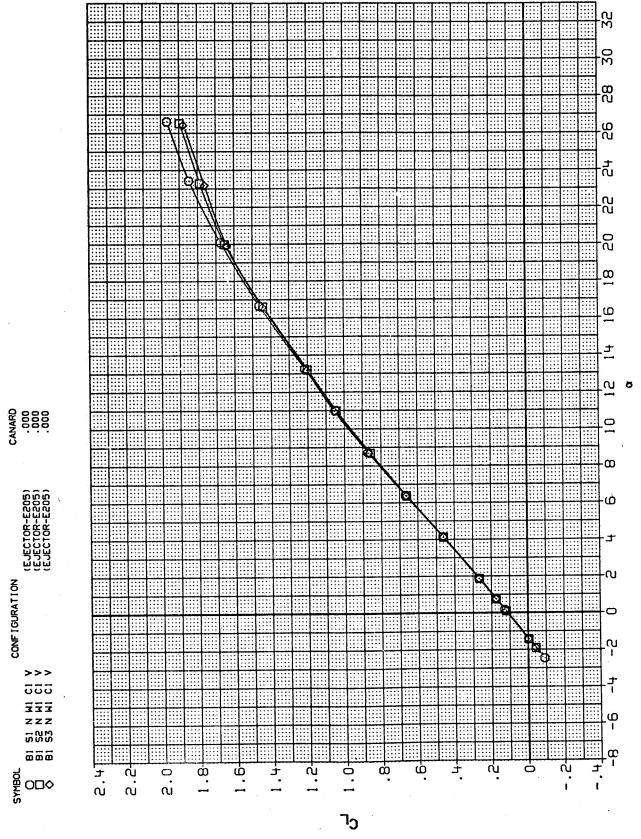
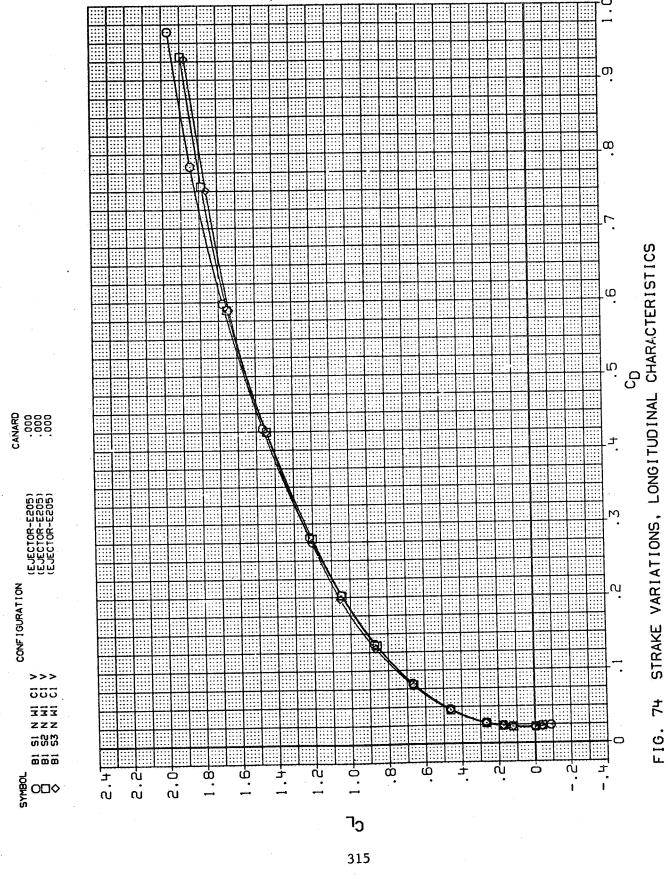


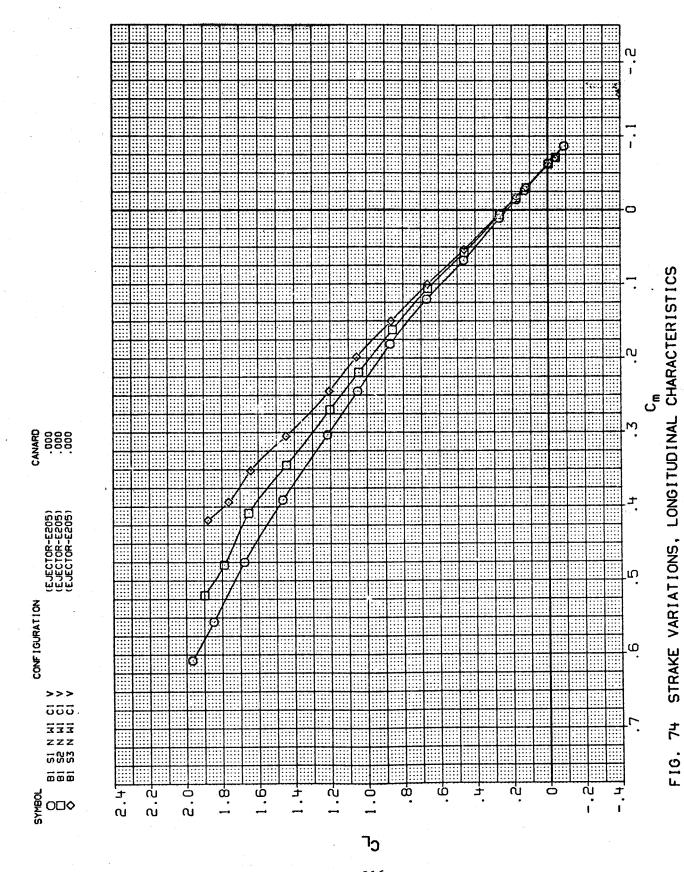
FIG. 74 STRAKE VARIATIONS, LONGITUDINAL CHARACTERISTICS

.60

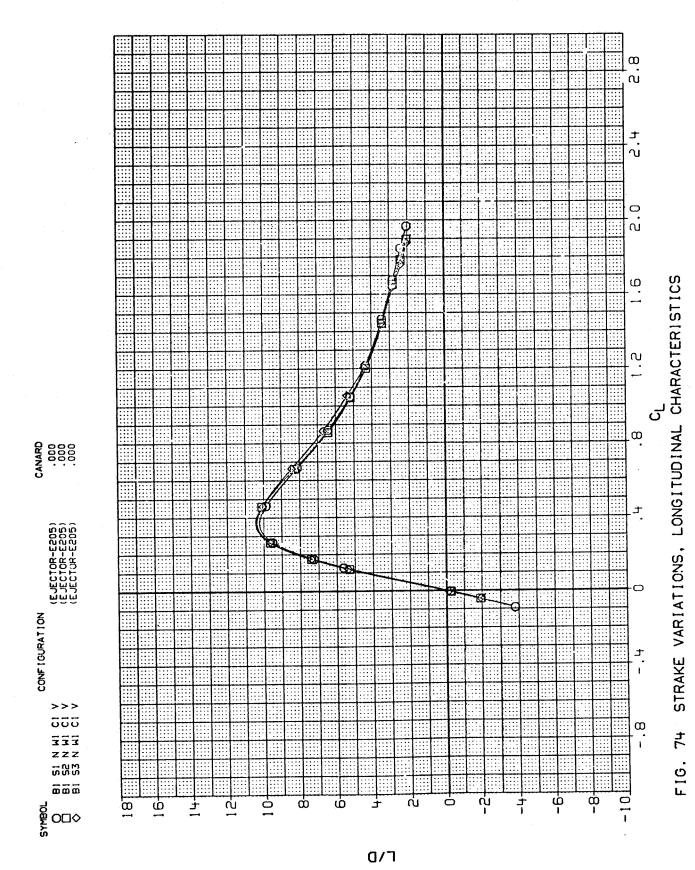
IJ



MACH = .60



MACH = .60



MACH = .6

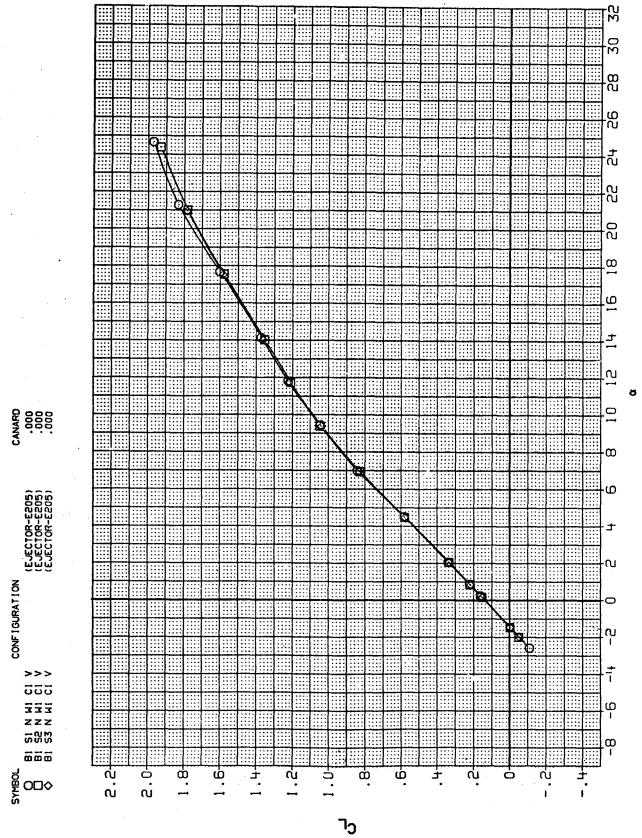
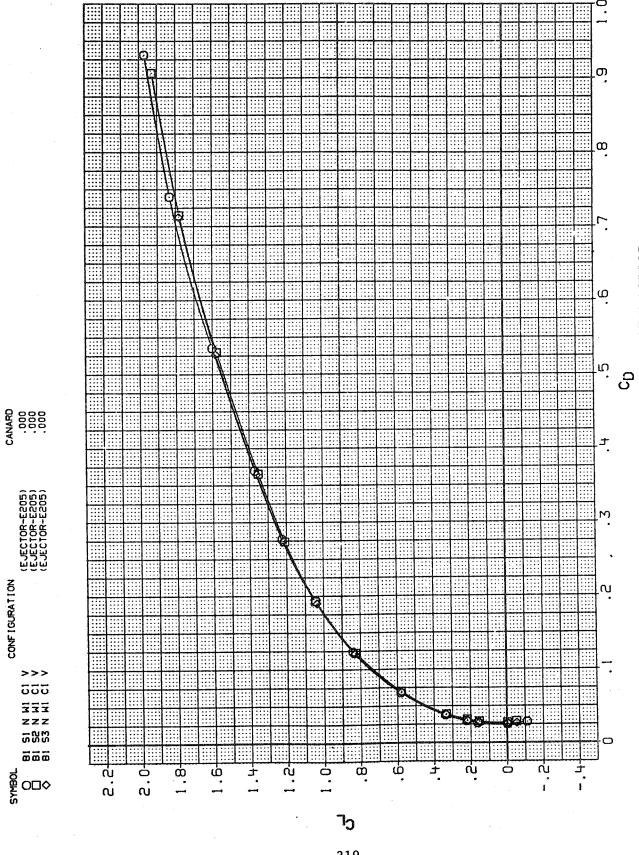
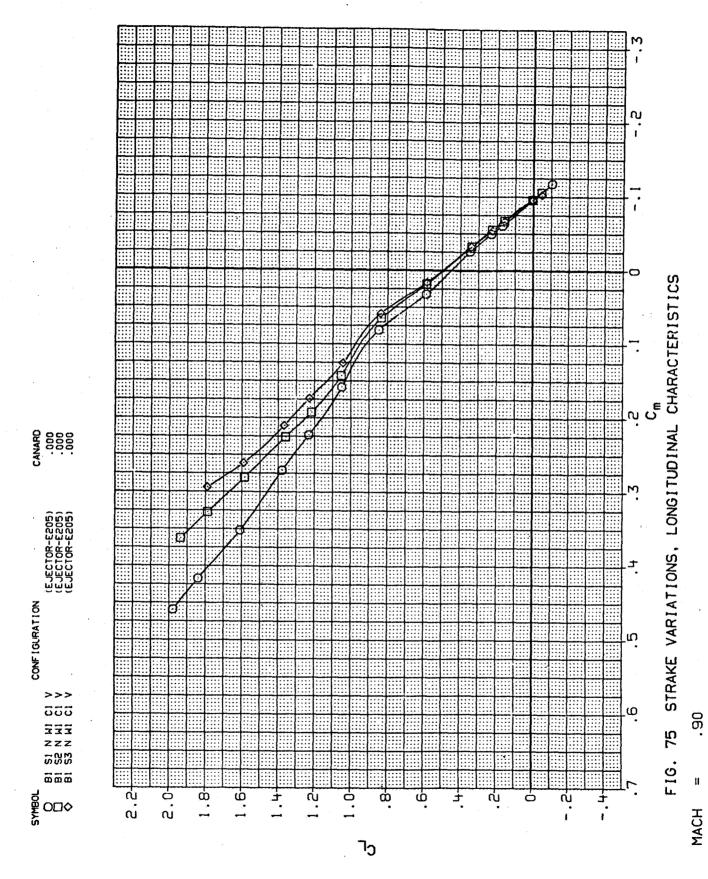


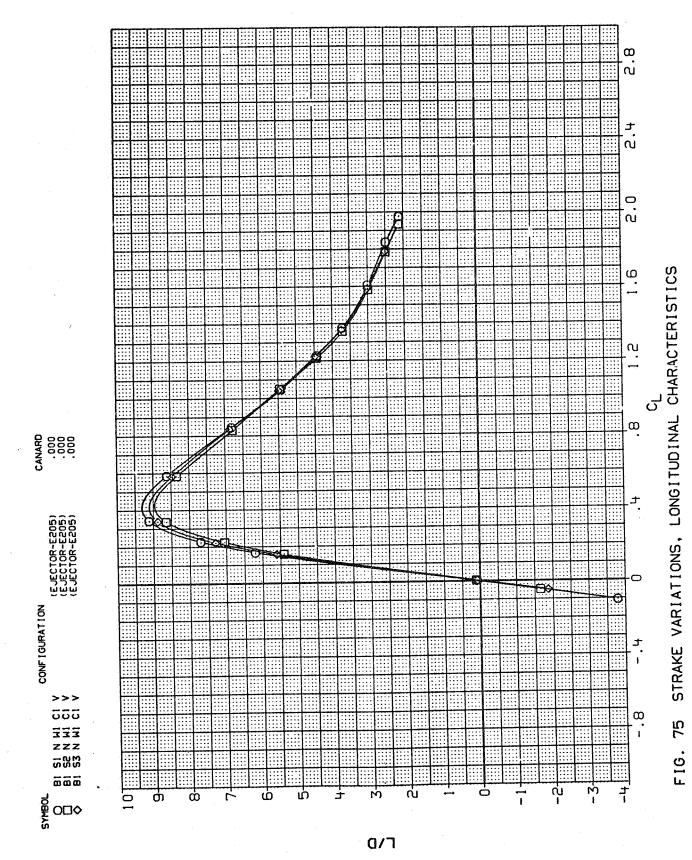
FIG. 75 STRAKE VARIATIONS, LONGITUDINAL CHARACTERISTICS

96.



STRAKE VARIATIONS, LONGITUDINAL CHARACTERISTICS 75 F16.





MACH = .90

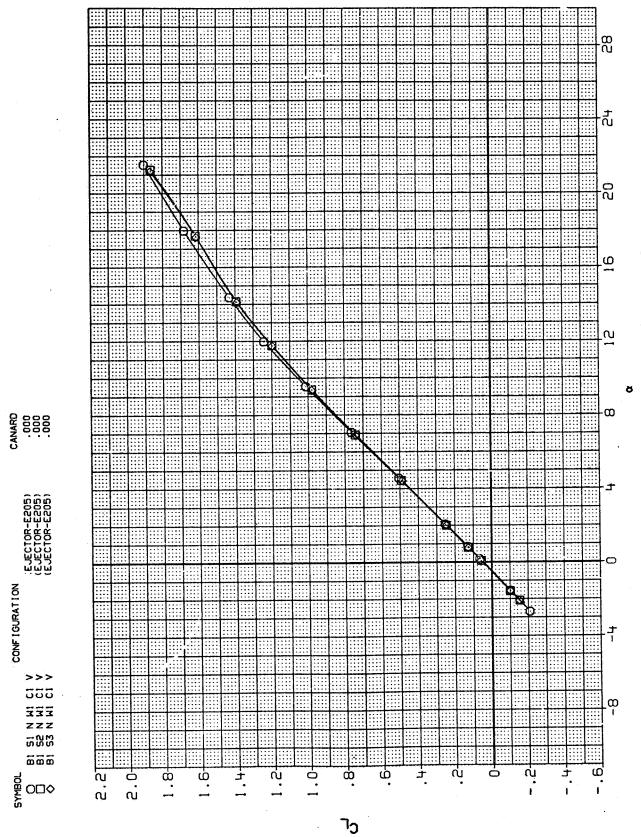
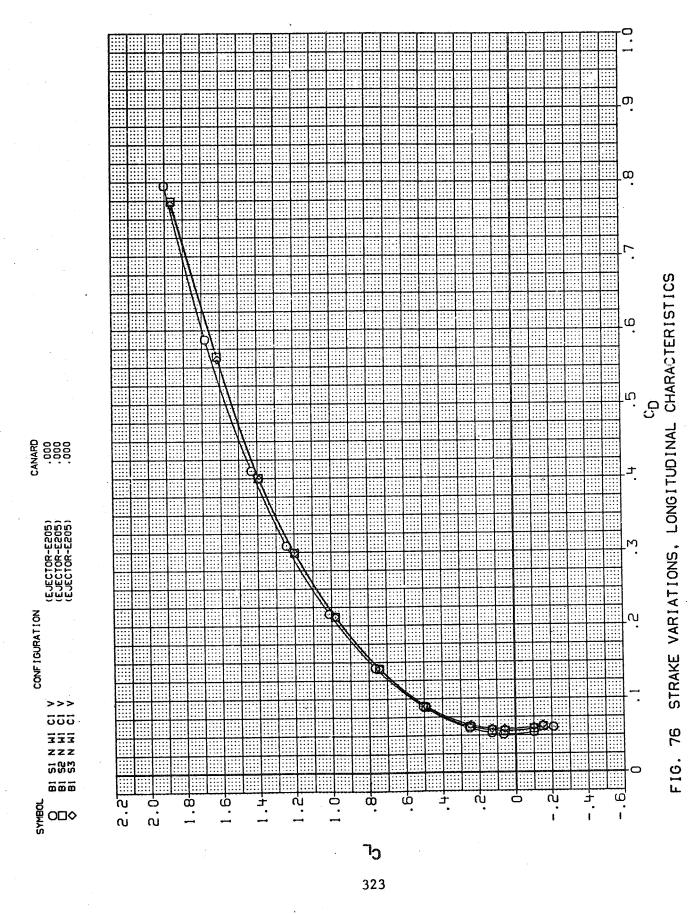
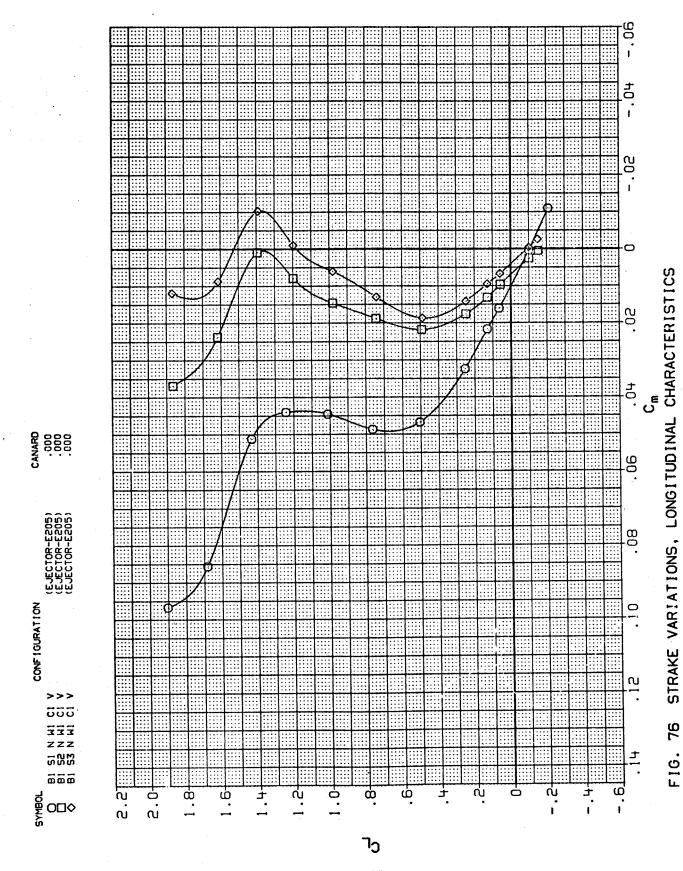


FIG. 76 STRAKE VARIATIONS, LONGITUDINAL CHARACTERISTICS



MACH = 1.20



MACH = 1.20

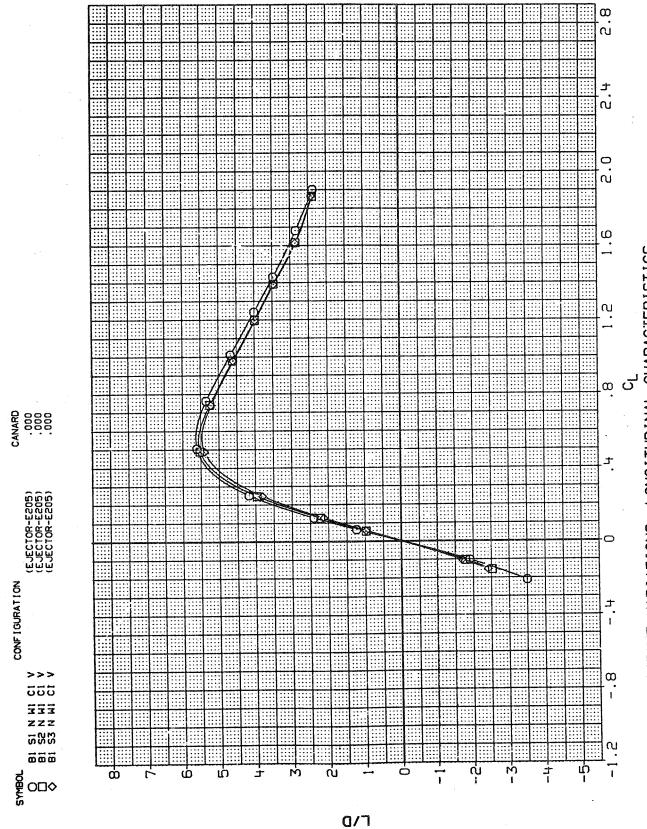
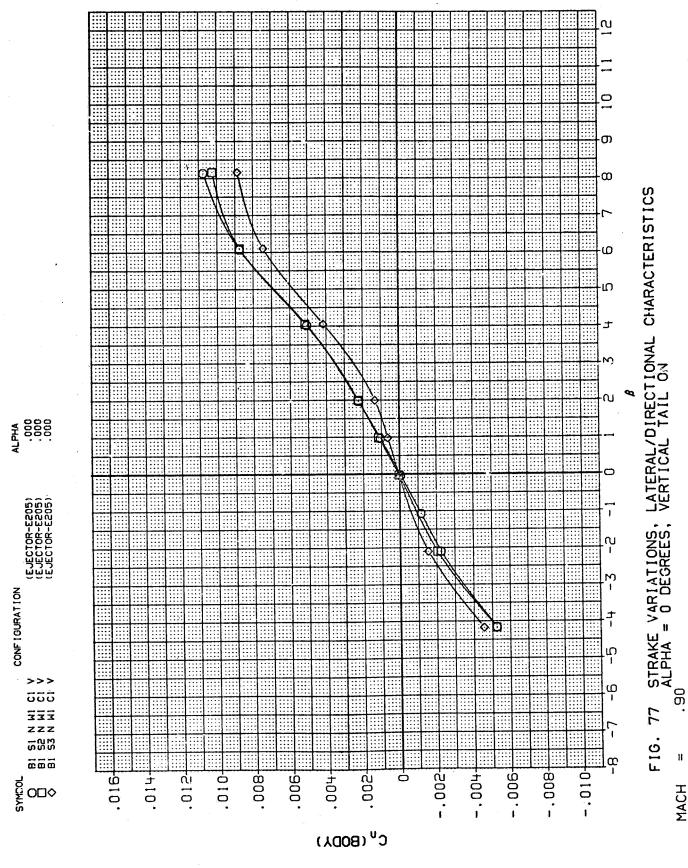
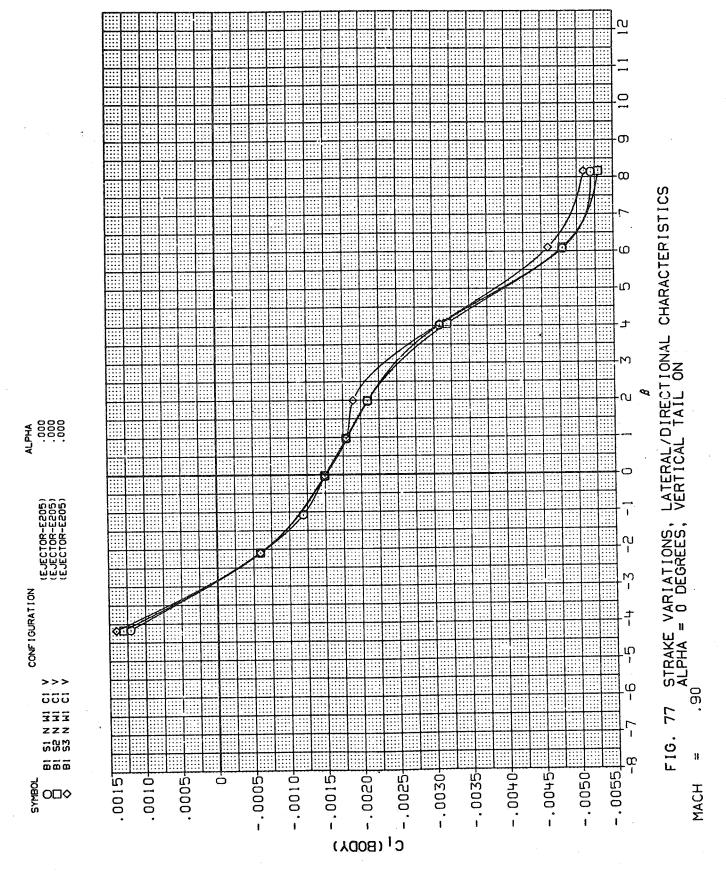
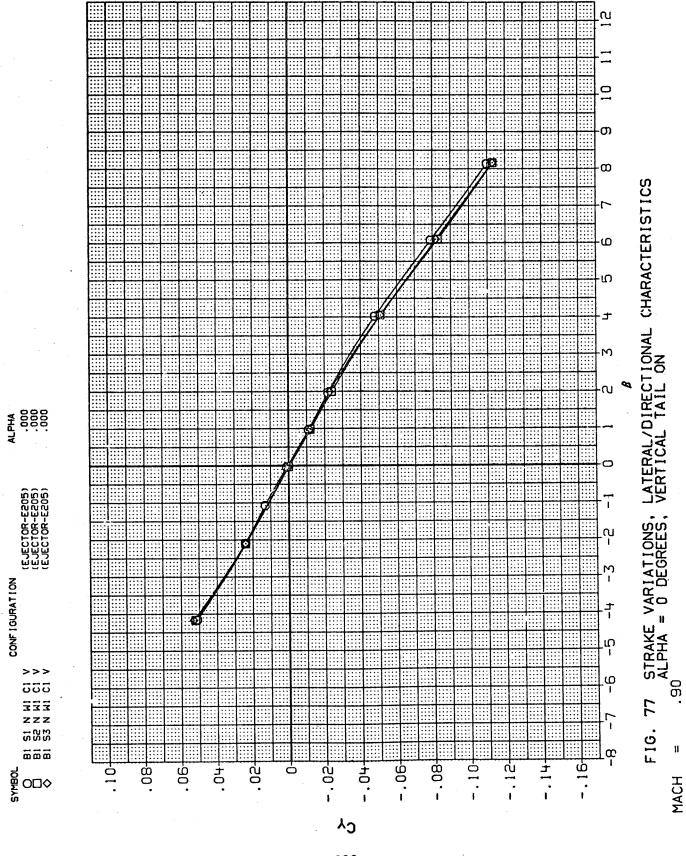
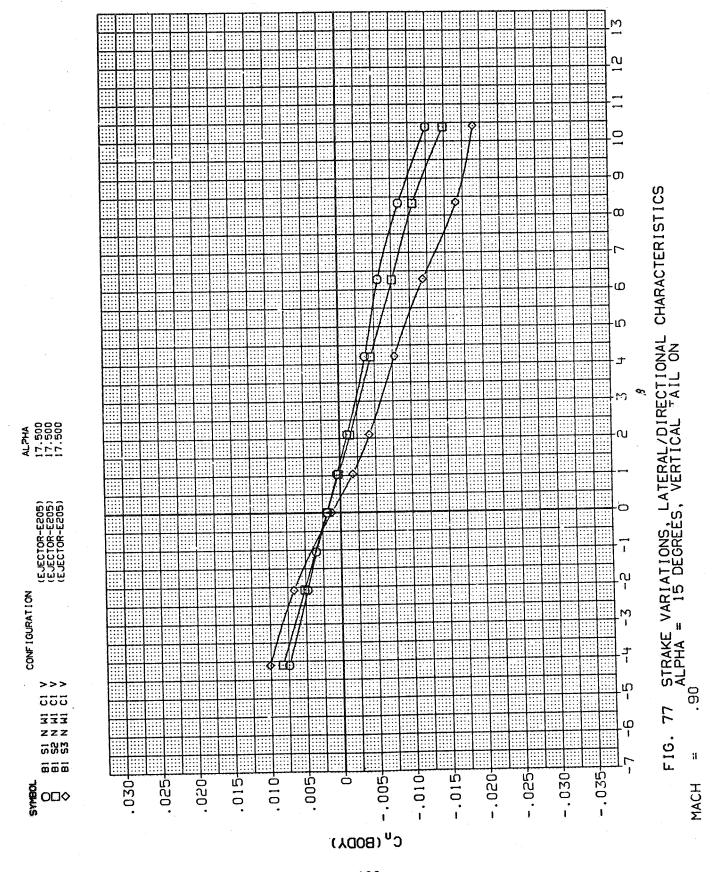


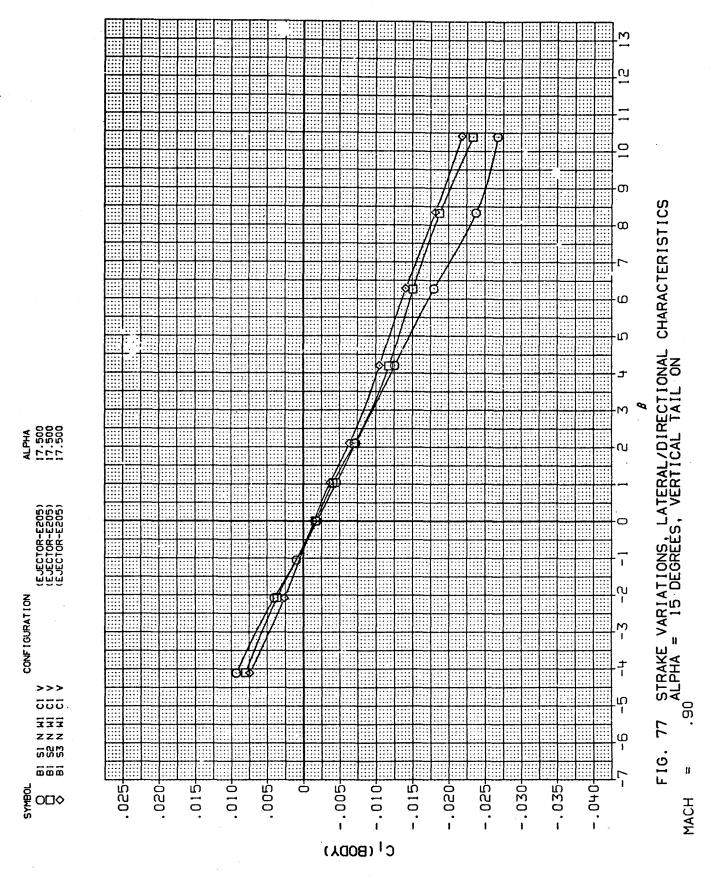
FIG. 76 STRAKE VARIATIONS, LONGITUDINAL CHARACTERISTICS

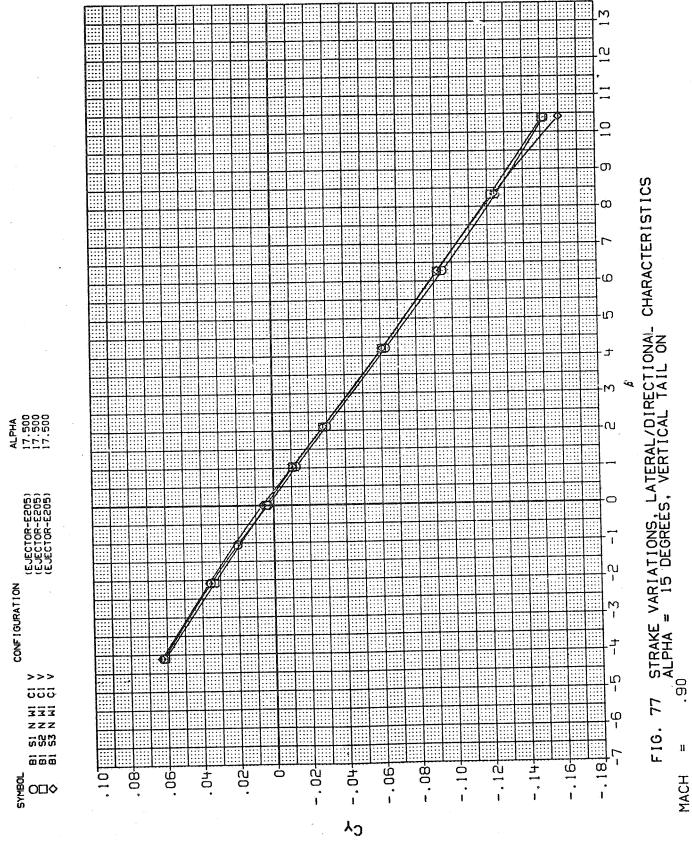


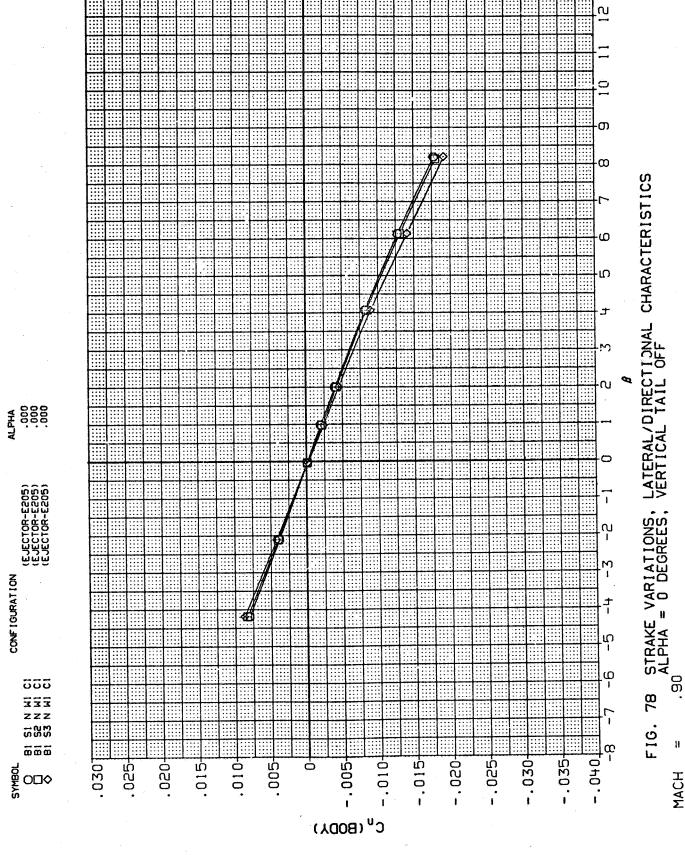


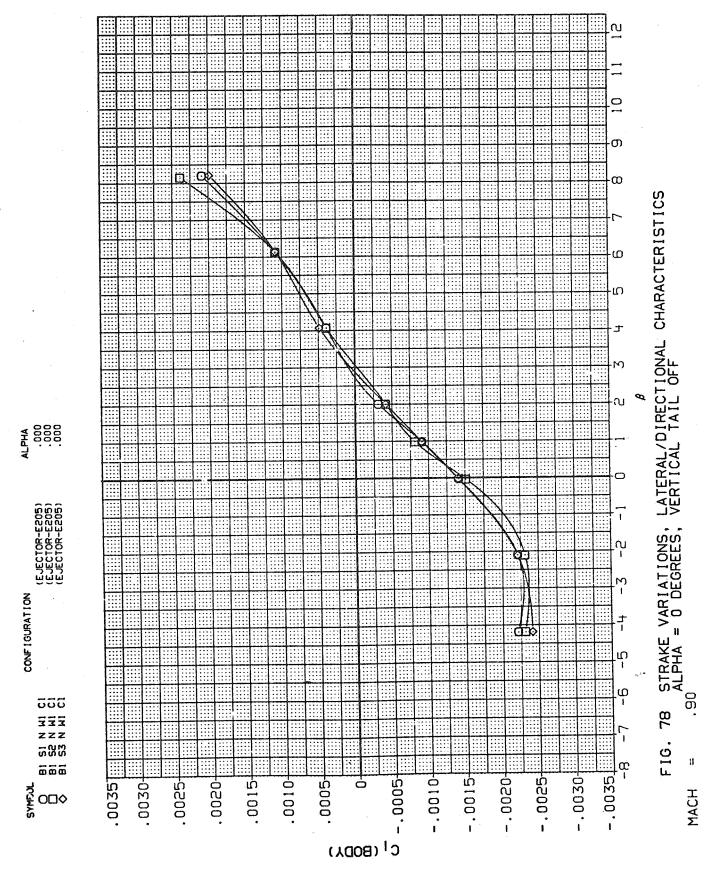


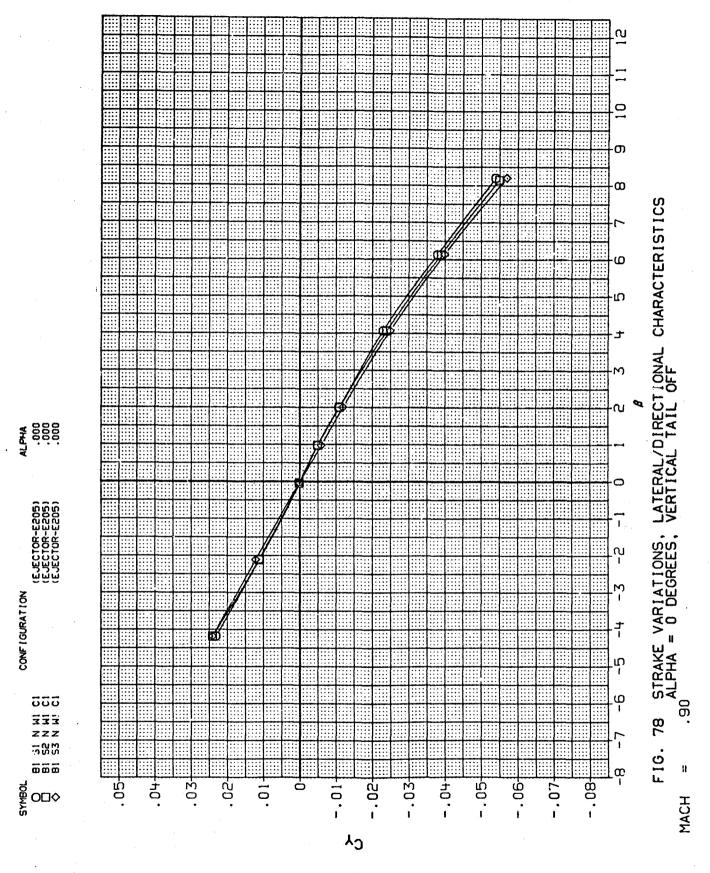


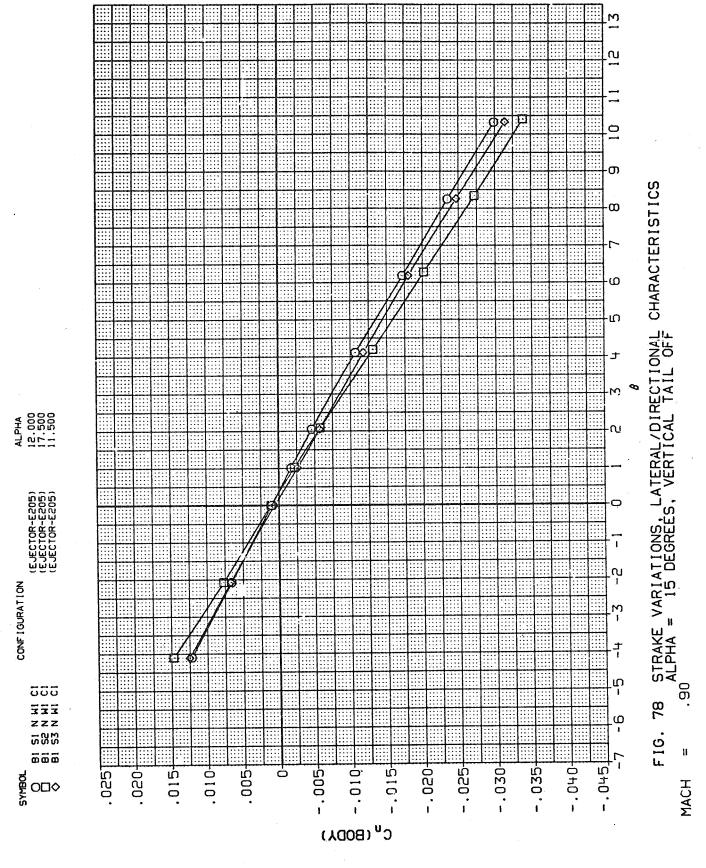


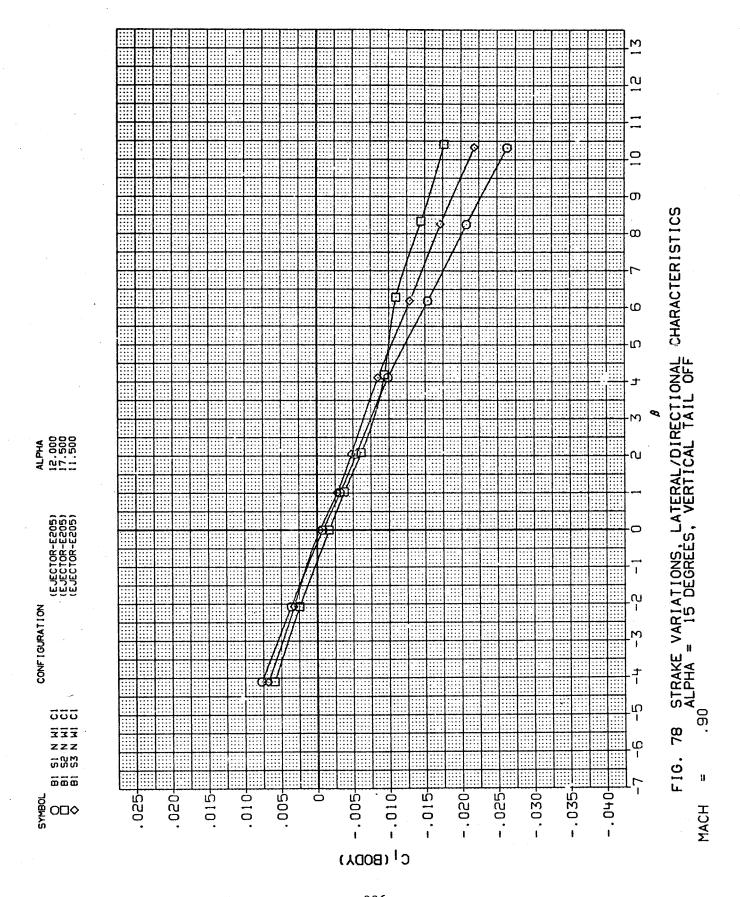


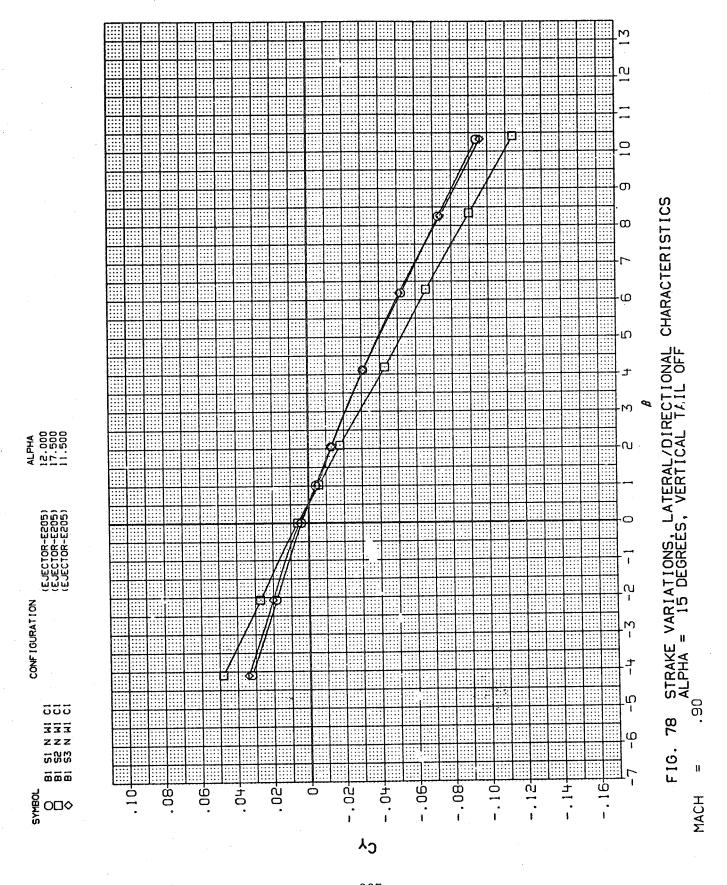


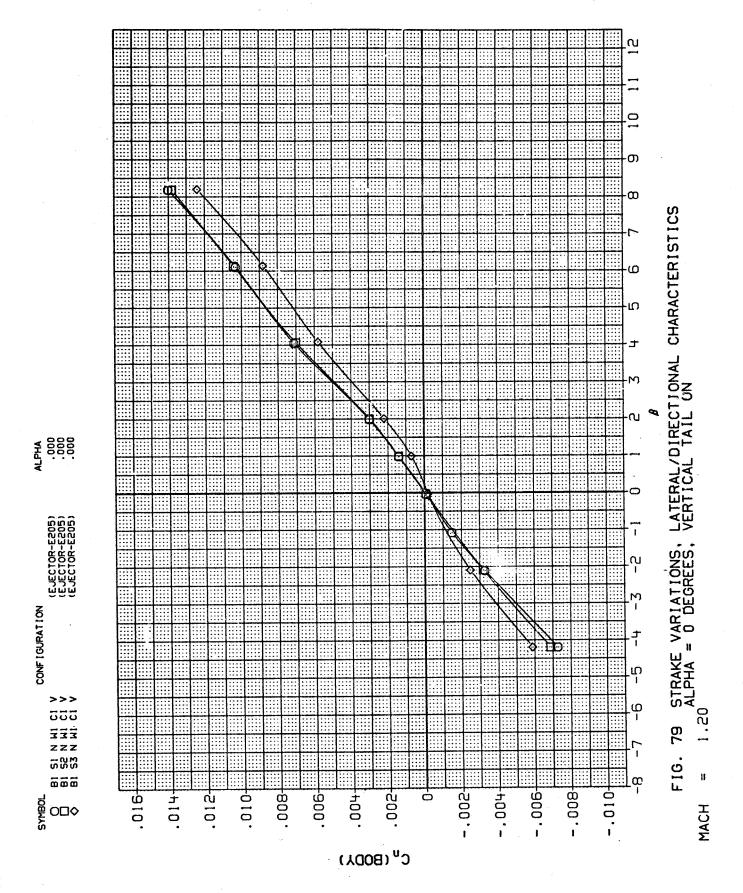


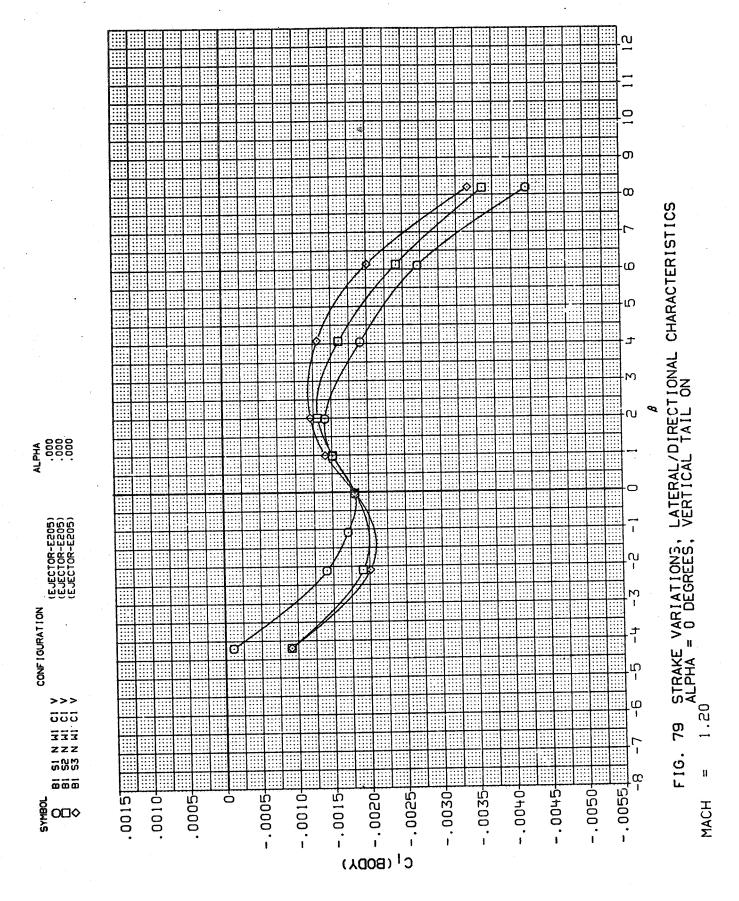


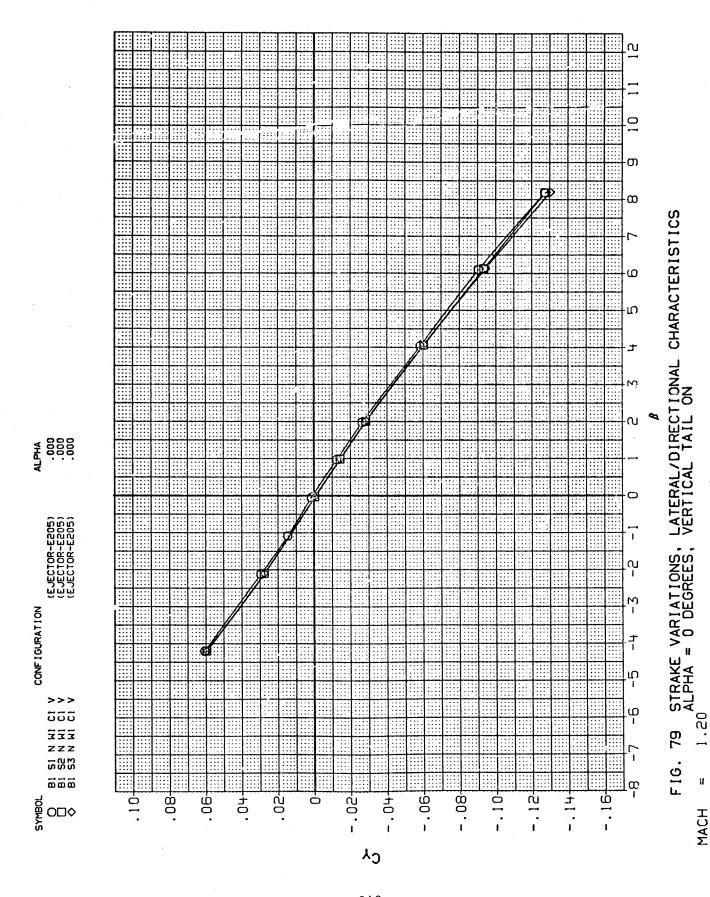




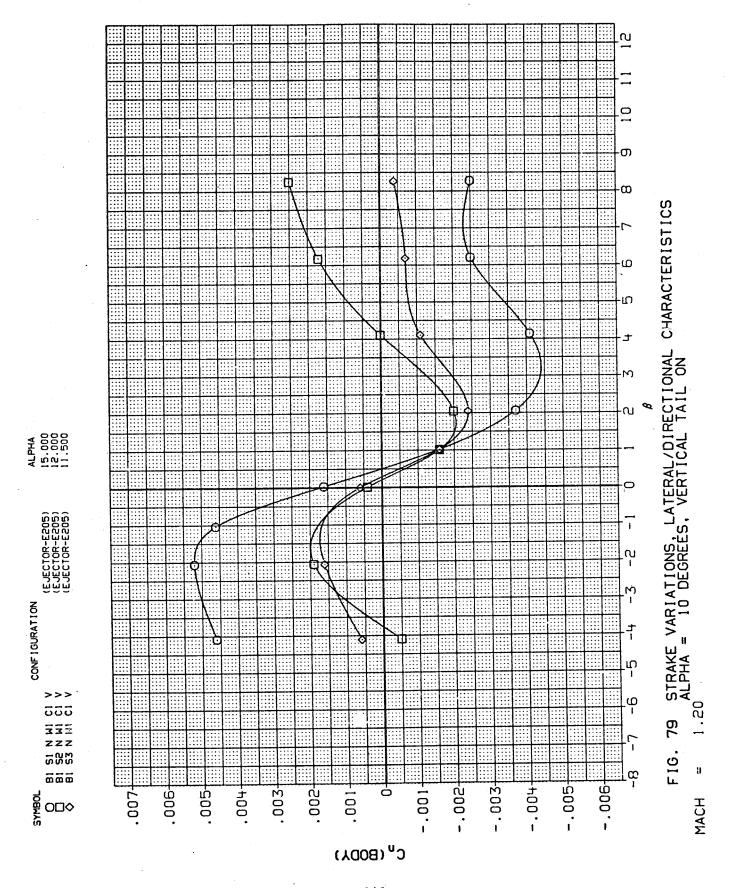


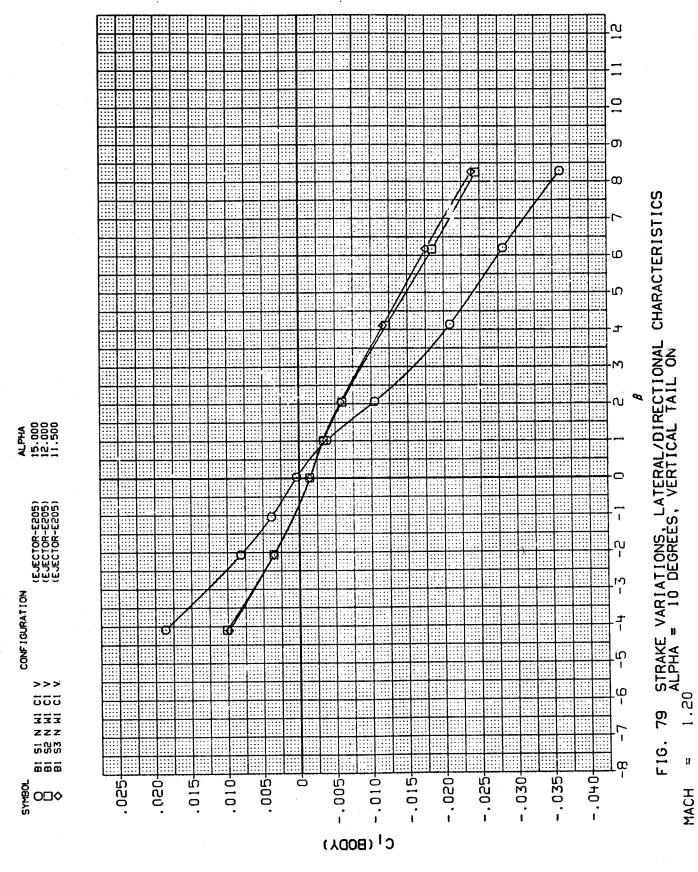


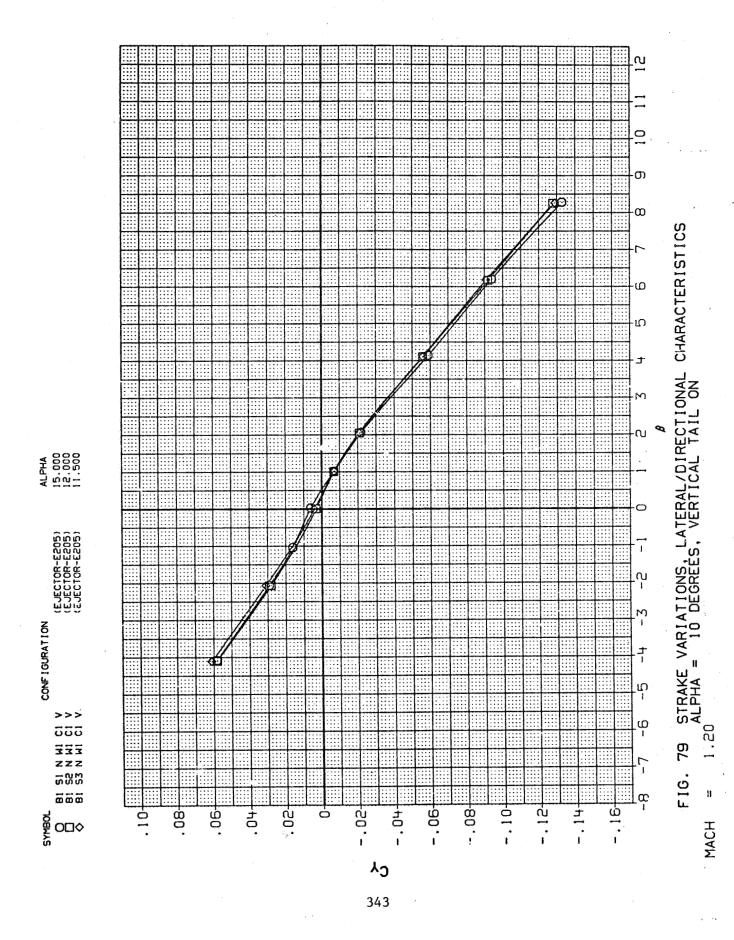


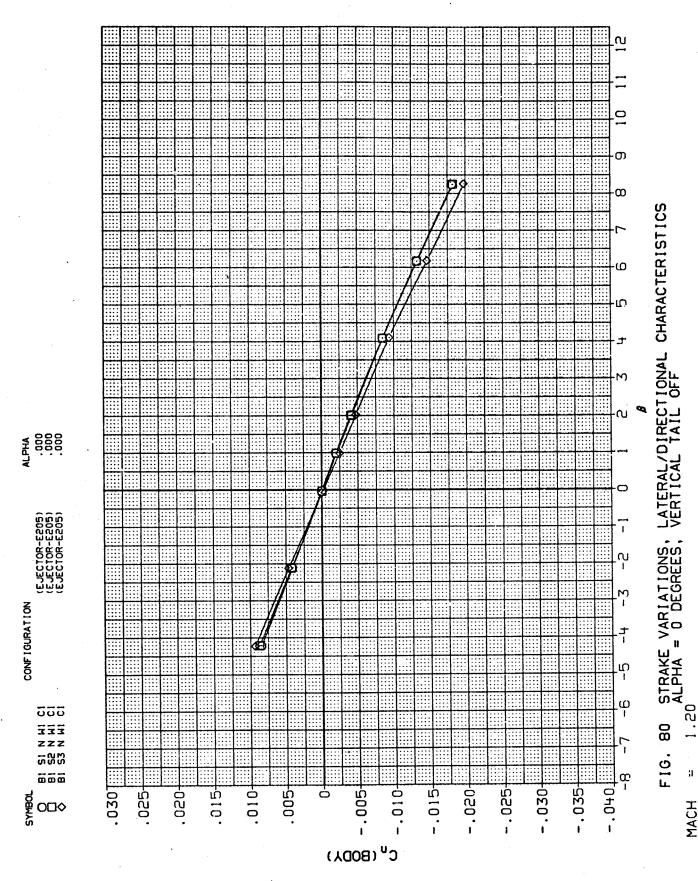


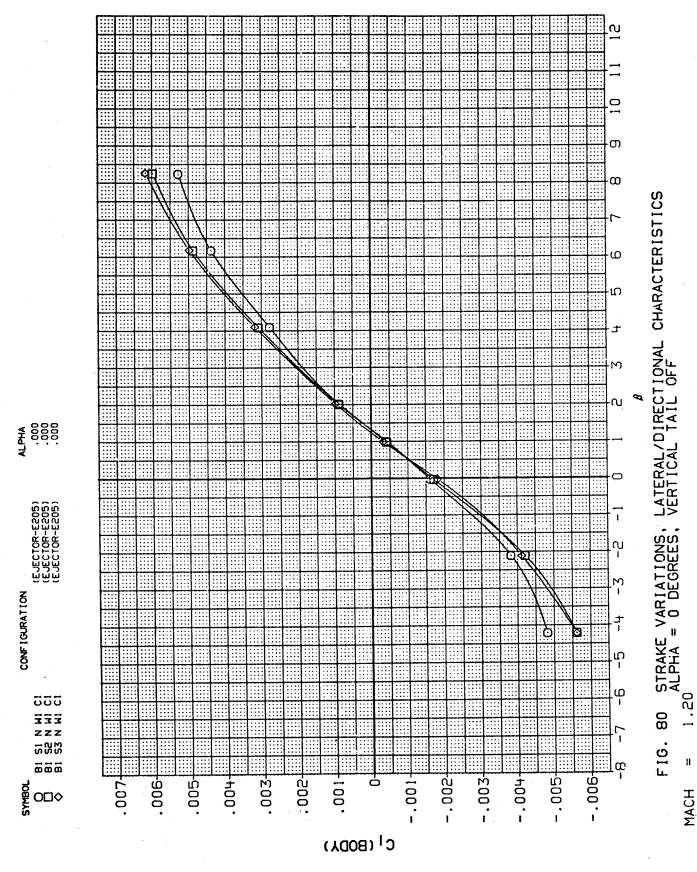
340

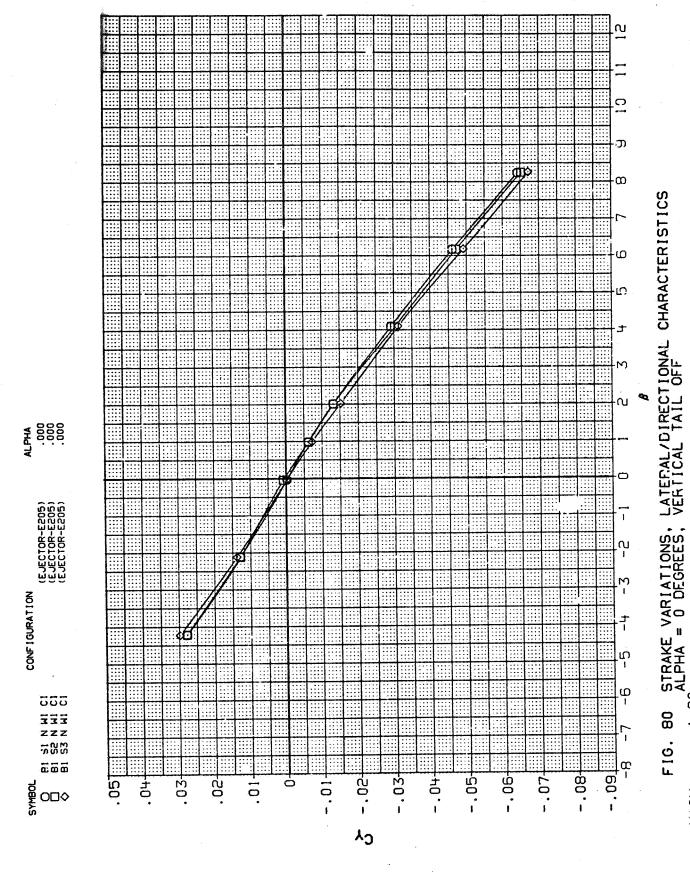




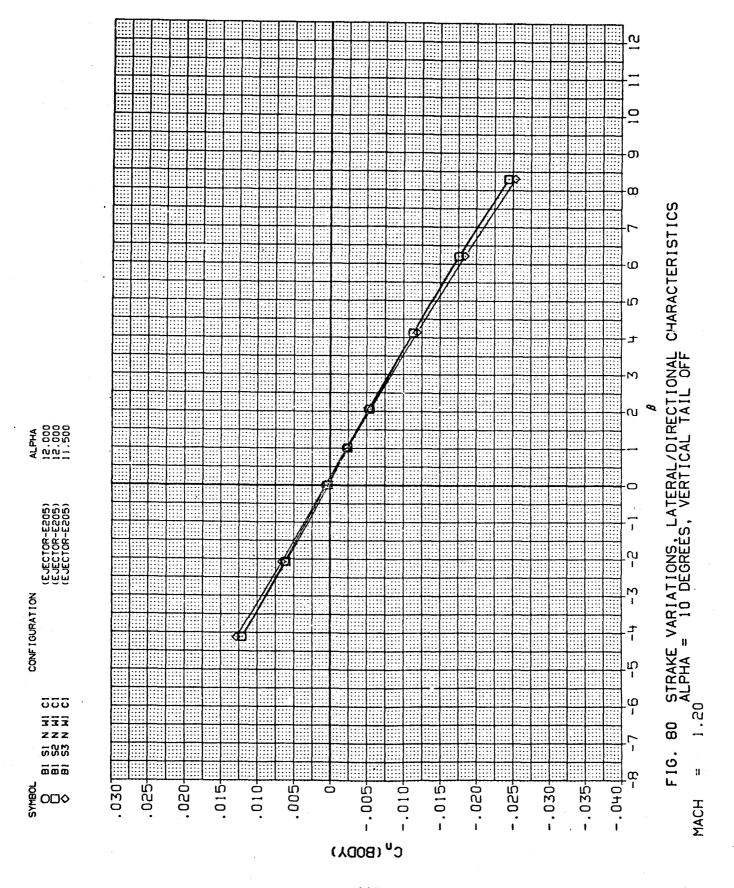


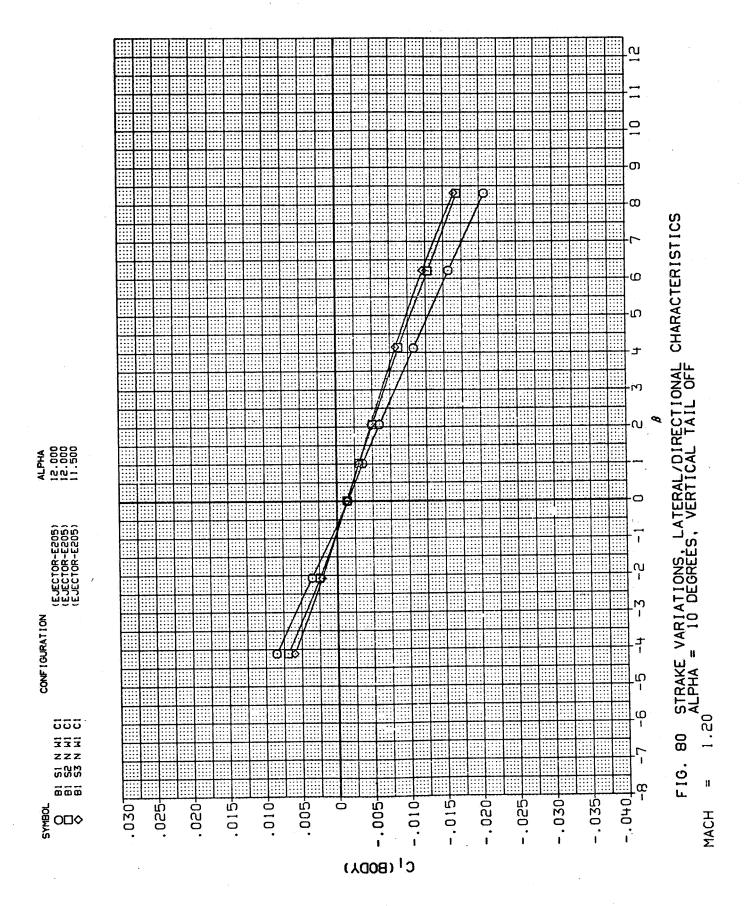


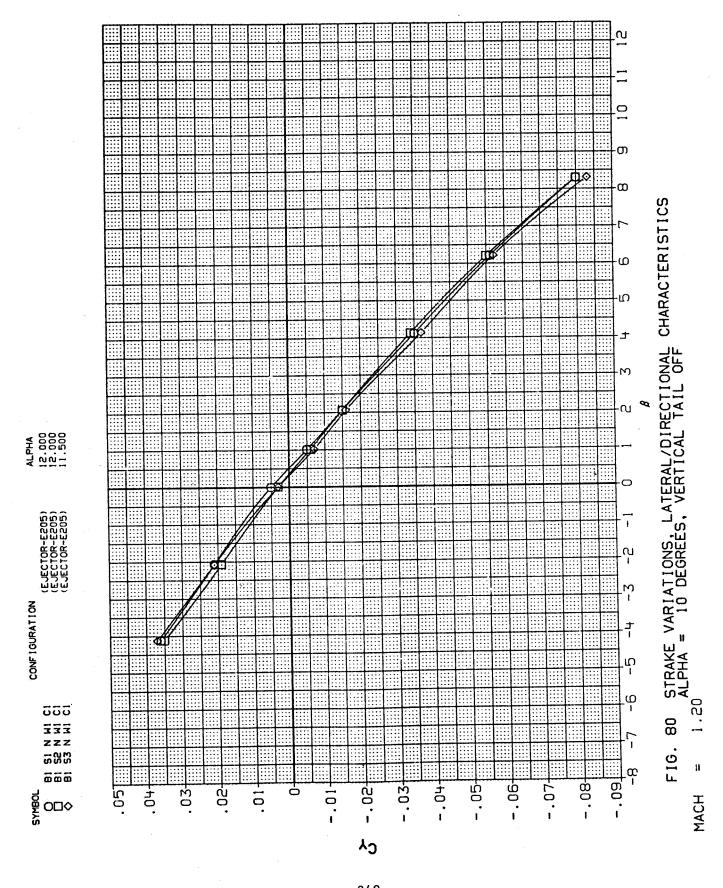




н







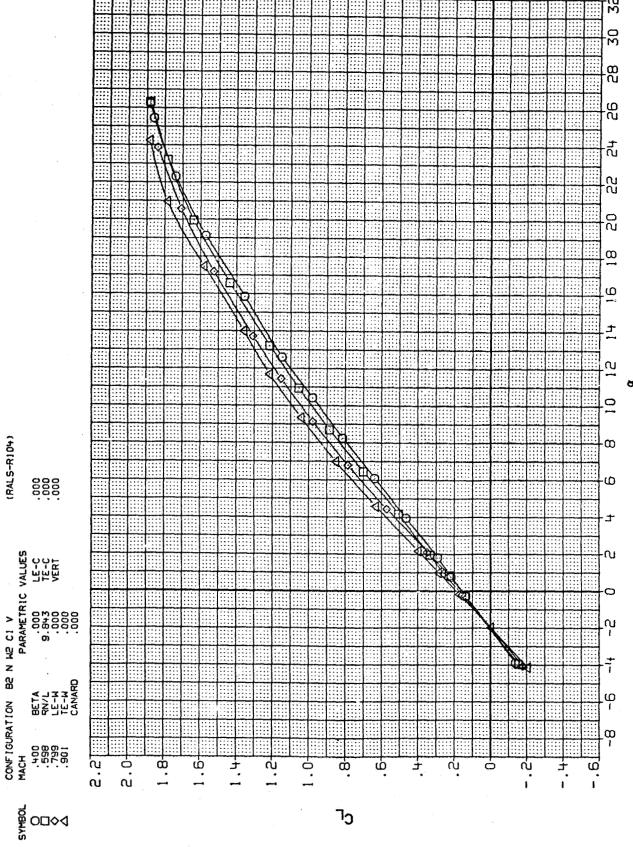
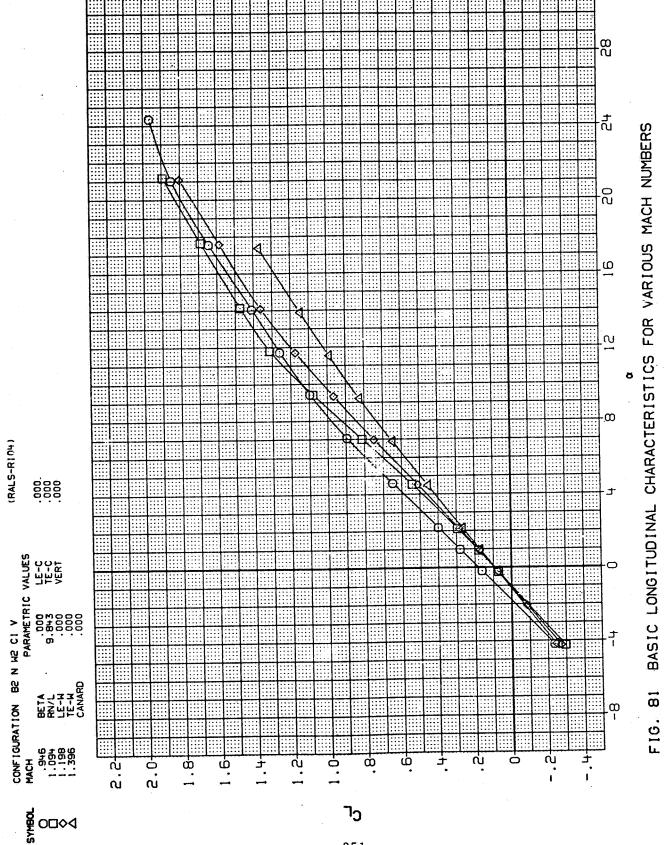
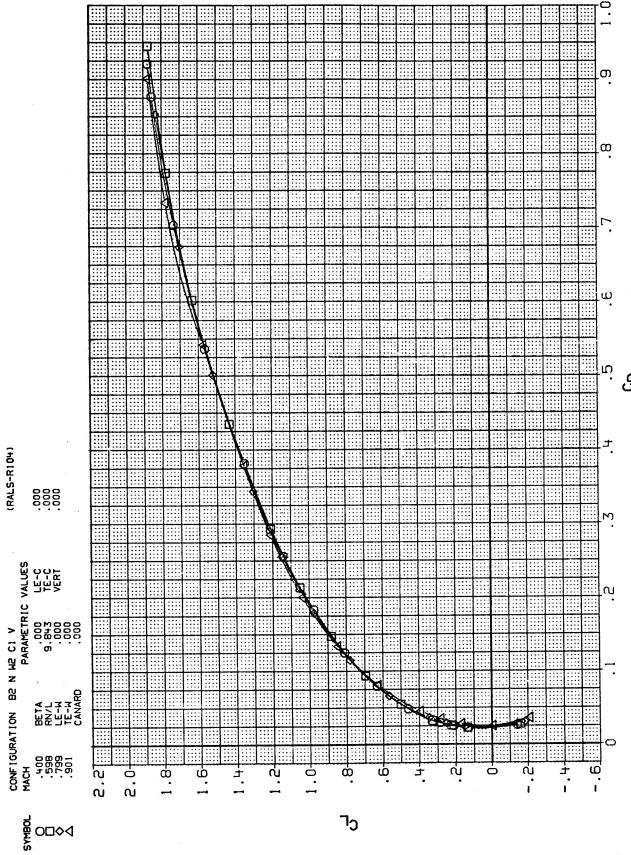


FIG. 81 BASIC LONGITUDINAL CHARACTERISTICS FOR VARIOUS MACH NUMBERS

350

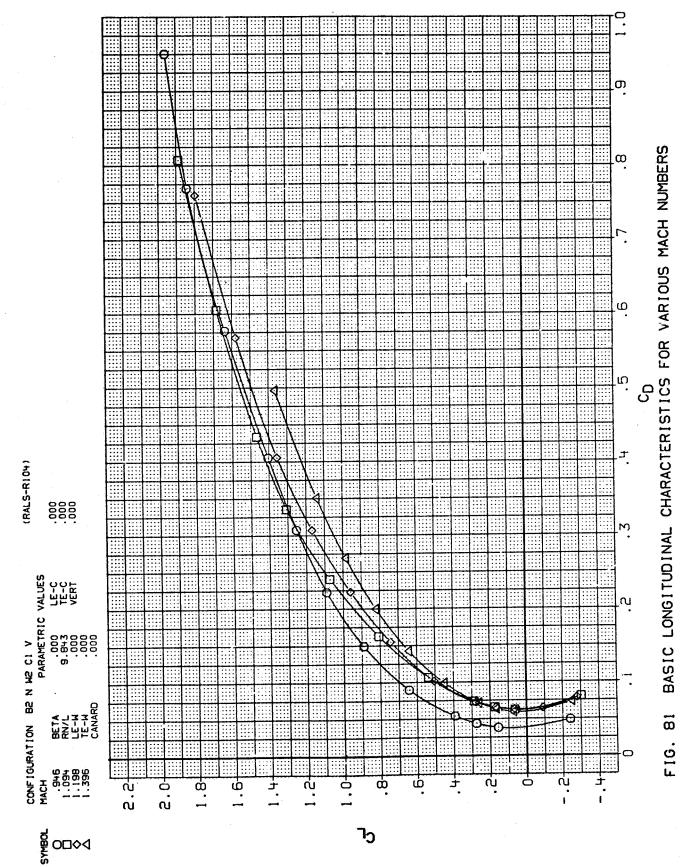


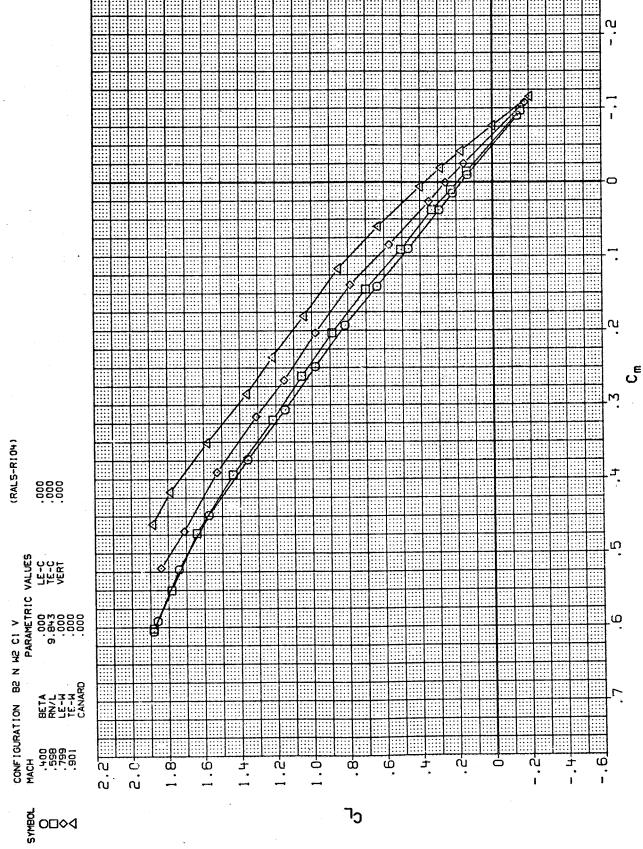


BASIC LONGITUDINAL CHARACTERISTICS FOR VARIOUS MACH NUMBERS

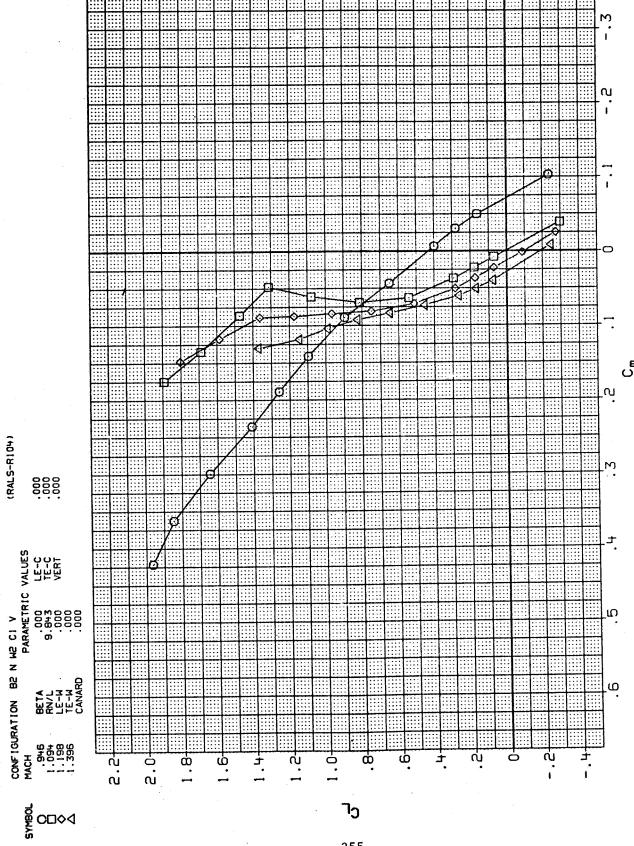
FIG. 81

352





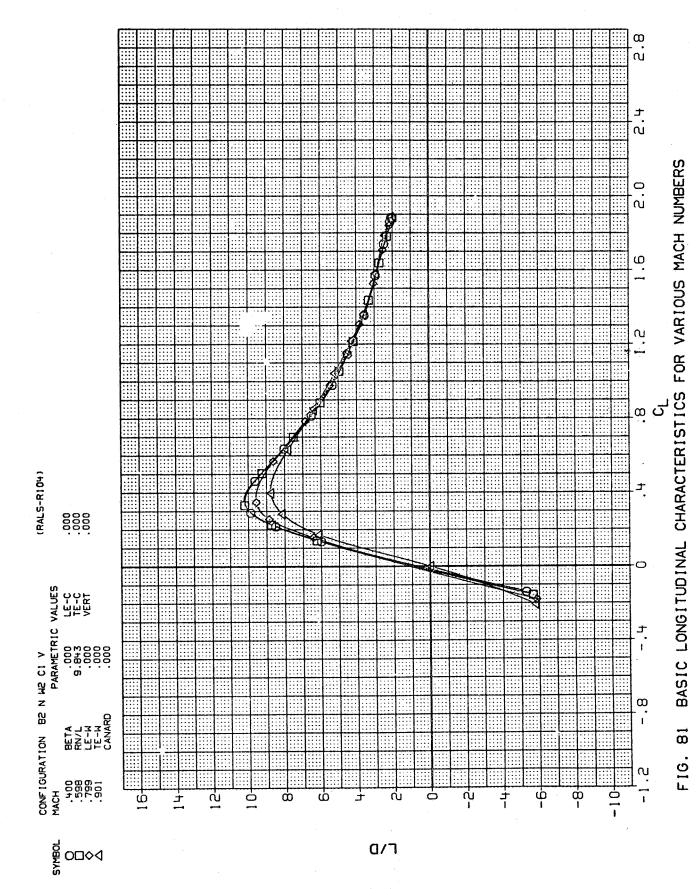
BASIC LONGITUDINAL CHARACTERISTICS FOR VARIOUS MACH NUMBERS F16. 81

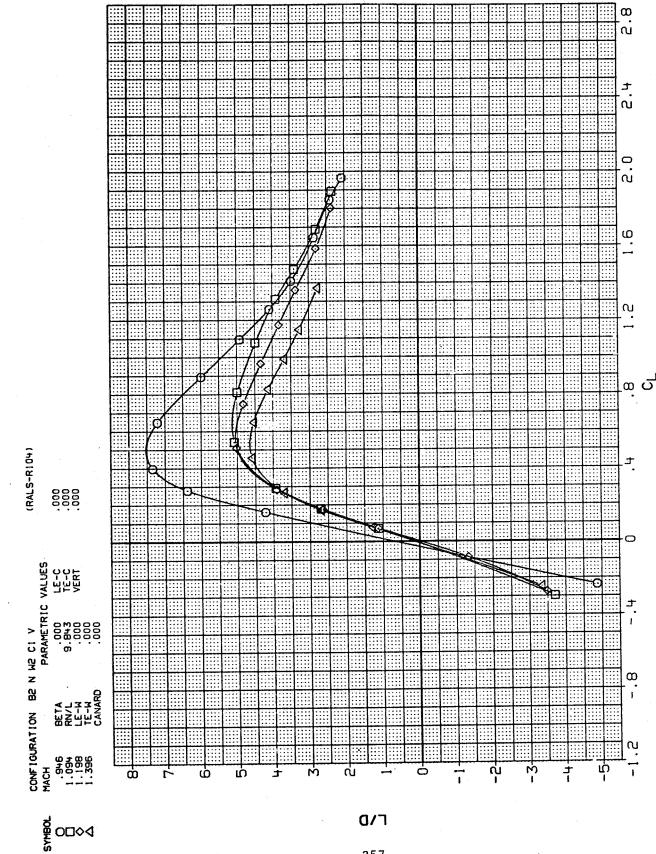


BASIC LONGITUDINAL CHARACTERISTICS FOR VARIOUS MACH NUMBERS

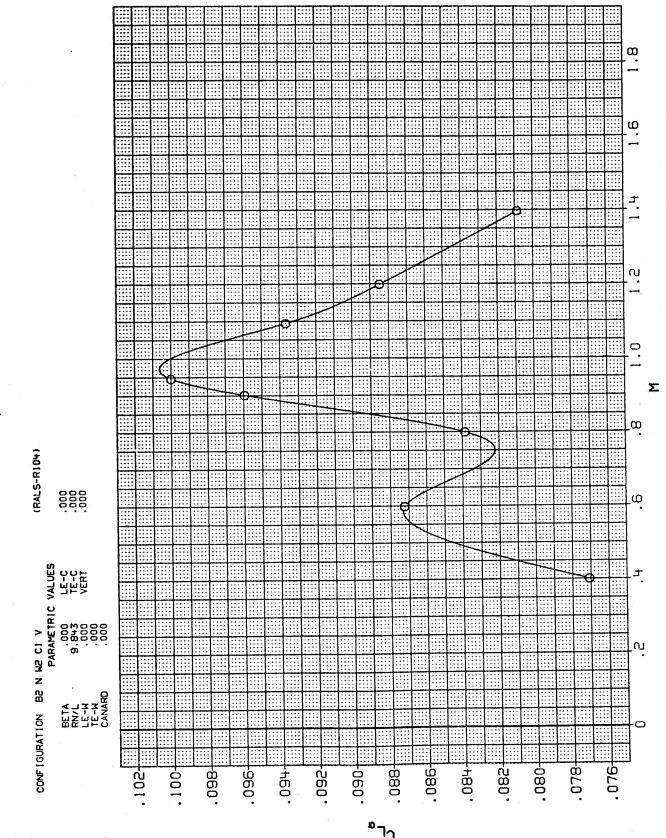
F16. 81

355

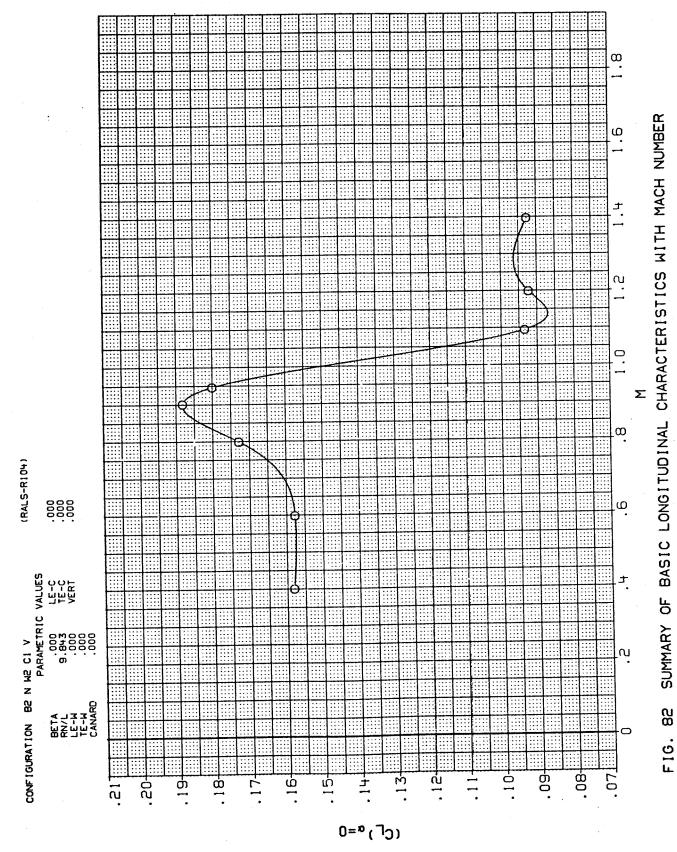


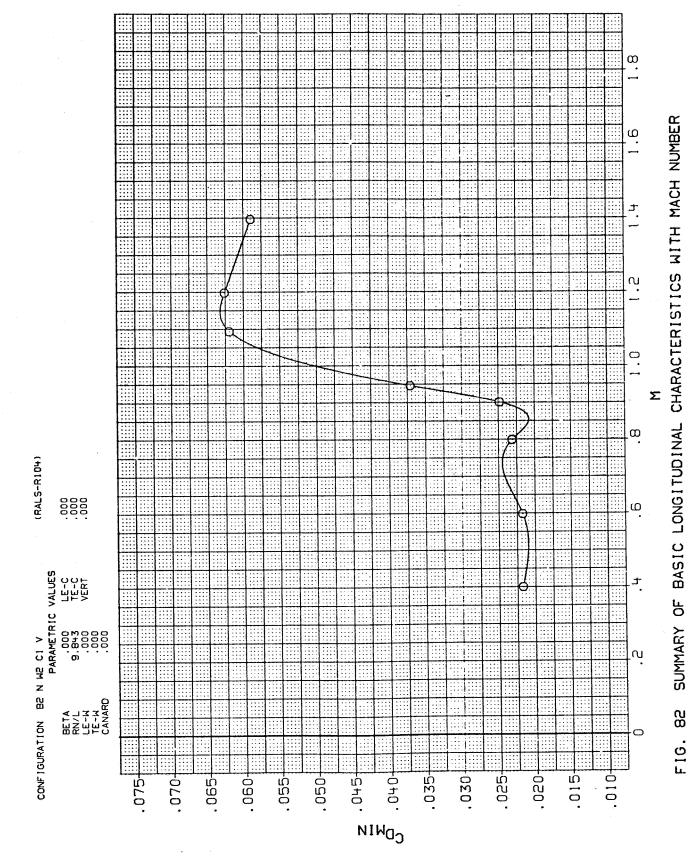


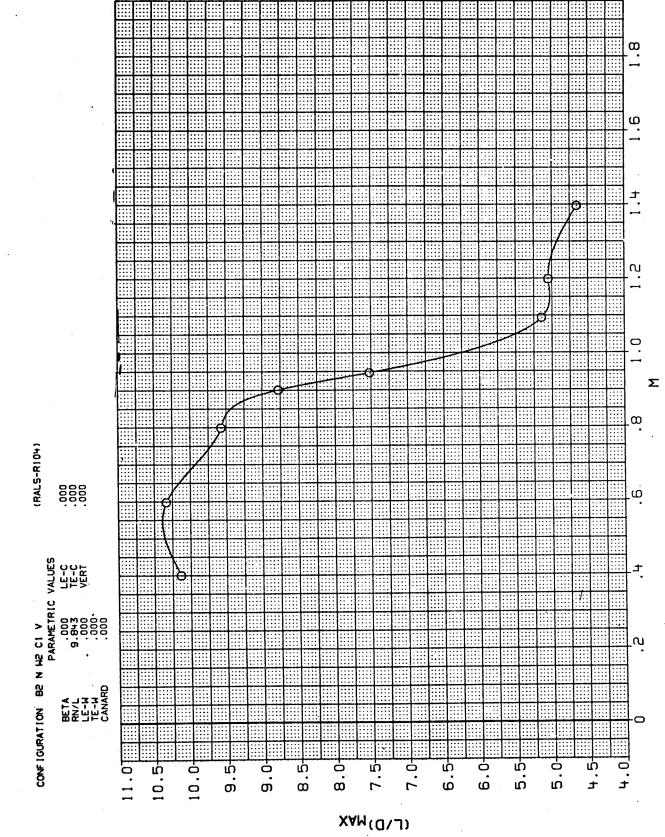
BASIC LONGITUDINAL CHARACTERISTICS FOR VARIOUS MACH NUMBERS F16. 81



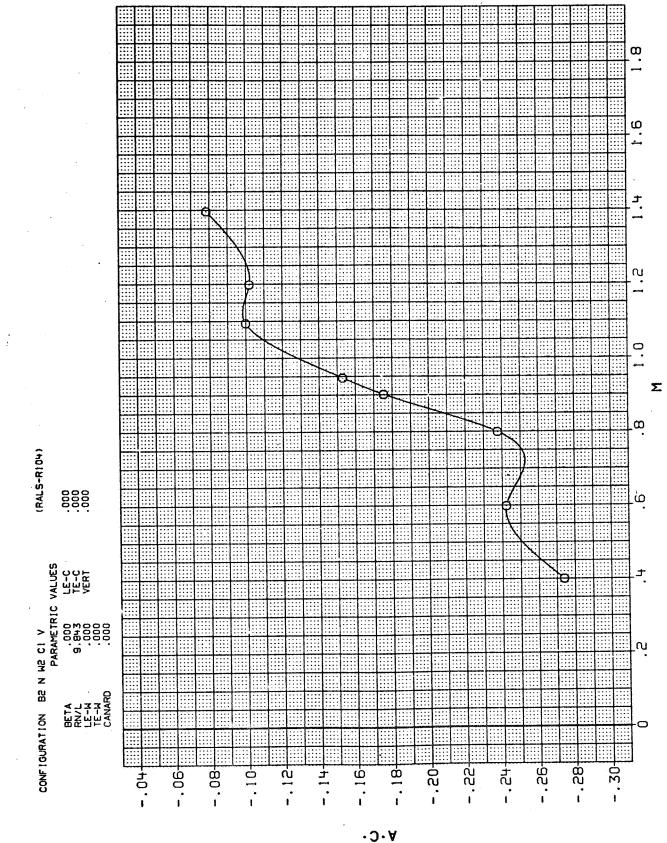
SUMMARY OF BASIC LONGITUDINAL CHARACTERISTICS WITH MACH NUMBER F16. 82



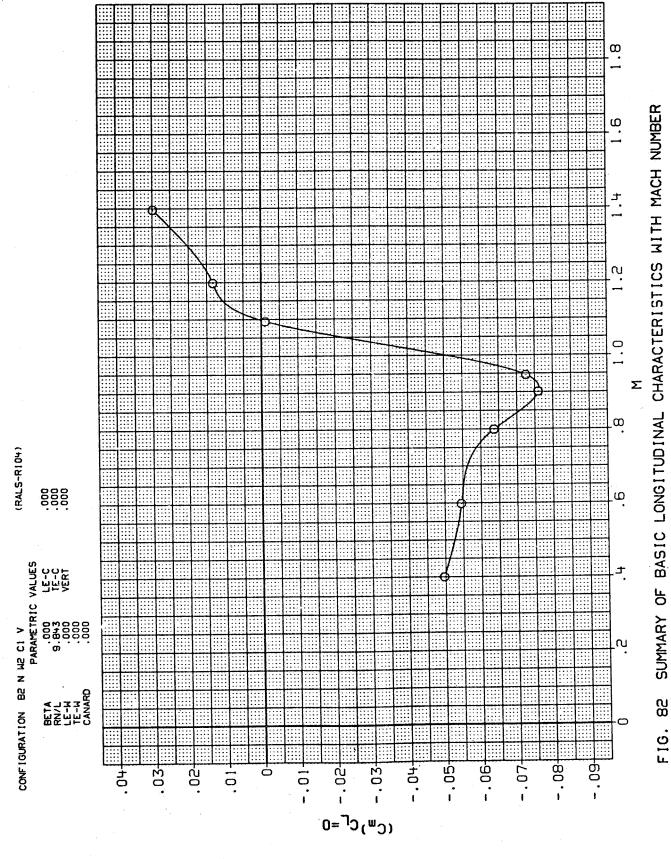




SUMMARY OF BASIC LONGITUDINAL CHARACTERISTICS WITH MACH NUMBER F16.82

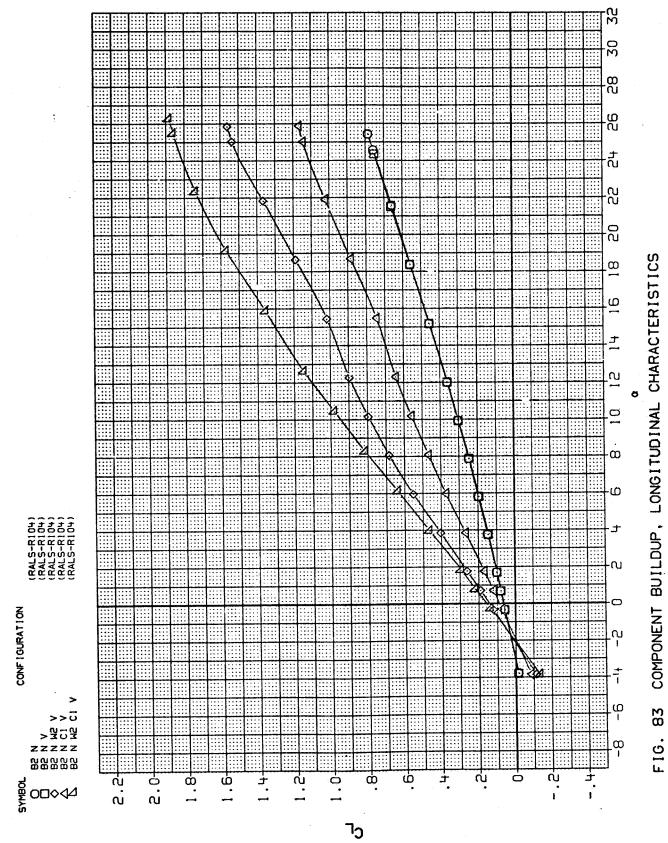


SUMMARY OF BASIC LONGITUDINAL CHARACTERISTICS WITH MACH NUMBER F16.82

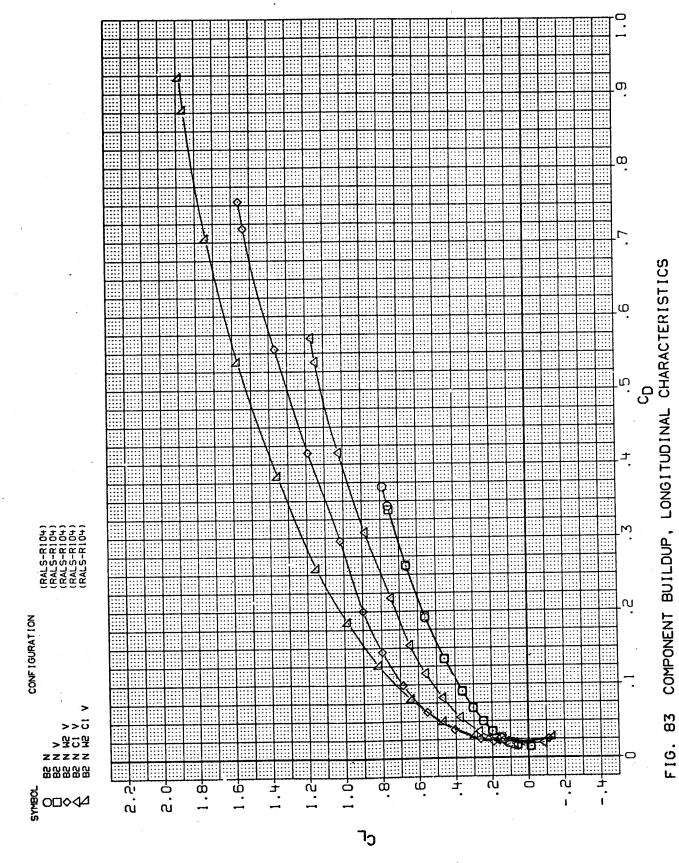


363

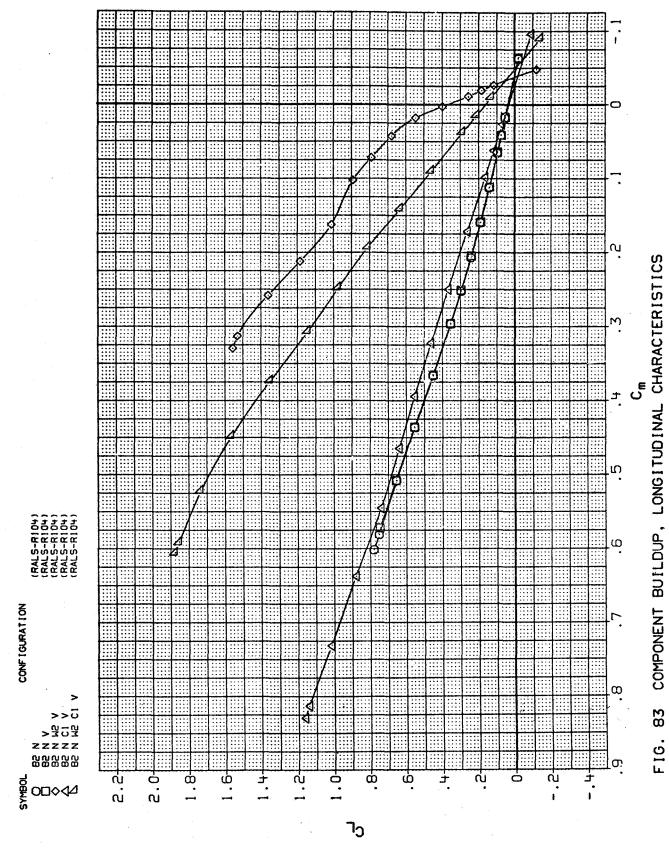
F16.82



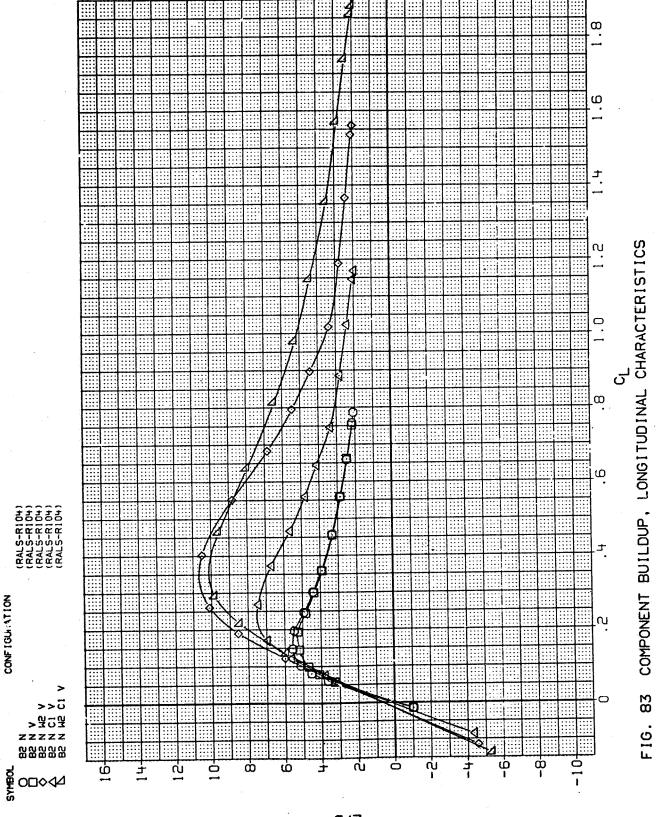
ACH = 140



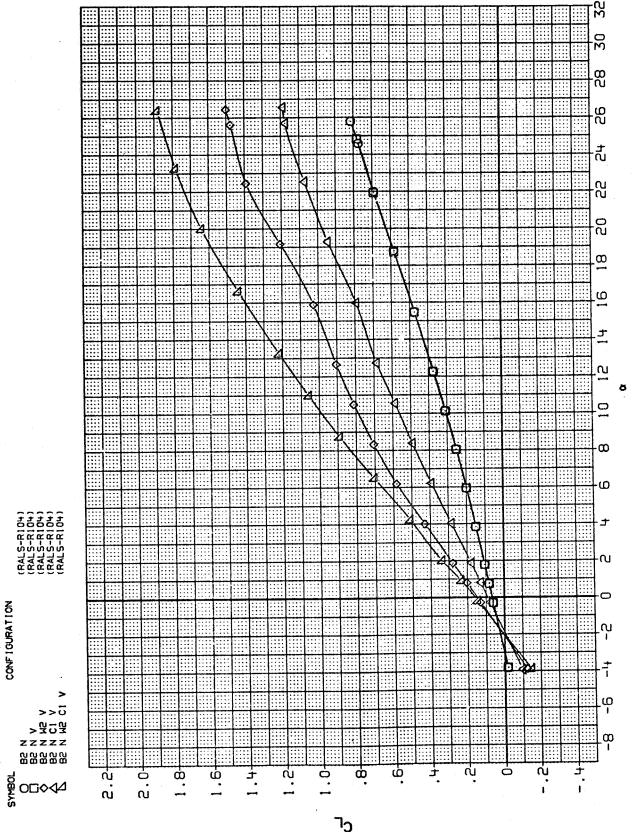
365



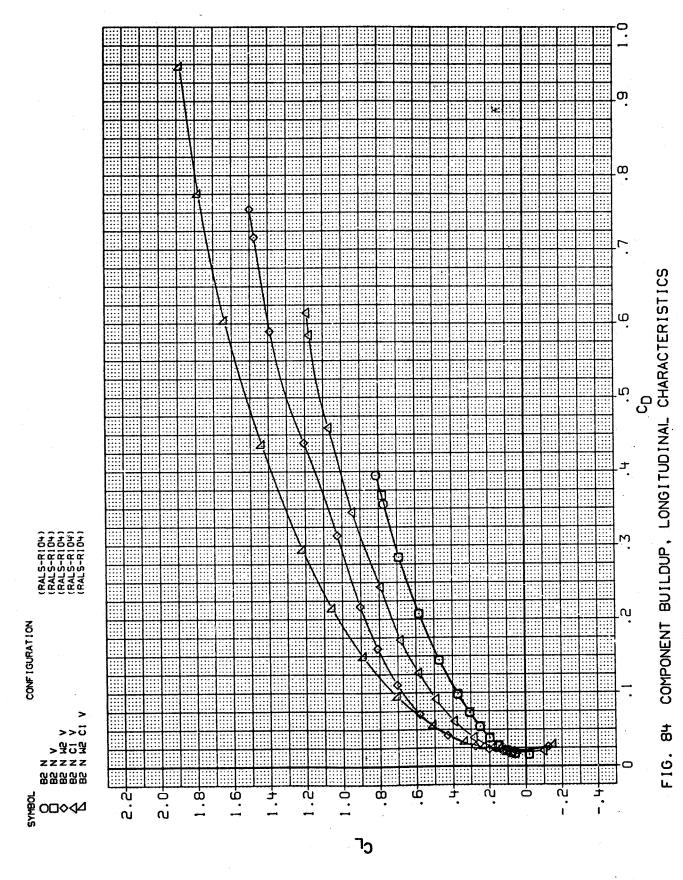
366



MACH = .40

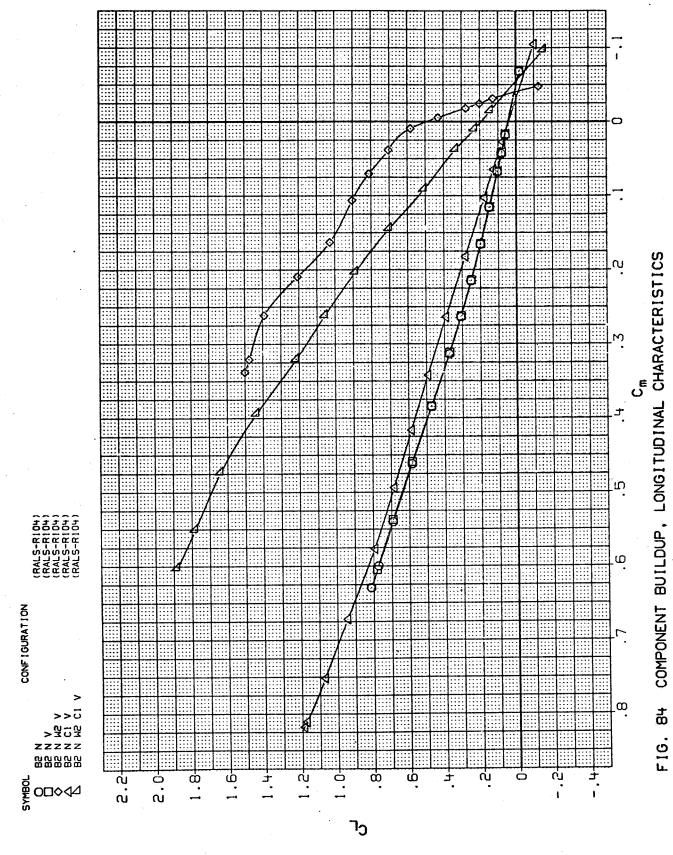


84 COMPONENT BUILDUP, LONGITUDINAL CHARACTERISTICS F16.



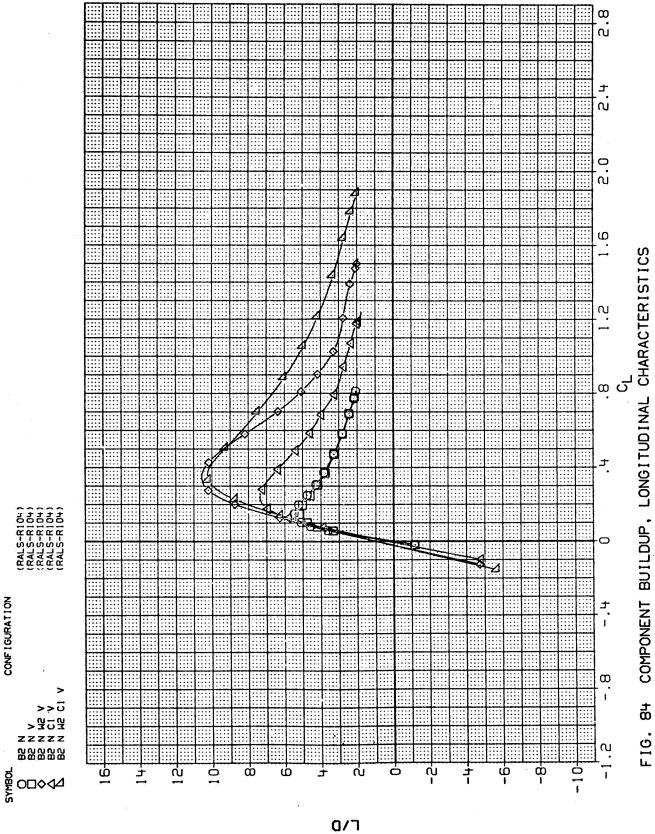
369

Ħ



370

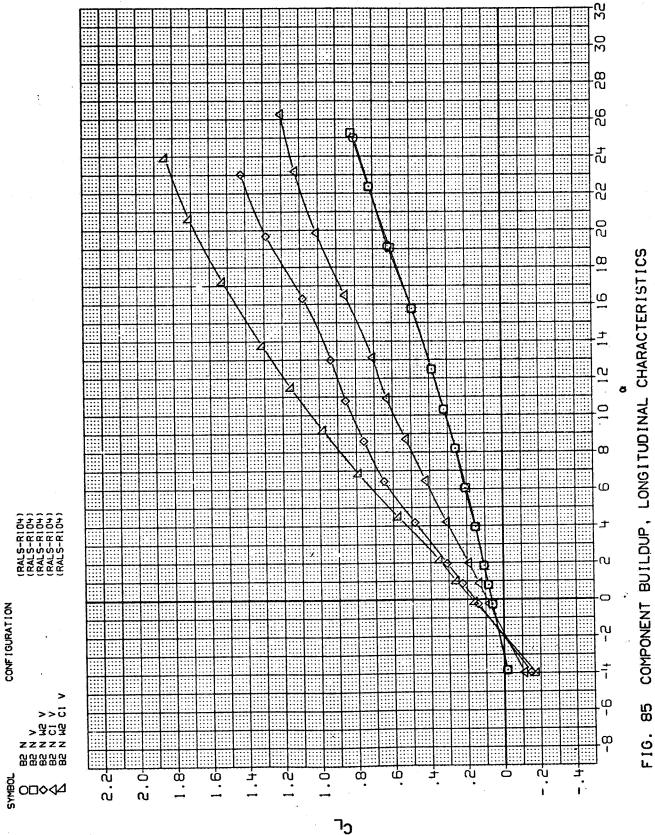
Ħ



11

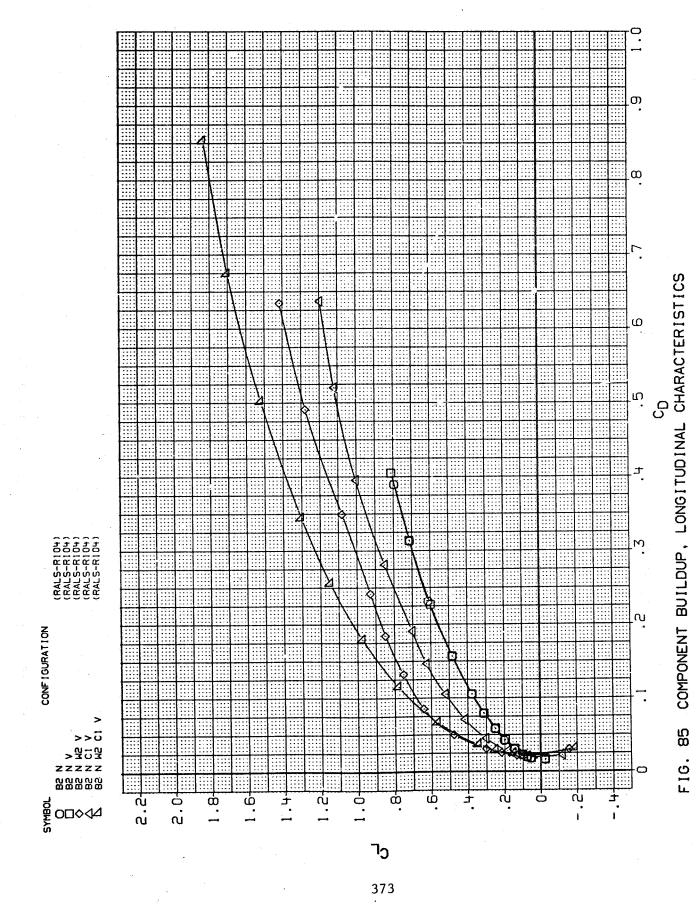
MACH

₩

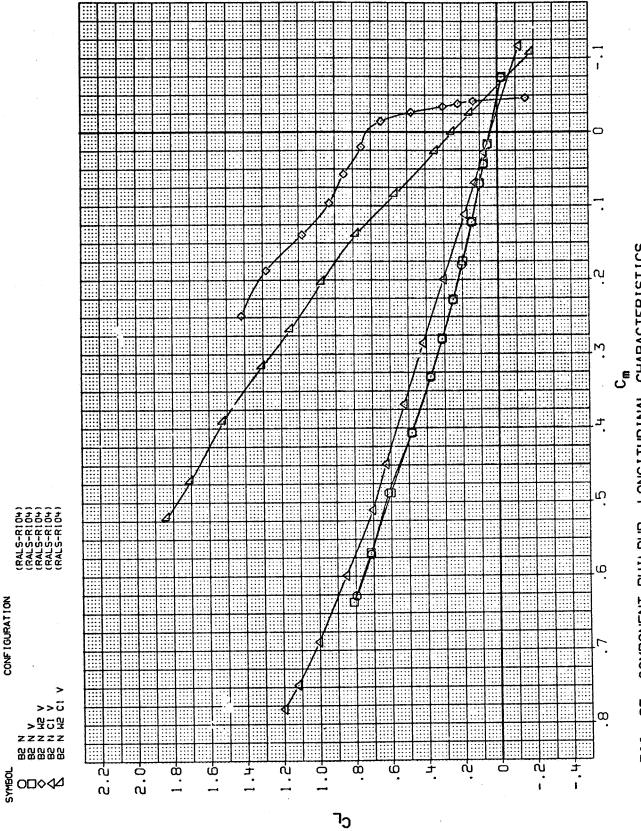


മ

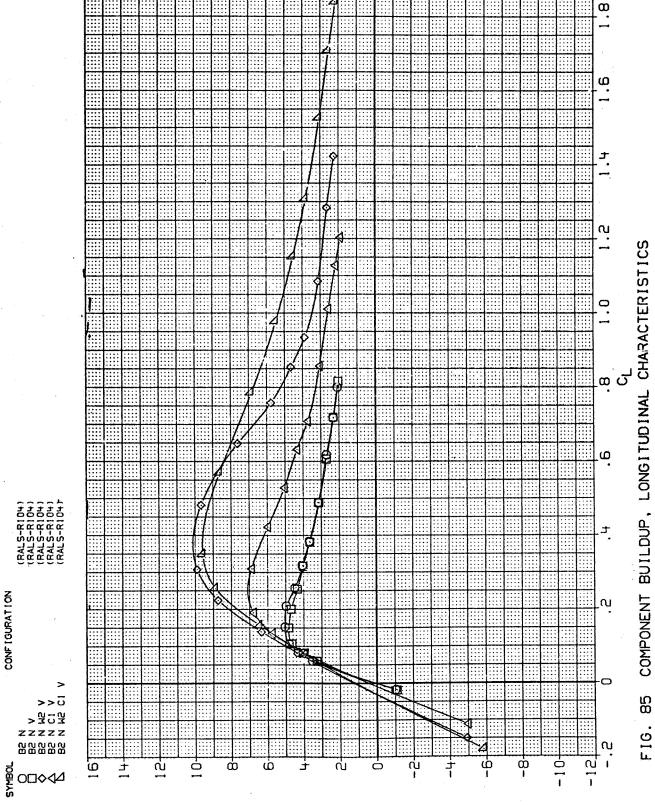
F16.



MACH = .80

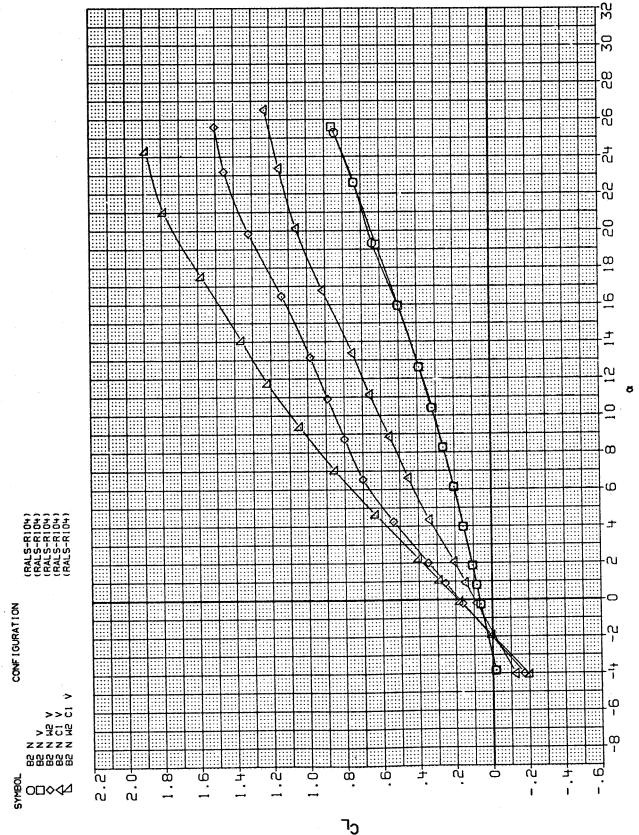


COMPONENT BUILDUP, LONGITUDINAL CHARACTERISTICS F16. 85

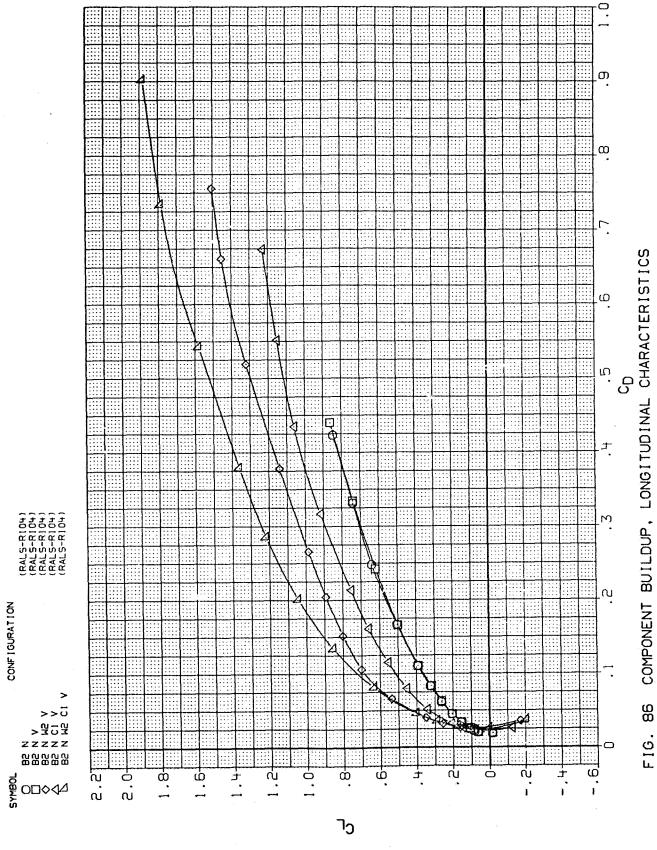


רום

.11

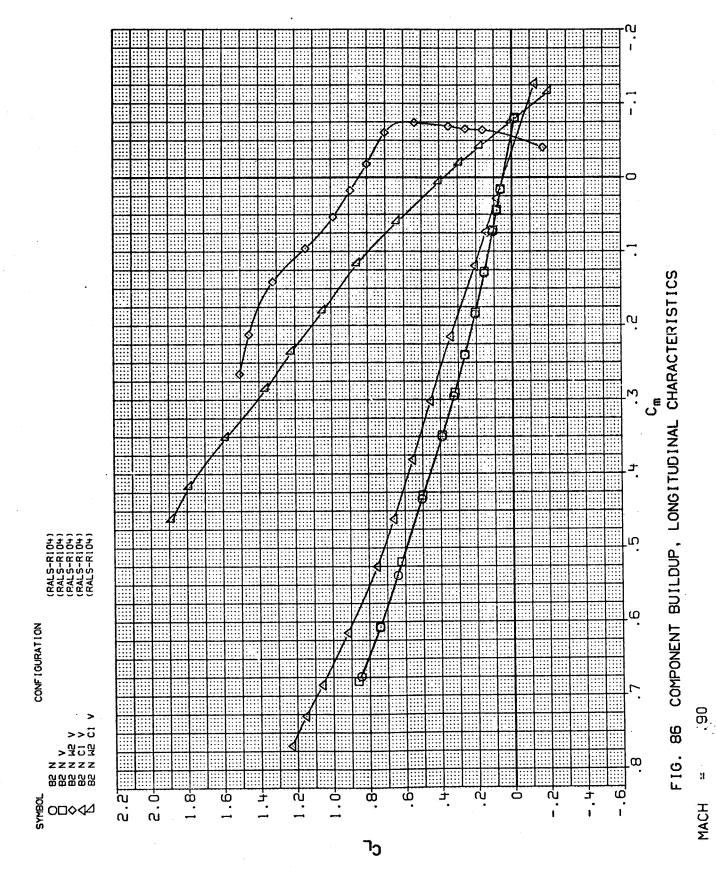


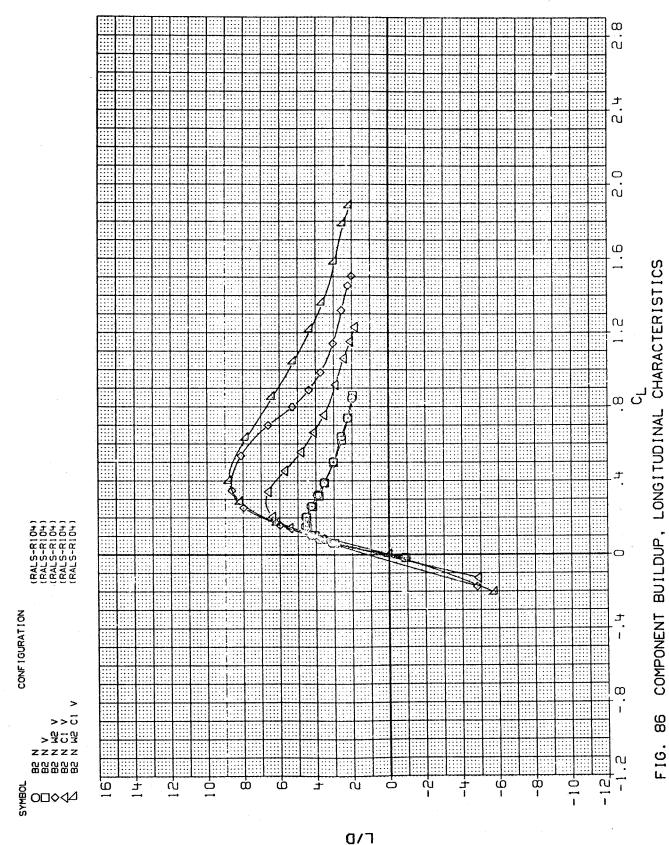
86 COMPONENT BUILDUP, LONGITUDINAL CHARACTERISTICS F16.



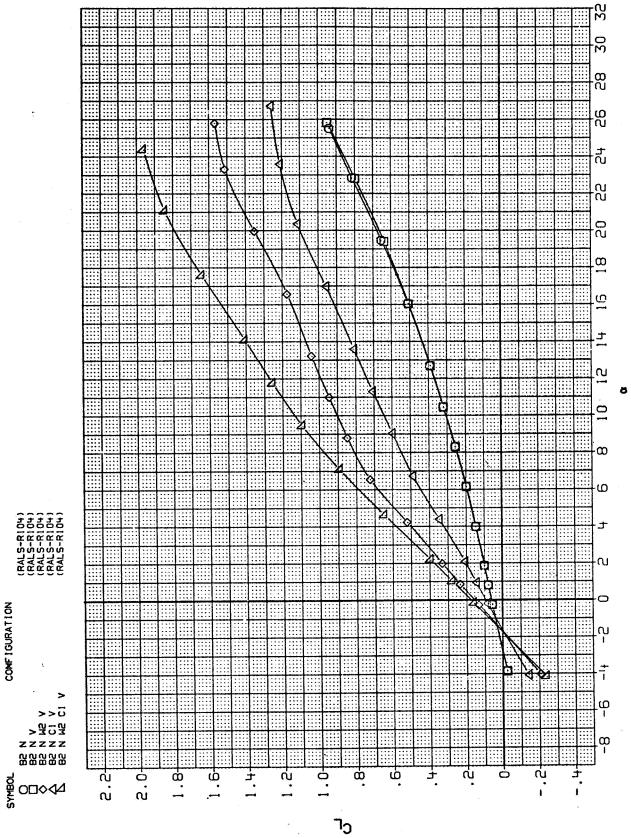
377

Ä



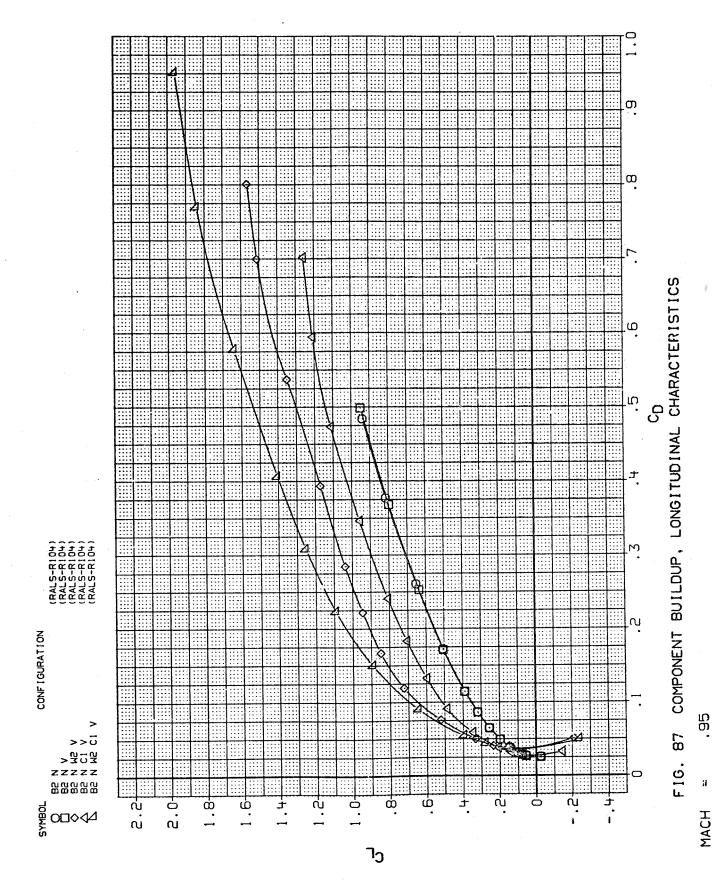


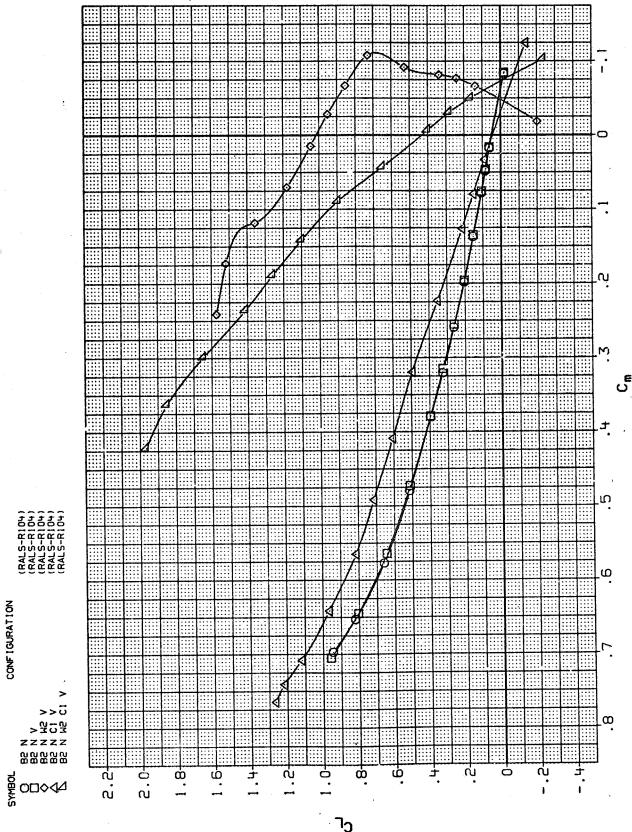
MACH = .90



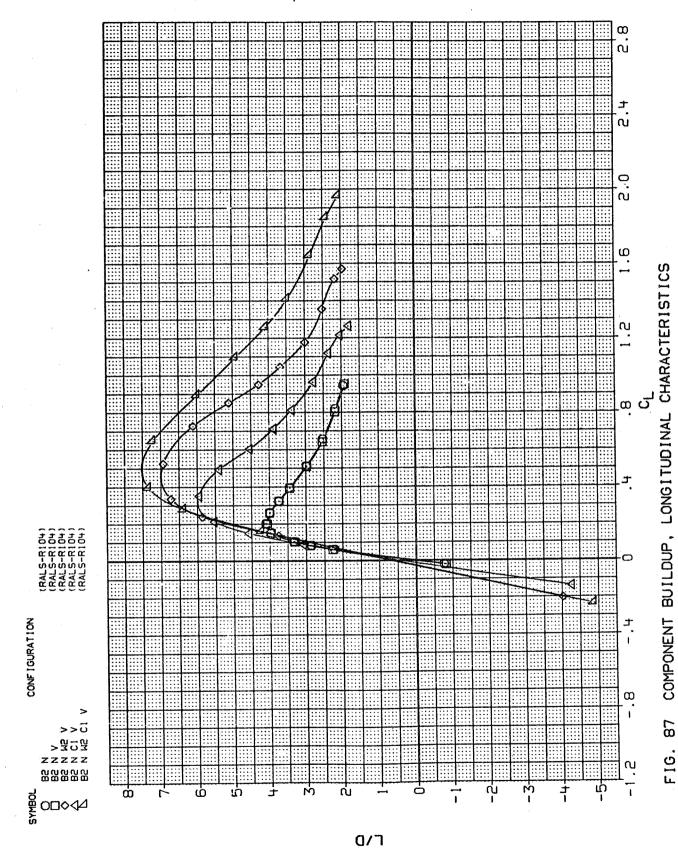
87 COMPONENT BUILDUP, LONGITUDINAL CHARACTERISTICS F16.

. წ

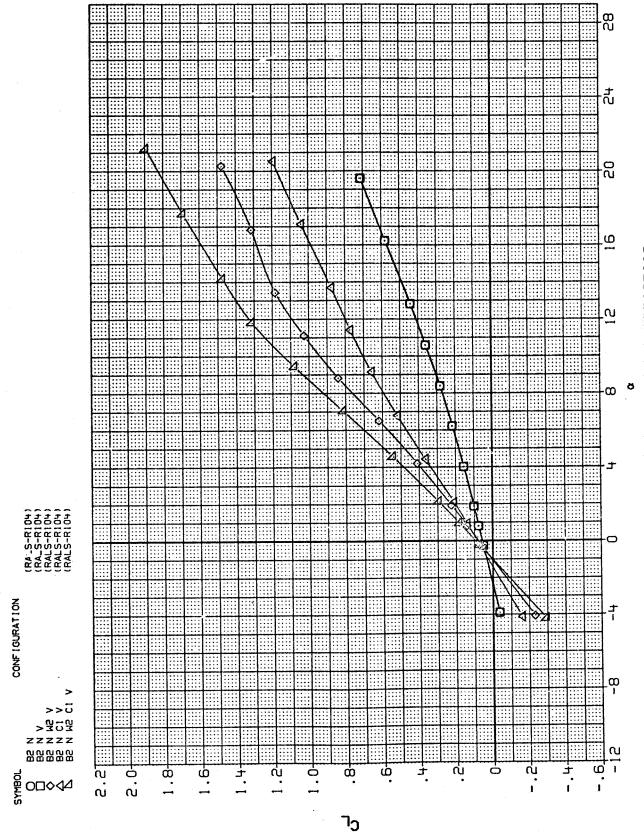




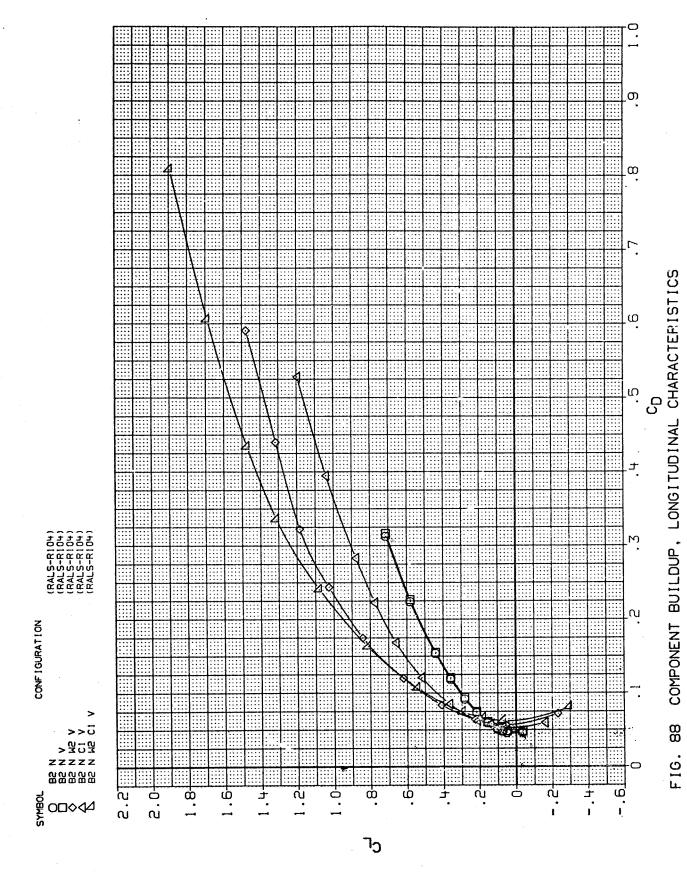
COMPONENT BUILDUP, LONGITUDINAL CHARACTERISTICS F16. 87

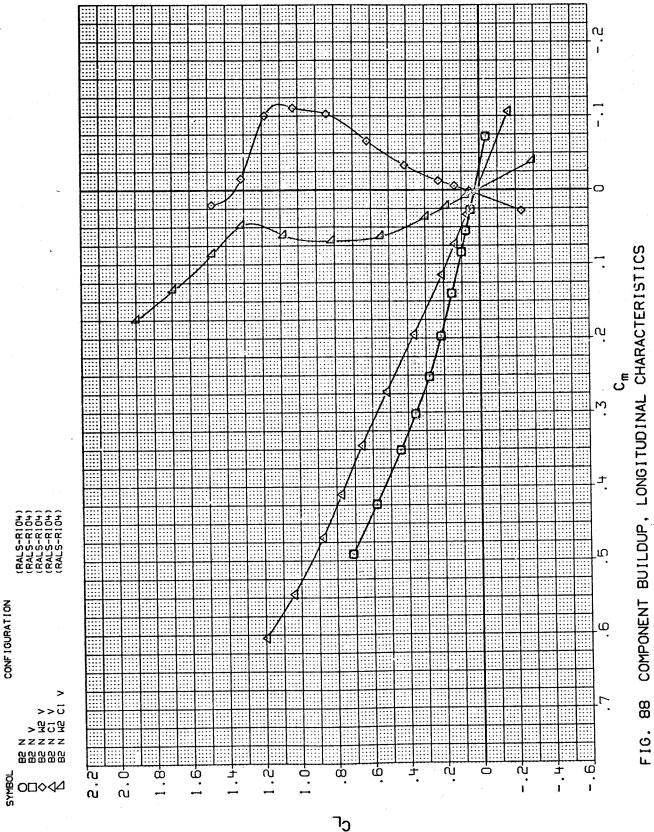


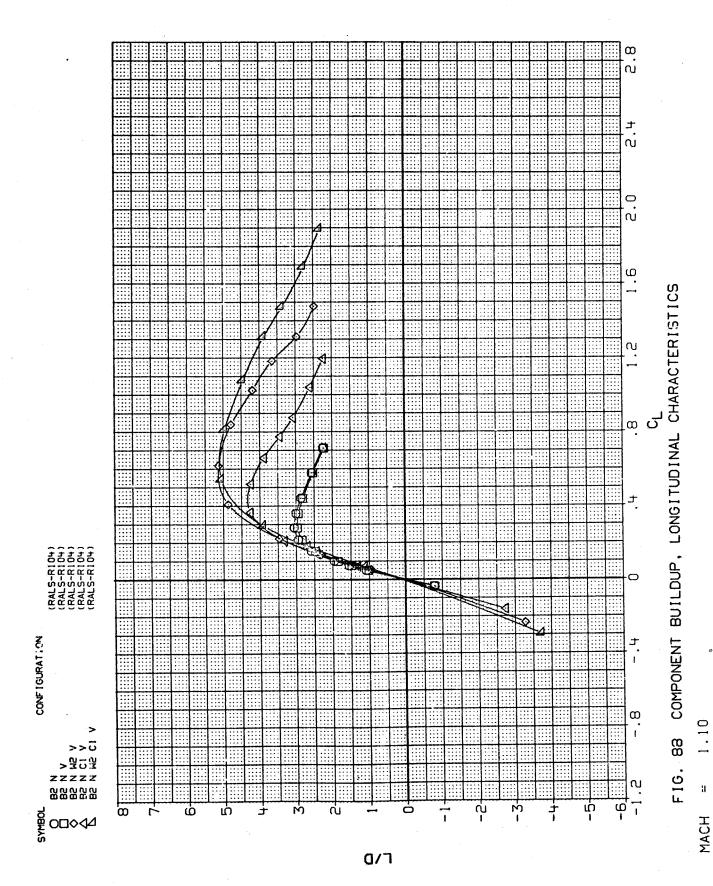
MACH = .95

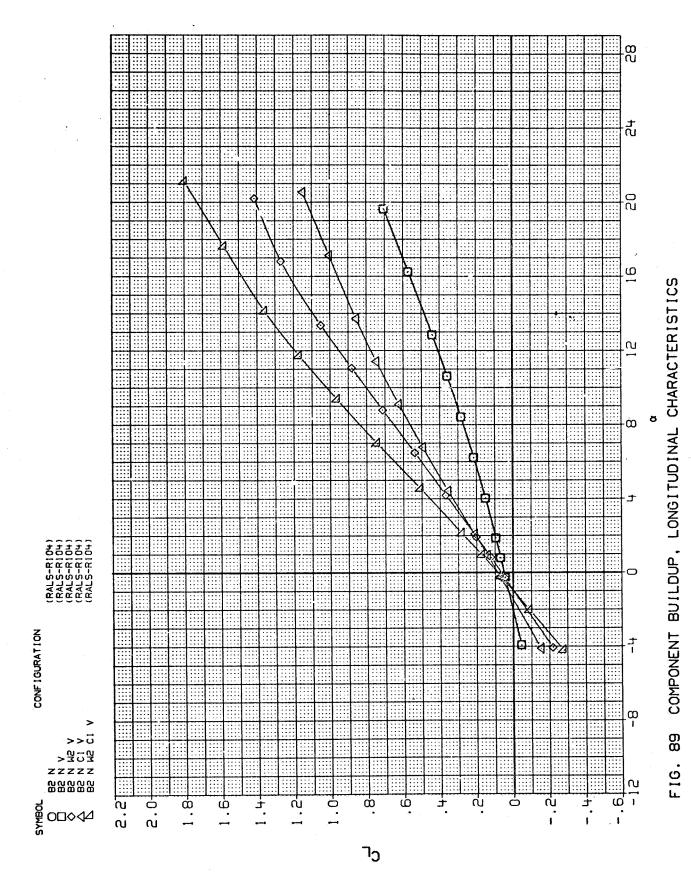


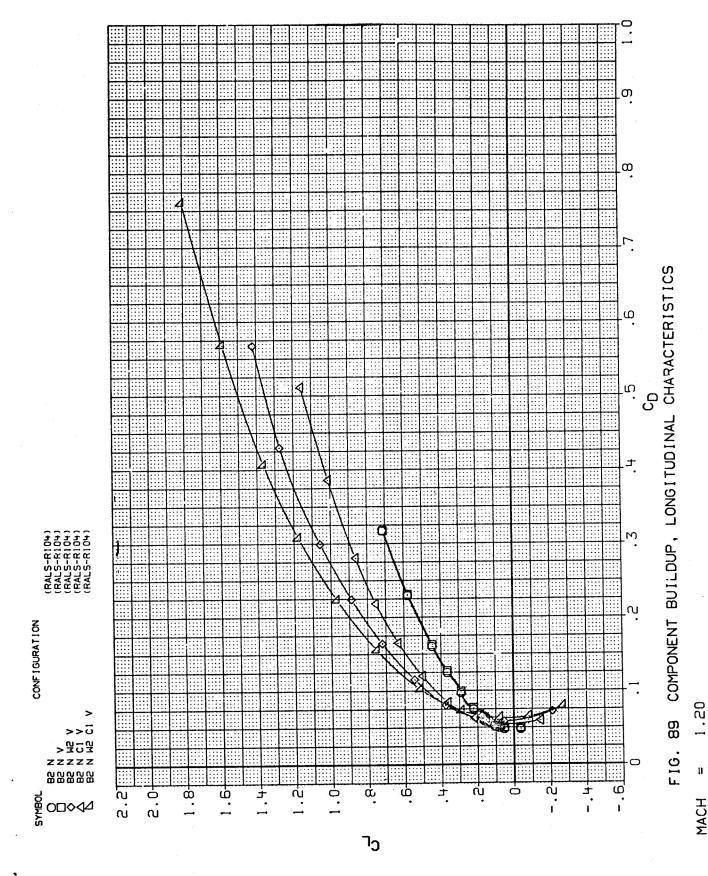
COMPONENT BUILDUP, LONGITUDINAL CHARACTERISTICS 88 F16.

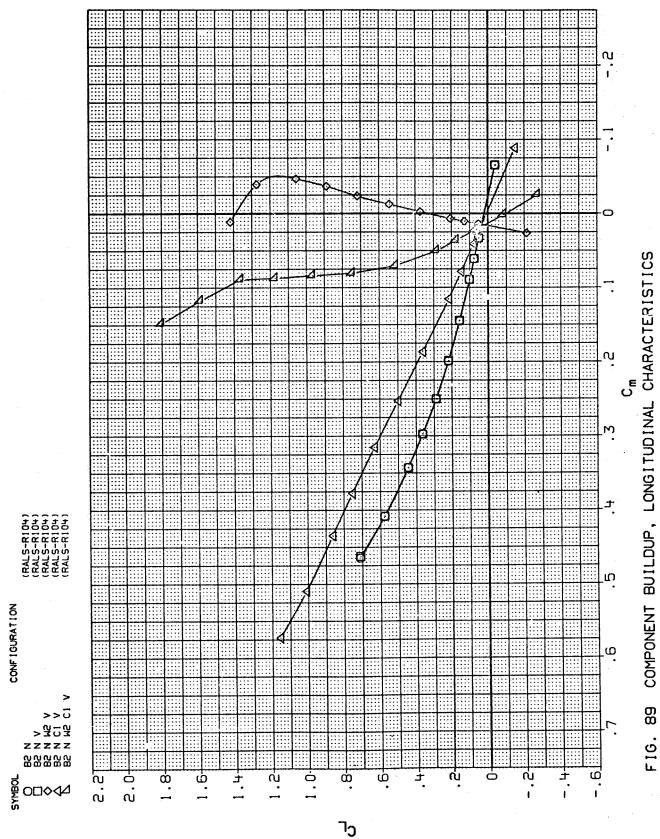




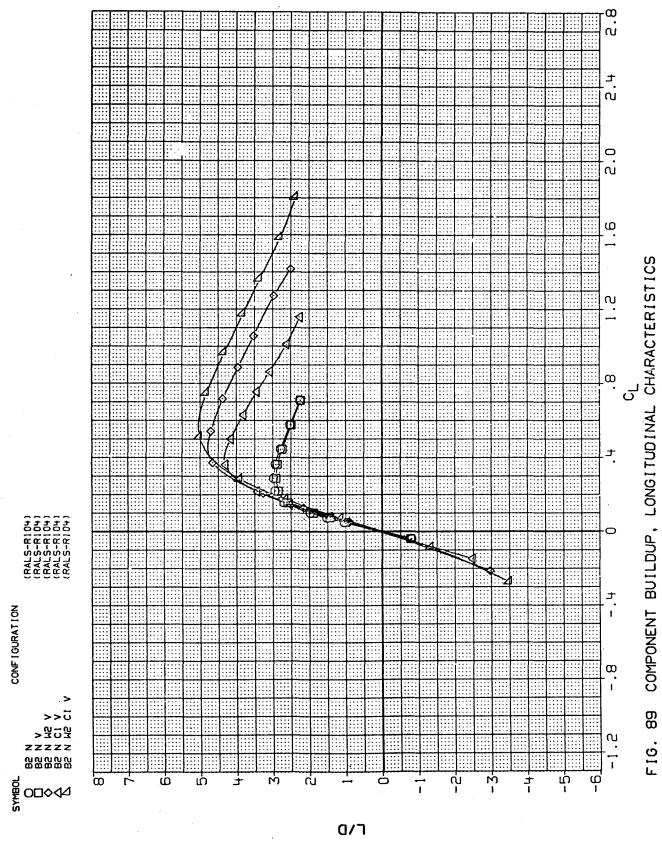




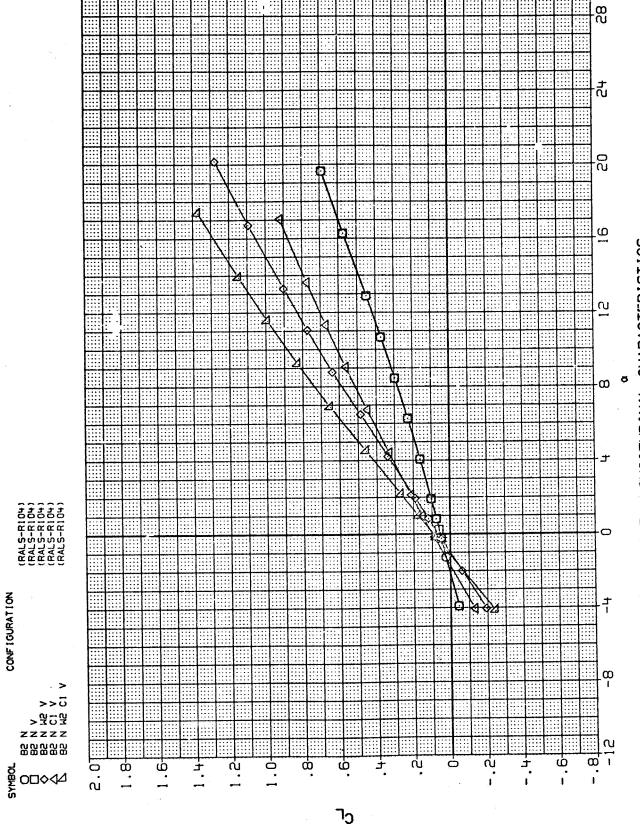




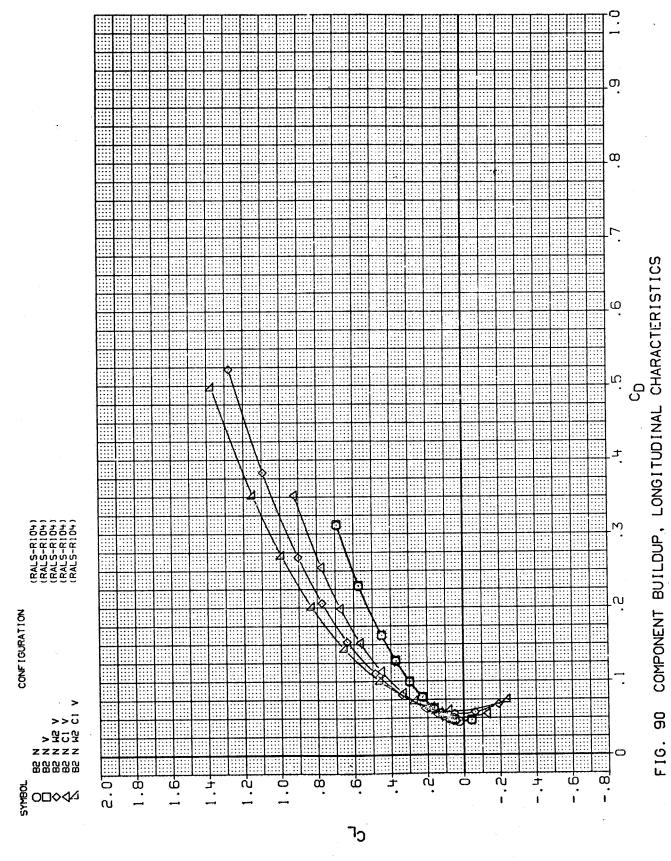
11



.H = 1.20



90 COMPONENT BUILDUP, LONGITUDINAL CHARACTERISTICS F16.



MACH = 1.40

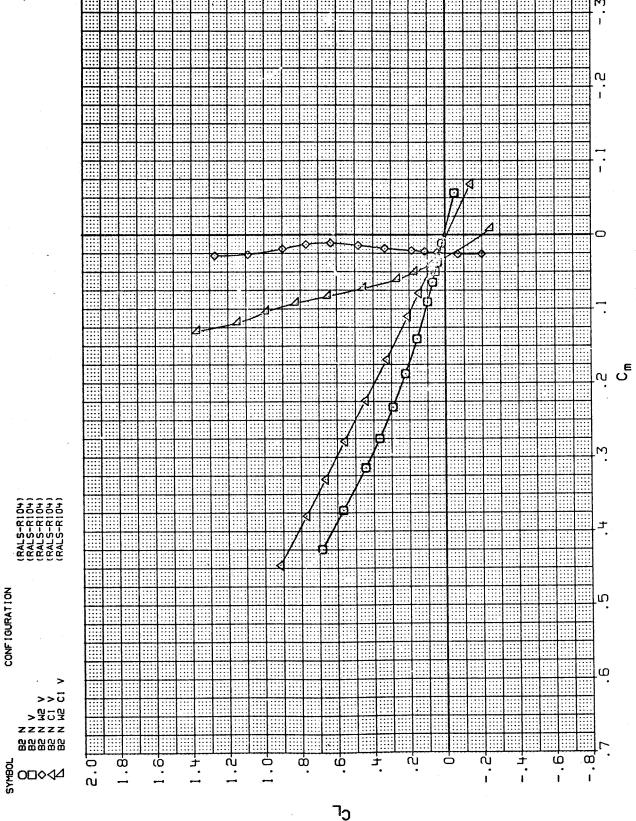


FIG. 90 COMPONENT BUILDUP, LONGITUDINAL CHARACTERISTICS

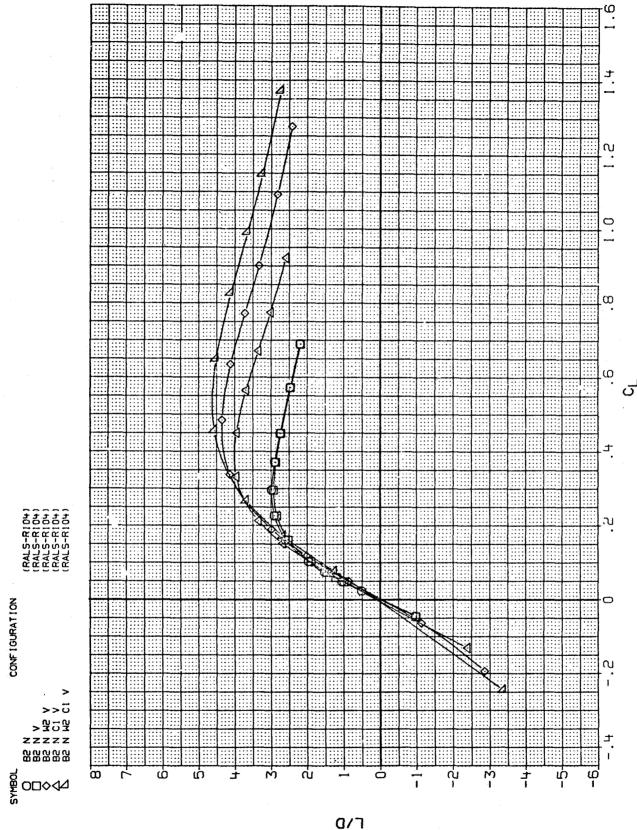
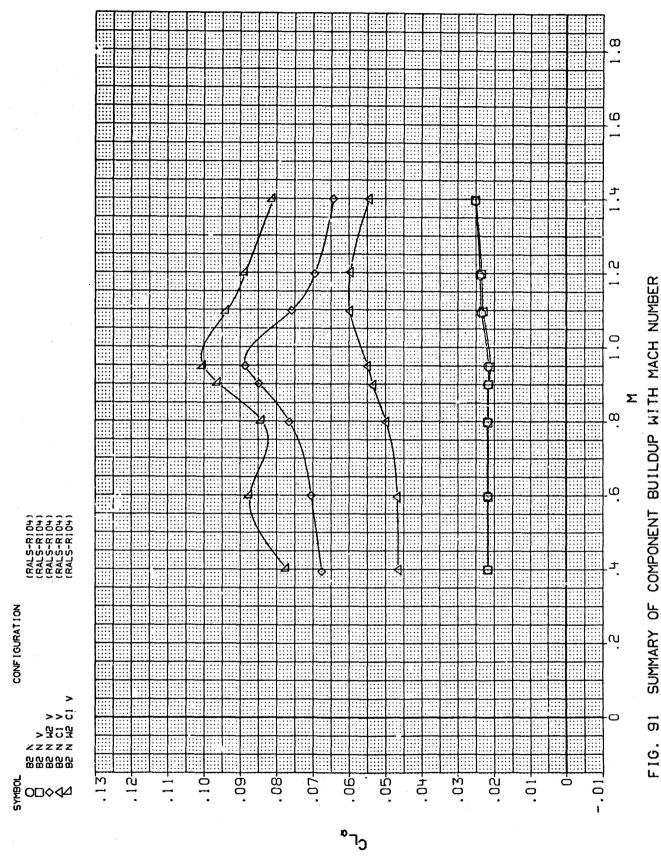
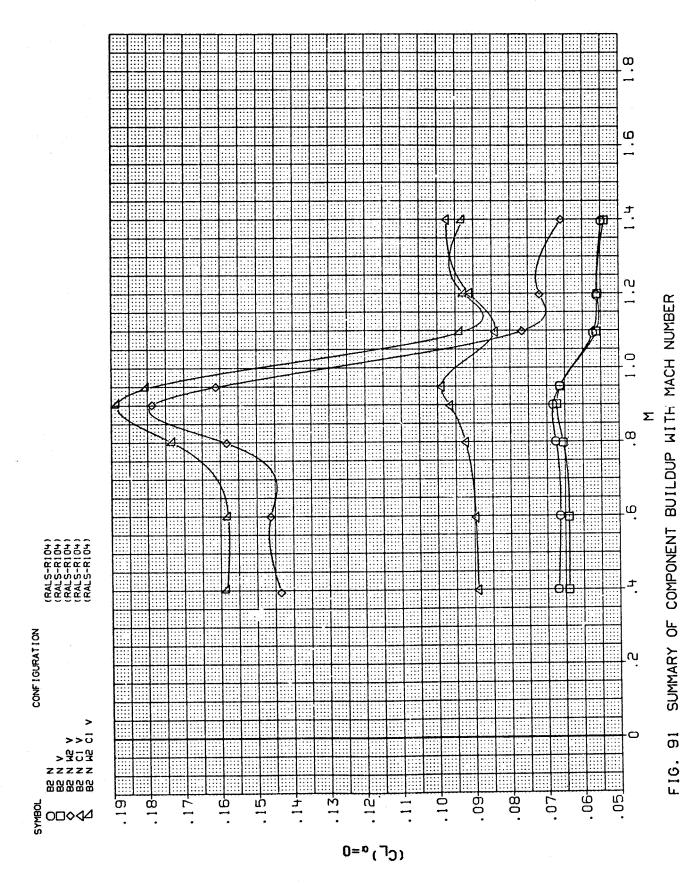
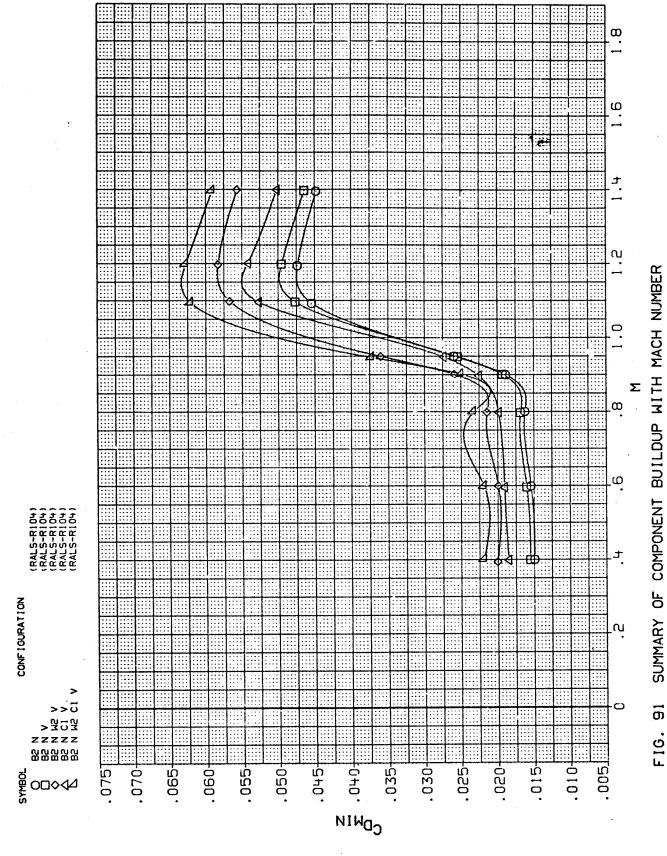


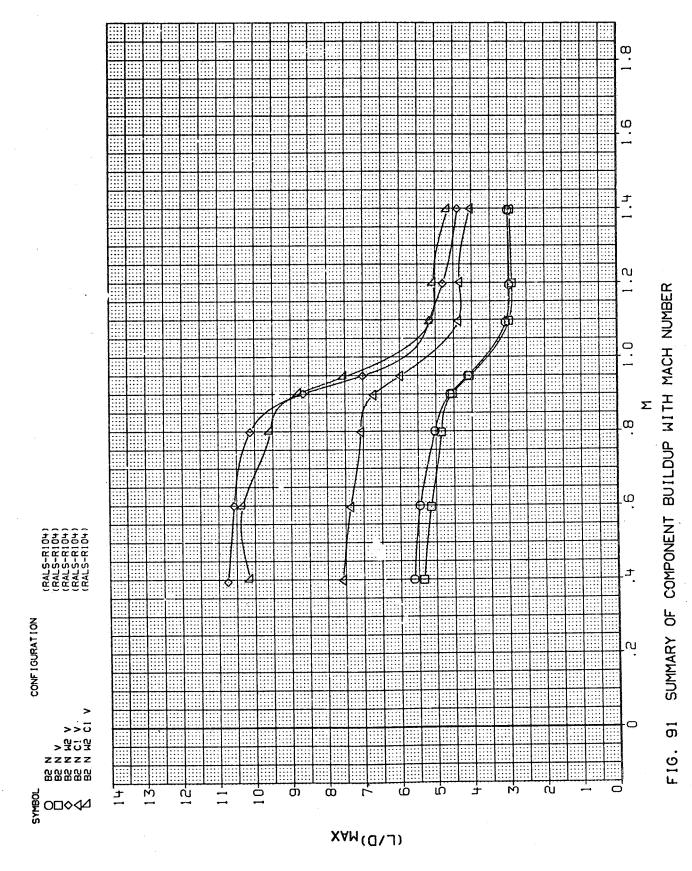
FIG. 90 COMPONENT BUILDUP, LONGITUDINAL CHARACTERISTICS

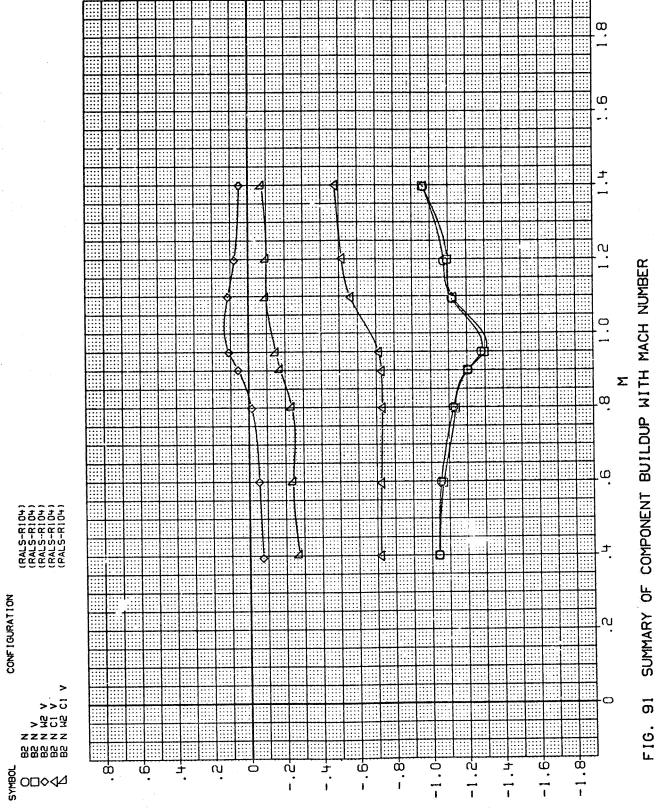


. .

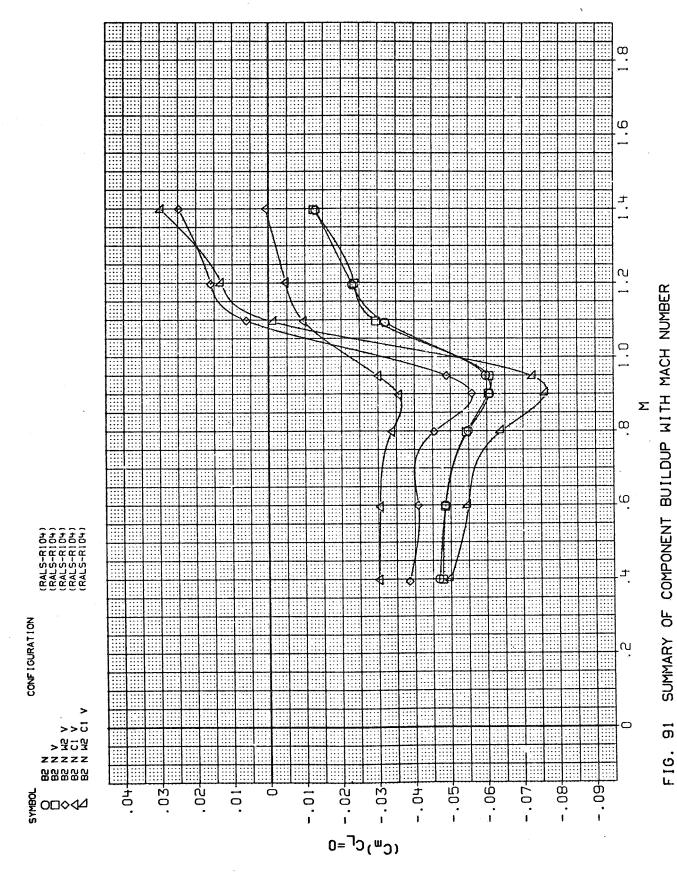


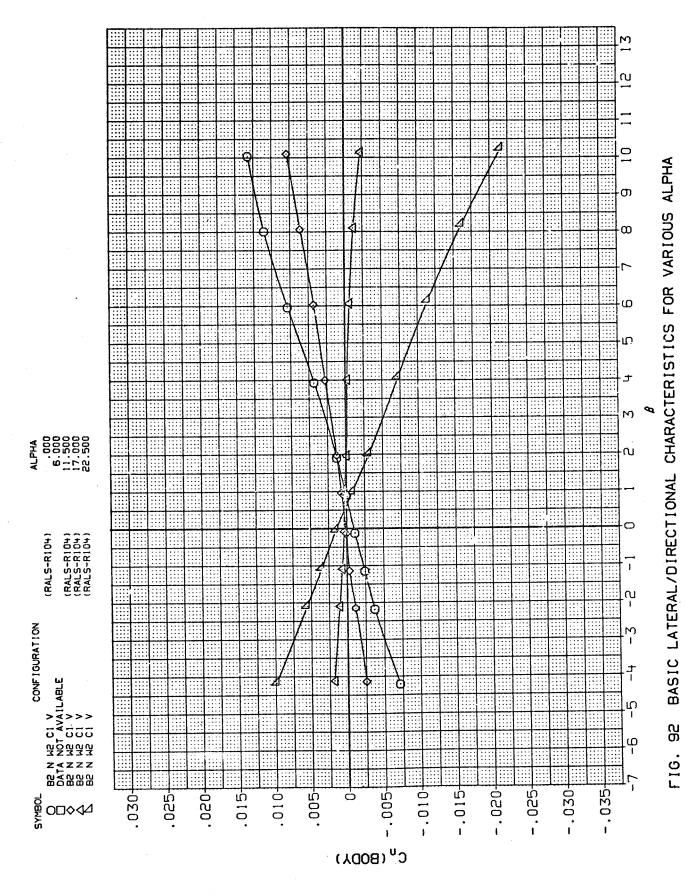


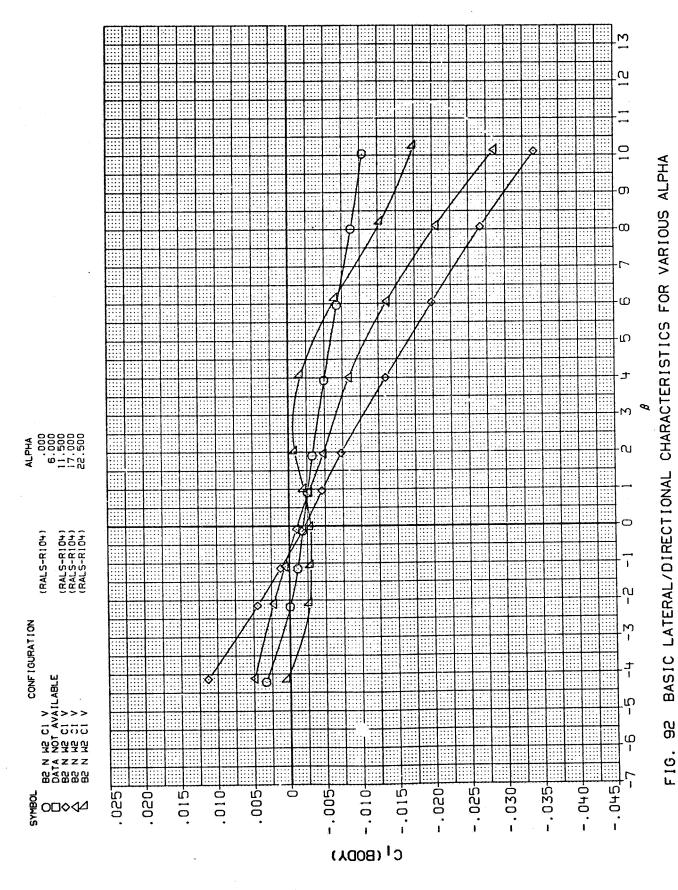




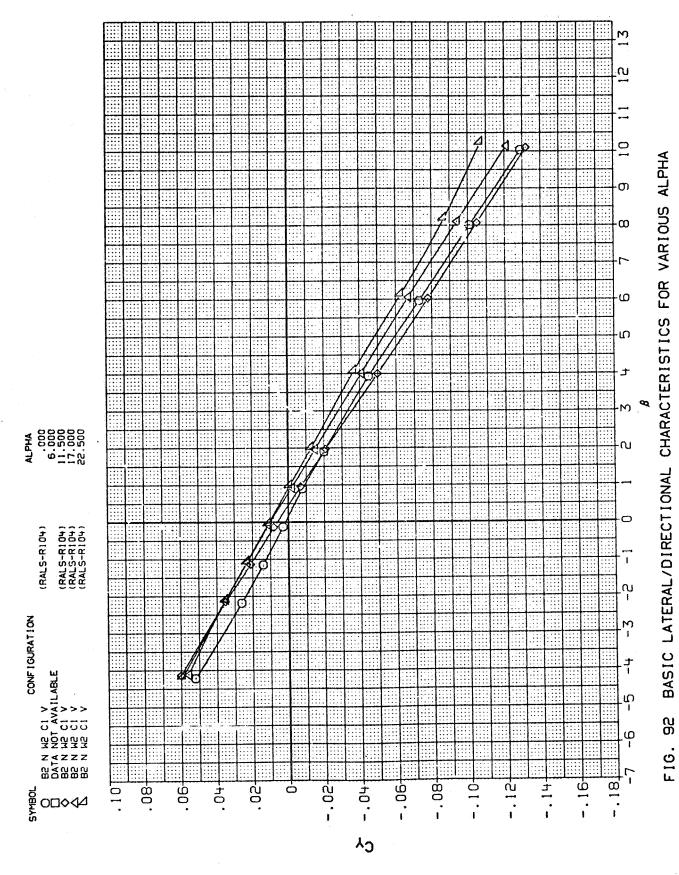
۷.C.



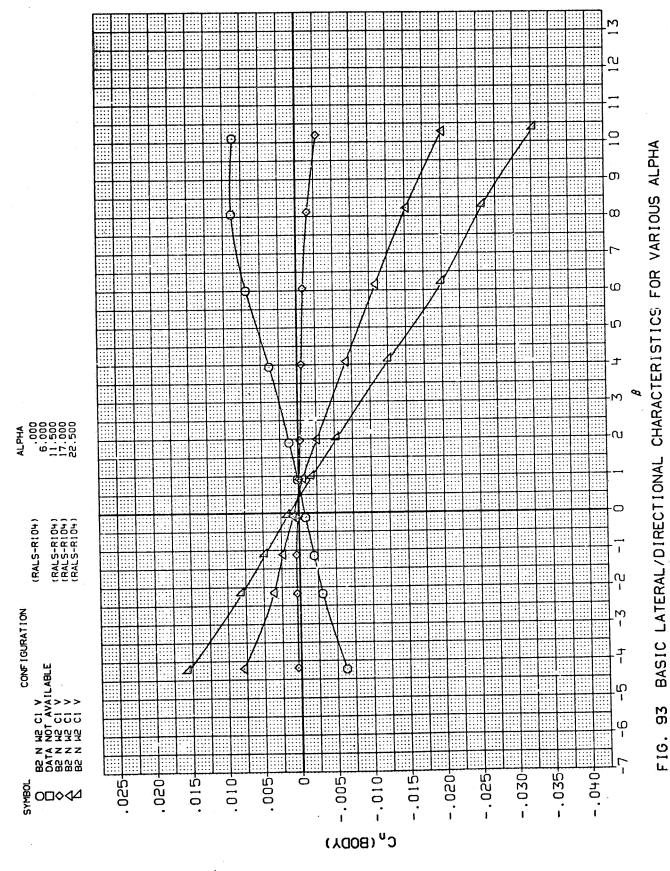




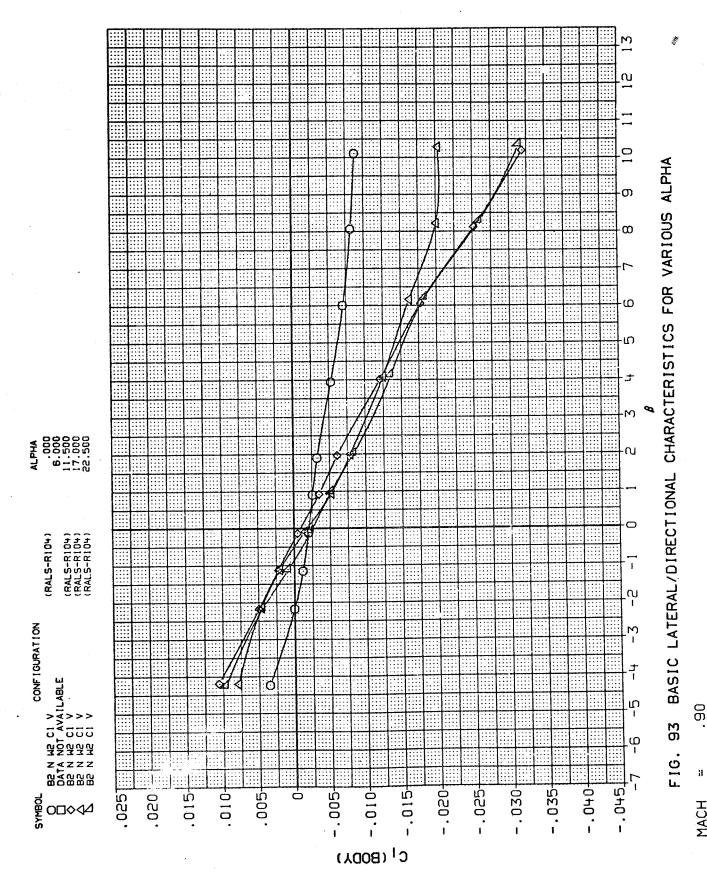
403



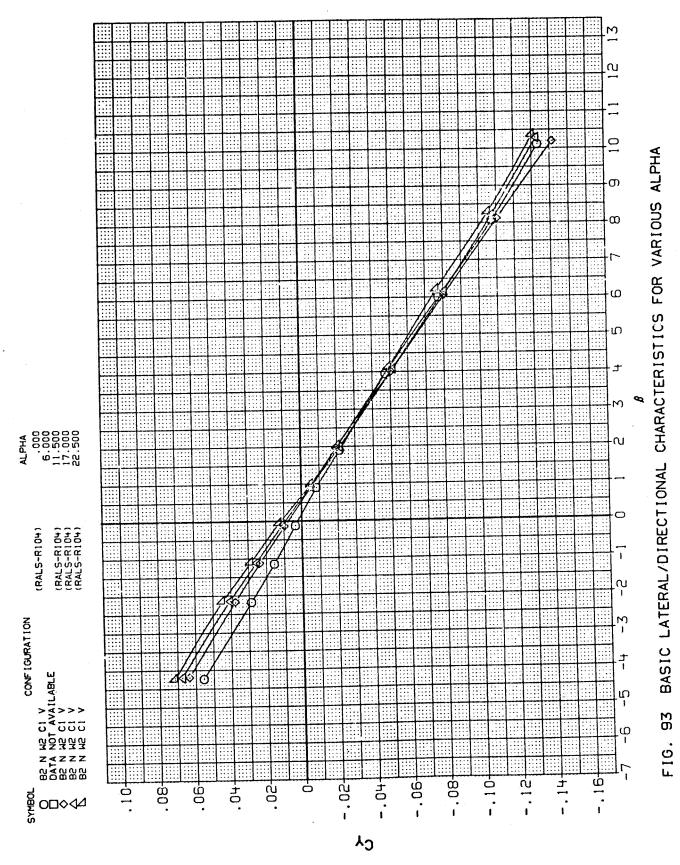
404

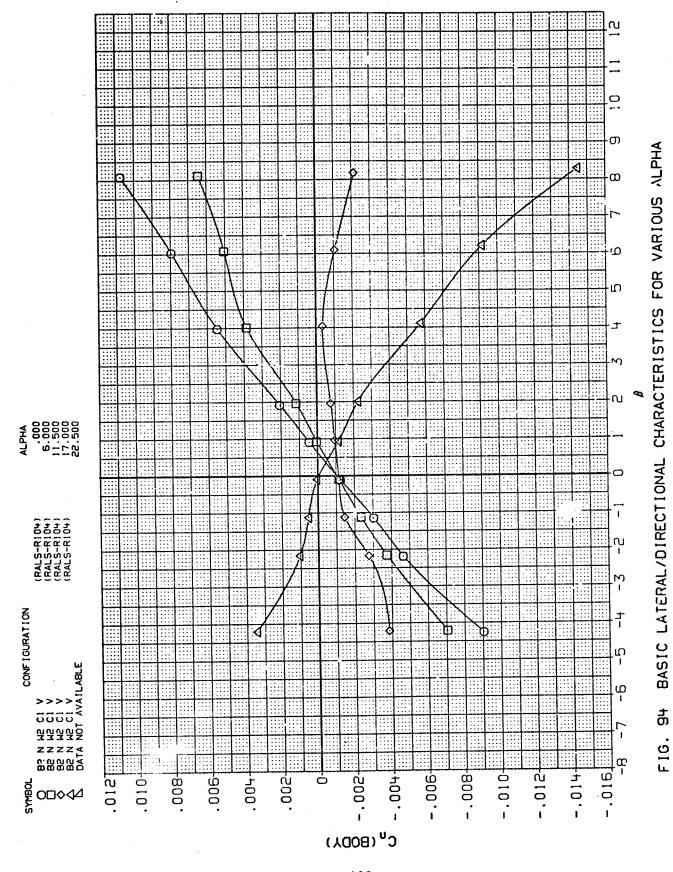


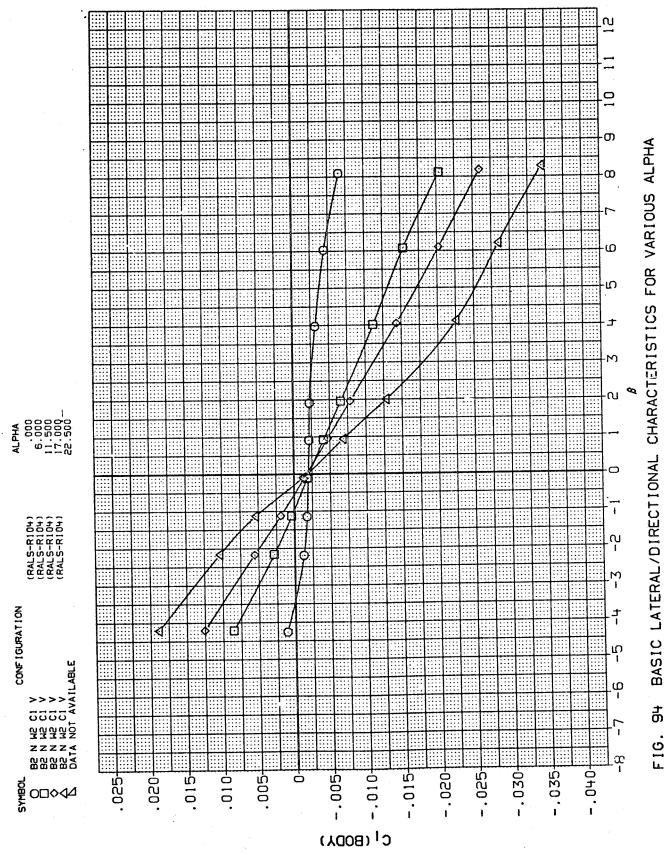
93 FIG.



н





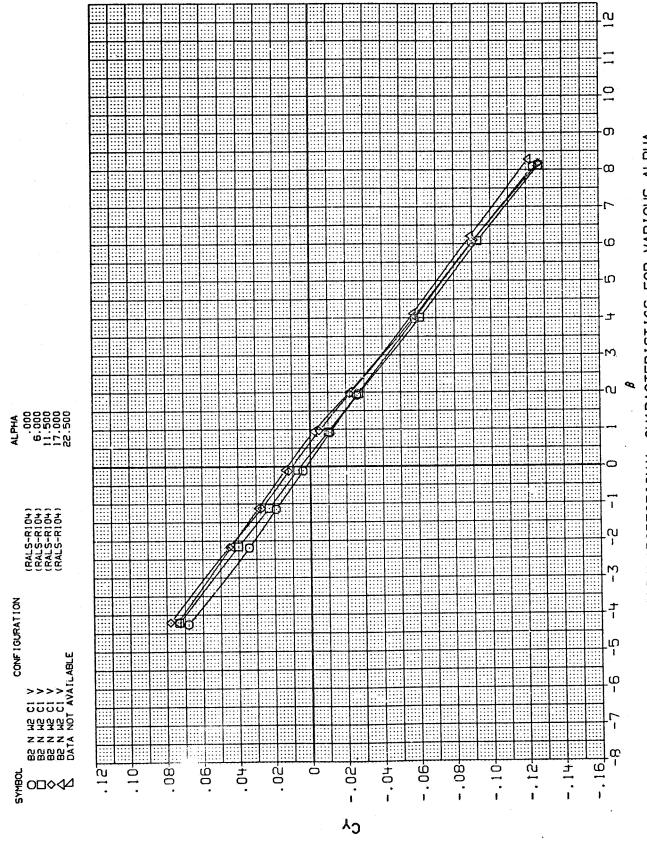


409

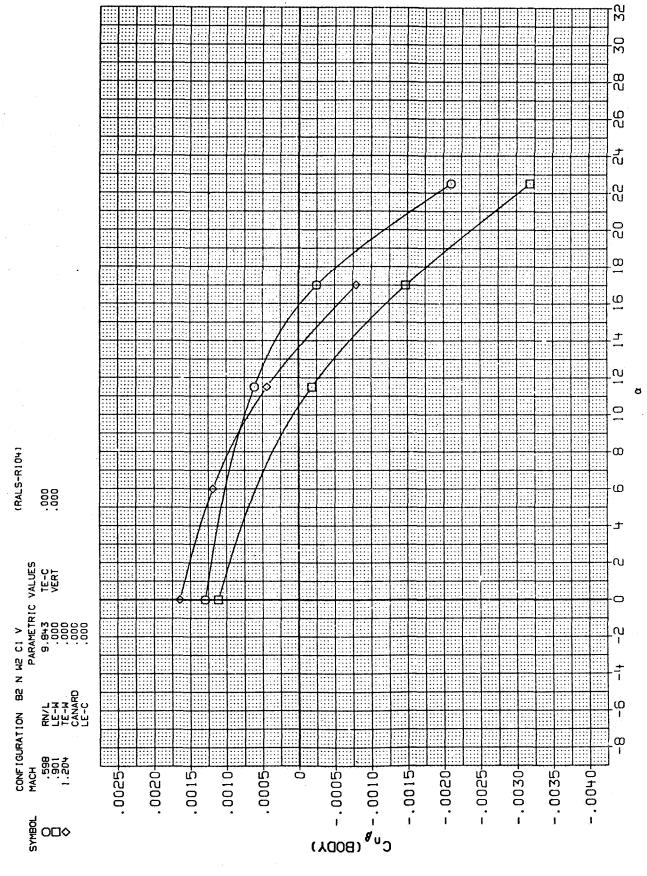
11

MACH

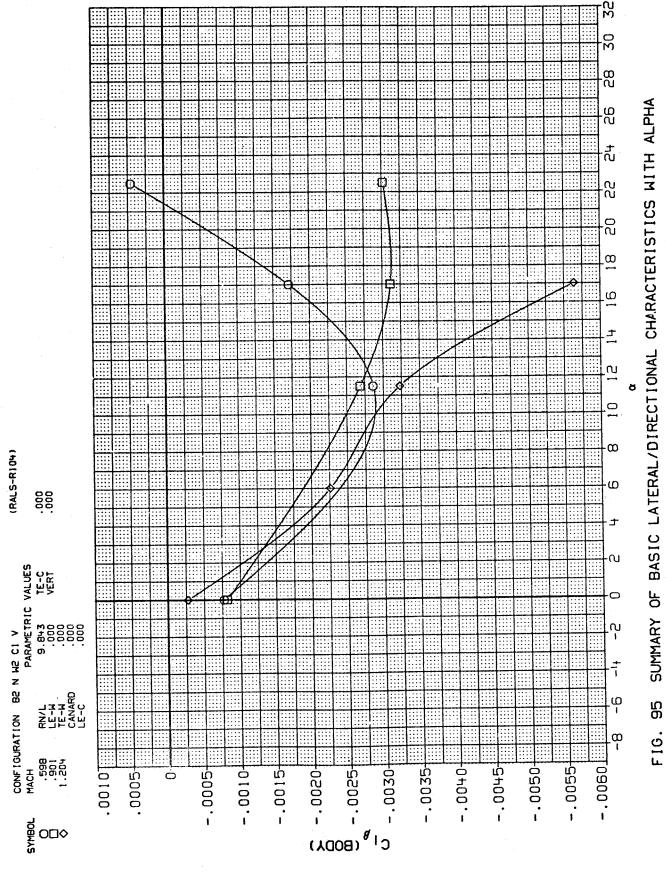
F1G. 94



BASIC LATERAL/DIRECTIONAL CHARACTERISTICS FOR VARIOUS ALPHA ф ф F16.

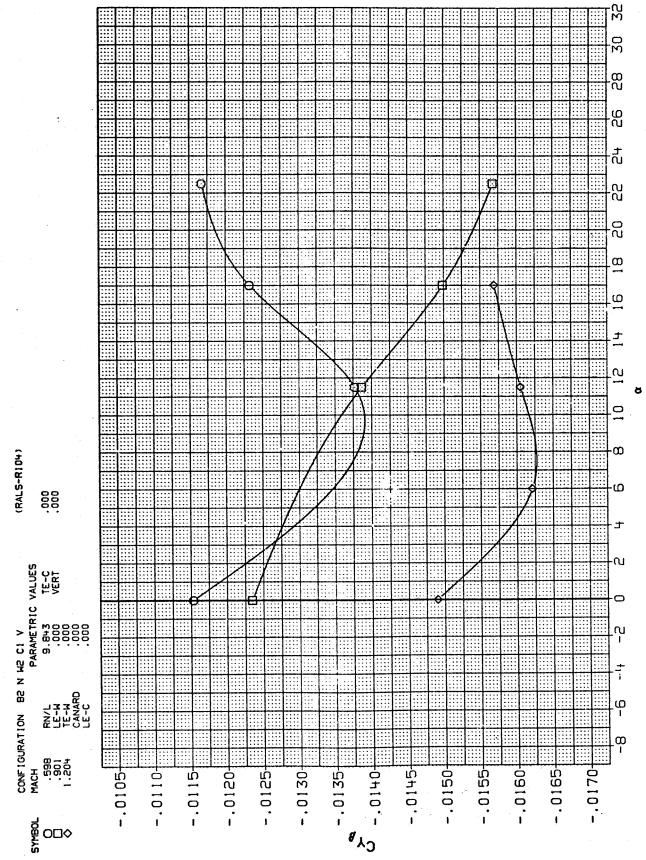


SUMMARY OF BASIC LATERAL/DIRECTIONAL CHARACTERISTICS WITH ALPHA FIG. 95

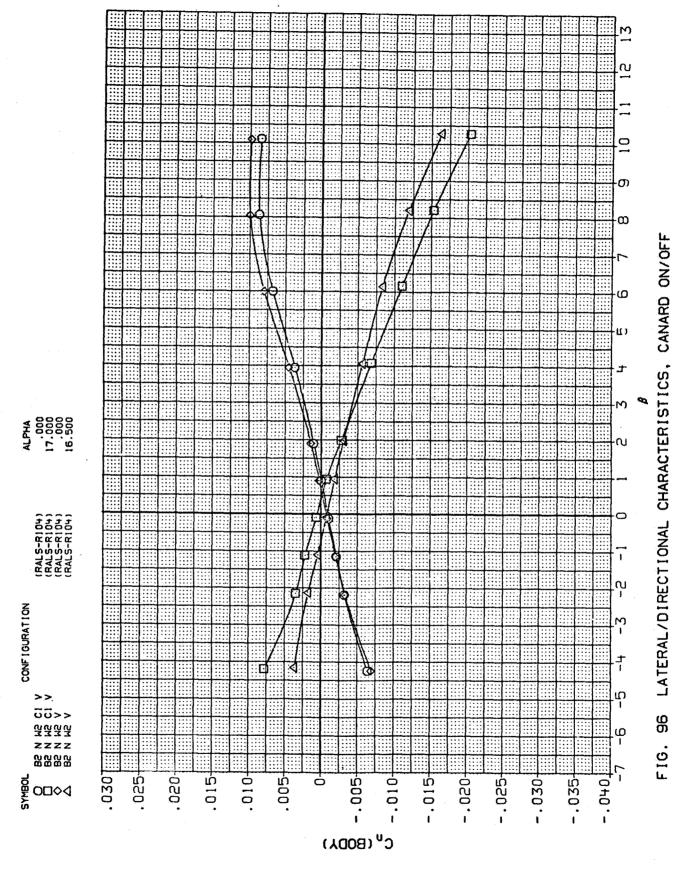


412

F16. 95

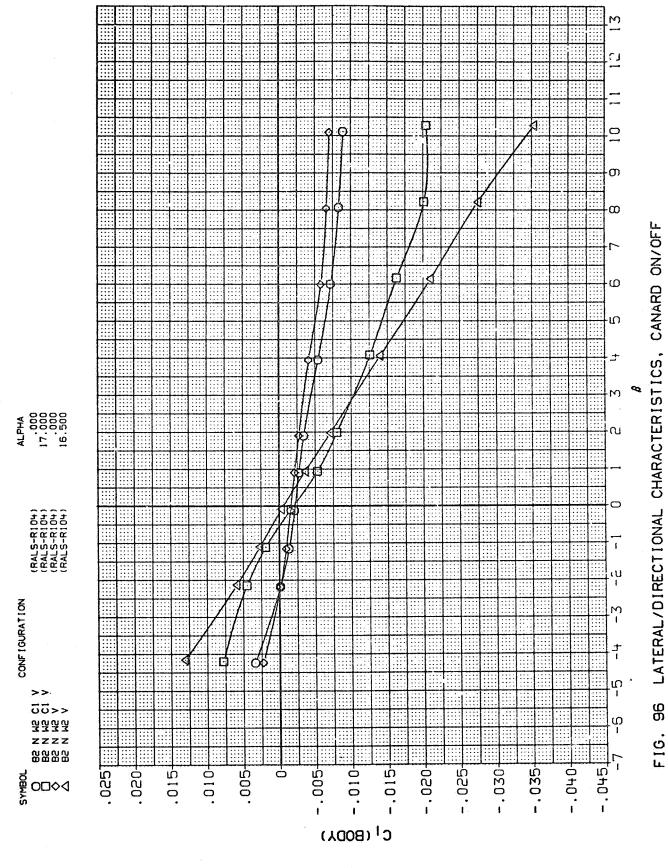


SUMMARY OF BASIC LATERAL/DIRECTIONAL CHARACTERISTICS WITH ALPHA F16. 95



414

11



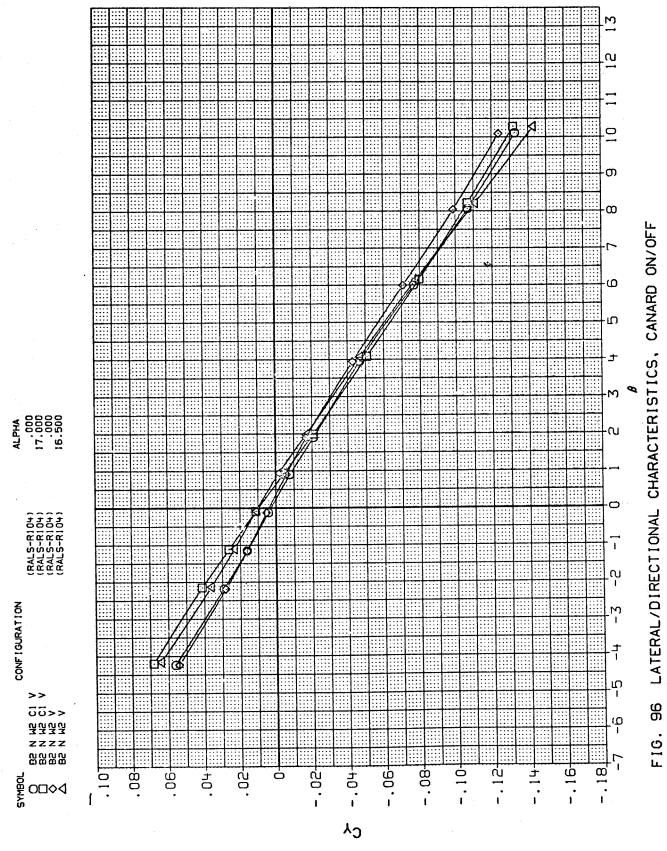
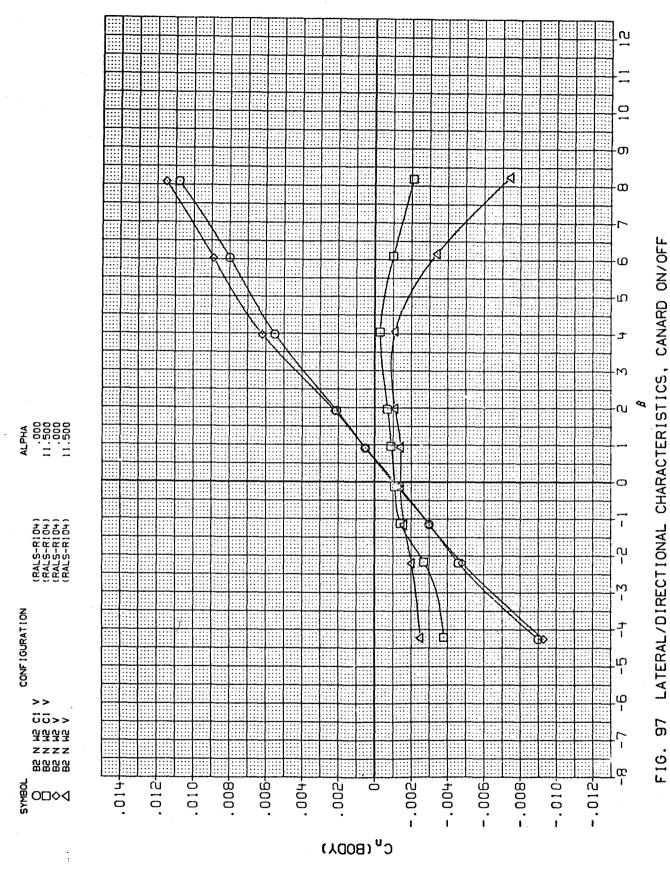
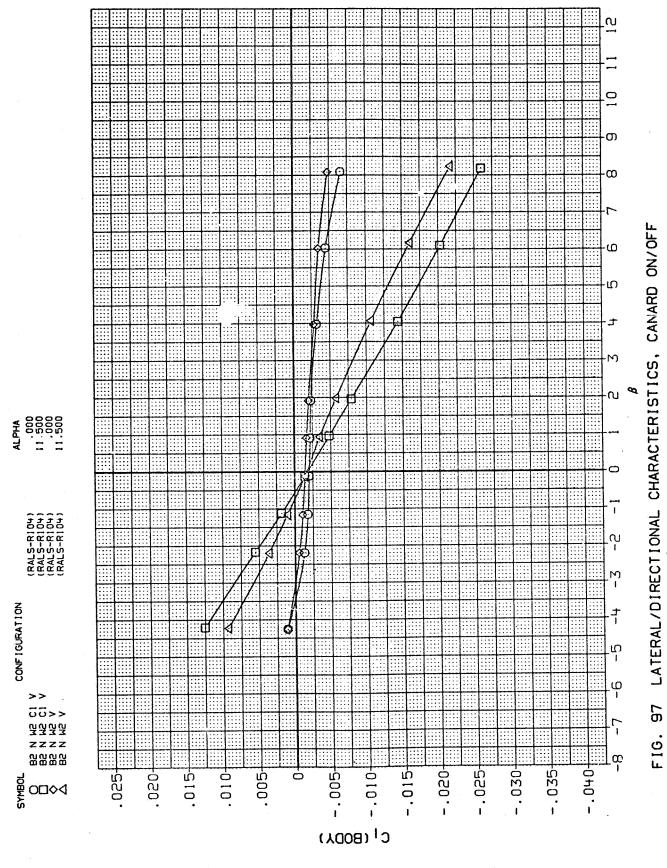
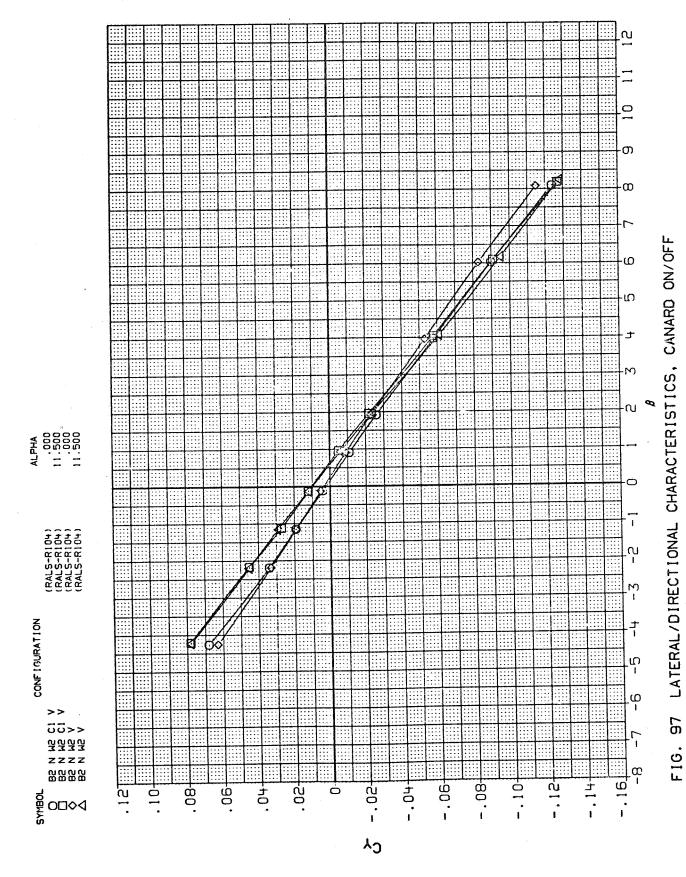


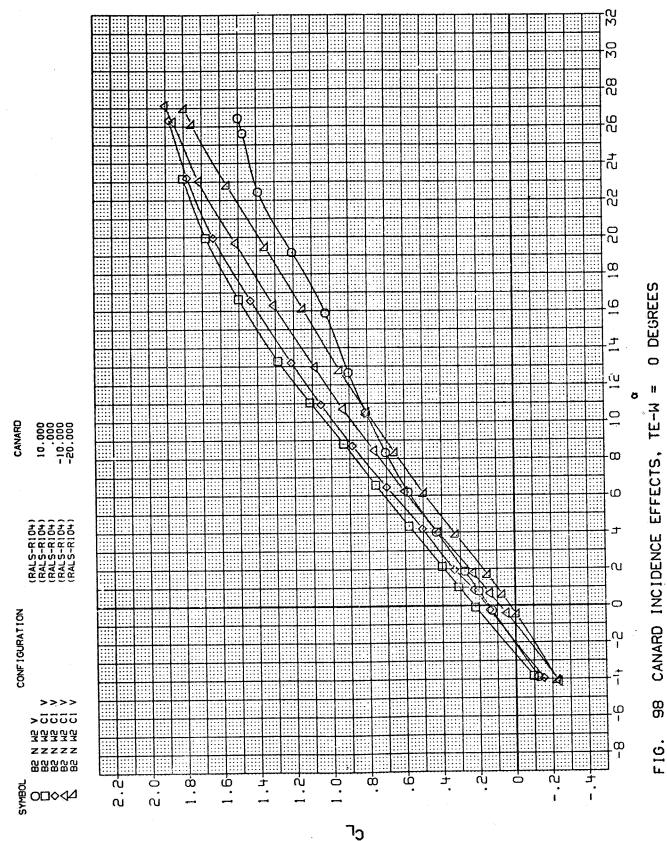
FIG. 95 LAIERAL/DIRECTIONAL = .90



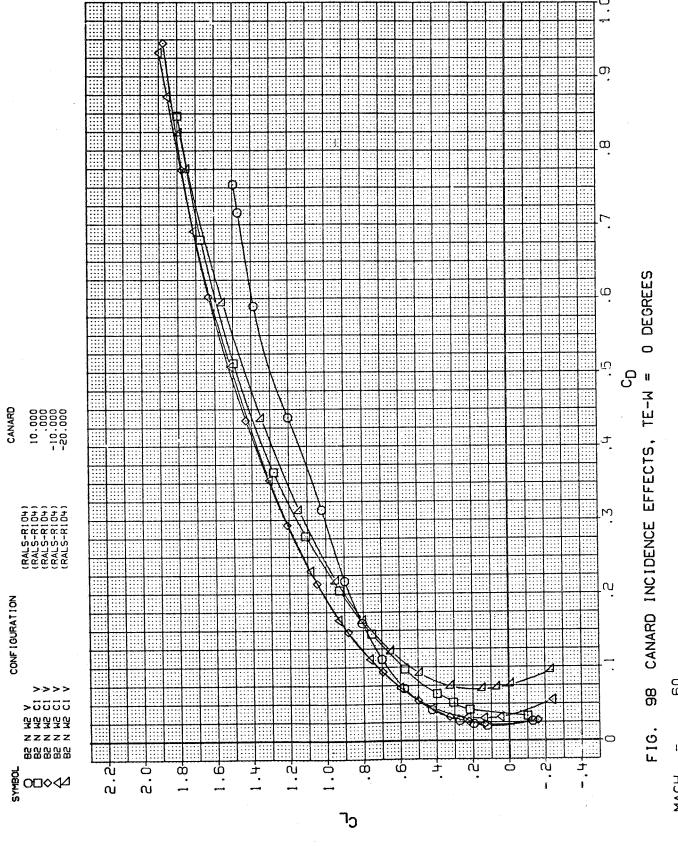


418





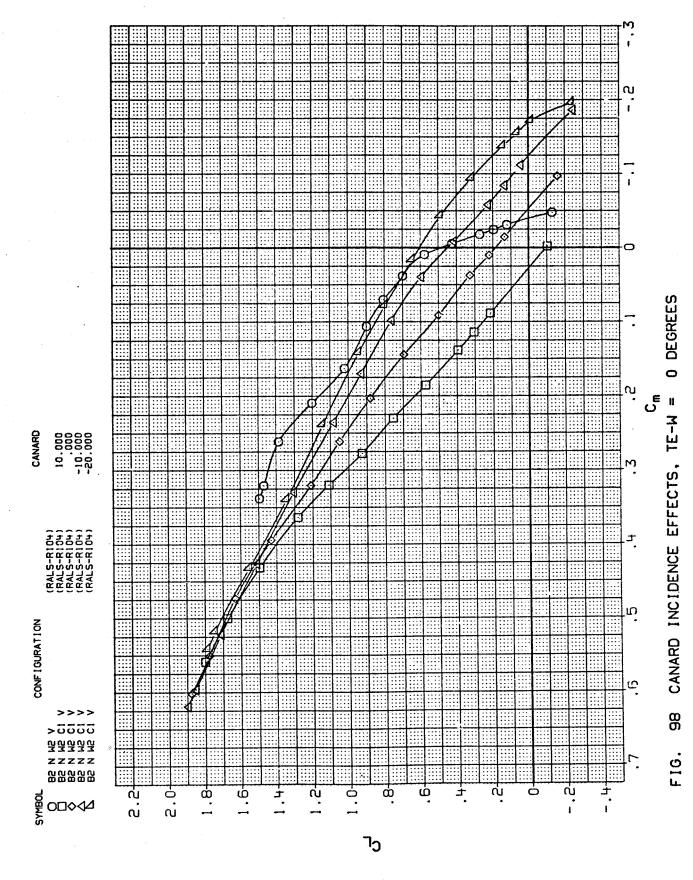
09· ≈ H



421

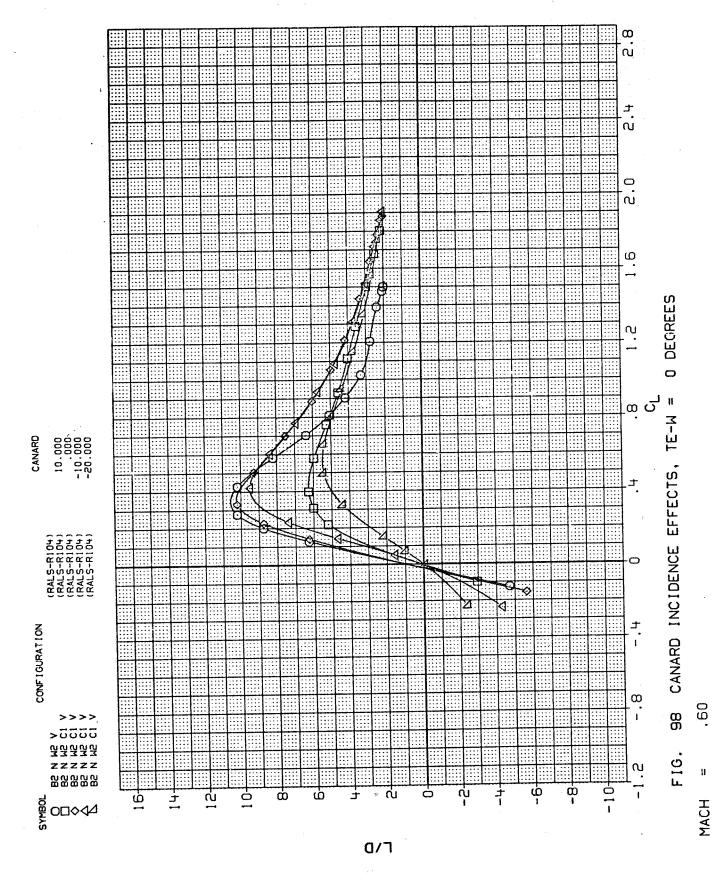
MACH

F1G.

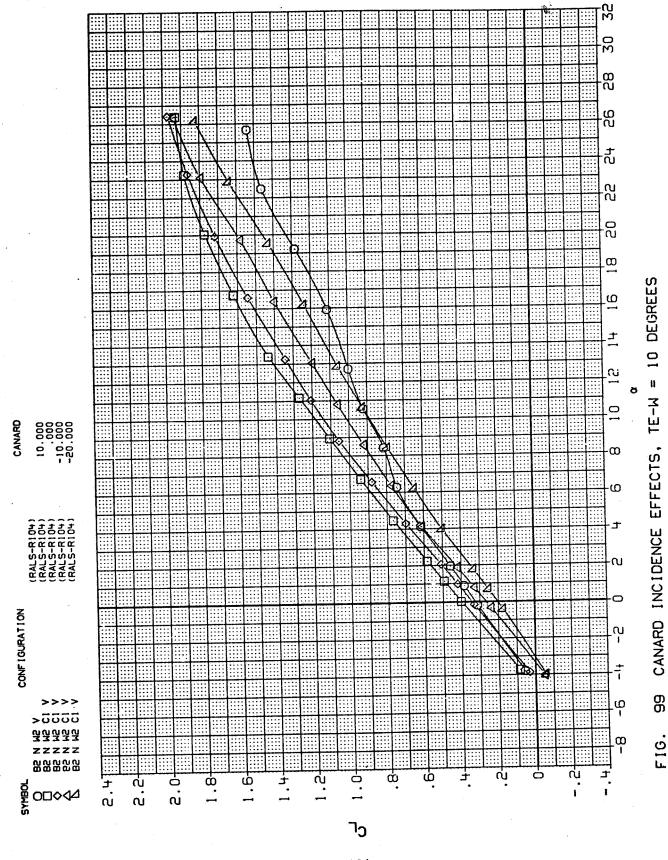


422

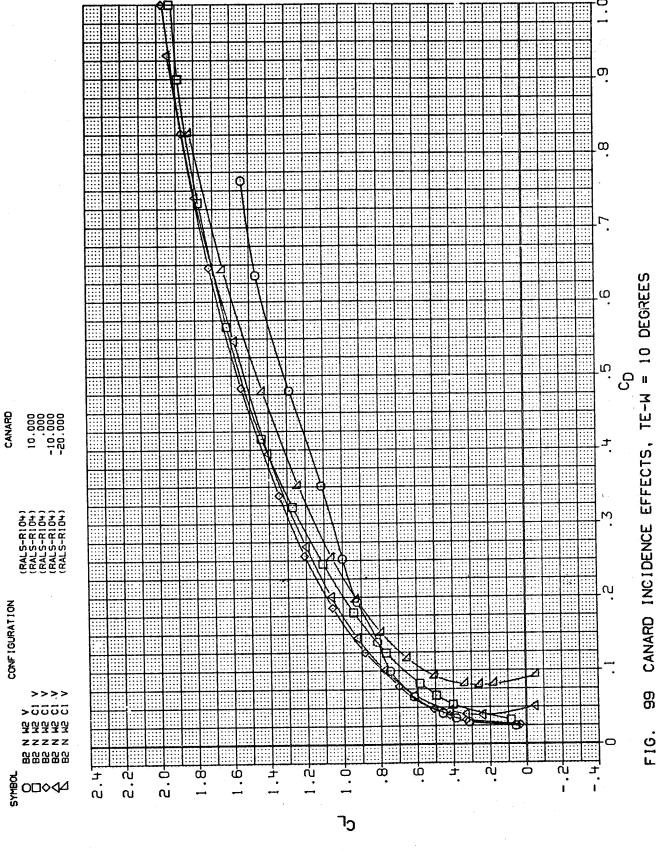
11



. . .

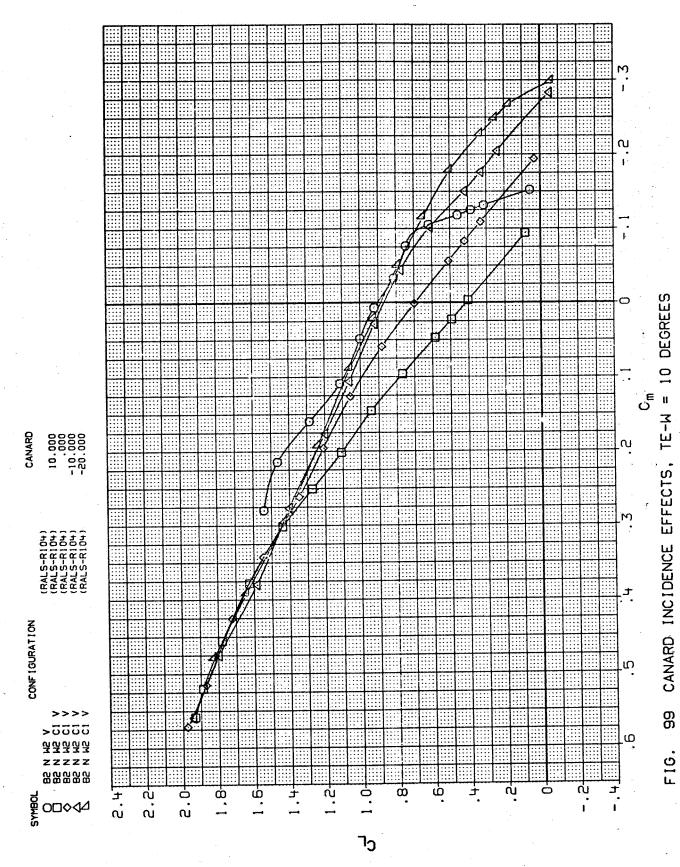


66 .60 F16.

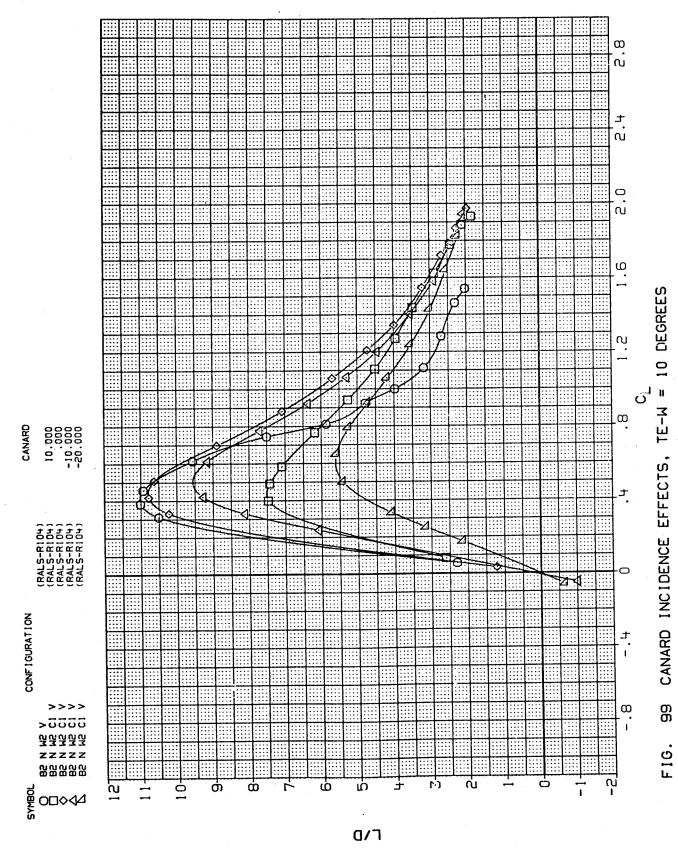


425

11



426



CH = +0.00

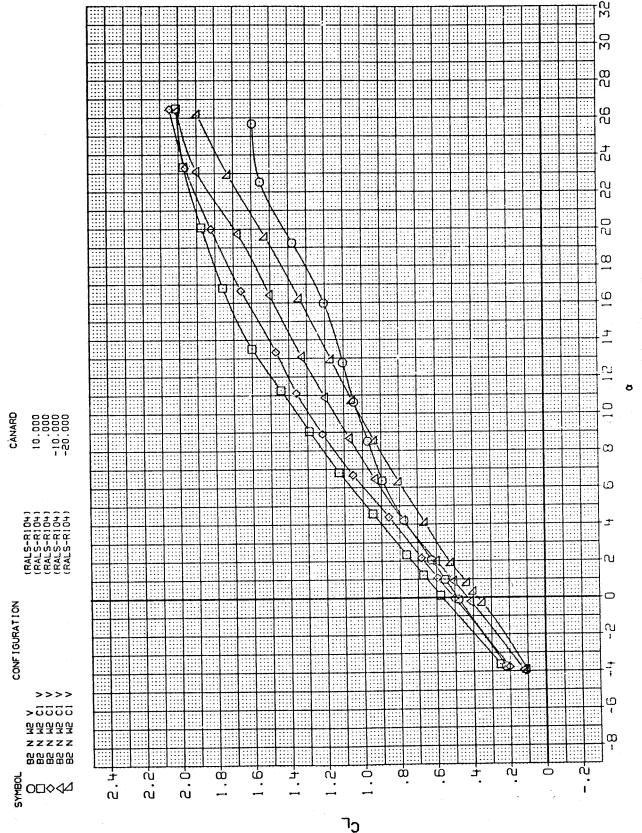
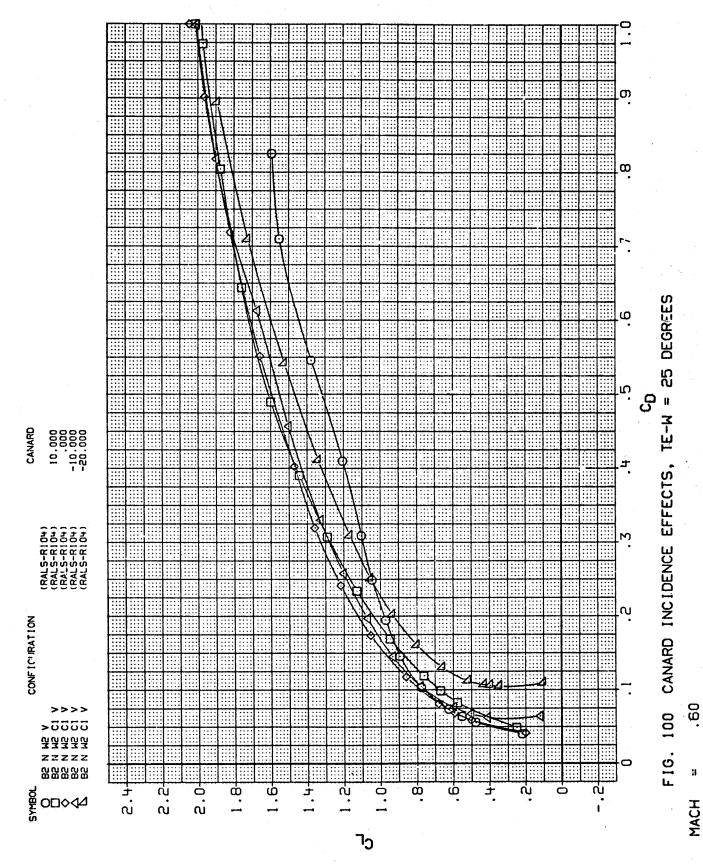
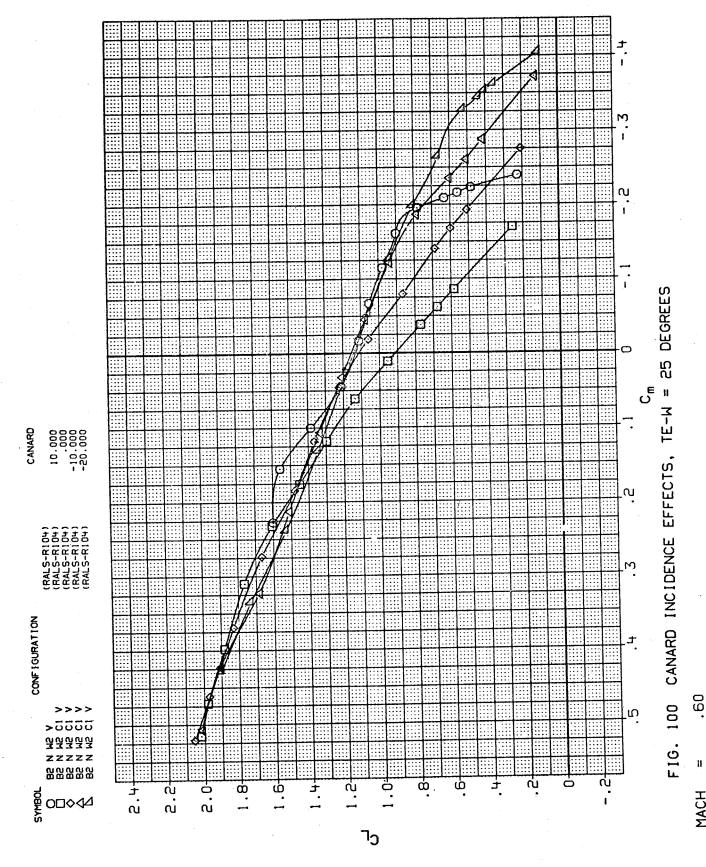
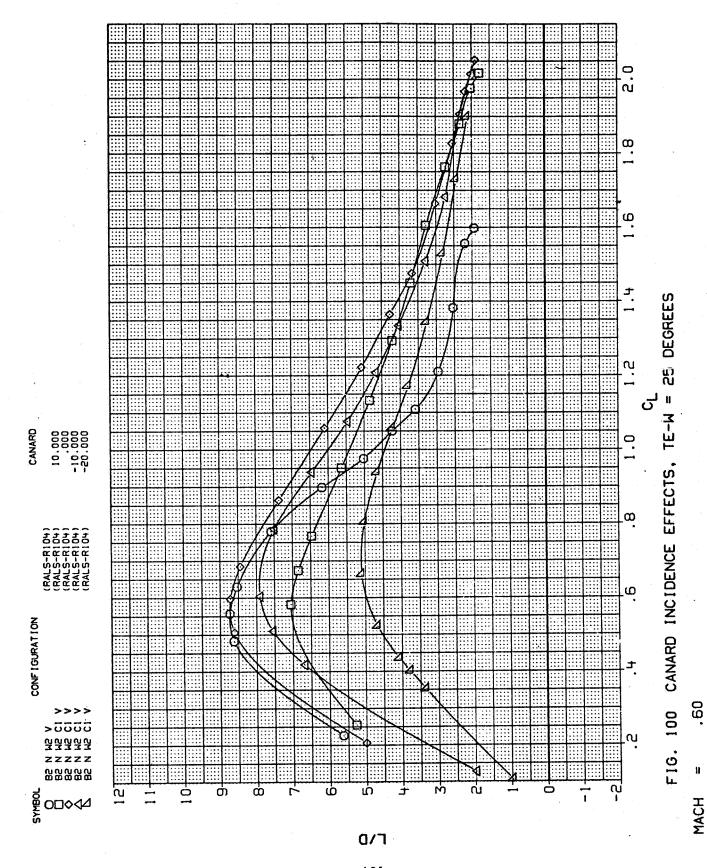
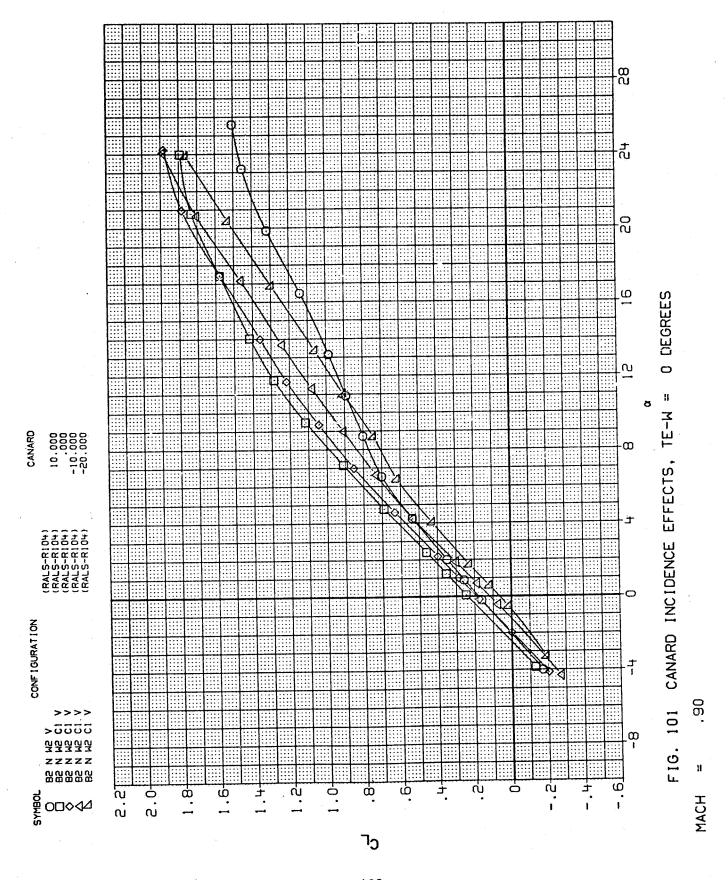


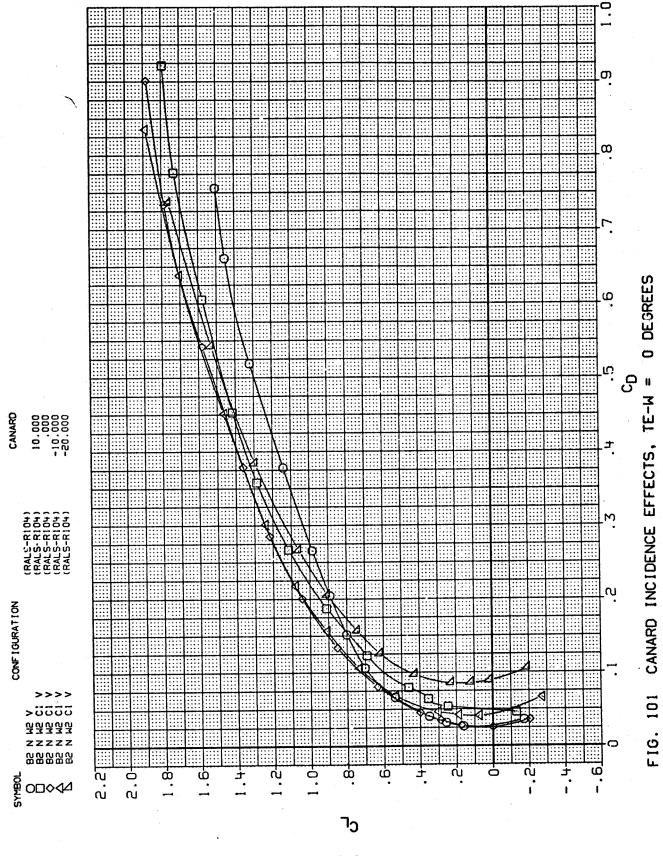
FIG. 100 CANARD INCIDENCE EFFECTS, TE-W = 25 DEGREES





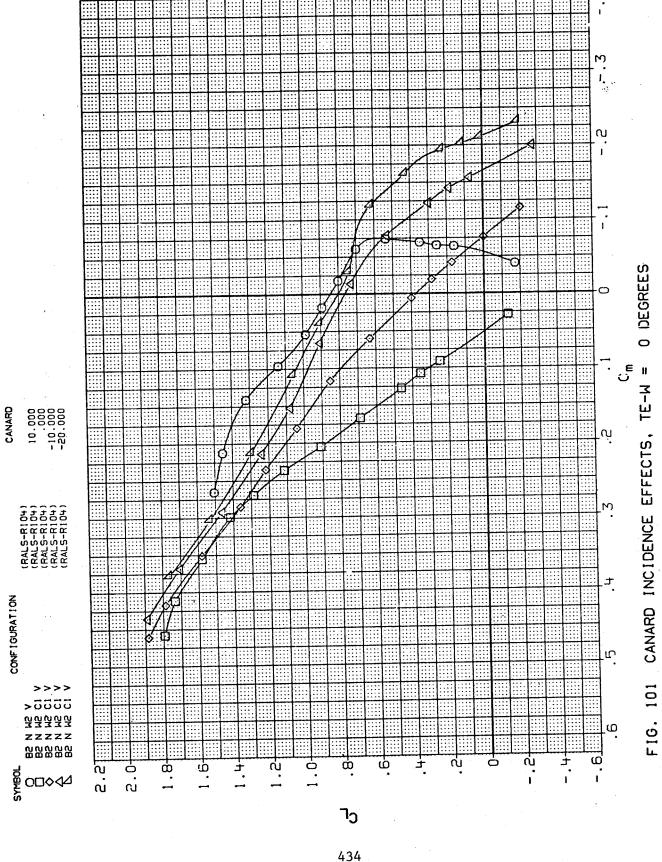




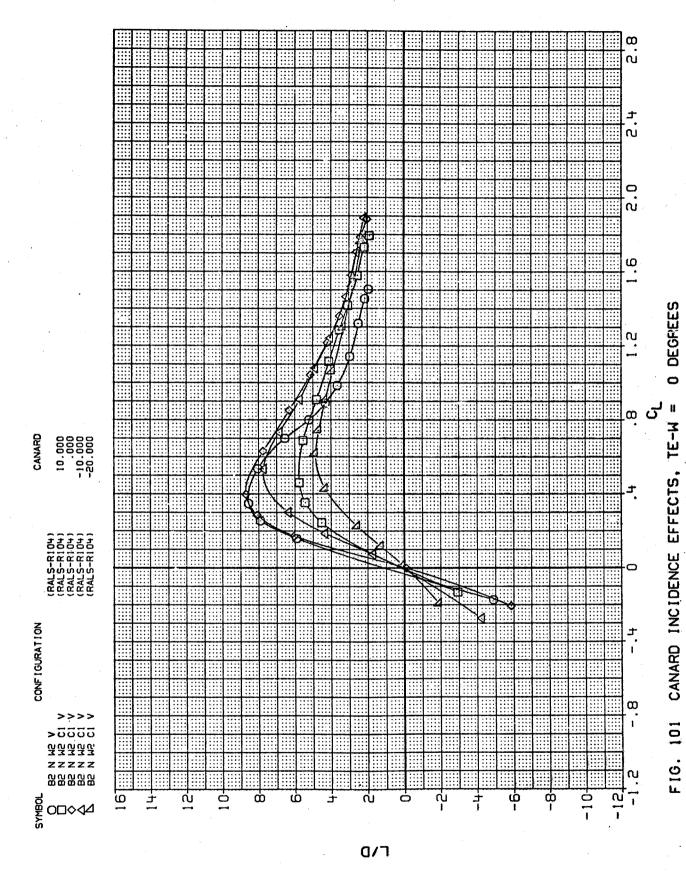


433

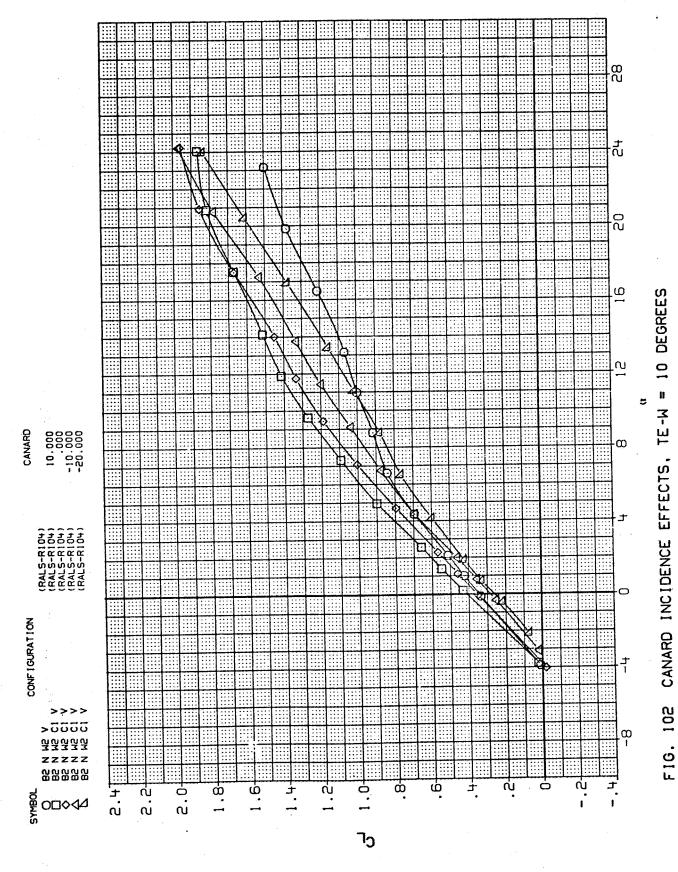
;;



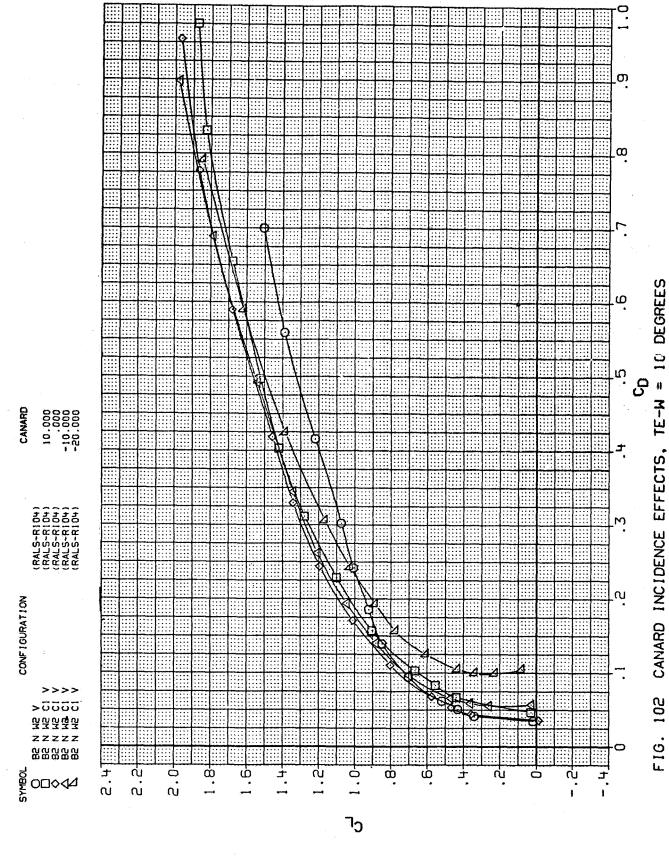
Ħ

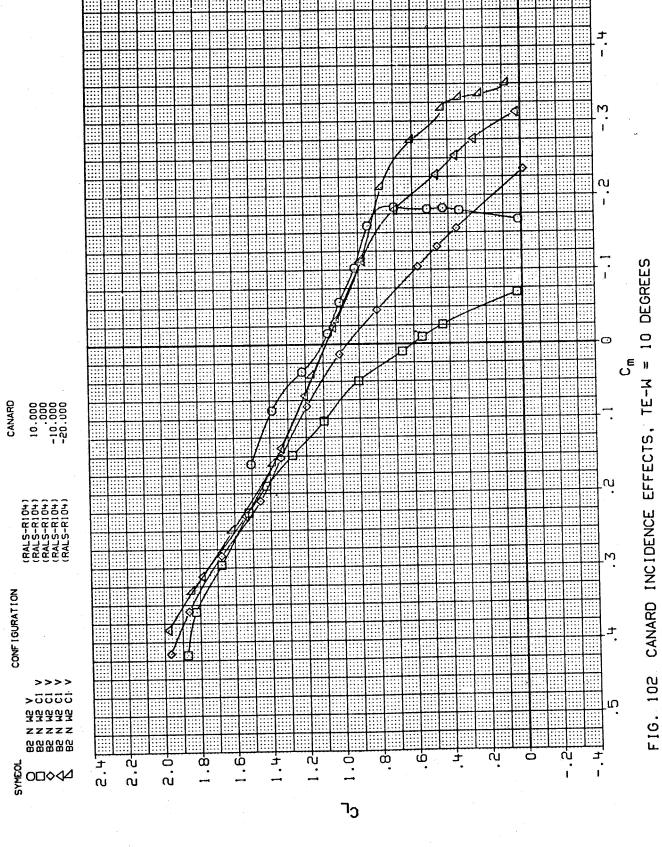


06. H

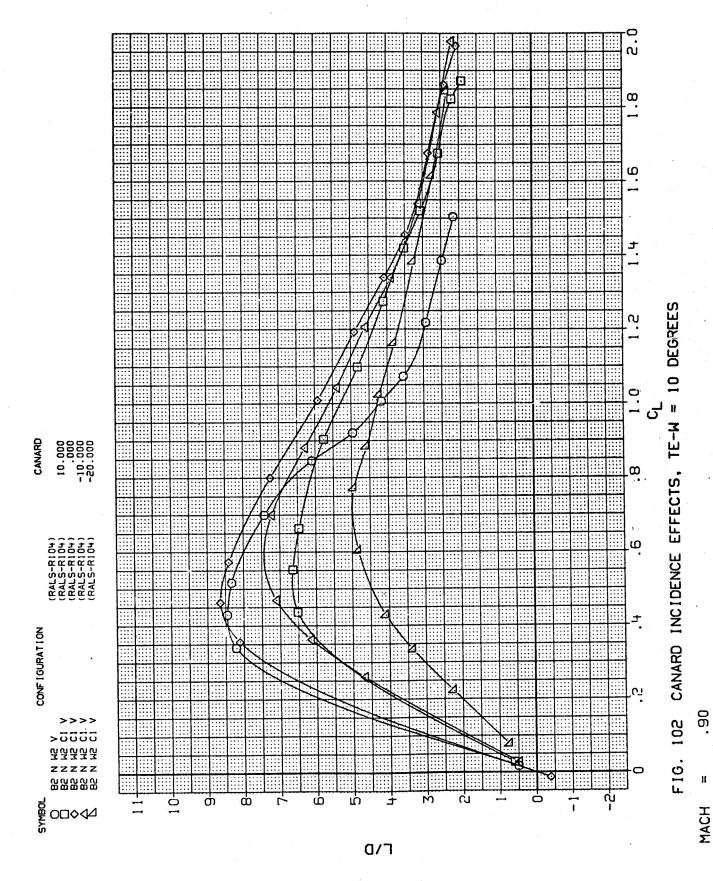


436





438



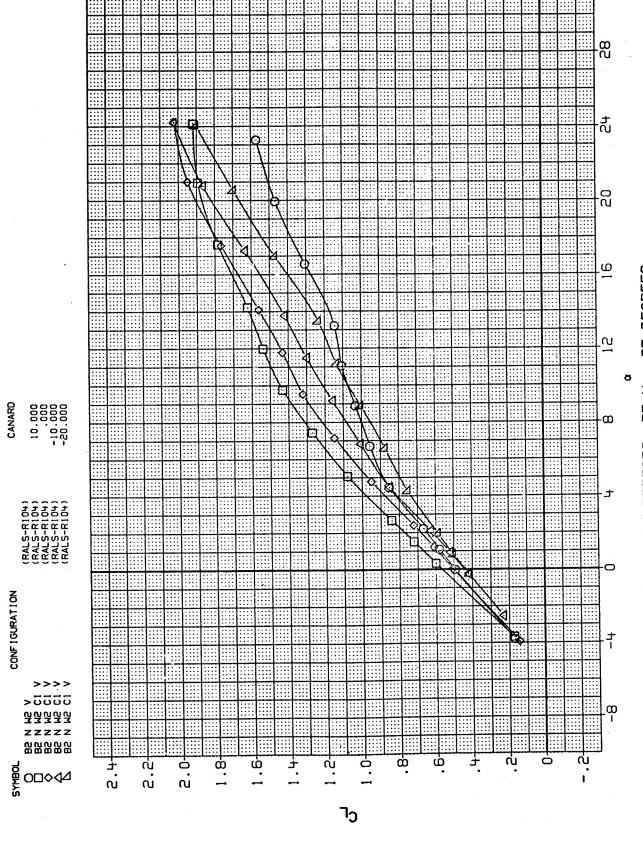
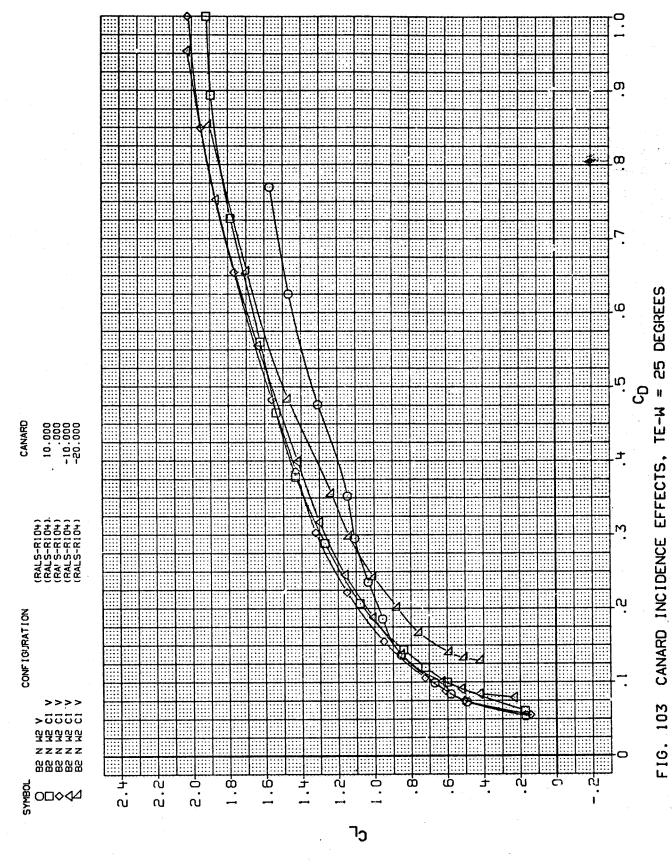
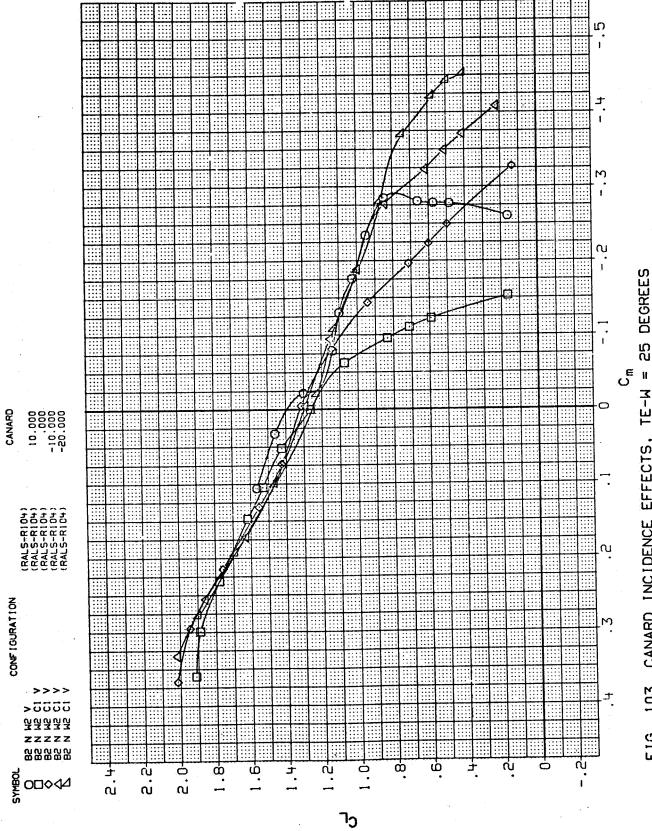
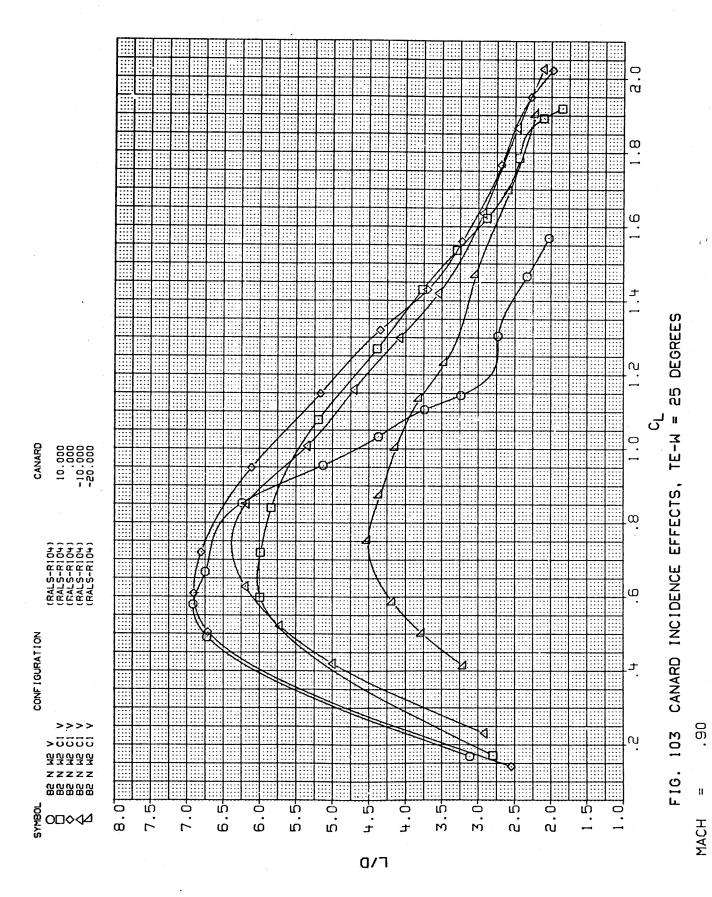


FIG. 103 CANARD INCIDENCE EFFECTS, TE-W = 25 DEGREES





H TE-M CANARD INCIDENCE EFFECTS, F16. 103



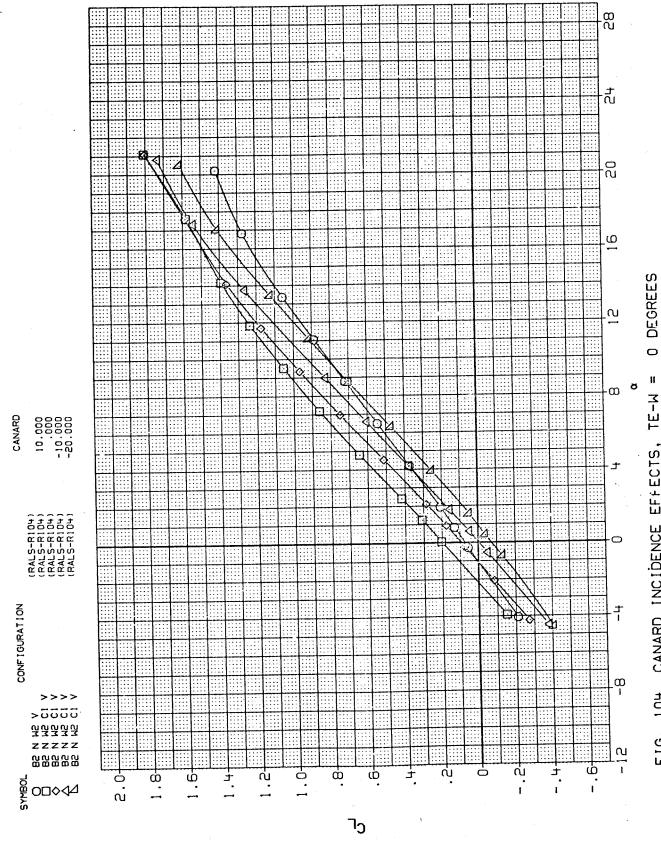
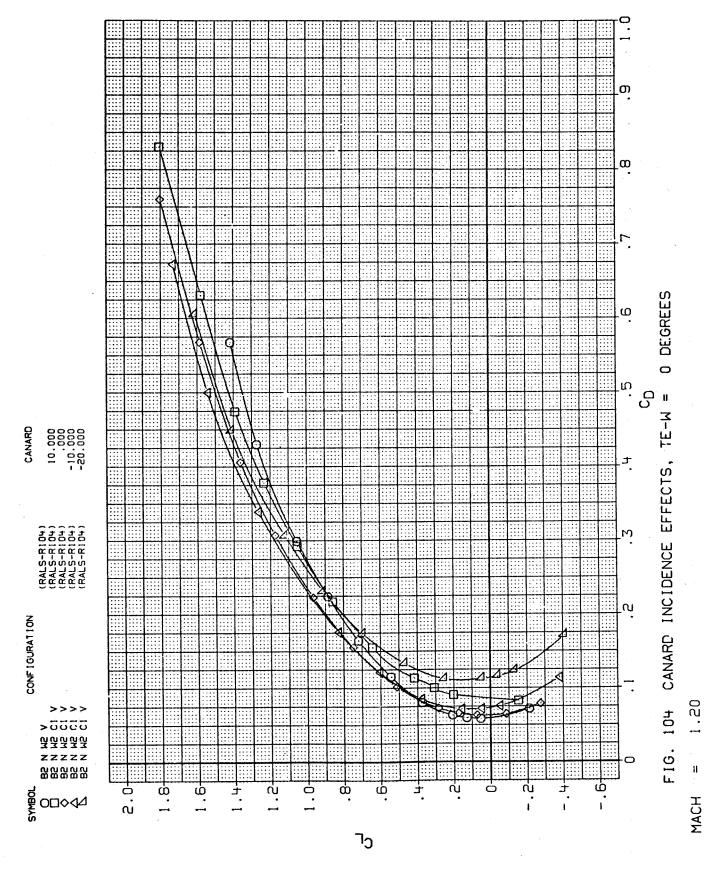
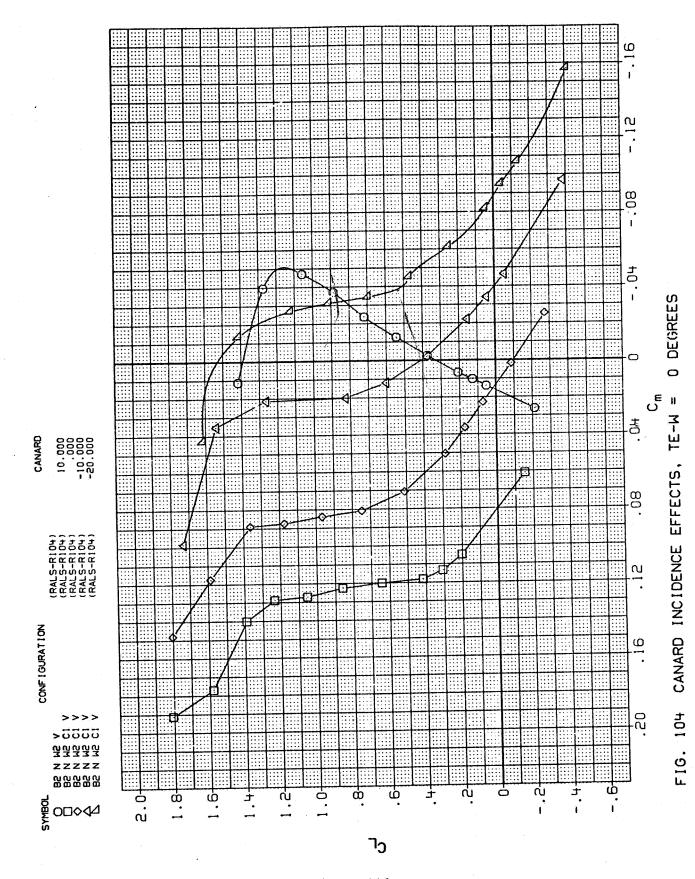


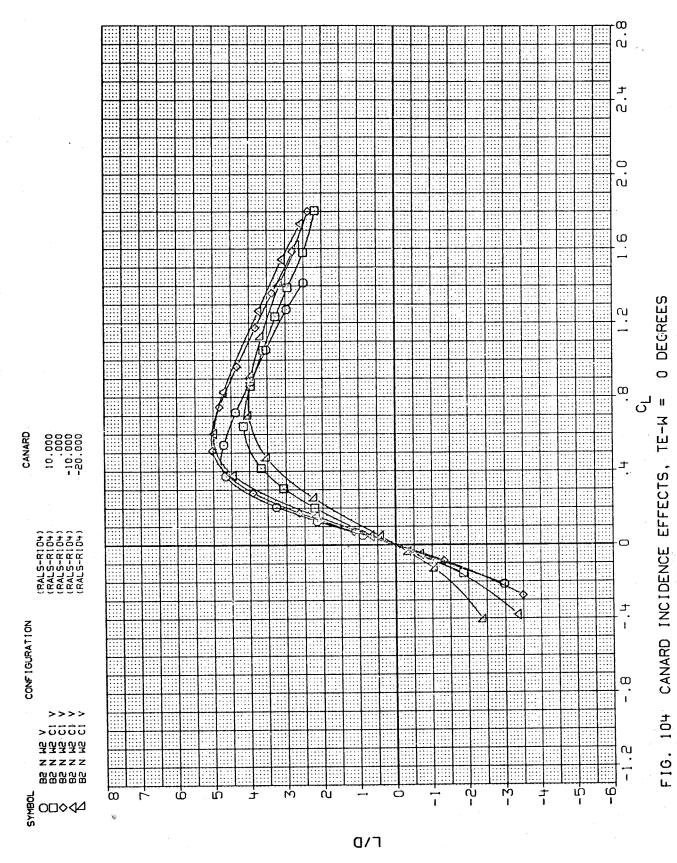
FIG. 104 CANARD INCIDENCE EFFECTS.

H





MACH = 1.20



MACH = 1.20

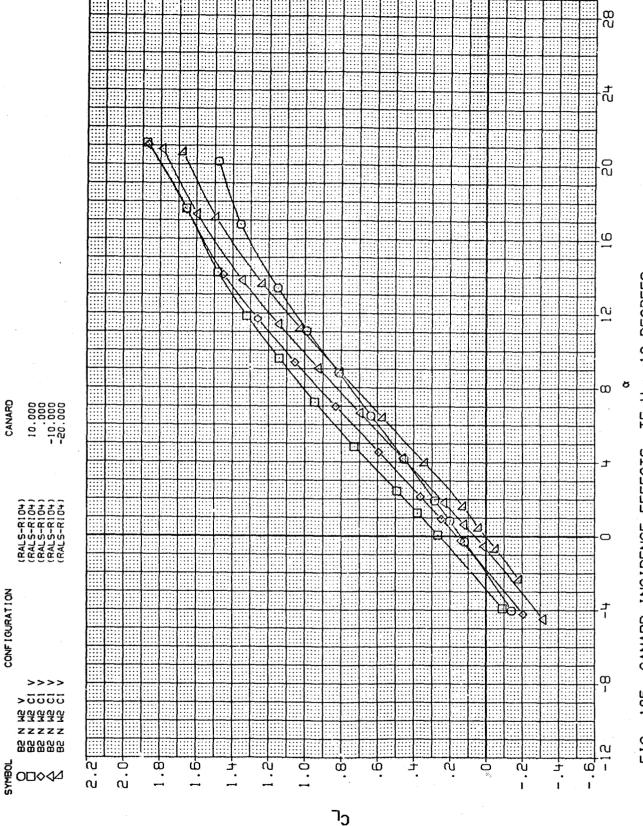
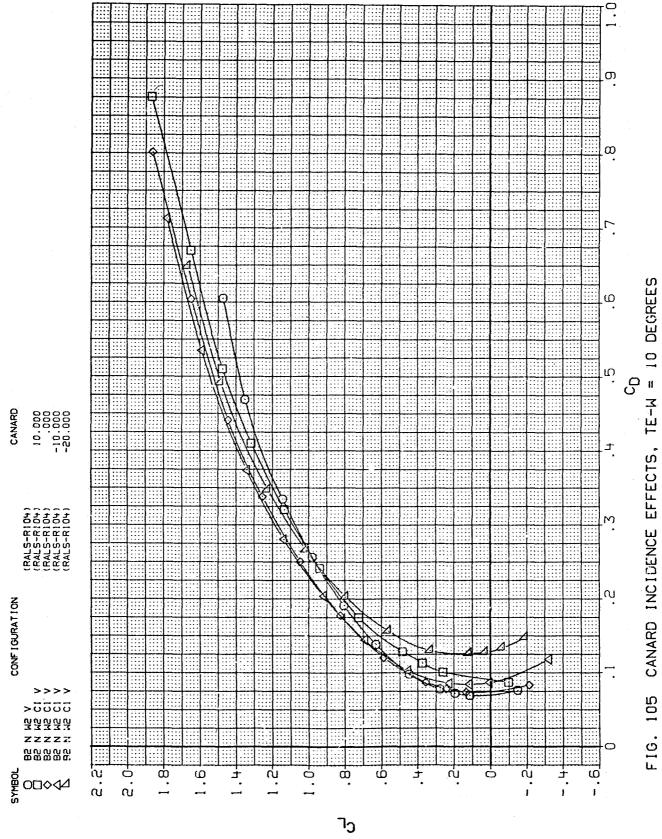


FIG. 105 CANARD INCIDENCE EFFECTS, TE-W = 10 DEGREES



MACH = 1.20

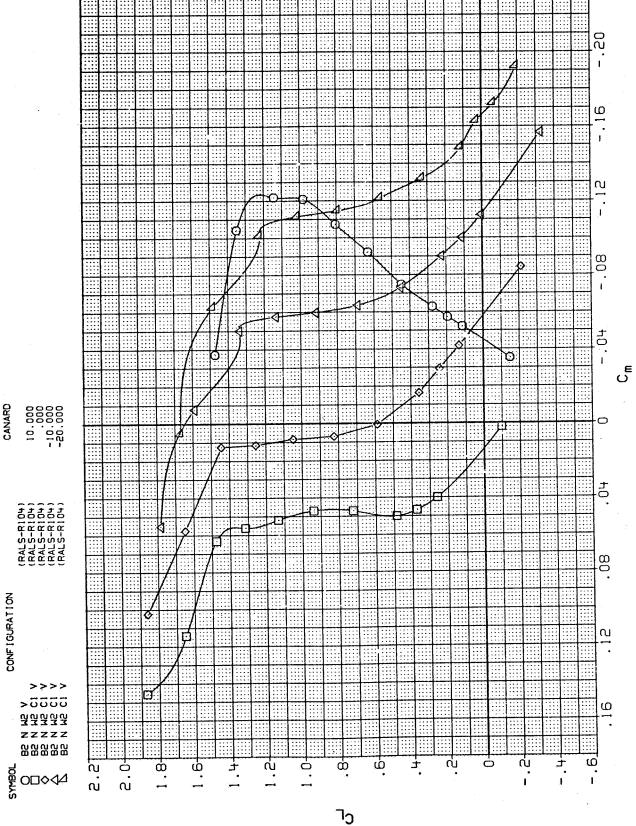


FIG. 105 CANARD INCIDENCE EFFECTS, TE-W = 10 DEGREES

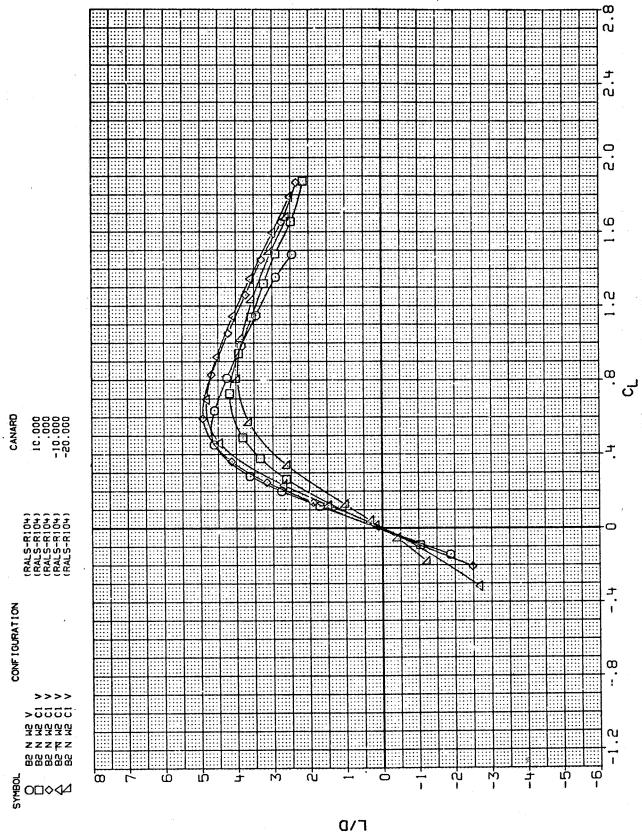


FIG. 105 CANARD INCIDENCE EFFECTS, TE-W = 10 DEGREES

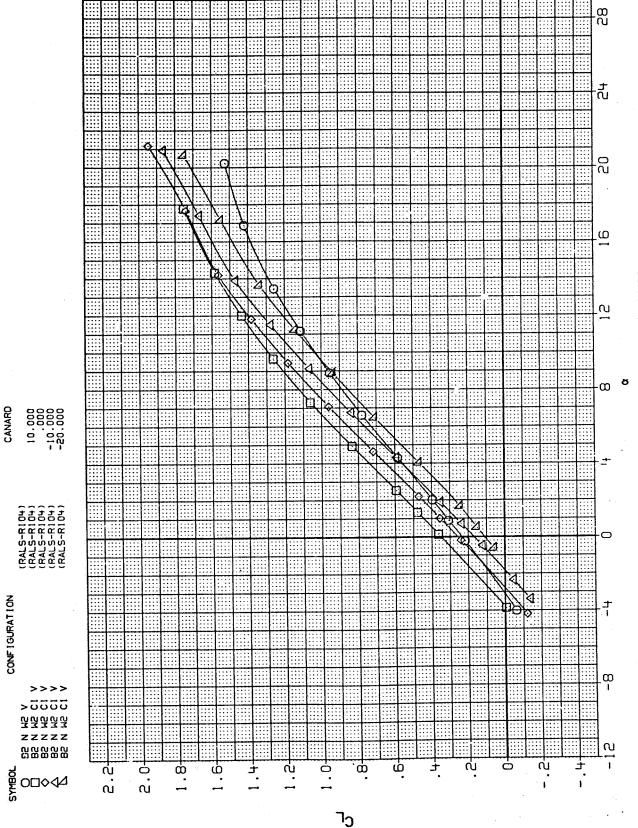
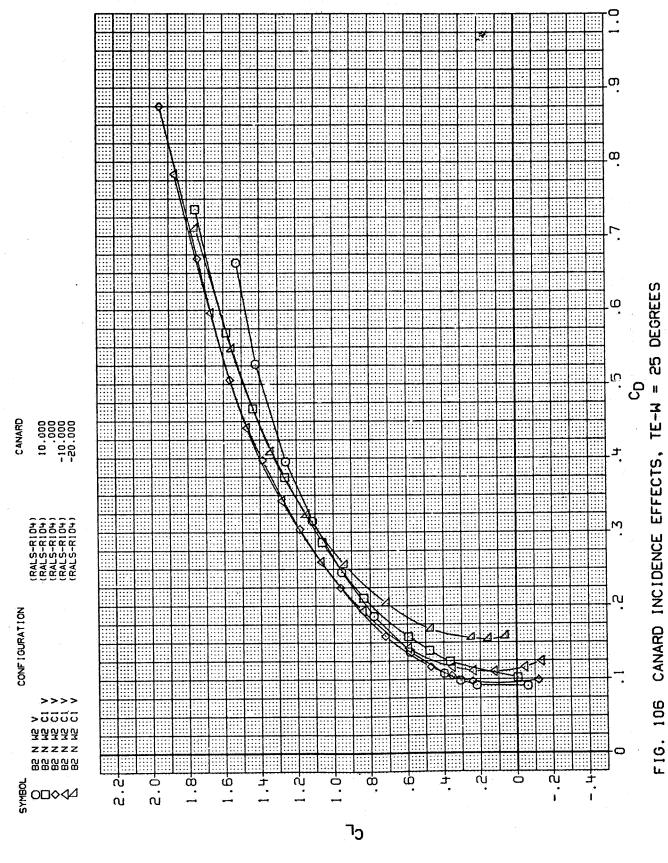


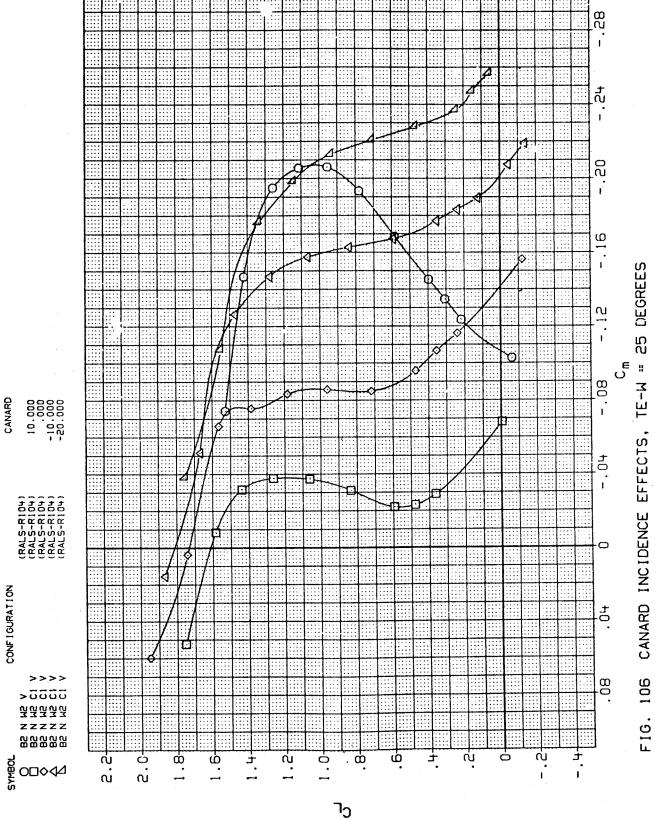
FIG. 106 CANARD INCIDENCE EFFECTS, TE-W = 25 DEGREES

11

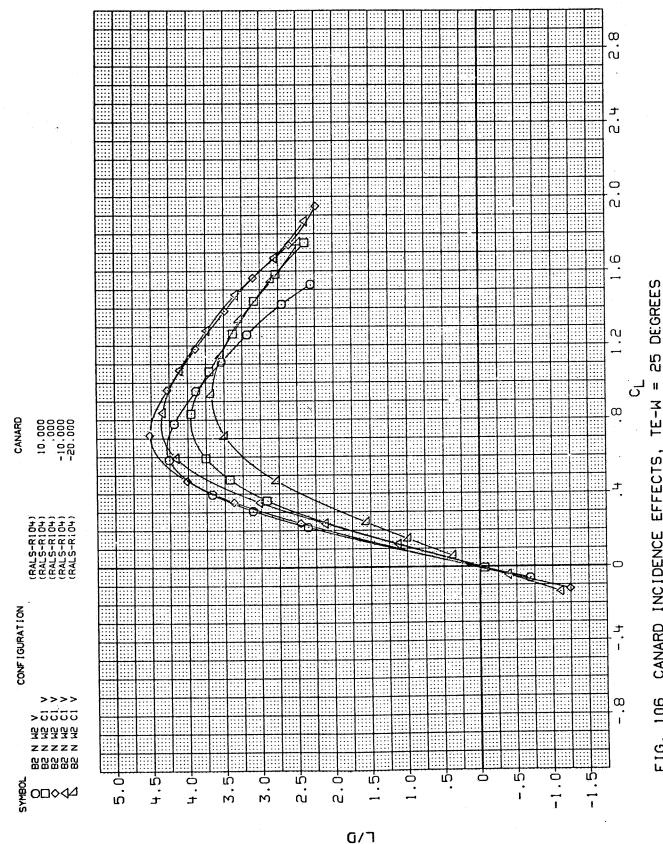


453

Ħ



1.20



Ħ TE-M FIG. 106 CANARD INCIDENCE EFFECTS,

H

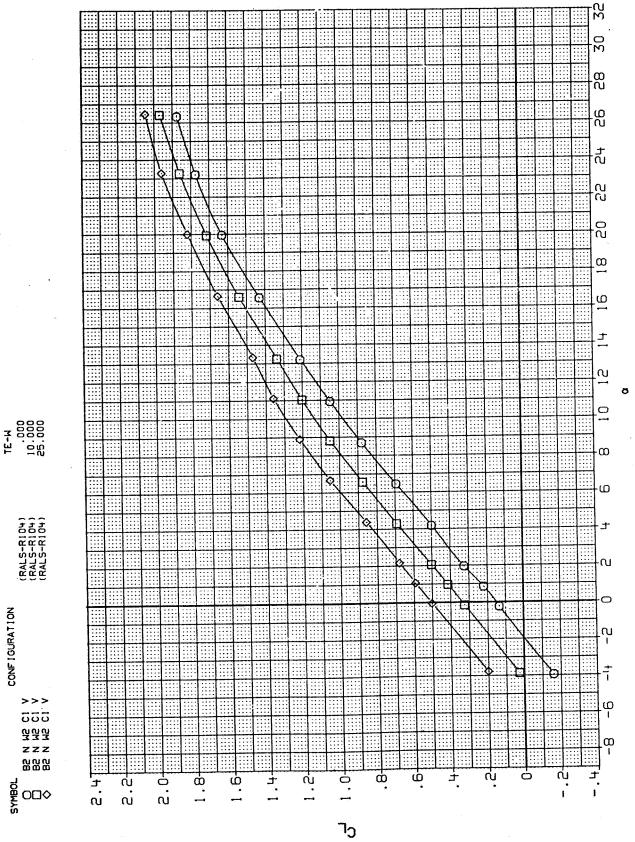
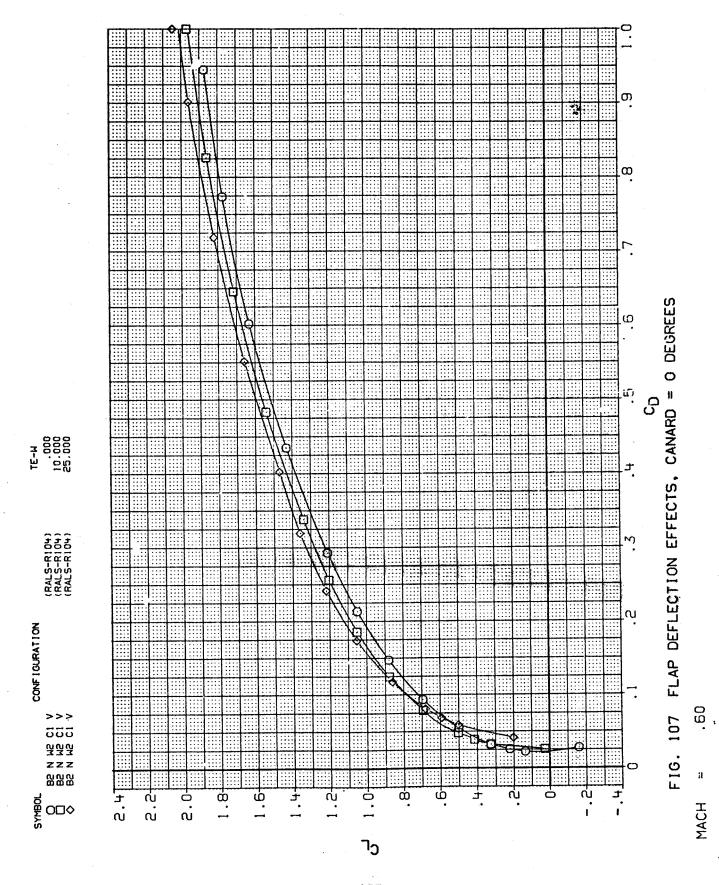
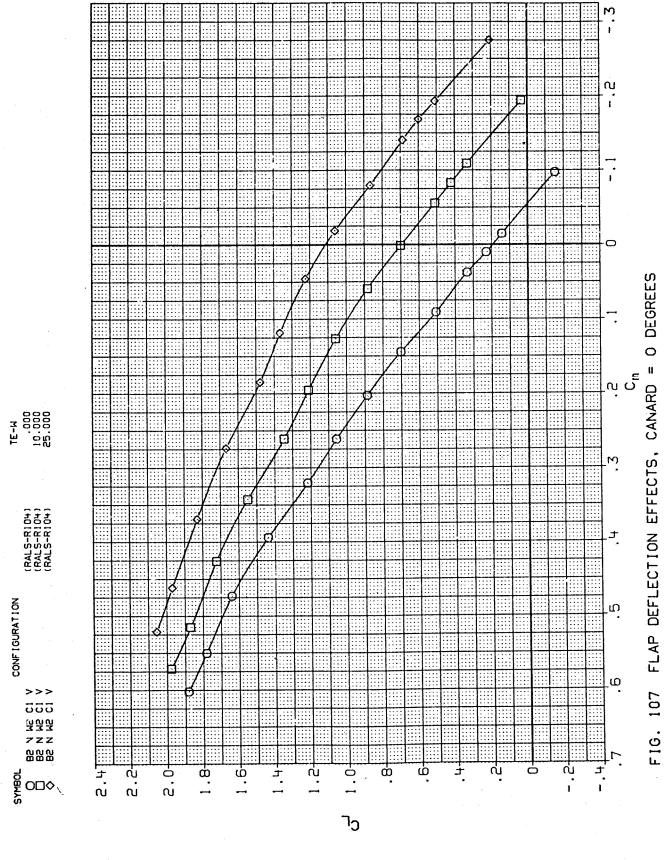
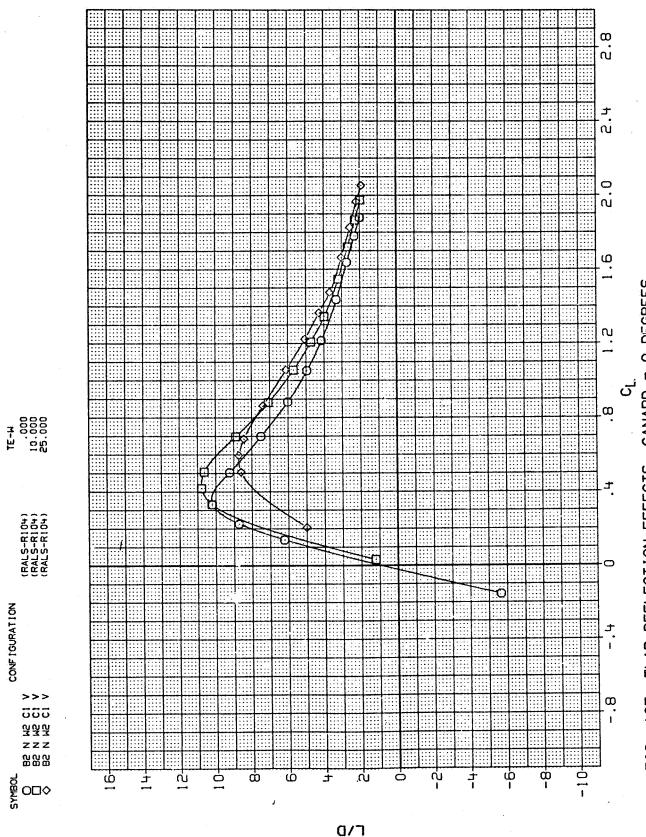


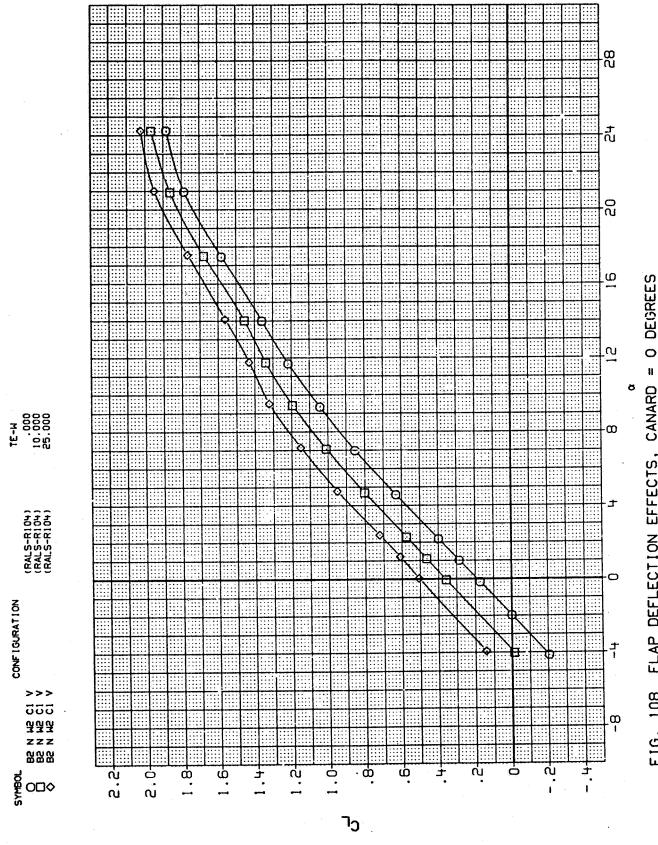
FIG. 107 FLAP DEFLECTION EFFECTS, CANARD = 0 DEGREES



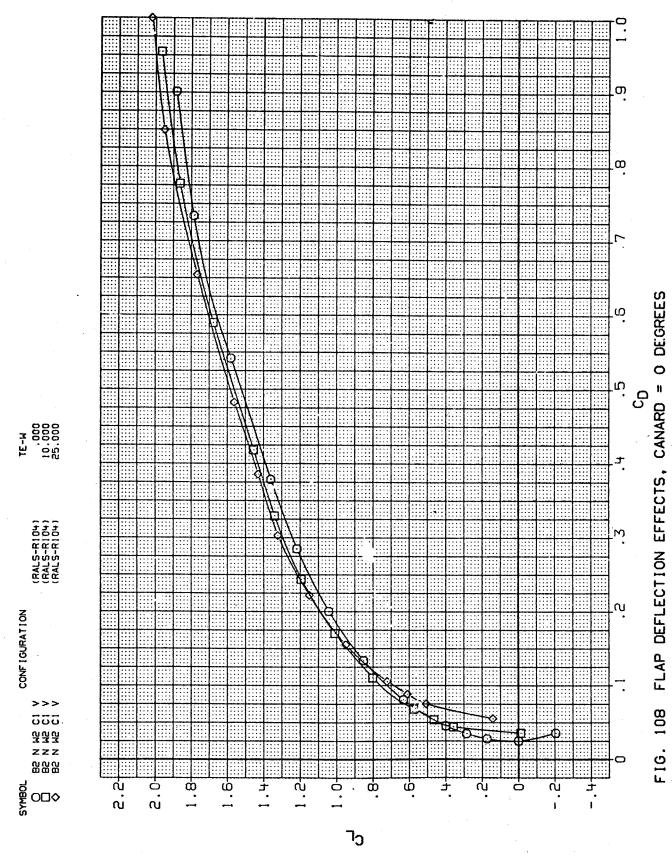




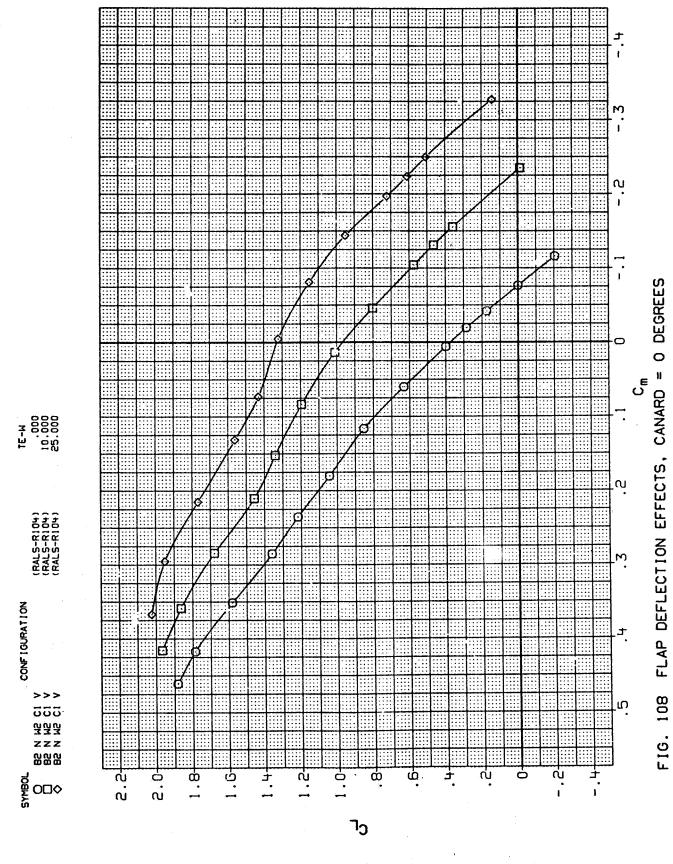
FIG, 107 FLAP DEFLECTION EFFECTS, CANARD = 0 DEGREES CH = .60

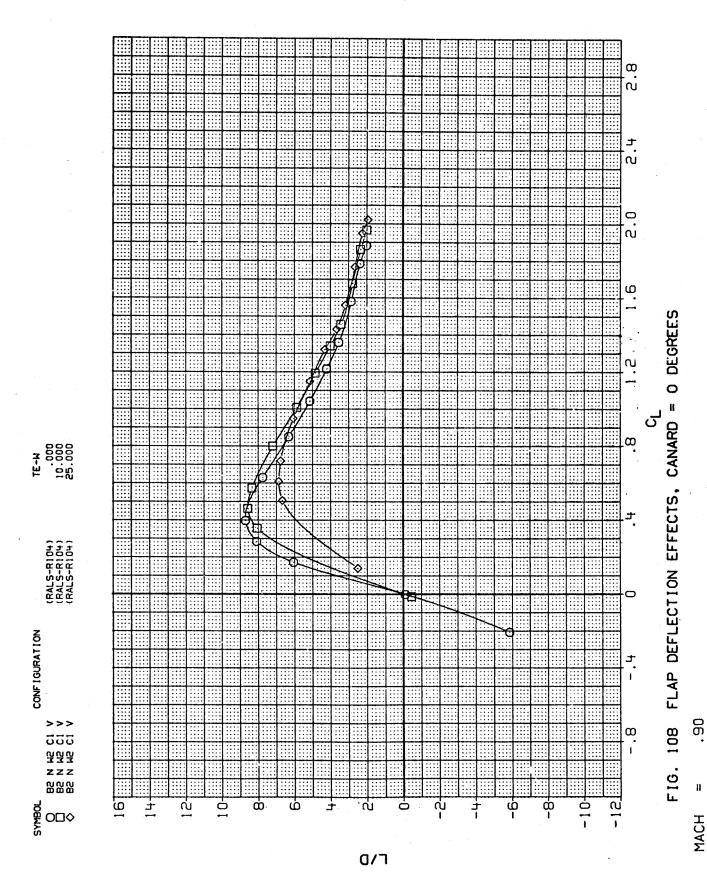


11 FLAP DEFLECTION EFFECTS, CANARD FIG. 108



461





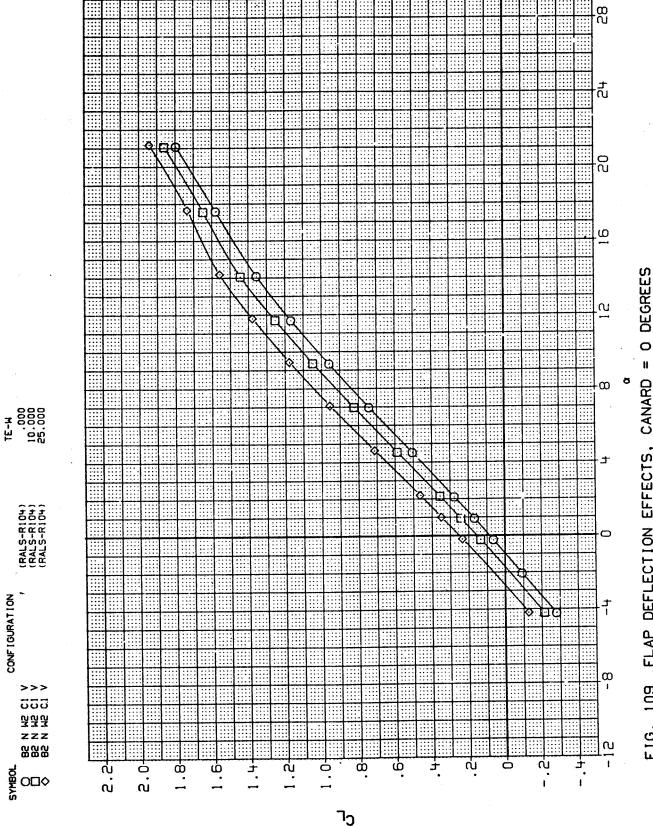
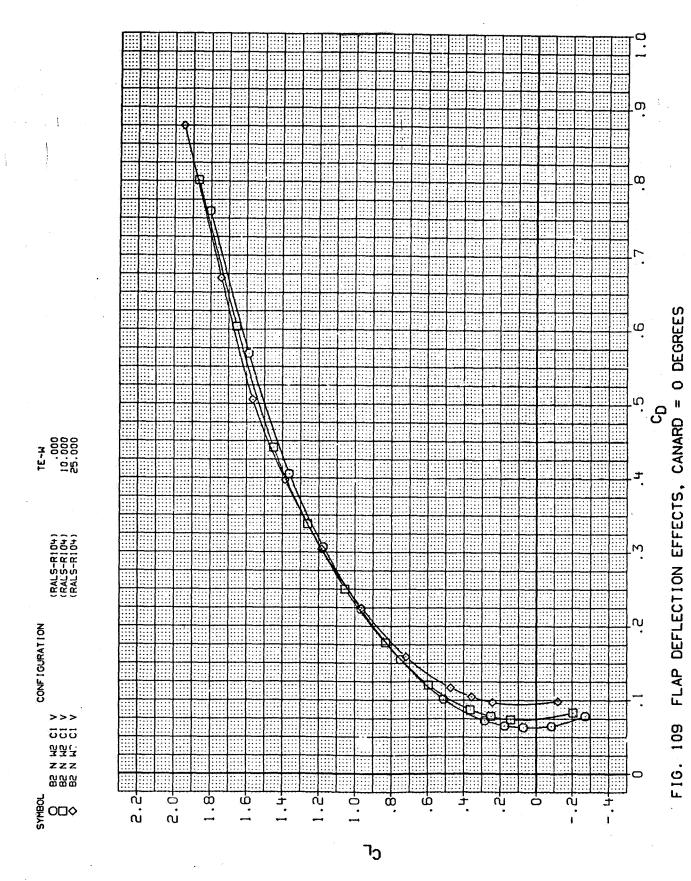
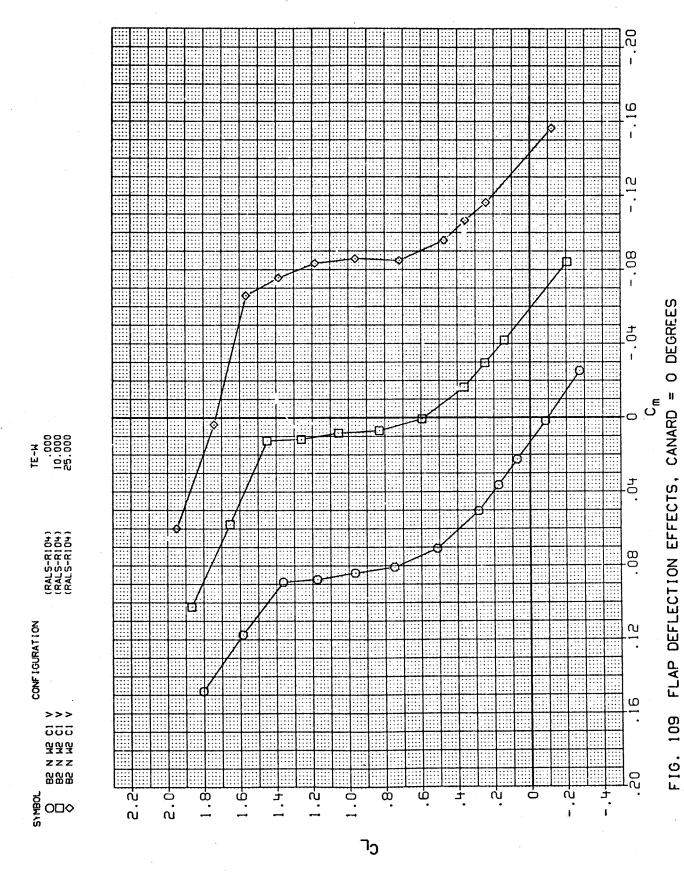


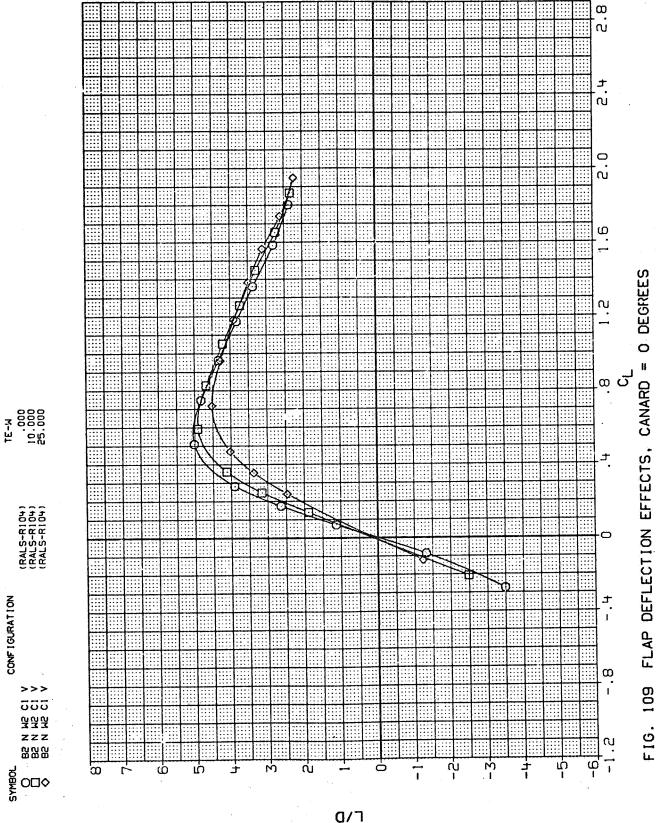
FIG. 109 FLAP DEFLECTION EFFECTS, CANARD =

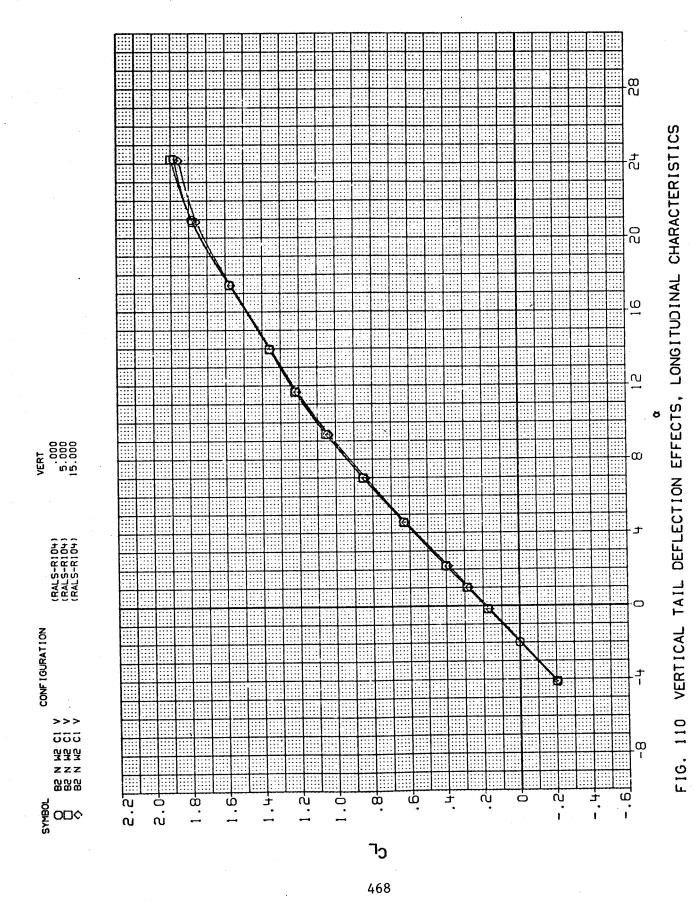
Ü



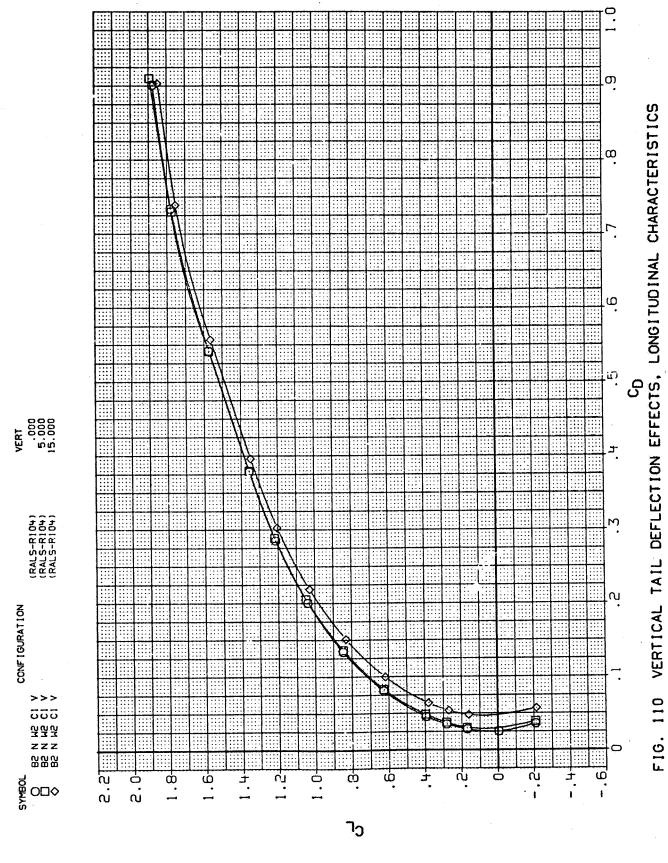


MACH = 1.20

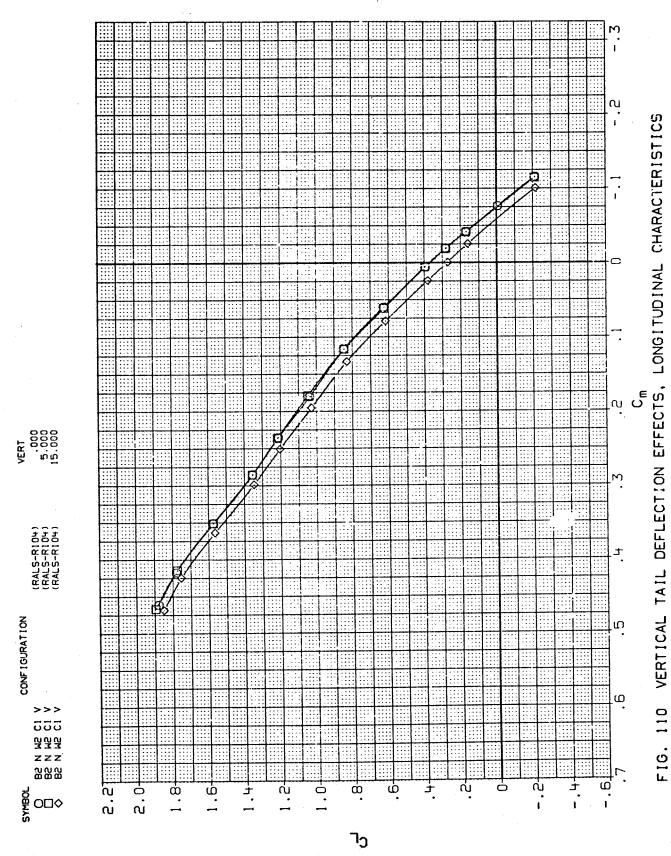


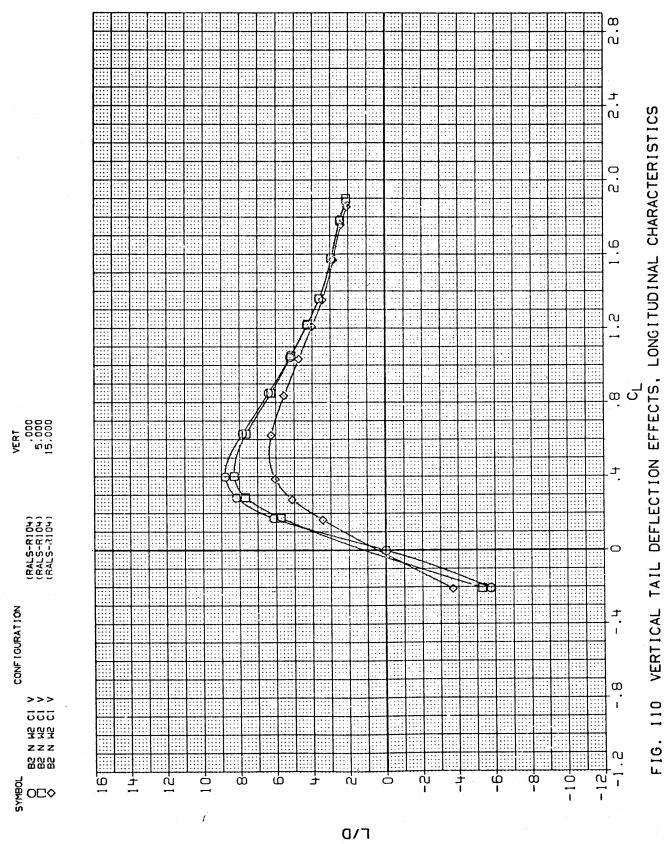


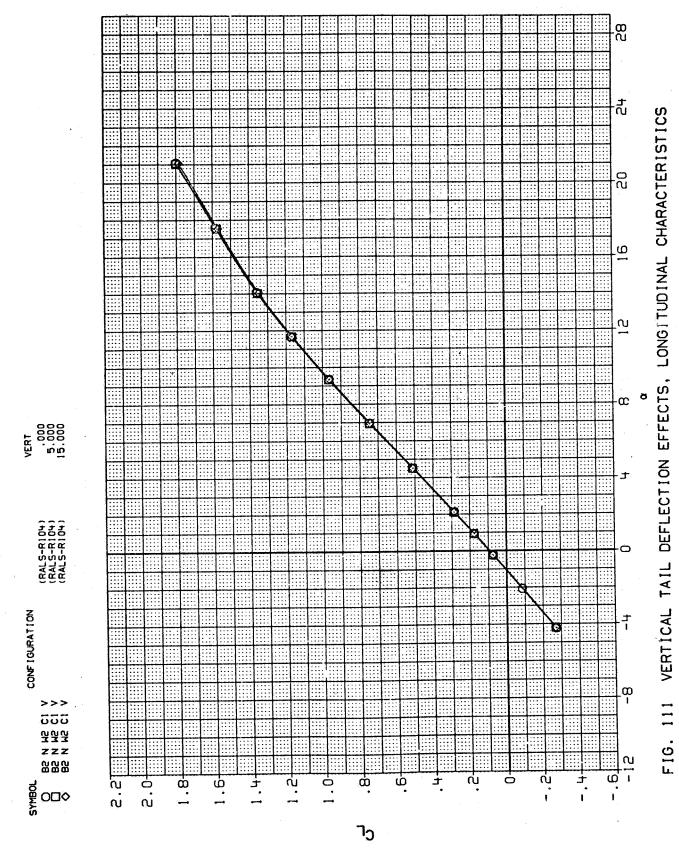
MACH ≃ .90



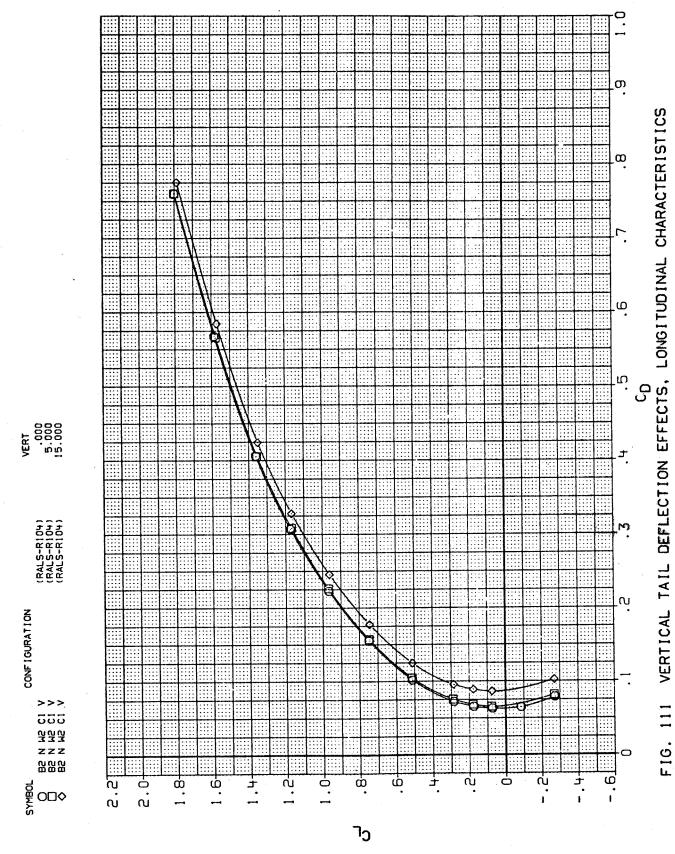
ij





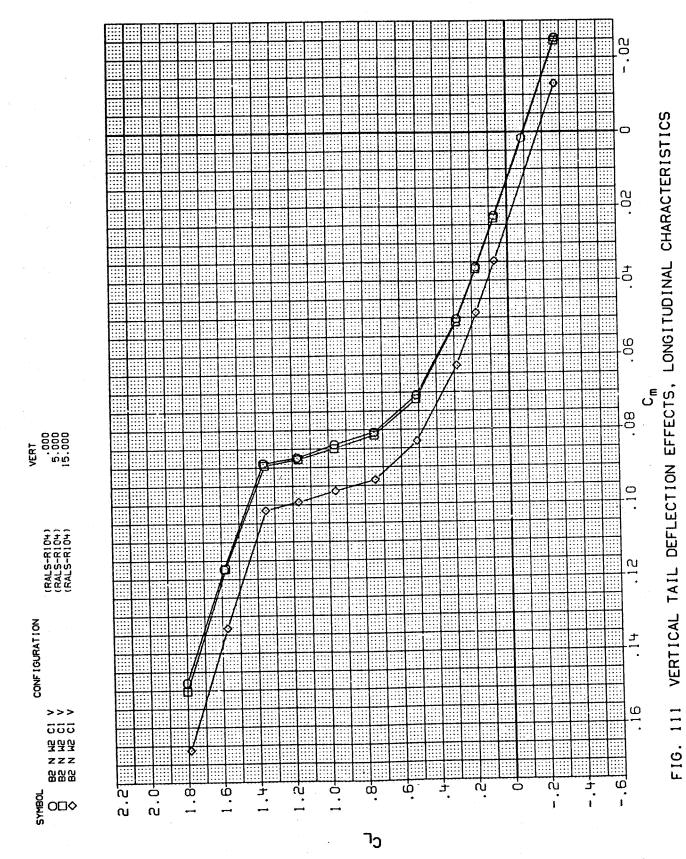


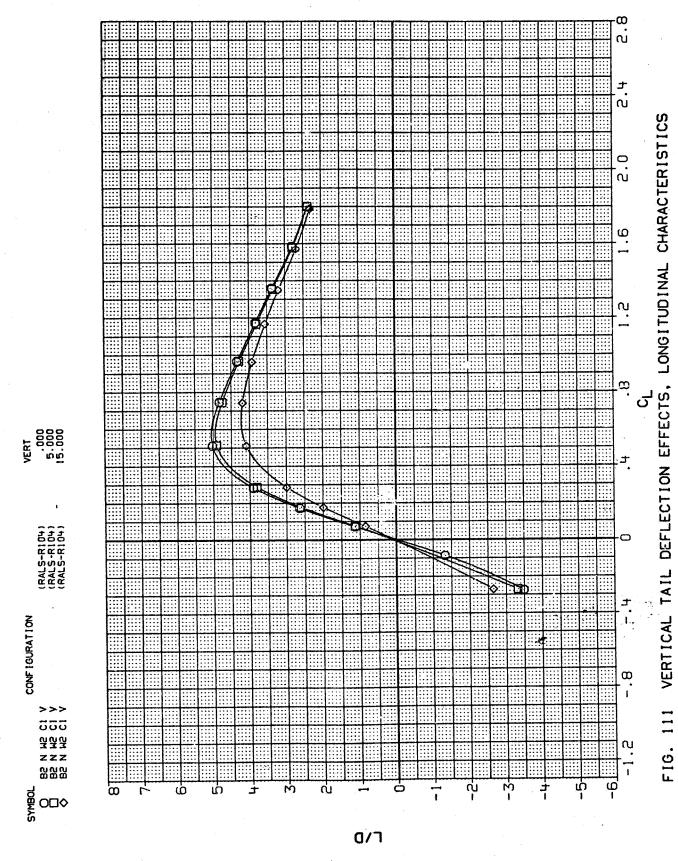
MACH = 1.20



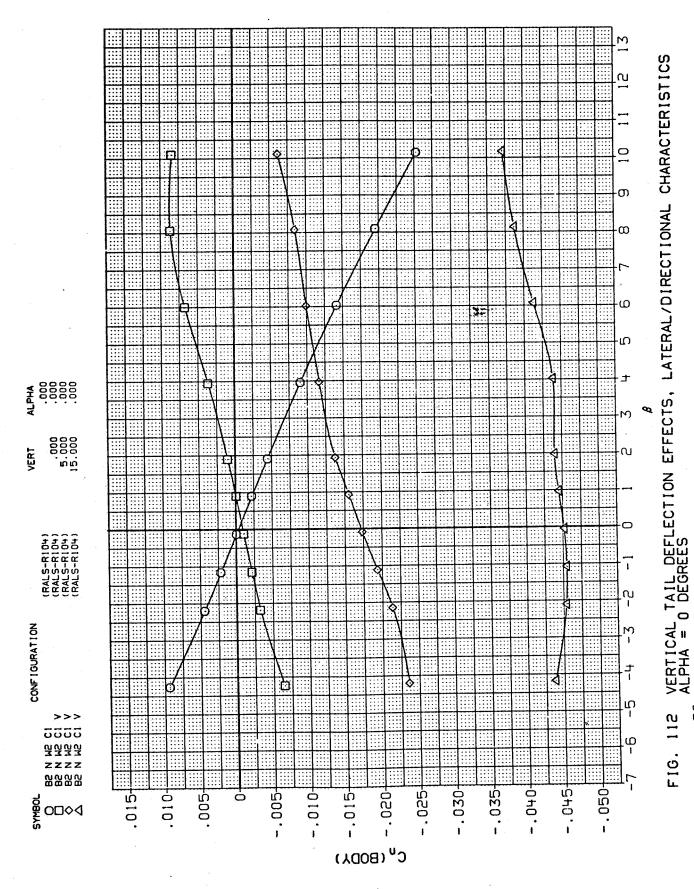
473

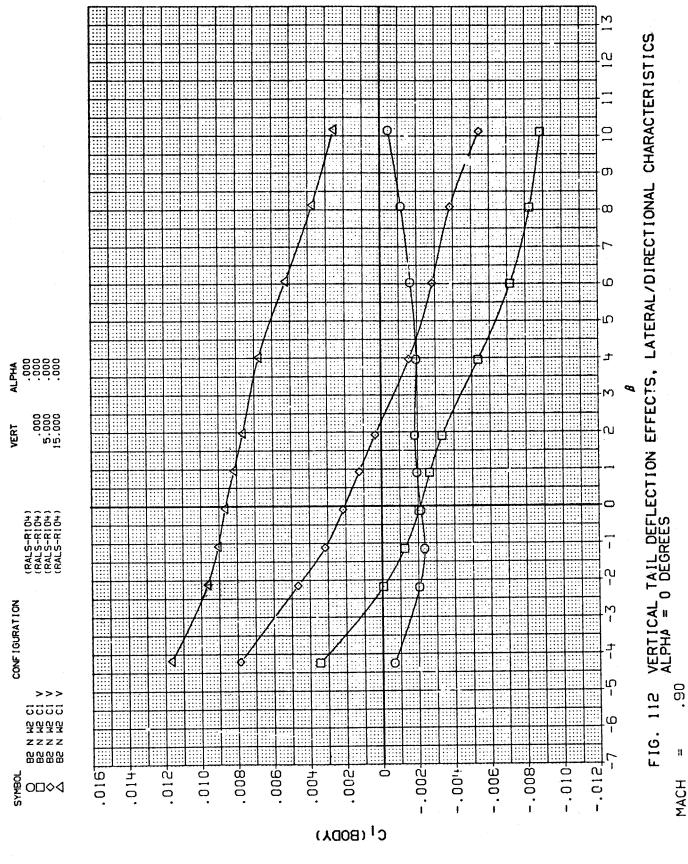
.3

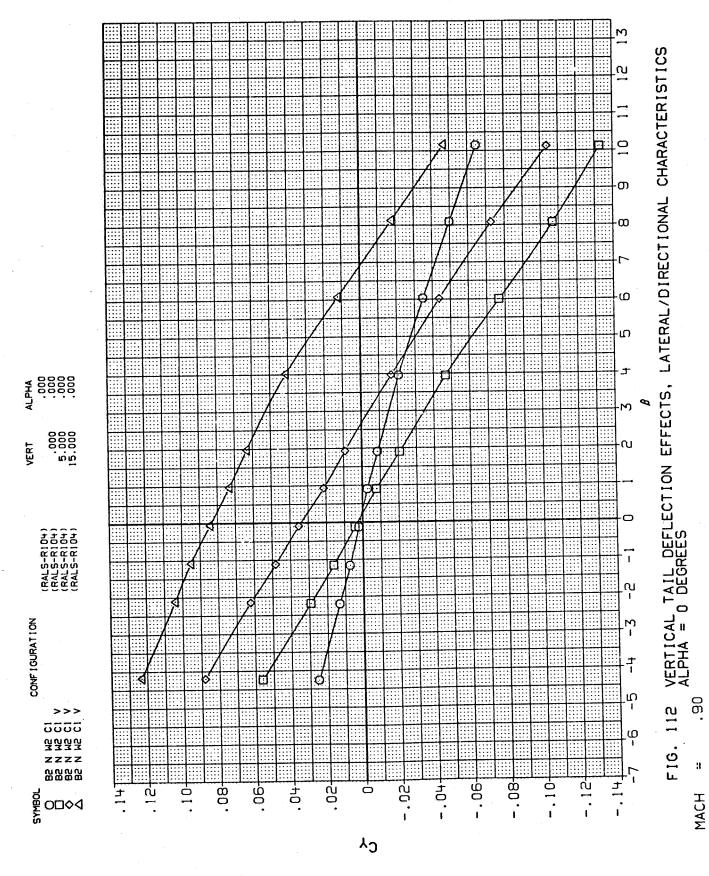


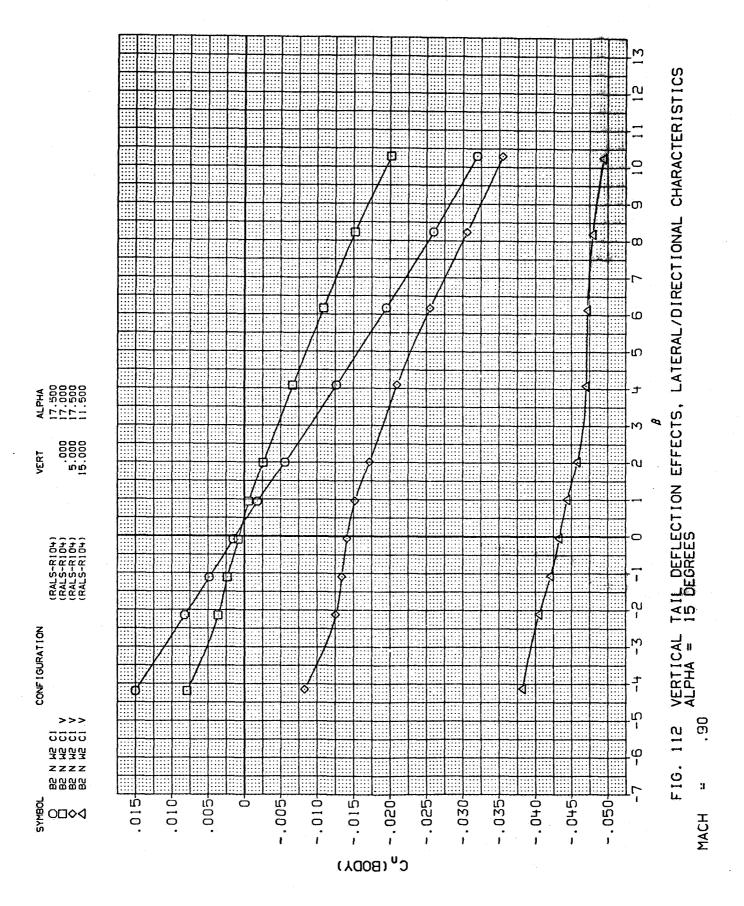


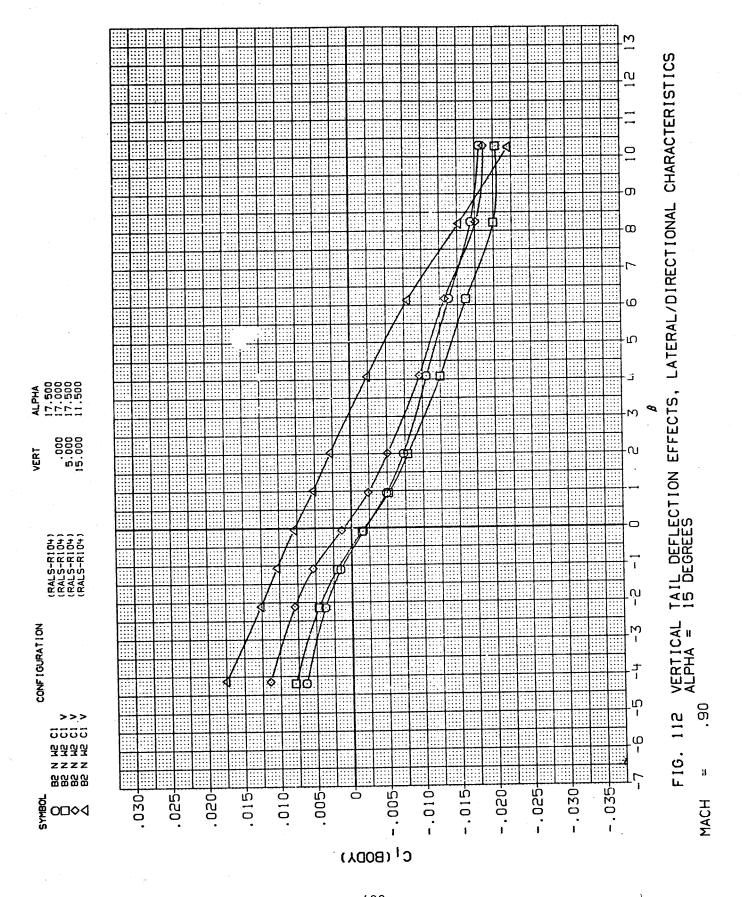
475

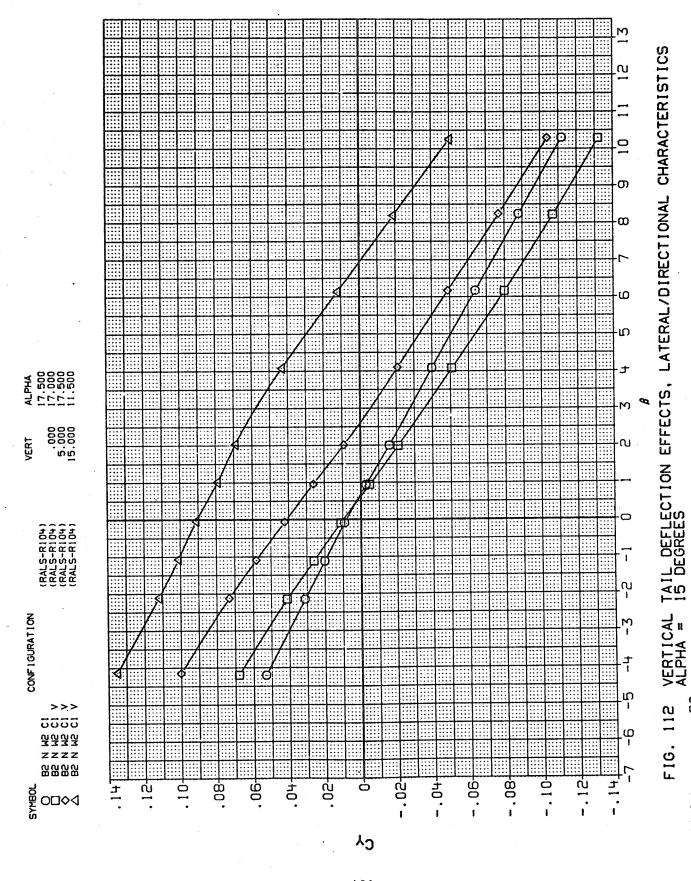


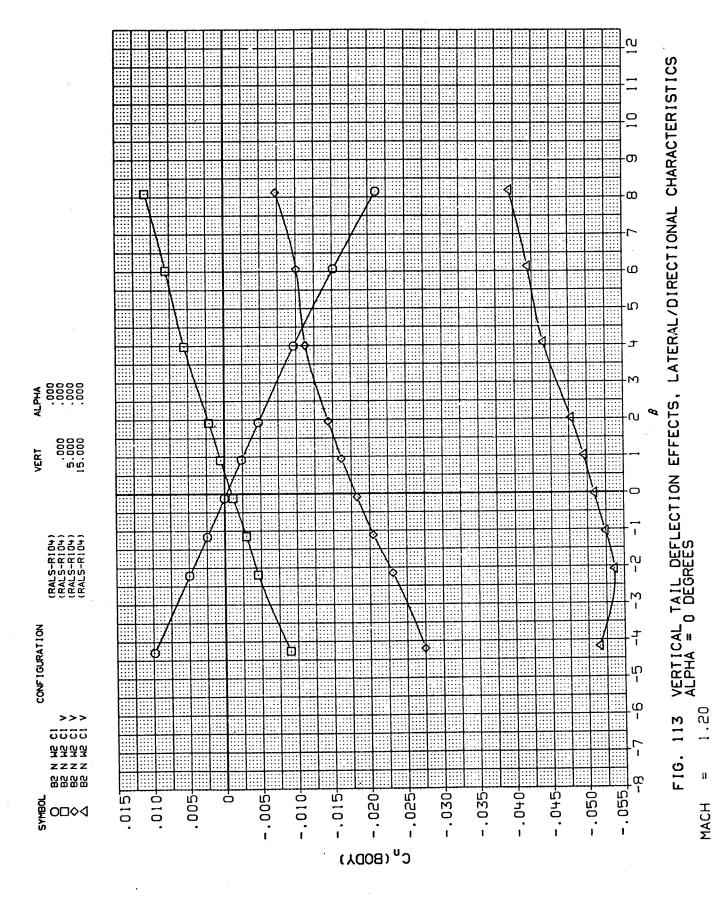


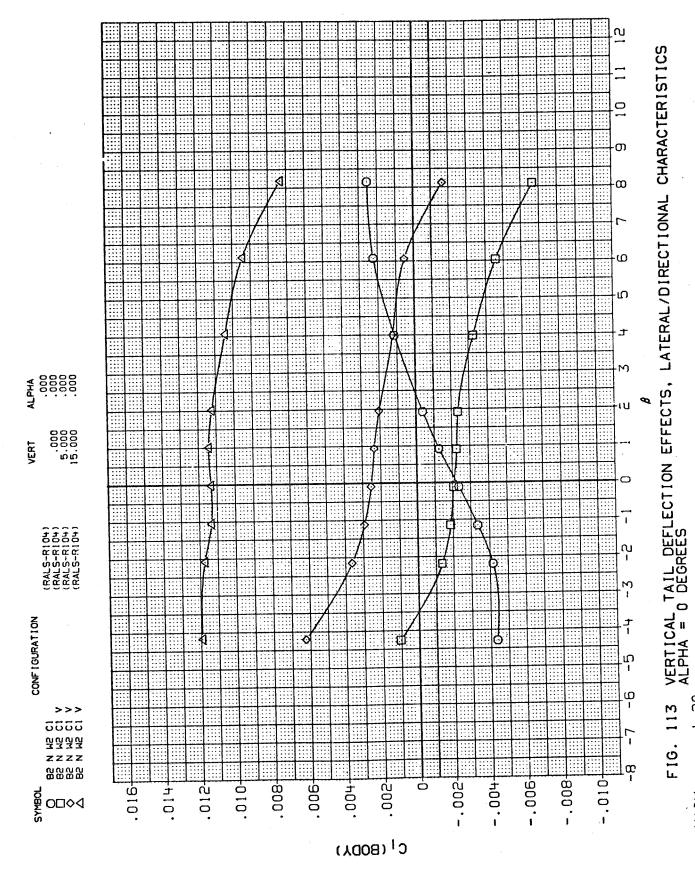


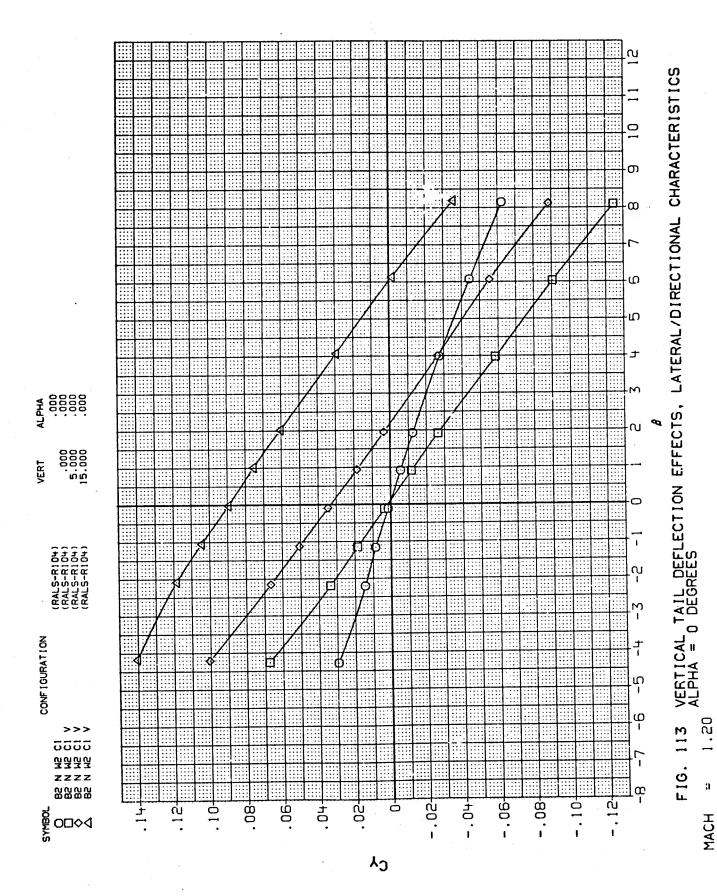




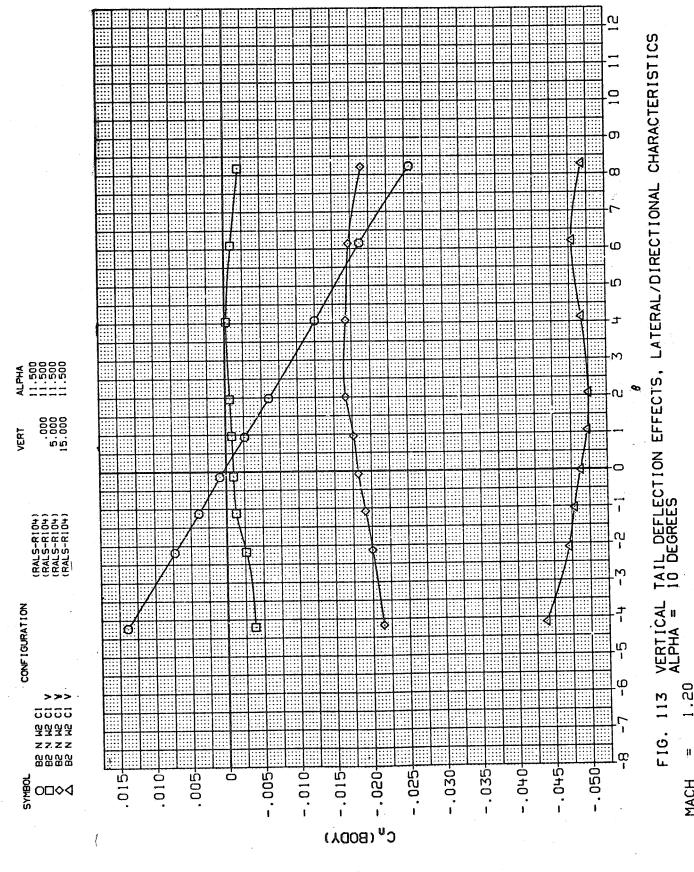


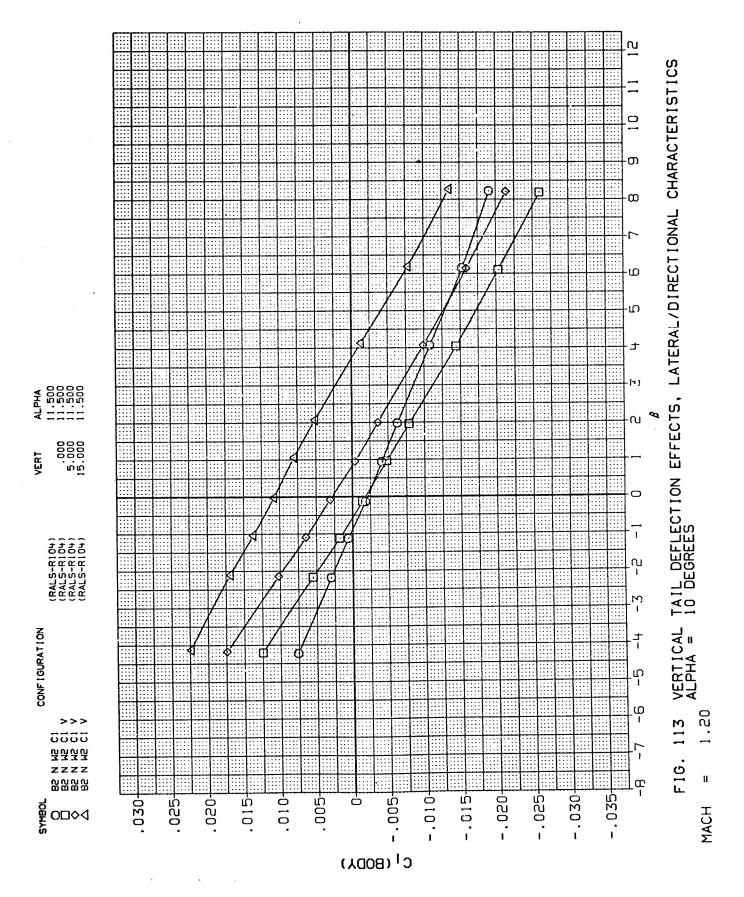


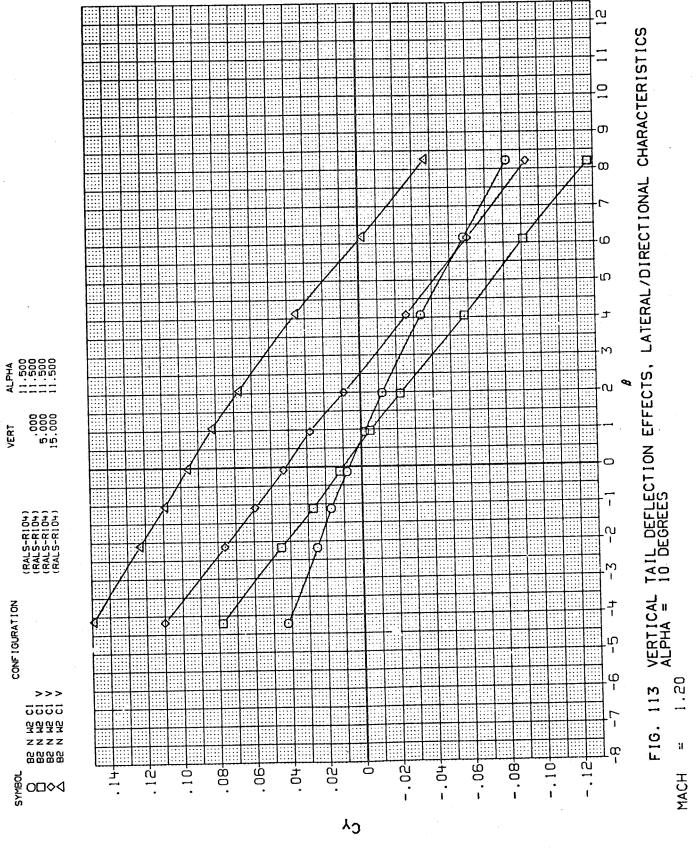


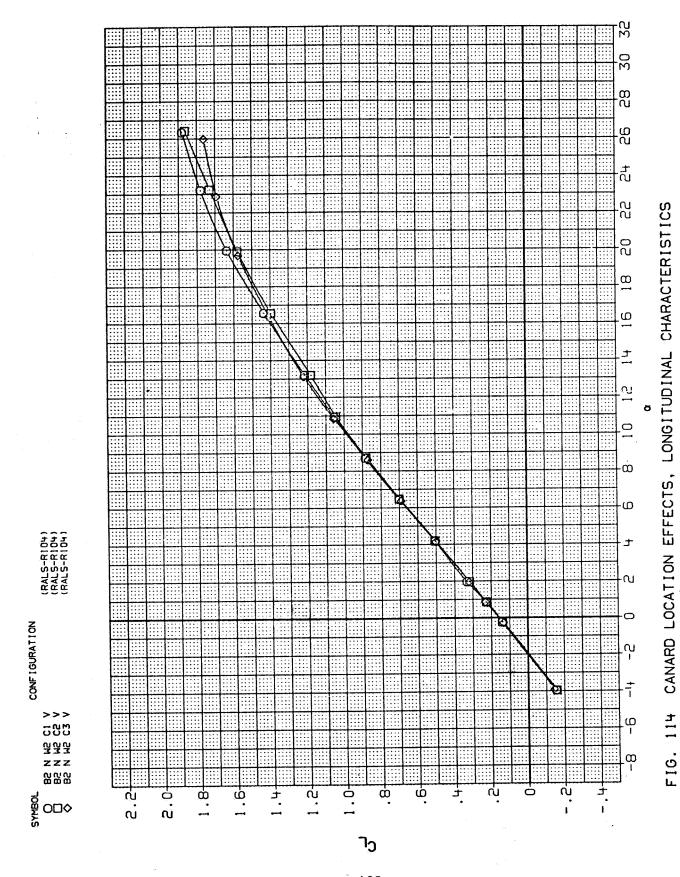


484

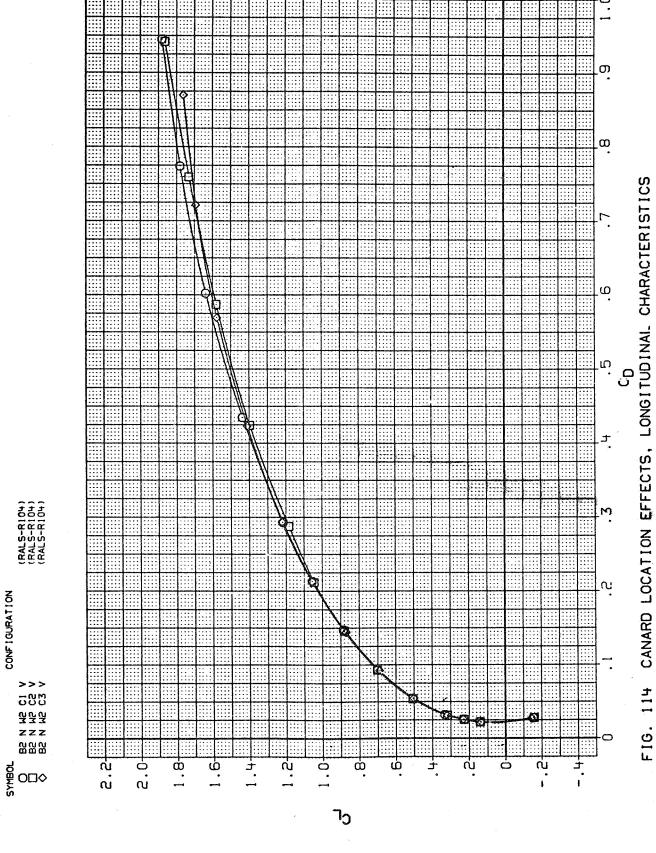




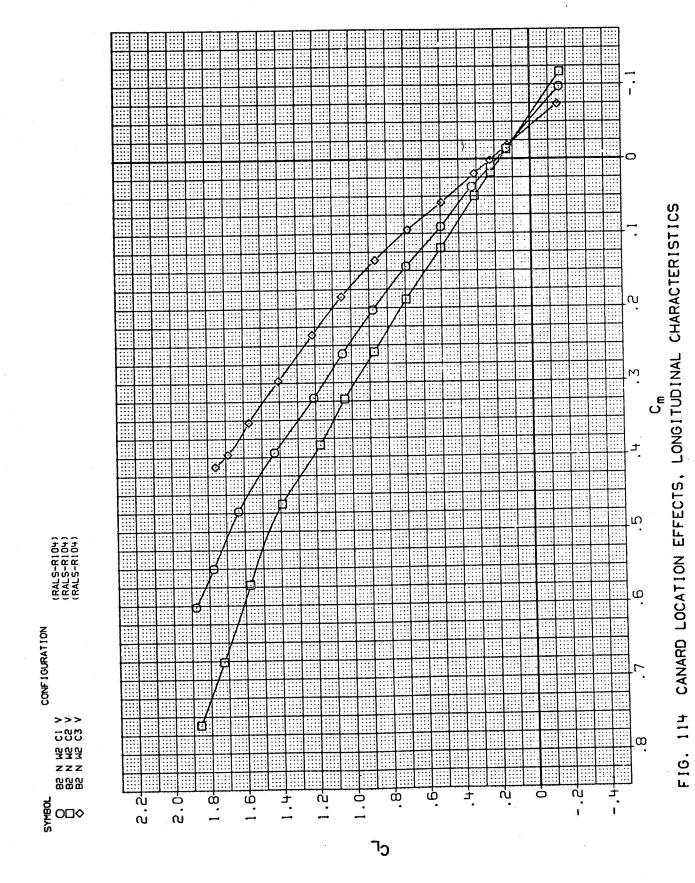




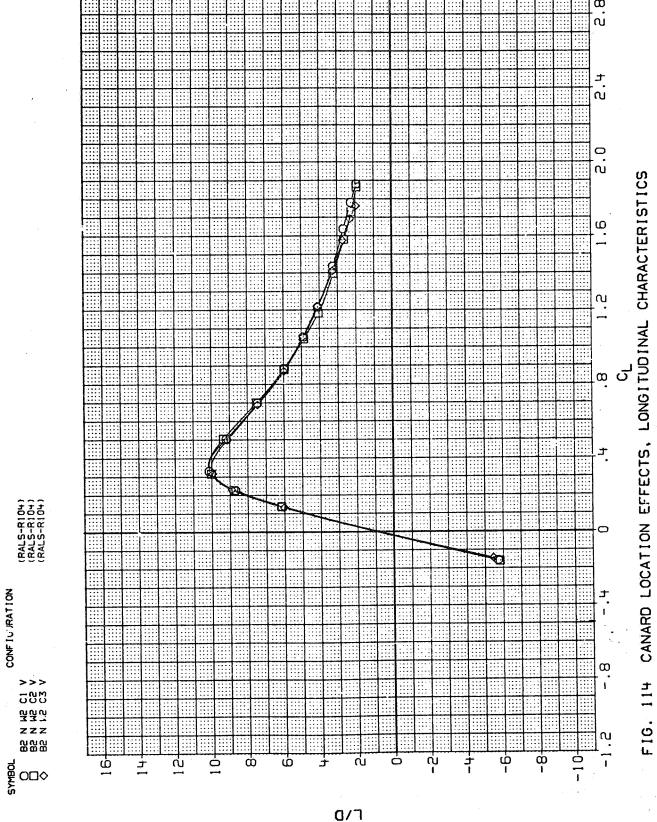
MACH = .60



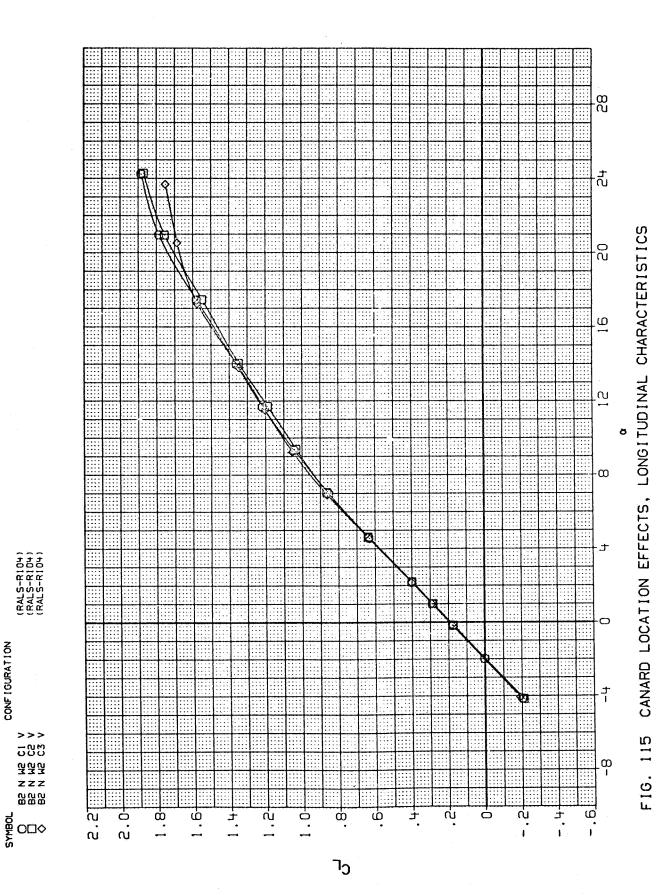
li



490



MACH



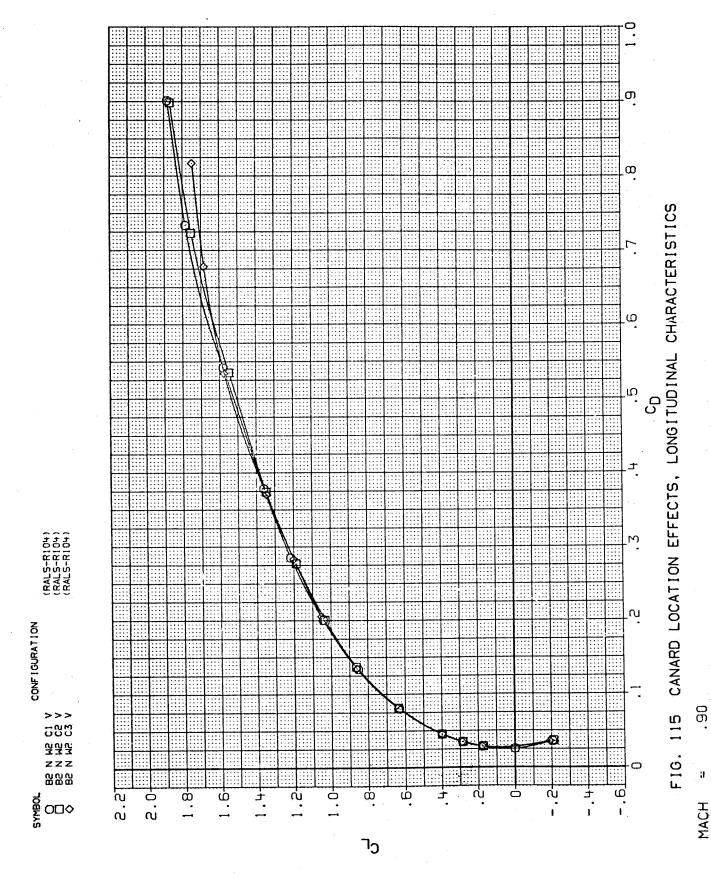
492

н

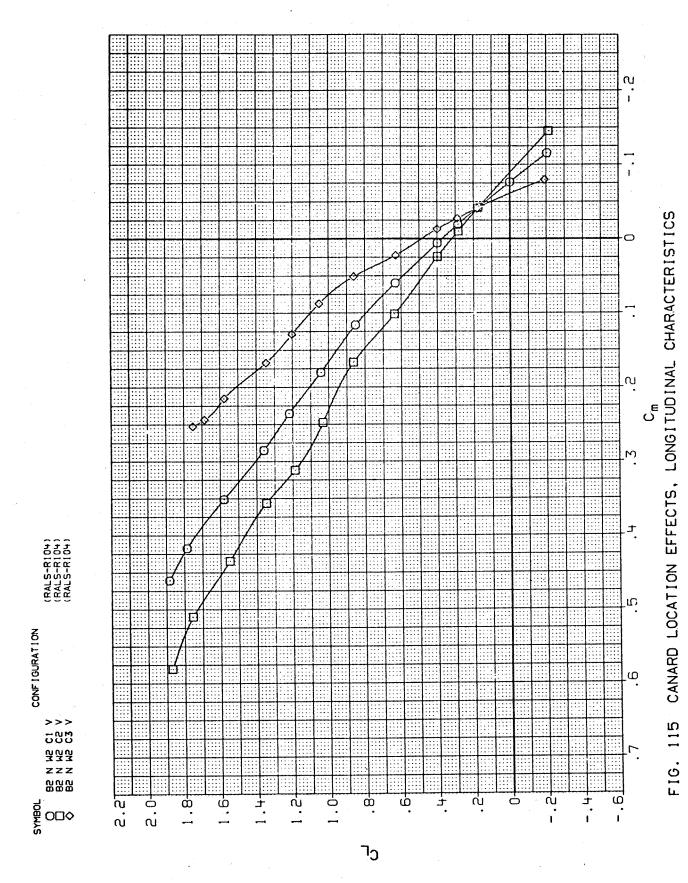
MACH

CONFIGURATION

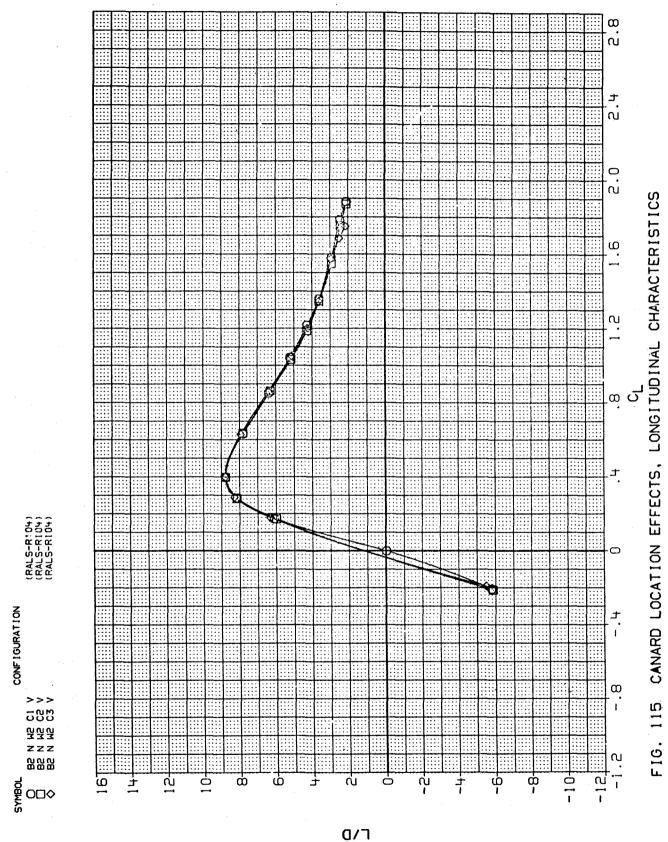
>>>



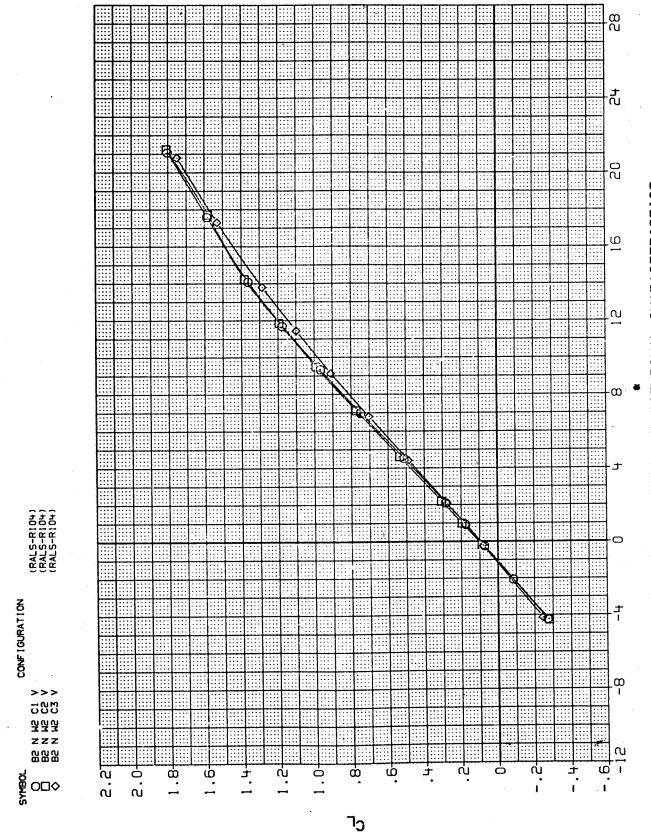
493



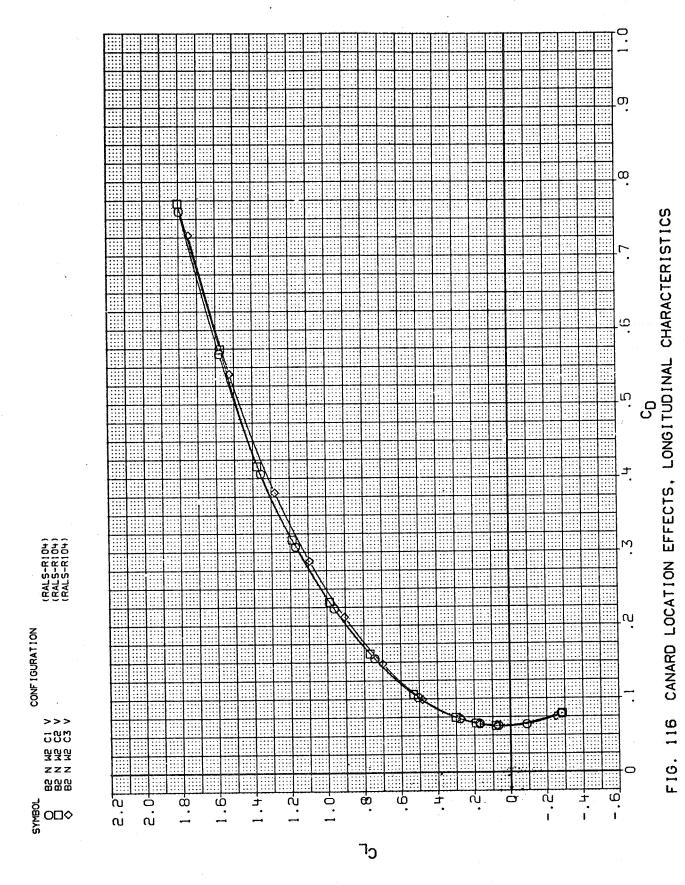
MACH = .90



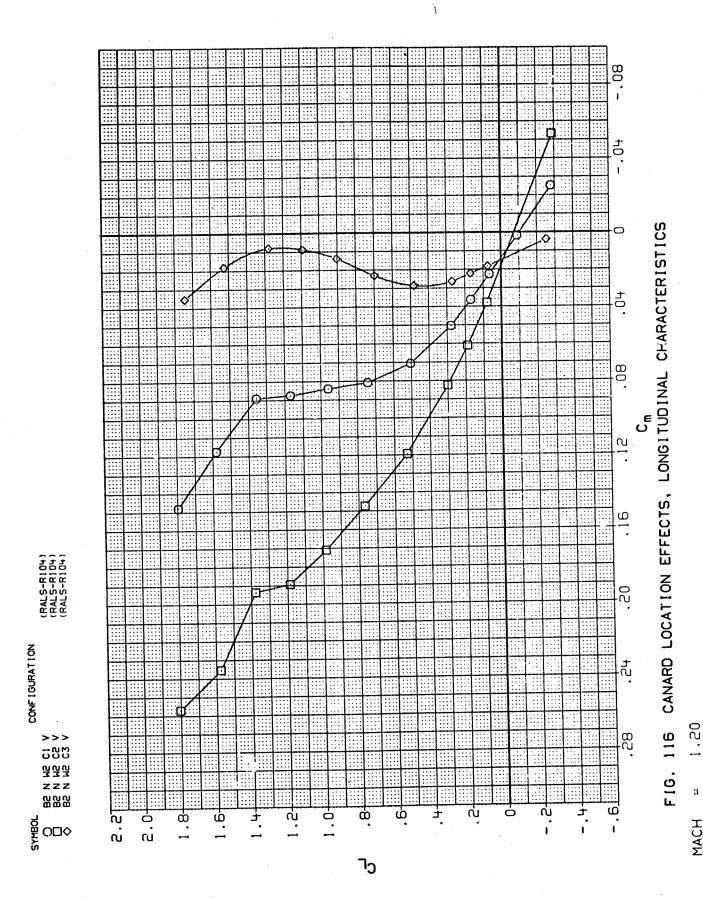
MACH = .90



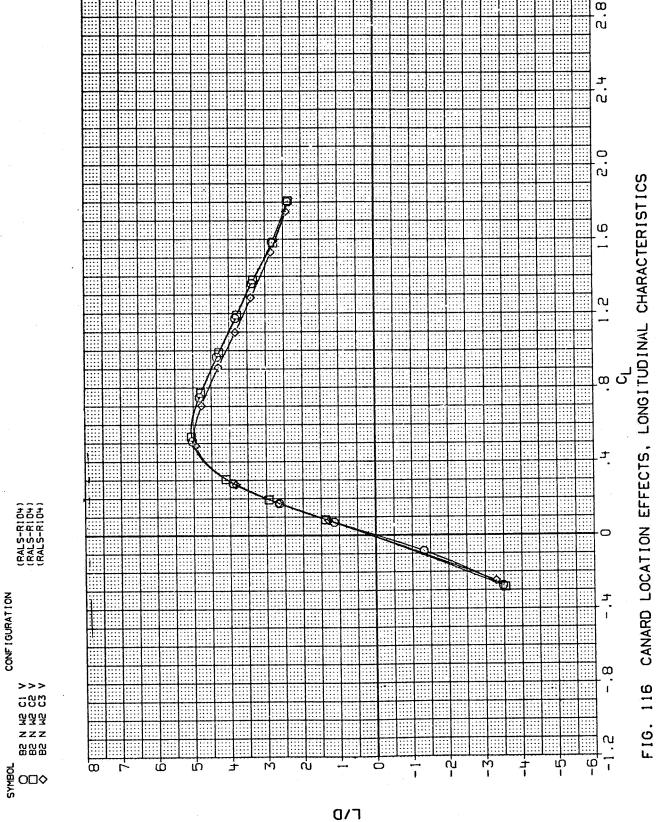
116 CANARD LOCATION EFFECTS, LONGITUBINAL CHARACTERISTICS F16.



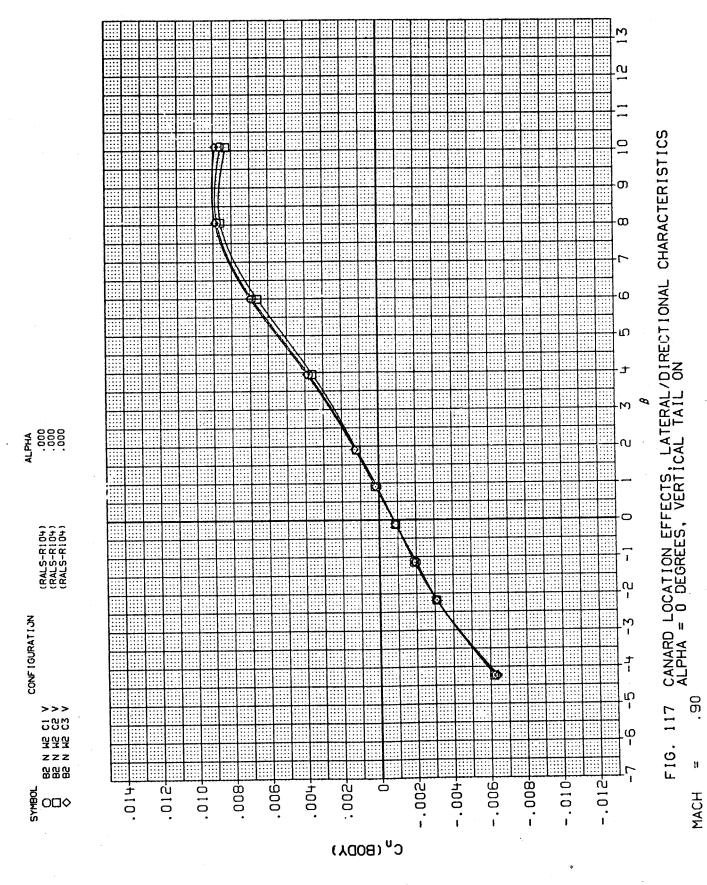
MACH = 1.2

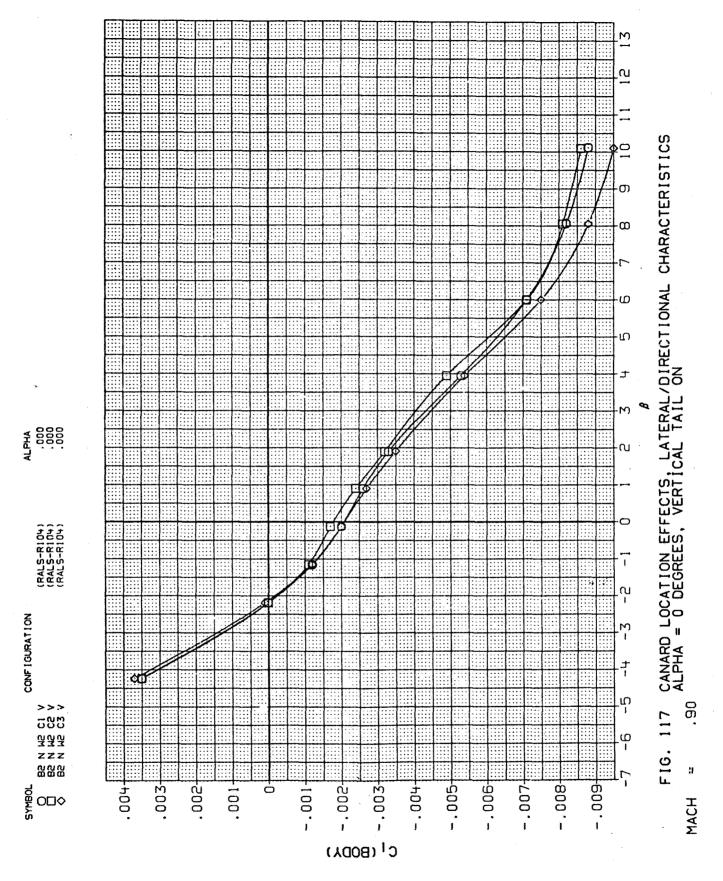


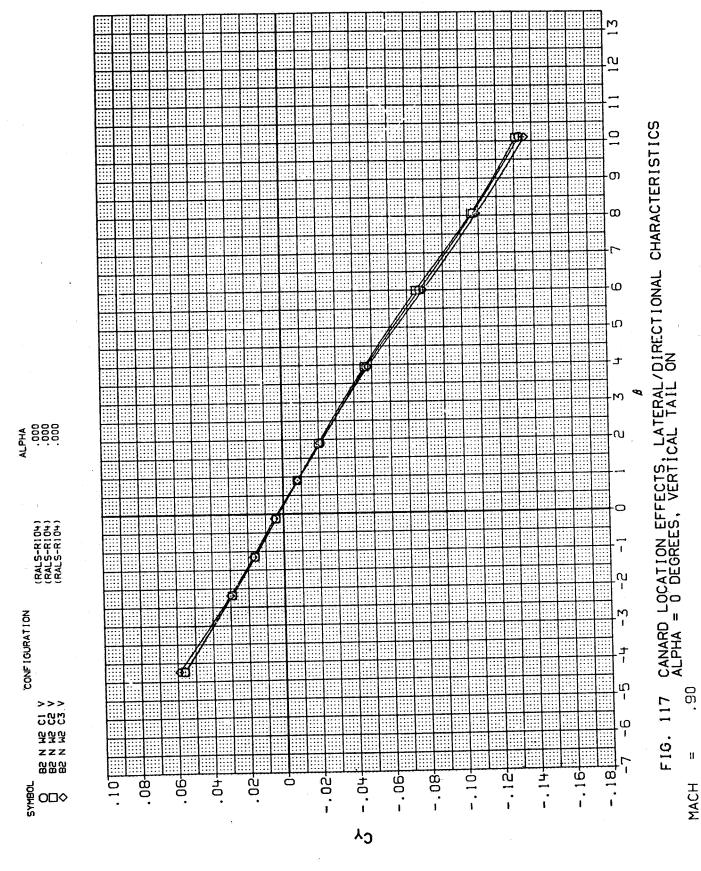
MACH

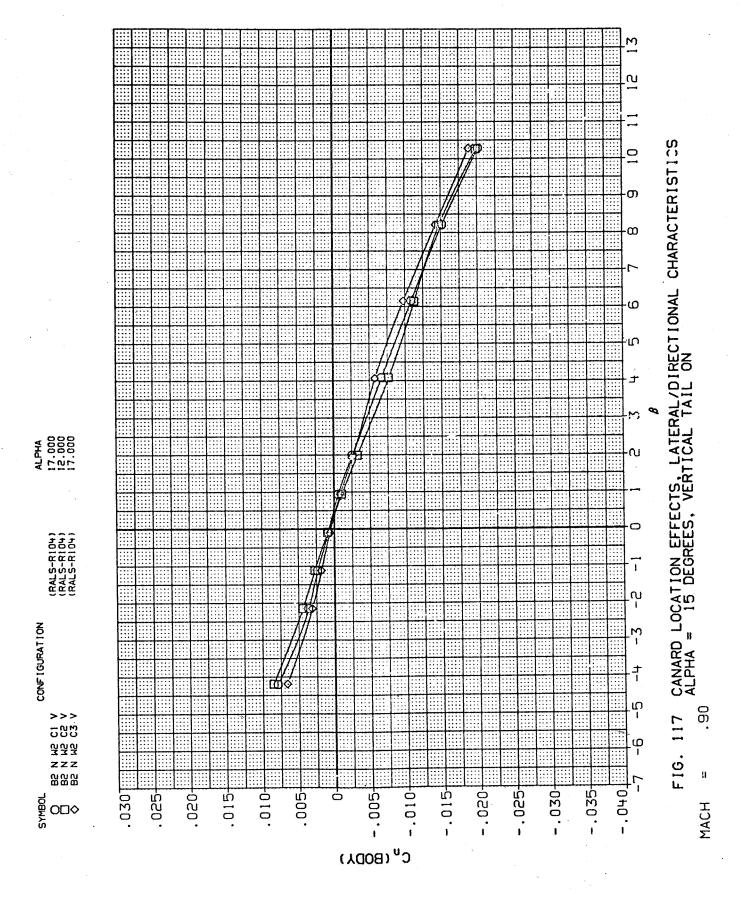


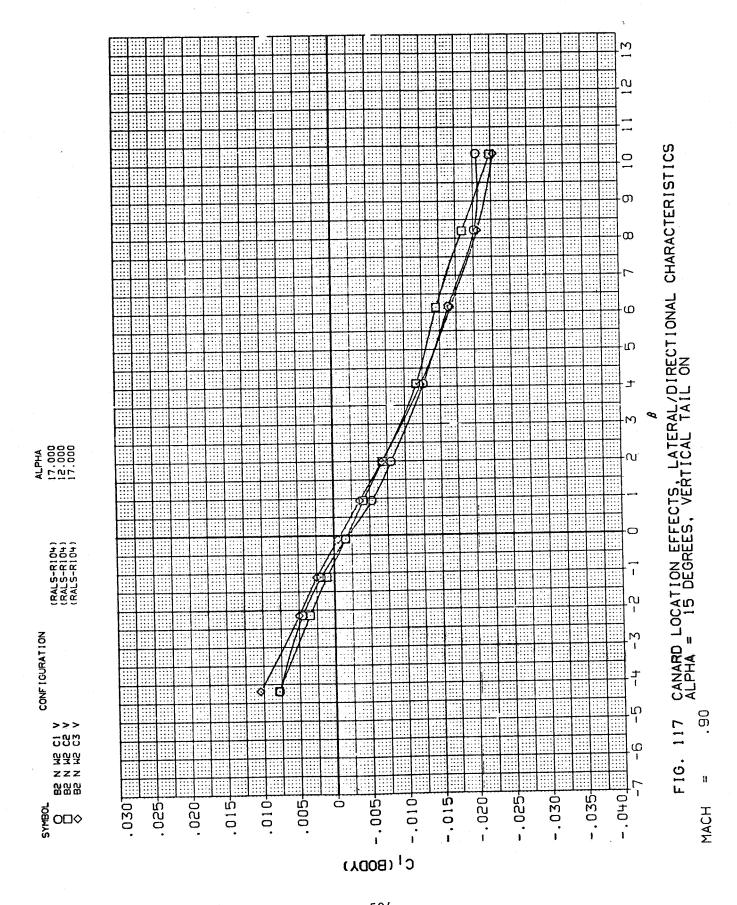
1.20

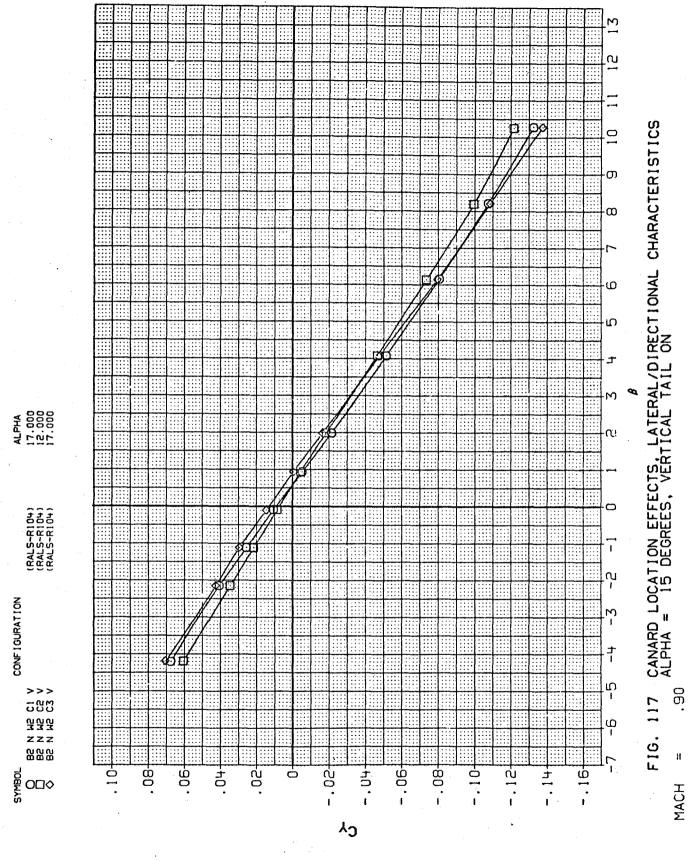




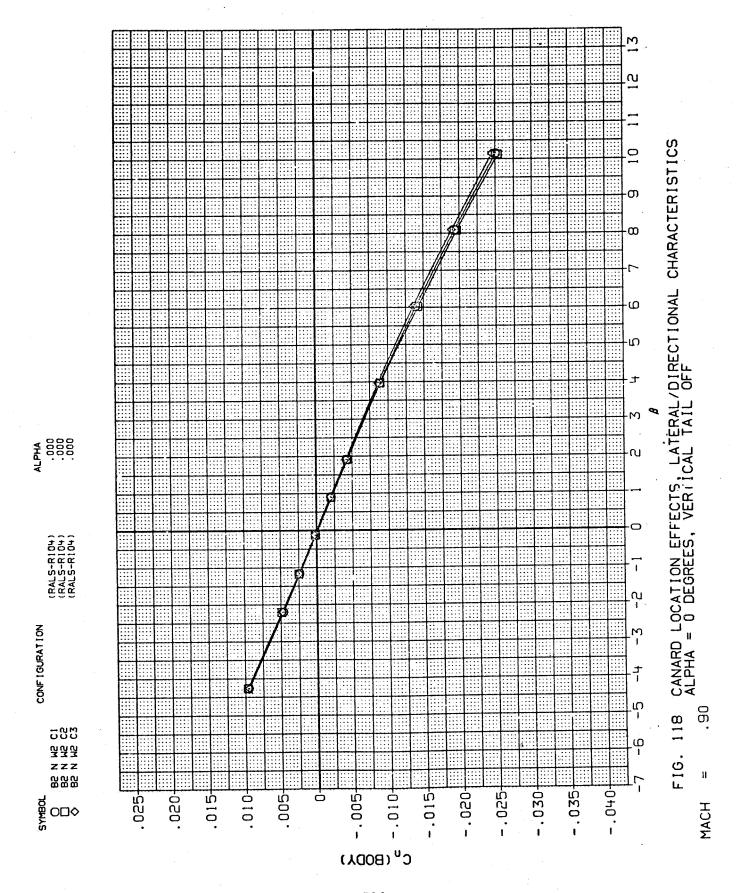


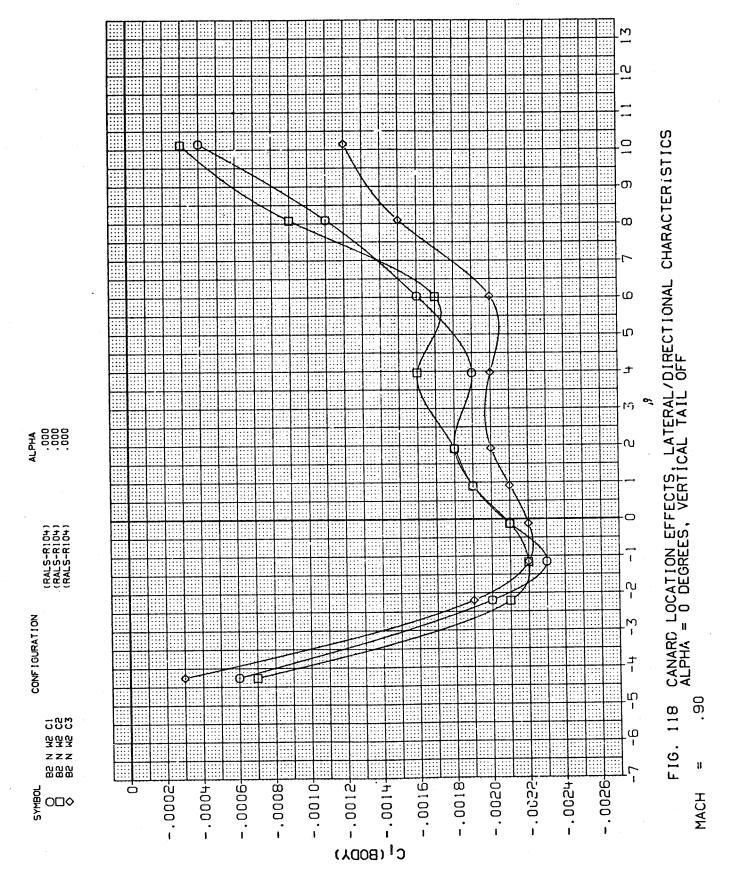


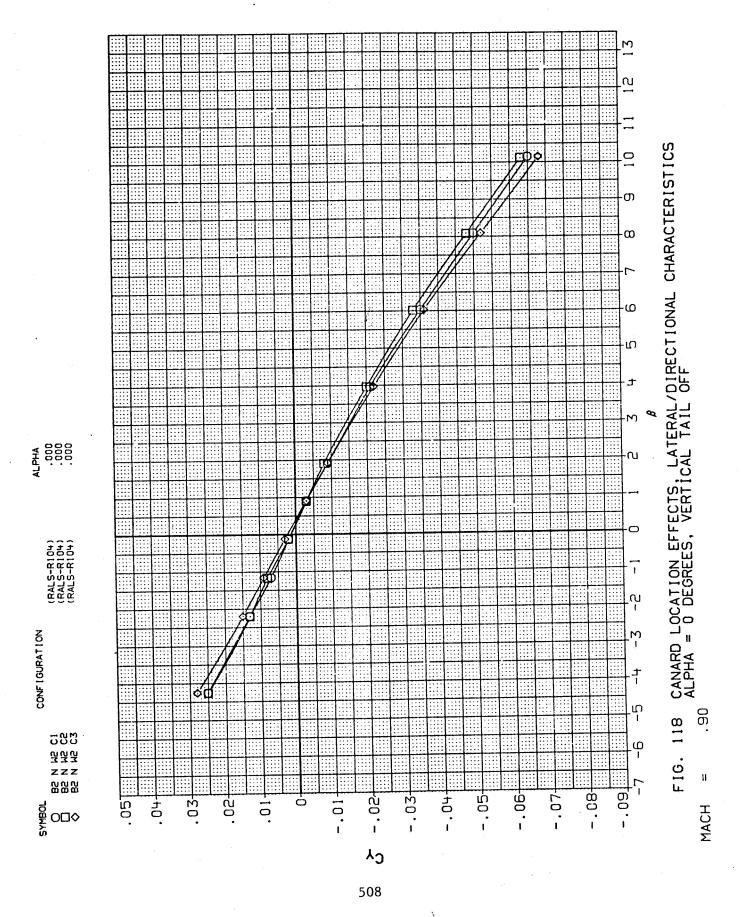


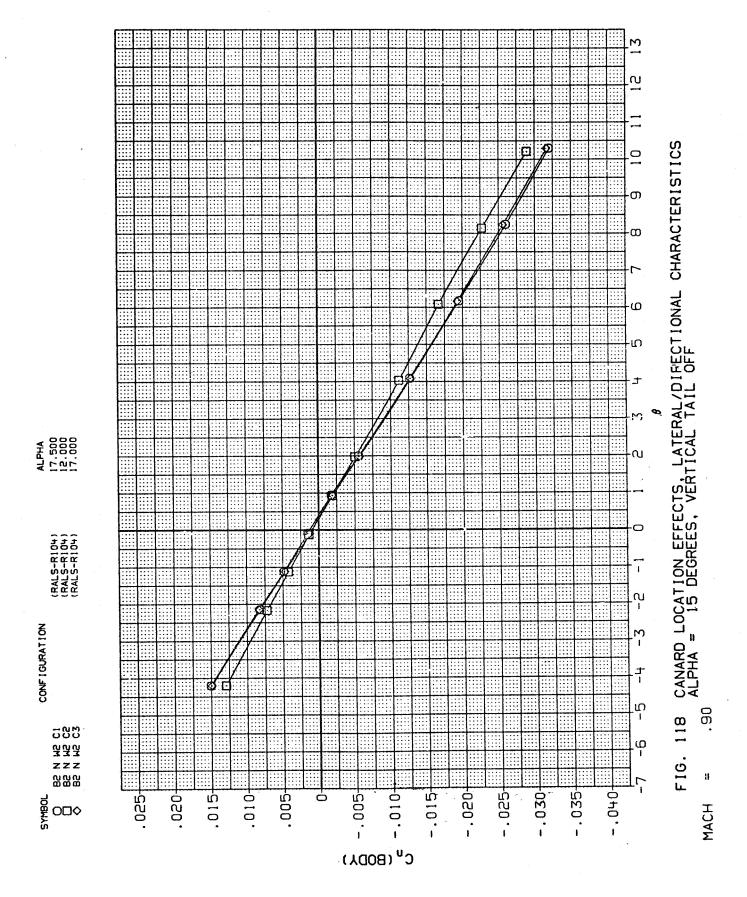


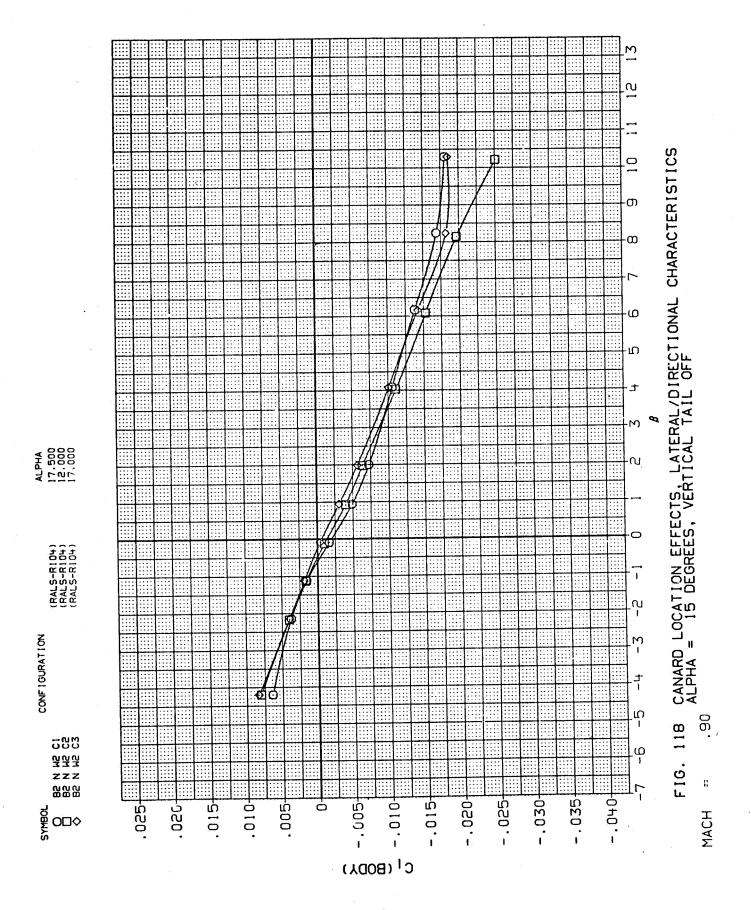
MACH

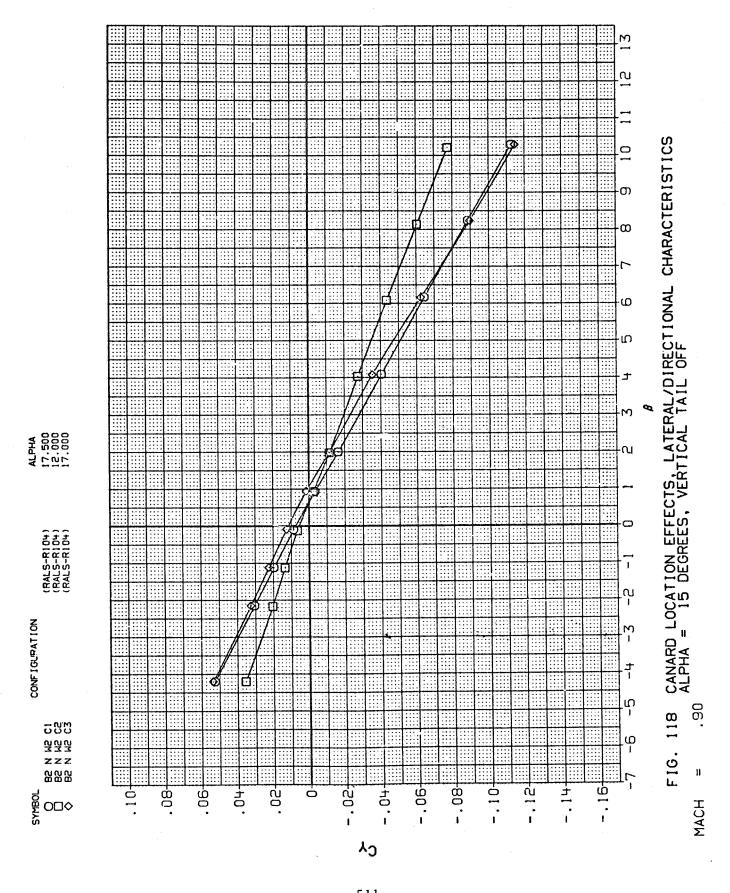


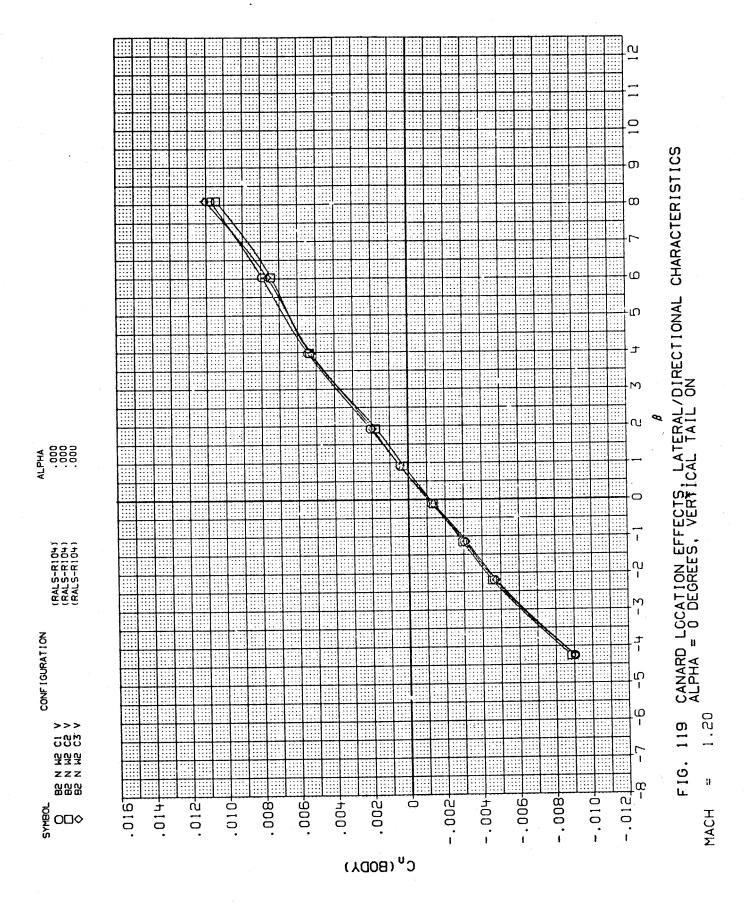


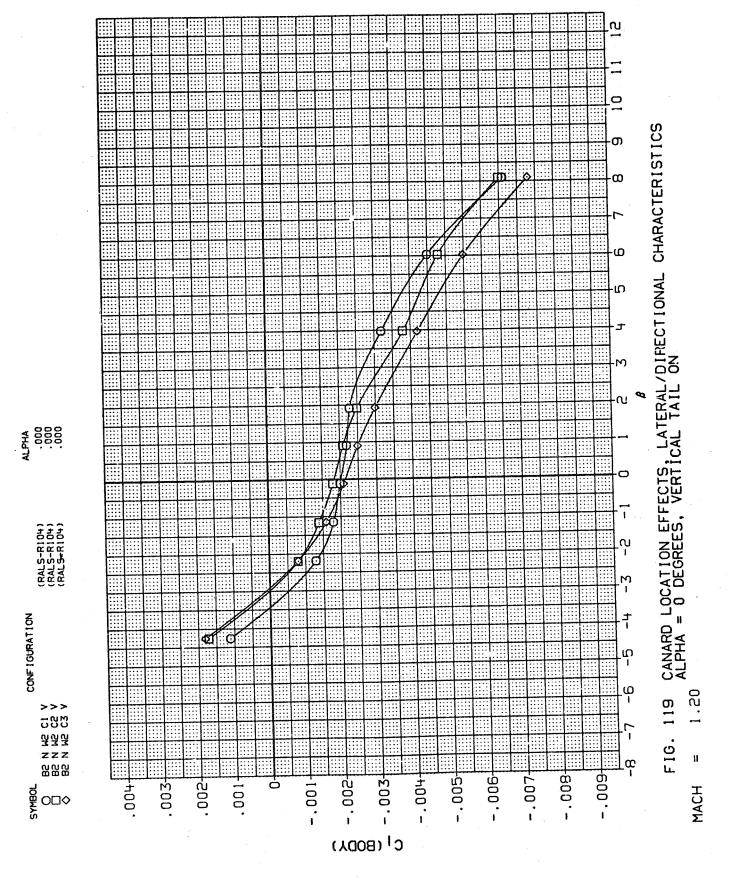


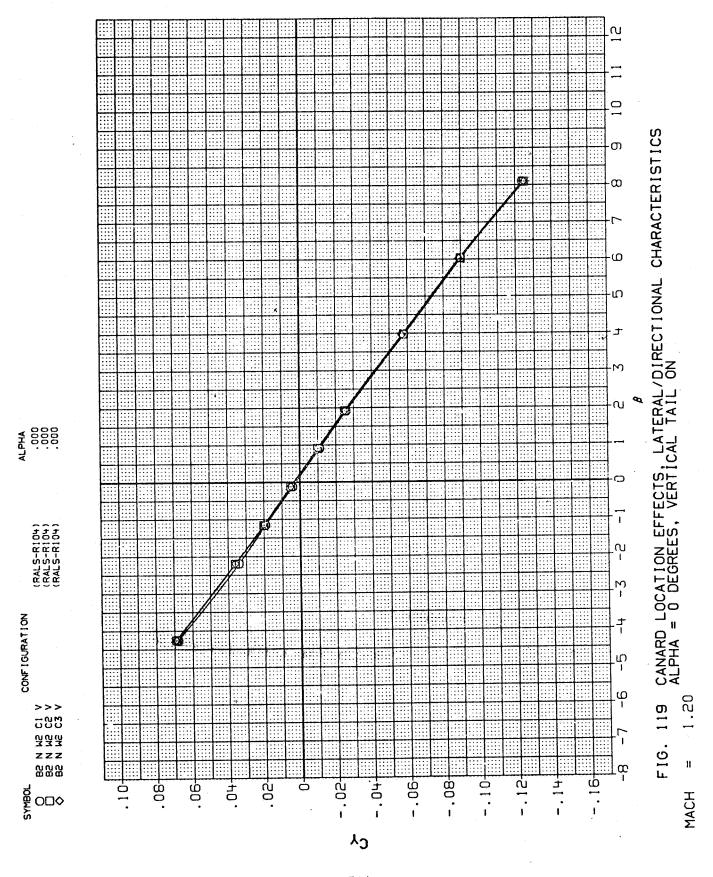


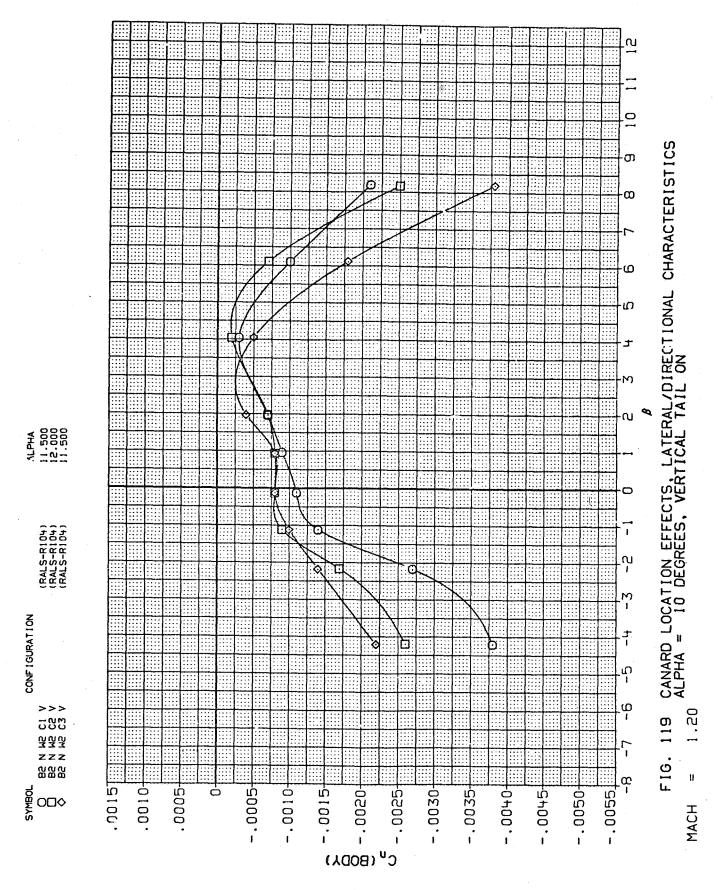


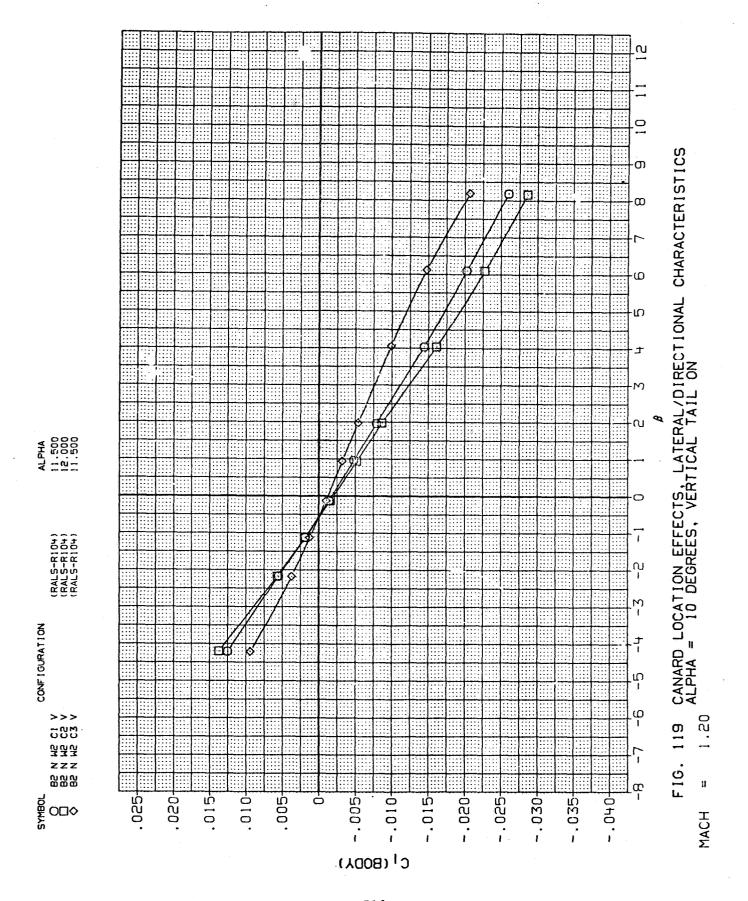


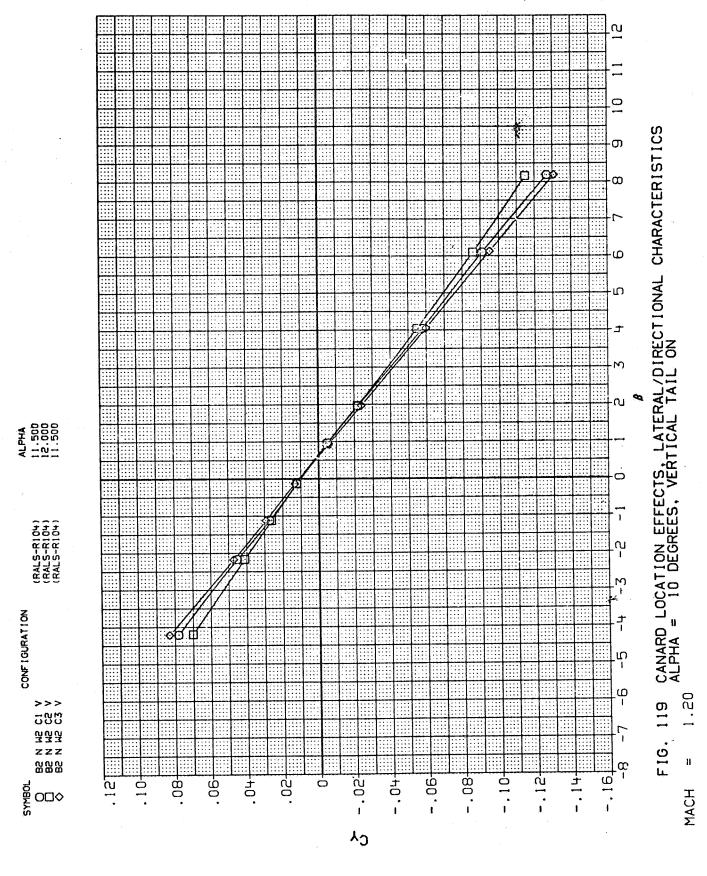


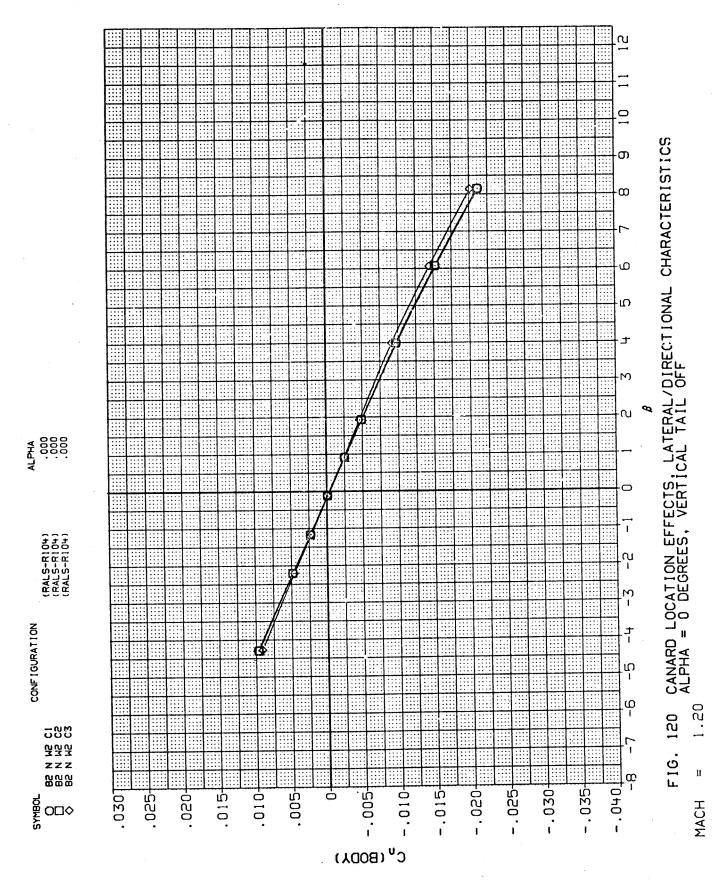


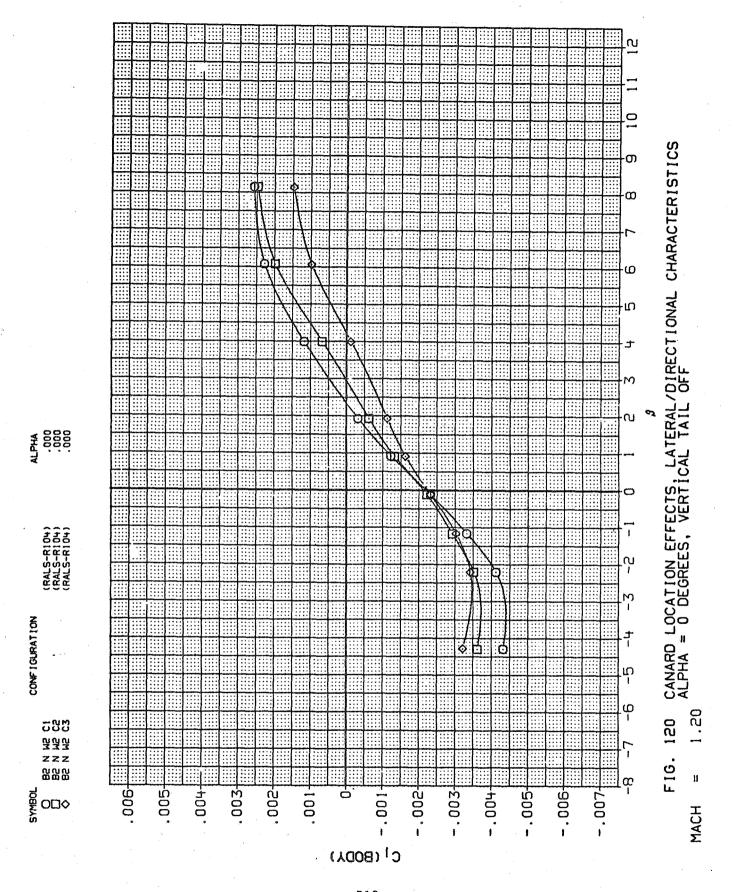


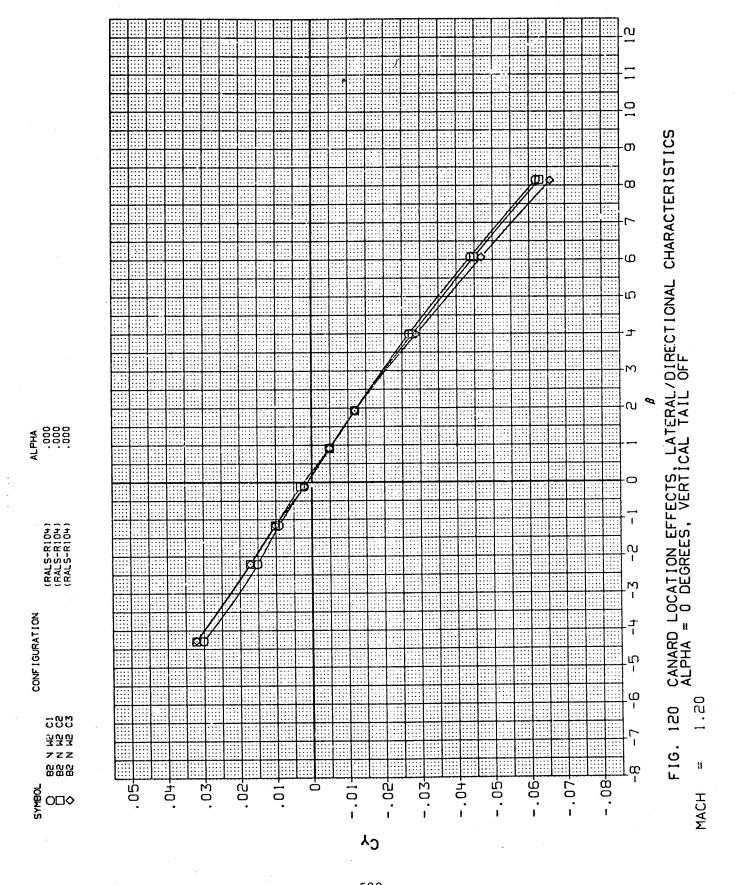


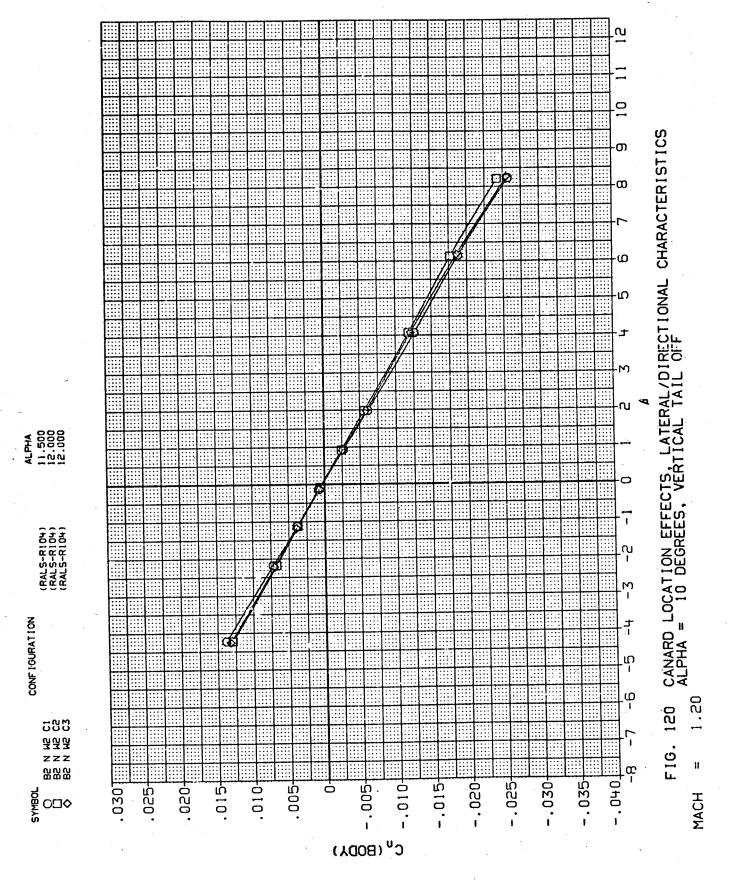


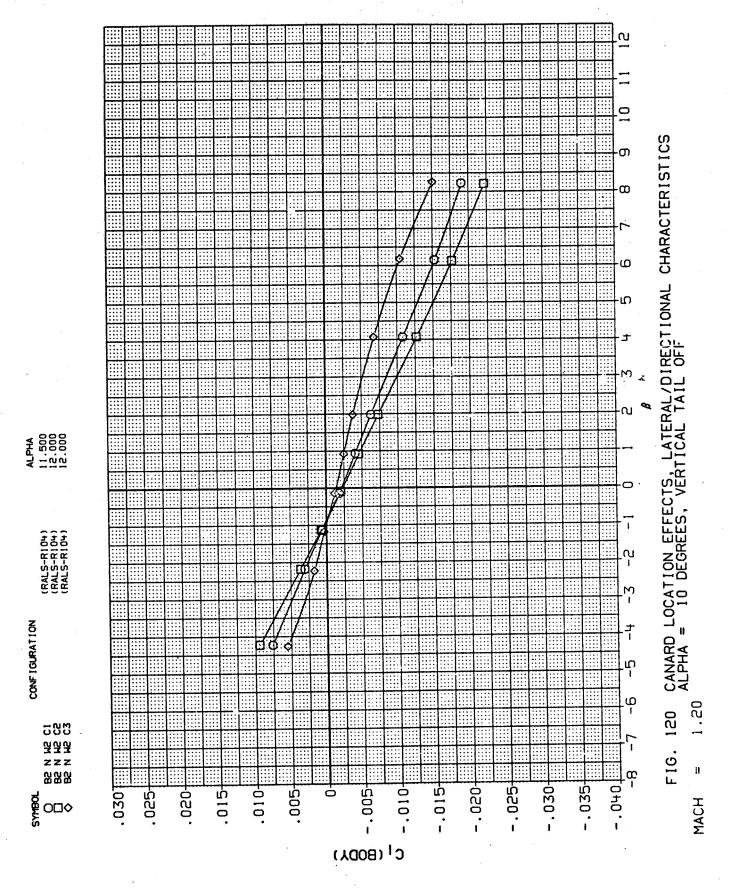


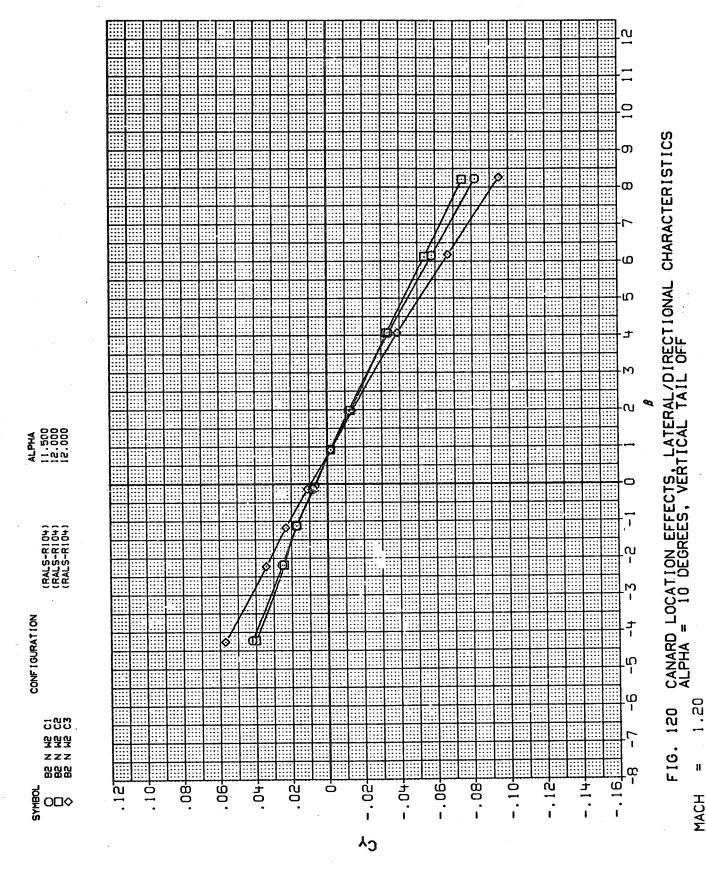












1. Re	eport No.	2. Government Acces	sion No.	3. Recipient's Catalog	No.	
N.A	ASA TM-81234					
4. Tit	itle and Subtitle			5. Report Date		
EX	XPERIMENTAL AERODYNAMIC CHARAC	TERISTICS OF TWO	WO V/STOL FIGHTER/			
1	ATTACK AIRCRAFT CONFIGURATIONS AT MACH NUMBERS FROM 0.4 TO 1.4			6. Performing Organization Code		
7. Au	uthor(s)				ation Report No.	
Wa	alter P. Nelms, Donald A. Durs	ton, and J. R. Lu	. Lummus*	A-8338		
				10. Work Unit No.		
9. Per	erforming Organization Name and Address			505-42-71		
	ASA, Ames Research Center offett Field, Calif. 94035	Division , Texas	11. Contract or Grant			
				13. Type of Report an		
12. Sp	2. Sponsoring Agency Name and Address			Technical Memorandum		
	ational Aeronautics and Space ashington, D.C. 20546		14. Sponsoring Agency	Code		
15. Su	upplementary Notes	**************************************	,,,,,,,,,,,,,,,,,,,,,,,,,,,,,,,,,,,,,,	· · · · · · · · · · · · · · · · · · ·		
16. Ab	bstract		<u> </u>	······································		
cc ir De li ir ce	A wind-tunnel test was conducted at Ames Research Center (ARC) to measure the aerodynamic characteristics of two horizontal-attitude takeoff and landing V/STOL fighter/attack aircraft concepts. The concepts were developed by the General Dynamics Corporation, Fort Worth Division, in a contract study for Ames Research Center and the David Taylor Naval Ship Research and Development Center (DTNSRDC). In one concept, a jet diffuser ejector was used for the vertical lift system; the other used a remote augmentation lift system (RALS). Wind-tunnel tests to investigate the aerodynamic uncertainties and to establish a data base for these types of concepts have been conducted at ARC over a Mach number range from 0.2 to 2.0. The present report covers tests, conducted in the Ames 11-Foot Transonic Wind Tunnel, for Mach numbers from 0.4 to 1.4. Detailed effects of varying the angle of attack (up to 27°), angle of sideslip (-4° to +8°), Mach number, Reynolds number, and configuration buildup were investigated. In addition, the effects of wing trailing-edge flap deflections, canard incidence, and vertical tail deflections were explored. Variable canard longitudinal location and different shapes of the inboard nacelle-body strakes were also investigated.					
ac ta	ddition, the effects of wing t ail deflections were explored.	railing-edge flap Variable canard	configuration builds deflections, canard longitudinal locat	up were investiga I incidence, and	from 0.4 Slip ated. In vertical	
ad ta th	ddition, the effects of wing t ail deflections were explored.	railing-edge flap Variable canard	configuration builds deflections, canard longitudinal locat	up were investigated incidence, and lon and different	from 0.4 Slip ated. In vertical	
ad ta th	ey Words (Suggested by Author(s))	railing-edge flap Variable canard	configuration builds deflections, canard longitudinal locations trigated.	up were investigated incidence, and lon and different	from 0.4 Slip ated. In vertical	
17. Ke	ey Words (Suggested by Author(s)) Cighter/attack aircraft Decreosystem of the company of the com	railing-edge flap Variable canard s were also inves	configuration builds deflections, canard longitudinal locations at least the second second location with the second location loca	up were investigated incidence, and lon and different	from 0.4 Slip ated. In vertical	
17. Ke Fi Ae Ve	ey Words (Suggested by Author(s)) Cighter/attack aircraft Lerodynamic technology Vectored-engine-over-wing (VEO-	railing-edge flap Variable canard s were also inves	configuration builds deflections, canard longitudinal locations trigated.	up were investigated incidence, and lon and different	from 0.4 slip nted. In vertical shapes of	
17. Ke Fi Ae Ve Re	ey Words (Suggested by Author(s)) Cighter/attack aircraft Decreosystem of the company of the com	railing-edge flap Variable canard s were also inves	configuration builds deflections, canard longitudinal locations trigated.	up were investigated incidence, and lon and different	from 0.4 slip nted. In vertical shapes of	
17. Ke Fi Ae Ve Re P1	ey Words (Suggested by Author(s)) Cighter/attack aircraft Lerodynamic technology Cectored-engine-over-wing (VEO- Lemote augmentation lift system	railing-edge flap Variable canard s were also inves	configuration builds deflections, canard longitudinal locations trigated.	up were investigated incidence, and lon and different	from 0.4 slip nted. In vertical shapes of	
17. Ker Fi Ae Ve Re Pi VS	ey Words (Suggested by Author(s)) Cighter/attack aircraft Lerodynamic technology Cectored-engine-over-wing (VEO- Emote augmentation lift system Cropulsive lift	railing-edge flap Variable canard s were also inves	configuration builds deflections, canard longitudinal locations trigated. 18. Distribution Statement Unlimited	up were investigated incidence, and lon and different	from 0.4 slip nted. In vertical shapes of	